



The Ohio State University

DAA/Langley p.425
LANGLEY GRANT
11-32-CR
93173

A UNIFORM GTD ANALYSIS OF THE EM DIFFRACTION BY A THIN
DIELECTRIC/FERRITE HALF-PLANE AND RELATED CONFIGURATIONS

by

Roberto G. Rojas

The Ohio State University

ElectroScience Laboratory

Department of Electrical Engineering
Columbus, Ohio 43212

Technical Report No. 716199-5
Grant No. NSG-1498
March 1985

National Aeronautics and Space Administration
Langley Research Center
Hampton, Virginia 23665

(NASA-CR-181251) A UNIFORM GTD ANALYSIS OF
THE EM DIFFRACTION BY A THIN
DIELECTRIC/FERRITE HALF-PLANE AND RELATED
CONFIGURATIONS (Ohio State Univ.) 425 P
Avail: NTIS HC A18/MF A01 CSCL 20N G3/32

N87-27871

Unclass
0093173

NOTICES

When Government drawings, specifications, or other data are used for any purpose other than in connection with a definitely related Government procurement operation, the United States Government thereby incurs no responsibility nor any obligation whatsoever, and the fact that the Government may have formulated, furnished, or in any way supplied the said drawings, specifications, or other data, is not to be regarded by implication or otherwise as in any manner licensing the holder or any other person or corporation, or conveying any rights or permission to manufacture, use, or sell any patented invention that may in any way be related thereto.

REPORT DOCUMENTATION PAGE	1. REPORT NO.	2.	3. Recipient's Accession No.
4. Title and Subtitle A UNIFORM GTD ANALYSIS OF THE EM DIFFRACTION BY A THIN DIELECTRIC/FERRITE HALF-PLANE AND RELATED CONFIGURATIONS			5. Report Date March 1985
7. Author(s) Roberto G. Rojas			6.
9. Performing Organization Name and Address The Ohio State University ElectroScience Laboratory 1320 Kinnear Road Columbus, Ohio 43212			8. Performing Organization Rept. No. 716199-5
12. Sponsoring Organization Name and Address National Aeronautics and Space Administration Langley Research Center Hampton, Virginia 23665			10. Project/Task/Work Unit No.
			11. Contract(C) or Grant(G) No. (C) (G) NSG-1498
			13. Type of Report & Period Covered Technical
15. Supplementary Notes			14.
16. Abstract (Limit: 200 words) A uniform geometrical theory of diffraction (UTD) solution is developed for the problem of the diffraction by a thin dielectric/ferrite half-plane when it is excited by either a plane, cylindrical, or a surface wave field. Both transverse electric (TE) and transverse magnetic (TM) cases are considered. The solution to this problem is synthesized from the solutions to the related problems of EM diffraction by configurations involving perfectly conducting electric and magnetic walls covered by a dielectric/ferrite half-plane of one half the thickness of the original half-plane. The solutions to these related canonical problems are referred to as the dielectric/ferrite bisection (DFB) solutions. For a sufficiently thin half-plane, the DFB solutions can be approximately obtained by using an impedance boundary condition which facilitates the use of the Wiener-Hopf technique. The DFB solutions are then superposed to get the solution to the original dielectric/ferrite half-plane case. It is shown that the TE and TM diffracted fields are coupled for the general case of oblique incidence; however, they decouple for the special case of normal incidence. The accuracy of this new solution is established by comparing the UTD results obtained for the scattering by a dielectric strip with an independent moment method solution.			
17. Document Analysis a. Descriptors			
b. Identifiers/Open-Ended Terms			
c. COSATI Field/Group			
18. Availability Statement	19. Security Class (This Report) Unclassified	21. No. of Pages 409	
	20. Security Class (This Page) Unclassified	22. Price	

TABLE OF CONTENTS

	<u>Page</u>
LIST OF TABLES	vii
LIST OF FIGURES	viii
<u>Chapter</u>	
I. INTRODUCTION	1
II. FORMULATION OF THE PROBLEM	17
A. STATEMENT OF THE PROBLEM	17
B. SCALARIZATION OF THE 3-D VECTOR PROBLEM (OBLIQUE INCIDENCE)	24
C. SCALARIZATION OF THE 2-D VECTOR PROBLEM (NORMAL INCIDENCE)	34
D. METHODS OF SOLUTION	37
1. Maliuzhinets' Method	37
2. Wiener-Hopf Method	38
3. Solution of the Wiener-Hopf Equation	40
III. IMPEDANCE BISECTION PROBLEM (NORMAL INCIDENCE CASE)	46
A. STATEMENT OF THE PROBLEM	46
B. JONES' METHOD	52
1. Even Problem	52
2. Odd Problem	70
C. ASYMPTOTIC ANALYSIS	83
1. Angular Spectral Mapping	83
2. Even Problem	84
3. Odd Problem.	103

<u>Chapter</u>	<u>Page</u>
D. EVALUATION OF THE DIFFRACTED FIELD ON THE IMPEDANCE SURFACE	111
E. SLOPE DIFFRACTED FIELD	116
F. SURFACE WAVE EXCITATION	119
1. Even Problem	121
2. Odd Problem	125
3. Analytic Continuation	127
IV. IMPEDANCE BISECTION PROBLEM (OBLIQUE INCIDENCE)	138
A. STATEMENT OF THE PROBLEM	138
B. PEC CASE	139
1. TM_y polarization (E_y^e , even problem)	139
2. TE_y polarization (H_y^o , odd problem)	147
3. Determination of the constants C_a^e and d_h^o	152
C. PMC CASE	160
1. TM_y Polarization (E_y^o , odd problem)	160
2. TE_y Polarization (H_y^e , even problem)	162
D. ASYMPTOTIC ANALYSIS	164
1. PEC Case, TM_y Polarization (E_y^e , even problem)	164
2. PEC Case, TE_y Polarization (H_y^o , odd problem)	169
3. PMC Case, TM_y Polarization (E_y^o , odd problem)	172
4. PMC Case, TE_y Polarization (H_y^e , even problem)	174
E. SURFACE WAVE EXCITATION	177
1. PEC Case	178
2. PMC Case	184
F. RELATIONSHIP BETWEEN THE (E_z, H_z) AND THE (E_y, H_y) FIELDS	188
G. DIFFRACTED E_z^d AND H_z^d FIELDS	191

<u>Chapter</u>	<u>Page</u>
V. DIELECTRIC/FERRITE BISECTION PROBLEM	198
A. FIRST APPROACH	199
B. SECOND APPROACH	201
1. Modification of the Reflected Geometrical Optics Field	203
2. Diffraction Coefficients for the Normal Incidence Case ($\theta'=\pi/2$)	210
3. Modification of Surface Wave Field Excited by a Plane Wave (Normal Incidence)	218
4. Modification of Reflected and Diffracted Surface Wave Fields Excited by an Incident Surface Wave (Normal Incidence)	221
C. MODIFICATION OF DIFFRACTED FIELD FOR PLANE WAVE INCIDENCE (OBLIQUE INCIDENCE CASE)	224
D. MODIFICATION OF SURFACE WAVE FIELD EXCITED BY A PLANE WAVE (OBLIQUE INCIDENCE)	226
E. MODIFICATION OF REFLECTED AND DIFFRACTED SURFACE WAVE FIELDS (OBLIQUE INCIDENCE)	230
VI. THE DIELECTRIC/FERRITE HALF-PLANE PROBLEM	231
A. STATEMENT OF THE PROBLEM	231
B. GEOMETRICAL OPTICS FIELD	232
C. DIFFRACTED FIELD	245
D. SURFACE WAVE FIELD EXCITED BY A PLANE WAVE (OBLIQUE INCIDENCE)	249
E. REFLECTED SURFACE WAVE (OBLIQUE INCIDENCE)	251
F. DIFFRACTED SURFACE WAVE (OBLIQUE INCIDENCE)	254
G. LINE SOURCE EXCITATION	256
VII. MOMENT METHOD	260
VIII. RESULTS AND DISCUSSION	270
APPENDICES	
A FOURIER TRANSFORM IN COMPLEX S-PLANE	342
B RADIATION AND EDGE CONDITIONS	346
C SPECIFICATION OF THE VALUE OF $\beta = (k^2 - s^2)^{1/2}$	349

APPENDICES	<u>Page</u>
D FACTORIZATION OF THE FUNCTIONS $G^e(s)$ AND $G^0(s)$	356
E DECOMPOSITION OF THE FUNCTIONS $D^e(s)$ AND $D^0(s)$	364
F ANGULAR SPECTRAL MAPPING	368
G SADDLE POINT METHOD I	372
H SADDLE POINT METHOD II	378
I EXPRESSIONS FOR $\hat{E}_{x,z}$ AND $\hat{H}_{x,z}$ IN TERMS OF \hat{H}_y AND \hat{E}_y	381
J CALCULATION OF THE FRESNEL REFLECTION COEFFICIENTS OF A GROUNDED DIELECTRIC/FERRITE SLAB USING THE TRANSVERSE RESONANCE METHOD	384
K RAY-FIXED COORDINATE SYSTEM FOR GO FIELDS	390
L RAY-FIXED COORDINATE SYSTEM FOR DIFFRACTED FIELDS	396
REFERENCES	405

LIST OF TABLES

<u>Table</u>	<u>Page</u>
8.1 IBS SOLUTIONS	338
8.2 DFB SOLUTIONS	430
8.3 DIELECTRIC/FERRITE HALF-PLANE SOLUTIONS	341
C.1 SIGNS OF $\text{Re } (\beta)$ and $\text{Im } (\beta)$	353

LIST OF FIGURES

<u>Figure</u>	<u>Page</u>
1.1. Absorber coated aircraft.	2
1.2. Dielectric/ferrite half-plane problem. Note that TE and TM signify that both a transverse electric and magnetic polarizations are included in the total solution.	6
1.3. Dielectric/ferrite bisection problem. Note that PEC and PMC indicate, respectively, a perfect conductor of electricity and magnetism.	8
1.4. Normal incident case.	9
2.1. Dielectric/Ferrite Half-plane Geometry.	18
2.2. Decomposition of incident field into symmetrical and asymmetrical excitation.	21
2.3. Symmetrical and asymmetrical configurations are replaced by the even and odd dielectric/ferrite bisections, respectively.	23
2.4. Even and odd incident surface wave.	25
2.5. Dielectric/ferrite bisection is replaced by impedance bisection.	26
2.6. Impedance Bisection Geometry.	28
2.7. Regions of regularity of all the functions involved in Equations (2.65) and (2.69).	44
3.1. Impedance bisection geometry for plane wave excitation.	47
3.2. Unperturbed geometry.	50
3.3. Regions of analyticity of functions in Equations (3.58) and (3.131).	61
3.4. Integration path in Equations (3.86) and (3.152) for $k_2 \neq 0$.	67
3.5. Integration path in Equations (3.86) and (3.152) for lossless case ($k_2=0$).	67

<u>Figure</u>	<u>Page</u>
3.6. Location of the poles $\tilde{s}_{-}^{e,0}$ and $\tilde{s}_{+}^{e,0}$ on the improper Riemann sheet.	71
3.7. The angular spectral w-plane.	85
3.8. Polar coordinates.	86
3.9. Integration paths Γ_w and C_{SDP} in the periodic w-plane for $k=k_1$ (real).	90
3.10. Poles located in shaded area will be captured as C_{SDP} moves from SDP^- to SDP^+ .	91
3.11. Different wave types as a function of pole location in the periodic w-plane.	94
3.12. Slow and Fast waves in the periodic w-plane.	94
3.13. Demarcation of regions of w-plane about the saddle point characterizing the rate of exponential growth or decay of waves associated with the pole locations.	99
3.14. \sqrt{x} plane.	113
3.15. Top sheet of $x^{1/2}$ function where $\frac{-3\pi}{2} < \arg(x) < \frac{\pi}{2}$.	114
3.16. Geometry for slope diffracted field.	117
3.17. Geometry for surface wave excitation.	120
3.18. Integration paths Γ_w and C_{SDP} in the periodic w-plane for $k=k_1$ (real).	130
4.1. Integration paths on top Riemann sheet: $\text{Im}(\beta) > 0$.	155
5.1. Grounded Dielectric/Ferrite Slab.	199
5.2. Reflection coefficient for TM_y polarization (E_y), even case.	206
5.3. Reflection coefficient for TM_y polarization (E_y), odd case.	207
5.4. Reflection coefficient for TE_y polarization (H_y), even case.	208
5.5. Reflection coefficient for TE_y polarization (H_y), odd case.	209
5.6. Sign of $\tilde{\epsilon}$ near the reflection shadow boundary.	212

<u>Figure</u>	<u>Page</u>
5.7. Dielectric/ferrite bisection problem.	217
6.1. Ray fixed coordinate system used for 3D reflection and transmission.	233
6.2. Reflection coefficient of R^{\parallel} .	237
6.2. (continued)	238
6.3. Reflection Coefficient R^{\perp} .	239
6.3. (continued)	240
6.4. Transmission Coefficient T^{\parallel} .	241
6.4. (continued).	242
6.5. Transmission Coefficient T^{\perp} .	243
6.5. (continued).	244
6.6. Ray fixed coordinate system used for 3D diffraction.	246
6.7. Edge excited surface waves E_y^{sw} and H_y^{sw} where	250
6.8. Reflected surface wave field.	253
6.9. Edge diffracted surface wave fields E_y^{dsw} and H_y^{dsw} .	255
6.10. Line Source Excitation	256
6.11. Surface waves excited by a line source above a dielectric/ferrite slab.	259
7.1. Plane wave (\vec{E}^i, \vec{H}^i) incident on a dielectric object.	261
7.2. Polarization current \vec{J} replaces dielectric object.	263
7.3. Dielectric slab divided into square cells.	264
7.4. Square cell is replaced by a circular cell of the same area.	267
8.1. Plane wave excitation.	271
8.2. Line source excitation.	272

<u>Figure</u>	<u>Page</u>
8.3. Field components that contribute to the total field at the observation point.	273
8.4. Magnitude of the total H_z field for the geometry shown in Figure 8.2. (a) $\phi'=90^\circ$, $\rho'=1\lambda$. (b) $\phi'=30^\circ$, $\rho'=2\lambda$.	276
8.5. Magnitude of the total H_z field for the geometry shown in Figure 8.2.	277
8.6. Magnitude of the E_z field for the geometry shown in Figure 8.2. (a) $\phi'=10^\circ$, $\rho=40\lambda$. $\rho'=2\lambda$. (b) $\phi'=90^\circ$, $\rho=90\lambda$, $\rho'=0.25\lambda$.	278
8.7. Magnitude of the total H_z field for the geometry shown in Figure 8.2. (a) $\epsilon_r=4.+i0$. (b) $\epsilon_r=4.+i0.8$	280
8.8. Magnitude of the total H_z field for the geometry shown in Figure 8.2. (a) $\epsilon_r=4.+i2.$, $\phi'=15^\circ$ (b) $\epsilon_r=4.+i0.$, $\phi'=10^\circ$	281
8.9. Magnitude of the total H_z field for the geometry shown in Figure 8.2. (a) $\ell=7\lambda$, $\epsilon_r=4.+i2$. (b) $\ell=5\lambda$, $\epsilon_r=4.+i0$.	283
8.10. Magnitude of the total E_z field for the geometry shown in Figure 8.2. (a) $\epsilon_r=4.+i0$. (b) $\epsilon_r=4.+i2$.	284
8.11. Magnitude of the total E_z field for the geometry shown in Figure 8.2. (a) $\epsilon_r=4.+i0$. (b) $\epsilon_r=4.+i2$.	285
8.12. Magnitude of the total E_z field for the geometry shown in Figure 8.2. (a) $\ell=7\lambda$, $\epsilon_r=4.+i2.8$, $\phi'=5^\circ$ (b) $\ell=5\lambda$, $\epsilon_r=4.+i0.$, $\phi'=10^\circ$	286
8.13. Magnitude of the total E_z field for the geometry shown in Figure 8.2. (a) Without ² diffracted surface wave, (b) Field components V and VI included (diffracted surface wave included).	287
8.14. Doubly Edge Diffracted Field.	288
8.15. Magnitude of the total E_z field for the geometry shown in Figure 8.2. (a) $\epsilon_r=4.+i1.$, $\phi'=1^\circ$, (b) $\epsilon_r=4.+i0.$, $\phi'=0.1^\circ$	289
8.16. Magnitude of the total E_z field for the geometry shown in Figure 8.2. (a) $\epsilon_r=4.+i0.$, (b) $\epsilon_r=4.+i1$.	290
8.17. Magnitude of the total E_z field for the geometry shown in Figure 8.2. (a) Without diffracted surface wave (b) Field components V and VI included (diffracted surface wave included).	291

Figure	Page
8.18 Magnitude of the scattered E_z^S and H_z^S fields for an E_z^i -polarized plane wave incident on the geometry shown in Figure 8.1.	293
8.19 Magnitude of the scattered H_z^S and E_z^S fields for an H_z^i -polarized plane wave incident on the geometry shown in Figure 8.1.	294
8.20 Magnitude of the scattered E_z^S and H_z^S fields for an E_z^i -polarized plane wave incident on the geometry shown in Figure 8.1.	295
8.21 Magnitude of the scattered H_z^S and E_z^S fields for an H_z^i -polarized plane wave incident on the geometry shown in Figure 8.1.	296
8.22 Magnitude of the scattered E_z^S and H_z^S fields for an E_z^i -polarized plane wave incident on the geometry shown in Figure 8.1.	297
8.23 Magnitude of the scattered H_z^S and E_z^S fields for an H_z^i -polarized plane wave incident on the geometry shown in Figure 8.1.	298
8.24 Magnitude of the scattered E_z^S and H_z^S fields for an E_z^i -polarized plane wave incident on the geometry shown in Figure 8.1.	299
8.25 Magnitude of the scattered H_z^S and E_z^S fields for an H_z^i -polarized plane wave incident on the geometry shown in Figure 8.1.	300
8.26 Magnitude of the scattered field H_z^S for the geometry depicted in Figure 8.2. (a) $\epsilon_r = 4. + i0.$, $\rho' = 7\lambda$, (b) $\epsilon_r = 3. + i0.3$, $\rho' = 15\lambda$.	301
8.27 Magnitude of the scattered H_z^S field for the geometry depicted in Figure 8.2. (a) $\epsilon_r = 5. + i0.5$, $\mu_r = 1. + i0.$, (b) $\epsilon_r = 1. + i0.$, $\mu_r = 3. + i0.3$.	302
8.28 Magnitude of the scattered H_z^S field for the geometry depicted in Figure 8.1 (normal incidence). (a) $\ell = 5\lambda$, $\epsilon_r = 7. + i0.7$, (b) $\ell = 10\lambda$, $\epsilon_r = 5. + i0.5$.	304
8.29 Magnitude of the scattered E_z^S field for the geometry depicted in Figure 8.2. (a) $\epsilon_r = 3. + i0.$, (b) $\epsilon_r = 3. + i0.3$, (c) $\epsilon_r = 3. + i1.2$.	305

<u>Figure</u>	<u>Page</u>
8.30. Magnitude of the field E_z for the geometry depicted in Figure 8.1. (a) Scattered field E_z^S without diffracted surface wave, (b) diffracted surface wave E_z^{dsw} (field components V and VI).	306
8.31. Magnitude of the scattered field E_z^S with the diffracted surface wave field E_z^{dsw} included (see Figure 8.30).	308
8.32. Magnitude of the field E_z for the geometry depicted in Figure 8.2. (a) Scattered field E_z^S without diffracted surface wave, (b) Diffracted surface wave field E_z^{dsw} (field component V).	309
8.33. Magnitude of the field E_z for the geometry depicted in Figure 8.2. (a) Scattered field E_z^S with field component V included, (b) Diffracted surface wave field E_z^{dsw} (field component VI).	310
8.34. Magnitude of the field E_z for the geometry depicted in Figure 8.2. (a) Diffracted surface wave field E_z^{dsw} (field components V+VI), (b) Scattered field E_z^S with the field components V and VI included.	311
8.35. Magnitude of the scattered E_z^S and H_z^S fields for an E_z^i -polarized plane wave incident on the geometry shown in Figure 8.1. The diffracted surface wave is not included in the solution.	312
8.36. Magnitude of the diffracted surface wave fields E_z^{dsw} and H_z^{dsw} (field component V) for a E_z^i -polarized plane wave incident on the geometry shown in Figure 8.1.	313
8.37. Magnitude of the scattered fields E_z^S and H_z^S for an E_z^i -polarized plane wave. The diffracted surface wave (see Figure 8.36) is included in the solution.	314

<u>Figure</u>	<u>Page</u>
8.38. Magnitude of the scattered fields H_z^S and E_z^S for a H_z^i -polarized plane wave incident on the geometry depicted in Figure 8.1. The diffracted surface wave is not included in the solution.	315
8.39. Magnitude of the diffracted surface wave fields H_z^{dsw} and E_z^{dsw} (component V) for a H_z^i -polarized plane wave.	316
8.40. Magnitude of the scattered fields H_z^S and E_z^S for a H_z^i -polarized plane wave. The diffracted surface wave field (see Figure 8.39) is included in the solution.	317
8.41. Magnitude of the E_z field for the geometry depicted in Figure 8.2. (a) Scattered E_z^S field without the diffracted surface wave field, (b) Diffracted surface wave field E_z^{dsw} (see Figure 6.11).	318
8.42. Magnitude of the scattered E_z^S field with the diffracted surface wave field E_z^{dsw} included (see Figure 8.41).	319
8.43. Magnitude of the H_z field for the geometry depicted in Figure 8.2. (a) Scattered H_z^S field without the diffracted surface wave field. (b) Diffracted surface wave field H_z^{dsw} (see Figure 6.11).	320
8.44. Magnitude of the scattered H_z^S field with the diffracted surface wave field H_z^{dsw} included (see Figure 8.43).	321
8.45. Magnitude of the scattered E_z field for the geometry depicted in Figure 8.1 (normal incidence). (a) $\epsilon_r=4.+i0.$, (b) $\epsilon_r=4.+i1.$	322
8.46. Magnitude of the scattered E_z^S field for the geometry depicted in Figure 8.2. (a) $\epsilon_r=4.+i0.$, (b) $\epsilon_r=4.+i1.$	323
8.47. Magnitude of the scattered E_z^S field for the geometry depicted in figure 8.2.	325

<u>Figure</u>	<u>Page</u>
8.48. Even reflection coefficient (TM_z polarization) for a grounded (PMC) dielectric/ferrite slab.	326
8.49. Odd reflection coefficient (TM_z polarization) for a grounded (PEC) dielectric/ferrite slab.	327
8.50. Magnitude of diffracted E_z^d field for the geometry depicted in Figure 8.2. (a) $\epsilon_r=3.+i0.3$, $\mu_r=1.+i0.$, (b) $\epsilon_r=3.+i0.3$, $\mu_r=3.+i0.3$.	328
8.51. Magnitude of the scattered E_z^s field for the geometry depicted in Figure 8.2.	330
8.52. Echo width per wavelength of a thin dielectric strip, TM_z polarization.	331
8.52. Echo width per wavelength of a thin dielectric strip, TM_z polarization.	331
8.53. Echo width per wavelength of a thin dielectric strip, TE_z polarization.	332
8.54. Echo width per wavelength of a thin dielectric strip, TM_z polarization.	333
8.55. Echo width per wavelength of a thin dielectric strip, TM_z polarization.	334
8.56. Grounded dielectric slab.	335
C.1. Domain of $\beta = (K^2 - s^2)^{1/2}$.	352
C.2. Top sheet: $\text{Im}(\beta) > 0$.	354
C.3. Bottom sheet: $\text{Im}(\beta) < 0$.	354
C.4. Top sheet: $\text{Im}(\beta) > 0$, $K = K_1$.	355
C.5. Bottom sheet: $\text{Im}(\beta) < 0$, $K = K_1$.	355
D.1. Integration path of Equation D.15	360
D.2. Integration path of Equation D.25 in periodic α -plane.	360
F.1. Periodic ψ -plane.	371
G.1. Definition of the angle ϕ_s . The direction of integration along the path SDP is indicated by the arrowhead.	377

<u>Figure</u>	<u>Page</u>
J.1. Grounded Dielectric/ferrite slab.	384
J.2. Equivalent transmission-line circuit for Figure J.1.	385
L.1 Relationship between the unit vectors $\hat{\theta}$, $\hat{\beta}$, \hat{R} and \hat{S} .	404

CHAPTER I

INTRODUCTION

It is well known that the electromagnetic (EM) scattering properties of a body are a function of both, its geometrical and electrical (or material) parameters. In the last few years, there has been a renewed interest in understanding the effect of the material properties of a body on its EM scattering behavior. This subject is of great importance in many applications. Radar absorbing materials are often used to cover targets in order to reduce their EM scattering; however, in most cases the materials are designed to reduce the specular contributions [1] from the body without taking into account the diffraction from edges of the absorber coatings, creeping waves, and surface waves on the coatings. Thus, it is necessary to examine the effect that the material properties have on these non-specular contributions to the scattered field which may dominate over a certain range of aspects. Figure 1.1 shows an aircraft which is covered by an absorber in several places to control its EM echo area. Furthermore, since a typical airplane has many antennas mounted on its surface, the absorbers, which are not perfectly conducting materials, will have an

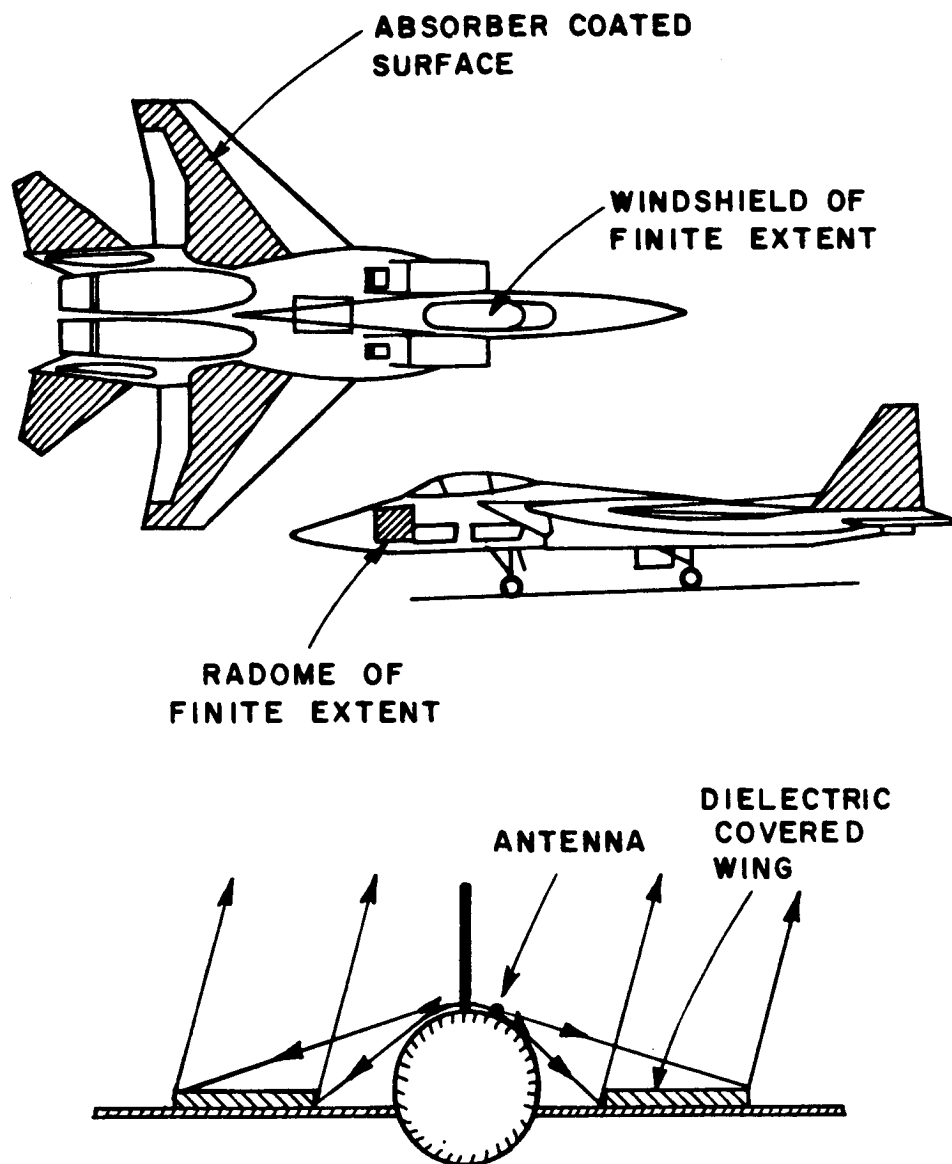


Figure 1.1. Absorber coated aircraft.

important effect on the radiation patterns of the antennas. As mentioned in Reference [2], when the radiation patterns of antennas mounted on a small private aircraft were being studied, it was found that the windshield scattering was a major contributor to the total pattern.

Single layer and multilayered coated surfaces have been investigated using a transmission line approach [3], however, this approach does not consider diffraction effects. Computer programs have also been developed [4,5] to solve the integral equations for the surface fields on two-dimensional bodies subject to the impedance boundary conditions. These programs can calculate the values of impedances which will minimize the backscattering from objects of various shapes.

Another important approach to solve these types of problems are the high frequency approximation techniques such as the geometrical theory of diffraction (GTD) and its uniform version, the uniform geometrical theory of diffraction (UTD) which has been used with great success to solve a wide variety of electromagnetic problems. One great advantage of high frequency solutions such as UTD over other types of solutions is that complex structures can be modelled by simpler ones whose solutions are known.

The Geometrical Theory of Diffraction (GTD) was developed around 1951 by J.B. Keller [6,7,8]. The GTD is a significant extension of classical geometrical optics (GO) in which a class of diffracted rays are systematically introduced in addition to the usual GO rays. According to the GTD, diffracted rays originate from certain localized

regions of a radiating/scattering structure such as at discontinuities in the geometrical and electrical properties of the structure. Furthermore, diffracted rays can also be produced at points of grazing incidence on a smooth convex surface. The diffracted rays, like the ordinary GO rays, satisfy the generalized Fermat's principle [6] proposed by Keller.

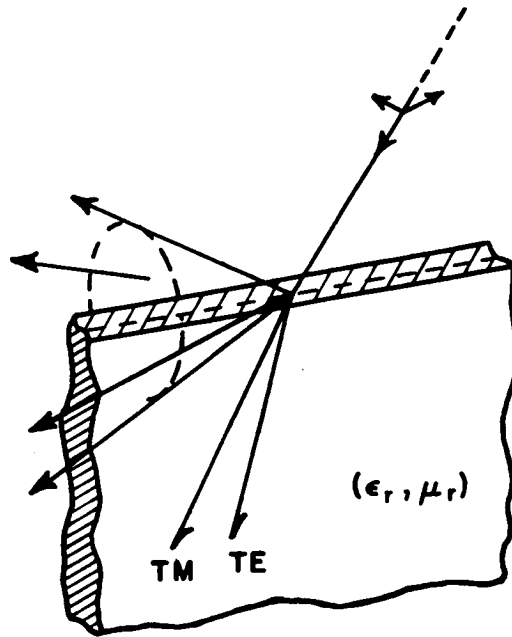
The initial value of a diffracted ray is given in terms of a diffraction coefficient which plays a role analogous to the reflection and transmission coefficients of the GO reflected and transmitted rays. These diffraction coefficients can be found from the asymptotic solutions to appropriate canonical problems, i.e., half-plane. These canonical problems are usually simple geometries which locally simulate parts of a complex structure that dominate the reflection, transmission and diffraction effects.

One defect of the GTD is that it fails in the transition region adjacent to shadow and reflection boundaries. In order to overcome this and other limitations, the uniform geometrical theory of diffraction (UTD) has been introduced [9,10,11]. The UTD requires that the diffracted field compensate the discontinuity in the GO field at the shadow and reflection boundaries so that the total high-frequency field is continuous everywhere away from the radiating or scattering body. It is noted that the diffracted field generally assumes its largest value near these boundaries where the GTD fails.

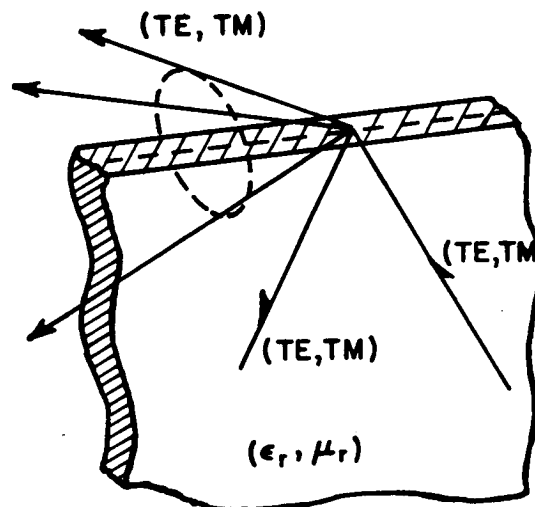
The object of this study is to obtain an approximate UTD solution to the problem of scattering by a thin dielectric/ferrite half-plane

either by itself or when it is placed on a perfect conductor of electricity or magnetism as shown in Figures 1.2 and 1.3. The half-plane in Figures 1.2 and 1.3 can be excited by either an obliquely incident EM plane or surface wave field. In the present work, the thickness of the dielectric/ferrite half-plane is restricted so that only the dominant TE and TM type surface wave fields can exist at any given operating frequency. This problem has many applications in the study of diffraction by dielectric/ferrite obstacles with edges as shown in Figure 1.1, and in the theory of surface wave antennas. Furthermore, it is an important canonical problem for the UTD since it extends the UTD edge diffraction solutions from perfectly conducting to penetrable geometries. As shown in Chapter VI, the solution to the problem of the diffraction by the dielectric/ferrite half-plane of Figure 1.2 will be synthesized from the solutions to the related problems of the diffraction by a dielectric/ferrite half-plane of half the original thickness when it is placed on perfectly conducting electric or magnetic surfaces of infinite extent as depicted in Figure 1.3. This geometry pertaining to the latter set of problems, which is referred to throughout this report as the dielectric/ferrite bisection, can be excited by either an obliquely incident plane or surface wave field.

An interesting phenomenon which does not take place in the case of diffraction by a perfectly conducting half-plane is the coupling between the TE and TM modes which is present in the dielectric/ferrite half-plane case. This coupling exists only for an obliquely incident field. Thus, for the special case of normal incidence on the edge,



Obliquely incident arbitrary ray optical field.

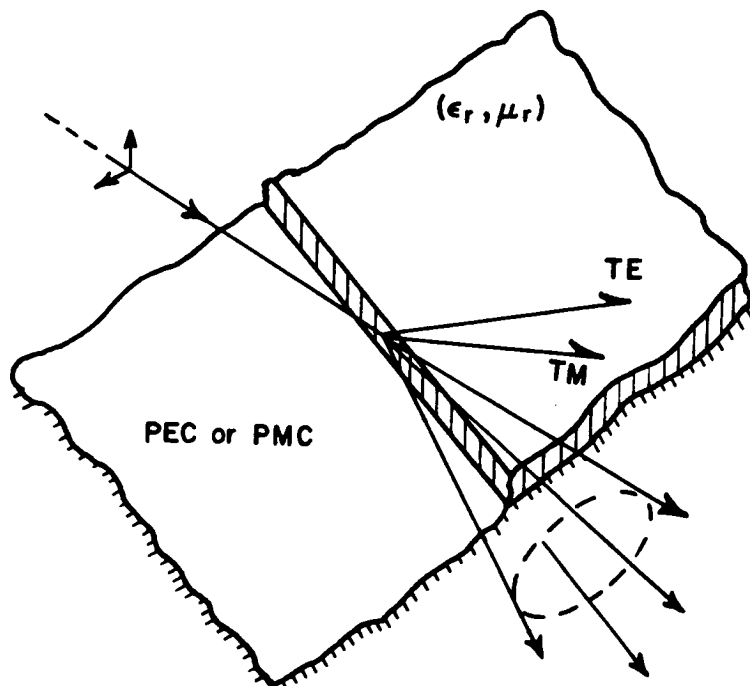


Obliquely incident surface wave field.

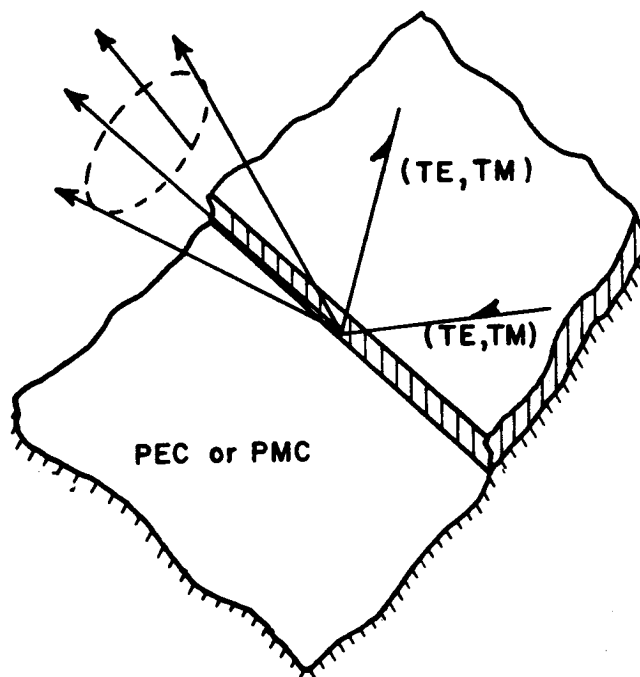
Figure 1.2. Dielectric/ferrite half-plane problem. Note that TE and TM signify that both a transverse electric and magnetic polarizations are included in the total solution.

which is depicted in Figure 1.4, there is no coupling between the TE and TM modes and obviously its solution is less complicated.

The problem of the diffraction by a dielectric half-plane has been studied by several authors in the past. Pistol'kors [12] uses the Fresnel reflection coefficient of the dielectric half-plane in a vector Kirchhoff approximation. His solution violates reciprocity except in the shadow boundary directions, and he does not include surface waves. Khrebet [13] also uses the Fresnel reflection coefficient to approximately satisfy the boundary conditions on the field which in turn is expressed in terms of an integral representation similar to Oberhettinger's half-plane diffraction integral [14]. As in Pistol'kor's case, the solution obtained by Khrebet also does not include surface waves, and it does not satisfy reciprocity except in the directions of the shadow boundaries. Mohsen and Hamid [15,16] solved the problem of the diffraction by a dielectric loaded, perfectly conducting wedge. Their solution is similar to Khrebet's solution except that they use the more general Oberhettinger wedge diffraction type integral. More recently, Anderson [17] has solved the problem of the diffraction by a thin dielectric half-plane by replacing the dielectric with an equivalent polarization current sheet. He solves only for the TM_z polarization using the Wiener-Hopf procedure, and his solution can not be directly extended to the other polarization. Furthermore, Anderson considers only the special case of normal incidence. Burnside [2] has proposed a heuristic extension of the UTD solution for a perfectly-conducting wedge to treat the diffraction by a

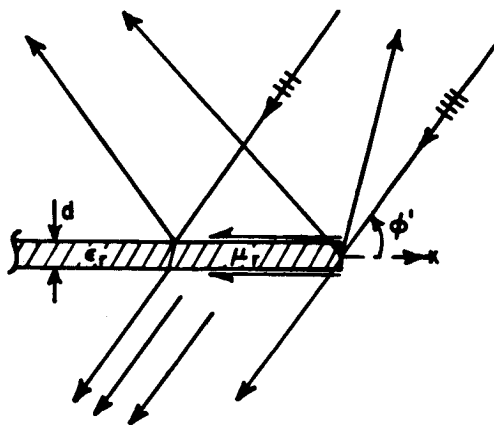


Obliquely incident arbitrary ray optical field.

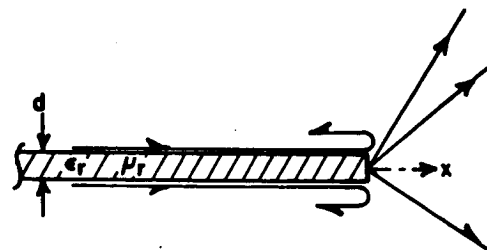


Obliquely incident surface wave field.

Figure 1.3. Dielectric/ferrite bisection problem. Note that PEC and PMC indicate, respectively, a perfect conductor of electricity and magnetism.

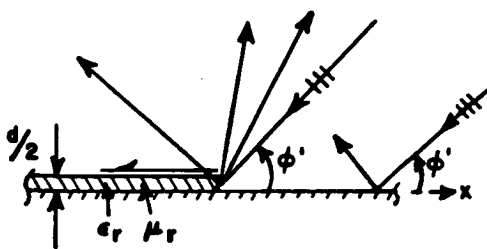


Plane Wave Excitation

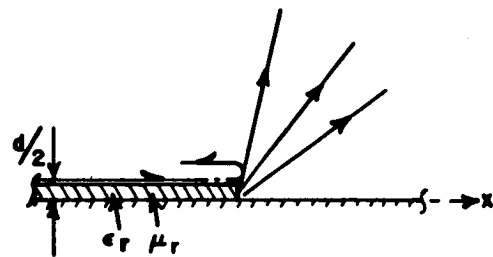


Surface Wave Excitation

Dielectric/ferrite half-plane problem.



Plane Wave Excitation



Surface Wave Excitation

Dielectric/ferrite bisection problem.

Figure 1.4. Normal incident case.

lossless dielectric half-plane by incorporating the Fresnel reflection and transmission coefficients for a dielectric slab. This solution which is somewhat similar to that in [13,15,16] has been shown [18,19] to give good accuracy for angles of incidence away from grazing. However, it also does not satisfy reciprocity away from the optical shadow boundaries and it does not include the surface waves excited at the edge of the half-plane, which are important in many applications. Nevertheless, unlike the previous two-dimensional solutions [13,15,16], the solution in [2] has been developed to approximately analyze both the two dimensional as well as the three-dimensional case of obliquely incident EM plane and spherical waves on the edge of a dielectric half-plane.

As mentioned earlier, the solution to the problem of the diffraction by a dielectric/ferrite half-plane in Figure 1.2 is synthesized in the present work from the solutions to the bisection problems shown in Figure 1.3, which can have an even or odd excitation. The dielectric/ferrite bisection (DFB) problem is still a fairly complicated problem, so the solution to the DFB problem of Figure 1.3 is obtained approximately via UTD considerations from the solution to the related problem of the diffraction by a two-part planar surface in which one part is a perfect conductor (of electricity or magnetism) and the other part is an impedance surface as shown in Figure 2.5. The new geometry, which is depicted in Figure 2.5, is referred to as the impedance bisection and it is amenable to solution by the Wiener-Hopf technique. Since it is desirable to deal with a scalar problem rather

than a vector problem, the scalarization of the impedance bisection problem is addressed in Chapter II together with the details of the original DFB problem. It is shown that the field or vector potential components that scalarize the vector problem depend on whether the incident field is obliquely or normally incident on the edge.

As stated before, there is no coupling between the TE and TM fields for the special case of normal incidence, which makes it simpler than the more general case of oblique incidence. Thus, in Chapter III, the impedance bisection problem for the case of normal incidence is solved first, using the Wiener-Hopf method. The Wiener-Hopf equation is obtained by Jones' method, which is briefly described in Section D of Chapter II. It is shown that the solutions to the Wiener-Hopf equations for both TE_z and TM_z polarizations can be expressed as integrals, which in general can not be integrated in closed form; here, z is parallel to the edge formed by the impedance discontinuity. Next, the integrals are evaluated asymptotically by the saddle point method.

The more general case of oblique incidence is discussed in Chapter IV. It is shown that identical Wiener-Hopf equations to the ones obtained in Chapter III are also obtained for the field components E_y and H_y which are normal to the surface. However, because of the different edge behavior of the normal field components E_y and H_y in the 3-D case as compared to those of the tangential components E_z and H_z used in the 2-D case, the final solutions are not the same in these two cases. Furthermore, it is shown that the edge condition requires that

there be a coupling between the TM_y and TE_y fields as mentioned above. The integral expressions for the fields E_y and H_y are then evaluated asymptotically by the saddle point method in Chapter IV.

Having obtained the solutions for the simpler impedance bisection problem, the next task is to modify them according to the UTD recipe so as to arrive at an approximate but accurate solution to the problem in Figure 1.3 and then subsequently synthesize the solution to the problem in Figure 1.2. In Chapter V, two methods are discussed for obtaining the DFB solutions from the impedance bisection solutions already obtained in Chapters III and IV. The first method addresses the problem of obtaining a value for the impedance Z_s in terms of the permeability, permittivity, and thickness of the grounded dielectric/ferrite half-plane. The second method, which is considered more accurate than the first one, starts by casting the impedance bisection solutions into the UTD form involving reflection and diffraction coefficients, and also the surface wave propagation ($\vec{\zeta}_p$) and attenuation ($\vec{\zeta}_a$) vectors, respectively. Note that the vectors, $\vec{\zeta}_p$ and $\vec{\zeta}_a$ can be easily obtained from the surface wave field parameters $\tilde{\beta}$ and $\tilde{\alpha}$. The reflection coefficients, and the surface wave constants $\tilde{\alpha}$ and $\tilde{\beta}$ of the IBS are replaced by the corresponding exact coefficients for the grounded dielectric/ferrite slab case which are well known. It is noted that for a specific ϵ_r , μ_r , and kd , the $\tilde{\alpha}$ and $\tilde{\beta}$ must be computed from the roots of a transcendental equation. Once this is done, the exact geometrical optics field for the grounded dielectric/ferrite slab is obtained. Also, the resulting diffracted field for the dielectric/ferrite bisection (DFB) case of Figure 1.3 maintains

continuity of the total field at the reflection shadow boundary. However, an additional minor modification is introduced heuristically in the resulting diffracted field so that it now also satisfies reciprocity.

Since the final goal of this study is to obtain the solution for the half-plane problem of Figure 1.2, Chapter VI discusses the manner in which the dielectric/ferrite bisection solutions are superposed to obtain the solution for this dielectric/ferrite half-plane problem. Furthermore, it is also shown in this chapter how the geometrical optics and diffracted fields can be written in a compact form by expressing these fields in their natural "ray-fixed" coordinate systems.

In order to verify the accuracy of the results for the half-plane problem of Figure 1.2, the UTD solutions developed in this study are used to compute the scattering by a dielectric/ferrite strip which can be excited by either a plane wave or a line source. These solutions are compared with the solutions obtained via the moment method (MM). Chapter VII discusses the moment method solution for a dielectric strip. In this chapter, the impedance matrix is computed for the general case of oblique incidence by a plane wave of TE or TM polarization. It is shown that the impedance matrix can be simplified when the plane wave is normally incident or for the case of line source excitation.

In Chapter VIII, the UTD solutions for the dielectric strip are compared with the independent moment method solutions, and both results are shown to agree very well. It is shown how the UTD solutions give insight into the type of scattering that occurs from the strip. Examples are shown, where by adding more surface wave interactions on

the strip, the agreement between the UTD and moment method solutions improves for near grazing angles of incidence on the strip. As expected, these surface wave effects become significant for grazing angles of incidence and diffraction. Thus, a useful characteristic of the UTD technique is identified, which is that the UTD provides a means of pinpointing the significant contributions to the total scattered field that can arise from different parts of a complex structure. Furthermore, the limitations of the new UTD solutions obtained in Chapters III through VI and further areas of research related to this topic are also discussed in Chapter VIII. Finally, in Appendices A through L, various analytical details are given.

Note that a dielectric/ferrite slab can sustain several surface wave modes. However, as mentioned in the beginning, it is assumed in this study that the thickness, permittivity, and permeability of the slab are adjusted such that only the lowest order (even) surface wave mode can propagate. Under this restriction, the solution of the half-plane problem may be constructed approximately with the assumption that the dielectric/ferrite half-plane has one equivalent diffracting edge only, even though a half-plane of finite thickness has actually two edges instead of one. It is found that very accurate solutions for engineering applications can be obtained under this approximation when the thickness does not exceed one quarter of a wavelength inside the dielectric/ferrite medium.

Before proceeding to the development of the UTD solutions for the problems in Figures 1.2 and 1.3, it is worthwhile at this juncture to comment on the notation and time convention employed in this work.

Since the Wiener-Hopf technique is heavily used in the development which follows, the time convention $e^{-i\omega t}$ will be adopted for ease of notation and suppressed from now on. As a result of this convention, Maxwell's equations in a homogeneous, isotropic and source-free region take the following form:

$$\nabla \times \vec{E} = i\omega\mu \vec{H} = ik\eta_0 \vec{H} \quad (1.1)$$

$$\nabla \times \vec{H} = -i\omega\epsilon \vec{E} = -ikY_0 \vec{E} \quad (1.2)$$

$$\nabla \cdot \vec{E} = 0 \quad (1.3)$$

$$\nabla \cdot \vec{H} = 0 \quad (1.4)$$

where \vec{E} is the electric field, \vec{H} is the magnetic field, ω is the angular frequency, η_0 is the free-space impedance, and Y_0 is the free-space admittance.

The dielectric/ferrite media to be considered here can be completely specified by the complex permeability μ and complex permittivity ϵ which are complex numbers in the first quadrant such that

$$\epsilon = \epsilon' + i\epsilon'' \quad \text{with} \quad (\epsilon', \epsilon'') > 0 \quad , \quad (1.5)$$

and

$$\mu = \mu' + i\mu'' \quad \text{with} \quad (\mu', \mu'') > 0 \quad . \quad (1.6)$$

The complex wave number k is also located in the first quadrant, and it is written as

$$k = k_r + ik_I \text{ with } (k_r, k_I) > 0 \quad . \quad (1.7)$$

Because the Fourier transform will be used throughout this report, it is convenient to discuss the notation at this point. The function $\hat{F}(s)$ will denote the Fourier transform of the spatial domain function $f(x)$. The Fourier Transform in the complex s -plane is defined in Appendix A where its most important properties relevant to the Wiener-Hopf technique are summarized.

CHAPTER II

FORMULATION OF THE PROBLEM

A. STATEMENT OF THE PROBLEM

As mentioned in Chapter I, the main canonical problem considered here is the EM diffraction by a thin dielectric/ferrite half-plane as shown in Figure 1.2 which is excited by a plane or surface wave field. It is, of course, recalled that the solution to this canonical problem in Figure 1.2 is synthesized in terms of the other two related canonical problems depicted in Figure 1.3. First, consider the case of plane wave excitation as illustrated in Figure 2.1, where u^i is the plane wave incident on the dielectric/ferrite half-plane and (u_1, u_2) , as defined below, represent the total field at the observation point (x, y, z) . It will be shown in Sections B and C, where the vector problem is scalarized, that for the case of oblique incidence on the edge of the half-plane, it is convenient to define u^i , u_1 and u_2 as

$$u^i(x, y, z) = E_y^i(x, y, z) \text{ or } H_y^i(x, y, z) \quad (2.1)$$

$$u_1(x, y, z) = E_y(x, y, z) \quad (2.2)$$

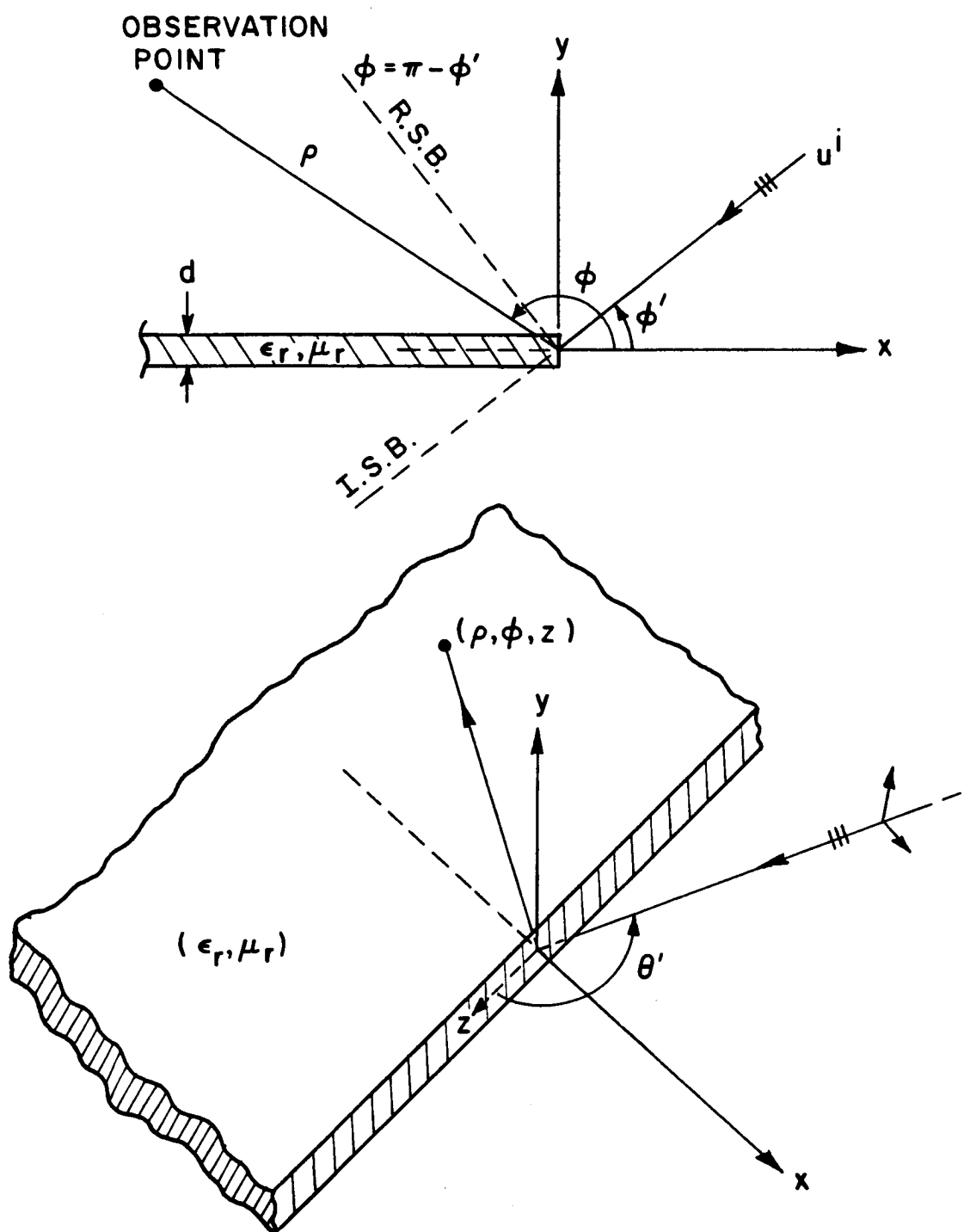


Figure 2.1. Dielectric/Ferrite Half-plane Geometry.

$$u_2(x,y,z) = H_y(x,y,z) \quad (2.3)$$

Note that both E_y and H_y are non-zero for oblique incidence, because a coupling occurs between these two field components.

On the other hand, for the special case of normal incidence to the edge of the half-plane, it is convenient to define u^i , u_1 and u_2 as:

$$u^i(x,y,z) = u^i(x,y) = E_z^i(x,y) \text{ or } H_z^i(x,y) \quad (2.4)$$

$$u_1(x,y,z) = u_1(x,y) \equiv u(x,y) = E_z(x,y) \text{ or } H_z(x,y) \quad (2.5)$$

$$u_2(x,y) \equiv 0 \quad (2.6)$$

It is clear from the definitions in Equations (2.4), (2.5) and (2.6), that u^i , u_1 and u_2 are replaced by u^i and u only. It is shown later that no coupling exists between E_z and H_z for the case of normal incidence because one can deal independently with either E_z alone or H_z alone, respectively.

Specifically, the approach for solving the half-plane diffraction problem of Figure 2.1 consists of the following steps. First of all, the incident field is expressed as the superposition of four incident plane waves as indicated in Figure 2.2. In other words, the original problem is expressed as the superposition of even and odd excitations.

It follows that the total fields u_1^e and u_2^e are even functions of y , that is

$$u_1^e(x,y,z) = u_1^e(x,-y,z) \quad (2.7)$$

$$u_2^e(x,y,z) = u_2^e(x,-y,z) \quad (2.8)$$

while the fields u_1^0 and u_2^0 are odd functions of y such that

$$u_1^0(x,y,z) = -u_1^0(x,-y,z) \quad (2.9)$$

$$u_2^0(x,y,z) = -u_2^0(x,-y,z) \quad (2.10)$$

Because of Equations (2.7) through (2.10) the configuration with symmetrical or even excitation will be referred to as the even problem, while the configuration with the asymmetrical or odd excitation will be referred to as the odd problem. Due to the even and odd symmetry of the solutions, it is enough to solve the even and odd problems for the half-space $y \geq 0$.

After solving the even and odd problems individually, the total field $u(x,y,z)$ is obtained by a simple superposition of u^e and u^0 . Thus,

$$u_1(x,y,z) = u_1^e(x,|y|,z) + \text{sign}(y)u_1^0(x,|y|,z) \quad (2.11)$$

and

$$u_2(x,y,z) = u_2^e(x,|y|,z) + \text{sign}(y)u_2^0(x,|y|,z) \quad (2.12)$$

Using image theory [20], one can obtain problems equivalent to the even and odd configurations as depicted in Figure 2.3. The configuration corresponding to the even problem will be referred to as the even bisection problem, while the configuration pertaining to the odd problem will be referred to as the odd bisection problem.

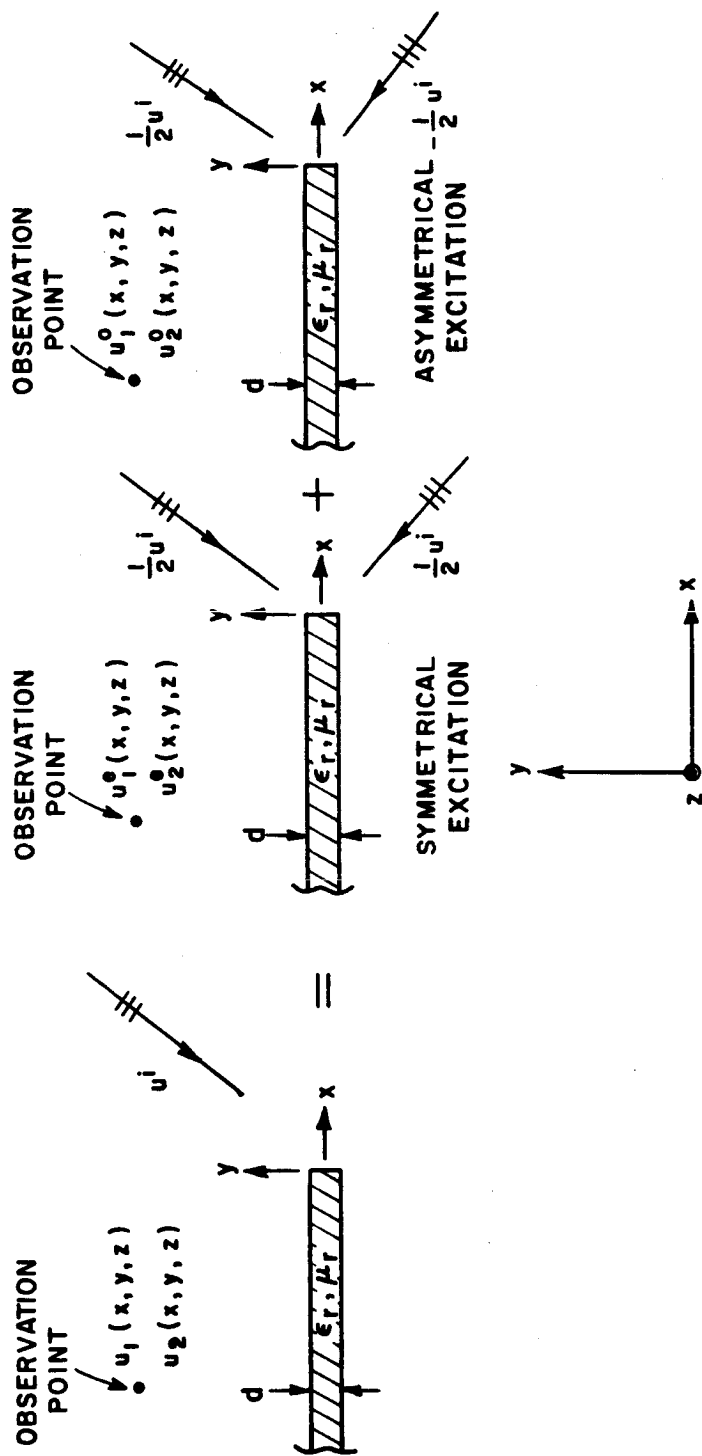


Figure 2.2. Decomposition of incident field into symmetrical and asymmetrical excitation.

Next, consider the case of surface wave excitation. As in the case of plane wave excitation,

$$u^{isw}(x,y,z) = E_y^{isw}(x,y,z) \text{ or } H_y^{isw}(x,y,z) \quad (2.13)$$

for oblique incidence, or

$$u^{isw}(x,y) = E_z^{isw}(x,y) \text{ or } H_z^{isw}(x,y) \quad (2.14)$$

for the special case of normal incidence.

It is well known [21] that surface wave modes guided along a dielectric/ferrite slab can be classified as even or odd modes. Thus, an equivalent problem for an even mode incident surface wave field is the even bisection problem shown in Figure 2.4. On the other hand, if the incident surface wave is an odd mode, the equivalent problem is the odd-bisection problem which is also depicted in Figure 2.4.

The even and odd bisection problems are still fairly complicated, so the next step in this procedure is to temporarily replace the thin grounded dielectric/ferrite slab by an impedance wall as shown in Figure 2.5. The reason for doing this is because the simpler impedance boundary contains all the essential characteristics of the thin grounded dielectric/ferrite slab and because the latter impedance configuration can be analyzed directly by the Wiener-Hopf procedure. This technique of replacing the original boundary value problem by an approximate

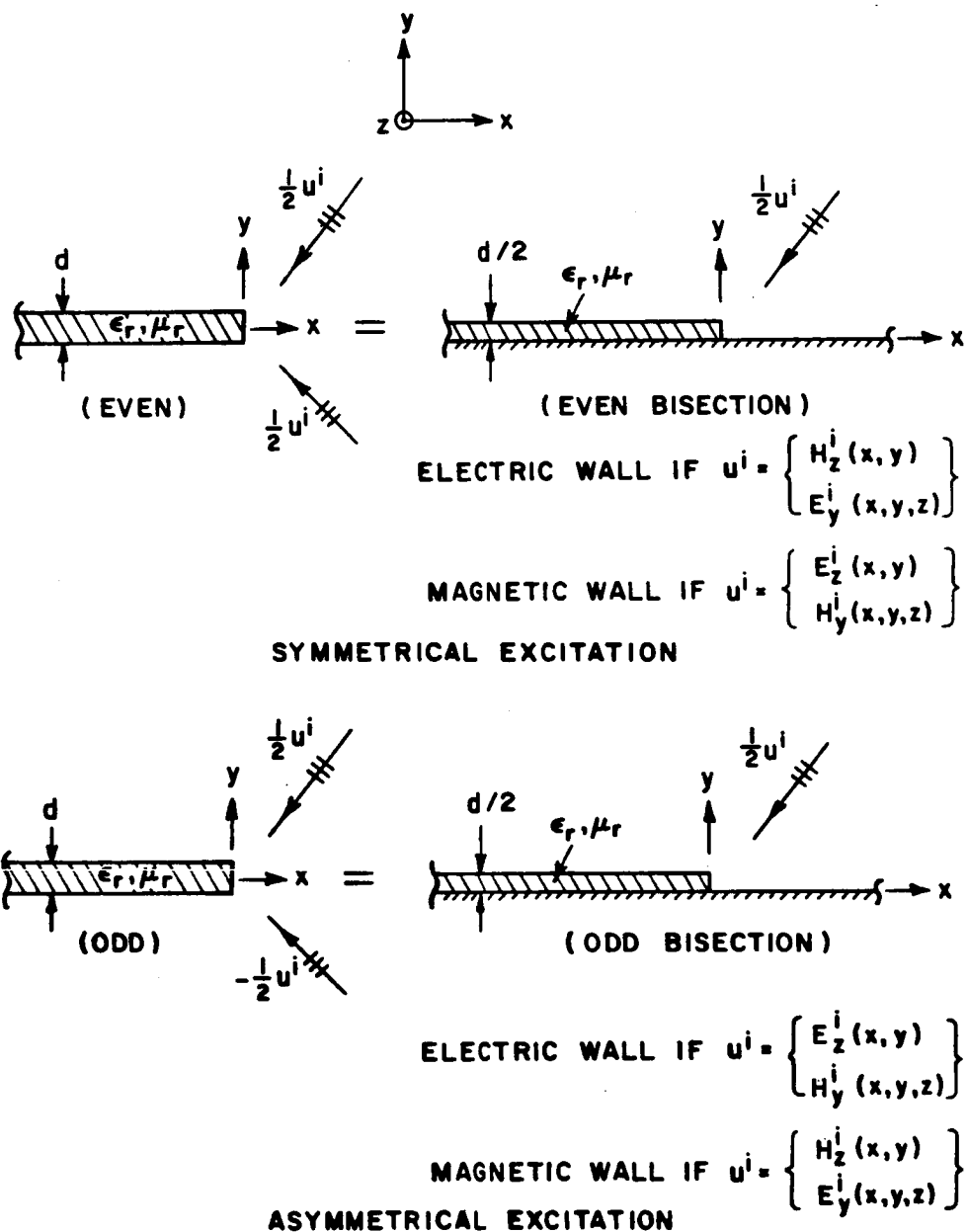


Figure 2.3. Symmetrical and asymmetrical configurations are replaced by the even and odd dielectric/ferrite bisections, respectively.

impedance boundary condition, also known as the Leontovich boundary condition, has been used extensively in the past [21,22,23]. It has been found that the surface impedance boundary conditions provide a useful model in analyzing the effect of the material properties ϵ_r and μ_r on edge diffraction. Once the solutions to the two part impedance problems in Figure 2.5 are obtained, they can be modified heuristically via the UTD recipe to arrive at the solutions to the canonical dielectric/ferrite bisection problems of Figures 2.3 and 2.4, or of Figure 1.3. Finally, the solution to the canonical problem in Figure 1.2 can be constructed directly via a superposition of the even and odd bisection solutions.

B. SCALARIZATION OF THE 3-D VECTOR PROBLEM (OBLIQUE INCIDENCE)

The canonical problem that is considered in this section is illustrated in Figure 2.6. The electric field \vec{E} and magnetic field \vec{H} satisfy the Helmholtz vector equation

$$(\nabla^2 + k^2)\vec{E} = 0 \quad , y > 0, |x| \text{ and } |z| < \infty \quad (2.15)$$

and

$$(\nabla^2 + k^2)\vec{H} = 0 \quad , y > 0, |x| \text{ and } |z| < \infty \quad (2.16)$$

where k is the free space wave number which is given by

$$k = \frac{2\pi}{\lambda} = \omega \sqrt{\mu_0 \epsilon_0} \quad . \quad (2.17)$$

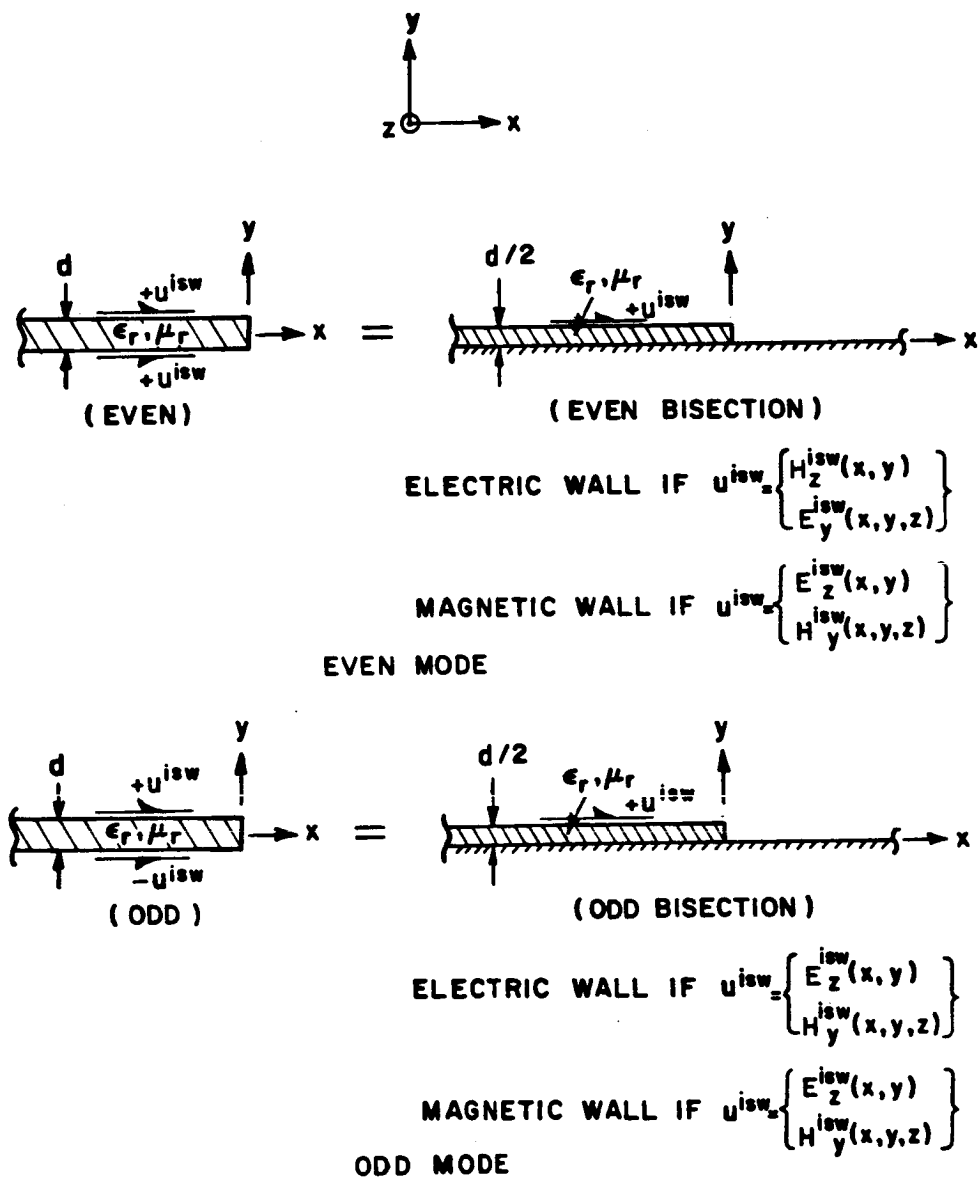


Figure 2.4. Even and odd incident surface wave.

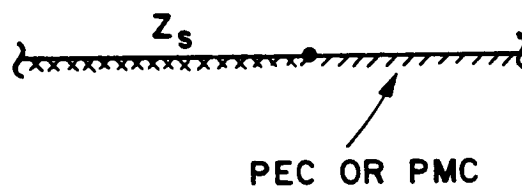
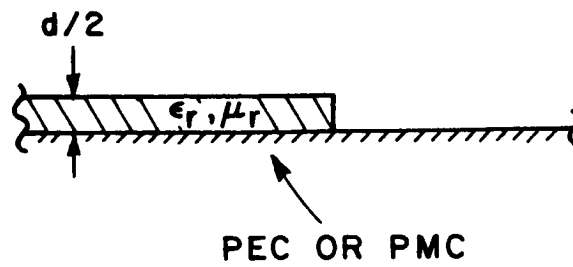


Figure 2.5. Dielectric/ferrite bisection is replaced by impedance bisection.

The fields \vec{E} and \vec{H} also satisfy the following boundary conditions:

$$\vec{E} - (\hat{y} \cdot \vec{E}) \hat{y} = Z_S \hat{y} \times \vec{H} \quad , \quad x < 0, y = 0, |z| < \infty \quad (2.18)$$

or

$$E_x = Z_S H_z \quad ; \quad E_z = -Z_S H_x \quad , \quad x < 0, y = 0, |z| < \infty \quad (2.19)$$

which constitute the impedance or Leontovich boundary conditions and

$$\hat{y} \times \vec{E} = 0 \quad , \quad x > 0, y = 0, |z| < \infty \quad (2.20)$$

or

$$E_x = 0; \quad E_z = 0 \quad , \quad x > 0, y = 0, |z| < \infty \quad (2.21)$$

on a perfect electric conductor. When the region $\{x > 0, y = 0, |z| < \infty\}$, is a perfect magnetic conductor, one requires

$$\hat{y} \times \vec{H} = 0 \quad , \quad x > 0, y = 0, |z| < \infty \quad (2.22)$$

or

$$H_x = 0; H_z = 0 \quad , \quad x > 0, y = 0, |z| < \infty \quad . \quad (2.23)$$

It is simpler to solve a scalar problem than a vector problem, thus, the goal of this section is to scalarize the canonical problem depicted in Figure 2.6. In other words, it is desirable to have decoupled scalar boundary conditions, and scalar differential equations. This can be accomplished in two ways:

(1) Choose the normal field components (E_y, H_y) to decouple the Leontovich boundary condition.

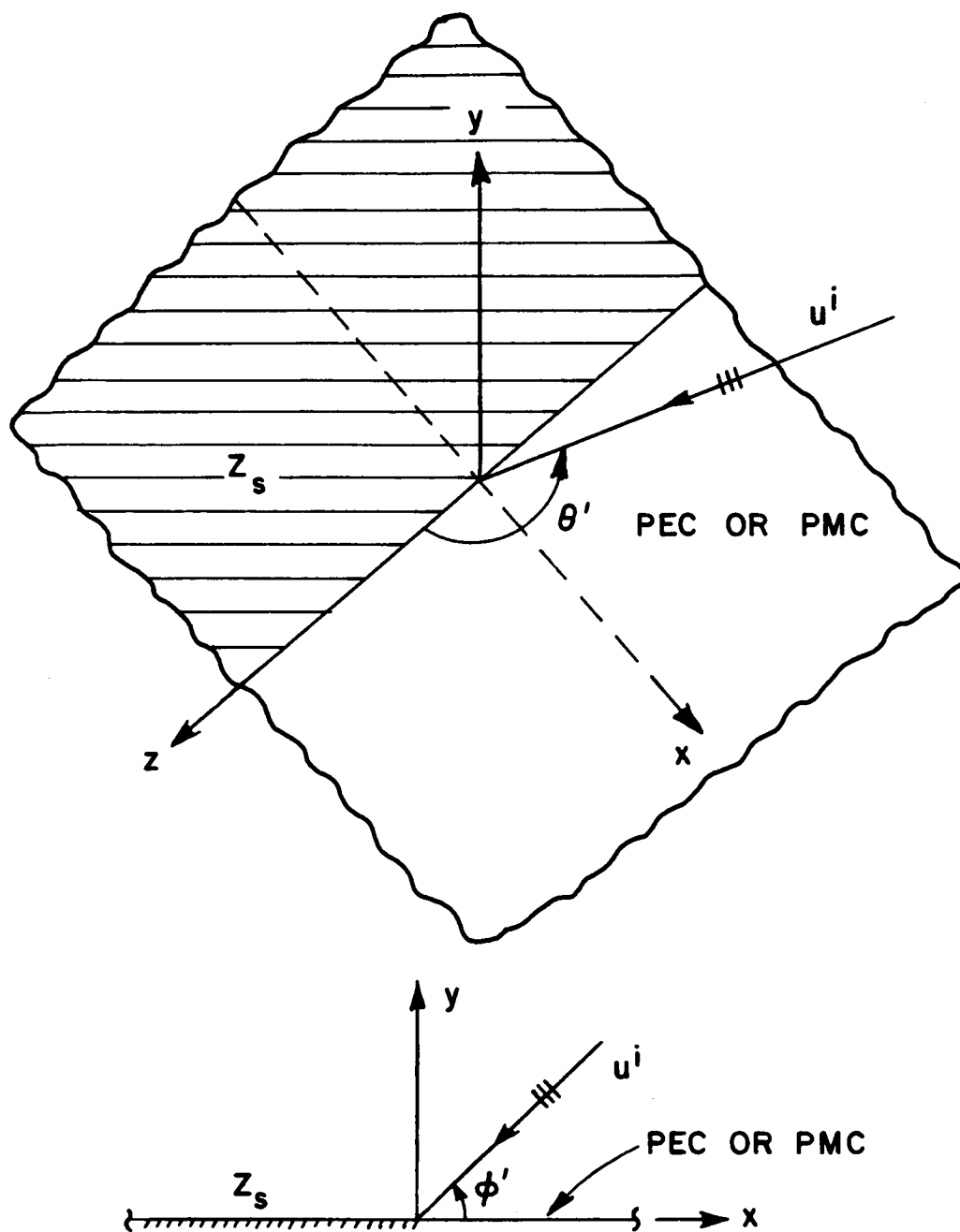


Figure 2.6. Impedance Bisection Geometry.

To prove this statement, one starts with Maxwell equations in a source-free, homogeneous, isotropic medium. These equations are given in (1.1) through (1.4).

Next, the tangential derivatives of Equation (2.19) are taken. That is, the derivatives with respect to x and z such that

$$\frac{\partial E_x}{\partial z} = Z_s \frac{\partial H_z}{\partial z} \quad \text{for } x < 0, y = 0, |z| < \infty \quad (2.24)$$

$$\frac{\partial E_z}{\partial z} = -Z_s \frac{\partial H_x}{\partial z} \quad \text{for } x < 0, y = 0, |z| < \infty \quad (2.25)$$

$$\frac{\partial E_x}{\partial x} = Z_s \frac{\partial H_z}{\partial x} \quad \text{for } x < 0, y = 0, |z| < \infty \quad (2.26)$$

$$\frac{\partial E_z}{\partial x} = -Z_s \frac{\partial H_x}{\partial x} \quad \text{for } x < 0, y = 0, |z| < \infty . \quad (2.27)$$

Adding Equations (2.25) and (2.26) and using Equation (1.2), one gets

$$\frac{\partial E_x}{\partial x} + \frac{\partial E_z}{\partial z} = Z_s \left[\frac{\partial H_z}{\partial x} - \frac{\partial H_x}{\partial z} \right] = ik \frac{Z_s}{\eta_0} E_y , \quad (2.28)$$

$x < 0, y = 0, |z| < \infty .$

Subtracting Equation (2.27) from Equation (2.24), and using Equation (1.1) yields

$$\frac{\partial E_x}{\partial z} - \frac{\partial E_z}{\partial x} = ik \eta_0 H_y = Z_s \left[\frac{\partial H_z}{\partial z} + \frac{\partial H_x}{\partial x} \right] , \quad (2.29)$$

$x < 0, y = 0, |z| < \infty .$

Substituting Equation (1.3) into the left-hand side of Equation (2.28), one finally obtains

$$\frac{\partial E_y}{\partial y} + ik \frac{Z_s}{\eta_0} E_y = 0 \quad , \quad x < 0, y = 0, |z| < \infty \quad (2.30)$$

which is one of the decoupled Leontovich boundary conditions. The other decoupled boundary condition is obtained by substituting Equation (1.4) into the right side of Equation (2.29), that is

$$\frac{\partial H_y}{\partial y} + ik \frac{\eta_0}{Z_s} H_y = 0 \quad , \quad x < 0, y = 0, |z| < \infty \quad . \quad (2.31)$$

To obtain the boundary conditions for the region $\{x > 0, y = 0, |z| < \infty\}$ one can follow the same procedure as above, but there is a simpler way of obtaining them by using the results already derived above.

If the half-plane described by $\{x > 0, y = 0, |z| < \infty\}$ is a perfect electric conductor, which is the limiting case of Z_s approaching zero, it follows from Equations (2.30) and (2.31) that

$$\frac{\partial E_y}{\partial y} = 0 \quad , \quad x > 0, y = 0, |z| < \infty \quad (2.32)$$

and

$$H_y = 0 \quad , \quad x > 0, y = 0, |z| < \infty \quad . \quad (2.33)$$

On the other hand, if the half-plane described by $\{x > 0, y = 0, |z| < \infty\}$ is a perfect magnetic conductor, which is the limiting case of $Z_s \rightarrow \infty$, one obtains from Equation (2.30) and (2.31) the following expressions:

$$E_y = 0 \quad , \quad x > 0, y = 0, |z| < \infty \quad (2.34)$$

and

$$\frac{\partial H_y}{\partial y} = 0, \quad x > 0, y = 0, |z| < \infty. \quad (2.35)$$

Thus, the decoupling of the boundary conditions has been accomplished. It is straightforward to decouple the Helmholtz vector equation. This is done by rewriting equations (2.15) and (2.16) in rectangular coordinates such that

$$(\nabla^2 + k^2) E_y = \left[\frac{\partial^2}{\partial x^2} + \frac{\partial^2}{\partial y^2} + \frac{\partial^2}{\partial z^2} + k^2 \right] E_y = 0, \quad (2.36)$$

$y > 0, |x| \text{ and } |z| < \infty$

$$(\nabla^2 + k^2) H_y = \left[\frac{\partial^2}{\partial x^2} + \frac{\partial^2}{\partial y^2} + \frac{\partial^2}{\partial z^2} + k^2 \right] H_y = 0, \quad (2.37)$$

$y > 0, |x| \text{ and } |z| < \infty.$

This shows that E_y and H_y satisfy Helmholtz scalar equation and completes the scalarization of the original vector problem.

(2) Choose the vector potentials $\vec{A} = \hat{y} A_y$ and $\vec{F}_y = \hat{y} F_y$ to decouple the Leontovich boundary condition.

It follows from [20], and the Lorentz condition for the potentials, that the fields \vec{E} and \vec{H} can be expressed in terms of A_y and F_y as follows:

$$\vec{E} = -\nabla(\hat{y} F_y) + ik\eta_0 \left[\hat{y} A_y + \frac{\nabla(\nabla \cdot (\hat{y} A_y))}{k^2} \right] \quad (2.38)$$

and

$$\vec{H} = \nabla(\hat{y} A_y) + ikY_0 \left[\hat{y} F_y + \frac{\nabla(\nabla \cdot (\hat{y} F_y))}{k^2} \right] \quad (2.39)$$

where A_y and F_y satisfy the Helmholtz scalar equation, that is

$$(\nabla^2 + k^2) A_y = \left[\frac{\partial^2}{\partial x^2} + \frac{\partial^2}{\partial y^2} + \frac{\partial^2}{\partial z^2} + k^2 \right] A_y = 0, \quad (2.40)$$

$y > 0, |x| \text{ and } |z| < \infty$

$$(\nabla^2 + k^2) F_y = \left[\frac{\partial^2}{\partial x^2} + \frac{\partial^2}{\partial y^2} + \frac{\partial^2}{\partial z^2} + k^2 \right] F_y = 0, \quad (2.41)$$

$y > 0, |x| \text{ and } |z| < \infty$

Thus, the differential equation has been already decoupled, and the next step is to decouple the boundary condition given by Equation (2.19).

First, replacing E_x , E_z , H_x and H_z in Equations (2.19)-(2.23) by the expressions given in Equations (2.38) and (2.39), one obtains

$$\frac{\partial}{\partial z} \left[Z_s A_y + \frac{1}{ikY_0} \frac{\partial A_y}{\partial y} \right] = - \frac{\partial}{\partial x} \left[F_y + \frac{Z_s}{ik\eta_0} \frac{\partial F_y}{\partial y} \right], \quad (2.42)$$

$x < 0, y = 0, |z| < \infty$

and

$$\frac{\partial}{\partial x} \left[Z_s A_y + \frac{1}{ikY_0} \frac{\partial A_y}{\partial y} \right] = \frac{\partial}{\partial z} \left[F_y + \frac{Z_s}{ik\eta_0} \frac{\partial F_y}{\partial y} \right], \quad (2.43)$$

$x < 0, y = 0, |z| < \infty$

for the impedance wall. Likewise, one obtains

$$\frac{\partial}{\partial z} [F_y] = \frac{1}{ikY_0} \frac{\partial}{\partial x} \left[\frac{\partial A_y}{\partial y} \right]; \quad \frac{\partial}{\partial x} [F_y] = - \frac{1}{ikY_0} \frac{\partial}{\partial z} \left[\frac{\partial A_y}{\partial y} \right], \quad (2.44)$$

$x > 0, y = 0, |z| < \infty$

for a perfect electric conductor, and

$$\frac{\partial}{\partial z} [A_y] = -\frac{1}{ik\eta_0} \frac{\partial}{\partial x} \left[\frac{\partial F_y}{\partial y} \right] ; \quad \frac{\partial}{\partial x} [A_y] = \frac{1}{ik\eta_0} \frac{\partial}{\partial z} \left[\frac{\partial}{\partial y} F_y \right], \quad (2.45)$$

$$x > 0, y = 0, |z| < \infty$$

for a perfect magnetic conductor.

Next, one arbitrarily assumes that the following two equations are satisfied by A_y and F_y ; namely,

$$Z_s A_y + \frac{1}{ik\eta_0} \frac{\partial A_y}{\partial y} = 0, \quad x < 0, y=0, |z| < \infty \quad (2.46)$$

and

$$F_y + \frac{Z_s}{ik\eta_0} \frac{\partial F_y}{\partial y} = 0, \quad x < 0, y=0, |z| < \infty. \quad (2.47)$$

Using the Expressions (2.46) and (2.47) in Equations (2.42) and (2.43), it is easy to see that both Equations (2.42) and (2.43) are simultaneously satisfied. It follows that the original assumptions (2.46) and (2.47) are indeed correct. Rewriting (2.46) and (2.47), one gets for the impedance wall,

$$\left[\frac{\partial}{\partial y} + ik \frac{Z_s}{\eta_0} \right] A_y = 0, \quad x < 0, y = 0, |z| < \infty \quad (2.48)$$

$$\left[\frac{\partial}{\partial y} + ik \frac{\eta_0}{Z_s} \right] F_y = 0, \quad x < 0, y = 0, |z| < \infty \quad (2.49)$$

which are the decoupled Leontovich boundary conditions for A_y and F_y .

Now, assume the following two equations are true for the perfect electric conductor:

$$F_y = 0; \quad \frac{\partial A_y}{\partial y} = 0 \quad , \quad x > 0, y = 0, |z| < \infty \quad . \quad (2.50)$$

Substituting (2.50) into (2.44) one verifies that both expressions in Equation (2.44) are simultaneously satisfied. Therefore, the original assumption given by Equation (2.50) is correct.

Finally, assume that the following is true for the perfect magnetic conductor:

$$A_y = 0; \quad \frac{\partial F_y}{\partial y} = 0 \quad , \quad x > 0, y = 0, |z| < \infty \quad . \quad (2.51)$$

Again, substituting for A_y and $\frac{\partial F_y}{\partial y}$ in Equation (2.45) by the expressions given in Equation (2.51), one concludes that both expressions in Equation (2.45) are simultaneously satisfied. It follows that the expressions in Equation (2.51) are also true.

Thus, by choosing the normal vector potentials A_y and F_y , one can also scalarize the original vector problem.

C. SCALARIZATION OF THE 2-D VECTOR PROBLEM (NORMAL INCIDENCE)

As in the more general case of oblique incidence, the vector problem for the special case of normal incidence can also be scalarized in two ways:

(1) Choose the tangential field components (E_z and H_z) to decouple the Leontovich boundary conditions.

Following a procedure similar to that in Part (1) of Section B, it can be shown that the Leontovich boundary condition can be decoupled as follows:

$$\left[\frac{\partial}{\partial y} + ik \frac{\eta_0}{Z_s} \right] E_z = 0, \quad x < 0, y = 0 \quad (2.52)$$

$$\left[\frac{\partial}{\partial y} + ik \frac{Z_s}{\eta_0} \right] H_z = 0, \quad x < 0, y = 0 \quad (2.53)$$

Also, for the case of the perfectly conducting electric wall, the boundary conditions satisfied by E_z and H_z are

$$E_z = 0; \quad \frac{\partial H_z}{\partial y} = 0, \quad x > 0, y = 0 \quad (2.54)$$

and the boundary conditions for the perfectly conducting magnetic wall are

$$\frac{\partial E_z}{\partial y} = 0; \quad H_z = 0, \quad x > 0, y = 0 \quad (2.55)$$

Next, rewriting Equations (2.15) and (2.16) in rectangular coordinates, one obtains

$$(\nabla_t^2 + k^2) E_z = 0 = \left[\frac{\partial^2}{\partial x^2} + \frac{\partial^2}{\partial y^2} + k^2 \right] E_z = 0, \quad |x| < \infty, y > 0 \quad (2.56)$$

$$(\nabla_t^2 + k^2) H_z = 0 = \left[\frac{\partial^2}{\partial x^2} + \frac{\partial^2}{\partial y^2} + k^2 \right] H_z = 0, \quad |x| < \infty, y > 0 \quad (2.57)$$

which completes the process of scalarizing the original vector problem.

(2) Choose the tangential vector potentials (A_z, F_z) to decouple the Leontovich boundary condition.

Again, one can follow a similar procedure as in Part (2) of Section B to show that the following is true. The tangential vector potentials A_z and F_z satisfy the following decoupled boundary conditions on the impedance wall:

$$\left[\frac{\partial}{\partial y} + ik \frac{\eta_0}{Z_s} \right] A_z = 0 \quad , \quad x < 0, y = 0 \quad (2.58)$$

$$\left[\frac{\partial}{\partial y} + ik \frac{Z_s}{\eta_0} \right] F_z = 0 \quad , \quad x < 0, y = 0 \quad (2.59)$$

On the region $\{x > 0, y = 0\}$, A_z and F_z satisfy the boundary conditions given by

$$\frac{\partial F_z}{\partial y} = 0 \quad ; \quad A_z = 0 \quad , \quad x > 0, y = 0 \quad (2.60)$$

for a perfect electric conductor, and

$$F_z = 0 \quad ; \quad \frac{\partial A_z}{\partial y} = 0 \quad , \quad x > 0, y = 0 \quad (2.61)$$

for a perfect magnetic conductor.

As in Part (2) of Section B, it follows from [20] and the Lorentz condition that A_z and F_z satisfy the Helmholtz scalar equation, that is

$$(\nabla_t^2 + k^2) A_z(x,y) = \left[\frac{\partial^2}{\partial x^2} + \frac{\partial^2}{\partial y^2} + k^2 \right] A_z(x,y) = 0 \quad (2.62)$$

and

$$(\nabla_t^2 + k^2) F_z(x,y) = \left[\frac{\partial^2}{\partial x^2} + \frac{\partial^2}{\partial y^2} + k^2 \right] F_z(x,y) = 0 \quad (2.63)$$

In conclusion, for the general case of oblique incidence on the edge, the normal field components (E_y , H_y) or the normal vector potentials (A_y , F_y) will scalarize the vector problem. On the other hand, for the special case of normal incidence on the edge, the tangential field components (E_z , H_z) or the tangential vector potentials (A_z , F_z) will scalarize the original vector problem. Thus, essentially what has been done is to transform the vector problem to two scalar ones.

This study will only consider the case when Z_s is a constant and scalar, corresponding to a homogeneous, isotropic impedance sheet. For the more general case when Z_s is a tensor and is a function of position, it is much more difficult and usually not possible to scalarize the Leontovich boundary conditions. In [1], Senior studies the case when Z_s is a tensor, but not a function of position, corresponding to a homogeneous, anisotropic impedance sheet.

D. METHODS OF SOLUTION

1. Maliuzhinets' Method

As mentioned in [1], there are two basic methods of solution of the canonical problem presented in Sections B and C. The first method is that of Maliuzhinets [24] and is the more general of the two, because it is applicable to wedge-shaped regions as well. The total field is expressed in cylindrical coordinates in the form of a Sommerfeld integral with an unknown weight function in the integrand which is deduced via the use of boundary conditions and complicated function

theoretic manipulations. For more details, refer to [24] where only the case of normal incidence is considered.

Different high-frequency approximations of the exact solution obtained by Maliuzhinets [24] in 1959 have been derived in [25] through [30] for various geometries which are special cases of the wedge. Recently, the high frequency solution of Maliuzhinets [24] has been made uniformly valid across the shadow boundaries and it has been cast into the UTD form [31] which is useful for further generalization of this solution. The solution presented in [31] is thus expressed in terms of a UTD diffraction coefficient which has the same general structure as that for the perfectly conducting wedge [11].

2. Wiener-Hopf Method

The second method which will be used in this study is the Wiener-Hopf method. When the fields and currents are expressed in cartesian (rectangular) coordinates, the canonical problem presented in Sections B and C becomes a planar two-part boundary value problem which can be solved by the Wiener-Hopf technique. It can not be solved by the more common method of separation of variables because the boundary conditions are different in the two semi-infinite regions $\{x < 0, y = 0, |z| < \infty\}$ and $\{x > 0, y = 0, |z| < \infty\}$.

As indicated by Noble [32], there are three basic ways of arriving at the Wiener-Hopf equation which must then be solved via the Wiener-Hopf procedure.

(i) Jones' Method

This method due to D.S. Jones [33] obtains the Wiener-Hopf equation by simply applying Fourier transforms directly to the partial differential equation and boundary conditions. One minor disadvantage of this method is that sometimes in very complicated problems it may not be immediately obvious that the transform equations can be reduced to the Wiener-Hopf equation. Jones' method will be used in Chapters III and IV to derive the Wiener-Hopf equation.

(ii) Integral Equation Method

In this method, the integral equation is usually obtained by the Green's function technique. A typical integral equation has the following form:

$$\int_0^{\infty} Q(x) g(z-x) dx = q(z) , \quad 0 < z < \infty \quad (2.64)$$

where $g(z-x)$ and $q(z)$ are known functions, and $Q(x)$ is the unknown function. The function $g(z-x)$ is usually referred to as the kernel of the integral equation and is generally related to a Green's function used in the formulation of the integral equation.

In many cases, it is not obvious which Green's function should be chosen, and the Fourier transforms of the kernels (Green's functions) introduced by this method may not be easy to obtain. This is completely avoided in Jones' method. The main advantage of the integral equation

method seems to be that it is very easy to recognize problems that can be solved by the Wiener-Hopf technique, because the integral equation in (2.64) has a semi-infinite range. For more details refer to [32] and [34] where a more complete treatment of this method is done. This method will not be used in this study. In [35], Senior obtains the solution for the diffraction by an impedance half-plane by solving coupled Wiener-Hopf integral equations for the Fourier transforms of the electric and magnetic currents.

(iii) Dual Integral Method

The main characteristic of this method is that the partial differential equation is solved in the transform domain, but unlike Jones' method, the solution is inverted to the space-domain where the boundary conditions are applied. This gives rise to a pair of coupled integral equations. Edge conditions do not appear explicitly in this method, but they are assumed implicitly, because one assumes that certain orders of integration can be interchanged and certain integrals are convergent. After the solution has been completed, one can check if these assumptions were valid or not. Questions of rigor and uniqueness are not as obviously addressed here as in the first two methods.

3. Solution of the Wiener-Hopf Equation

In this section, a brief outline of the formal procedure for solving the Wiener-Hopf equation will be given. A more detailed

discussion is available in Noble [32], and in Mittra and Lee [34].

A typical Wiener-Hopf equation is given by

$$\hat{F}_+(x) G(s) = K(s) - \hat{C}_-(s) \quad , \quad \tau_- < \tau < \tau_+ \quad (2.65)$$

where $\hat{F}_+(s)$ and $\hat{C}_-(s)$ are unknown functions; whereas, $K(s)$ and $G(s)$ are known functions. Note that there are two unknown functions and only one equation. Furthermore, Equation (2.65) holds only in the strip defined by $\tau_- < \tau < \tau_+$ of the complex s -plane. With the Wiener-Hopf procedure one can accomplish the apparently impossible task of solving for two unknown functions from only one equation. However, there is one more piece of information that is crucial for solving Equation (2.65). As the notation in (2.65) implies, $\hat{F}_+(s)$ is regular in the upper half-plane described by $\tau > \tau_-$, while $\hat{C}_-(s)$ is regular in the lower half s -plane $\tau < \tau_+$. Furthermore, $G(s)$ and $K(s)$ are regular in the strip defined by $\tau_- < \tau < \tau_+$.

The fundamental step in the Wiener-Hopf procedure is the factorization of the function $G(s)$ into the product of two functions such that

$$G(s) = G_+(s) G_-(s) \quad (2.66)$$

where $G_+(s)$ is regular in the upper half s -plane defined by $\tau > \tau_-$ and $G_-(s)$ is regular in the lower half s -plane defined by $\tau < \tau_+$. For reasons that will become obvious, it is required that $G_+(s)$ and $G_-(s)$ be free of zeros in the respective half-planes where each function is regular. This is possible only if $G(s)$ is free of zeros in the strip $\tau_- < \tau < \tau_+$ [34].

There is a formal procedure for factorizing $G(s)$ which is discussed in Appendix D. Sometimes $G_+(s)$ and $G_-(s)$ can be found by inspection when $G(s)$ is a simple function. Substituting (2.66) into (2.65) and dividing by $G_-(s)$ gives

$$\hat{F}_+(s) G_+(s) = \frac{K(s)}{G_-(s)} - \frac{\hat{C}_-(s)}{G_-(s)} \quad , \quad \tau_- < \tau < \tau_+ \quad . \quad (2.67)$$

Note that it is possible to divide by $G_-(s)$ because it was assumed $G_-(s)$ is nonzero in the half-plane $\tau < \tau_+$. The function $\hat{F}_+(s)G_+(s)$ is analytic in the upper half s-plane $\tau > \tau_-$, while the function $\hat{C}_-(s)/G_-(s)$ is analytic in the lower half s-plane $\tau < \tau_+$. However, $K(s)/G_-(s)$ can have singularities in both half planes.

The second most important step in the Wiener-Hopf procedure is to decompose the function $K(s)/G_-(s)$ into the sum of two functions such that

$$\frac{K(s)}{G_-(s)} = D_+(s) + D_-(s) \quad (2.68)$$

where $D_+(s)$ is regular in the upper half s-plane $\tau > \tau_-$, and $D_-(s)$ is regular in the lower half s-plane $\tau < \tau_+$. As in the case of factorization, there is a formal procedure for the decomposition of a function which is discussed in Appendix E. In this study, the function $K(s)/G_-(s)$ will be simple enough such that it can be decomposed by inspection as shown in Chapter III. Substituting (2.68) into (2.67) and rearranging terms yields

$$\hat{F}_+(s) G_+(s) - D_+(s) = D_-(s) - \frac{\hat{C}_-(s)}{G_-(s)} \quad , \quad \tau_- < \tau < \tau_+ \quad . \quad (2.69)$$

Figure 2.7 shows the regions of regularity of all the functions involved in Equations (2.65) and (2.69).

By a careful examination of Equation (2.69) one concludes that the function on the right-hand side of (2.69) is analytic in the lower s-plane $\tau < \tau_+$, and the function on the left-hand side of (2.69) is analytic in the upper half s-plane defined by $\tau > \tau_-$. Since both half planes have a common overlapping region described by $\tau_- < \tau < \tau_+$, it follows by analytic continuation [32] that both sides are equal to an entire function $J(s)$ (regular in the whole s-plane) such that

$$J(s) = F_+(s) G_+(s) - D_+(s) = D_-(s) - \frac{\hat{C}_-(s)}{G_-(s)} \quad \text{for all } s \quad (2.70)$$

where Equation (2.70) holds over the entire s-plane.

Now suppose it can be shown that

$$|\hat{F}_+(s) G_+(s) - D_+(s)| < |s|^p \quad \text{as } s \rightarrow \infty \quad \text{for } \tau > \tau_- \quad (2.71)$$

and

$$|D_-(s) - \frac{\hat{C}_-(s)}{G_-(s)}| < |s|^q \quad \text{as } s \rightarrow \infty \quad \text{for } \tau < \tau_+ \quad (2.72)$$

Then, by the extended form of Liouville's theorem [32], $J(s)$ is a polynomial $P(s)$ of a degree less than or equal to the integral part of $\min(p, q) = n$ such that

$$P(s) = a_0 + a_1 s + a_2 s^2 + \dots + a_n s^n = \sum_{i=0}^n a_i s^i \quad (2.73)$$

where the constants a_i are unknown.

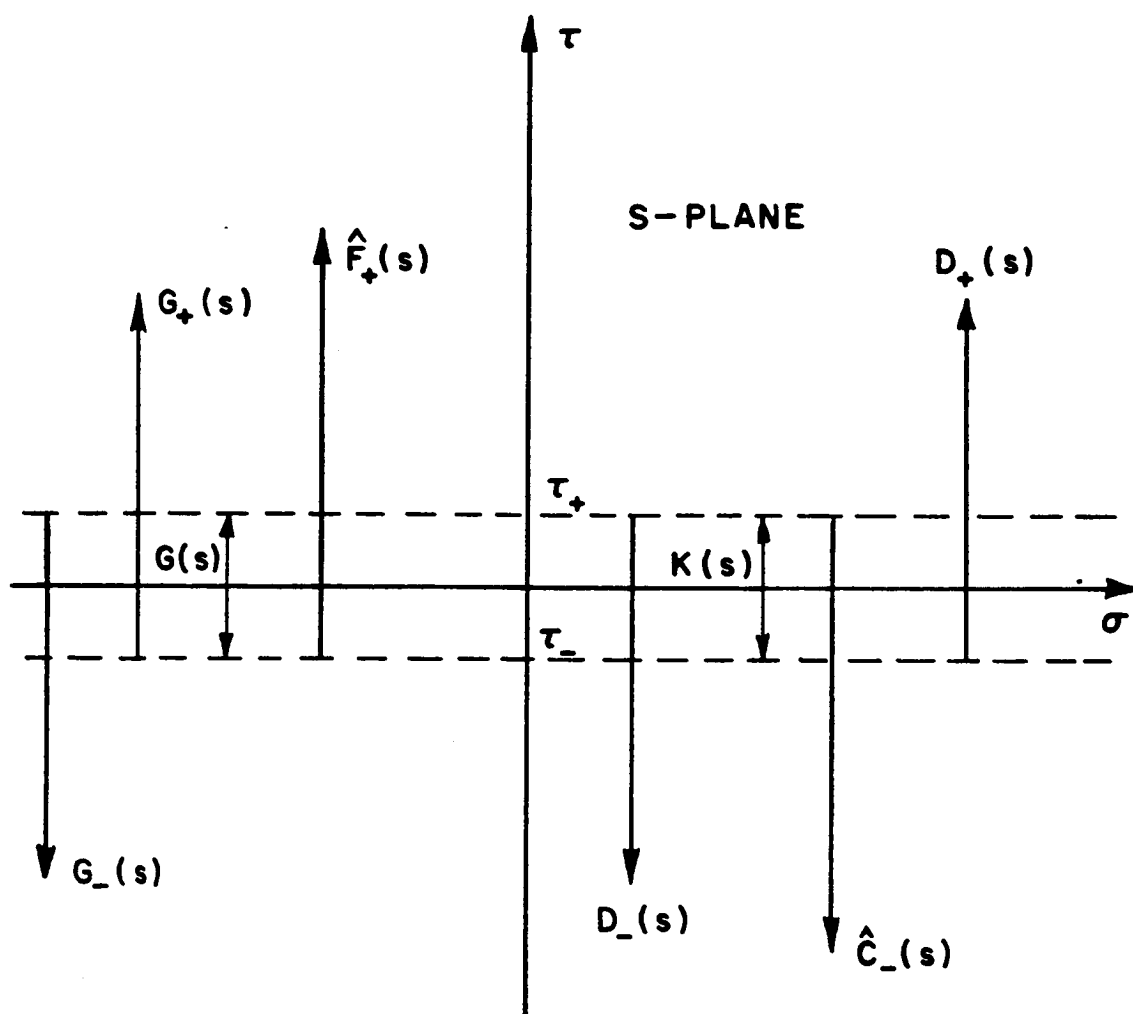


Figure 2.7. Regions of regularity of all the functions involved in Equations (2.65) and (2.69).

Solving for the two unknown functions $F_+(s)$ and $C_-(s)$ one gets

$$\hat{F}_+(s) = \frac{P(s) + D_+(s)}{G_+(s)} \quad (2.74)$$

and

$$\hat{C}_-(s) = [D_-(s) - P(s)] G_-(s) \quad (2.75)$$

It follows from (2.73), (2.74) and (2.75) that $\hat{F}_+(s)$ and $\hat{C}_-(s)$ are determined to within a finite number of arbitrary constants which must be determined otherwise.

The assumption that $J(s)$ is a polynomial is true when one is dealing with electromagnetic problems, because the functions involved in Equations (2.71) and (2.72) are restricted to have algebraic growth. This is due to the edge conditions that the fields have to satisfy near geometrical singularities. The edge conditions are discussed in Appendix B. In most problems in electromagnetics, $P(s)$ will be zero, in which case $\hat{F}_+(s)$ and $\hat{C}_-(s)$ will be uniquely determined. Sometimes $P(s)$ may be a nonzero constant which still has to be determined. Chapter IV shows how this can be accomplished.

CHAPTER III

IMPEDANCE BISECTION PROBLEM (NORMAL INCIDENCE CASE)

A. STATEMENT OF THE PROBLEM

This chapter deals with the analysis of the problem of diffraction by the two-part impedance geometry depicted in Figure 3.1. An infinitely thin screen which is either a perfect electric conductor (PEC) or a perfect magnetic conductor (PMC) lies on the half-plane $\{x > 0, y = 0\}$. It is joined to another half-plane $\{x < 0, y = 0\}$ which consists of a homogeneous, isotropic impedance wall characterized by the impedance Z_s which is a constant. Note that the PEC screen can be characterized by a zero impedance, while the PMC screen is equivalent to an infinite impedance screen. A plane wave u^i is incident from free-space at an angle ϕ' to the x -axis ($0 < \phi' < \pi$). The incident wave may be of the transverse magnetic (TM_z , $u^i = E_z^i$) or transverse electric (TE_z , $u^i = H_z^i$) type field relative to the z -axis. Note that there is no variation of the incident field and the geometry in the z -direction, hence it is a two-dimensional problem. The total field will be determined everywhere in the half-space $y > 0$.

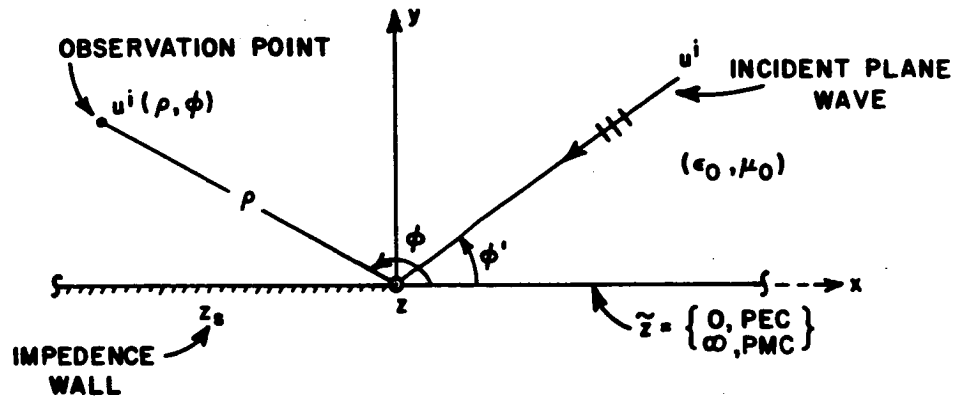


Figure 3.1. Impedance bisection geometry for plane wave excitation.

As shown in Section C of Chapter II, this problem can be scalarized by dealing with either the tangential field components (E_z , H_z) or the \hat{z} -directed potentials ($\tilde{A}=\hat{z}A_z$, $\tilde{F}=\hat{z}F_z$). The tangential field components will be used here. It follows that the boundary conditions for both TE_z and TM_z polarizations are (see Section C, Chapter II) given by

TE_z case: $E_z = 0$

$$\left[\frac{d}{dy} + ik \frac{Z_s}{\eta_0} \right] H_z = 0 \quad , \quad y = 0 \quad , \quad x < 0 \quad (3.1)$$

$$\frac{d}{dy} H_z = 0 \quad \text{for PEC} \quad , \quad y = 0 \quad , \quad x > 0 \quad (3.2)$$

or

$$H_z = 0 \quad \text{for PMC} \quad , \quad y = 0 \quad , \quad x > 0 \quad . \quad (3.3)$$

TM_z case: $H_z = 0$

$$\left[\frac{d}{dy} + ik \frac{\eta_0}{Z_s} \right] E_z = 0 \quad , \quad y = 0 \quad , \quad x < 0 \quad (3.4)$$

$$E_z = 0 \quad \text{for PEC} \quad , \quad y = 0 \quad , \quad x > 0 \quad (3.5)$$

or

$$\frac{d}{dy} E_z = 0 \quad \text{for PMC} \quad , \quad y = 0 \quad , \quad x > 0 \quad (3.6)$$

where $\eta_0 = (\mu_0/\epsilon_0)^{1/2}$ is the free space impedance.

Instead of solving four different problems (two polarizations and PEC or PMC screen), only two problems will be solved: even and odd problems. For both cases, the function $u(x,y)$ is equal to

$$u(x,y) = \begin{cases} E_z & \text{for TM}_z \text{ polarization, or} \\ H_z & \text{for TE}_z \text{ polarization} \end{cases} \quad (3.7)$$

and it satisfies the scalar Helmholtz equation

$$(\nabla_t^2 + k^2) u(x,y) = \left(\frac{\partial^2}{\partial x^2} + \frac{\partial^2}{\partial y^2} + k^2 \right) u(x,y) = 0 \quad \text{for } y > 0 \quad \text{and } |x| < \infty . \quad (3.8)$$

For the even problem, $u(x,y) = u_e(x,y)$, and the boundary conditions become

$$\left[\frac{d}{dy} + ik\delta_e \right] u_e(x,y) = 0 \quad , \quad x < 0, y = 0 \quad (3.9)$$

and

$$\frac{d}{dy} u_e(x,y) = 0 \quad , \quad x > 0, y = 0 \quad (3.10)$$

where

$$\delta_e = \begin{cases} Z_s/\eta_0 = \text{normalized impedance, TE}_z \text{ polarization} \\ \eta_0/Z_s = \text{normalized admittance, TM}_z \text{ polarization} \end{cases} \quad (3.11)$$

For the odd problem, $u(x,y) = u_o(x,y)$, and the boundary conditions are given by

$$\left[\frac{d}{dy} + ik\delta_o \right] u_o(x,y) = 0 \quad , \quad x < 0, y = 0 \quad (3.12)$$

and

$$u_o(x,y) = 0 \quad , \quad x > 0, y = 0 \quad (3.13)$$

where δ_o has the same definition as δ_e . The subscript "e" refers to the even problem while the subscript "o" refers to the odd problem. Let the incident field be denoted by

$$u^i(x,y) = v e^{i(k_x^i x - k_y^i y)} \quad , \quad y > 0 \quad (3.14)$$

where

$$k_x^i = -k \cos \phi' \quad ; \quad k_y^i = k \sin \phi' \quad (3.15)$$

and v is an arbitrary constant. In cylindrical coordinates, $u^i(x,y)$ is equal to

$$u^i(\rho, \phi) = v e^{-ik\rho \cos(\phi - \phi')} \quad , \quad \rho > 0, 0 < (\phi, \phi') < \pi \quad (3.16)$$

The first step in solving this problem is to consider the geometry shown in Figure 3.2 where a homogeneous, isotropic impedance wall occupies the plane $y = 0$. The reason for doing this will become obvious in the following steps of the analysis.

The field $\tilde{u}(\rho, \phi)$ will be referred to as the unperturbed total field in the presence of the impedance wall. This problem can be solved by the well known separation of variables technique [36], because the boundary conditions given in Equations (3.9) and (3.12) hold for all values of x such that

$$\left[\frac{\partial}{\partial y} + ik\delta \right] \tilde{u}(x, y) = 0 \quad \text{for } |x| < \infty, y = 0 \quad (3.17)$$

where the subscripts "e" and "o" will be temporarily dropped for convenience.

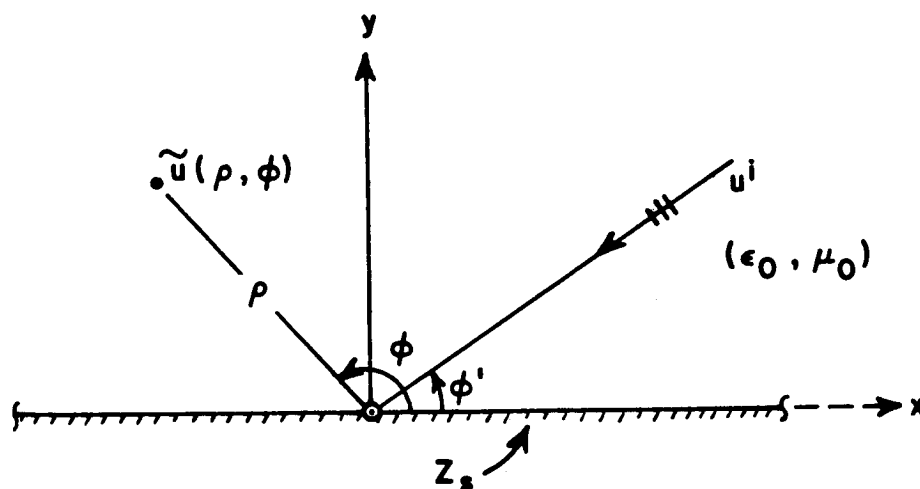


Figure 3.2. Unperturbed geometry.

Without going over the details of the solution, the final result can be written as

$$\tilde{u}(x,y) = u^i(x,y) + \tilde{u}^r(x,y) \quad (3.18)$$

where $\tilde{u}^r(x,y)$ is the reflected field given by

$$\tilde{u}^r(x,y) = vR(\delta, \phi') e^{i(k'_x x + k'_y y)}, \quad |x| < \infty, y > 0 \quad (3.19)$$

and $R(\delta, \phi')$ is the Fresnel reflection coefficient.

$$R(\delta, \phi') = \frac{k'_y - k\delta}{k'_y + k\delta} = \frac{\sin\phi' - \delta}{\sin\phi' + \delta} \quad (3.20)$$

Note that the unperturbed field $\tilde{u}(x,y)$ still satisfies Equation (3.8) (or the scalar, two-dimensional Helmholtz equation).

As stated in Section D of Chapter II, there are two basic methods for solving the canonical two part impedance problem being considered in this chapter. In this analysis, the Wiener-Hopf method will be used, and the Wiener-Hopf equation will be obtained by Jones' method in Section B.

B. JONES' METHOD

In order to have some order in the analysis, the even problem is solved first, and then the odd problem will be considered.

1. Even Problem

The total even field $u_e(x,y)$ can be written as

$$u_e(x,y) = \tilde{u}_e(x,y) + u_e^S(x,y) \quad \text{for } y > 0, \quad |x| < \infty \quad (3.21)$$

where $\tilde{u}_e(x,y)$ is the even unperturbed field which was defined in Section A.

The field $u_e^S(x,y)$ which is referred to as the scattered field is necessary to properly account for the effects of the PEC or PMC screen lying in the half-plane $\{x > 0, y = 0\}$. Note that the definition of the scattered field $u_e^S(x,y)$ is different from the usual definition of scattered field.

Since the total field $u_e(x,y)$, and the unperturbed field $\tilde{u}_e(x,y)$ satisfy the scalar Helmholtz equation, it follows that $u_e^S(x,y)$ also satisfies the same equation, that is

$$\left[\frac{\partial^2}{\partial x^2} + \frac{\partial^2}{\partial y^2} + k^2 \right] u_e^S(x,y) = 0 \quad \text{for } |x| < \infty, y > 0 \quad . \quad (3.22)$$

Furthermore, it follows from Equations (3.9), (3.17) and (3.21) that

$$\left[\frac{\partial}{\partial y} + ik\delta_e \right] u_e^S(x,y) = 0 \quad \text{for } y = 0, \quad x < 0 \quad . \quad (3.23)$$

Thus, the field $u_e^S(x,y)$ also satisfies the Leontovich boundary condition for $\{y = 0, x < 0\}$. For the half-plane $\{x > 0, y = 0\}$, the boundary condition given in Equation (3.10) becomes

$$\frac{\partial}{\partial y} u_e^S(x,y) = - \frac{\partial}{\partial y} \tilde{u}_e(x,y) = - \frac{\partial}{\partial y} [u^i(x,y) + \tilde{u}_e^r(x,y)] \quad (3.24)$$

for $y = 0, x > 0$

Following the notation of Appendix A, let

$$u_e^S(x,y) = u_{e+}^S(x,y) + u_{e-}^S(x,y) \quad (3.25)$$

where $u_{e+}^S(x,y)$ and $u_{e-}^S(x,y)$ are the half-range functions defined in Appendix A. Also, let

$$u_e^{i+r}(x,y) = u^i(x,y) + \tilde{u}_e^r(x,y) = u_{e+}^{i+r}(x,y) + u_{e-}^{i+r}(x,y) \quad (3.26)$$

It follows that Equations (3.23) and (3.24) can be rewritten as follows:

$$\left[\frac{\partial}{\partial y} + ik\delta_e \right] u_{e-}^S(x,y) = 0 \quad \text{for } y = 0, |x| < \infty \quad (3.27)$$

and

$$\frac{\partial}{\partial y} u_{e+}^S(x,y) = - \frac{\partial}{\partial y} (u_{e+}^{i+r}(x,y)) \quad \text{for } y = 0, |x| < \infty \quad (3.28)$$

As stated in Section D of Chapter II, the principal feature of Jones' method is that the Fourier transform is applied directly to the differential equation and the boundary conditions. Note that the Fourier transform being used here is carefully defined in Appendix A, and it will not be repeated in this chapter. Applying one-sided Fourier

transforms to Equations (3.27) and (3.28) with respect to the variable x , one gets

$$\left[\frac{\partial}{\partial y} + ik\delta_e \right] \hat{u}_{e-}^s(s,y) = 0 \quad \text{for } y = 0, \tau = \text{Im}(s) < \tau_+ \quad (3.29)$$

and

$$\frac{\partial}{\partial y} \hat{u}_{e+}^s(s,y) = - \frac{\partial}{\partial y} (\hat{u}_{e+}^{i+r}(s,y)) \quad \text{for } y = 0, \tau = \text{Im}(s) > \tau_- \quad (3.30)$$

where s is the complex variable in the Fourier transform domain and the constants τ_+ and τ_- , which are defined in Appendix A, will be determined later in the analysis. Next, Fourier transforming Equation (3.22) and using Equation (A.16), one obtains that

$$\left[\frac{\partial^2}{\partial y^2} + \beta^2 \right] \hat{u}_e^s(s,y) = 0 \quad \text{for } y > 0, \tau_- < \tau < \tau_+ \quad (3.31)$$

where $\hat{u}_e^s(s,y)$ is regular in the strip $\tau_- < \tau < \tau_+$, and β , which is carefully defined in Appendix C, is given by

$$\beta = (k^2 - s^2)^{1/2} \quad (3.32)$$

Since (3.31) is a second order differential equations, it has two solutions, that is

$$\hat{u}_e^s(s,y) = A_e(s)e^{i\beta y} + B_e(s)e^{-i\beta y} \quad \text{for } y > 0, \tau_- < \tau < \tau_+ \quad (3.33)$$

Let

$$\beta = \beta_r + i\beta_I \quad (3.34)$$

where β_r and β_I are real variables. In Appendix C, the branch cut of β is defined such that $\beta_I > 0$ in the entire top (proper) Riemann sheet of the complex s -plane. It is obvious that the second solution of (3.33) will become unbounded as $y \rightarrow \infty$. It follows from the radiation condition given in Appendix B that

$$B_e(s) = 0 \quad (3.35)$$

and $\hat{u}_e^S(s,y)$ becomes

$$\hat{u}_e^S(s,y) = A_e(s)e^{i\beta y} \quad \text{for } y > 0, \tau_- < \tau < \tau_+ \quad (3.36)$$

where $A_e(s)$ is still unknown at this point. The function $\hat{u}_e^S(x,y)$ can be rewritten in terms of one-sided Fourier transforms as

$$\hat{u}_e^S(s,y) = A_e(s)e^{i\beta y} = \hat{u}_{e+}^S(s,y) + \hat{u}_{e-}^S(s,y) \quad (3.37)$$

for $y > 0, \tau_- < \tau < \tau_+$

where $\hat{u}_{e+}^S(s,y)$ is regular in the upper half s -plane defined by $\tau > \tau_-$

and $\hat{u}_{e-}^S(s,y)$ is regular in the lower half s -plane defined by $\tau < \tau_+$.

Letting $y = 0$ in Equation (3.37), one gets

$$A_e(s) = \hat{u}_{e+}^S(s,0) + \hat{u}_{e-}^S(s,0) \quad , \quad \tau_- < \tau < \tau_+ \quad (3.38)$$

which indicates that $A_e(s)$ is also regular in the strip defined by

$$\tau_- < \tau < \tau_+.$$

Following a similar procedure as above, the one-sided Fourier transform of $u_{e+}^{i+r}(x,y)$ will be computed next. Substituting u_{e+}^{i+r} into (A.7) yields

$$\hat{u}_{e+}^{i+r}(s,y) = \frac{1}{\sqrt{2\pi}} \int_0^{\infty} u_{e+}^{i+r}(x,y) e^{isx} dx \quad \text{for } y > 0 \quad (3.39)$$

or

$$\hat{u}_{e+}^{i+r}(s,y) = \frac{v}{\sqrt{2\pi}} \left[e^{-ik_y' y} + R_e(\delta_e, \phi') e^{ik_y' y} \right] \quad (3.40)$$

$$\cdot \lim_{a \rightarrow \infty} \int_0^a e^{i(s+k_x')x} dx \quad \text{for } y > 0 ,$$

but

$$\lim_{a \rightarrow \infty} \int_0^a e^{i(s+k_x')x} dx = \lim_{a \rightarrow \infty} \left[\frac{e^{i(s+k_x')a}}{i(s+k_x')} - \frac{1}{i(s+k_x')} \right] \quad (3.41)$$

If $\text{Im}(s+k_x') = \text{Im}(\sigma + i\tau - (k_1 + ik_2) \cos \phi') = \tau - k_2 \cos \phi'$ is greater than zero, one finds that

$$\lim_{a \rightarrow \infty} \frac{e^{i(s+k_x')a}}{i(s+k_x')} = 0 \quad \text{for } \tau > k_2 \cos \phi' \quad (3.42)$$

and

$$\hat{u}_{e+}^{i+r}(s,y) = \frac{v}{\sqrt{2\pi}} \left[e^{-ik_y' y} + R_e(\delta_e, \phi') e^{ik_y' y} \right] \frac{i}{s+k_x'} \quad (3.43)$$

$$\text{for } \tau > k_2 \cos \phi' .$$

It follows that

$$\tau_- = k_2 \cos \phi' \quad (3.44)$$

and $\hat{u}_{e+}^{i+r}(s,y)$ is a regular function in the upper s -plane defined by

$$\tau > \tau_-.$$

Taking the derivative of $\hat{u}_{e+}^{i+r}(s,y)$ with respect to y , one gets

$$\frac{\partial}{\partial y} \hat{u}_{e+}^{i+r}(s,y) = \frac{v}{\sqrt{2\pi}} \left[e^{-ik_y' y} - R_e e^{ik_y' y} \right] \frac{k_y'}{s+k_x'} \quad (3.45)$$

Evaluating (3.45) at $y = 0$ and substituting into Equation (3.30), one obtains that

$$\frac{\partial}{\partial y} \hat{u}_{e+}^s(s,y) = -\frac{v}{\sqrt{2\pi}} \frac{k_y'}{s+k_x'} (1 - R_e) \quad \text{for } y = 0, \tau > \tau_- \quad (3.46)$$

If the following notation is used:

$$\frac{\partial}{\partial y} \hat{u}_{e+}^s(s,y) \Big|_{y=0} = \frac{\partial}{\partial y} \hat{u}_{e+}^s(s,0) \quad , \quad (3.47)$$

Equation (3.46) becomes

$$\frac{\partial}{\partial y} \hat{u}_{e+}^s(s,0) = \frac{-v}{\sqrt{2\pi}} \frac{k_y'}{(s+k_x')} (1 - R_e) \quad \text{for } \tau > \tau_- \quad (3.48)$$

It is obvious from Equation (3.48) that $\frac{\partial}{\partial y} \hat{u}_{e+}^s(s,0)$ is also regular in the upper s -plane $\tau > \tau_-$.

As stated above, the scattered field $u_e^S(x,y)$ is needed to account for the effects of the PEC or PMC screen lying on the half-plane $\{x > 0, y = 0\}$. This means that $u_{e+}^S(x,0)$ has to have the same asymptotic behavior as $u_{e+}^{i+r}(x,0)$ for $x \rightarrow \infty$, that is

$$\lim_{x \rightarrow +\infty} u_{e+}^S(x,0) \sim c e^{k_2 \cos \phi' x} = c e^{\tau_- x} \quad . \quad (3.49)$$

It follows from Equations (A.4) and (A.7) that $\hat{u}_{e+}^S(s,0)$ is regular in the upper s -plane defined by $\tau > \tau_-$.

The next step in the analysis is to take the derivative of Equation (3.37) with respect to y , and after setting $y = 0$, one finds that

$$i\beta A_e(s) = \frac{\partial}{\partial y} \hat{u}_{e+}^S(s,0) + \frac{\partial \hat{u}_{e-}^S(s,0)}{\partial y} \quad , \quad \tau_- < \tau < \tau_+ \quad . \quad (3.50)$$

Substituting Equations (3.29), (3.38) and (3.48) into (3.50), one obtains

$$i\beta \left[\hat{u}_{e+}^S(s,0) + \hat{u}_{e-}^S(s,0) \right] = -\frac{v}{\sqrt{2\pi}} \frac{k_y'(1-R_e)}{(s+k_x')} - ik\delta_e \hat{u}_{e-}^S(s,0), \quad (3.51)$$

$\tau_- < \tau < \tau_+$

or

$$\frac{-v}{\sqrt{2\pi}} \frac{k_y'(1-R_e)}{(s+k_x')} = i\beta \hat{u}_{e+}^S(s,0) + \hat{u}_{e-}^S(s,0) (i\beta + ik\delta_e) \quad , \quad (3.52)$$

$\tau_- < \tau < \tau_+ \quad .$

At this point in the analysis, the regions of regularity of $\hat{u}_{e+}^S(s,0)$ and $\frac{\partial}{\partial y} \hat{u}_{e+}^S(s,0)$ have been established. Furthermore, from the

definition of β in Appendix C, it is easily determined that β is regular in the strip defined by $-k_2 < \tau < k_2$. Thus, it remains to determine the regions of regularity of $\hat{u}_{e-}^s(s,0)$ which can be established by knowing the asymptotic behavior of $u_{e-}^s(x,0)$ as $x \rightarrow -\infty$. Note that besides the contribution to $u_{e-}^s(x,y)$ from the currents lying on the PEC or PMC screen, there will be a contribution from the region $\{x = 0, y = 0\}$ where the impedance discontinuity occurs [6,10]. This contribution can be interpreted as coming from an equivalent source [6,10] located at $\{x = 0, y = 0\}$. It follows from Equation (B.4) that the asymptotic behavior of $u_{e-}^s(x,0)$ due to this contribution will be

$$u_{e-}^s(x,0) \sim \frac{ce^{-ikx}}{|x|^{(1/2 \text{ or } 3/2)}} = \frac{ce^{-ik_1x} e^{k_2x}}{|x|^{(1/2 \text{ or } 3/2)}} \text{ as } x \rightarrow -\infty. \quad (3.53)$$

Therefore, τ_+ is equal to

$$\tau_+ = \text{Im}(k) = k_2 \quad (3.54)$$

and $\hat{u}_{e-}^s(s,0)$ is regular in the lower half s -plane defined by $\tau < \tau_+$.

Dividing (3.52) by $i\beta$, one gets

$$\frac{vi k_y (1-R_e)}{\sqrt{2\pi} (s+k_x')\beta} = \hat{u}_{e+}^s(s,0) + \left[\frac{-k\delta_e + \beta}{\beta} \right] \hat{u}_{e-}^s(s,0), \quad (3.55)$$

$$\tau_- < \tau < \tau_+.$$

Since $\tau_+ > \tau_-$, all the functions of Equation (3.55) have a common overlapping region of regularity. In a well-posed physical problem, this is always the case [34]. Let $G^e(s)$ and $\Phi^e(s)$ be defined as follows:

$$G^e(s) = \frac{\beta}{k\delta_e + \beta} \quad (3.56)$$

$$\phi^e(s) = \frac{ivk_y'(1-R_e)}{\sqrt{2\pi\beta}(s+k_x')} \quad (3.57)$$

where $G^e(s)$ is regular in the strip $-k_2 < \tau < k_2$ which includes the strip $\tau_- < \tau < \tau_+$, and $\phi^e(s)$ is regular in the strip $\tau_- < \tau < \tau_+$. Substituting (3.56) and (3.57) into Equation (3.55), and multiplying by $G^e(s)$, one obtains

$$\phi^e(s) G^e(s) = \hat{u}_{e-}^s(s,0) + G^e(s) \hat{u}_{e+}^s(s,0) \quad , \quad \tau_- < \tau < \tau_+ \quad (3.58)$$

which is known as the Wiener-Hopf equation. Figure (3.3) shows the regions of regularity of all the functions in Equation (3.58). Note that there are two unknown functions in (3.58); namely, $\hat{u}_{e+}^s(s,0)$ and $\hat{u}_{e-}^s(s,0)$. This equation can be solved using the Wiener-Hopf technique which was invented around 1931 to solve a special type of integral equation [32]. This technique was summarized in Section D.3 of Chapter II. Comparing Equations (2.65) and (3.58) one concludes that

$$K(s) = \phi^e(s) G^e(s) \quad (3.59)$$

$$\hat{F}_+(s) = \hat{u}_{e+}^s(s,0) \quad (3.60)$$

$$\hat{C}_-(s) = \hat{u}_{e-}^s(s,0) \quad . \quad (3.61)$$

It is required that $G^e(s)$ be free of zeros in the strip $\tau_- < \tau < \tau_+$. It is obvious that $G^e(s)$ in Equation (3.56) does not have zeros in the

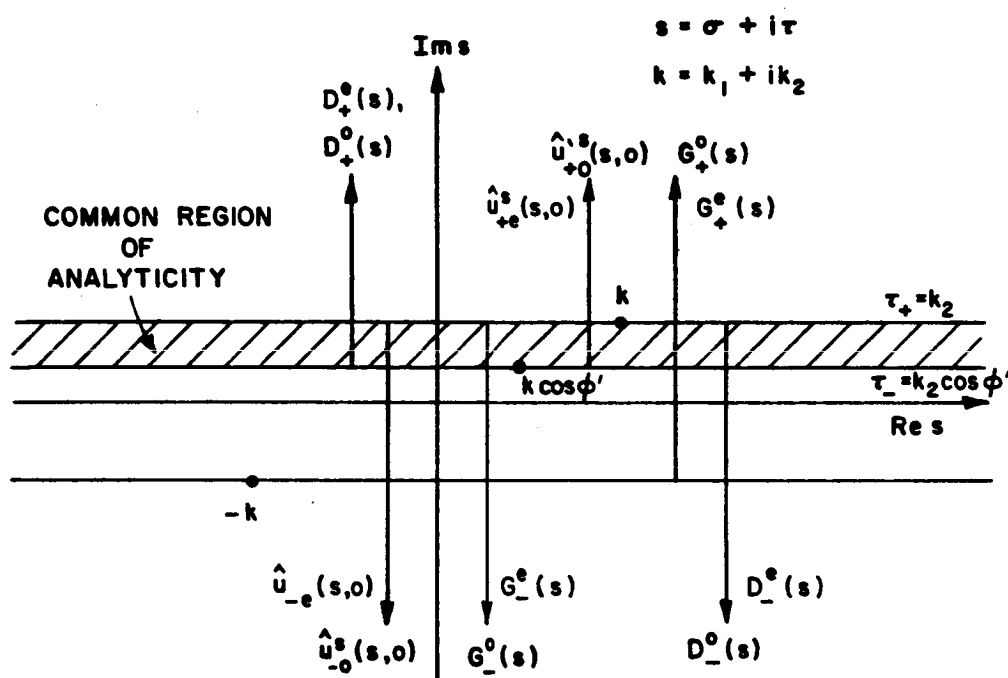


Figure 3.3. Regions of analyticity of functions in Equations (3.58) and (3.131).

strip $\tau_- < \tau < \tau_+$. The factorization of $G^e(s)$ is possible if $G^e(s)$ satisfies certain conditions [32], which are satisfied by this particular $G^e(s)$. The functions $G_+^e(s)$ and $G_-^e(s)$ are obtained by following the same procedure as Weinstein [37] and the details are shown in Appendix D.

As mentioned in Section D.3, Chapter II, the functions $D_+^e(s)$ and $D_-^e(s)$ in this particular problem can be obtained by inspection. Recall that

$$\frac{K(s)}{G_-^e(s)} = \Phi^e(s) G_+^e(s) = D_+^e(s) + D_-^e(s) \quad , \quad \tau_- < \tau < \tau_+ \quad . \quad (3.62)$$

It is shown in Appendix E that D_+^e and $D_-^e(s)$ are given, respectively, by

$$D_+^e(s) = \frac{ivk_y'(1-R_e)}{\sqrt{2\pi} k \delta_e(s+k_x')} \left[\frac{1}{G_-^e(-k_x')} - G_+^e(s) \right] \quad (3.63)$$

and

$$D_-^e(s) = \frac{ivk_y'(1-R_e)}{\sqrt{2\pi} k \delta_e(s+k_x')} \left[\frac{1}{G_-^e(s)} - \frac{1}{G_-^e(-k_x')} \right] \quad . \quad (3.64)$$

Substituting (3.62) into (3.58) and using the results of (2.70) yields

$$D_+^e(s) - \hat{u}_{e+}^s(s,0) G_+^e(s) = \hat{u}_{e-}^s(s,0) \frac{1}{G_-^e(s)} - D_-^e(s) = P(s) \quad (3.65)$$

for all s

where $P(s)$ is still an unknown entire function which can be expressed as a polynomial in s .

Solving for $\hat{u}_{e+}^s(s,0)$ and $\hat{u}_{e-}^s(s,0)$ in terms of $P(s)$, one obtains

$$\hat{u}_{e+}^s(s,0) = \frac{D_+^e(s) - P(s)}{G_+^e(s)} \quad (3.66)$$

and

$$\hat{u}_{e-}^s(s,0) = G_-^e(s) [P(s) + D_-^e(s)] \quad (3.67)$$

Since $P(s)$ is an unknown, $\hat{u}_{e+}^s(s,0)$ and $\hat{u}_{e-}^s(s,0)$ are not unique solutions. In other words, it is possible to obtain many solutions which satisfy the scalar Helmholtz equation and all the boundary conditions. In order to obtain a unique solution, the asymptotic behavior of both sides of Equation (3.65) has to be determined for the specific problem at hand.

It follows from Equation (3.56) that

$$G^e(s) \sim 1 \text{ as } |s| \rightarrow \infty \quad \text{for } \tau_- < \tau < \tau_+ \quad (3.68)$$

It is shown in Appendix D that

$$G_+^e(s) \sim 1 \text{ as } |s| \rightarrow \infty \quad \text{for } \tau > \tau_- \quad (3.69)$$

and

$$G_-^e(s) \sim 1 \text{ as } |s| \rightarrow \infty \quad \text{for } \tau < \tau_+ \quad (3.70)$$

The asymptotic behavior of $D_+^e(s)$ and $D_-^e(s)$ is easily determined from Equations (3.63) and (3.64), that is

$$D_+^e(s) \sim s^{-1} \text{ as } |s| \rightarrow \infty \quad \text{for } \tau > \tau_- \quad (3.71)$$

and

$$D_-^e(s) \sim s^{-1} \text{ as } |s| \rightarrow \infty \text{ for } \tau < \tau_+ \quad . \quad (3.72)$$

In order to determine the asymptotic behavior of $\hat{u}_{e-}^s(s,0)$ and $\hat{u}_{e+}^s(s,0)$, the edge conditions given in Appendix B have to be used. Recall that $u_e(x,y)$ represents the tangential electric field component E_z or the tangential magnetic component H_z . It follows from Equation (B.5) that

$$u_{e+}^s(x,0) = O(|x|^p) \quad \text{as } x \rightarrow 0+ \quad (3.73)$$

and

$$u_{e-}^s(x,0) \sim O(|x|^p) \quad \text{as } x \rightarrow 0- \quad (3.74)$$

where $p > 0$. Therefore, using Equations (A.12) through (A.15) yields

$$\hat{u}_{e+}^s(s,0) \sim s^{-p-1} \quad \text{as } |s| \rightarrow \infty \text{ for } \tau > \tau_- \quad (3.75)$$

$$\hat{u}_{e-}^s(s,0) \sim s^{-p-1} \quad \text{as } |s| \rightarrow \infty \text{ for } \tau < \tau_+ \quad . \quad (3.76)$$

Substituting Equations (3.69) through (3.72), (3.75) and (3.76) into (3.65), one gets

$$|D_+^e(s) - \hat{u}_{e+}^s(s,0) G_+^e(s)| \sim |s|^{-p-1} \text{ as } |s| \rightarrow \infty \text{ for } \tau > \tau_- \quad (3.77)$$

$$|\hat{u}_{e-}^s(s,0) / G_-^e(s) - D_-^e(s)| \sim |s|^{-p-1} \text{ as } |s| \rightarrow \infty \text{ for } \tau < \tau_+ \quad . \quad (3.78)$$

Although the constant p is unknown, it is at least known that $p > 0$.

Thus, it follows from (3.77) and (3.78) that

$$P(s) \rightarrow 0 \quad \text{as } |s| \rightarrow \infty \quad . \quad (3.79)$$

Finally, by an application of Liouville's theorem [32] which states that a bounded entire function is a constant; i.e.,

$$P(s) = 0 \quad \text{for all } s \quad . \quad (3.80)$$

Thus, by applying the edge conditions, unique solutions have been obtained. However, as shown in Chapter IV, this is not always true. Sometimes additional information is needed in order to uniquely determine the polynomial $P(s)$.

Substituting (3.66) and (3.67) into (3.38) one obtains

$$A_e(s) = D_+^e(s) G_+^{e-1}(s) + G_-^e(s) D_-^e(s) \quad \text{for all } s. \quad (3.81)$$

Since the functions $D_+^e(s)$ and $D_-^e(s)$ are given in (3.63) and (3.64), respectively, $A_e(s)$ can be rewritten as

$$A_e(s) = \frac{ivk_y'(1-R_e) G_-^e(s)}{\sqrt{2\pi} k \delta_e(s+k_x)'} \left[\frac{1}{G_-^e(s)} - \frac{1}{G_-^e(-k_x')} \right. \\ \left. + \frac{1}{G^e(s) G_-^e(-k_x')} - \frac{1}{G_-^e(s)} \right] \quad (3.82)$$

and solving for $\frac{1}{\beta}$ in Equation (3.56) yields

$$\frac{1}{\beta} = \frac{1}{k \delta_e} \left[\frac{1}{G^e(s)} - 1 \right] \quad . \quad (3.83)$$

Therefore, $A_e(s)$ is given by

$$A_e(s) = \frac{ivk_y'(1-R_e) G_-^e(s)}{\sqrt{2\pi} (s+k_x') \beta G_-^e(-k_x')} \quad (3.84)$$

Substituting (3.84) into (3.37) leads to

$$\hat{u}_e^s(s,y) = \frac{ivk_y'(1-R_e) G_-^e(s)}{\sqrt{2\pi} (s+k_x') \beta G_-^e(-k_x')} e^{i\beta y} \quad \text{for all } s, \text{ and } y > 0. \quad (3.85)$$

The final step is to take the inverse Fourier transform of $\hat{u}_e^s(s,y)$ to obtain $u_e^s(x,y)$. Using Equations (A.10) and (3.85) one gets

$$u_e^s(x,y) = \frac{1}{\sqrt{2\pi}} \int_{-\infty+ia}^{\infty+ia} \frac{ivk_y'(1-R_e) G_-^e(s)}{\sqrt{2\pi} (s+k_x') \beta G_-^e(-k_x')} e^{i\beta y} e^{-isx} ds \quad (3.86)$$

for $\tau_- < a < \tau_+$
and $y > 0, |x| < \infty$

where the path of integration is shown in Figure (3.4). Note that the integration path lies entirely in the proper (top) sheet of the s -plane ($\text{Im}\beta > 0$) as required. When $\text{Im}(k) \rightarrow 0$, the medium becomes lossless, and the new path of integration ($a=0$) is shown in Figure (3.5.).

Furthermore, notice that $\hat{u}_e^s(x,y)$ has a pole $s_p^e = -k_x'$ in the lower half-plane $\tau < \tau_-$ and a pole due to $G_-^e(s)$ in the upper half-plane $\tau > \tau_+$. The contribution to the integral in (3.86) arising from these poles is evaluated next.

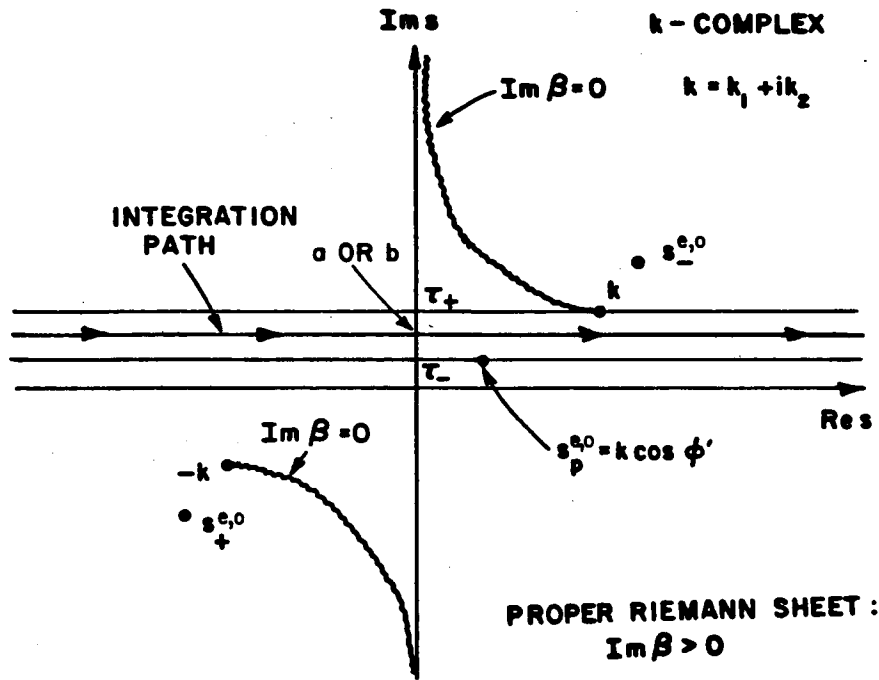


Figure 3.4. Integration path in Equations (3.86) and (3.152) for $k_2 \neq 0$.

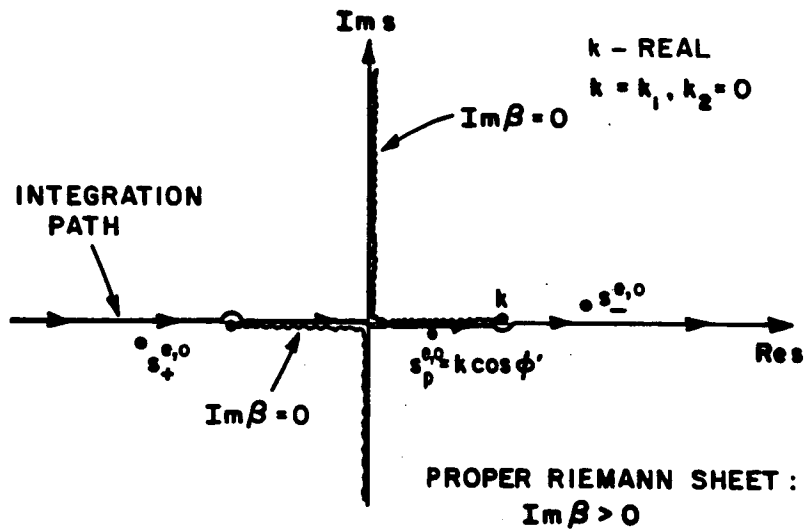


Figure 3.5. Integration path in Equations (3.86) and (3.152) for lossless case ($k_2 = 0$).

Assume that the medium is lossless, i.e., $\text{Im } k = k_2 = 0$, and $k = k_1$. It follows from Equation (3.56) that the poles of $G^e(s)$ satisfy the equation

$$\beta = (k^2 - s^2)^{1/2} = -k\delta_e = -k_1(\delta_{er} + i\delta_{eI}) \quad (3.87)$$

where $k_1 > 0$, and it will be shown that $\delta_{er} > 0$. Since $\text{Im}\beta > 0$ on the proper (top) Riemann sheet, the poles of $G^e(s)$ will lie on this top Riemann sheet if

$$\text{Im } \delta_e = \delta_{eI} < 0 \quad . \quad (3.88)$$

Otherwise, the poles of $G^e(s)$ will lie on the improper (bottom) Riemann sheet. This observation is important because, as will be shown later, the poles of $G^e(s)$ will give rise to the surface wave fields if they lie on the proper (top) Riemann sheet.

Solving for s in (3.87) and assuming (3.88) is true, one obtains

$$s_-^e = k(1 - \delta_e^2)^{1/2} \quad (3.89)$$

$$s_+^e = -k(1 - \delta_e^2)^{1/2} \quad (3.90)$$

where s_-^e lies in the upper half s -plane $\tau > \tau_+$, and it is the pole of $G_-^e(s)$. Similarly, s_+^e lies in the lower half s -plane $\tau < \tau_-$ and it is the pole of $G_+^e(s)$. To show that the last two statements are true, recall that

$$\delta_e = \begin{cases} \tilde{R}_s + i\tilde{X}_s & \text{for TE}_z \text{ Polarization, or} \\ \tilde{G}_s + i\tilde{B}_s & \text{for TM}_z \text{ Polarization} \end{cases} \quad (3.91)$$

Since $\{\tilde{R}_s, \tilde{G}_s\} > 0$ for a passive impedance sheet, and because it was assumed that $\text{Im}(\delta_e) < 0$, δ_e will lie in the fourth quadrant of the s-plane, such that

$$\delta_e = |\delta_e| e^{i\phi} \quad , \quad -\frac{\pi}{2} < \phi < 0 \quad . \quad (3.92)$$

Squaring (3.92) yields

$$\delta_e^2 = |\delta_e|^2 e^{i2\phi} \quad , \quad -\pi < \phi < 0 \quad (3.92)$$

and

$$1 - \delta_e^2 = |1 - \delta_e^2| e^{i\tilde{\phi}} \quad , \quad 0 < \tilde{\phi} < \pi \quad . \quad (3.93)$$

Thus,

$$(1 - \delta_e^2)^{1/2} = |1 - \delta_e^2|^{1/2} e^{i\tilde{\phi}/2} \quad , \quad 0 < \frac{\tilde{\phi}}{2} < \frac{\pi}{2} \quad . \quad (3.95)$$

It follows from (3.95) that $(1 - \delta_e^2)^{1/2}$ always lies in the first quadrant of the s-plane when $\text{Im}(\delta_e) < 0$. Therefore, s_-^e lies in the first quadrant of the s-plane above the line $\tau = \tau_+$ as shown in Figure 3.4. The pole s_+^e lies in the third quadrant of the s-plane below the line $\tau = \tau_-$ and it is also depicted in Figure 3.4.

It is shown in Appendix D that in order to factorize $G^e(s)$, it is convenient to express δ_e as

$$\delta_e = \cos \xi^e = \cos(\xi_r^e + i\xi_I^e) = \cos \xi_r^e \cosh \xi_I^e - i \sin \xi_r^e \sinh \xi_I^e \quad ,$$

$$0 < \left[\text{Re}(\xi^e) = \xi_r^e \right] < \frac{\pi}{2} \quad . \quad (3.96)$$

The restriction in the real part of ξ^e is due to the fact that $\text{Re}(\delta_e) =$

$\delta_{er} = \left\{ \begin{smallmatrix} \tilde{R}_s \\ \tilde{G}_s \end{smallmatrix} \right\}$ is always greater than or equal to zero. Substituting

(3.96) into (3.89) and (3.90), s_-^e and s_+^e can be written as

$$s_-^e = k \sin \xi^e, \quad 0 < \text{Re}(\xi^e) < \frac{\pi}{2} \quad (3.97)$$

$$s_+^e = -k \sin \xi^e, \quad 0 < \text{Re}(\xi^e) < \frac{\pi}{2} \quad (3.98)$$

where

$$\text{Im}(\xi^e) = \xi_I^e > 0 \quad \text{if} \quad \text{Im}(\delta_e) = \delta_{eI} < 0. \quad (3.99)$$

Note that if $\text{Im}(\delta_e) > 0$, then the poles of $^eG(s)$ will lie on the improper (bottom) Riemann sheet such that

$$\tilde{s}_-^e = -k \sin \xi^e, \quad \text{Im}(\xi^e) < 0, \quad 0 < \text{Re}(\xi^e) < \frac{\pi}{2} \quad (3.100)$$

$$\tilde{s}_+^e = k \sin \xi^e, \quad \text{Im}(\xi^e) < 0, \quad 0 < \text{Re}(\xi^e) < \frac{\pi}{2} \quad (3.101)$$

where \tilde{s}_-^e is the pole of $G_-^e(s)$ and \tilde{s}_+^e is the pole of $G_+^e(s)$ as depicted in Figure 3.6.

2. Odd Problem

For the odd problem, the unperturbed field is

$$\tilde{u}_0(x, y) = u_0^i(x, y) + u_0^r(x, y) = v e^{+ik_y^i x} \left[e^{-ik_y^i y} + R_0(\delta_0, \phi') e^{ik_y^i y} \right], \quad (3.102)$$

$y > 0, \quad |x| < \infty$

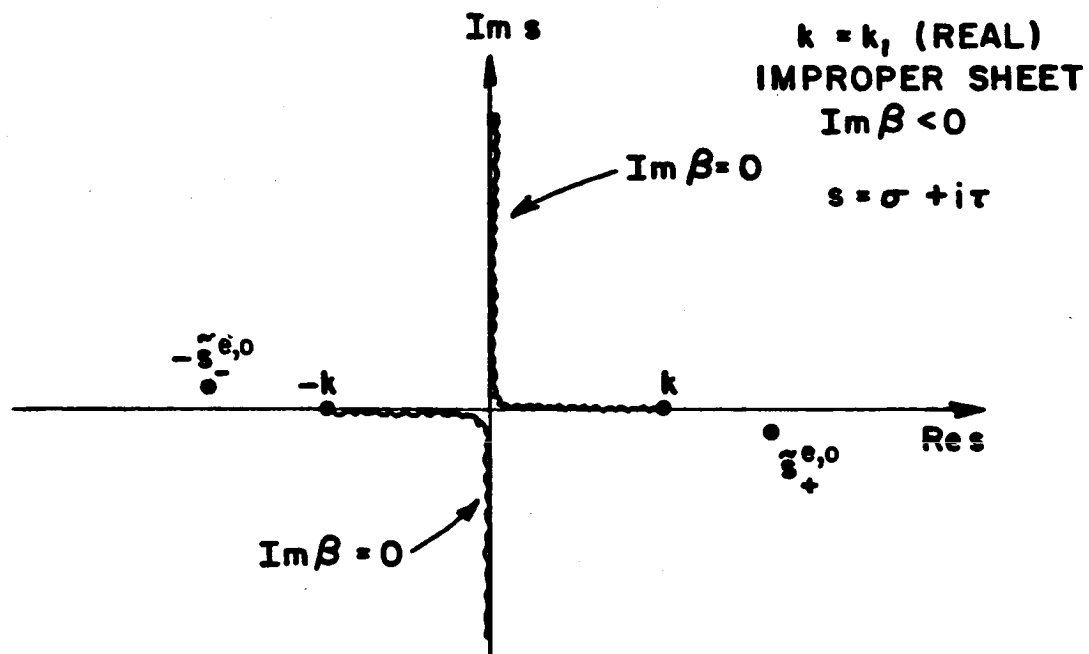


Figure 3.6. Location of the poles $\tilde{s}_{-}^{e,0}$ and $\tilde{s}_{+}^{e,0}$ on the improper Riemann sheet.

where v is a constant and the subscript "o" in u_o^i , u_o^r , R_o and δ_o refers to the odd problem. The scattered field $u_o^s(x,y)$ still satisfies the scalar Helmholtz equation

$$\left[\frac{\partial^2}{\partial x^2} + \frac{\partial^2}{\partial y^2} + k^2 \right] u_o^s(x,y) = 0 \quad , \quad |x| < \infty \quad , \quad y > 0 \quad (3.103)$$

and the following boundary conditions:

$$\left[\frac{\partial}{\partial y} + ik\delta_o \right] u_o^s(x,y) = 0 \quad \text{for } x < 0 \quad , \quad y = 0 \quad (3.104)$$

and

$$u_o^s(x,y) = -u_o^i(x,y) - \hat{u}_o^r(x,y) \quad \text{for } x > 0 \quad , \quad y = 0 \quad . \quad (3.105)$$

Using the half-range functions defined in Appendix A, (3.104) and (3.105) can be rewritten as

$$\left[\frac{\partial}{\partial y} + ik\delta_o \right] u_{o-}^s(x,y) = 0 \quad \text{for } y = 0 \quad , \quad |x| < \infty \quad (3.106)$$

$$u_{o+}^s(x,y) = -u_{o+}^{i+r}(x,y) \quad \text{for } y = 0 \quad , \quad |x| < \infty \quad . \quad (3.107)$$

Taking the Fourier transform of Equations (3.103), (3.106) and (3.107) with respect to x , one obtains

$$\left[\frac{\partial^2}{\partial y^2} + \beta^2 \right] \hat{u}_o^s(s,y) = 0 \quad \text{for } y > 0 \quad , \quad \tau_- < \tau < \tau_+ \quad (3.108)$$

$$\left[\frac{\partial}{\partial y} + ik\delta_o \right] \hat{u}_{o-}^s(s,y) = 0 \quad \text{for } y = 0 \quad , \quad \tau < \tau_+ \quad (3.109)$$

$$\hat{u}_{o+}^s(s,y) = -\hat{u}_{o+}^{i+r}(s,y) \quad \text{for } y = 0 \quad , \quad \tau > \tau_- \quad (3.110)$$

where β has been defined in Equation (3.32) and the constants τ_+ and τ_- are unknown at this point. The most general solution of (3.108) is

$$\hat{u}_0^s(s,y) = A_0(s)e^{i\beta y} + B_0(s)e^{-i\beta y} = \hat{u}_{0+}^s(s,y) + \hat{u}_{0-}^s(s,y) \quad (3.111)$$

for $y > 0$, $\tau_- < \tau < \tau_+$.

Since $\hat{u}_0^s(s,y)$ satisfies the radiation condition and $\text{Im}(\beta) > 0$ on the proper Riemann sheet, $e^{-i\beta y}$ is not bounded as $y \rightarrow \infty$. It follows that

$$B_0(s) \equiv 0 \quad (3.112)$$

so that

$$\hat{u}_0^s(s,y) = \hat{u}_{0+}^s(s,y) + \hat{u}_{0-}^s(s,y) = A_0(s)e^{i\beta y} \quad (3.113)$$

for $y > 0$, $\tau_- < \tau < \tau_+$

and

$$A_0(s) = \hat{u}_{0+}^s(s,0) + \hat{u}_{0-}^s(s,0) \quad \text{for } \tau_- < \tau < \tau_+ \quad (3.114)$$

where $A_0(s)$ is analytic in the strip defined by $\tau_- < \tau < \tau_+$.

Proceeding with the solution, the next step is to take the derivative of (3.113) with respect to y and then set $y = 0$ to arrive at

$$i\beta A_0(s) = \frac{\partial}{\partial y} \hat{u}_{0+}^s(s,y) + \frac{\partial}{\partial y} \hat{u}_{0-}^s(s,y) , y = 0 , \tau_- < \tau < \tau_+ . \quad (3.115)$$

Using (3.114) in (3.115) to eliminate $A_0(s)$

$$i\beta \left[\hat{u}_{0+}^s(s,0) + \hat{u}_{0-}^s(s,0) \right] = \frac{\partial}{\partial y} \hat{u}_{0+}^s(s,y) + \frac{\partial}{\partial y} \hat{u}_{0-}^s(s,y) , \quad (3.116)$$

$$y = 0 , \quad \tau_- < \tau < \tau_+ .$$

Now, substituting the boundary conditions given in equations (3.109) and (3.110) into (3.116), one gets

$$i\beta \left[-\hat{u}_{0+}^{i+r}(s,0) + \hat{u}_{0-}^s(s,0) \right] = -ik\delta_0 \hat{u}_{0-}^s(s,0) + \hat{u}_{0+}^{i+s}(s,0) , \quad (3.117)$$

$$\tau_- < \tau < \tau_+$$

or, rewriting (3.117)

$$-i\beta \hat{u}_{0+}^{i+r}(s,0) = -i(\beta + k\delta_0) \hat{u}_{0-}^s(s,0) + \hat{u}_{0+}^{i+s}(s,0) , \quad (3.118)$$

$$\tau_- < \tau < \tau_+$$

where

$$\hat{u}_{0+}^{i+s}(s,0) = \frac{\partial}{\partial y} \hat{u}_{0+}^s(s,y) \Big|_{y=0} . \quad (3.119)$$

In order to compute $\hat{u}_{0+}^{i+r}(s,0)$, it is enough to observe that $u_0^{i+r}(x,y)$ has exactly the same form as $u_e^{i+r}(x,y)$. Therefore, $\hat{u}_{0+}^{i+r}(s,y)$ can be obtained from Equation (3.43); i.e.,

$$\hat{u}_{0+}^{i+r}(s,y) = \frac{v}{\sqrt{2\pi}} \left[e^{-ik_y^i y} + R_0 e^{ik_y^i y} \right] \frac{i}{s+k_x^i} , \quad \tau > \tau_- \quad (3.120)$$

where τ_- has been defined in (3.44) and $\hat{u}_{0+}^{i+r}(s,y)$ is regular in the upper half s -plane defined by $\tau > \tau_-$.

Next, the functions $G^0(s)$ and $\Phi^0(s)$ are defined as follows:

$$G^0(s) = \frac{1}{\beta + k\delta_0} \quad (3.121)$$

and

$$\Phi^0(s) = \hat{u}_{0+}^{i+r}(s,0) = \beta \frac{v}{\sqrt{2\pi}} (1 + R_0) \frac{i}{s+k'_x} \quad (3.122)$$

Since β is regular in the strip $-k_2 < \tau < k_2$, and as shown later, $G^0(s)$ is free of poles in the same strip, it follows that $G^0(s)$ is a regular function in the strip $-k_2 < \tau < k_2$. Also, since $\hat{u}_{0+}^{i+r}(s,0)$ is regular in the upper half s -plane $\tau > \tau_-$, $\Phi^0(s)$ is regular in the strip $\tau_- < \tau < k_2$. Furthermore, $G^0(s)$ is free of zeros in the strip $-k_2 < \tau < \tau_2$ as required ($G^0(s)$ does not have any finite zeros in the s -plane). Substituting (3.121) and (3.122) into (3.118) yields

$$\Phi^0(s) G^0(s) = \hat{u}_{0-}^s(s,0) + iG^0(s) \hat{u}_{0+}^{i's}(s,0), \quad \tau_- < \tau < \tau_+ \quad (3.123)$$

which is the Wiener-Hopf equation. Note that $\Phi^0(s)$ and $G^0(s)$ are known functions, but there are two unknown functions; namely, $\hat{u}_{0-}^s(s,0)$ and $\hat{u}_{0+}^{i's}(s,0)$. In order to determine the constant τ_+ , it is necessary to know the asymptotic behavior of $u_{0-}^s(x,0)$ and $u_{0+}^{i's}(x,0)$ and use Equations (A.12) through (A.15).

Recall that $u_0^s(x,y)$ represents the electric field E_z , or the magnetic field H_z . It follows from Maxwell's Equations (1.1) - (1.4) that $u_0^{i's}(x,y)$ is proportional to either E_x or H_x . Following the same argument as in part 1, the asymptotic behavior of $u_{0-}^s(x,0)$ and $u_{0+}^{i's}(x,0)$ is

$$u_{0-}^s(x,0) \sim \frac{ce^{-ikx}}{|x|^{(1/2 \text{ or } 3/2)}} = \frac{ce^{-ik_1x} e^{k_2x}}{|x|^{(1/2 \text{ or } 3/2)}} \text{ as } x \rightarrow -\infty. \quad (3.124)$$

and

$$u_{0+}^s(x,0) \sim c_2 e^{+ik_1'x} = c_2 e^{-ik_1 \cos \phi' x} e^{k_2 \cos \phi' x}, \text{ as } x \rightarrow +\infty. \quad (3.125)$$

Since $u_{0-}^s(x,0)$ has the same asymptotic behavior as u_{e-}^s (see Equation (3.53)), τ_+ is given by (3.54).

As in the even problem, the next step is to factorize $G^0(s)$ into a product of two functions such that

$$G^0(s) = G_-^0(s) G_+^0(s) \quad (3.126)$$

where $G_+^0(s)$ is regular in the upper half s -plane $\tau > -\text{Im}(k) = -k_2$ and $G_-^0(s)$ in the lower half s -plane $\tau < \text{Im}(k) = k_2$. It is shown in Appendix D how one obtains $G_+^0(s)$ and $G_-^0(s)$. Using (3.126) in (3.123) and dividing by $G_-^0(s)$, which is possible since $G_-^0(s)$ is free of zeros in the lower s -plane $\tau < \tau_+$, one gets

$$\Phi^0(s) G_+^0(s) = \frac{\hat{u}_{0-}^s(s,0)}{G_-^0(s)} + i G_+^0(s) \hat{u}_{0+}^s(s,0), \quad \tau_- < \tau < \tau_+. \quad (3.127)$$

The left hand side of Equation (3.127) is similar to the left hand side of Equation (3.58) in the even problem. Thus, $\Phi^0(s) G_+^0(s)$ can be decomposed into a sum of two functions such that

$$\Phi^0(s) G_+^0(s) = D_+^0(s) + D_-^0(s) \quad (3.128)$$

where $D_+^0(s)$ is regular in the upper half s-plane $\tau > \tau_-$ and $D_-^0(s)$ is regular in the lower half s-plane $\tau < \tau_+$. As in part 1, this decomposition can be done by inspection. The details are given in Appendix E and only the final expressions for $D_+^0(s)$ and $D_-^0(s)$ are shown here:

$$D_+^0(s) = \frac{vi(1+R_0)}{\sqrt{2\pi} (s+k'_x)} \left[\frac{1}{G_-^0(-k'_x)} - k\delta_0 G_+^0(s) \right] \quad (3.129)$$

$$D_-^0(s) = \frac{vi(1+R_0)}{\sqrt{2\pi} (s+k'_x)} \left[\frac{1}{G_-^0(s)} - \frac{1}{G_-^0(-k'_x)} \right] \quad (3.130)$$

Substituting (3.129) and (3.130) into (3.127), one obtains

$$D_+^0(s) - iG_+^0(s) \hat{u}_{0+}^s(s,0) = \frac{\hat{u}_{0-}^s(s,0)}{G_-^0(s)} - D_-^0(s), \quad \tau_- < \tau < \tau_+ \quad (3.131)$$

where the regions of regularity in the s-plane of all the functions in Equations (3.131) are depicted in Figure 3.3.

The right hand side of Equation (3.131) is regular in the lower half s-plane $\tau < \tau_+$, and the left hand side is regular in the upper half s-plane $\tau > \tau_-$, so both sides have a common region of regularity. By analytic continuation, both sides of Equation (3.131) are equal to an entire function $B(s)$ which is yet to be determined. Thus,

$$D_+^0(s) - iG_+^0(s)\hat{u}_{0+}^1(s,0) = \frac{\hat{u}_{0-}^s(s,0)}{G_-^0(s)} - D_-^0(s) = B(s) , \quad (3.132)$$

for all s .

As stated in Section D.3 of Chapter II, $B(s)$ is a polynomial in s such that

$$B(s) = a_0 + a_1 s + a_2 s^2 + \dots + a_n s^n \quad (3.133)$$

where the unknown coefficients $\{a_i\}$ can be determined by examining the asymptotic behavior of the functions of Equation (3.132).

It follows from (3.121) that

$$G^0(s) \sim s^{-1} \text{ as } |s| \rightarrow \infty \text{ for } \tau_- < \tau < \tau_+ \quad (3.134)$$

and from the expressions of $G_-^0(s)$ and $G_+^0(s)$ given in Appendix D, one concludes that

$$G_-^0(s) \sim s^{-1/2} \text{ as } |s| \rightarrow \infty \text{ for } \tau < \tau_+ \quad (3.135)$$

and

$$G_+^0(s) \sim s^{-1/2} \text{ as } |s| \rightarrow \infty \text{ for } \tau > \tau_- . \quad (3.136)$$

The asymptotic behavior of $D_+^0(s)$ and $D_-^0(s)$ is easily obtained from (3.129) and (3.130), that is

$$D_+^0(s) \sim s^{-1} \text{ as } |s| \rightarrow \infty \text{ for } \tau > \tau_- \quad (3.137)$$

and

$$D_-^0(s) \sim s^{-1/2} \text{ as } |s| \rightarrow \infty \text{ for } \tau < \tau_+ . \quad (3.138)$$

In order to determine the asymptotic behavior of $\hat{u}_{0-}^s(s,0)$ and $\hat{u}_{0+}^{i's}(s,0)$ it is necessary to apply the edge conditions given in Appendix B.

Recall that $u_0^s(x,y)$ is either equal to E_z (perfect electric conductor for $x > 0, y = 0$) or H_z (perfect magnetic conductor for $x > 0, y = 0$).

Also, as stated before, it follows from Maxwell's equations that

$u_0^{i's}(x,y)$ is then proportional to either H_x or E_x . Using Equations (B.5) and (B.6), one obtains

$$u_{0-}^s(x,0) = O(|x|^p) \quad \text{as } x \rightarrow 0- \quad (3.139)$$

$$\left. \frac{\partial}{\partial y} u_{0+}^s(x,y) \right|_{y=0} = u_{0+}^{i's}(x,0) = O(|x|^{p-1}) \quad \text{as } x \rightarrow 0+ \quad (3.140)$$

where

$$p > 0 \quad . \quad (3.141)$$

It follows that the asymptotic behavior of \hat{u}_{0-}^s and $\hat{u}_{0+}^{i's}$ is:

$$\hat{u}_{0-}^s(s,0) \sim s^{-p-1} \quad \text{as } |s| \rightarrow \infty, \quad \tau < \tau_+ \quad (3.142)$$

$$\hat{u}_{0+}^{i's}(s,0) \sim s^{-p} \quad \text{as } |s| \rightarrow \infty, \quad \tau > \tau_- \quad . \quad (3.143)$$

Since $p > 0$, it is easily verified from above that $B(s) \rightarrow 0$ as $|s| \rightarrow \infty$, and then by the application of Liouville's theorem [32], $B(s)$ is uniquely determined as $B(s) = 0$ for all s . Therefore, $\hat{u}_{0-}^s(s,0)$ and $\hat{u}_{0+}^{i's}(s,0)$ can be solved simultaneously from Equation (3.132) such that

$$\hat{u}_{0-}^s(s,0) = D_-^0(s) G_-^0(s) \quad \text{for all } s \quad (3.144)$$

$$\hat{u}_{0+}^s(s,0) = \frac{-iD_+^0(s)}{G_+^0(s)} \quad \text{for all } s \quad . \quad (3.145)$$

Substituting (3.129) and (3.130) into (3.144) and (3.145) yields

$$\hat{u}_{0-}^s(s,0) = \frac{iv(1+R_0)}{\sqrt{2\pi} (s+k_x)} G_-^0(s) \left[\frac{1}{G_-^0(s)} - \frac{1}{G_-^0(-k_x)} \right] \quad (3.146)$$

$$\hat{u}_{0+}^s(s,0) = \frac{v(1+R_0)}{\sqrt{2\pi} (s+k_x)} \left[\frac{1}{G_-^0(-k_x)} - k\delta_0 G_+^0(s) \right] \frac{1}{G_+^0(s)} \quad . \quad (3.147)$$

Since $\hat{u}_{0+}^{i+r}(s,y)$ is known and it is given in (3.120), it follows from (3.110) that

$$\hat{u}_{0+}^s(s,0) = \frac{-iv (1+R_0)}{\sqrt{2\pi} (s+k_x)} \quad . \quad (3.148)$$

Furthermore, substituting (3.146) and (3.148) into (3.114), the expression for $A_0(s)$ becomes

$$A_0(s) = \frac{-iv (1+R_0)}{\sqrt{2\pi} (s+k_x)} + \frac{iv (1+R_0)}{\sqrt{2\pi} (s+k_x)} G_-^0(s) \left[\frac{1}{G_-^0(s)} - \frac{1}{G_-^0(-k_x)} \right] \quad (3.149)$$

for all s

which can be simplified to

$$A_0(s) = \frac{-iv (1+R_0) G_-^0(s)}{\sqrt{2\pi} (s+k_x) G_-^0(-k_x)} \quad \text{for all } s \quad . \quad (3.150)$$

Therefore, $\hat{u}_0^s(s,y)$ can be obtained from (3.150) and (3.113) as

$$\hat{u}_0^s(s,y) = \frac{-iv (1+R_0) G_-^0(s)}{\sqrt{2\pi} (s+k_x') G_-^0(-k_x')} e^{i\beta y} \quad \text{for } y > 0, \text{ and all } s. \quad (3.151)$$

Finally, the last step in this analysis is to take the inverse Fourier transform of $\hat{u}_0^s(s,y)$ to obtain $u_0^s(x,y)$. It follows from Equation (A.10) that

$$u_0^s(x,y) = \frac{i}{\sqrt{2\pi}} \int_{-\infty+ib}^{\infty+ib} \frac{-iv (1+R_0) G_-^0(s)}{\sqrt{2\pi} (s+k_x') G_-^0(-k_x')} e^{i\beta y} e^{-isx} ds \quad (3.152)$$

for $y > 0, |x| < \infty,$
 $\tau_- < b < \tau_+$

where the path of integration, as depicted in Figure 3.4, lies entirely on the proper (top) Riemann sheet where $\text{Im}\beta > 0$. When $\text{Im}(k)=k_2 \rightarrow 0$, the medium becomes lossless and the new path of integration ($b=0$) is shown in Figure 3.5. Note that $\hat{u}_0^s(s,y)$ has a pole $s_p^0 = -k_x'$ in the lower half s -plane $\tau < \tau_-$ of the top and bottom Riemann sheets, and a pole due to $G_-^0(s)$ in the upper half s -plane $\tau > \tau_+$ which is evaluated next.

In order to evaluate the poles of $G^0(s)$, note that the denominator of $G^0(s)$ is the same as the denominator of $G^e(s)$. Thus, the poles obtained in the even problem are the same for the odd problem. In other words, the poles of $G^0(s)$ will lie on the proper (top) Riemann sheet if

$$\text{Im}(\delta_0) = \text{Im} [\delta_{0r} + i\delta_{0I}] = \delta_{0I} < 0 \quad (3.153)$$

Otherwise, the poles of $G^0(s)$ will lie on the improper (bottom) Riemann sheet and will not contribute to the scattered fields as shown in Section C. Using the results of part 1, and assuming $\text{Im}(\delta_0) < 0$, the poles of $G^0(s)$ are

$$s_-^0 = k(1 - \delta_0^2)^{1/2} \quad (3.154)$$

and

$$s_+^0 = -k(1 - \delta_0^2)^{1/2} \quad (3.155)$$

where s_-^0 lies in the upper half s-plane $\tau > \tau_+$ and it is the pole of $G_-^0(s)$. Similarly, s_+^0 lies in the lower half s-plane $\tau < \tau_-$ and it is the pole of $G_+^0(s)$. The poles s_-^0 and s_+^0 are depicted in Figure 3.5. As in the even case, in order to factorize $G^0(s)$, it is convenient to express δ_0 as

$$\delta_0 = \cos \xi^0 = \cos(\xi_r^0 + i\xi_I^0) = \cos \xi_r^0 \cosh \xi_I^0 - i \sin \xi_r^0 \sinh \xi_I^0, \quad (3.156)$$

$$0 < \left[\text{Re}(\xi^0) = \xi_r^0 \right] < \frac{\pi}{2}.$$

Substituting (3.156) into (3.154) and (3.155), s_-^0 and s_+^0 become

$$s_-^0 = k \sin \xi^0, \quad 0 < \left[\text{Re}(\xi^0) = \xi_r^0 \right] < \frac{\pi}{2} \quad (3.157)$$

$$s_+^0 = -k \sin \xi^0, \quad 0 < \left[\text{Re}(\xi^0) = \xi_r^0 \right] < \frac{\pi}{2} \quad (3.158)$$

where $\text{Im}(\xi^0) = \xi_I^0 > 0$ because $\text{Im}(\delta_0) = \delta_{0I} < 0$.

When $\text{Im}(\delta_0) > 0$, the poles of $G^0(s)$ will lie on the improper (bottom) Riemann sheet. In this case, \tilde{s}_-^0 and \tilde{s}_+^0 are given by

$$\tilde{s}_-^0 = -k \sin \xi^0, \quad \text{Im}(\xi^0) < 0, \quad 0 < \text{Re}(\xi^0) < \frac{\pi}{2} \quad (3.159)$$

$$\tilde{s}_+^0 = k \sin \xi^0, \quad \text{Im}(\xi^0) < 0, \quad 0 < \text{Re}(\xi^0) < \frac{\pi}{2} \quad (3.160)$$

where \tilde{s}_-^0 is the pole of $G_-^0(s)$ and \tilde{s}_+^0 is the pole of $G_+^0(s)$ as shown in Figure 3.6.

C. ASYMPTOTIC ANALYSIS

The solutions of the even and odd problem given in Equations (3.86) and (3.152), respectively, are expressed in terms of an integral which, except for very simple cases, cannot be computed in closed form. Fortunately, in diffraction problems one is interested in the far field solutions which can be obtained by applying asymptotic integration techniques to (3.86) and (3.152). Here, the saddle point method [38] will be used to obtain the leading terms of $u_e^S(x,y)$ and $u_o^S(x,y)$ for large $k\sqrt{x^2+y^2}$.

1. Angular Spectral Mapping

It is common practice to introduce a change of variables via the transformations

$$s = \sigma + i\tau = -k\cos w = -k\cos(\alpha + i\gamma) \quad (3.161)$$

$$\beta = \sqrt{k^2 - s^2} = k\sin w = k\sin(\alpha + i\gamma) \quad (3.162)$$

where $k = k_1$ ($k_2 = 0$, lossless medium) is real. The above transformation is a mapping from the s -domain to the w -domain, which is conventionally referred to as the angular spectral domain. All the details of the mapping from the s -domain to the w -domain are given in Appendix F. The former two-sheeted plane of $\beta(s)$ becomes the periodic plane depicted in Figure 3.7 with the role of the branch cuts replaced by lines which are their images. It is obvious that the effect of this transformation is to open up the function $\beta(s)$ and thus remove the branch points and branch cuts associated with β .

It is also convenient to make a change of variables from the rectangular to polar coordinate system via the transformation

$$x = \rho\cos\phi \quad ; \quad y = \rho\sin\phi \quad (3.163)$$

where the quantities ρ and ϕ are shown in Figure 3.8.

2. Even Problem

Substituting Equations (3.161), (3.162) and (3.163) into (3.86), one obtains

$$u_e^s(\rho, \phi) = \frac{v(1-R_e)\sin\phi'}{2\pi i} \int_{\Gamma_w^e} \frac{G_-^e(-k\cos w) e^{ik\rho\cos(w-\phi)} dw}{(\cos w + \cos\phi') G_-^e(k\cos\phi')} \quad , \quad (3.164)$$

$0 < (\phi, \phi') < \pi$

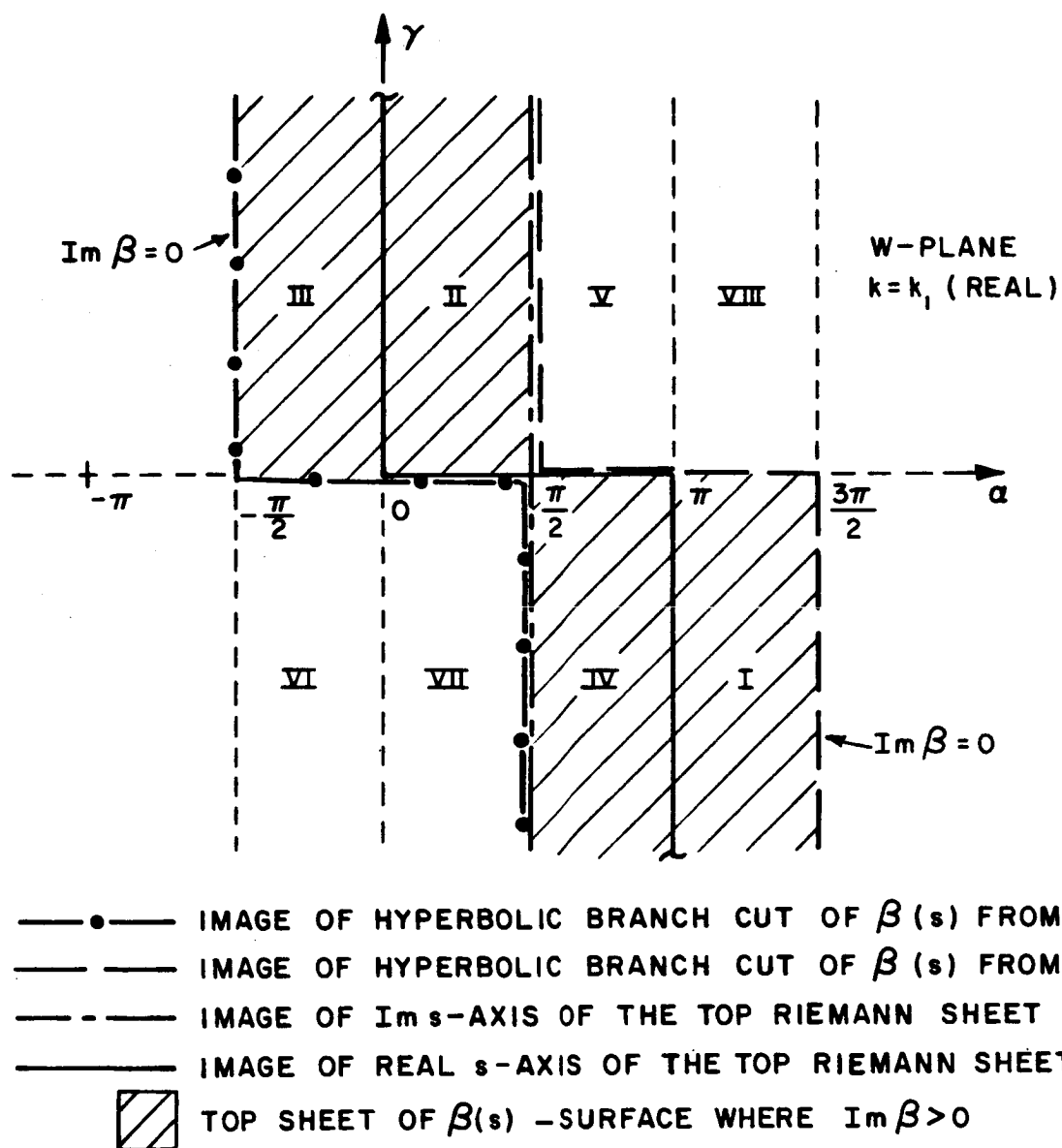


Figure 3.7. The angular spectral w-plane.

where Γ_w^e is the new integration path in the w -domain as shown in Figure 3.9. The pole $s_p^e = -k_x' = k \cos \phi'$ on the proper (top) Riemann sheet in the s -domain is mapped to

$$w_r^{e+} = \pi - \phi \quad (3.165)$$

in the w -domain, and the same pole on the improper (bottom) sheet in the s -domain is mapped to

$$w_r^{e-} = \pi + \phi' \quad (3.166)$$

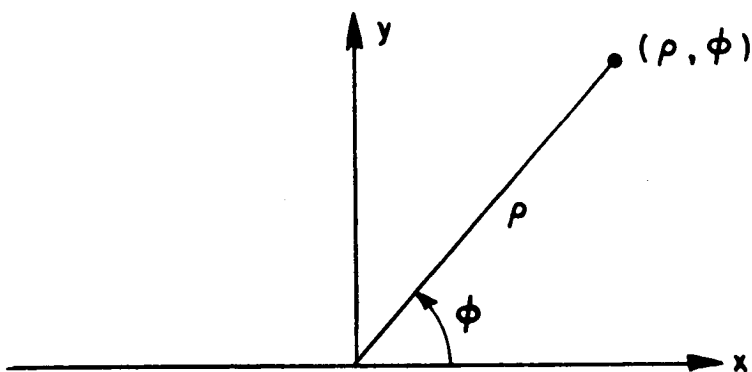


Figure 3.8. Polar coordinates.

in the w -domain. The pole of $G_-^e(s)$ at $s_-^e = k \sin \xi^e$, which is located in the first quadrant of the s -plane if $\text{Im}(\delta_e) < 0$ ($\text{Im}(\xi^e) > 0$), is mapped to

$$w_s^e = \frac{3\pi}{2} - \xi^e = \frac{3\pi}{2} - \xi_r^e - i\xi_I^e, \quad 0 < \text{Re}(\xi^e) < \frac{\pi}{2} \quad (3.167)$$

in the w -plane. Note that if $\text{Im}(\delta_e) > 0$, then $s_-^e = -k \sin \xi^e$ will lie in the second quadrant of the bottom Riemann sheet and its image in the w -plane is

$$w_s^e = \xi^e - \frac{\pi}{2} = \xi_r^e - \frac{\pi}{2} + i\xi_I^e, \quad 0 < \text{Re}(\xi^e) < \frac{\pi}{2}, \quad \text{Im}(\xi^e) < 0. \quad (3.168)$$

The next step in the asymptotic analysis of $u_e^s(\rho, \phi)$ is to deform the path of integration Γ_w^e to the steepest descent path (SDP) through the saddle point.

First, it is convenient to define the functions $f(w)$ and $M_e(w)$ such that

$$f(w) = i \cos(\phi - w) = f_r(\alpha, \gamma) + i f_I(\alpha, \gamma) \quad (3.169)$$

$$M_e(w) = \frac{v(1-R_e) \sin \phi' G_-^e(-k \cos w)}{2\pi i (\cos w + \cos \phi') G_-^e(+k \cos \phi')} \quad (3.170)$$

where

$$f_r(\alpha, \gamma) = -\sin(\phi - \alpha) \sinh \gamma = \sin(\alpha - \phi) \sinh \gamma \quad (3.171)$$

$$f_I(\alpha, \gamma) = \cos(\phi - \alpha) \cosh \gamma \quad (3.172)$$

The saddle point, denoted by $w_s = \alpha_s + i\gamma_s$, is a point in the w -plane at which the derivative of $f(w)$ vanishes [38], that is

$$f'(w_s) = \left. \frac{d}{dw} f(w) \right|_{w_s} = 0 \quad . \quad (3.173)$$

Next, taking the derivative of $f(w)$ and setting equal to zero yields

$$f'(w_s) = \left. \frac{d}{dw} i \cos(\alpha - w) \right|_{w_s} = i \sin(\alpha - w_s) = 0 \quad . \quad (3.174)$$

Since the real part of w is restricted to the interval $-\frac{\pi}{2} < \text{Re}(w) < \frac{3\pi}{2}$, it follows that

$$w_s = \phi, \quad \text{or} \quad \alpha_s = \phi \quad \text{and} \quad \gamma_s = 0, \quad 0 < \phi < \pi \quad . \quad (3.175)$$

The steepest descent path (SDP), where (α_p, γ_p) is a point on this curve, is given by

$$f_I(\alpha_p, \gamma_p) = f_I(\alpha_s, \gamma_s) ; \quad f_r(\alpha_p, \gamma_p) < f_r(\alpha_s, \gamma_s) \quad . \quad (3.176)$$

In specifying the contour of integration C_{SDP} along SDP, it is important to include the direction of integration as shown in Figure 3.9. From Equations (3.175) and (3.176), the path of integration C_{SDP} is determined by

$$\cos(\phi - \alpha_p) \cosh \gamma_p = 1 \quad (3.177)$$

and

$$\sin(\alpha_p - \phi) \sinh \gamma_p < 0 \quad . \quad (3.178)$$

Also, the angle ϕ_s depicted in Figure 3.9 has to be computed. This is accomplished [38] by twice differentiating (3.177) and evaluating the result at the saddle point. Without going over the details, one gets

$$\left[\frac{d}{d\alpha_p} \gamma_p \right]_{\alpha_p = \alpha_s}^2 = \cos(\phi - \alpha_p) \cosh \gamma_p \Big|_{w_p = \alpha_s + i\gamma_s} = 1 \quad (3.179)$$

From Figure 3.9, it is obvious that

$$\left[\frac{d}{d\alpha_p} \gamma_p \right]_{\alpha_p = \alpha_s} = -1 \quad (3.180)$$

which means that

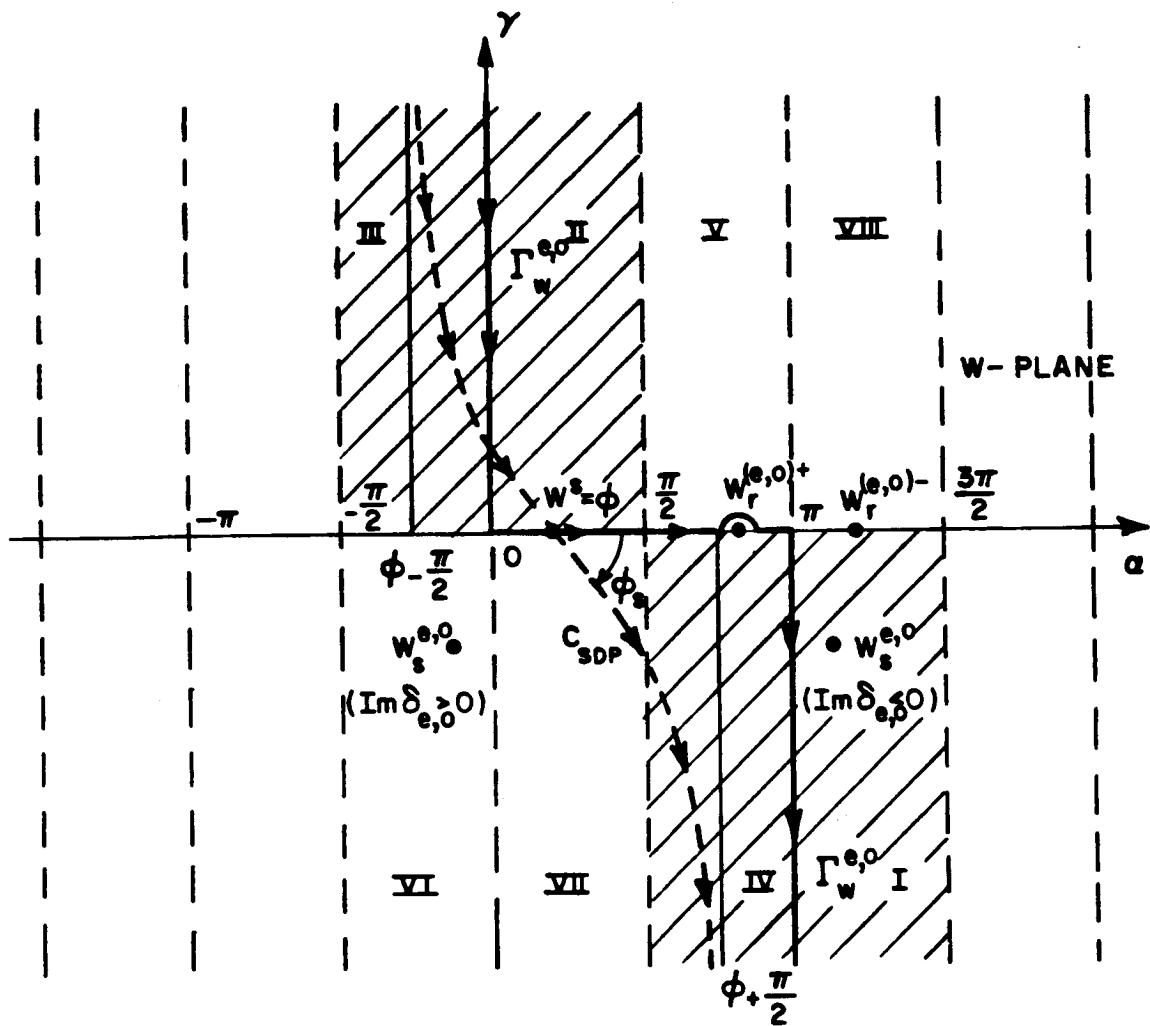
$$\phi_s = -\frac{\pi}{4} \quad (3.181)$$

Substituting (3.169) and (3.170) into (3.164), the expression for $u_e^S(\rho, \phi)$ becomes

$$u_e^S(\rho, \phi) = \int_{\Gamma_w^e} M_e(w) e^{k\rho f(w)} dw, \quad 0 < \phi < \pi \quad (3.182)$$

where $M_e(w)$ has poles at w_r^{e+} , w_r^{e-} and w_s^e as shown in Figure 3.9. After the deformation of Γ_w^e to the C_{SDP} , the field $u_e^S(\rho, \phi)$ is represented via Cauchy's residue theorem, as the sum of the residues arising from the pole singularities captured during this deformation and the integral along the C_{SDP} . Note that the steepest descent path C_{SDP} , depending on the angle ϕ , may run anywhere between the path SDP^- crossing the real axis at $\alpha=0$ to SDP^+ which crosses the real axis at $\alpha=\pi$.

The paths SDP^- and SDP^+ are depicted in Figure 3.10. Any pole located in the shaded area shown in Figure 3.10 will be captured as the path C_{SDP} runs between SDP^- and SDP^+ . Applying Cauchy's residue theorem in Equation (3.182) yields:



TOP RIEMANN SHEET IN S-DOMAIN WHERE $\text{Im}\beta > 0$

Figure 3.9. Integration paths Γ_w and C_{SDP} in the periodic w-plane for $k=k_1$ (real).

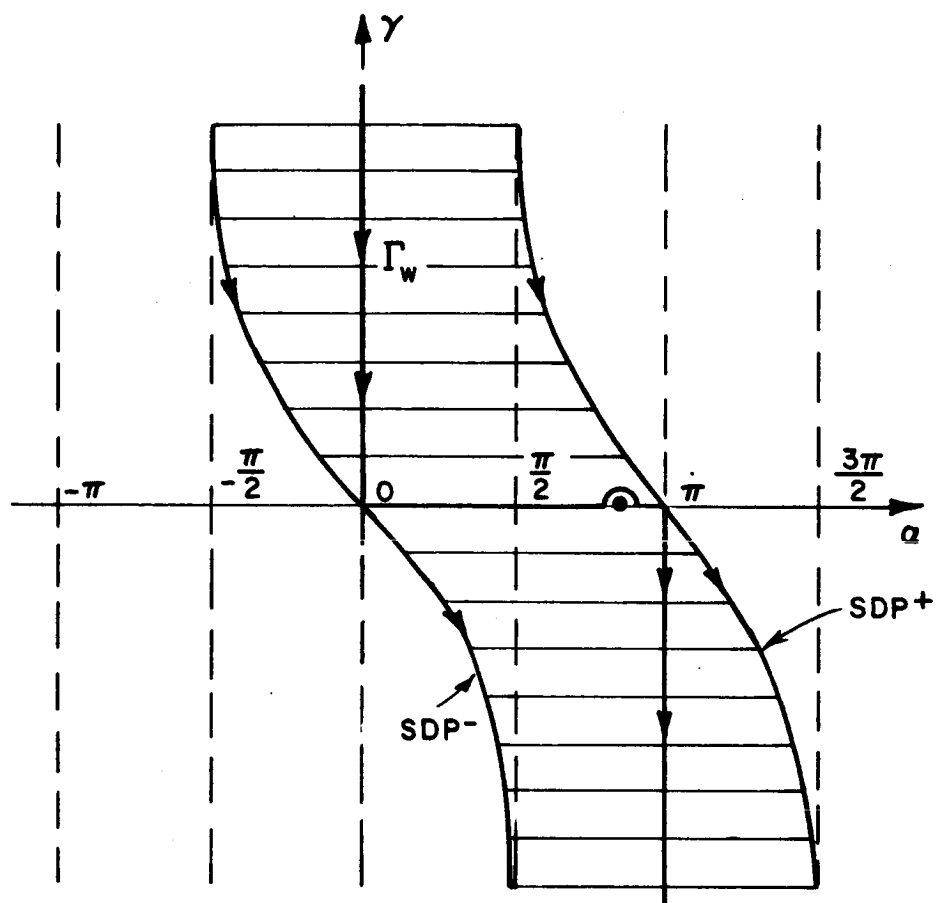


Figure 3.10. Poles located in shaded area will be captured as C_{SDP} moves from SDP^- to SDP^+ .

$$\begin{aligned}
u_e^S(\rho, \phi) = & 2\pi i \left[\text{Res} \left[M_e(w_s^e) e^{k\rho f(w_s^e)} \right] U(\phi - \tilde{\phi}_s^e) \right. \\
& \left. - \text{Res} \left[M_e(w_r^{e+}) e^{k\rho f(w_r^{e+})} \right] U(w_r^{e+} - \phi) \right] \\
& + \int_{C_{SDP}} M_e(w) e^{k\rho f(w)} dw, \quad 0 < \phi < \pi
\end{aligned} \tag{3.183}$$

where $\tilde{\phi}_s^e$ is computed later and $U(\phi - \tilde{\phi}_s^e)$, $U(w_r^{e+} - \phi)$ are the usual unit step functions. The various types of waves that contribute to the field $u_e^S(\rho, \phi)$ are those arising from the following poles and saddle point of the integrand in (3.182); namely from:

- (i) The pole w_r^{e+} which is the zero of $(\cos w + \cos \phi')$. It contributes to the geometrical optics field when it is captured. This pole is captured when $0 < \phi < \pi - \phi'$.
- (ii) The pole w_s^e which is the zero of $G_-^e(s)$. It contributes to the surface wave field excited at the edge $(x=0, y=0)$ by the incident plane wave. This pole may be captured only if $\text{Im}(\delta_e) < 0$.
- (iii) C_{SDP} integral contribution. This contribution is always present and when $k\rho \rightarrow \infty$, it is asymptotic to a term containing the value of the integrand $M(w)e^{k\rho f(w)}$ at the saddle point $w=w^S$. It is usually known as the diffracted field.

The location of the poles in the w -plane determines the type of guided waves they will contribute. Figure 3.11 illustrates the different types of waves corresponding to poles located in the various regions of the w -plane [39]. This diagram was obtained by examining the exponential function $e^{k\rho f(w)}$ in Equation (3.182). The vectors $\vec{\zeta}_p$ and $\vec{\zeta}_a$ are the propagation and attenuation vectors, respectively, and they will be defined more carefully in section F. It is sufficient to mention at this point that the waves propagate in the direction of $\vec{\zeta}_p$, and $\vec{\zeta}_a$ is the direction of most rapid attenuation. As shown in section F, $\vec{\zeta}_p$ and $\vec{\zeta}_a$ are always orthogonal to each other. Note that the proper surface waves are located in quadrants I and III; the improper surface waves are located in quadrants VI and VIII; and the leaky waves in quadrants V and VII. It can be shown that the magnitude of the propagation vector is $|\vec{\zeta}_p| = k \cosh \tilde{w}_I$ where \tilde{w}_I is the imaginary part of the pole \tilde{w} . This states that for a pole with nonzero imaginary part, the wave that it contributes will always be a slow wave in the direction of propagation. However, the projection of $\vec{\zeta}_p$ on the x -direction may correspond to either a fast or slow wave [39]. That is, $|\vec{\zeta}_p \cdot \hat{x}| = |\zeta_{px}| = k \cos \tilde{w}_r \cosh \tilde{w}_I > 1$, where \tilde{w}_r is the real part of the pole \tilde{w} . Figure 3.12 illustrates the regions where the waves are either fast or slow. Poles corresponding to slow waves are located in the clear region, while those corresponding to fast waves are found in the shaded regions of the strip $-\pi/2 < \alpha < 3\pi/2$.

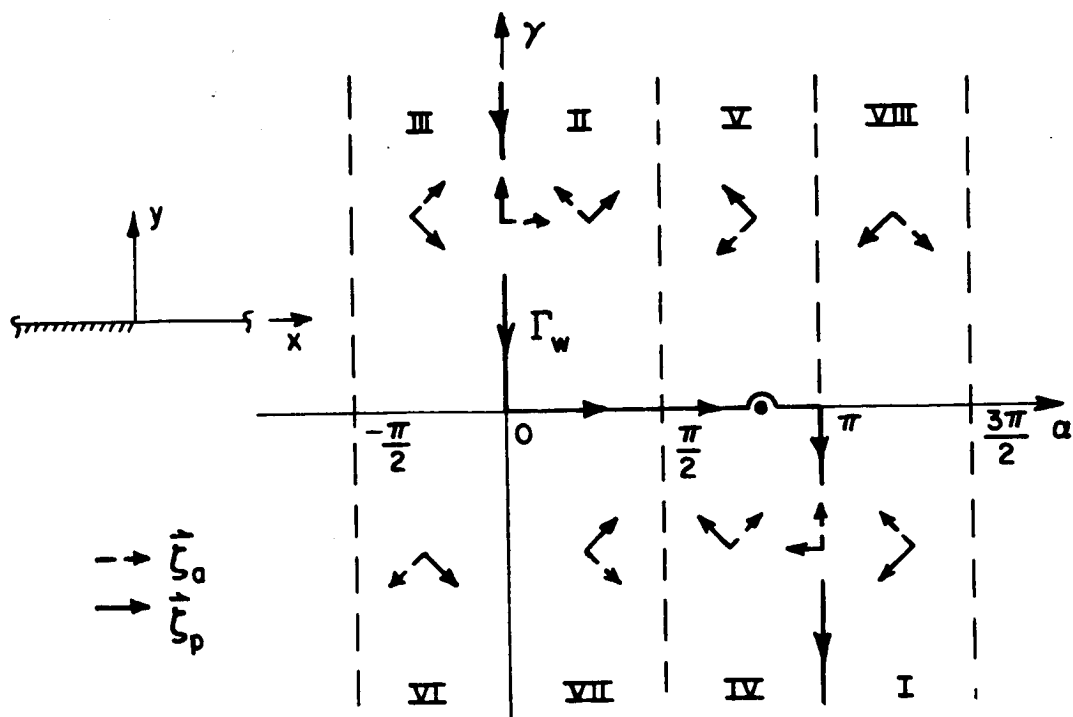


Figure 3.11. Different wave types as a function of pole location in the periodic w-plane.

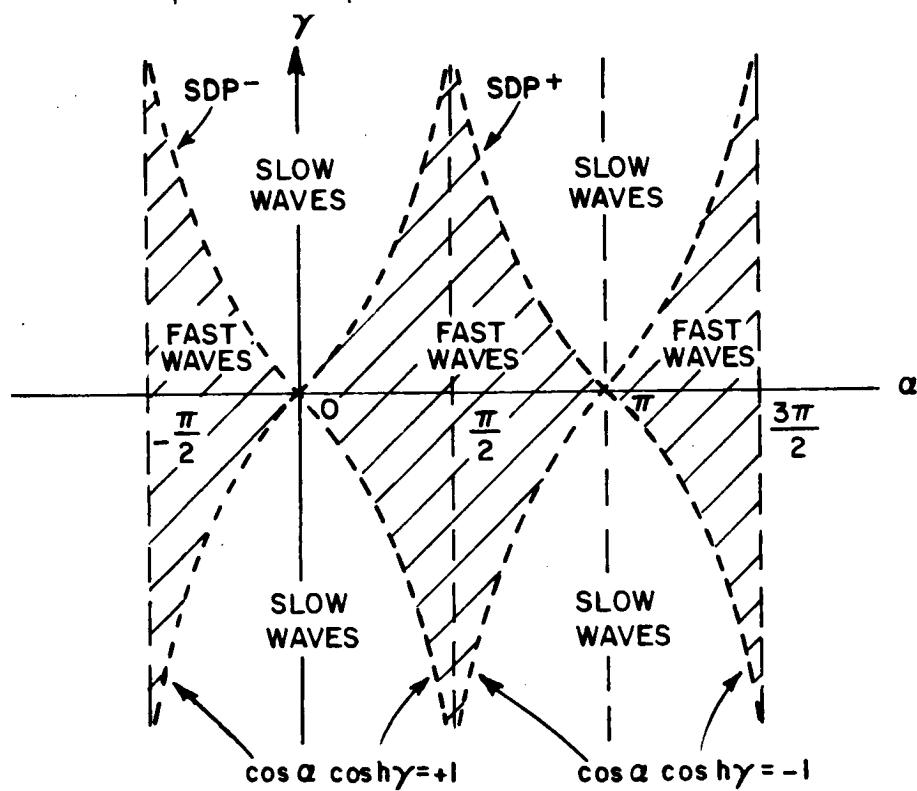


Figure 3.12. Slow and Fast waves in the periodic w-plane.

First, the residue at w_r^{e+} in (3.183) will be computed, that is

$$\text{Res} \left[M_e(w_r^{e+}) e^{k\rho f(w_r^{e+})} \right] = \lim_{w \rightarrow w_r^{e+}} (w - w_r^{e+}) M_e(w) e^{k\rho f(w)} \quad (3.184)$$

Substituting Equations (3.169) and (3.170) into (3.184) yields

$$\text{Res} \left[M_e(w_r^{e+}) e^{k\rho f(w_r^{e+})} \right] = \frac{-v(1-R_e)}{2\pi i} e^{-ik\rho \cos(\phi+\phi')} \quad (3.185)$$

In order to compute the residue at $w = w_s^e$, it is necessary to write the expressions for $G_-^e(-k\cos w)$. Using the results given in Appendix D and Equations (3.162) and (3.96) yields

$$G_-^e(-k\cos w) = \frac{k \sin w}{k \sin w + k \cos \xi^e} = \frac{\sin w}{\sin w + \cos \xi^e}, \quad 0 < \text{Re}(\xi^e) < \frac{\pi}{2} \quad (3.186)$$

$$G_+^e(-k\cos w) = \left[\frac{1 - \cos w}{\sin \xi^e - \cos w} \right]^{1/2} \exp \left[\frac{1}{2\pi} \int_{\frac{3\pi}{2} - w - \xi^e}^{\frac{\pi}{2} - w + \xi^e} \frac{t}{\sin t} dt \right] \quad (3.187)$$

$$G_-^e(-k\cos w) = \left[\frac{1 + \cos w}{\sin \xi^e + \cos w} \right]^{1/2} \exp \left[\frac{1}{2\pi} \int_{w + \frac{\pi}{2} - \xi^e}^{w - \frac{\pi}{2} + \xi^e} \frac{t}{\sin t} dt \right] \quad (3.188)$$

Evaluating Equation (3.188) at $w = w_r^{e+}$, one obtains

$$G_-^e(-k\cos w_r^{e+}) = G_-^e(k\cos \phi') = \frac{\sqrt{2} \sin(\phi'/2)}{(\sin \xi^e - \cos \phi')}^{1/2} \exp \left[\frac{1}{2\pi} \int_0^{\phi'} \frac{t}{\sin t} dt \right] \quad (3.189)$$

where

$$J_1^e(\phi') = \int_{\frac{3\pi}{2} - \phi' - \xi^e}^{\frac{\pi}{2} - \phi' + \xi^e} \frac{t}{\sin t} dt \quad . \quad (3.190)$$

It is convenient to express $G_-^e(-k\cos w)$ in terms of $G^e(-k\cos w)$ and $G_+^e(-k\cos w)$. This can be accomplished by solving for $G_-^e(-k\cos w)$; i.e.,

$$G_-^e(-k\cos w) = \frac{G^e(-k\cos w)}{G_+^e(-k\cos w)} \quad . \quad (3.191)$$

Thus, $M_e(w)$ can be rewritten as

$$M_e(w) = \frac{v(1-R_e)\sin\phi' \sin w}{2\pi i(\cos w + \cos\phi') (\sin w + \cos\xi^e) G_-^e(k\cos\phi') G_+^e(-k\cos w)} \quad . \quad (3.192)$$

Substituting Equations (3.187) and (3.189) into (3.192) and using trigonometric identities, the expression for $M_e(w)$ becomes

$$M_e(w) = \frac{v}{2\pi i} \left[\frac{1-R_e}{2} \right] \frac{[(\sin\xi^e - \cos w) (\sin\xi^e - \cos\phi')]^{1/2}}{\sin w + \cos\xi^e} \cdot \left[\sec((w-\phi')/2) + \sec((w+\phi')/2) \right] e^{-\frac{1}{2\pi} [J_1^e(\phi') + J_1^e(w)]} \quad . \quad (3.193)$$

Now, the residue at $w_s^e = \frac{3\pi}{2} - \xi^e$, $\text{Im}(\xi^e) > 0$ can be computed such that

$$\text{Res} \left[M_e(w_s^e) e^{k\rho f(w_s^e)} \right] = \lim_{w \rightarrow w_s^e} (w - w_s^e) M_e(w) e^{k\rho f(w)} \quad (3.194)$$

Substituting (3.193) into (3.194), one obtains

$$\begin{aligned} \text{Res} \left[M_e(w_s^e) e^{k\rho f(w_s^e)} \right] &= \frac{-v}{2\pi i} \frac{\cos \xi^e}{\sin \phi' + \cos \xi^e} \left[\frac{2(\sin \xi^e - \cos \phi')}{\sin \xi^e} \right]^{1/2} \\ &\cdot \left[\sec((w_s^e - \phi')/2) + \sec((w_s^e + \phi')/2) \right] e^{-ik\rho \sin(\phi + \xi^e)} \\ &\cdot \exp \left[-\frac{1}{2\pi} (J_1^e(\phi') + J_1^e(w_s^e)) \right], \quad \xi_1^e > 0, \quad 0 < \xi_r^e < \frac{\pi}{2}. \quad (3.195) \end{aligned}$$

The final step is the asymptotic evaluation of the integral along the path C_{SDP} . Before the diffracted field is computed, it is important to examine the exponential behavior of the various contributors to the field $u_e^S(\rho, \phi)$. A plot of the zero exponential decay contours is shown in Figure (3.13). It is seen that these contours divide the w -plane into two regions: one in which the exponential decay is greater than that at the saddle point, and the other region in which there is exponential growth which represents non-physical fields.

Since the pole w_r^{e+} lies in the $\text{Re}(w) = \alpha$ axis, it has the same exponential decay as the saddle point, namely, zero exponential decay. On the other hand, the exponential decay of the surface wave field is

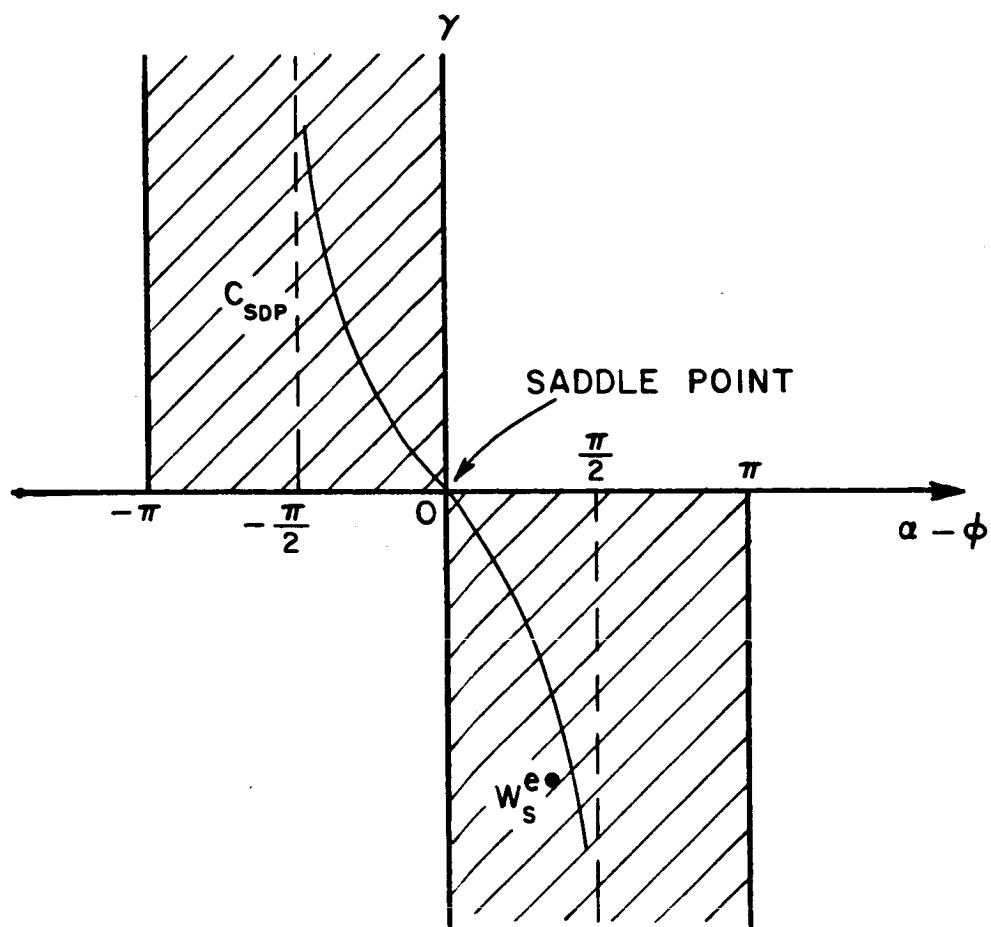
greater than that at the saddle point as shown in Figure 3.13. There is one special case when the surface wave field will have zero exponential decay: when $\text{Re}(\delta_e) = \delta_{er} = 0$ ($\xi_r^e = \frac{\pi}{2}$, lossless impedance wall) and $\phi = \pi$. In this case, the pole w_s^e will lie on a zero decay contour.

In order to perform a uniform asymptotic evaluation of the steepest descent integral, it is necessary to assume that $|\text{Im} \delta_e|$ is large enough so that the surface wave pole w_s^e is never close to the saddle point $w_s = \phi$ or the poles w_r^{e+} and w_r^{e-} . All the details of the saddle point analysis are shown in Appendix G and note that the largeness parameter is $k\rho$. Thus, for large $k\rho$, the resulting expression is given by

$$\begin{aligned}
 \int_{C_{SDP}} M_e(w) e^{k\rho f(w)} dw = u_e^d(\rho, \phi) \sim & \frac{-ve^{i\pi/4}}{\sqrt{2\pi k}} \left[\frac{1-R_e}{2} \right] \\
 & \cdot \frac{[(\sin \xi^e - \cos \phi') (\sin \xi^e - \cos \phi)]^{1/2}}{\sin \phi + \cos \xi^e} \exp(-[J_1^e(\phi') + J_1^e(\phi)]/(2\pi)) \\
 & \cdot \left[\sec((\phi + \phi')/2) F^*(kLa^+) + \sec((\phi - \phi')/2) F^*(kLa^-) \right] \frac{e^{ik\rho}}{\sqrt{\rho}}
 \end{aligned} \tag{3.196}$$

where $F(x)$, which is referred to as the transition function [11], is defined as follows:

$$F(x) = 2i\sqrt{x} e^{ix} \int_{\sqrt{x}}^{\infty} e^{-it^2} dt \tag{3.197}$$





- ZERO DECAY CONTOURS
-  REGION WITH GREATER EXPONENTIAL DECAY THAN AT THE SADDLE POINT
-  REGION WITH EXPONENTIAL GROWTH NON-PHYSICAL

Figure 3.13. Demarcation of regions of w -plane about the saddle point characterizing the rate of exponential growth or decay of waves associated with the pole locations.

and

$$a^{\pm} = -i[f(\phi) - f(w_r^{e\pm})] = -i[i - i\cos(\phi - w_r^{e\pm})] = 2\cos^2(\phi \pm \phi')/2 \quad (3.198)$$

Furthermore, for the case of plane wave incidence: $L=\rho$, and the field $u_e^d(\rho, \phi)$ defined in Equation (3.196) is commonly referred to as the diffracted field.

The expression for the scattered field $u_e^s(\rho, \phi)$ is obtained by substituting equations (3.185), (3.195) and (3.196) into (3.183). Thus, for large $k\rho$

$$u_e^s(\rho, \phi) \sim v(1-R_e)e^{-ik\rho\cos(\phi+\phi')}U(\pi-\phi-\phi') + u_e^{sw}(\rho, \phi) + u_e^d(\rho, \phi), \quad 0 < (\phi, \phi') < \pi \quad (3.199)$$

where $u_e^{sw}(\rho, \phi)$ is the surface wave field which is excited only if $\text{Im}(\delta_e) < 0$ ($\text{Im}(\xi^e) > 0$). The expression for $u_e^{sw}(\rho, \phi)$ is given by

$$\begin{aligned} u_e^{sw}(\rho, \phi) = & - \frac{v \cos \xi^e}{\sin \phi' + \cos \xi^e} \left[\frac{2(\sin \xi^e - \cos \phi')}{\sin \xi^e} \right]^{1/2} \\ & \cdot \left[\sec((w_s^e - \phi')/2) + \sec((w_s^e + \phi')/2) \right] \\ & \cdot \exp \left[\frac{-1}{2\pi} (J_1^e(w_s^e) + J_1^e(\phi')) \right] \exp \left[-ik(x \sin \xi^e + y \cos \xi^e) \right] U(\phi - \tilde{\phi}_s^e), \\ & 0 < (\phi, \phi'), < \pi \quad (3.200) \end{aligned}$$

where $\tilde{\phi}_S^e$ is computed next. Note that if $\xi_I^e < 0$ or $\text{Re}(\xi^e) = \xi_r^e = 0$, the pole w_S^e is not captured. Thus, assuming $0 < \xi_r^e < \pi/2$ and $\xi_I^e > 0$, it follows from (3.177) and (3.178) that

$$-\sin(\tilde{\phi}_S^e + \xi_r^e) \cosh \xi_I^e = 1 ; \quad \cos(\xi_r^e + \tilde{\phi}_S^e) \sinh \xi_I^e < 0 . \quad (3.201)$$

Therefore, one concludes from (3.201) that

$$\frac{\pi}{2} < \tilde{\phi}_S^e + \xi_r^e < \frac{3\pi}{2} . \quad (3.202)$$

Then, solving for $\tilde{\phi}_S^e$ from (3.201) yields

$$\tilde{\phi}_S^e = \pi - \xi_r^e + \arcsin \left[\frac{1}{\cosh \xi_I^e} \right] , \quad 0 < \xi_r^e < \frac{\pi}{2} , \quad \xi_I^e > 0 . \quad (3.203)$$

Since ϕ is restricted to the interval $0 < \phi < \pi$, the pole w_S^e will be captured only if

$$\xi_r^e > \arcsin \left[\frac{1}{\cosh \xi_I^e} \right] , \quad \xi_I^e > 0 . \quad (3.204)$$

Finally, the expression for the total field $u_e(\rho, \phi)$ is obtained by substituting Equations (3.18) and (3.199) into (3.21) such that

$$u_e(\rho, \phi) \sim u_e^i(\rho, \phi) + u_e^r(\rho, \phi) + u_e^{sw}(\rho, \phi) + u_e^d(\rho, \phi) , \quad 0 < \phi < \pi \quad (3.205)$$

where $u_e^i(\rho, \phi)$ is the incident field defined in Equation (3.16) and $u_e^r(\rho, \phi)$ is the reflected field given by

$$u_e^r(\xi, \phi) = v \Lambda_e(\phi') e^{-ik\rho \cos(\phi + \phi')} , \quad 0 < (\phi, \phi') < \pi \quad (3.206)$$

where

$$\Lambda_e(\phi') = \begin{cases} 1 & \text{for } \phi + \phi' < \pi \\ R_e(\phi') & \text{for } \phi + \phi' > \pi \end{cases} \quad (3.207)$$

Before the odd problem is solved, it is convenient to write the diffracted field in standard form [11]. Let QE be the diffraction point at the edge which in this case is the origin ($x=0, y=0$). It follows from [11] that the diffracted field $u_e^d(\rho, \phi)$ can be expressed as follows:

$$u_e^d(\rho, \phi) = u_e^i(QE) D_e^d(\phi, \phi') \frac{e^{ik\rho}}{\sqrt{\rho}} \quad (3.208)$$

where

$$u_e^i(QE) = u_e^i(0,0) = v \quad (3.209)$$

Substituting (3.196) into (3.208) yields

$$D_e^d(\phi, \phi') = \frac{-e^{i\pi/4}}{\sqrt{2\pi k}} \left[\frac{1-R_e}{2} \right] \frac{[(\sin \xi^e - \cos \phi)(\sin \xi^e - \cos \phi')]^{1/2}}{\sin \phi + \cos \xi^e} \\ \cdot e^{-1/(2\pi)(J_1^e(\phi) + J_1^e(\phi'))} \left[\sec(\beta^+/2) F^*(kLa^+) + \sec(\beta^-/2) F^*(kLa^-) \right], \\ 0 \leq (\phi, \phi') \leq \pi \quad (3.210)$$

where $D_e^d(\phi, \phi')$ is the even UTD diffraction coefficient, and

$$\beta^\pm = \phi \pm \phi' \quad (3.211)$$

Note that the transition function F in (3.210) makes the diffraction coefficient D_e^e uniform such that the diffracted field of (3.208) exactly compensates the discontinuity of the reflected field in (3.206) across the reflection shadow boundary. Consequently, the total high frequency UTD field as given in (3.205) is continuous everywhere away from the diffracting edge as long as the surface wave field is insignificant away from the impedance wall.

3. Odd Problem.

Exactly the same procedure as in the even problem is followed to obtain the uniform asymptotic solution for the odd problem. Thus, the first step is to express the integral representation of $u_0^s(x,y)$ in the w -plane. Substituting Equations (3.161)-(3.163) into (3.152) yields

$$u_0^s(\rho, \phi) = \frac{-v(1+R_0)}{2\pi i} \int_{\Gamma_w^0} \frac{G_-^0(-k \cos w) \sin w e^{ik\rho \cos(w-\phi)}}{(\cos \phi' + \cos w) G_-^0(k \cos \phi')} dw, \quad (3.212)$$

$0 < \phi < \pi$

where the path of integration Γ_w^0 is shown in Figure 3.9. The steepest descent path C_{SDP} and the angle ϕ_s are the same as in the even problem. That is, $\phi_s = -\pi/4$ and C_{SDP} is depicted in Figure 3.9. The pole $s_p^0 = -k_x' = k \cos \phi'$ of the integrand in Equation (3.152) on the top Riemann sheet of the s -domain is mapped to

$$w_r^{0+} = \pi - \phi' \quad (3.213)$$

in the w -plane, and the same pole on the bottom Riemann sheet is mapped to

$$w_r^{0-} = \pi + \phi' \quad (3.214)$$

in the w -plane. Furthermore, the pole of $G_-^0(s)$ at $s_-^0 = k \sin \xi^0$ ($\text{Im}(\delta_0) < 0$) is mapped to

$$w_s^0 = \frac{3\pi}{2} - \xi^0 = \frac{3\pi}{2} - \xi_r^e - i\xi_I^e, \quad 0 < \text{Re}(\xi^0) < \frac{\pi}{2} \quad (3.215)$$

On the other hand, if $\text{Im}(\delta_0) > 0$, the image of the pole $s_-^0 = k \sin \xi^0$ in the w -plane is

$$w_s^0 = \xi^0 - \frac{\pi}{2} = \xi_r^0 - \frac{\pi}{2} + i\xi_I^0, \quad 0 < \text{Re}(\xi^0) < \frac{\pi}{2}, \quad \text{Im}\xi^0 < 0. \quad (3.216)$$

Next, it is convenient to define the function $M_0(w)$ such that

$$M_0(w) = \frac{-v(1+R_0) G_-^0(-k \cos w) \sin w}{2\pi i (\cos \phi' + \cos w) G_-^0(k \cos \phi')} \quad (3.217)$$

Substituting Equations (3.169) and (3.217) into (3.212), one obtains

$$u_0^S(\rho, \phi) = \int_{r_w^0} M_0(w) e^{k\rho f(w)} dw, \quad 0 < \phi < \pi. \quad (3.218)$$

Note that Equations (3.182) and (3.218) are similar. Thus, the results obtained in Section 2 can be used here. It follows from Equation (3.183) that

$$\begin{aligned}
u_S^0(\rho, \phi) = 2\pi i & \left[\text{Res} \left[\left[M_0(w_S^0) e^{k\rho f(w_S^0)} \right] U(\phi - \tilde{\phi}_S^0) \right. \right. \\
& \left. \left. - \text{Res} \left[\left[M_0(w_r^{0+}) e^{k\rho f(w_r^{0+})} \right] U(w_r^{0+} - \phi) \right] \right] + \int_{C_{SDP}} M_0(w) e^{k\rho f(w)} dw \right]
\end{aligned} \quad (3.219)$$

where $\tilde{\phi}_S^0$ is unknown at this point.

The residues at w_S^0 and w_r^{0+} are computed in the same way as in Section 2. The residue at w_r^{0+} is

$$\text{Res} \left[\left[M_0(w_r^{0+}) e^{k\rho f(w_r^{0+})} \right] \right] = \frac{v(1+R_0)}{2\pi i} e^{-ik\rho \cos(\phi + \phi')} \quad (3.220)$$

Using the results of Appendix D, the functions $G^0(s)$, $G_-^0(s)$ and $G_+^0(s)$ can be expressed in the w -domain as follows:

$$G^0(-k\cos w) = \frac{1}{k(\sin w + \cos \xi^0)} \quad , \quad 0 < \text{Re}(\xi^0) < \frac{\pi}{2} \quad (3.221)$$

$$G_+^0(-k\cos w) = \left[\frac{1}{k(\sin \xi^0 - \cos w)} \right]^{1/2} \exp \left[\frac{1}{2\pi} \int_{3\pi/2 - w - \xi^0}^{\pi/2 - w + \xi^0} \frac{t}{\sin t} dt \right] \quad (3.222)$$

$$G_-^0(-k\cos w) = \left[\frac{1}{k(\sin \xi^0 + \cos w)} \right]^{1/2} \exp \left[\frac{1}{2\pi} \int_{w + \pi/2 - \xi^0}^{w - \pi/2 + \xi^0} \frac{t}{\sin t} dt \right] \quad (3.223)$$

Evaluating $G_-^0(-k\cos w)$ at w_r^{0+} , one obtains

$$G_-^0(-k\cos w_r^{0+}) = G_-^0(k\cos \phi') = \left[\frac{1}{k(\sin \xi^0 - \cos \phi)} \right]^{1/2} \cdot \exp \left[\int_{3\pi/2 - \phi' - \xi^0}^{\pi/2 - \phi' + \xi^0} \frac{t}{\sin t} dt \right] \quad (3.224)$$

The function $G_-^0(-k\cos w)$ can be expressed in terms of $G_+^0(-k\cos w)$ and $G_-^0(k\cos w)$ such that

$$G_-^0(-k\cos w) = \frac{G_-^0(-k\cos w)}{G_+^0(-k\cos w)} = \frac{(k(\sin \xi^0 - \cos w))^{1/2}}{k(\sin w + \cos \xi^0)} e^{-1/(2\pi)J_1^0(w)} \quad (3.225)$$

where

$$J_1^0(w) = \int_{3\pi/2 - w - \xi^0}^{\pi/2 - w + \xi^0} \frac{t}{\sin t} dt \quad (3.226)$$

Consequently, $M_0(w)$ can be written as

$$M_0(s) = \frac{v(1+R_0)\cos(w/2)[\sin \xi^0 - \cos w](\sin \xi^0 - \cos \phi')^{1/2}}{2\pi i (\sin w + \cos \xi^0) 2\sin(\phi'/2)} e^{-\frac{1}{2\pi}(J_1^0(w) + J_1^0(\phi'))} \cdot \left[\sec((w - \phi')/2) - \sec((w + \phi')/2) \right] \quad (3.227)$$

where the following trigonometric identity has been used in (3.227):

$$\frac{-4\sin(w/2) \sin(\phi'/2)}{\cos w + \cos \phi'} = \sec((w-\phi')/2) - \sec((w+\phi')/2) \quad (3.228)$$

Now it is possible to compute the residue at $w_s^0 = \frac{3\pi}{2} - \xi^0$ (where it is assumed that $\text{Im}(\xi^0) > 0$) such that

$$\begin{aligned} \text{Res} \left[M_0(w_s^0) e^{k\rho f(w)} \right] &= \frac{-v \, 2\cos(\phi'/2)}{2\pi i} \left[\frac{2(\sin \xi^0 - \cos \phi')}{\sin \xi^0} \right]^{1/2} \\ &\cdot \left[\sec((w_s^0 - \phi')/2) - \sec((w_s^0 + \phi')/2) \right] \frac{\cos(w_s^0/2)}{\sin \phi' + \cos \xi^0} \\ &\cdot e^{-ik\rho \sin(\phi + \xi^0)} \cdot \exp \left[\frac{-1}{2\pi} (J_1^0(w_s^0) + J_1^0(\phi')) \right], \\ &0 < \text{Re}(\xi^0) < \frac{\pi}{2} \end{aligned} \quad (3.229)$$

where the following equality has been employed:

$$\frac{1+R_0}{2} = \frac{\sin \phi'}{\sin \phi' + \delta_0} = \frac{2\sin(\phi'/2) \cos(\phi'/2)}{\sin \phi' + \cos \xi^0} \quad (3.230)$$

In order to complete the solution of $u_s^S(\rho, \phi)$, it is necessary to evaluate the integral over C_{SDP} asymptotically using the saddle point method. As in Section 2, assume, that $|\text{Im} \delta_0|$ is large enough so that the pole w_s^0 is not close to the saddle point or the poles w_r^{0+} and w_r^{0-} .

Therefore, for large $k\rho$ (see Appendix G), one obtains

$$\begin{aligned}
 \int_{C_{SDP}} M_0(w) e^{k\rho f(w)} dw = u_0^d(\rho, \phi) \sim & \frac{-ve^{i\pi/4}}{\sqrt{2\pi k}} \left[\frac{1+R_0}{2} \right] \frac{\cos(\phi/2)}{\sin(\phi'/2)} \\
 & \cdot \exp \left[-\frac{1}{2\pi} (J_1^0(\phi) + J_1^0(\phi')) \right] \cdot \frac{[(\sin \xi^0 - \cos \phi)(\sin \xi^0 - \cos \phi')]^{1/2}}{\sin \phi + \cos \xi^0} \\
 & \cdot \left[\sec((\phi - \phi')/2) F^*(kLa^-) - \sec((\phi + \phi')/2) F^*(kLa^+) \right] \frac{e^{ik\rho}}{\sqrt{\rho}}, \\
 & 0 < (\phi, \phi') < \pi \quad (3.231)
 \end{aligned}$$

where the functions $F(x)$ and a^\pm were defined in Equations (3.197) and (3.198), respectively. Furthermore, the field $u_0^d(\rho, \phi)$ is the diffracted field and L , as in the even problem, is equal to ρ for the case of plane wave incidence.

The expression for $u_0^S(\rho, \phi)$ is obtained by substituting equations (3.220), (3.229) and (3.231) into (3.219). Thus, for large $k\rho$

$$\begin{aligned}
 u_0^S(\rho, \phi) \sim & -v(1+R_0)e^{-ik\rho \cos(\phi+\phi')} U(\pi - \phi - \phi') + u_0^{SW}(\rho, \phi) + u_0^d(\rho, \phi), \\
 & 0 < (\phi, \phi') < \pi \quad (3.232)
 \end{aligned}$$

where $u_0^{SW}(\rho, \phi)$ is the surface wave field excited by the incident plane wave when $\text{Im}(\delta_0) < 0$ ($\text{Im}(\xi^0) > 0$). $u_0^{SW}(\rho, \phi)$ is given by

$$\begin{aligned}
u_0^{sw}(x,y) = & \frac{-v2\cos(\phi'/2)\cos(w_s^0/2)}{\sin\phi' + \cos\xi^0} \left[\frac{2(\sin\xi^0 - \cos\phi')}{\sin\xi^0} \right]^{1/2} \\
& \cdot \left[\sec((w_s^0 - \phi')/2) - \sec((w_s^0 + \phi')/2) \right] e^{-1/(2\pi)(J_1^0(\phi') + J_1^0(w_s^0))} \\
& \cdot e^{-ik(x\sin\xi^0 + y\cos\xi^0)} U(\phi - \tilde{\phi}_s^0) , \quad y > 0 \quad (3.233)
\end{aligned}$$

where

$$\tilde{\phi}_s^0 = \pi - \xi_r^0 + \arcsin \left[\frac{1}{\cosh \xi_I^0} \right] . \quad (3.234)$$

As in the even case, ϕ is restricted to the interval $0 < \phi < \pi$. It follows that the pole w_s^0 will be captured only if

$$\xi_r^0 > \arcsin \left[\frac{1}{\cosh \xi_I^0} \right] , \quad \xi_I^0 > 0 . \quad (3.235)$$

Recall that the total field $u_0(\rho, \phi)$ is given by

$$u_0(\rho, \phi) = u_0^i(\rho, \phi) + \tilde{u}_0^r(\rho, \phi) + u_0^s(\rho, \phi) , \quad 0 < (\phi, \phi') < \pi . \quad (3.236)$$

Substituting (3.232) into (3.236) yields

$$\begin{aligned}
u_0(\rho, \phi) = & u_0^i(\rho, \phi) + u_0^r(\rho, \phi) + u_0^{sw}(\rho, \phi) + u_0^d(\rho, \phi) , \\
& 0 < (\phi, \phi') < \pi \quad (3.237)
\end{aligned}$$

where $u_0^i(\rho, \phi)$ is the incident field given by Equation (3.16) and $u_0^r(\rho, \phi)$ is the reflected field which can be written as

$$u_r^0(\rho, \phi) = v \Lambda_0(\phi') e^{-ik\rho \cos(\phi + \phi')} \quad (3.238)$$

where

$$\Lambda_0(\phi') = \begin{cases} -1 & , \quad \phi + \phi' < \pi \\ R_0(\phi') & , \quad \phi + \phi' > \pi \end{cases} \quad (3.239)$$

Finally, as in Section 2, the diffracted field can be expressed as follows:

$$u_0^d(\rho, \phi) = u_0^i(QE) D_0^d(\phi, \phi') \frac{e^{ik\rho}}{\sqrt{\rho}} \quad (3.240)$$

where

$$u_0^i(QE) = u_0^i(0, 0) = v \quad (3.241)$$

and substituting (3.231) into (3.240) yields

$$D_0^d(\phi, \phi') = \frac{-e^{i\pi/4}}{\sqrt{2\pi k}} \left[\frac{1+R_0}{2} \right] \frac{\cos(\phi/2) [(\sin \xi^0 - \cos \phi)(\sin \xi^0 - \cos \phi')]^{1/2}}{\sin(\phi'/2) \sin \phi + \cos \xi^0} \\ \cdot e^{-1/(2\pi)[J_1^0(\phi) + J_1^0(\phi')]} [\sec(\beta^-/2) F^*(kLa^-) - \sec(\beta^+/2) F^*(kLa^+)] , \quad (3.242)$$

$$0 < (\phi, \phi') < \pi$$

which is the odd UTD diffraction coefficient. The diffraction coefficients D_e^d and D_0^d will be referred to as the two-dimensional coefficients to differentiate them from the diffraction coefficients that will be obtained in Chapter IV for the more general case of oblique incidence. Again, D_0^d in (3.242) makes u_0^d uniformly valid across the RSB

where u_r^0 becomes discontinuous such that the total high frequency UTD field in (3.237) is continuous there (assuming u_0^{sw} is insignificant away from the impedance wall).

D. EVALUATION OF THE DIFFRACTED FIELD ON THE IMPEDANCE SURFACE

The asymptotic solutions presented in Equations (3.196) and (3.231) include terms up to the order $k^{-1/2}$ with respect to the incident field. It is easy to show that both even and odd diffracted fields to order $k^{-1/2}$ vanish when the observation point is on the impedance surface, i.e., $\phi=\pi$. However, there are some applications when a better high-frequency description of the diffracted field is necessary; for example, when analyzing antennas mounted on an impedance wall [31]. In this section, a more accurate asymptotic evaluation of the integral along the steepest descent path is considered.

Recall that the function $M_e(w)$ defined in Equation (3.170) has three poles in the periodic w -plane. When the even diffracted field was evaluated in Section C, it was assumed that the pole w_s^e was never close to the saddle point, so only the geometrical optics poles were allowed to be near the saddle point. In this section, the pole w_s^e will also be allowed to be close to the saddle point, and details of the method [40] are given in Appendix G.

Using the results of Appendix G, the uniform asymptotic evaluation of the integral in (3.196), which takes into account the presence of the poles w_r^{e+} , w_r^{e-} and w_s^e , is given by (for large $k\rho$)

$$\begin{aligned}
\int_{C_{SDP}} M_e(w) e^{i\rho f(w)} dw = u_e^d(\rho, \phi) \sim & \frac{-ve^{i\pi/4}}{\sqrt{2\pi k}} \left[\frac{1-R_e}{2} \right] \\
& \cdot \frac{[(\sin \xi^e - \cos \phi)(\sin \xi^e - \cos \phi')]^{1/2}}{\sin \phi + \cos \xi^e} \cdot e^{-1/(2\pi)(J_1^e(\phi) + J_1^e(\phi'))} \\
& \cdot \left[\sec(\beta^+/2) T(a^+, a_p^e) + \sec(\beta^-/2) T(a^-, a_p^e) \right] \frac{e^{ik\rho}}{\sqrt{\rho}} \quad (3.243)
\end{aligned}$$

where the function T , which is referred to as the composite transition function, can be expressed as follows:

$$T(a^\pm, a_p^e) = \frac{(a_p^e)^{1/2} F(-kLa^\pm) - (a^\pm)^{1/2} F(-kLa_p^e)}{(a_p^e)^{1/2} - (a^\pm)^{1/2}} \quad (3.244)$$

The function a^\pm was defined in Equation (3.198) and $F(x)$ is the same transition function as in Equation (3.197) but generalized to the case of complex argument [41]. In order for (3.244) to converge, the argument of \sqrt{x} is restricted to [41]

$$\frac{-3\pi}{4} < \arg(\sqrt{x}) < \frac{\pi}{4} \quad (3.245)$$

as shown in Figure 3.14. Furthermore, the complex function a_p^e is given by

$$a_p^e = 2 \sin^2 \left[\frac{\phi - w_s^e}{2} \right] \quad (3.246)$$

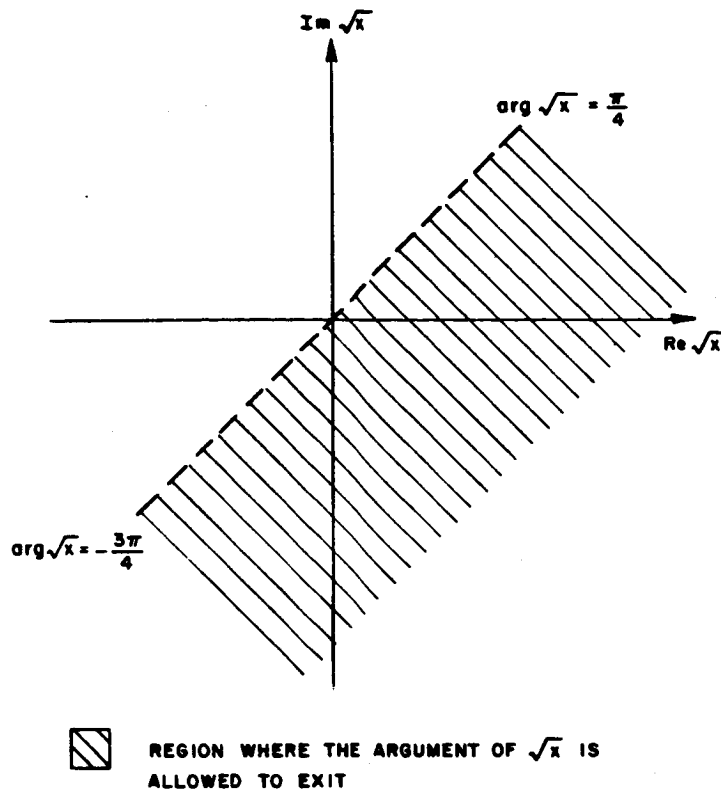


Figure 3.14. \sqrt{x} plane.

It follows from (3.245) that

$$\frac{-3\pi}{2} < \arg [a_p^e] < \frac{\pi}{2} \quad (3.247)$$

and

$$\frac{-3\pi}{2} < \arg [a^\pm] < \frac{\pi}{2} \quad . \quad (3.248)$$

In other words, the square root function \sqrt{x} in (3.245) has a branch cut in the x -plane as depicted in Figure 3.15.

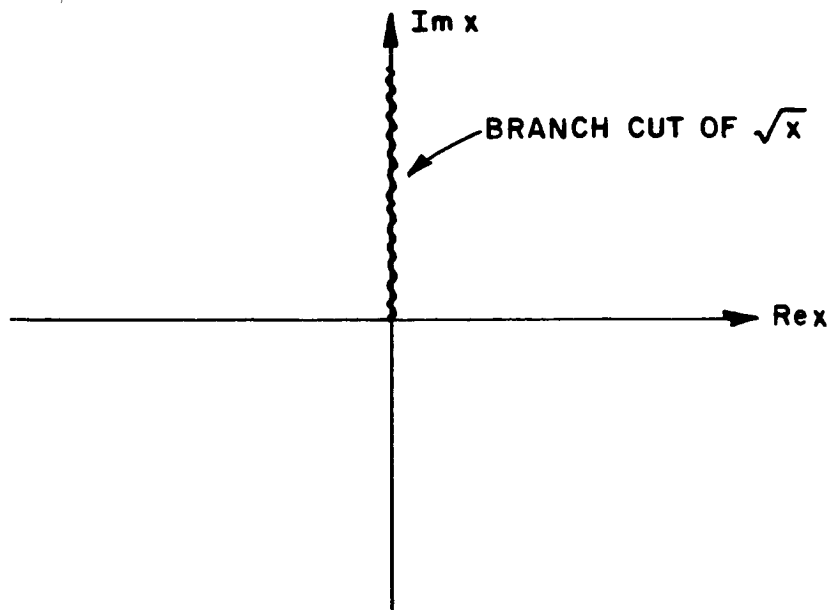


Figure 3.15. Top sheet of $x^{1/2}$ function where $\frac{-3\pi}{2} < \arg(x) < \frac{\pi}{2}$.

Note that the new more accurate expression for the diffracted field $u_e^d(\rho, \phi)$ given in (3.243) does not vanish when $\phi = \pi$, that is

$$u_e^d(\rho, \pi) \neq 0. \quad (3.249)$$

In order to obtain a new more accurate expression for the odd diffracted field $u_0^d(\rho, \phi)$, which does not vanish on the impedance surface, a different procedure is followed. The function $M_0(w)$ given in (3.227) is zero when the saddle point is equal to $\phi = \pi$, which means that a higher order term is required. Instead of computing a higher order term by the method described in Appendix G, another approach which is given by Felsen and Marcuvitz [42] is followed. The details are given

in Appendix H and only the final result is presented here. Thus, when $\phi=\pi$, and $k\rho$ is large

$$\begin{aligned}
 u_0^d(\rho, \pi) \sim & \left[2i \sqrt{\pi} e^{-ik\rho(1-\cos 2\phi')} Q[-ib \sqrt{k\rho}] + \left(\frac{\pi}{k\rho}\right)^{1/2} \frac{1}{b} \right] \cdot e^{ik\rho} \\
 & \cdot \frac{v}{2\pi i} \frac{\sin \phi' (\sin^2 \xi^0 - \cos^2 \phi')^{1/2} e^{-1/(2\pi) J_1^0(\phi')}}{(\sin \phi' + \cos \xi^0)} \\
 & \cdot \left[\frac{e^{-1/(2\pi) J_1^0(\pi+\phi')}}{\cos \xi^0 - \sin \phi'} - \frac{e^{-1/(2\pi) J_1^0(\pi-\phi')}}{\sin \phi' + \cos \xi^0} \right] \quad (3.250)
 \end{aligned}$$

where

$$b = \sqrt{2} e^{i\pi/4} \sin(\phi'/2) \quad (3.251)$$

and

$$Q(x) = \int_y^\infty e^{-x^2} dx \quad (3.252)$$

The new expression in (3.250) is not identically zero at $\phi=\pi$ for a finite ρ . However, as shown in Appendix H, when the parameter $|b\sqrt{k\rho}| \rightarrow \infty$, $u_0^d(\rho, \pi) \rightarrow 0$.

E. SLOPE DIFFRACTED FIELD

When the diffracted field was obtained in Section C, it was implicitly assumed that the incident field $u^i(\rho, \phi')$ had a slow spatial variation in the vicinity of the diffraction point ($x=0, y=0$), except for the phase along the incident ray. When this is not the case, it has been shown in [10] that the diffracted field must be supplemented by a higher-order term in the asymptotic expansion of the integral along C_{SDP} . This higher order term which is referred to as the slope diffracted field $u^{sd}(\rho, \phi)$, is given by the following expression [10]:

$$u^{sd}(\rho, \phi) = \left[\frac{\partial u^i}{\partial \hat{n}'} \right]_{(QE)} d^s(\phi, \phi') \frac{e^{ik\rho}}{\sqrt{\rho}} \quad (3.253)$$

where the vector \hat{n}' , and the point of diffraction (QE) are shown in Figure 3.16. The expression for the slope diffraction coefficient $d^s(\phi, \phi')$ is as follows:

$$d^s(\phi, \phi') = \frac{1}{ik} \frac{\partial D^d}{\partial \phi'}(\phi, \phi') \quad (3.254)$$

where $D^d(\phi, \phi')$ is the diffraction coefficient which was defined in Section C. Substituting Equation (3.210) into (3.254) yields

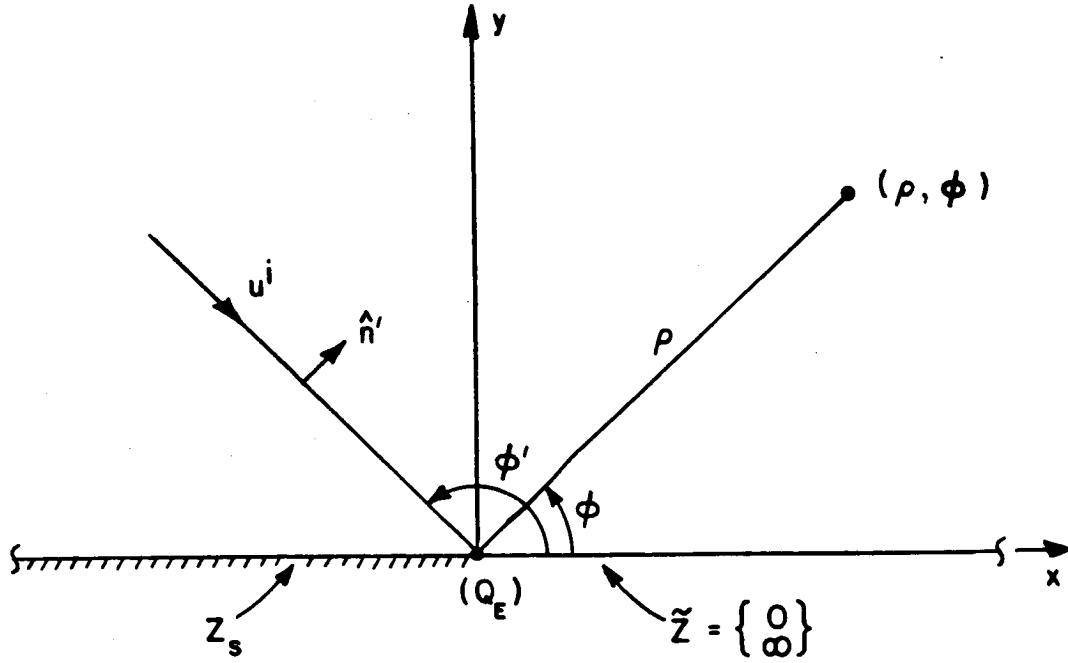


Figure 3.16. Geometry for slope diffracted field.

$$\begin{aligned}
 d^{se}(\phi, \phi') &= \frac{-1}{ik} \left[\frac{1-R_e}{2} \right] \frac{e^{i\pi/4}}{\sqrt{2\pi k}} \frac{[(\sin \xi^e - \cos \phi)(\sin \xi^e - \cos \phi')]^{1/2}}{\sin \phi + \cos \xi} e \\
 &\cdot e^{-1/(2\pi)(J_1^e(\phi) + J_1^e(\phi'))} \\
 &\cdot \left[\begin{aligned} &[\sin(\beta^-/2)F_s^*(kLa^-) - \sin(\beta^+/2)F_s^*(kLa^+)] \\ &+ [\sec(\beta^+/2)F^*(kLa^+) + \sec(\beta^-/2)F^*(kLa^-)] \\ &\cdot \left[\frac{\sin \phi'}{2(\sin \xi^e - \cos \phi')} - \frac{\cos \phi'}{(\sin \phi' + \cos \xi^e)} + \frac{\pi/2 + \xi^e - \phi'}{2\pi \cos(\xi^e - \phi')} + \frac{3\pi/2 - \phi' - \xi^e}{2\pi \cos(\phi' + \xi^e)} \right] \end{aligned} \right]
 \end{aligned}
 \tag{3.255}$$

for the even slope diffraction coefficient. The function $F_s^*(kLa)$ is given by

$$F_s^*(kLa) = 2ikL (1 - F^*(kLa)) \quad (3.256)$$

Similarly, the odd diffraction coefficient can be obtained by substituting (3.242) into (3.354). After some simplification, one obtains

$$d^{SO}(\phi, \phi') = \frac{-2}{ik} \frac{e^{i\pi/4}}{\sqrt{2\pi k}} \frac{\cos(\phi/2)[(\sin \xi^0 - \cos \phi)(\sin \xi^0 - \cos \phi')]^{1/2}}{(\sin \phi + \cos \xi^0)(\sin \phi' + \cos \xi^0)} \\ \cdot e^{-1/(2\pi)(J_1^0(\phi) + J_1^0(\phi'))} \\ \cdot \left[\begin{aligned} & \cos(\phi'/2)[\sin(\beta^-/2)F_s^*(kLa^-) + \sin(\beta^+/2)F_s^*(kLa^+)] \\ & + [\sec(\beta^-/2)F^*(kLa^-) - \sec(\beta^+/2)F^*(kLa^+)] \\ & \cdot \left[\frac{\cos(\phi'/2)\sin \phi'}{2(\sin \xi^0 - \cos \phi')} - \frac{\cos(\phi'/2)\cos \phi'}{(\sin \phi' + \cos \xi^0)} - \frac{\sin(\phi'/2)}{2} \right. \\ & \left. + \frac{\cos(\phi'/2)(\pi/2 + \xi^0 - \phi')}{2\pi \cos(\xi^0 - \phi')} + \frac{\cos(\phi'/2)(3\pi/2 - \phi' - \xi^0)}{2\pi \cos(\phi' + \xi^0)} \right] \end{aligned} \right] \quad (3.257)$$

Adding the slope diffracted field to Equations (3.205) and (3.237), the total fields $u_e(\rho, \phi)$ and $u_o(\rho, \phi)$ become

$$u_e(\rho, \phi) \sim u_e^i(\rho, \phi) + u_e^r(\rho, \phi) + u_e^{sw}(\rho, \phi) + u_e^d(\rho, \phi) + u_e^{sd}(\rho, \phi), \quad 0 < \phi < \pi \quad (3.258)$$

and

$$u_o(\rho, \phi) \sim u_o^i(\rho, \phi) + u_o^r(\rho, \phi) + u_o^{sw}(\rho, \phi) + u_o^d(\rho, \phi) + u_o^{sd}(\rho, \phi), \quad 0 < \phi < \pi \quad (3.259)$$

F. SURFACE WAVE EXCITATION

Let the incident wave be a surface wave field as shown in Figure 3.17. Assume that

$$u_{sw}^i = v e^{i\vec{\zeta}^i \cdot \vec{r}} = v e^{i\tilde{\beta}x - \tilde{\alpha}y} \quad (3.260)$$

is the incident surface wave field, where

$$\vec{\zeta}^i = \hat{x}\tilde{\beta} + i\hat{y}\tilde{\alpha} \quad (3.261)$$

is the complex propagation constant. Note that the constants $\tilde{\beta}$ and $\tilde{\alpha}$ are also complex, that is

$$\tilde{\beta} = \tilde{\beta}_r + i\tilde{\beta}_I \quad (3.262)$$

and

$$\tilde{\alpha} = \tilde{\alpha}_r + i\tilde{\alpha}_I \quad (3.263)$$

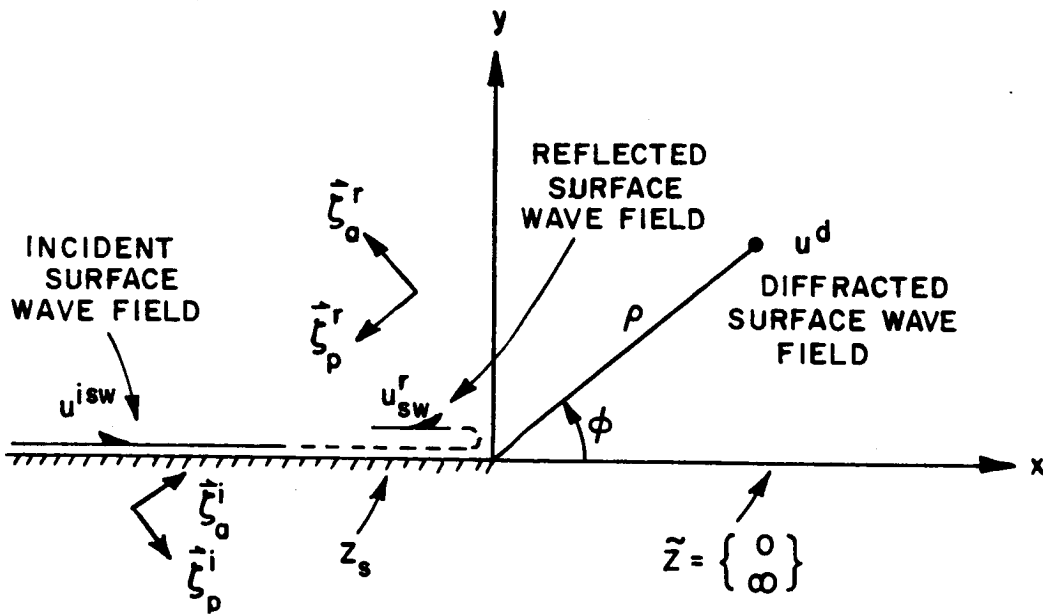


Figure 3.17. Geometry for surface wave excitation.

Rewriting ζ_p^i in terms of real and imaginary parts, one gets

$$\zeta^i = \zeta_p^i + i\zeta_a^i \quad (3.264)$$

where ζ_p^i and ζ_a^i are the real and imaginary parts of ζ^i , respectively.

It follows from Equations (3.262) and (3.263) that

$$\zeta_p^i = \hat{x} \tilde{\beta}_r - \hat{y} \tilde{\alpha}_I \quad (3.265)$$

and

$$\zeta_a^i = \hat{x} \tilde{\beta}_I + \hat{y} \tilde{\alpha}_r \quad (3.266)$$

1. Even Problem

The total field can be expressed in terms of the unperturbed and scattered fields such that

$$u_e(x,y) = \tilde{u}_e(x,y) + u_e^s(x,y) \quad (3.267)$$

where

$$\tilde{u}_e(x,y) = u_e^{isw}(x,y) = v \exp(i\tilde{\beta}^e x - \tilde{\alpha}^e y) \quad \text{for } |x| < \infty, \quad y > 0 \quad (3.268)$$

is the unperturbed field. It follows from Equations (3.8) and (3.17) that

$$\begin{aligned} \tilde{\alpha}^e &= \tilde{\alpha}_r^e + i\tilde{\alpha}_I^e = ik\delta_e = ik\cos\xi^e = ik\cos\xi_r^e \cosh h\xi_I^e \\ &\quad + k\sin\xi_r^e \sinh\xi_I^e \end{aligned} \quad (3.269)$$

and

$$\begin{aligned} \tilde{\beta}^e &= \tilde{\beta}_r^e + i\tilde{\beta}_I^e = k(1-\delta_e^2)^{1/2} = k\sin\xi^e = k\sin\xi_r^e \cosh\xi_I^e \\ &\quad + ik\sinh\xi_I^e \cos\xi_r^e \end{aligned} \quad (3.270)$$

Note that the unperturbed field exists on the whole impedance plane shown in Figure 3.2. Substituting Equations (3.269) and (3.270) into (3.265) and (3.266) yields

$$\tilde{\zeta}_p^{ie} = k\cosh\xi_I^e (\hat{x} \sin\xi_r^e - \hat{y} \cos\xi_r^e) \quad (3.271)$$

and

$$\tilde{\zeta}_a^{ie} = k\sinh\xi_I^e (\hat{x} \cos\xi_r^e + \hat{y} \sin\xi_r^e) \quad (3.272)$$

The vector $\vec{\zeta}_p^{ie}$ is usually referred to as the propagation vector, while $\vec{\zeta}_a^{ie}$ is known as the attenuation vector. It is easy to show that $\vec{\zeta}_p^{ie}$ and $\vec{\zeta}_a^{ie}$ satisfy the following identity:

$$\vec{\zeta}_p^{ie} \cdot \vec{\zeta}_a^{ie} = 0 \quad . \quad (3.273)$$

Recall that δ_e is either the normalized impedance (TE_z) or the normalized admittance (TM_z). It follows from (3.269) that the surface wave field u_{sw}^i exists if and only if $\text{Im}(\delta_e) < 0$. In other words, it exists if

$$\text{Im}(Z_s) < 0 \quad \text{for the } TE_z \text{ polarization } (H_z) \quad (3.274)$$

or

$$\text{Im}(Z_s) > 0 \quad \text{for the } TM_z \text{ polarization } (E_z) \quad (3.275)$$

Thus, for a given surface impedance Z_s , only one polarization of the surface wave field can exist.

The next step is to solve for the scattered field $u_e^s(\rho, \phi)$. Exactly the same procedure as in the case for plane wave incidence is followed to solve for $u_e^s(\rho, \phi)$. The scattered field satisfies Equations (3.22), (3.23), and

$$\frac{\partial}{\partial y} u_e^s(x, y) = \frac{-\partial}{\partial y} \tilde{u}_e(x, y) \quad \text{for } y = 0, x > 0. \quad (3.276)$$

Details of the solution are shown in [46] and in [43] where the dual integral method is employed. For large $k\rho$, the total field $u_e(\rho, \phi)$ can be expressed as

$$u_e(\rho, \phi) \sim u_e^{isw}(\rho, \phi) U(\phi - \tilde{\phi}_e^i) + u_e^{rsw}(\rho, \phi) U(\phi - \tilde{\phi}_s^e) + u_e^{dsw}(\rho, \phi) ,$$

$$0 < \phi < \pi \quad (3.277)$$

where

$$u_e^{rsw}(\rho, \phi) = \frac{-(1 - \sin \xi^e) v}{\sin \xi^e} \exp \left[\frac{-1}{\pi} \int_0^{2\xi^e - \pi} \frac{t}{\sin t} dt \right] \exp(-i\tilde{\beta}^e x - \tilde{\alpha}^e y) \quad (3.278)$$

is the reflected field and

$$u_e^{dsw}(\rho, \phi) = \frac{v e^{-i\pi/4} i \cos \xi^e}{\sqrt{2\pi k} (\sin \xi^e - \cos \phi)}$$

$$\cdot \left[\frac{2 \sin \xi^e (1 + \cos \phi)}{(1 + \sin \xi^e)(\sin \xi^e + \cos \phi)} \right]^{1/2} \exp(J_2^e(\phi)/(2\pi)) \frac{e^{ik\rho}}{\sqrt{\rho}} \quad (3.279)$$

is the diffracted field. The function $J_2^e(\phi)$ is given by

$$J_2^e(\phi) = \int_{\phi - \xi^e + \pi/2}^{\phi + \xi^e - \pi/2} \frac{u}{\sin u} du - \int_0^{2\xi^e - \pi} \frac{u}{\sin u} du . \quad (3.280)$$

The diffracted field $u_e^{dsw}(\rho, \phi)$ was computed assuming that no poles were close to the saddle point. In other words, Equation (3.279) is not a uniform asymptotic expression. This means that u_e^{dsw} is a valid expression away from the shadow boundaries $\phi = \tilde{\phi}_e^i$ and $\phi = \tilde{\phi}_s^e$. However, near the same shadow boundaries $u_e^{dsw}(\rho, \phi)$ is not correct because the

total field will be discontinuous when $\phi = \tilde{\phi}_e^i$ and $\phi = \tilde{\phi}_s^e$. In the next section, a uniform asymptotic expression for $u_e^{dsw}(\rho, \phi)$ will be obtained.

The surface wave fields u_e^{isw} and u_e^{rsw} are not very significant with respect to $u_e^{dsw}(\rho, \phi)$ when the observation point is away from $\phi \approx \pi$.

Therefore, they can be ignored when the angle ϕ is away from the impedance surface and the expression for u_e^{dsw} given in Equation (3.279) is quite accurate.

The angle $\tilde{\phi}_s^e$ was defined in Equation (3.203) and $\tilde{\phi}_e^i$, which is computed in exactly the same way as $\tilde{\phi}_s^e$, is given by

$$\tilde{\phi}_e^i = \xi^e - \arcsin \left[\frac{1}{\cos \xi_I^e} \right], \quad 0 < \xi_r^e < \pi/2, \quad \xi_I^e > 0. \quad (3.281)$$

As in Equation (3.261), one can define a vector $\vec{\zeta}^{re}$ such that

$$\vec{\zeta}^{re} = -\hat{x} \tilde{\beta}^e + i\hat{y} \tilde{\alpha}^e = \vec{\xi}_p^{re} + i\vec{\xi}_a^{re} \quad (3.282)$$

where $\vec{\xi}_p^{re}$ and $\vec{\xi}_a^{re}$ are the propagation and attenuation vectors of the reflected surface wave field u_e^{rsw} , respectively.

It follows from (3.282), (3.269), and (3.270) that

$$\vec{\xi}_p^{re} = -\hat{x} \tilde{\beta}_r^e - \hat{y} \tilde{\alpha}_I^e = k \cosh \xi_I^e (-\hat{x} \sin \xi_r^e - \hat{y} \cos \xi_r^e) \quad (3.283)$$

$$\vec{\xi}_a^{re} = -\hat{x} \tilde{\beta}_I^e + \hat{y} \tilde{\alpha}_r^e = k \sinh \xi_I^e (-\hat{x} \cos \xi_r^e + \hat{y} \sin \xi_r^e) \quad (3.284)$$

The vectors $\vec{\xi}_p^{re}$ and $\vec{\xi}_a^{re}$ are shown in Figure 3.17. Furthermore, $\vec{\xi}_p^{re}$ and $\vec{\xi}_a^{re}$ satisfy identity (3.273), and ξ^e has to satisfy Equation (3.204) so that the pole contributing to the reflected field u_e^{rsw} can be captured.

2. Odd Problem

In this case, the scattered field $u_0^s(\rho, \phi)$ satisfies Equations (3.103), (3.104) and

$$u_0^s(x, y) = -\tilde{u}_0(x, y) \quad \text{for } x > 0, \quad y = 0 \quad (3.285)$$

where $\tilde{u}_0(x, y)$ is the unperturbed field given by

$$\tilde{u}_0(x, y) = u_0^{isw}(x, y) = v \exp(i\tilde{\beta}^0 x - \tilde{\alpha}^0 y) \quad (3.286)$$

where

$$\tilde{\alpha}^0 = ik \cos \xi^0 = ik \delta_0 \quad (3.287)$$

$$\tilde{\beta}^0 = k \sin \xi^0 = k(1 - \delta_0^2)^{1/2} \quad (3.288)$$

It follows from [43] that the total field $u_0(\rho, \phi)$ is asymptotically equal to

$$u_0(\rho, \phi) \sim u_0^{isw}(\rho, \phi) U(\phi - \tilde{\phi}_0^i) + u_0^{rsw}(\rho, \phi) U(\phi - \tilde{\phi}_s^0) + u_0^{dsw}(\rho, \phi), \quad 0 < \phi < \pi \quad (3.289)$$

where $\tilde{\phi}_s^0$ was defined in Equation (3.234) and $\tilde{\phi}_0^i$ is given by

$$\tilde{\phi}_0^i = \xi_r^0 - \arcsin \left[\frac{1}{\cosh \xi_I^0} \right], \quad 0 < \xi_r^0 < \pi/2, \quad \xi_I^0 > 0. \quad (3.290)$$

The field u_0^{rsw} is the reflected field which is given by the following expression:

$$u_0^{rsw}(\rho, \phi) = \frac{v \cos \xi^0}{\sin \xi^0} \exp \left[\frac{-1}{\pi} \int_0^{2\xi^0 - \pi} \frac{u}{\sin u} du \right] e^{i \vec{\zeta}^{ro} \cdot \vec{r}} \quad (3.291)$$

where

$$\vec{\zeta}^{ro} = -\hat{x} \tilde{\beta}^0 + i \tilde{\alpha}^0 \hat{y} = \vec{\zeta}_p^{ro} + i \vec{\zeta}_a^{ro}. \quad (3.292)$$

The propagation vector $\vec{\zeta}_p^{ro}$ is equal to

$$\vec{\zeta}_p^{ro} = -\hat{x} \tilde{\beta}_r^0 - \hat{y} \tilde{\alpha}_I^0 = k \cosh \xi_I^0 (-\hat{x} \sin \xi_r^0 - \hat{y} \cos \xi_r^0) \quad (3.293)$$

and the attenuation vector $\vec{\zeta}_a^{ro}$ is given by

$$\vec{\zeta}_a^{ro} = -\hat{x} \tilde{\beta}_I^0 + \hat{y} \tilde{\alpha}_r^0 = k \sinh \xi_I^0 (-\hat{x} \cos \xi_r^0 + \hat{y} \sin \xi_r^0). \quad (3.294)$$

The diffracted field u_0^{dsw} can be expressed as follows:

$$u_0^{dsw}(\rho, \phi) = \frac{-ie^{-\pi/4} v}{\sqrt{2\pi k}} \left[\frac{\sin \phi}{\sin \xi^0 - \cos \phi} \right] \cdot \left[\frac{2 \sin \xi^0}{\sin \xi + \cos \phi} \right]^{1/2} \exp \left[\frac{1}{(2\pi) J_2^0(\phi)} \right] \frac{e^{ik\rho}}{\sqrt{\rho}}, \quad 0 < \phi < \pi \quad (3.295)$$

where

$$J_2^0(\phi) = \int_{\phi-\xi^0+\pi/2}^{\phi+\xi^0-\pi/2} \frac{u}{\sin u} du - \int_0^{2\xi^0-\pi} \frac{u}{\sin u} du \quad . \quad (3.296)$$

As in the even case, the diffracted field is computed assuming no poles are close to the saddle point. In other words, the expression for $u_0^{\text{dsw}}(\rho, \phi)$ in (3.295) is not uniform. Therefore, the total field $u_0(\rho, \phi)$ is not continuous at the shadow boundaries $\phi = \tilde{\phi}_0^i$ and $\phi = \tilde{\phi}_s^0$. A uniform expression for $u_0(\rho, \phi)$ will be obtained in Section 3. Furthermore, in order for the field u_0^{rsw} to exist, ξ^0 has to satisfy Equation (3.235).

3. Analytic Continuation

There is another way to obtain the total fields $u_e(x, y)$ and $u_o(x, y)$ by an analytic continuation of the angle ϕ' into the complex domain for the case of plane wave excitation [24].

Recall that when the angle of incidence is equal to the Brewster angle $\tilde{\phi}_b$, the Fresnel reflection coefficient vanishes [21] such that

$$R(\phi' = \tilde{\phi}_b) = \frac{\sin \tilde{\phi}_b - \cos \xi}{\sin \tilde{\phi}_b + \cos \xi} = 0 \quad . \quad (3.297)$$

It follows from Equation (3.297) that

$$\tilde{\phi}_b = \pi/2 \pm \xi \quad . \quad (3.298)$$

Substituting Equation (3.298) into (3.16), one concludes that the only possible solution is

$$\tilde{\phi}_b = \pi/2 + \xi \quad . \quad (3.299)$$

EVEN PROBLEM

Substituting Equation (3.299) into (3.16) yields

$$u_e^{isw}(\phi, \tilde{\phi}_b^e) = v e^{-ik\rho \cos(\phi - \pi/2 - \xi^e)} = v e^{-ik\rho \sin(\phi - \xi^e)} \quad (3.300)$$

or

$$u_e^{isw}(\phi, \tilde{\phi}_b^e) = v \exp(i\tilde{\beta}^e x - \tilde{\alpha}^e y) \quad (3.301)$$

which is identical to Equation (3.268). The expression for $u_e^s(\rho, \tilde{\phi}_b^e, \phi)$ becomes

$$u_e^s(\rho, \tilde{\phi}_b^e, \phi) = \frac{v \cos \xi^e}{2\pi i} \int_{\Gamma_w^e} \frac{G_-^e(-k \cos w) e^{ik\rho \cos(w - \phi)}}{(\cos w - \sin \xi^e) G_-^e(-k \sin \xi^e)} dw \quad . \quad (3.302)$$

The original geometrical optics poles w_r^{e+} and w_r^{e-} become

$$\tilde{w}_r^{e+} = \pi - \tilde{\phi}_b^e = \pi/2 - \xi^e \quad , \quad 0 < \xi_r^e < \pi/2 \quad , \quad \xi_I^e > 0 \quad (4.303)$$

and

$$\tilde{w}_r^{e-} = -\pi + \tilde{\phi}_b^e = -\pi/2 + \xi^e \quad , \quad 0 < \xi_r^e < \pi/2 \quad , \quad \xi_I^0 > 0 \quad (3.304)$$

where the new poles \tilde{w}_r^{e+} and \tilde{w}_r^{e-} are depicted in Figure 3.18. Note that in this case, the pole \tilde{w}_r^{e-} will contribute to the total field unlike the case for plane wave excitation where w_r^{e+} contributes to the total field. Deforming the contour of integration Γ_w^e , one gets

$$\begin{aligned}
u_e^S(\rho, \phi) = & 2\pi i [-\text{Res}(\tilde{w}_r^{e-})U(\tilde{\phi}_e^i - \phi) + \text{Res}(w_s^e)U(\phi - \tilde{\phi}_s^e)] \\
& + \frac{v \cos \xi^e}{2\pi i} \int_{C_{SDP}} \frac{G_-^e(-k \cos w) e^{ik\rho \cos(w-\phi)}}{(\cos w - \sin \xi^e) G_-^e(-k \cos \tilde{w}_r^{e-})} dw \quad (3.305)
\end{aligned}$$

where the steepest descent path C_{SDP} is shown in Figure 3.18.

The residue at \tilde{w}_r^{e-} is given by

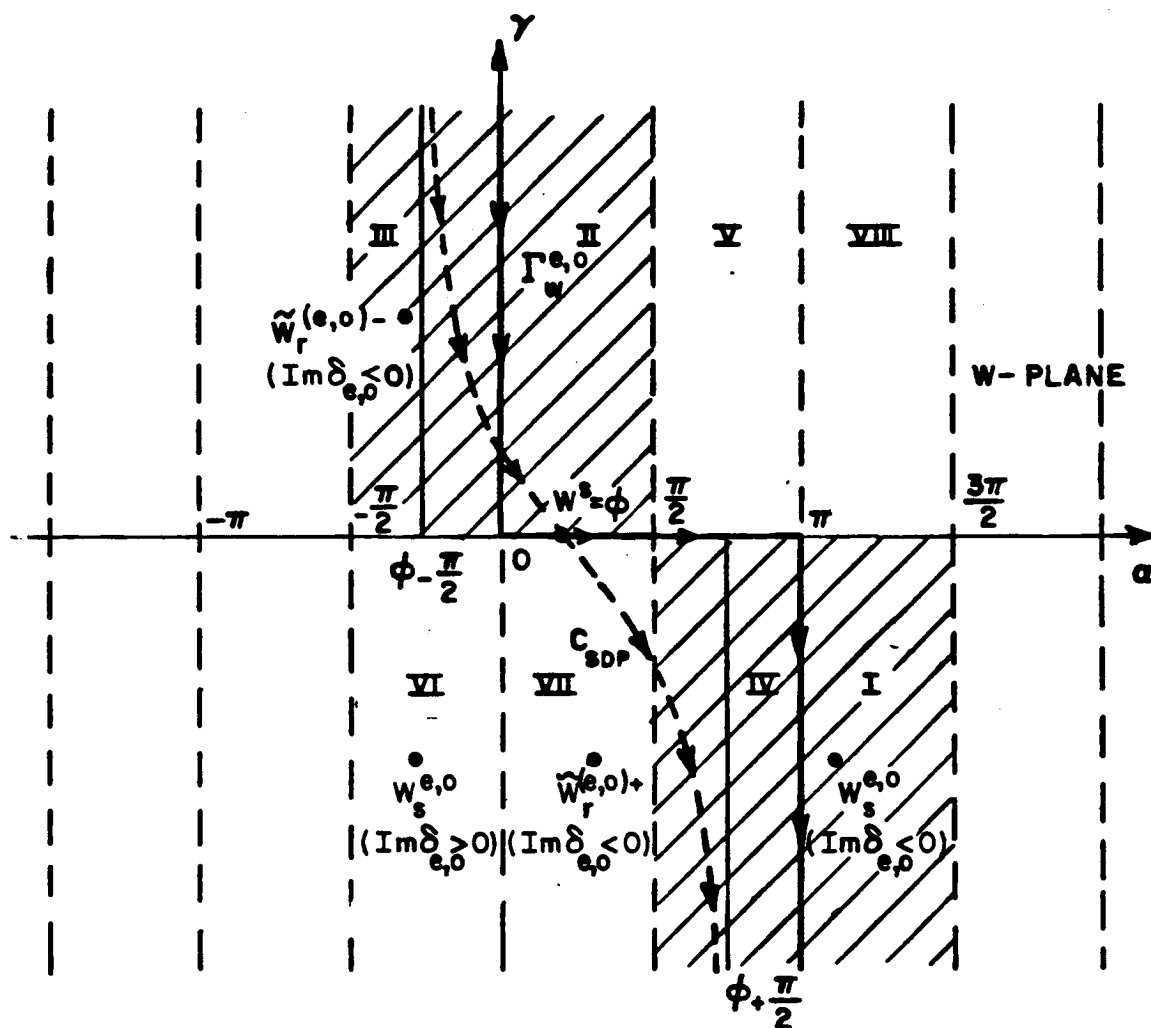
$$\begin{aligned}
\text{Res}(\tilde{w}_r^{e-}) &= \frac{v \cos \xi^e G_-^e(-k \sin \xi^e)}{\cos \xi^e 2\pi i G_-^e(-k \cos \tilde{w}_r^{e-})} e^{ik\rho \cos(\xi^e - \pi/2 - \phi)} \\
&= \frac{v}{2\pi i} \exp(i\tilde{\beta}^e x - \tilde{\alpha}^e y) \quad (3.306)
\end{aligned}$$

In order to compute the residue at w_s^e it is necessary to rewrite $G_-^e(-k \cos w)/G_-^e(-k \cos \tilde{w}_r^{e-})$. Substituting Equation (3.167) into (3.304) yields

$$\tilde{w}_r^{e-} = -\pi/2 + 3\pi/2 - w_s^e = \pi - w_s^e \quad (3.307)$$

Thus,

$$\begin{aligned}
G_-^e(-k \cos w)/G_-^e(-k \cos \tilde{w}_r^{e-}) &= \frac{G_-^e(-k \cos w)}{G_-^e(k \cos w_s^e)} = \frac{G^e(-k \cos w)}{G_+^e(-k \cos w) G_-^e(k \cos w_s^e)} \quad (3.308)
\end{aligned}$$



 TOP RIEMANN SHEET IN S-DOMAIN WHERE $\text{Im}\beta > 0$

Figure 3.18. Integration paths Γ_w and C_{SDP} in the periodic w -plane for $k=k_1$ (real).

Substituting Equations (3.186)-(3.188) into (3.308) one obtains

$$\frac{G^e(-k\cos w)}{G_-^e(-k\cos w_r^e)} = \left[\frac{\sin w}{\sin w + \cos \xi^e} \right] \frac{[(\sin \xi^e - \cos w)(\sin \xi^e - \cos w_s^e)]^{1/2}}{2\sin(w/2) \sin(w_s^e/2)} \cdot \exp \left[- (J_1^e(w_s^e) + J_1^e(w))/(2\pi) \right] \quad (3.309)$$

Now the residue at w_s^e can be computed. After some simplification, the residue at w_s^e can be expressed the following way:

$$\text{Res}(w_s^e) = \frac{v(1+\cos w_s^e)}{2\pi i \cos w_s^e} \exp(-J_1^e(w_s^e)/\pi) \exp(i\tilde{\beta}^e x - \tilde{\alpha}^e y), \quad y > 0 \quad (3.310)$$

where

$$J_1^e(w_s^e) = J_1^e(3\pi/2 - \xi^e) = \int_0^{2\xi^e - \pi} t/\sin t \, dt \quad (3.311)$$

For the case of plane wave excitation, the uniform asymptotic evaluation of the integral along C_{SDP} was equal to the diffracted field $u_e^d(\rho, \phi)$. Therefore, the diffracted surface wave field can be obtained directly from Equation (3.196) by letting $\phi' = \tilde{\phi}_b^e = \pi/2 + \xi^e$ such that

$$\begin{aligned}
u_e^{\text{dsw}}(\rho, \phi) = & \frac{-ve^{i\pi/4}}{\sqrt{2\pi k}} \frac{[(\sin \xi^e - \cos \phi) 2\sin \xi^e]^{1/2}}{2(\sin \phi + \cos \xi^e)} \\
& \cdot \exp \left[- (J_1^e(\phi) + J_1^e(w_s^e)) / (2\pi) \right] \\
& \cdot \left[\sec((\phi + \pi/2 + \xi^e)/2) T(a_e^+, a_p^e) + \sec((\phi - \pi/2 - \xi^e)/2) T(a_e^-, a_p^e) \right] \frac{e^{ik\rho}}{\sqrt{\rho}}
\end{aligned}
\tag{3.312}$$

where T was defined in (3.244), a_e^\pm is given by

$$a_e^\pm = 2\cos^2 \left[(\phi \pm (\pi/2 + \xi^e))/2 \right]
\tag{3.313}$$

and $F(x)$ is the generalized transition function where x can be a complex number. As stated before, the argument of \sqrt{x} has to satisfy Equation (3.245) in order for (3.312) to converge.

Substituting Equations (3.306), (3.310) and (3.12) into (3.05) yields

$$\begin{aligned}
u_e^S(\rho, \phi) \sim & -v \exp(i\tilde{\beta}^e x - \tilde{\alpha}^e y) U(\tilde{\phi}_e^i - \phi) + u_e^{\text{rsw}}(\rho, \phi) + u_e^{\text{dsw}}(\rho, \phi), \\
& 0 < \phi < \pi
\end{aligned}
\tag{3.314}$$

where $u_e^{\text{rsw}}(\rho, \phi)$ is the reflected surface wave field given by

$$u_e^{rsw}(\rho, \phi) = \frac{v(1+\cos w_s^e)}{\cos w_s^e} \exp(-J_1^e((w_s^e)/\pi)) \exp(-i\tilde{\beta}^e x - i\tilde{\alpha}^e y) U(\phi - \tilde{\phi}_s^e) \quad (3.315)$$

which is identical to Equation (3.278). The total field $u_e(\rho, \phi)$ is obtained by substituting Equation (3.314) into (3.267). Thus, for large $k\rho$

$$u_e(\rho, \phi) \sim u_e^{isw}(\phi, \tilde{\phi}_b^e) U(\phi - \tilde{\phi}_e^i) + u_e^{rsw}(\rho, \phi) + u_e^{dsw}(\rho, \phi) \quad (3.316)$$

where $u_e^{isw}(\phi, \tilde{\phi}_b^e)$ was defined in Equation (3.301).

Note that the expression for $u_e^{dsw}(\rho, \phi)$ in Equation (3.312) is uniform, whereas the non-uniform result was previously given in Equation (3.279). Thus, one can get the expression in (3.279) from (3.312) by assuming that $|\text{Im}(\delta_e)|$ is large. In other words, for large $|kLa_e^\pm|$ and $|kLa_p^e|$, it can be shown that [11] $F(-kLa_p^e) = F(-kLa_e^\pm) \approx 1$. It follows from (3.244) that

$$T(a_{e,p}^\pm) \approx 1 \quad (3.317)$$

Substituting Equation (3.317) into (3.312) yields

$$u_e^{dsw}(\rho, \phi) = \frac{ve^{-i\pi/4} i \cos \xi^e}{\sqrt{2\pi k} (\sin \xi^e - \cos \phi)} \left[\frac{2 \sin \xi^e (1 + \cos \phi)}{(1 + \sin \xi^e)(\sin \xi^e + \cos \phi)} \right]^{1/2} \cdot \left[\frac{\sin \phi - \cos \xi^e}{\sin \phi + \cos \xi^e} \right]^{1/2} e^{-1/(2\pi)[J_1^e(\phi) + J_1^e(w_s^e)]} \frac{e^{ik\rho}}{\sqrt{\rho}} \quad (3.318)$$

where $J_1^e(w_s^e)$ was defined in Equation (3.311) and

$$J_1^e(\phi) \int_{3\pi/2-\phi-\xi^e}^{\pi/2-\phi+\xi^e} \frac{t}{\sin t} dt = - \int_{\phi+\xi^e-3\pi/2}^{\phi-\pi/2-\xi^e} \frac{t}{\sin t} dt = \int_{\phi-\pi/2-\xi^e}^{\phi+\xi^e-3\pi/2} \frac{t}{\sin t} dt. \quad (3.319)$$

Letting $u = t + \pi$, J_1^e becomes

$$J_1^e(\phi) = \int_{\phi-\xi^e+\pi/2}^{\phi+\xi^e-\pi/2} \frac{u-\pi}{\sin(u-\pi)} du = - \int_{\phi-\xi^e+\pi/2}^{\phi+\xi^e-\pi/2} \frac{u}{\sin u} du + \int_{\phi-\xi^e+\pi/2}^{\phi+\xi^e-\pi/2} \frac{\pi}{\sin u} du. \quad (3.320)$$

The second integral in Equation (3.320) can be evaluated in closed form such that [44]

$$\int_{\phi-\xi^e+\pi/2}^{\phi+\xi^e-\pi/2} \frac{\pi}{\sin u} du = \pi \log \left[\frac{\tan \left[\frac{\phi+\xi^e-\pi/2}{2} \right]}{\tan \left[\frac{\phi-\xi^e+\pi/2}{2} \right]} \right] = \pi \log \left[\frac{\sin \phi - \cos \xi^e}{\sin \phi + \cos \xi^e} \right]. \quad (4.321)$$

Using Equation (3.320) and (3.321), one obtains the following expression:

$$\exp \left[-\frac{1}{2\pi} (J_1^e(\phi) + J_1^e(w_s^e)) \right] = e^{1/(2\pi) J_2^e(\phi)} \left[\frac{\sin \phi + \cos \xi^e}{\sin \phi - \cos \xi^e} \right]^{1/2}. \quad (3.322)$$

Finally, substituting (3.322) into (3.318), one obtains

$$u_e^{dsw}(\rho, \phi) = \frac{ve^{-i\pi/4} i \cos \xi^e}{\sqrt{2\pi k} (\sin \xi^e - \cos \phi)} \left[\frac{2 \sin \xi^e (1 + \cos \phi)}{(1 + \sin \xi^e)(\sin \xi^e + \cos \phi)} \right]^{1/2} \cdot \exp(J_2^e(\phi)/(2\pi)) \frac{e^{ik\rho}}{\sqrt{\rho}} \quad (3.323)$$

which is identical to Equation (3.279).

ODD PROBLEM

In this case, letting $\phi' = \tilde{\phi}_b^0 = \pi/2 + \xi^0$ in Equation (3.16) yields

$$u_0^{isw}(\phi, \tilde{\phi}_b^0) = ve^{-ik\rho \sin(\phi - \xi^0)} = v \exp(i\tilde{\beta}_0^0 x - \tilde{\alpha}_0^0 y) = \tilde{u}_0(\phi, \tilde{\phi}_b^0), \quad 0 < \phi < \pi \quad (3.324)$$

where $\tilde{u}_0(\phi, \tilde{\phi}_b^0)$ is the unperturbed field. Furthermore, Equation (3.212) becomes

$$u_0^S(\rho, \tilde{\phi}_b^0, \phi) = \frac{-v}{2\pi i} \int_{\Gamma_w^0} \frac{G_-^0(-k \cos w) e^{ik\rho \cos(w - \phi)} \sin w \, dw}{(\cos w - \sin \xi^0) G_-^0(-k \sin \xi^0)} \quad (3.325)$$

The geometrical optics poles w_r^{0+} and w_r^{0-} become

$$\tilde{w}_r^{0+} = \pi/2 - \xi^0 \quad (3.326)$$

and

$$\tilde{w}_r^{0-} = -\pi/2 + \xi^0 \quad (3.327)$$

where $0 < \text{Re}(\xi^0) < \pi/2$ and $\text{Im}(\xi^0) > 0$. The above two poles

are depicted in Figure 3.18. Note that the integrand in (3.325) still has three poles, namely, \tilde{w}_r^{0+} , \tilde{w}_r^{0-} and w_s^0 . Following the same procedure as in the even case, the total field $u_0(\rho, \phi)$ is given by

$$u_0(\rho, \phi) \sim u_0^{isw}(\rho, \phi) U(\phi - \tilde{\phi}_0^i) + u_0^{rsw}(\rho, \phi) + u_0^{dsw}(\rho, \phi), \quad 0 < \phi < \pi \quad (3.328)$$

where

$$u_0^{rsw}(\rho, \phi) = v \tan(w_s^0) \exp(-J_1^0(w_s^0)/\pi) \exp(-i\tilde{\beta}^0 x - \tilde{\alpha}^0 y) U(\phi - \tilde{\phi}_s^0) \quad (3.329)$$

is the reflected field, and

$$u_0^{dsw}(\rho, \phi) \sim \frac{-ve^{i\pi/4}}{\sqrt{2\pi k}} \frac{\cos(\phi/2)}{2\sin(w_s^0/2)} \frac{[2\sin\xi^0(\sin\xi^0 - \cos\phi)]^{1/2}}{\sin\phi + \cos\xi^0} \cdot e^{-1/(2\pi)[J_1^0(\phi) + J_1^0(w_s^0)]} \cdot \left[\sec((\phi - \pi/2 - \xi^0)/2) T(a_0^-, a_p^0) - \sec((\phi + \pi/2 + \xi^0)/2) T(a_0^+, a_p^0) \right] \frac{e^{ik\rho}}{\sqrt{\rho}}, \quad 0 < \phi < \pi \quad (3.330)$$

is the odd diffracted field. The constants a_0^\pm and a_p^0 are given by

$$a_0^\pm = 2\cos^2 \left[\frac{\phi \pm (\pi/2 + \xi^0)}{2} \right]; \quad a_p^0 = 2\sin^2((\phi - w_s^0)/2) \quad (3.331)$$

and they satisfy Equation (3.248). Note that T is the composite transition function which was defined in (3.244).

As expected, the diffracted field in (3.330) is not the same as the one given in (3.295). However, assuming that $|\text{Im } \delta_0|$ is large enough so that Equation (3.317) is true, Equation (3.330) becomes

$$u_0^{\text{dsw}}(\rho, \phi) \sim \frac{-i e^{-i\pi/4}}{\sqrt{2\pi k}} \frac{\sin \phi}{(\sin \xi^0 - \cos \phi)} \left[\frac{2 \sin \xi^0}{\sin \xi^0 + \cos \phi} \right]^{1/2} \\ \cdot \left[\frac{\sin \phi - \cos \xi^0}{\sin \phi + \cos \xi^0} \right]^{1/2} \cdot \exp \left[\frac{-1}{2\pi} (J_1^0(\phi) + J_1^0(w_s^0)) \right] \frac{e^{ik\rho}}{\sqrt{\rho}}, \quad 0 < \phi < \pi. \quad (3.332)$$

As in the even case, it can be shown that

$$\exp \left[\frac{-1}{2\pi} (J_1^0(\phi) + J_1^0(w_s^0)) \right] = \exp(J_2^0(\phi)/(2\pi)) \left[\frac{\sin \phi + \cos \xi^0}{\sin \phi - \cos \xi^0} \right]^{1/2}. \quad (3.333)$$

Substituting (3.333) into (3.332) yields

$$u_0^{\text{dsw}}(\rho, \phi) \sim \frac{-i e^{-i\pi/4}}{\sqrt{2\pi k}} \left[\frac{\sin \phi}{\sin \xi^0 - \cos \phi} \right] \left[\frac{2 \sin \xi^0}{\sin \xi^0 + \cos \phi} \right]^{1/2} \\ \cdot \exp(J_2^0(\phi)/(2\pi)) \frac{e^{ik\rho}}{\sqrt{\rho}}, \quad 0 < \phi < \pi \quad (3.334)$$

which is the nonuniform expression obtained in Equation (3.295).

CHAPTER IV

IMPEDANCE BISECTION PROBLEM

(OBLIQUE INCIDENCE)

A. STATEMENT OF THE PROBLEM

Chapter III was restricted to the case where the fields had no z -variation; hence, it was a two dimensional problem. In this chapter the more general case of oblique incidence will be considered. The geometry of the problem is shown in Figure 2.6. It was shown in Chapter II that there are two ways to scalarize this vector problem. In this chapter, the normal field components E_y and H_y will be used. Recall that these fields satisfy the scalar Helmholtz differential equation as shown in Equations (2.36) and (2.37). Furthermore, as indicated in Chapter II, the normal field components E_y and H_y independently satisfy the following impedance (or Leontovich) boundary conditions for $x < 0, y = 0$:

$$\left[\frac{\partial}{\partial y} + ik\delta_a \right] E_y = 0, \quad x < 0, y = 0, \quad |z| < \infty \quad (4.1)$$

$$\left[\frac{\partial}{\partial y} + ik\delta_h \right] H_y = 0, \quad x < 0, y = 0, \quad |z| < \infty, \quad (4.2)$$

where

$$\delta_a = \begin{cases} Z_s/\eta_0 = \text{normalized impedance, TM}_y \text{ polarization} \\ \eta_0/Z_s = \text{normalized admittance, TE}_y \text{ polarization} \end{cases} \quad (4.3)$$

The subscript "a" refers to the E_y field, while the subscript "h" refers to the H_y field.

When the region $\{x>0, y=0, |z|<\infty\}$ is a PEC, the boundary conditions are given by Equations (2.32) and (2.33). On the other hand, if a PMC occupies the region $\{x>0, y=0, |z|<\infty\}$, the boundary conditions satisfy by E_y and H_y are given by Equations (2.34) and (2.35), respectively. Thus, there are four problems that need to be solved. The case when a PEC occupies the half-plane $\{x>0, y=0, |z|<\infty\}$ will be solved for both polarizations. The other case, when the PMC occupies the same half-plane as the PEC, will be obtained by duality for both E_y and H_y fields.

B. PEC CASE

1. TM_y polarization (E_y^e , even problem)

Let the incident field be equal to

$$E_y^i(x,y,z) = E_{cy} \exp[i(k_x^i x - k_y^i y + k_z^i z)] \quad (4.4)$$

where E_{cy} is an arbitrary constant, and the constants k_x^i , k_y^i , and k_z^i are given by

$$k'_x = -K \cos \phi' ; \quad k'_y = K \sin \phi' ; \quad k'_z = -k \cos \theta' ; \quad 0 < \theta' < \pi, \quad 0 \leq \phi' < \pi \quad (4.5)$$

where

$$K = K_1 + iK_2 = k \sin \theta' = (k_1 + ik_2) \sin \theta' \quad (4.6)$$

Substituting Equation (4.5) into (4.4) and using cylindrical coordinates yields

$$E_y^i(x, y, z) = E_{cy} \exp[-ik\rho \cos(\phi - \phi') + ik'_z z] \quad (4.7)$$

Note that the boundary conditions are not a function of z , and since the geometry depicted in Figure 2.6 is a two-dimensional geometry, it follows that all components of the total field E_y , i.e., E_y^i , E_y^r , E_y^d , etc., will have the same z -variation. In other words, they will have the common term $\exp(ik'_z z)$. Consequently, the differential Equation (2.36) becomes

$$(\nabla_t^2 + K^2)E_y = 0, \quad y > 0, \quad |x| \text{ and } |z| < \infty \quad (4.8)$$

Following the same procedure as in Chapter III, the total field E_y can be expressed as

$$E_y^e(x, y, z) = E_y^{se} + \tilde{E}_y^r + \tilde{E}_y^i, \quad y > 0 \quad (4.9)$$

where \tilde{E}_y^r is the unperturbed reflected field given by

$$\tilde{E}_y^r(x,y,z) = E_{cy} R_a(\phi', \theta', \delta_a) \exp[i(k_x' x + k_y' y + k_z' z)] \quad (4.10)$$

where

$$R_a(\phi', \theta', \delta_a) = \frac{\sin \phi' - \delta_a / \sin \theta'}{\sin \phi' + \delta_a / \sin \theta'} \quad (4.11)$$

is the Fresnel reflection coefficient for an impedance wall. Note that the superscript "e" refers to the even problem.

Since the field $E_y^{se}(x,y,z)$ satisfies the same boundary conditions (Equations (4.1) and (2.32)) and differential equation (except that k is replaced by K in Equation (4.8)) as the field $u_e^s(x,y)$ in Chapter III, it is not necessary to repeat all the analysis for E_y^{se} . However, the similarities end when the edge conditions satisfied by E_y^e have to be used. Therefore, it follows that \hat{E}_{y+} and \hat{E}_{y-} satisfy Equation (3.58), that is

$$\phi^{ae}(s) G^{ae}(s) = \hat{E}_{y-}^{se}(s, 0) + \hat{E}_{y+}^{se}(s, 0) G^{ae}(s) \quad , \quad \tau_- < \tau < \tau_+ \quad (4.12)$$

where the common term $e^{ik_z' z}$ has been dropped and

$$\tau_{-} = (\text{Im } K) \cos \phi' = K_2 \cos \phi' = k_2 \sin \theta' \cos \phi' \quad (4.13)$$

$$\tau_{+} = (\text{Im } K) = K_2 = k_2 \sin \theta' \quad (4.14)$$

The constants $G^{ae}(s)$ and $\Phi^{ae}(s)$ are defined as follows:

$$G^{ae}(s) = \frac{\beta}{\beta + k \delta_a} \quad (4.15)$$

$$\Phi^{ae}(s) = \frac{i E_{cy} k_y' (1 - R_a)}{\sqrt{2\pi} (s + k_x') \beta} \quad (4.16)$$

where the function β , given by

$$\beta = (K^2 - s^2)^{1/2} \quad (4.17)$$

is defined in exactly the same way as in Chapter III, except that k has been replaced by K . Factorizing $G^{ae}(s)$ and decomposing $G_+^{ae}(s) \Phi^{ae}(s)$, one obtains

$$G^{ae}(s) = G_+^{ae}(s) G_-^{ae}(s) \quad (4.18)$$

$$G_+^{ae}(s) \Phi^{ae}(s) = D_+^{ae}(s) + D_-^{ae}(s) \quad (4.19)$$

where $G_-^{ae}(s)$ is regular and free of zeros in the lower half s -plane defined by $\tau < K_2$, while $G_+^{ae}(s)$ is regular and free of zeros in the upper half s -plane $\tau > -K_2$. The details of the factorization of $G^{ae}(s)$ are shown in Appendix D. As shown in Appendix E, the decomposition of $G_+^{ae}(s)\Phi^{ae}(s)$ can be done by inspection. The functions $D_+^{ae}(s)$ and $D_-^{ae}(s)$ are given by

$$D_+^{ae}(s) = \frac{iE_{cy}k_y'(1-R_a)}{\sqrt{2\pi}k\delta_a(s+k_x')} \left[\frac{1}{G_-^{ae}(-k_x')} - G_+^{ae}(s) \right] \quad (4.20)$$

$$D_-^{ae}(s) = \frac{iE_{cy}k_y'(1-R_a)}{\sqrt{2\pi}k\delta_a(s+k_x')} \left[\frac{1}{G_-^{ae}(s)} - \frac{1}{G_-^{ae}(-k_x')} \right] \quad (4.21)$$

where $D_+^{ae}(s)$ is regular in the upper half s -plane $\tau > \tau_-$, while $D_-^{ae}(s)$ is regular in the lower half s -plane $\tau < \tau_+$. Furthermore, by the same arguments as in Chapter III, $\hat{E}_{y+}(s,0)$ is regular in the upper half s -plane defined by $\tau > \tau_-$ and $\hat{E}_{y-}(s,0)$ is regular in the lower half s -plane defined by $\tau < \tau_+$.

Substituting Equations (4.18) and (4.19) into (4.12) yields

$$D_+^{ae}(s) - \hat{E}_{y+}^{se}(s,0)G_+^{ae}(s) = \hat{E}_{y-}^{se}(s,0)/G_-^{ae}(s) - D_-^{ae}(s), \tau_- < \tau < \tau_+. \quad (4.22)$$

By analytic continuation, both sides of equation (4.22) are equal to a polynomial $P(s)$ ($P(s)$ is an entire function which is unknown at this point) such that

$$D_+^{ae}(s) - \hat{E}_{y+}^{se}(s,0)G_+^{ae}(s) = \hat{E}_{y-}^{se}(s,0)/G_-^{ae}(s) - D_-^{ae}(s) = P(s) \text{ for all } s \quad (4.23)$$

where

$$P(s) = C_0 + C_1s + C_2s^2 + \dots + C_ns^n \quad (4.24)$$

In order to obtain unique solutions for \hat{E}_{y+}^{se} and \hat{E}_{y-}^{se} , it is necessary to determine the unknown coefficients $\{C_i\}_{i=0}^n$. In Chapter III, the coefficients of the polynomial $P(s)$ were determined by examining the asymptotic behavior of both sides of equation (3.65). The same procedure will be followed in this chapter. Using the results of Chapter III, one obtains

$$G_+^{ae}(s) \sim 1 \quad \text{as } |s| \rightarrow \infty \quad \text{for } \tau > \tau_- \quad (4.25)$$

$$G_-^{ae}(s) \sim 1 \quad \text{as } |s| \rightarrow \infty \quad \text{for } \tau < \tau_+ \quad (4.26)$$

$$D_+^{ae}(s) \sim s^{-1} \quad \text{as } |s| \rightarrow \infty \quad \text{for } \tau > \tau_- \quad (4.27)$$

$$D_-^{ae}(s) \sim s^{-1} \quad \text{as } |s| \rightarrow \infty \quad \text{for } \tau < \tau_+ \quad (4.28)$$

Thus, the asymptotic behavior of \hat{E}_{y+}^{se} and \hat{E}_{y-}^{se} remains to be determined. It is shown in Appendix B that the behavior of the transverse components E_y and H_y near an edge is more singular than that of the tangential

components E_z and H_z by a factor of ρ^{-1} (see Equation (B.6)). It follows from Equations (A.13) and (A.15) that

$$\hat{E}_{y+}^{se}(s,0) \sim \hat{u}_{e+}^s(s,0)s \quad \text{as } |s| \rightarrow \infty \text{ for } \tau > \tau_- \quad (4.29)$$

$$\hat{E}_{y-}^{se}(s,0) \sim \hat{u}_{e-}^s(s,0)s \quad \text{as } |s| \rightarrow \infty \text{ for } \tau < \tau_+ \quad (4.30)$$

Substituting Equations (3.66) and (3.67) into (4.29) and (4.30), respectively, one obtains

$$\hat{E}_{y+}^{se}(s,0) \sim s^0 \quad \text{as } |s| \rightarrow \infty \text{ for } \tau > \tau_- \quad (4.31)$$

$$\hat{E}_{y-}^{se}(s,0) \sim s^0 \quad \text{as } |s| \rightarrow \infty \text{ for } \tau < \tau_+ \quad (4.32)$$

Moreover, substituting (4.25)-(4.32) into (4.22) yields

$$\left| D_+^{ae}(s) - \hat{E}_{y+}^{se}(s,0)G_+^{ae}(s) \right| \sim s^0 \quad \text{as } |s| \rightarrow \infty \text{ for } \tau > \tau_- \quad (4.33)$$

$$\left| \hat{E}_{y-}^{se}(s,0)/G_-^{ae}(s) - D_-^{ae}(s) \right| \sim s^0 \quad \text{as } |s| \rightarrow \infty \text{ for } \tau < \tau_+ \quad (4.34)$$

It follows from (4.23) that

$$P(s) \sim s^0 \quad \text{as } |s| \rightarrow \infty \quad (4.35)$$

Thus, at most the polynomial $P(s)$ can be a constant such that

$$P(s) = C_a^e \quad (4.36)$$

It will be shown later that indeed, $P(s)$ has to be a nonzero constant in order to obtain solutions that satisfy the radiation condition.

Substituting Equation (4.36) into (4.23) and solving for $\hat{E}_{y+}^{se}(s,0)$ and $\hat{E}_{y-}^{se}(s,0)$, one obtains

$$\hat{E}_{y+}^{se}(s,0) = (D_+^{ae}(s) - C_a^e)/G_+^{ae}(s) \quad (4.37)$$

$$\hat{E}_{y-}^{se}(s,0) = (C_a^e + D_-^{ae}(s))G_-^{ae}(s) \quad (4.38)$$

where the unknown constant C_a^e has to be determined. Combining Equations (4.37) and (4.38), the expression for \hat{E}_y^{se} becomes

$$\hat{E}_y^{se}(x,y,z) = [\hat{E}_{y+}^{se}(s,0) + \hat{E}_{y-}^{se}(s,0)] \exp(ik_z^i z + i\beta y), \quad y > 0, \quad \tau_- < \tau < \tau_+. \quad (4.39)$$

Substituting Equations (4.20), (4.21), (4.37) and (4.38) into (4.39) yields

$$\hat{E}_y^{se} = \frac{G_-^{ae}(s)}{\beta} \left[\frac{iE_{cy} k_y^i (1-R_a)}{\sqrt{2\pi} (s+k_x^i) G_-^{ae}(-k_x^i)} - k \delta_a C_a^e \right] e^{i(\beta y + k_z^i z)}, \quad y > 0, \quad \tau_- < \tau < \tau_+. \quad (4.40)$$

Finally, taking the inverse Fourier transform of (4.40), one gets

$$E_y^{se}(x,y,z) = \frac{1}{\sqrt{2\pi}} \int_{-\infty+ia}^{\infty+ia} \hat{E}_y^{se}(s,y,z) \exp(-isx) ds \quad (4.41)$$

where the path of integration is shown in Figure 3.4. Before the

constant C_a^e is determined, the general form of the solution for the TE_y polarization will also be obtained next.

2. TE_y polarization (H_y^0 , odd problem)

In this case, the incident field is

$$H_y^i(x,y,z) = H_{cy} \exp(i(k_x^i x - k_y^i y + k_z^i z)) \quad , \quad y > 0 \quad (4.42)$$

where H_{cy} is an arbitrary constant. The total field H_y satisfies the boundary conditions given in Equations (4.2) and (2.33), and the differential equation (2.37).

Since $H_y^0(x,y,z)$ satisfies the same boundary conditions and differential equation as the odd field $u_0(x,y)$ in Chapter III, one can use the results of Chapter III in this section. On the other hand, one notes that $u_0(x,y)$ and $H_y^0(x,y,z)$ satisfy different edge conditions at the origin $x=y=0$, and as shown in the previous section, this difference has an important effect in the final solution for $\hat{H}_y^0(s,y,z)$.

As in Chapter III, let H_y^0 be equal to

$$H_y^0(x,y,z) = H_y^{s0}(x,y,z) + H_y^i(x,y,z) + \tilde{H}_y^r(x,y,z) \quad , \quad y > 0 \quad (4.43)$$

where $\tilde{H}_y^r(x,y,z)$ is the unperturbed reflected field given by

$$\tilde{H}_y^r(x,y,z) = H_{cy} R_h(\phi', \theta', \delta_h) \exp(i(k_x^i x + k_y^i y + k_z^i z)) \quad , \quad (4.44)$$

in which

$$R_h(\phi', \theta', \delta_h) = \frac{\sin \phi' - \delta_h / \sin \theta'}{\sin \phi' + \delta_h / \sin \theta'} \quad (4.45)$$

is the Fresnel reflection coefficient for an impedance wall.

The scattered field $H_y^{SO}(x, y, z)$ can be obtained by the same approach used in Chapter III. Without repeating the analysis, it follows from (3.131) that the Wiener-Hopf equation is given by

$$iD_+^{ho}(s) + G_+^{ho}(s) \hat{H}_{y+}^{SO}(s, 0) = \frac{-\hat{H}_{y-}^{SO}(s, 0)}{iG_-^{ho}(s)} - iD_-^{ho}(s), \quad \tau_- < \tau < \tau_+ \quad (4.46)$$

where τ_- and τ_+ were defined in (4.13) and (4.14), respectively. It follows from Equations (3.129) and (3.130) that D_+^{ho} and D_-^{ho} are given by

$$D_+^{ho}(s) = \frac{H_{cy} i(1+R_h)}{\sqrt{2\pi} (s+k_x')} \left[\frac{1}{G_-^{ho}(-k_x')} - k\delta_h G_+^{ho}(s) \right] \quad (4.47)$$

$$D_-^{ho}(s) = \frac{H_{cy} i(1+R_h)}{\sqrt{2\pi} (s+k_x')} \left[\frac{1}{G_-^{ho}(s)} - \frac{1}{G_-^{ho}(-k_x')} \right] \quad (4.48)$$

and

$$G^{ho}(s) = 1/(\beta + k\delta_h) = G_+^{ho}(s) G_-^{ho}(s) \quad (4.49)$$

The expressions for $G_-^{ho}(s)$ and $G_+^{ho}(s)$ are given in Appendix D, and the

notation $\hat{H}_{y+}^{so}(s,0)$ means

$$\hat{H}_{y+}^{so}(s,0) = \frac{d}{dy} \hat{H}_{y+}^{so}(s,y) \quad \text{at } y=0 \quad . \quad (4.50)$$

Since all the functions in Equation (4.46) have a common region of regularity (the strip defined by $\tau_+ < \tau < \tau_-$), one concludes (by analytic continuation) that both sides of (4.46) are equal to an entire function $D(s)$ which happens to be a polynomial in s such that

$$iD_+^{ho}(s) + G_+^{ho}(s) \hat{H}_{y+}^{so}(s,0) = \frac{-\hat{H}_{y-}^{so}(s,0)}{iG_-^{ho}(s)} - iD_-^{ho}(s) = D(s) \quad \text{for all } s \quad (4.51)$$

where

$$D(s) = d_0 + d_1 s + d_2 s^2 + \dots + d_n s^n \quad . \quad (4.52)$$

Note that all the coefficients $\{d_i\}$ are unknown at this point in the analysis. Moreover, as in the TMy polarization, the asymptotic behavior of all the functions in Equation (4.51) have to be determined. It was shown in Chapter III that

$$G_+^{ho}(s) \sim s^{-1/2} \quad \text{as } |s| \rightarrow \infty \quad \text{for } \tau > \tau_- \quad (4.53)$$

$$G_-^{ho}(s) \sim s^{-1/2} \quad \text{as } |s| \rightarrow \infty \quad \text{for } \tau < \tau_+ \quad (4.54)$$

$$D_+^{ho}(s) \sim s^{-1} \quad \text{as } |s| \rightarrow \infty \quad \text{for } \tau > \tau_- \quad (4.55)$$

$$D_-^{ho}(s) \sim s^{-1/2} \quad \text{as } |s| \rightarrow \infty \quad \text{for } \tau < \tau_+ \quad . \quad (4.56)$$

By the same arguments as in the case of TMy polarization, the asymptotic behavior of $\hat{H}_{y+}^{so}(s,0)$ and $\hat{H}_{y-}^{so}(s,0)$ can be obtained as follows:

$$\hat{H}_{y-}^{so}(s,0) \sim \hat{u}_{0-}^s(s,0)s \quad \text{as } |s| \rightarrow \infty \quad \text{for } \tau < \tau_+ \quad (4.57)$$

$$\hat{H}_{y+}^{so}(s,0) \sim \hat{u}_{0+}^s(s,0)s \quad \text{as } |s| \rightarrow \infty \quad \text{for } \tau > \tau_- \quad . \quad (4.58)$$

Substituting Equations (3.144) and (3.145) into (4.57) and (4.58), respectively, yields

$$\hat{H}_{y-}^{so}(s,0) \sim s^0 \quad \text{as } |s| \rightarrow \infty \quad \text{for } \tau < \tau_+ \quad (4.59)$$

$$\hat{H}_{y+}^{so}(s,0) \sim s^{1/2} \quad \text{as } |s| \rightarrow \infty \quad \text{for } \tau > \tau_- \quad . \quad (4.60)$$

Using Equations (4.53)-(4.60) in (4.51), one obtains

$$\left| iD_+^{ho}(s) + \hat{H}_{y+}^{so}(s,0)G_+^{ho}(s) \right| \sim s^0 \quad \text{as } |s| \rightarrow \infty \quad \text{for } \tau > \tau_- \quad (4.61)$$

$$\left| i\hat{H}_{y-}^{so}(s,0)/G_-^{ho}(s) - iD_-^{ho}(s) \right| \sim s^{1/2} \quad \text{as } |s| \rightarrow \infty \quad \text{for } \tau < \tau_+ \quad . \quad (4.62)$$

By the extended form of Liouville's theorem [32], the polynomial $D(s)$ is of degree less than or equal to the integral part of $\min(0, 1/2)$.

That is,

$$D(s) = d_h^0 \quad (4.63)$$

where d_h^0 is still an unknown constant.

Solving for $\hat{H}_{y-}^{so}(s,0)$ in (4.51), one obtains

$$\hat{H}_{y-}^{so}(s,0) = -iG_-^{ho}(s)[d_h^0 + i D_-^{ho}(s)] \quad (4.64)$$

The expression for $\hat{H}_+^{so}(s,0)$ can be obtained from (3.148) by replacing v by H_{cy} such that

$$\hat{H}_{y+}^{so}(s,0) = \frac{-iH_{cy}(1+R_h)}{\sqrt{2\pi}(s+k_x^i)} \quad (4.65)$$

It follows from (3.113) that $\hat{H}_y^{so}(s,y,z)$ is given by

$$\hat{H}_y^{so}(s,y,z) = [\hat{H}_{y+}^{so}(s,0) + \hat{H}_{y-}^{so}(s,0)] \exp(ik_z^i z + i\beta y), \quad y > 0, \tau_- < \tau < \tau_+ \quad (4.66)$$

Substituting Equations (4.48), (4.64) and (4.65) into (4.66) yields

$$\hat{H}_y^{so} = \frac{G_-^{ho}(s)}{i} \left[\frac{H_{cy}(1+R_h)}{\sqrt{2\pi}(s+k_x^i)G_-^{ho}(-k_x^i)} + d_h^0 \right] e^{i(\beta y + k_z^i z)}, \quad y > 0, \tau_- < \tau < \tau_+ \quad (4.67)$$

Finally, taking the inverse Fourier transform of (4.67), one obtains

$$H_y^{SO}(x,y,z) = \frac{1}{\sqrt{2\pi}} \int_{-\infty+ib}^{\infty+ib} \hat{H}_y^{SO}(s,y,z) \exp(-isx) ds, \quad y>0, \quad \tau_- < \tau < \tau_+ \quad (4.68)$$

where the path of integration is shown in Figure 3.4.

3. Determination of the constants C_a^e and d_h^0

In order to determine the unknown constants C_a^e and d_h^0 , it is necessary to solve for the other field components, i.e., \hat{E}_x , \hat{E}_z , \hat{H}_x , \hat{H}_z , in terms of the normal field components \hat{E}_y and \hat{H}_y . It is shown in Appendix I that the following relations hold; namely,

$$\hat{E}_x(s,y,z) = \frac{ik_z' k \hat{H}_y(s,y,z) + i\gamma_0 s \beta \hat{E}_y(s,y,z)}{i\gamma_0 (s^2 + k_z'^2)} \quad (4.69)$$

$$\hat{E}_z(s,y,z) = \frac{k\eta_0 s \hat{H}_y(s,y,z) - k_z' \beta \hat{E}_y(s,y,z)}{(s^2 + k_z'^2)} \quad (4.70)$$

$$\hat{H}_x(s,y,z) = \frac{-ik_z' k \hat{E}_y(s,y,z) + i\eta_0 s \beta \hat{H}_y(s,y,z)}{i\eta_0 (s^2 + k_z'^2)} \quad (4.71)$$

$$\hat{H}_z(s,y,z) = \frac{-k\gamma_0 s \hat{E}_y(s,y,z) - k_z' \hat{H}_y(s,y,z)}{(s^2 + k_z'^2)} \quad (4.72)$$

Note that all the four expressions above have two poles at

$$s = ik_z' = -ik\cos\theta' \quad , \quad 0 < \theta' < \pi \quad (4.73)$$

and

$$s = -ik_z' = ik\cos\theta' \quad , \quad 0 < \theta' < \pi \quad (4.74)$$

Taking the inverse Fourier transform of Equations (4.69)-(4.72), one gets

$$E_x^S(x,y,z) = \frac{1}{\sqrt{2\pi}} \int_{-\infty+ic}^{\infty+ic} \hat{E}_x^S(s,y,z) \exp(-isx) ds \quad , \quad y>0 \quad \tau_- < \tau < \tau_+ \quad (4.75)$$

$$E_z^S(x,y,z) = \frac{1}{\sqrt{2\pi}} \int_{-\infty+ic}^{\infty+ic} \hat{E}_z^S(s,y,z) \exp(-isx) ds \quad , \quad y>0 \quad \tau_- < \tau < \tau_+ \quad (4.76)$$

$$H_x^S(x,y,z) = \frac{1}{\sqrt{2\pi}} \int_{-\infty+ic}^{\infty+ic} \hat{H}_x^S(s,y,z) \exp(-isx) ds \quad , \quad y>0 \quad \tau_- < \tau < \tau_+ \quad (4.77)$$

$$H_z^S(x,y,z) = \frac{1}{\sqrt{2\pi}} \int_{-\infty+ic}^{\infty+ic} \hat{H}_z^S(s,y,z) \exp(-isx) ds \quad , \quad y>0 \quad \tau_- < \tau < \tau_+ \quad (4.78)$$

The next step in the analysis is to examine the poles at $\pm ik \cos \theta'$ and determine what kind of fields they contribute, and whether or not these fields are physically possible. Let s_1 and s_2 , shown in Figure (4.1), be defined as follows:

$$s_1 = ik |\cos \theta'| \quad (4.79)$$

$$s_2 = -ik |\cos \theta'| \quad (4.80)$$

For $x < 0$, the path of integration in Equations (4.75)-(4.78) can be closed in the upper s -plane as depicted in Figure 4.1 such that

$$\int_{-\infty+ic}^{\infty+ic} g(s) e^{-isx} ds + \int_{\Gamma_1} g(s) e^{-isx} ds = \int_{\Gamma_1} g(s) e^{-isx} ds, \quad x < 0, y > 0 \quad (4.81)$$

where $g(s)$ represents any of the fields in Equations (4.69)-(4.72). Note that for $x < 0$, only the pole s_1 will be captured. Applying Cauchy's Residue Theorem in (4.81) yields an expression of the form

$$\exp(iky - is_1 x) = \exp(ik_1 y + ik_2 |\cos \theta'| x) \exp(-k_2 y + k_1 |\cos \theta'| x), \quad x < 0 \quad (4.82)$$

where k was defined in Equation (1.7). At $s=s_1$ or s_2 , the function β is equal to

$$\beta(s=s_1 \text{ or } s_2) = (K^2 + k^2 \cos^2 \theta')^{1/2} = k_1 + ik_2 = k \quad (4.83)$$

on the top Riemann sheet ($\text{Im} \beta > 0$).

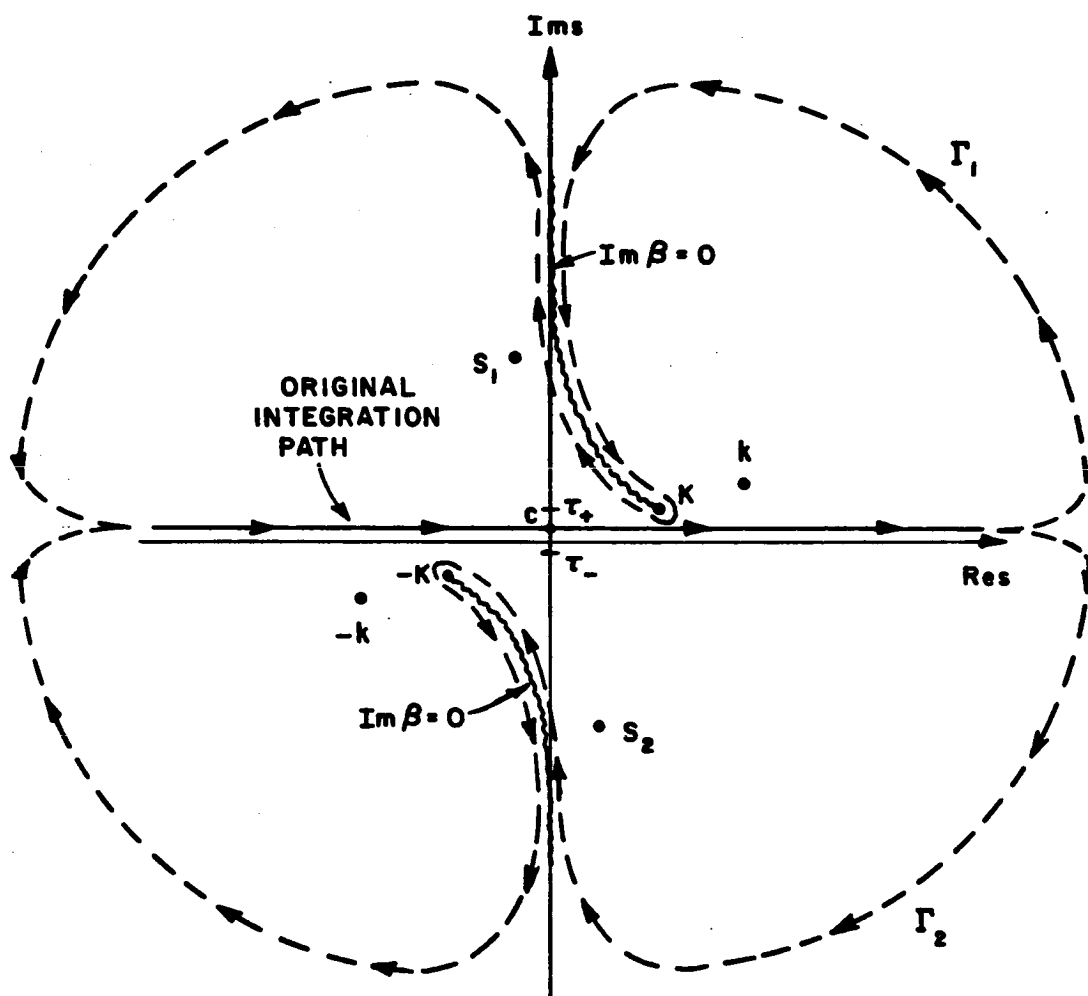


Figure 4.1. Integration paths on top Riemann sheet: $\text{Im}(\beta) > 0$.

The expression in (4.82) does not satisfy the radiation condition since it represents a wave which propagates towards the origin ($x=0=y=z$). Likewise, for $x > 0$, the path of integration in Equations (4.75)-(4.78) can be closed in the lower s -plane as illustrated in Figure 4.1 such that

$$\int_{-\infty+ic}^{\infty+ic} g(s) e^{-isx} ds + \int_{\Gamma_2} g(s) e^{-isx} ds = \oint g(s) e^{-isx} ds, \quad x > 0, y > 0. \quad (4.84)$$

As shown in Figure 4.1, only the pole s_2 is captured for $x > 0$. Applying Cauchy's Residue Theorem in (4.84), one obtains an expression which is proportional to

$$\exp(iky - is_2x) = \exp(ik_1y - ik_2|\cos\theta'|x) \exp(-k_2y - k_1|\cos\theta'|x), \quad x > 0. \quad (4.85)$$

This expression also represents a wave which propagates towards the origin in violation of the radiation condition.

Thus, the poles s_1 and s_2 , which contribute waves that do not satisfy the radiation condition, are not valid poles. Consequently, the numerators of Equations (4.69)-(4.72) should be equal to zero when s is equal to s_1 or s_2 . It can be shown that by setting the numerators of (4.69)-(4.72) equal to zero at $s=s_1$ and s_2 , one obtains only two equations:

$$i\eta_0 \hat{H}_y'(ik_z) - \hat{E}_y'(ik_z) = 0 \quad (4.86)$$

$$i\eta_0 \hat{H}_y(-ik_z') + \hat{E}_y(-ik_z') = 0 \quad (4.87)$$

Substituting (4.40) and (4.67) into (4.86) and (4.87) yields

$$\begin{aligned} G_-^{ae}(ik_z') \left[\frac{iE_{cy} k_y' (1-R_a)}{\sqrt{2\pi} (ik_z' + k_x') G_-^{ae}(-k_x') k} - \delta_a C_a^e \right] = \\ \eta_0 G_-^{ho}(ik_z') \left[\frac{H_{cy} (1+R_h)}{\sqrt{2\pi} (k_x' + ik_z') G_-^{ho}(-k_x')} + d_h^o \right] \end{aligned} \quad (4.88)$$

$$\begin{aligned} \eta_0 G_-^{ho}(-ik_z') \left[\frac{H_{cy} (1+R_h)}{\sqrt{2\pi} (k_x' - ik_z') G_-^{ho}(-k_x')} + d_h^o \right] = \\ -G_-^{ae}(-ik_z') \left[\frac{iE_{cy} k_y' (1-R_a)}{\sqrt{2\pi} (-ik_z' + k_x') G_-^{ae}(-k_x') k} - \delta_a C_a^e \right] \end{aligned} \quad (4.89)$$

The last two equations can be used to determine the two constants C_a^e and d_h^o such that

$$C_a^e = \frac{iE_{cy}k_y'(1-R_a)k_x'}{\sqrt{2\pi}(k_z'^2 + k_x'^2)G_-^{ae}(-k_x')k\delta_a} + \frac{ik_z'k}{\sqrt{2\pi}(k_z'^2 + k_x'^2)k\delta_a|\bar{B}_{ce}|} \cdot \left[\frac{-iE_{cy}k_y'(1-R_a)|\bar{A}_{ce}|}{G_-^{ae}(-k_x')k} + \frac{H_{cy}\eta_0 2(1+R_h)G_-^{ho}(ik_z')}{G_-^{ho}(-k_x')} \right] \quad (4.90)$$

$$d_h^o = \frac{-H_{cy}(1+R_h)k_x'}{\sqrt{2\pi}(k_z'^2 + k_x'^2)G_-^{ho}(-k_x')} + \frac{ik_z'}{\sqrt{2\pi}(k_z'^2 + k_x'^2)|\bar{B}_{ce}|} \cdot \left[\frac{H_{cy}(1+R_h)|\bar{A}_{ce}|}{G_-^{ho}(-k_x')} + \frac{2E_{cy}k_y'(1-R_a)G_-^{ae}(ik_z')}{ik\eta_0 G_-^{ae}(-k_x')} \right] \quad (4.91)$$

where

$$\bar{\bar{A}}_{ce} = \begin{bmatrix} G_-^{ho}(ik_z') & G_-^{ae}(ik_z') \\ G_-^{ho}(-ik_z') & G_-^{ae}(-ik_z') \end{bmatrix} \quad (4.92)$$

$$\bar{\bar{B}}_{ce} = \begin{bmatrix} G_-^{ho}(ik_z') & G_-^{ae}(ik_z') \\ -G_-^{ho}(-ik_z') & G_-^{ae}(-ik_z') \end{bmatrix} \quad (4.93)$$

Note that the two bars above \bar{A} and \bar{B} denote a matrix. Furthermore, $|\bar{A}|$ and $|\bar{B}|$ are the determinants of the matrices \bar{A} and \bar{B} , respectively.

Evaluating Equations (4.15) and (4.49) at $s = \mp i k_z'$, one gets

$$G_-^{ae}(i k_z') = G_-^{ae}(-i k_z') = \frac{1}{1 + \delta_a} \quad (4.94)$$

$$G_-^{ho}(i k_z') = G_-^{ho}(-i k_z') = \frac{1}{(1 + \delta_h)k} \quad (4.95)$$

The functions $G_-^{ae}(\mp i k_z')$ and $G_-^{ho}(\mp i k_z')$ will be defined in section D.

It is easy to show that C_a^e is proportional to k^{-1} , while d_h^o is proportional to $k^{-1/2}$. Furthermore, note that both C_a^e and d_h^o are functions of H_{cy} and E_{cy} . This implies that if the incident wave is TE_y or TM_y polarized, it will excite a diffracted field that has both polarizations. In other words, there is coupling between the TE_y and TM_y polarizations, which was not the case in Chapter III where the direction of propagation of the incident field was normal to the edge (z-axis). In order to show that the TE_y and TM_y polarizations decoupled for the case of normal incidence, let $k_z = 0$ ($\theta' = \pi/2$) in Equations (4.90) and (4.91) such that

$$C_a^e = \frac{i E_{cy} k_y' (1 - R_a)}{\sqrt{2\pi} k_x' G_-^{ae}(-k_x') k \delta_a}, \quad k_z' = 0 \quad (4.96)$$

$$d_h^o = \frac{-H_{cy} (1 + R_h)}{\sqrt{2\pi} k_x' G_-^{ho}(-k_x')}, \quad k_z' = 0 \quad (4.97)$$

As expected, the constant C_a^e is only a function of E_{cy} , while d_h^0 is only a function of H_{cy} .

Following the work in Chapter III, let the constant ξ be defined as done earlier; i.e.,

$$\cos \xi = \cos(\xi_r + i\xi_i) = \delta / \sin \theta' \quad , \quad \begin{array}{l} 0 \leq \text{Re}(\xi) < \pi/2 \\ 0 < \theta' < \pi/2 \end{array} \quad (4.98)$$

Thus, for the TMy polarization (E_y)

$$\cos \xi^a = \delta_a / \sin \theta' = Z_s / (n_0 \sin \theta') \quad (4.99)$$

and for the TEy polarization (H_y)

$$\cos \xi^h = \delta_h / \sin \theta' = n_0 / (Z_s \sin \theta') \quad (4.100)$$

C. PMC CASE

1. TMy Polarization (E_y^0 , odd problem)

In this case, the field \hat{E}_y^0 satisfies the same type of boundary conditions as \hat{H}_y^0 in section B. Thus, the solution for \hat{E}_y^0 can be simply obtained by duality [20]; i.e.,

$$\hat{E}_y^0(E_{cy}, H_{cy}, \xi^a, \xi^h, n_0, Y_0) = \hat{H}_y^0(H_{cy}, -E_{cy}, \xi^h, \xi^a, Y_0, n_0) \quad (4.101)$$

Substituting (4.67) into (4.101) yields

$$\hat{E}_y^{so} = \frac{G_-^{ao}(s)}{i} \left[\frac{E_{cy} (1+R_a)}{\sqrt{2\pi} (s+k_x') G_-^{ao}(-k_x')} + C_a^0 \right] e^{i(\beta y + k_z' z)}, \quad \tau_- < \tau < \tau_+, \quad y > 0. \quad (4.102)$$

The constant C_a^0 is given by

$$C_a^0 = \frac{-E_{cy}(1+R_a)k_x'}{\sqrt{2\pi} (k_z'^2 + k_x'^2) G_-^{ao}(-k_x')} + \frac{ik_z'}{\sqrt{2\pi} (k_z'^2 + k_x'^2) |\bar{B}_{co}|} \cdot \left[\frac{E_{cy}(1+R_a) |\bar{A}_{co}|}{G_-^{ao}(-k_x')} - \frac{2H_{cy} \eta_0 k_y' (1-R_h) G_-^{he}(ik_z')}{ik G_-^{he}(-k_x')} \right] \quad (4.103)$$

where

$$\bar{A}_{co} = \begin{bmatrix} G_-^{ao}(ik_z') & G_-^{he}(ik_z') \\ G_-^{ao}(-ik_z') & G_-^{he}(-ik_z') \end{bmatrix} \quad (4.104)$$

$$\bar{B}_{co} = \begin{bmatrix} G_-^{ao}(ik_z') & G_-^{he}(ik_z') \\ -G_-^{ao}(-ik_z') & G_-^{he}(-ik_z') \end{bmatrix} \quad (4.105)$$

and

$$G^{he}(ik_z') = G^{he}(-ik_z') = \frac{1}{1 + \delta_h} \quad . \quad (4.106)$$

The functions $G_-^{ao}(\mp ik_z)$ and $G_-^{he}(\mp ik_z)$ will be defined in section D. Furthermore, the constant C_a^0 is proportional to $k^{-1/2}$ which is not surprising, since it was derived from d_h^0 .

Taking the inverse Fourier transform of (4.102), one obtains

$$E_y^{so}(x,y,z) = \frac{1}{\sqrt{2\pi}} \int_{-\infty+ib}^{\infty+ib} \hat{E}_y^{so}(s,y,z) \exp(-isx) ds, \quad y \geq 0, \quad \tau_- < \tau < \tau_+ \quad (4.107)$$

where the path of integration is depicted in Figure 3.4. Finally, the total field E_y^0 can be expressed as follows:

$$E_y^0(x,y,z) = E_y^i(x,y,z) + \tilde{E}_y^r(x,y,z) + E_y^{so}(x,y,z), \quad y \geq 0 \quad . \quad (4.108)$$

2. TE_y Polarization (H_y^e , even problem)

For this polarization, the field H_y^e satisfies similar boundary conditions as E_y^e in section B. As in the odd TMy case, the solution for H_y can be obtained by duality such that

$$\hat{H}_y^e(H_{cy}, -E_{cy}, \xi^h, \xi^a, \eta_0, \gamma_0) = \hat{E}_y^e(E_{cy}, H_{cy}, \xi^a, \xi^h, \gamma_0, \eta_0) \quad . \quad (4.109)$$

Substituting (4.40) into (4.109) yields

$$\hat{H}_y^{se} = \frac{G_-^{he}(s)}{\beta} \left[\frac{-iH_{cy} k_y' (1-R_h)}{\sqrt{2\pi} (s+k_x') G_-^{he}(-k_x')} - k\delta_h d_h^e \right] e^{i(\beta y + k_z' z)} , \quad \begin{matrix} \tau_- < \tau < \tau_+ \\ y > 0 \end{matrix} \quad (4.110)$$

The constant d_h^e , which is proportional to k^{-1} , is given by

$$d_h^e = \frac{iH_{cy} k_y' (1-R_h) k_x'}{\sqrt{2\pi} (k_z'^2 + k_x'^2) G_-^{he}(-k_x') k\delta_h} + \frac{ik_z' k}{\sqrt{2\pi} (k_z'^2 + k_x'^2) k\delta_h |\bar{B}_{co}|} \cdot \left[\frac{-iH_{cy} k_y' (1-R_h) |\bar{A}_{co}|}{G_-^{he}(-k_x') k} - \frac{E_{cy} \gamma_o^2 (1+R_a) G^{ao}(ik_z')}{G_-^{ao}(-k_x')} \right] \quad (4.111)$$

where

$$G^{ao}(ik_z') = G^{ao}(-ik_z') = \frac{1}{(1 + \delta_a)k} \quad (4.112)$$

The scattered field H_y^{se} is obtained by taking the inverse Fourier transform of (4.110), that is

$$H_y^{se}(x,y,z) = \frac{1}{\sqrt{2\pi}} \int_{-\infty+ia}^{\infty+ia} \hat{H}_y^{se}(s,y,z) \exp(-isx) ds , \quad \begin{matrix} y > 0 \\ \tau_- < \tau < \tau_+ \end{matrix} \quad (4.113)$$

where the path of integration is depicted in Figure 3.4. The last step in this section is to determine the total field H_y^e which can be

obtained from Equation (4.43) as follows:

$$H_y^e(x,y,z) = H_y^i(x,y,z) + \tilde{H}_y^r(x,y,z) + H_y^{se}(x,y,z), \quad y > 0 \quad (4.114)$$

where H_y^i and \tilde{H}_y^r are given in Equations (4.42) and (4.44), respectively.

D. ASYMPTOTIC ANALYSIS

As in Chapter III, before the asymptotic analysis is performed, it is necessary to map from the s -domain to the periodic w -domain where the saddle point method can be applied conveniently. Thus, define w such that

$$s = -K \cos w \quad . \quad (4.115)$$

Substituting (4.115) into (4.17) yields

$$\beta = K \sin w \quad (4.116)$$

where it is assumed that $K=K_1=k_1 \sin \theta'$ is real ($K_2=0$, lossless medium). Equations (4.115) and (4.116) are the same as Equations (3.161) and (3.162), respectively, except that k has been replaced by K .

1. PEC Case, TM_y Polarization (E_y^e , even problem)

Substituting Equations (4.115), (4.116), (3.163), and (4.5) into (4.41), one gets

$$E_y^{se}(\rho, \phi, z) = \frac{e^{ik_z' z}}{2\pi i} \int_{\Gamma_w^e} G_-^{ae}(-K \cos w) \left[\frac{E_{cy} \sin \phi' (1 - R_a^e)}{(\cos w + \cos \phi') G_-^{ae}(K \cos \phi')} \right. \\ \left. - i\sqrt{2\pi} k \delta_a^e C_a^e \right] e^{iK\rho \cos(w-\phi)} dw, \quad \begin{matrix} 0 < \phi < \pi \\ 0 < \phi' < \pi \end{matrix} \quad (4.117)$$

where the path of integration is shown in Figure (3.9). Note that the integrand in Equation (4.117) has the same poles as the integrand in Equation (3.164) which are also shown in Figure (3.9).

At this point in the analysis, it is convenient to write the expressions for the functions G^e and G^0 . Substituting Equations (4.116) and (4.98) into (4.15) and (4.49) one obtains an expression for G^e identical to Equation (3.186), while the expression for G^0 is the same as Equation (3.221), except that k is replaced by K . It follows that $G_+^e(-K \cos w)$ is given by (3.187), while $G_-^e(-K \cos w)$ is given by (3.188). Likewise, the expressions for $G_+^0(-K \cos w)$ and $G_-^0(-K \cos w)$ are given by Equations (3.222) and (3.223), respectively, except that k is replaced by K . The superscript a or h is attached to the functions G^a , G^h , G_+^a , G_+^h when $\xi = \xi^a$ (TM_y) or $\xi = \xi^h$ (TE_y), respectively.

Following the same procedure as in Chapter III, the total field E_y^e can be expressed as follows:

$$E_y^e(\rho, \phi, z) = E_y^i(\rho, \phi, z) + E_y^{re}(\rho, \phi, z) + E_{ye}^{sw}(\rho, \phi, z) + E_y^{de}(\rho, \phi, z) \quad (4.118)$$

where the incident field E_y^i is given in Equation (4.7) and

$$E_y^{re}(\rho, \phi, z) = E_{cy} \Lambda_a^e(\phi') \exp[i(-K\rho \cos(\phi + \phi') + k_z' z)] , \quad \begin{matrix} 0 < (\phi, \phi') < \pi \\ 0 < \theta' < \pi \end{matrix} \quad (4.119)$$

is the reflected field where Λ_a^e is given by

$$\Lambda_a^e(\phi') = \begin{cases} 1 & \text{for } \phi + \phi' < \pi \\ R_a^e(\phi') & \text{for } \phi + \phi' > \pi \end{cases} \quad (4.120)$$

The contribution from the pole w_s^{ae} (pole of $G_-^{ae}(-K \cos w)$), which was defined in Equation (3.167), is the surface wave field $E_{ye}^{sw}(\rho, \phi, z)$. This field is given by the following expression:

$$E_{ye}^{sw}(\rho, \phi, z) = \frac{-e^{ik_z' z} \sqrt{2}}{(\sin \xi^{ae})^{1/2}} \exp(-J_1^{ae}(w_s^{ae})/(2\pi)) U(\phi - \tilde{\phi}_s^{ae})$$

$$\cdot \left[\frac{E_{cy} \cos \xi^{ae}}{\sin \phi' + \cos \xi^{ae}} \exp(-J_1^{ae}(\phi')/(2\pi)) \left[\sec((w_s^{ae} + \phi')/2) + \sec((w_s^{ae} - \phi')/2) \right] \right.$$

$$\cdot (\sin \xi^{ae} - \cos \phi')^{1/2} - i\sqrt{2\pi} k \delta_a C_a^e \sqrt{2} \cos(w_s^{ae}/2) \left. \right]$$

$$\cdot \exp(iK(x \cos w_s^{ae} + y \sin w_s^{ae})) \quad (4.121)$$

where $\tilde{\phi}_s^{ae}$ was defined in Equation (3.203). Note that the superscript e has been added to δ and ξ . When this solution is generalized to treat dielectric/ferrite materials, δ_a^e in general will not be equal to δ_a^0 .

The last component of the total field E_y^e is the diffracted field E_y^{de} which is given by the following integral:

$$\begin{aligned}
 E_y^{de}(\rho, \phi, z) = & \frac{e^{ik_z' z}}{2\pi i} \int_{\text{CSDP}} \frac{e^{iK\rho \cos(w-\phi)}}{\sin w + \cos \xi^{ae}} \exp(-J_1^{ae}(w)/(2\pi)) \\
 & \cdot \left[\sec((w+\phi')/2) + \sec((w-\phi')/2) \right] \cdot (\sin \xi^{ae} - \cos w)^{1/2} \\
 & \cdot \left[E_{cy}(1 - R_a^e)/2 (\sin \xi^{ae} - \cos \phi')^{1/2} \exp(-J_1^{ae}(\phi')/(2\pi)) \right. \\
 & \left. + \sqrt{4\pi} k \delta_a^e C_a^e \frac{(\cos w + \cos \phi')}{4i \cos(\phi'/2)} \right] dw \quad . \quad (4.122)
 \end{aligned}$$

For large $K\rho$, the integral in (4.122) can be evaluated using the saddle point method. The expression for E_y^{de} becomes

$$\begin{aligned}
E_y^{de}(\rho, \phi, z) = & \frac{-e^{i\pi/4} \exp(-J_1^{ae}(\phi)/(2\pi))}{\sqrt{2\pi K\rho} (\sin\phi + \cos\xi^{ae})} (\sin\xi^{ae} - \cos\phi)^{1/2} e^{i(K\rho + k'_z z)} \\
& \cdot \left[\sec((\phi+\phi')/2)F(-KLa^+) + \sec((\phi-\phi')/2)F(-KLa^-) \right] \\
& \cdot \left[E_{cy}(1 - R_a^e)/2 (\sin\xi^{ae} - \cos\phi')^{1/2} \exp(-J_1^{ae}(\phi')/(2\pi)) \right. \\
& \left. + \sqrt{4\pi} k \delta_a^e C_a^e \frac{(\cos\phi + \cos\phi')}{4i\cos(\phi'/2)} \right] \quad (4.123)
\end{aligned}$$

where $L=\rho$ for plane wave incidence, and C_a^e has been defined in Equation (4.90).

The functions $G_-^e(\mp i k_z')$ and $G_-^0(\mp i k_z')$ which appear in Equations (4.92)-(4.93) and (4.104)-(4.105) are evaluated next. Using the results of Appendix F, it can be shown that $s_1 = i k_z'$ is mapped to

$$\tilde{w} = \pi/2 - i \sinh^{-1}(\cot\theta') \quad (4.124)$$

in the periodic w -domain. Substituting (4.124) into (3.187), (3.188), (3.222) and (3.223) yields

$$G_-^e(-i k_z') = \frac{e^{-i(\pi/4 - \theta'/2)} \exp(\tilde{J}^e(-\tilde{\tau})/(2\pi))}{(\sin\theta' \sin\xi^e - i \cos\theta')^{1/2}} \quad (4.125)$$

$$G_{-}^e(ik_z') = \frac{e^{i(\pi/4-\theta'/2)} \exp(\tilde{J}^e(\tilde{\tau})/(2\pi))}{(\sin\theta' \sin\xi^e + i \cos\theta')^{1/2}} \quad (4.126)$$

$$G_{-}^0(ik_z') = \frac{\exp(\tilde{J}^e(\tilde{\tau})/(2\pi))}{(k(\sin\theta' \sin\xi^0 + i \cos\theta'))^{1/2}} \quad (4.127)$$

$$G_{-}^0(-ik_z') = \frac{\exp(\tilde{J}^e(-\tilde{\tau})/(2\pi))}{(k(\sin\theta' \sin\xi^0 - i \cos\theta'))^{1/2}} \quad (4.128)$$

where

$$\tilde{\tau} = -i \sinh^{-1}(\cot\theta') \quad , \quad 0 < \theta' < \pi \quad (4.129)$$

$$\tilde{J}^{e,0}(\tau) = \int_{\tau+\xi^{e,0}+\pi}^{\tau+\xi^{e,0}} t/\sin t \, dt \quad (4.130)$$

2. PEC Case, TE_y Polarization (H_y^0 , odd problem)

The integral expression for H_y^{so} in the w -domain is given by

$$H_y^{so}(\rho, \phi, z) = \frac{e^{ik_z' z}}{2\pi i} \int_{\Gamma_w^0} G_{-}^{ho}(-K \cos w) \sin w \left[\frac{-H_{cy}^0 (1+R_h^0)}{(\cos w + \cos \phi') G_{-}^{ho}(K \cos \phi')} \right. \\ \left. + \sqrt{2\pi} K d_h^0 \right] e^{iK\rho \cos(w-\phi)} dw, \quad \begin{matrix} 0 < \phi < \pi \\ 0 < \theta' < \pi \end{matrix} \quad (4.131)$$

where the contour of integration Γ_w^0 is depicted in Figure 3.9. It is important to note that the integrand in (4.131) has the same poles (shown in Figure 3.9) as the integrand in Equation (3.212). Thus, the results of Chapter III can be used here to solve for the field H_y^{so} .

The scattered field H_y^{so} is represented, after deforming the contour Γ_w^0 to the steepest descend path C_{SDP} , as the sum of an integral along C_{SDP} and the contributions from the poles swept during the deformation. The total field H_y^0 can then be obtained by adding H_y^{so} to the unperturbed field. The expression for H_y^0 becomes

$$H_y^0(\rho, \phi, z) = H_y^i(\rho, \phi, z) + H_y^{ro}(\rho, \phi, z) + H_{y0}^{sw}(\rho, \phi, z) + H_y^{do}(\rho, \phi, z) \quad (4.132)$$

where H_y^i is the incident field defined in Equation (4.42) and

$$H_y^{ro}(\rho, \phi, z) = H_{cy} \Lambda_h^0(\phi') \exp[i(-K\rho \cos(\phi + \phi') + k_z z)] , \quad \begin{matrix} 0 < (\phi, \phi') < \pi \\ 0 < \theta' < \pi \end{matrix} \quad (4.133)$$

is the reflected field where Λ_h^0 is given by

$$\Lambda_h^0(\phi') = \begin{bmatrix} -1 & \text{for } \phi + \phi' < \pi \\ R_h^0(\phi') & \text{for } \phi + \phi' > \pi \end{bmatrix} \quad (4.134)$$

The surface wave field H_{y0}^{sw} is a contribution of w_s^{ho} which is a pole of $G_-^{ho}(-K \cos w)$ and was defined in Equation (3.215). Note that the pole w_s^{ho} is captured only if ξ^{ho} satisfies Equation (3.235). The expression for H_{y0}^{sw} is as follows:

$$\begin{aligned}
H_{y0}^{sw}(\rho, \phi, z) &= \frac{-e^{ik_z' z} \sqrt{2}}{(\sin \xi^{ho})^{1/2}} \exp(-J_1^{ho}(w_s^{ho})/(2\pi)) U(\phi - \tilde{\phi}_s^{ho}) \\
&\cdot \left[\frac{H_{cy}}{\sin \phi' + \cos \xi^{ho}} \exp(-J_1^{ho}(\phi')/(2\pi)) \left[\sec((w_s^{ho} - \phi')/2) - \sec((w_s^{ho} + \phi')/2) \right] \right. \\
&\quad \cdot \left. \cos(\phi'/2) \cos(w_s^{ho}/2) (\sin \xi^{ho} - \cos \phi')^{1/2} + \sqrt{2\pi K} d_h^0 \sin w_s^{ho} \right] \\
&\cdot \exp(iK(x \cos w_s^{ho} + y \sin w_s^{ho})) \quad (4.135)
\end{aligned}$$

where the angle $\tilde{\phi}_s^{ho}$ has been defined in Equation (3.234).

The integral along C_{SDP} , which is the diffracted field H_y^{do} , is given by

$$\begin{aligned}
H_y^{do}(\rho, \phi, z) &= \frac{e^{ik_z' z}}{2\pi i} \int_{C_{SDP}} \frac{e^{iK\rho \cos(w-\phi)}}{\sin w + \cos \xi^{ho}} \exp(-J_1^{ho}(w)/(2\pi)) \frac{\cos(w/2)}{2\sin(\phi'/2)} \\
&\cdot \left[\sec((w-\phi')/2) - \sec((w+\phi')/2) \right] \cdot (\sin \xi^{ho} - \cos w)^{1/2} \\
&\cdot \left[H_{cy}(1 + R_h^0) (\sin \xi^{ho} - \cos \phi')^{1/2} \exp(-J_1^{ho}(\phi')/(2\pi)) \right. \\
&\quad \left. - \sqrt{2\pi K} d_h^0 (\cos w + \cos \phi') \right] dw \quad (4.136)
\end{aligned}$$

For large $K\rho$, the integral along C_{SDP} is asymptotic to a term

containing the value of the integrand of (4.136) at the saddle point such that

$$\begin{aligned}
 H_y^{\text{do}}(\rho, \phi, z) = & \frac{-e^{i\pi/4} \exp(-J_1^{\text{ho}}(\phi)/(2\pi))}{\sqrt{2\pi K\rho} (\sin\phi + \cos\xi^{\text{ho}})} (\sin\xi^{\text{ho}} - \cos\phi)^{1/2} e^{i(K\rho + k_z' z)} \\
 & \cdot \left[\sec((\phi - \phi')/2) F(-KLa^-) - \sec((\phi + \phi')/2) F(-KLa^+) \right] \frac{\cos(\phi/2)}{\sin(\phi'/2)} \\
 & \cdot \left[H_{cy}(1 + R_h^0)/2 (\sin\xi^{\text{ho}} - \cos\phi')^{1/2} \exp(-J_1^{\text{ho}}(\phi')/(2\pi)) \right. \\
 & \quad \left. - \sqrt{2\pi K}/2 d_h^0 (\cos\phi + \cos\phi') \right] \quad (4.137)
 \end{aligned}$$

3. PMC Case, TM_y Polarization (E_y^0 , odd problem)

As in Section C, the total field E_y^0 can be obtained from H_y^0 by duality. It follows from Equation (4.101) and (4.132) that

$$E_y^0(\rho, \phi, z) = E_y^i(\rho, \phi, z) + E_y^{\text{ro}}(\rho, \phi, z) + E_{y0}^{\text{sw}}(\rho, \phi, z) + E_y^{\text{do}}(\rho, \phi, z) \quad (4.138)$$

where

$$E_y^{\text{ro}}(\rho, \phi, z) = E_{cy} \Lambda_a^0(\phi') \exp[i(-K\rho \cos(\phi + \phi') + k_z' z)] \quad , \quad \begin{matrix} 0 < (\phi, \phi') < \pi \\ 0 < \theta' < \pi \end{matrix} \quad (4.139)$$

is the reflected field and Λ_h^0 is given by

$$\Lambda_a^0(\phi') = \begin{bmatrix} -1 & \text{for } \phi + \phi' < \pi \\ R_a^0(\phi') & \text{for } \phi + \phi' > \pi \end{bmatrix} \quad (4.140)$$

The surface wave field E_{y0}^{SW} can also be obtained from (4.135) by duality. Substituting (4.135) into (4.101), one obtains

$$E_{y0}^{SW}(\rho, \phi, z) = \frac{-e^{ik_z z} \sqrt{2}}{(\sin \xi^{ao})^{1/2}} \exp(-j_1^{ao}(w_s^{ao})/(2\pi)) U(\phi - \tilde{\phi}_s^{ao})$$

$$\cdot \left[\frac{E_{cy}}{\sin \phi' + \cos \xi^{ao}} \exp(-j_1^{ao}(\phi')/(2\pi)) \left[\sec((w_s^{ao} - \phi')/2) - \sec((w_s^{ao} + \phi')/2) \right] \right.$$

$$\left. \cdot \cos(\phi'/2) \cos(w_s^{ao}/2) (\sin \xi^{ao} - \cos \phi')^{1/2} + \sqrt{2\pi K} C_a^0 \sin w_s^{ao} \right]$$

$$\cdot \exp(iK(x \cos w_s^{ao} + y \sin w_s^{ao})) \quad (4.141)$$

Finally, the diffracted field E_y^{do} is given by (for large $K\rho$)

$$\begin{aligned}
E_y^{do}(\rho, \phi, z) = & \frac{-e^{i\pi/4} \exp(-J_1^{a0}(\phi)/(2\pi))}{\sqrt{2\pi K\rho} (\sin\phi + \cos\xi^{a0})} (\sin\xi^{a0} - \cos\phi)^{1/2} e^{i(K\rho + k_z' z)} \\
& \cdot \left[\sec((\phi - \phi')/2) F(-KLa^-) - \sec((\phi + \phi')/2) F(-KLa^+) \right] \frac{\cos(\phi/2)}{\sin(\phi'/2)} \\
& \cdot \left[E_{cy} (1 + R_a^0)/2 (\sin\xi^{a0} - \cos\phi')^{1/2} \exp(-J_1^{a0}(\phi')/(2\pi)) \right. \\
& \quad \left. - \sqrt{2\pi K}/2 C_a^0 (\cos\phi + \cos\phi') \right] \quad (4.142)
\end{aligned}$$

4. PMC Case, TE_y Polarization (H_y^e , even problem)

As in the previous section, the total field H_y^e can be simply obtained by duality such that

$$H_y^e(\rho, \phi, z) = H_y^i(\rho, \phi, z) + H_y^{re}(\rho, \phi, z) + H_{ye}^{sw}(\rho, \phi, z) + H_y^{de}(\rho, \phi, z) \quad (4.143)$$

where

$$H_y^{re}(\rho, \phi, z) = H_{cy} \Lambda_h^e(\phi') \exp[i(-K\rho \cos(\phi + \phi') + k_z' z)] \quad , \quad \begin{matrix} 0 < (\phi, \phi') < \pi \\ 0 < \theta' < \pi \end{matrix} \quad (4.144)$$

$$\Lambda_h^e(\phi') = \begin{bmatrix} 1 & \text{for } \phi + \phi' < \pi \\ R_h^e(\phi') & \text{for } \phi + \phi' > \pi \end{bmatrix} \quad (4.145)$$

$$\begin{aligned}
H_{ye}^{sw}(\rho, \phi, z) &= \frac{-e^{ik_z^i z} \sqrt{2}}{(\sin \xi^{he})^{1/2}} \exp(-j_1^{he}(w_s^{he})/(2\pi)) U(\phi - \phi_s^{he}) \\
&\cdot \left[\frac{\bar{H}_{cy} \cos \xi^{he}}{\sin \phi' + \cos \xi^{he}} \exp(-j_1^{he}(\phi')/(2\pi)) \left[\sec((w_s^{he} + \phi')/2) + \sec((w_s^{he} - \phi')/2) \right] \right. \\
&\cdot \left. (\sin \xi^{he} - \cos \phi')^{1/2} - i\sqrt{2\pi} k \delta_h^e d_h^e \sqrt{2} \cos(w_s^{he}/2) \right] \\
&\cdot \exp(iK(x \cos w_s^{he} + y \sin w_s^{he})) \quad (4.146)
\end{aligned}$$

$$\begin{aligned}
H_y^{de}(\rho, \phi, z) &= \frac{-e^{i\pi/4} \exp(-j_1^{he}(\phi)/(2\pi))}{\sqrt{2\pi K\rho} (\sin \phi + \cos \xi^{he})} (\sin \xi^{he} - \cos \phi)^{1/2} e^{i(K\rho + k_z^i z)} \\
&\cdot \left[\sec((\phi + \phi')/2) F(-KLa^+) + \sec((\phi - \phi')/2) F(-KLa^-) \right] \\
&\cdot \left[H_{cy} (1 - R_h^e)/2 (\sin \xi^{he} - \cos \phi')^{1/2} \exp(-j_1^{he}(\phi')/(2\pi)) \right. \\
&\cdot \left. + \sqrt{4\pi} k \delta_h^e d_h^e \frac{(\cos \phi + \cos \phi')}{4 \cos(\phi'/2)} \right] \quad (4.147)
\end{aligned}$$

In the next section, the problem of surface wave excitation will

be considered. It will be helpful if the constants C_a^e , d_h^e , C_a^o and d_h^o are rewritten in terms of ϕ' and θ' . Thus, substituting (4.5) and (4.6) into (4.90), (4.91), (4.103) and (4.111) yields

$$C_a^e = \frac{E_{cy} 2\cos\xi^{ae} \sin\theta' \sin\phi' (\sin\theta' \cos\phi' + i\cos\theta' |\bar{A}_{ce}|/|\bar{B}_{ce}|)}{ik\delta_a^e \sqrt{2\pi} (\sin^2\theta' \cos^2\phi' + \cos^2\theta') G_-^{ae}(K\cos\phi') (\sin\phi' + \cos\xi^{ae})} \\ + \frac{2\eta_o H_{cy} 2\sin\phi' \cos\theta' G_-^{ho}(-ik\cos\theta')}{\sqrt{2\pi} ik\delta_a^e (\sin^2\theta' \cos^2\phi' + \cos^2\theta') G_-^{ho}(K\cos\phi') (\sin\phi' + \cos\xi^{ho}) |\bar{B}_{ce}|} \quad (4.148)$$

$$d_h^o = \frac{H_{cy} 2\sin\phi' (\sin\theta' \cos\phi' - i\cos\theta' |\bar{A}_{ce}|/|\bar{B}_{ce}|)}{\sqrt{2\pi} k (\sin^2\theta' \cos^2\phi' + \cos^2\theta') G_-^{ho}(K\cos\phi') (\sin\phi' + \cos\xi^{ho})} \\ - \frac{2E_{cy} 2\cos\xi^{ae} \sin\theta' \cos\theta' \sin\phi' G_-^{ae}(-ik\cos\theta')}{\sqrt{2\pi} k\eta_o (\sin^2\theta' \cos^2\phi' + \cos^2\theta') G_-^{ae}(K\cos\phi') (\sin\phi' + \cos\xi^{ae}) |\bar{B}_{ce}|} \quad (4.149)$$

$$C_a^o = \frac{E_{cy} 2\sin\phi' (\sin\theta' \cos\phi' - i\cos\theta' |\bar{A}_{co}|/|\bar{B}_{co}|)}{\sqrt{2\pi} k (\sin^2\theta' \cos^2\phi' + \cos^2\theta') G_-^{ao}(K\cos\phi') (\sin\phi' + \cos\xi^{ao})} \\ + \frac{2\eta_o H_{cy} 2\cos\xi^{he} \sin\theta' \cos\theta' \sin\phi' G_-^{he}(-ik\cos\theta')}{\sqrt{2\pi} k (\sin^2\theta' \cos^2\phi' + \cos^2\theta') G_-^{he}(K\cos\phi') (\sin\phi' + \cos\xi^{he}) |\bar{B}_{co}|} \quad (4.150)$$

$$d_h^e = \frac{H_{cy} 2\cos\xi^{he} \sin\theta' \sin\phi' (\sin\theta' \cos\phi' + i\cos\theta' |\bar{A}_{co}|/|\bar{B}_{co}|)}{ik\delta_h^e \sqrt{2\pi} (\sin^2\theta' \cos^2\phi' + \cos^2\theta') G_-^{he}(K\cos\phi') (\sin\phi' + \cos\xi^{he})} \\ - \frac{2Y_0 E_{cy} 2\sin\phi' \cos\theta' G_-^{a0}(-ik\cos\theta')}{\sqrt{2\pi} ik\delta_h^e (\sin^2\theta' \cos^2\phi' + \cos^2\theta') G_-^{a0}(K\cos\phi') (\sin\phi' + \cos\xi^{a0}) |\bar{B}_{co}|} \quad (4.151)$$

E. SURFACE WAVE EXCITATION

The surface wave excitation problem will be solved following the procedure of Section F.3 in Chapter III, that is, using the concept of analytic continuation. It was shown in Section F.3 that the Brewster angle $\tilde{\phi}_b$ is given by Equation (3.299). The unperturbed incident surface wave field (TM_y or TE_y) can be obtained by substituting (3.299) into (4.7) or (4.42). One obtains an expression (TM_y or TE_y) which is proportional to

$$\exp(-iKp\cos(\phi - \tilde{\phi}_b)) = \exp(-iKycos\xi) \exp(iKxsin\xi), \quad y > 0 \quad (4.152)$$

Recall that (see Equation (4.98))

$$K\cos\xi = k\delta = k(\delta_r + i\delta_I), \quad (4.153)$$

it follows from (4.152) and (4.153) that Equation (4.152) will be bounded as $y \rightarrow \infty$, if and only if

$$\delta_I < 0 \quad (4.154)$$

which is the same result obtained in Chapter III. For the TM_y polarization, Equation (4.154) implies that

$$\text{Im}(Z_S) = X_S < 0 \quad (4.155)$$

On the other hand, for the TE_y polarization (4.154) implies that

$$\text{Im}(Z_S) = X_S > 0 \quad (4.156)$$

Therefore, for a given surface impedance with nonzero reactance ($X_S \neq 0$), the surface wave field can have only one polarization.

1. PEC Case

Substituting Equation (3.299) into (4.117) and (4.131) yields

$$E_y^{se}(\rho, \phi, z) = \frac{e^{ik_z' z}}{2\pi i} \int_{\Gamma_w^e} G_-^{ae}(-K \cos w) \left[\frac{-E_{cy} \sin w_s^{ae}}{(\cos w + \cos w_s^{ae}) G_-^{ae}(K \cos w_s^{ae})} \right. \\ \left. - i\sqrt{2\pi} k \delta_a^e C_a^e \right] e^{iK\rho \cos(w-\phi)} dw, \quad \begin{matrix} 0 < \phi < \pi \\ 0 < \phi' < \pi \end{matrix} \quad (4.157)$$

for $\phi' = \tilde{\phi}_b^{ae} = 2\pi - w_s^{ae}$, and

$$H_y^{so}(\rho, \phi, z) = \frac{e^{ik_z' z}}{2\pi i} \int_{\Gamma_w^0} G_-^{ho}(-K \cos w) \sin w \left[\frac{-H_{cy}}{(\cos w + \cos w_s^{ho}) G_-^{ho}(K \cos w_s^{ho})} \right. \\ \left. + \sqrt{2\pi} K d_h^0 \right] e^{iK\rho \cos(w-\phi)} dw, \quad \begin{matrix} 0 < \phi < \pi \\ 0 < \theta' < \pi \end{matrix} \quad (4.158)$$

for $\phi' = \tilde{\phi}_b^{ho} = 2\pi - w_s^{ho}$.

For $x_s < 0$, the unperturbed incident surface wave field is

$$E_{ye}^{isw}(x, y, z) = E_{cy} \exp(iK(y \sin w_s^{ae} - x \cos w_s^{ae})) \exp(ik_z' z) \quad (4.159)$$

where $\tilde{\phi}_b^{ae} = 2\pi - w_s^{ae}$ and

$$H_{yo}^{isw} = 0 \quad (4.160)$$

Using the same method of analysis as in Section F.3 of Chapter III, the total field E_y^e can be expressed as follows:

$$E_y^e(x, y, z) = E_{ye}^{isw}(x, y, z) U(\phi - \tilde{\phi}_{ae}^i) + E_{ye}^{rsw}(x, y, z) + E_{ye}^{dsw}(\rho, \phi, z) \quad (4.161)$$

where E_{ye}^{rsw} and E_{ye}^{dsw} are the reflected and diffracted surface wave fields, respectively. The fields E_{ye}^{rsw} and E_{ye}^{dsw} can be expressed as follows:

$$\begin{aligned}
E_{ye}^{rsw}(x,y,z) &= E_{cy} (1 + \cos w_s^{ae}) / \cos w_s^{ae} \exp(-J_1^{ae}(w_s^{ae})/\pi) U(\phi - \phi_s^{ae}) \\
&\cdot \left[1 - \frac{2 \cos w_s^{ae} \sin \theta' (\sin \theta' \cos w_s^{ae} + i \cos \theta' |\bar{A}_{ce}| / |\bar{B}_{ce}|)}{(\cos^2 \theta' + \sin^2 \theta' \cos^2 w_s^{ae})} \right] \\
&\cdot \exp(ik(x \cos w_s^{ae} + y \sin w_s^{ae})) \exp(ik_z z) \quad (4.162)
\end{aligned}$$

$$\begin{aligned}
E_{ye}^{dsw}(\rho, \phi, z) &= \frac{E_{cy} e^{i\pi/4} \exp(-J_1^{ae}(\phi)/(2\pi)) \exp(-J_1^{ae}(w_s^{ae})/(2\pi))}{\sqrt{2\pi K} 2(\sin \phi - \sin w_s^{ae})} \\
&\cdot \left[\sec((\phi + w_s^{ae})/2) T(a_{ae}^+, a_p^{ae}) + \sec((\phi - w_s^{ae})/2) T(a_{ae}^-, a_p^{ae}) \right] \\
&\cdot \left[1 - \frac{(\cos \phi + \cos w_s^{ae}) \sin \theta' (\sin \theta' \cos w_s^{ae} + i \cos \theta' |\bar{A}_{ce}| / |\bar{B}_{ce}|)}{(\cos^2 \theta' + \sin^2 \theta' \cos^2 w_s^{ae})} \right] \\
&\cdot (2 \cos w_s^{ae} (\cos \phi + \cos w_s^{ae}))^{1/2} \exp(ik\rho + ik_z z) / \sqrt{\rho} \quad (4.163)
\end{aligned}$$

where

$$a_{ae}^\mp = 2 \cos^2((\phi \mp w_s^{ae})/2) \quad ; \quad a_p^{ae} = 2 \sin^2((\phi - w_s^{ae})/2) \quad (4.164)$$

and T was defined in Equation (3.244). Note that the expression in (4.163) takes into account the presence of two poles near the saddle point.

Substituting (4.160) into (4.158), one obtains

$$H_y^0 = H_{y0}^{dsw} = \frac{e^{ik_z' z}}{2\pi i} \int_{\Gamma_w^0} G_-^{ho}(-K \cos w) \sin w \sqrt{2\pi} K d_h^0 e^{iK\rho \cos(w-\phi)} dw \quad (4.165)$$

where d_h^0 is given in (4.149), except that $H_{cy}=0$. Note that by deforming the contour of integration Γ_w^0 to C_{SDP} , no poles of G_-^{ho} are crossed. Therefore, the total field H_y^0 becomes

$$H_y^0 = H_{y0}^{dsw} = \frac{e^{ik_z' z}}{2\pi i} \int_{C_{SDP}} G_-^{ho}(-K \cos w) \sin w \sqrt{2\pi} K d_h^0 e^{iK\rho \cos(w-\phi)} dw. \quad (4.166)$$

For large $K\rho$, the diffracted field H_{y0}^{dsw} can be obtained by substituting (3.299) and (4.149) into (G.13) such that

$$H_{y0}^{dsw}(\rho, \phi, z) = \frac{-E_{cy} e^{i\pi/4} \exp(-J_1^{ho}(\phi)/(2\pi)) \exp(-J_1^{ae}(w_s^{ae})/(2\pi))}{\sqrt{2\pi K} \eta_0 (\sin \phi - \sin w_s^{ho}) \sin(w_s^{ae}/2)} \\ \cdot \frac{F(-K\rho a_p^{ho}) (2\cos w_s^{ae} (\cos w_s^{ho} + \cos \phi))^{1/2} \cos \theta' \sin \theta' G^{ae}(-ik \cos \theta')}{k |\bar{B}_{ce}| (\sin^2 \theta' \cos^2 w_s^{ae} + \cos^2 \theta')} \\ \cdot \sqrt{2K} \sin \phi \sin w_s^{ae} \exp(ik_z' z + iK\rho)/\sqrt{\rho} \quad (4.167)$$

where a_p^{ho} was defined in (4.164) except that "ae" is replaced by "ho".

For $\lambda_s > 0$, the unperturbed surface wave field is

$$H_{y0}^{isw}(x,y,z) = H_{cy} \exp(iK(y \sin w_s^{ho} - x \cos w_s^{ho})) \exp(ik_z' z) \quad (4.168)$$

where $\phi' = \tilde{\phi}_b^{ho} = 2\pi - w_s^{ho}$, and

$$E_{ye}^{isw} = 0. \quad (4.169)$$

The total field H_y^0 can be expressed as follows:

$$H_y^0(x,y,z) = H_{y0}^{isw}(x,y,z)U(\phi - \tilde{\phi}_{ho}^i) + H_{y0}^{rsw}(x,y,z) + H_{y0}^{dsw}(\rho, \phi, z) \quad (4.170)$$

where H_{y0}^{rsw} and H_{y0}^{dsw} are the reflected and diffracted surface wave fields, respectively. The field H_{y0}^{rsw} is given by

$$H_{y0}^{rsw}(x,y,z) = H_{cy} \tan(w_s^{ho}) \exp(-J_1^{ho}(w_s^{ho})/\pi) U(\phi - \tilde{\phi}_s^{ho})$$

$$\cdot \left[1 - \frac{2 \cos w_s^{ho} \sin \theta' (\sin \theta' \cos w_s^{ho} - i \cos \theta' |\bar{A}_{ce}| / |\bar{B}_{ce}|)}{(\cos^2 \theta' + \sin^2 \theta' \cos^2 w_s^{ho})} \right]$$

$$\cdot \exp(iK(x \cos w_s^{ho} + y \sin w_s^{ho})) \exp(ik_z' z) \quad (4.171)$$

The diffracted field H_{y0}^{dsw} can be easily obtained by substituting (3.299) into (4.137). Thus, for large $K\rho$ (and taking into account the two poles near the saddle point)

$$\begin{aligned}
H_{yo}^{dsw}(\rho, \phi, z) = & \frac{-H_{cy} e^{i\pi/4} \exp(-j_1^{ho}(\phi)/(2\pi)) \exp(-j_1^{ho}(w_s^{ho})/(2\pi))}{\sqrt{2\pi K} 2(\sin\phi - \sin w_s^{ho}) \sin(w_s^{ho}/2)} \\
& \cdot \left[\sec((\phi - w_s^{ho})/2) T(a_{ho}^-, a_p^{ho}) - \sec((\phi + w_s^{ho})/2) T(a_{ho}^+, a_p^{ho}) \right] \\
& \cdot \left[1 - \frac{(\cos\phi + \cos w_s^{ho}) \sin\theta' (\sin\theta' \cos w_s^{ho} - i \cos\theta' |\bar{A}_{ce}|/|\bar{B}_{ce}|)}{(\cos^2\theta' + \sin^2\theta' \cos^2 w_s^{ho})} \right] \\
& \cdot \cos(\phi/2) (2 \cos w_s^{ho} (\cos\phi + \cos w_s^{ho}))^{1/2} \exp(ik\rho + ik_z' z)/\sqrt{\rho} \quad (4.172)
\end{aligned}$$

where a_{ho}^\mp was defined in (4.164) except that "ae" is replaced by "ho".

Furthermore, T is the composite transition function defined in (3.244).

Since $E_{cy}=0$, the expression for E_y^{se} becomes

$$E_y^{se} = \frac{e^{ik_z' z}}{2\pi i} \int_{\Gamma_w^e} G_-^{ae}(-K \cos w) \sqrt{2\pi} k \delta_a^e C_a^e / i e^{iK\rho \cos(w-\phi)} dw \quad (4.173)$$

The integrand in (4.173) has only one pole due to G_-^{ae} , but in deforming

the contour Γ_w^e to the contour C_{SDP} , the pole of G_-^{ae} is not captured.

Therefore, the total field E_y^e becomes

$$E_y^e = E_{ye}^{dsw} = \frac{e^{ik_z' z}}{2\pi i} \int_{C_{SDP}} G_-^{ae}(-K \cos w) \sqrt{2\pi} k \delta_a^e C_a^e / i e^{iK\rho \cos(w-\phi)} dw. \quad (4.174)$$

Furthermore, for large $K\rho$, E_{ye}^{dsw} can be obtained by substituting (3.299) and (4.148) into (G.13) such that

$$E_{ye}^{dsw}(\rho, \phi, z) = \frac{H_{cy} e^{i\pi/4} \exp(-j_1^{ae}(\phi)/(2\pi)) \exp(-j_1^{ho}(w_s^{ho})/(2\pi))}{\sqrt{2\pi K} Y_0(\sin\phi - \sin w_s^{ae})} \cdot \frac{F(-K\rho a_p^{ae}) (2\cos w_s^{ho} (\cos w_s^{ae} + \cos\phi))^{1/2} G^{ho}(-ik\cos\theta')}{|B_{ce}| (\sin^2\theta' \cos^2 w_s^{ho} + \cos^2\theta')} \cdot \sqrt{2K} 2\cos(\phi/2) \cos\theta' \exp(ik_z' z + iK\rho)/\sqrt{\rho}. \quad (4.175)$$

where a_p^{ae} was defined in (4.164).

2. PMC Case

Without repeating the analysis of Section 1., the total fields E_y^0 and H_y^e can be obtained from Section 1. by duality. Thus, for $X_s < 0$, the total field E_y^0 is given by

$$E_y^0(x, y, z) = E_{y0}^{isw}(x, y, z) U(\phi - \tilde{\phi}_{a0}^i) + E_{y0}^{rsw}(x, y, z) + E_{y0}^{dsw}(\rho, \phi, z) \quad (4.176)$$

where $\phi' = 2\pi - w_s^{a0}$ and

$$E_{y0}^{isw}(x,y,z) = E_{cy} \exp[iK(y \sin w_S^{ao} - x \cos w_S^{ao})] \exp(ik_z^i z) \quad (4.177)$$

$$E_{y0}^{rsw}(x,y,z) = E_{cy} \tan(w_S^{ao}) \exp(-j_1^{ao}(w_S^{ao})/\pi) U(\phi - \tilde{\phi}_S^{ao})$$

$$\cdot \left[1 - \frac{2 \cos w_S^{ao} \sin \theta' (\sin \theta' \cos w_S^{ao} - i \cos \theta' |\bar{A}_{co}|/|\bar{B}_{co}|)}{(\cos^2 \theta' + \sin^2 \theta' \cos^2 w_S^{ao})} \right]$$

$$\cdot \exp[iK(x \cos w_S^{ao} + y \sin w_S^{ao})] \exp(ik_z^i z) \quad (4.178)$$

$$E_{y0}^{dsw}(\rho, \phi, z) = \frac{-E_{cy} e^{i\pi/4} \exp(-j_1^{ao}(\phi)/(2\pi)) \exp(-j_1^{ao}(w_S^{ao})/(2\pi))}{\sqrt{2\pi K} 2(\sin \phi - \sin w_S^{ao}) \sin(w_S^{ao}/2)}$$

$$\cdot \left[\sec((\phi - w_S^{ao})/2) T(a_{ao}^-, a_p^{ao}) - \sec((\phi + w_S^{ao})/2) T(a_{ao}^+, a_p^{ao}) \right]$$

$$\cdot \left[1 - \frac{(\cos \phi + \cos w_S^{ao}) \sin \theta' (\sin \theta' \cos w_S^{ao} - i \cos \theta' |\bar{A}_{co}|/|\bar{B}_{co}|)}{(\cos^2 \theta' + \sin^2 \theta' \cos^2 w_S^{ao})} \right]$$

$$\cdot \cos(\phi/2) (2 \cos w_S^{ao} (\cos \phi + \cos w_S^{ao}))^{1/2} \exp(iK\rho + ik_z^i z)/\sqrt{\rho} \quad (4.179)$$

Since $H_{cy}=0$ for $x_S < 0$, the total field H_y^e is equal to the diffracted

field H_{ye}^{dsw} . Substituting (4.175) into (4.109) yields (for large $K\rho$)

$$H_y^e(\rho, \phi, z) = H_{ye}^{dsw} = \frac{-E_{cy} e^{i\pi/4} \exp(-J_1^{he}(\phi)/(2\pi)) \exp(-J_1^{ao}(w_s^{ao})/(2\pi))}{\sqrt{2\pi K} \eta_0 (\sin\phi - \sin w_s^{he})}$$

$$\cdot \frac{F(-K\rho a_p^{he}) (2\cos w_s^{ao} (\cos w_s^{he} + \cos\phi))^{1/2} G^{ao}(-ik\cos\theta')}{|\bar{B}_{co}| (\sin^2\theta' \cos^2 w_s^{ao} + \cos^2\theta')}$$

$$\cdot \sqrt{2K} 2\cos(\phi/2) \cos\theta' \exp(ik_z' z + iK\rho)/\sqrt{\rho} \quad (4.180)$$

As shown before, when $X_s > 0$, $E_y^{isw} = 0 = E_{cy}$, so the total field E_y^0 is equal to the diffracted field E_{yo}^{dsw} which can be also simply obtained from (4.167) by duality. Thus, for large $K\rho$ ($\phi' = \tilde{\phi}_b^{he} = 2\pi - w_s^{he}$)

$$E_{yo}^{dsw}(\rho, \phi, z) = \frac{H_{cy} e^{i\pi/4} \exp(-J_1^{ao}(\phi)/(2\pi)) \exp(-J_1^{he}(w_s^{he})/(2\pi))}{\sqrt{2\pi K} \gamma_0 (\sin\phi - \sin w_s^{ao}) \sin(w_s^{he}/2)}$$

$$\cdot \frac{F(-K\rho a_p^{ao}) (2\cos w_s^{he} (\cos w_s^{ao} + \cos\phi))^{1/2} \cos\theta' \sin\theta' G^{he}(-ik\cos\theta')}{k |\bar{B}_{co}| (\sin^2\theta' \cos^2 w_s^{he} + \cos^2\theta')}$$

$$\cdot \sqrt{2K} \sin\phi \sin w_s^{he} \exp(ik_z' z + iK\rho)/\sqrt{\rho} \quad (4.181)$$

Furthermore, for the TE_y polarization, the total field H_y^e , likewise, can be obtained by duality. It follows from Equations (4.161) and (4.109) that

$$H_y^e(x,y,z) = H_{ye}^{isw}(x,y,z)U(\phi - \tilde{\phi}_{he}^i) + H_{ye}^{rsw}(x,y,z) + H_{ye}^{dsw}(\rho, \phi, z) \quad (4.182)$$

where

$$H_{ye}^{isw}(x,y,z) = H_{cy} \exp[iK(y \sin w_s^{he} - x \cos w_s^{he})] \exp(ik_z' z) \quad (4.183)$$

is the incident field, and

$$H_{ye}^{rsw}(x,y,z) = H_{cy} (1 + \cos w_s^{he}) / \cos w_s^{he} \exp(-J_1^{he}(w_s^{he})/\pi) U(\phi - \tilde{\phi}_s^{he})$$

$$\cdot \left[1 - \frac{2 \cos w_s^{he} \sin \theta' (\sin \theta' \cos w_s^{he} + i \cos \theta' |\bar{A}_{co}| / |\bar{B}_{co}|)}{(\cos^2 \theta' + \sin^2 \theta' \cos^2 w_s^{he})} \right] \cdot \exp[iK(x \cos w_s^{he} + y \sin w_s^{he})] \exp(ik_z' z) \quad (4.184)$$

is the reflected field. The last field component in Equation (4.182) is given by

$$\begin{aligned}
H_{ye}^{dsw}(\rho, \phi, z) = & \frac{H_{cy} e^{i\pi/4} \exp(-J_1^{he}(\phi)/(2\pi)) \exp(-J_1^{he}(w_s^{he})/(2\pi))}{\sqrt{2\pi K} 2(\sin\phi - \sin w_s^{he})} \\
& \cdot \left[\sec((\phi + w_s^{he})/2) T(a_{he}^+, a_p^{he}) + \sec((\phi - w_s^{he})/2) T(a_{he}^-, a_p^{he}) \right] \\
& \cdot \left[1 - \frac{(\cos\phi + \cos w_s^{he}) \sin\theta' (\sin\theta' \cos w_s^{he} + i \cos\theta' |\bar{A}_{co}| / |\bar{B}_{co}|)}{(\cos^2\theta' + \sin^2\theta' \cos^2 w_s^{he})} \right] \\
& \cdot (2 \cos w_s^{he} (\cos\phi + \cos w_s^{he}))^{1/2} \exp(ik\rho + ik_z' z) / \sqrt{\rho} \quad (4.185)
\end{aligned}$$

F. RELATIONSHIP BETWEEN THE (E_z, H_z) AND THE (E_y, H_y) FIELDS

In Chapter III, the solution of the canonical problem was expressed in terms of E_z and H_z fields, while in Chapter IV, the normal fields E_y and H_y were used. It is necessary to know how to transform from one set of fields to the other in order to use both solutions together.

It is shown in [45] that if all the field components have the same exponential z dependence $\exp(-ik_z \cos\theta')$, then, all the fields can be expressed in terms of H_z and E_z as follows:

$$\vec{E}(x, y, z) = \nabla x (\nabla x (\hat{z} E_z) + ik \eta_0 (\hat{z} H_z)) / K^2 \quad (4.186)$$

$$\vec{H}(x,y,z) = \nabla x(\nabla x(\hat{z}H_z) - ikY_0(\hat{z}E_z))/K^2 \quad (4.187)$$

As mentioned in Section B.3, it is shown in Appendix I that the fields components E_x , E_z , H_x and H_z (in the s -domain) can be expressed in terms of E_y and H_y . The expressions for these fields components are given in Equations (4.69)-(4.72). It is more convenient to write these equations in the periodic w -domain. Thus, substituting (4.115) and (4.116) into (4.69)-(4.72) yields

$$\hat{H}_z(-K\cos w, y, z) = \frac{\sin\theta'[\cos\theta'\sin w\hat{H}_y(-K\cos w, y, z) + Y_0\cos w\hat{E}_y(-K\cos w, x, z)]}{1 - \sin^2\theta'\sin^2 w} \quad (4.188)$$

$$\hat{E}_z(-K\cos w, y, z) = \frac{\sin\theta'[\cos\theta'\sin w\hat{E}_y(-K\cos w, y, z) - \eta_0\cos w\hat{H}_y(-K\cos w, x, z)]}{1 - \sin^2\theta'\sin^2 w} \quad (4.189)$$

$$\hat{H}_x(-K\cos w, y, z) = \frac{Y_0\cos\theta'\hat{E}_y(-K\cos w, x, z) - \sin^2\theta'\cos w\sin w\hat{H}_y(-K\cos w, y, z)}{1 - \sin^2\theta'\sin^2 w} \quad (4.190)$$

$$\hat{E}_x(-K\cos w, y, z) = \frac{-\eta_0 \cos \theta' \hat{H}_y(-K\cos w, x, z) - \sin^2 \theta' \cos w \sin w \hat{E}_y(-K\cos w, y, z)}{1 - \sin^2 \theta' \sin^2 w} \quad (4.191)$$

Note that the roots of the denominator $(1 - \sin^2 \theta' \sin^2 w)$ are not poles of the above expressions. Furthermore, it will be useful for later use to obtain expressions for the incident H_y^i and E_y^i fields in terms of the tangential E_z^i and H_z^i fields. Thus, assume that the fields E_z^i and H_z^i are given by

$$E_z^i = E_{cz} \exp(i(k_x^i x - k_y^i y + k_z^i z)) \quad (4.192)$$

$$H_z^i = H_{cz} \exp(i(k_x^i x - k_y^i y + k_z^i z)) \quad (4.193)$$

where E_{cz} and H_{cz} are arbitrary constants. Substituting (4.192) and (4.193) into (4.186) and (4.187) yields

$$E_y^i = -(\eta_0 \cos \phi' H_z^i + \cos \theta' \sin \phi' E_z^i) / \sin \theta' \quad , \quad 0 < \theta' < \pi \quad (4.194)$$

$$H_y^i = (Y_0 \cos \phi' E_z^i - \cos \theta' \sin \phi' H_z^i) / \sin \theta' \quad , \quad 0 < \theta' < \pi \quad (4.195)$$

G. DIFFRACTED E_Z^d AND H_Z^d FIELDS

In this section, the diffracted fields $E_Z^d(x,y,z)$ and $H_Z^d(x,y,z)$ will be computed using the results of the previous section.

The first step is to take the inverse Fourier transform of \hat{H}_Z^S and \hat{E}_Z^S . The fields E_Z^S and H_Z^S are given in Equations (4.76) and (4.78), respectively. In the periodic w -domain, these equations can be written as follows:

$$H_Z^S = \frac{1}{\sqrt{2\pi}} \int_{\Gamma_w} \hat{H}_Z^S(-K \cos w, y, z) e^{iK \cos w x} K \sin w \, dw \quad (4.196)$$

$$E_Z^S = \frac{1}{\sqrt{2\pi}} \int_{\Gamma_w} \hat{E}_Z^S(-K \cos w, y, z) e^{iK \cos w x} K \sin w \, dw \quad (4.197)$$

Recall that the diffracted fields E_y^d and H_y^d were contributions from a integral along the steepest descend path which was evaluated asymptotically by the saddle point method. Thus, substituting $w=\phi$ (saddle point) into (4.188) and (4.189) yields

$$H_Z^d(\rho, \phi, z) = \frac{\sin \theta' [\cos \theta' \sin \phi H_y^d(\rho, \phi, z) + Y_0 \cos \phi E_y^d(\rho, \phi, z)]}{1 - \sin^2 \theta' \sin^2 \phi} \quad (4.198)$$

$$E_z^d(\rho, \phi, z) = \frac{\sin \theta' [\cos \theta' \sin \phi E_y^d(\rho, \phi, z) - \eta_0 \cos \phi H_y^d(\rho, \phi, z)]}{1 - \sin^2 \theta' \sin^2 \phi} \quad (4.199)$$

The next step is to write the constants E_{cy} and H_{cy} in terms of E_{cz} and H_{cz} so that the diffracted fields can be expressed in terms of E_{cz} and H_{cz} only.

PEC CASE.

Substituting (4.194), (4.195), (4.123) and (4.137) into (4.198) and (4.199), and after some rather tedious algebra, one obtains

$$E_z^{do}(\rho, \phi, z) = \left[\frac{-E_{cz} D_{zo}^{a1}(\phi', \phi) + \eta_0 H_{cz} \cos \theta' D_{zo}^{a2}(\phi', \phi)}{1 - \sin^2 \theta' \sin^2 \phi} \right] \frac{e^{(iK\rho + ik_z' z)}}{\sqrt{\rho}} \quad (4.200)$$

$$H_z^{de}(\rho, \phi, z) = \left[\frac{-H_{cz} D_{ze}^{h1}(\phi', \phi) + \gamma_0 E_{cz} \cos \theta' D_{ze}^{h2}(\phi', \phi)}{1 - \sin^2 \theta' \sin^2 \phi} \right] \frac{e^{(iK\rho + ik_z' z)}}{\sqrt{\rho}} \quad (4.201)$$

where the subscripts and superscripts attached to the diffraction coefficients $\{D_{zo}^{a1}, D_{zo}^{a2}, D_{ze}^{h1}, D_{ze}^{h2}\}$ refer to the following facts:

- (i) "a" refers to the electric field, while "h" refers to the magnetic field.

(ii) "z" refers to the fact that these diffraction coefficients pertain to the E_z and H_z fields.

(iii) "e" refers to the even case, whereas, "o" refers to the odd case.

The diffraction coefficients $\{D_{zo}^{a1}, D_{zo}^{a2}, D_{ze}^{h1}, D_{ze}^{h2}\}$ can be expressed in terms of the diffraction coefficients obtained in Chapter III as follows:

$$\begin{aligned} D_{ze}^{h1}(\phi', \phi) &= \cos \phi D_{ye}^{da}(\phi', \phi) [\cos \phi' - (\cos \phi + \cos \phi') \hat{F}_2^{ce}] \\ &+ \cos^2 \theta' \sin \phi \sin \phi' D_{yo}^{dh}(\phi', \phi) [1 - (\cos \phi + \cos \phi') \hat{F}_3^{ce}] \end{aligned} \quad (4.202)$$

$$\begin{aligned} D_{ze}^{h2}(\phi', \phi) &= \sin \phi D_{yo}^{dh}(\phi', \phi) [\cos \phi' - (\cos \phi + \cos \phi') \hat{F}_1^{ce}] \\ &+ \cos \phi D_{ye}^{da}(\phi', \phi) [-\sin \phi' + (\cos \phi + \cos \phi') \hat{F}_4^{ce}] \end{aligned} \quad (4.203)$$

$$\begin{aligned} D_{zo}^{a1}(\phi', \phi) &= \cos \phi D_{yo}^{dh}(\phi', \phi) [\cos \phi' - (\cos \phi + \cos \phi') \hat{F}_1^{ce}] \\ &+ \cos^2 \theta' \sin \phi D_{ye}^{da}(\phi', \phi) [\sin \phi' - (\cos \phi + \cos \phi') \hat{F}_4^{ce}] \end{aligned} \quad (4.204)$$

$$\begin{aligned} D_{zo}^{a2}(\phi', \phi) &= \cos \phi \sin \phi' D_{yo}^{dh}(\phi', \phi) [1 - (\cos \phi + \cos \phi') \hat{F}_3^{ce}] \\ &+ \sin \phi D_{ye}^{da}(\phi', \phi) [-\cos \phi' + (\cos \phi + \cos \phi') \hat{F}_2^{ce}] \end{aligned} \quad (4.205)$$

where the diffraction coefficients (D_{ye}^{da} , D_{yo}^{dh}) are exactly the same as the diffraction coefficients (D_e^d , D_o^d) of Chapter III, except that k is replaced by K . Therefore, it follows from (3.210) and (3.242) that:

$$D_{ye}^{da}(\phi, \phi') = \frac{-e^{i\pi/4} (1 - R_a^e)/2 [(\sin \xi^{ae} - \cos \phi)(\sin \xi^{ae} - \cos \phi')]^{1/2}}{\sqrt{2\pi K} (\sin \phi + \cos \xi^{ae})} \cdot \exp(-(J_1^{ae}(\phi) + J_1^{ae}(\phi'))/(2\pi)) \cdot (\sec(\beta^+/2)F(-KLa^+) + \sec(\beta^-/2)F(-KLa^-)) \quad (4.206)$$

$$D_{yo}^{dh}(\phi, \phi') = \frac{-e^{i\pi/4} (1 + R_h^o)/2 [(\sin \xi^{ho} - \cos \phi)(\sin \xi^{ho} - \cos \phi')]^{1/2}}{\sqrt{2\pi K} (\sin \phi + \cos \xi^{ho})} \cdot \exp(-(J_1^{ho}(\phi) + J_1^{ho}(\phi'))/(2\pi)) \cdot (\sec(\beta^-/2)F(-KLa^-) - \sec(\beta^+/2)F(-KLa^+)) \cdot \cos(\phi/2)/\sin(\phi'/2) \quad (4.207)$$

where the subscript "y" refers to the E_y and H_y fields.

The functions $\{\tilde{F}_i^{ce}\}_{i=1}^4$, which do not depend on the angles of observation (ϕ, θ) , are given by

$$\tilde{F}_1^{ce}(\phi', \theta') = \cos \phi' F_1^{ce} + 2\cos^2 \theta' \cos(\phi'/2) \sin(\phi') F_2^{ce} \quad (4.208)$$

$$\tilde{F}_2^{ce}(\phi', \theta') = \cos \phi' F_3^{ce} + \cos^2 \theta' \sin \phi' F_4^{ce} \quad (4.209)$$

$$F_3^{ce}(\phi', \theta') = F_1^{ce} - F_2^{ce} \cos \phi' / \sin(\phi'/2) \quad (4.210)$$

$$F_4^{ce}(\phi', \theta') = \sin \phi' F_3^{ce} - \cos \phi' F_4^{ce} \quad (4.211)$$

where

$$F_1^{ce}(\phi', \theta') = \sin \theta' (\sin \theta' \cos \phi' - i \cos \theta' |\bar{A}_{ce}| / |\bar{B}_{ce}|) / (1 - \sin^2 \theta' \sin^2 \phi') \quad (4.212)$$

$$F_3^{ce}(\phi', \theta') = \sin \theta' (\sin \theta' \cos \phi' + i \cos \theta' |\bar{A}_{ce}| / |\bar{B}_{ce}|) / (1 - \sin^2 \theta' \sin^2 \phi') \quad (4.213)$$

$$F_2^{ce}(\phi', \theta') = \frac{\sin \theta' \cos \xi^{ae} (\sin \phi' + \cos \xi^{ho}) \exp([J_1^{ho}(\phi') - J_1^{ae}(\phi')]/(2\pi))}{(1 - \sin^2 \theta' \sin^2 \phi') k |\bar{B}_{ce}| (\sin \phi' + \cos \xi^{ae}) (1 + \sin \theta' \cos \xi^{ae})} \\ \cdot \sqrt{2K} ((\sin \xi^{ae} - \cos \phi') / (\sin \xi^{ho} - \cos \phi'))^{1/2} / \sin \phi' \quad (4.214)$$

$$F_4^{ce}(\phi', \theta') = \frac{2 \sin(\phi'/2) (\sin \phi' + \cos \xi^{ae}) \exp([J_1^{ae}(\phi') - J_1^{ho}(\phi')]/(2\pi))}{(1 - \sin^2 \theta' \sin^2 \phi') k |\bar{B}_{ce}| (\sin \phi' + \cos \xi^{ho}) (1 + \sin \theta' \cos \xi^{ho})} \\ \cdot \sqrt{2K} ((\sin \xi^{ho} - \cos \phi') / (\sin \xi^{ae} - \cos \phi'))^{1/2} / \cos(\xi^{ae}) \quad (4.215)$$

Note that for a given ϕ' , θ' and ξ , the functions $\{\tilde{F}_i^{ce}\}_{i=1}^4$ are fixed, which is very helpful when the diffraction coefficients have to be computed.

PMC CASE.

The diffracted E_z^{de} and H_z^{do} fields can be simply obtained by duality from the results given for the PEC case, that is

$$E_z^{de}(\rho, \phi, z) = \left[\frac{-E_{cz} D_{ze}^{a1}(\phi', \phi) + \eta_0 H_{cz} \cos \theta' D_{ze}^{a2}(\phi', \phi)}{1 - \sin^2 \theta' \sin^2 \phi} \right] \frac{e^{(iK\rho + ik'_z z)}}{\sqrt{\rho}} \quad (4.216)$$

$$H_z^{do}(\rho, \phi, z) = \left[\frac{-H_{cz} D_{zo}^{h1}(\phi', \phi) + Y_0 E_{cz} \cos \theta' D_{zo}^{h2}(\phi', \phi)}{1 - \sin^2 \theta' \sin^2 \phi} \right] \frac{e^{(iK\rho + ik'_z z)}}{\sqrt{\rho}} \quad (4.217)$$

where

$$\begin{aligned} D_{ze}^{a1}(\phi', \phi) &= \cos \phi D_{ye}^{dh}(\phi', \phi) [\cos \phi' - (\cos \phi + \cos \phi') \tilde{F}_2^{co}] \\ &+ \cos^2 \theta' \sin \phi \sin \phi' D_{yo}^{da}(\phi', \phi) [1 - (\cos \phi + \cos \phi') \tilde{F}_3^{co}] \end{aligned} \quad (4.218)$$

$$\begin{aligned}
D_{ze}^{a2}(\phi', \phi) = & -\sin\phi D_{y0}^{da}(\phi', \phi)[\cos\phi' - (\cos\phi + \cos\phi')\hat{F}_1^{co}] \\
& - \cos\phi D_{ye}^{dh}(\phi', \phi)[- \sin\phi' + (\cos\phi + \cos\phi')\hat{F}_4^{co}] \quad (4.219)
\end{aligned}$$

$$\begin{aligned}
D_{zo}^{h1}(\phi', \phi) = & \cos\phi D_{y0}^{da}(\phi', \phi)[\cos\phi' - (\cos\phi + \cos\phi')\hat{F}_1^{co}] \\
& + \cos^2\theta' \sin\phi D_{ye}^{dh}(\phi', \phi)[\sin\phi' - (\cos\phi + \cos\phi')\hat{F}_4^{co}] \quad (4.220)
\end{aligned}$$

$$\begin{aligned}
D_{zo}^{h2}(\phi', \phi) = & -\cos\phi \sin\phi' D_{y0}^{da}(\phi', \phi)[1 - (\cos\phi + \cos\phi')\hat{F}_3^{co}] \\
& - \sin\phi D_{ye}^{dh}(\phi', \phi)[- \cos\phi' + (\cos\phi + \cos\phi')\hat{F}_2^{co}] \quad (4.221)
\end{aligned}$$

$$D_{ye}^{dh}(\phi, \phi', \xi^{he}) = D_{ye}^{da}(\phi, \phi', \xi^{ae}) \quad (4.222)$$

$$D_{y0}^{da}(\phi, \phi', \xi^{ao}) = D_{y0}^{dh}(\phi, \phi', \xi^{ho}) \quad (4.223)$$

$$\hat{F}_i^{co}(\phi', \theta', \xi^{ao}, \xi^{he}) = \hat{F}_i^{ce}(\phi', \theta', \xi^{ho}, \xi^{ae}) \quad , \quad i=1,2,3,4 \quad . \quad (4.224)$$

CHAPTER V

DIELECTRIC/FERRITE BISECTION PROBLEM

Recall that when the solution of the dielectric/ferrite bisection problem (even and odd) was being discussed in Chapter II, it was mentioned that this problem was still fairly complicated. In order to simplify the problem, the thin, grounded dielectric/ferrite slab was replaced by an impedance wall. In this chapter, two different ways of modifying the solutions obtained in Chapters III and IV will be shown.

The first approach is to try to obtain a value for Z_s from the parameters describing the dielectric/ferrite slab, i.e., d , ϵ_r , μ_r . This approach applies to thin dielectric slabs (a more specific condition on how thin will be given below). The second approach is to modify the solutions obtained in Chapters III and IV, so that the geometrical optics fields are the exact fields which can be obtained by applying the exact boundary conditions to the grounded dielectric/ferrite slab.

A. FIRST APPROACH

In order to obtain the value of the impedance Z_s assume the geometry is as depicted in Figure 5.1 where a dielectric/ferrite slab above a perfectly conducting electric or magnetic plane is shown.

Following the same procedure as in [21,46], it can be shown that if a dielectric/ferrite slab of thickness $d/2$ as shown in Figure 5.1 satisfies the condition

$$kd/2 |N| \ll 1 \quad (5.1)$$

where N , given by

$$N = (\epsilon_r \mu_r)^{1/2} \quad (5.2)$$

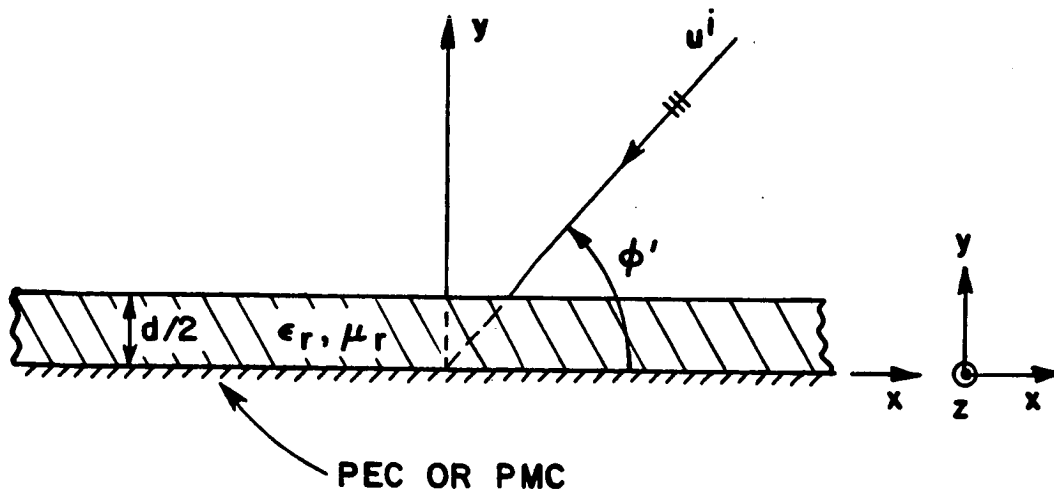


Figure 5.1 Grounded Dielectric/Ferrite Slab.

is the index of refraction, then Z_s can be approximately found as follows:

(i) TE_z polarization (H_z)

$$Z_s \approx -i \frac{\eta_0}{\epsilon_r} (N^2 - 1) k \frac{d}{2} \quad (\text{even case}) \quad (5.3)$$

$$Z_s \approx i \frac{2 \eta_0}{(\epsilon_r - 1) kd} \quad (\text{odd case}) \quad (5.4)$$

(ii) TM_z polarization (E_z)

$$\frac{1}{Z_s} = Y_s \approx \frac{-i}{\eta_0 \mu_r} (N^2 - 1) k \frac{d}{2} \quad (\text{even case}) \quad (5.5)$$

$$\frac{1}{Z_s} = Y_s \approx \frac{i}{\eta_0 (\mu_r - 1)} \frac{2}{kd} \quad (\text{odd case}) \quad (5.6)$$

(iii) TE_y polarization (H_y)

$$\frac{1}{Z_s} = Y_s \approx \frac{-i}{\eta_0 \mu_r} (N^2 - 1) k \frac{d}{2} \quad (\text{even case}) \quad (5.7)$$

$$\frac{1}{Z_s} = Y_s \approx \frac{i}{\eta_0 (\mu_r - 1)} \frac{2}{kd} \quad (\text{odd case}) \quad (5.8)$$

(iv) TM_y polarization (E_y)

$$Z_s \approx -i \frac{\eta_0}{\epsilon_r} (N^2 - 1) k \frac{d}{2} \quad (\text{even case}) \quad (5.9)$$

$$Z_s \approx \frac{i 2 \eta_0}{(\epsilon_r - 1) kd} \quad (\text{odd case}) \quad (5.10)$$

Recall that the final objective of this study is to obtain a solution for a thin dielectric/ferrite half-plane. As shown in Chapter II, this can be accomplished by adding the solutions of the even and odd bisections. The validity of this approximate representation for a thin dielectric/ferrite sheet (by an equivalent impedance Z_s) can be established [17] by comparing the corresponding reflection and transmission coefficients (obtained by substituting Equations (5.3)-(5.10) into (2.11) and (2.12)) for a plane wave incident on a sheet of infinite extent, with the expressions obtained by application of the exact boundary conditions. It is found [17] that the results agree provided that Equation (5.1) is satisfied.

B. SECOND APPROACH

As stated above, the second approach is to modify the solutions of Chapters III and IV, so that the geometrical optics field is exact. This implies that the diffracted field has to be modified also in order to obtain a continuous total field at the shadow boundaries.

Thus, a modification of the reflected geometrical optics field will be considered first. This will be followed by a modification of the diffracted field component. Finally, the expressions for the surface wave field (excited by a plane wave incident on the even and odd bisections), reflected surface wave field, and diffracted surface wave field will be modified.

It is well known that an infinite number of surface wave modes (even and odd) can exist in the dielectric/ferrite slab [21] with all the modes, but one, having a lower frequency cutoff. The only mode

without lower frequency cutoff is the lowest order even mode. In this second approach, it will be assumed that the dielectric/ferrite slab parameters are such that only the lowest order even mode (TE and/or TM) can exist.

For example, for a lossless dielectric slab, the values of $\frac{d}{\lambda}$ at cutoff for both TE and TM polarizations are given by [21]

$$\frac{d}{\lambda} = \frac{n}{2(\epsilon_r - 1)^{1/2}} \quad n = 0, 1, 2, 3, \dots \quad (5.11)$$

where λ is the free space wavelength, ϵ_r is real and $\mu_r=1$. The even integers refer to the even modes, while the odd integers refer to the odd modes. Thus, if

$$0 < \frac{d}{\lambda} < \frac{1}{2(\epsilon_r - 1)^{1/2}} \quad , \quad (5.12)$$

only the lowest order mode can exist.

Note that an important assumption is being made here in treating the diffraction problem from a dielectric/ferrite half-plane. Since the solutions obtained in Chapters III and IV are being modified in order to treat the dielectric/ferrite half-plane problem, it is assumed that the dielectric/ferrite half-plane has only one equivalent diffracting edge instead of the two geometrical edges at the end of a half-plane of finite thickness. This assumption is found to be valid as long as the dielectric/ferrite half-plane is less than one quarter wavelength inside the dielectric/ferrite medium.

1. Modification of the Reflected Geometrical Optics Field

It was shown in Chapters III and IV that the unperturbed reflected field can be written as follows:

$$\tilde{u}^r(\rho, \phi, z) = v R(\phi') e^{-iK\rho\cos(\phi+\phi')} e^{ik_z' z} \quad (5.13)$$

where $R(\phi')$ is the Fresnel reflection coefficient of an impedance wall, and $k_z' = 0$, $K=k$ for the special case of normal incidence.

It is easy to show that an expression similar to (5.13) is obtained for the geometry of Figure 5.1 if the exact boundary conditions are applied. It is shown in Appendix J that the reflection coefficients for the TE_z , TE_y , TM_z and TM_y polarizations can be obtained by the Transverse Resonance Method. Note that the reflection coefficients obtained in Appendix J are referred to the x-z plane.

It follows from Appendix J, that the reflection coefficients of Figure 5.1 (referred to the x-z plane) for the different polarizations can be expressed as follows ($e^{-i\omega t}$ time convention):

EVEN Reflection Coefficients

$$\tilde{R}_h^e(\phi', \theta') = \frac{\sin\phi' - \mu_r^{-1} \gamma^e(\phi', \theta')/\sin\theta'}{\sin\phi' + \mu_r^{-1} \gamma^e(\phi', \theta')/\sin\theta'} e^{-ik\psi(\phi', \theta')}; (H_y^e), 0 < \theta' < \pi \quad (5.14)$$

$$\tilde{R}_a^e(\phi', \theta') = \frac{\sin\phi' - \epsilon_r^{-1} \gamma^e(\phi', \theta')/\sin\theta'}{\sin\phi' + \epsilon_r^{-1} \gamma^e(\phi', \theta')/\sin\theta'} e^{-ik\psi(\phi', \theta')}; (E_y^e), 0 < \theta' < \pi \quad (5.15)$$

$$\hat{R}_a^e(\phi', \theta'=\pi/2) = \frac{\sin\phi' - \mu_r^{-1} \gamma^e(\phi', \theta'=\pi/2)}{\sin\phi' + \mu_r^{-1} \gamma^e(\phi', \theta'=\pi/2)} e^{-ik\psi(\phi', \theta'=\pi/2)} ;$$

(E_Z^e), $\theta'=\pi/2$

(5.16)

$$\hat{R}_h^e(\phi', \theta'=\pi/2) = \frac{\sin\phi' - \epsilon_r^{-1} \gamma^e(\phi', \theta'=\pi/2)}{\sin\phi' + \epsilon_r^{-1} \gamma^e(\phi', \theta'=\pi/2)} e^{-ik\psi(\phi', \theta'=\pi/2)} ;$$

(H_Z^e), $\theta'=\pi/2$

(5.17)

ODD Reflection Coefficients

$$\hat{R}_h^o(\phi', \theta') = \frac{\sin\phi' - \mu_r^{-1} \gamma^o(\phi', \theta')/\sin\theta'}{\sin\phi' + \mu_r^{-1} \gamma^o(\phi', \theta')/\sin\theta'} e^{-ik\psi(\phi', \theta')} ; (H_y^o), 0 < \theta' < \pi$$

(5.18)

$$\hat{R}_a^o(\phi', \theta') = \frac{\sin\phi' - \epsilon_r^{-1} \gamma^o(\phi', \theta')/\sin\theta'}{\sin\phi' + \epsilon_r^{-1} \gamma^o(\phi', \theta')/\sin\theta'} e^{-ik\psi(\phi', \theta')} ; (E_y^o), 0 < \theta' < \pi$$

(5.19)

$$\hat{R}_a^o(\phi', \theta'=\pi/2) = \frac{\sin\phi' - \mu_r^{-1} \gamma^o(\phi', \theta'=\pi/2)}{\sin\phi' + \mu_r^{-1} \gamma^o(\phi', \theta'=\pi/2)} e^{-ik\psi(\phi', \theta'=\pi/2)} ;$$

(E_Z^o), $\theta'=\pi/2$

(5.20)

$$\tilde{R}_h^0(\phi', \theta' = \pi/2) = \frac{\sin \phi' - \epsilon_r^{-1} \gamma^0(\phi', \theta' = \pi/2)}{\sin \phi' + \epsilon_r^{-1} \gamma^0(\phi', \theta' = \pi/2)} e^{-ik\psi(\phi', \theta' = \pi/2)} ;$$

(H_Z⁰), $\theta' = \pi/2$.

(5.21)

The expressions for γ^e , γ^0 and ψ are such that

$$\gamma^e(\phi', \theta') = -i[N^2 - \cos^2 \theta' \sin^2 \phi' - \cos^2 \phi']^{1/2} \cdot \tan \left[[N^2 - \cos^2 \theta' \sin^2 \phi' - \cos^2 \phi']^{1/2} k \frac{d}{2} \right]$$

(5.22)

$$\gamma^0(\phi', \theta') = +i[N^2 - \cos^2 \theta' \sin^2 \phi' - \cos^2 \phi']^{1/2} \cdot \cot \left[[N^2 - \cos^2 \theta' \sin^2 \phi' - \cos^2 \phi']^{1/2} k \frac{d}{2} \right]$$

(5.23)

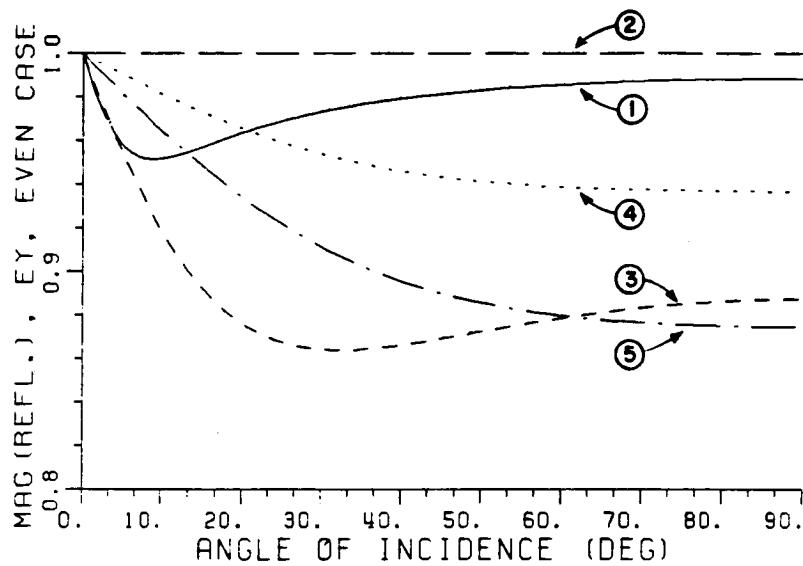
and

$$\psi(\phi', \theta') = d \sin \theta' \sin \phi' \quad (5.24)$$

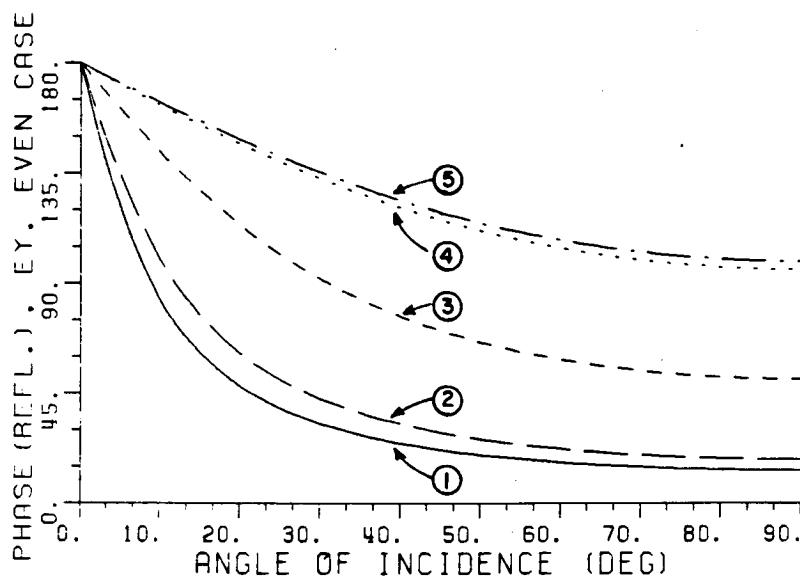
where N is the index of refraction and it was defined in Equation (5.2).

The reflection coefficients defined in Equations (5.15), (5.19), (5.14) and (5.18) are shown in Figures (5.2)-(5.5), respectively, for $\theta' = \pi/6$, $d/2 = 0.025\lambda$, and for the following values of ϵ_r and μ_r :

- | | |
|----------------------------------|--------------------------|
| (1) $\epsilon_r = 2.(1 + i0.05)$ | $\mu_r = 1.(1 + i0.0)$ |
| (2) $\epsilon_r = 3.(1 + i0.0)$ | $\mu_r = 1.(1 + i0.0)$ |
| (3) $\epsilon_r = 3.(1 + i0.1)$ | $\mu_r = 2.(1 + i0.1)$ |
| (4) $\epsilon_r = 3.(1 + i0.05)$ | $\mu_r = 4.(1 + i0.05)$ |
| (5) $\epsilon_r = 4.(1 + i0.1)$ | $\mu_r = 4.(1 + i0.1)$. |

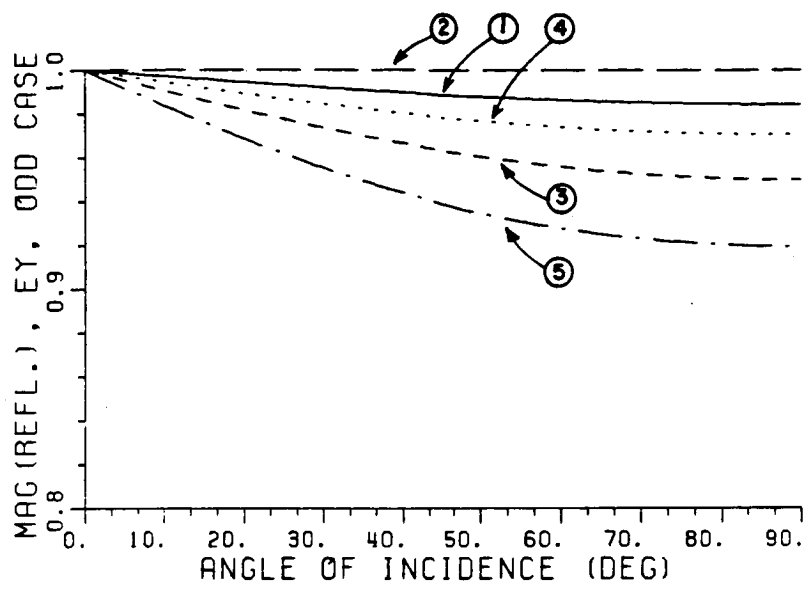


Magnitude of Reflection Coefficient

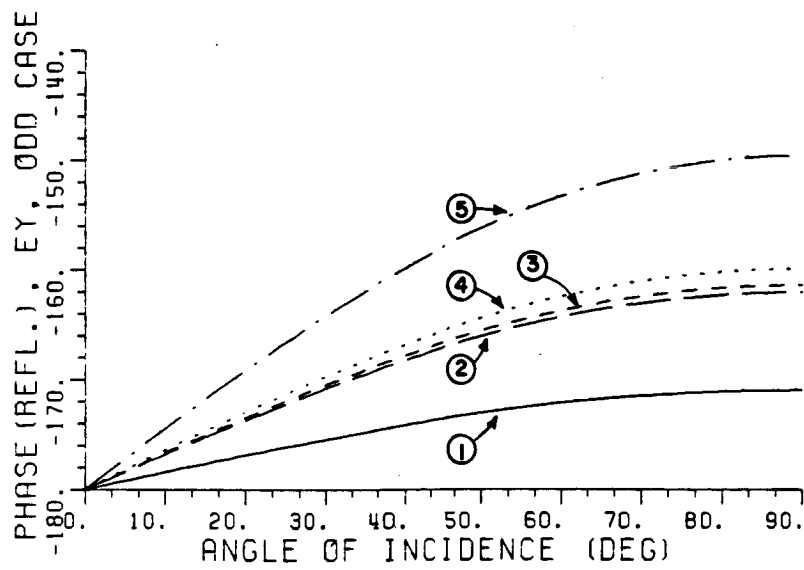


Phase of Reflection Coefficient (Degrees)

Figure 5.2. Reflection coefficient for TM_y polarization (E_y), even case.

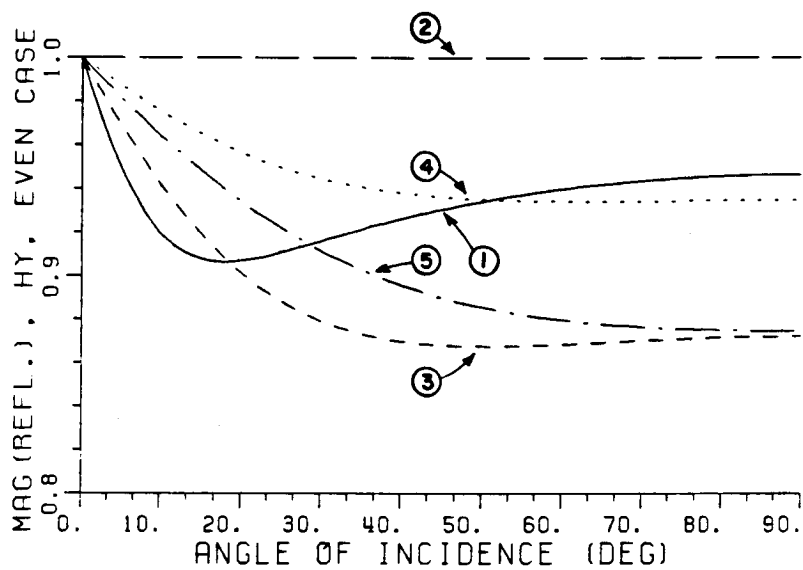


Magnitude of Reflection Coefficient

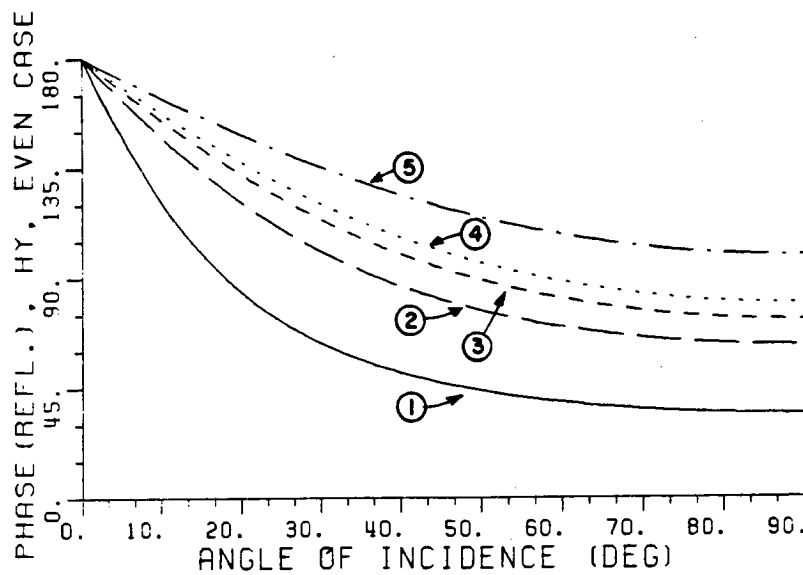


Phase of Reflection Coefficient (Degrees)

Figure 5.3. Reflection coefficient for TM_y polarization (E_y), odd case.

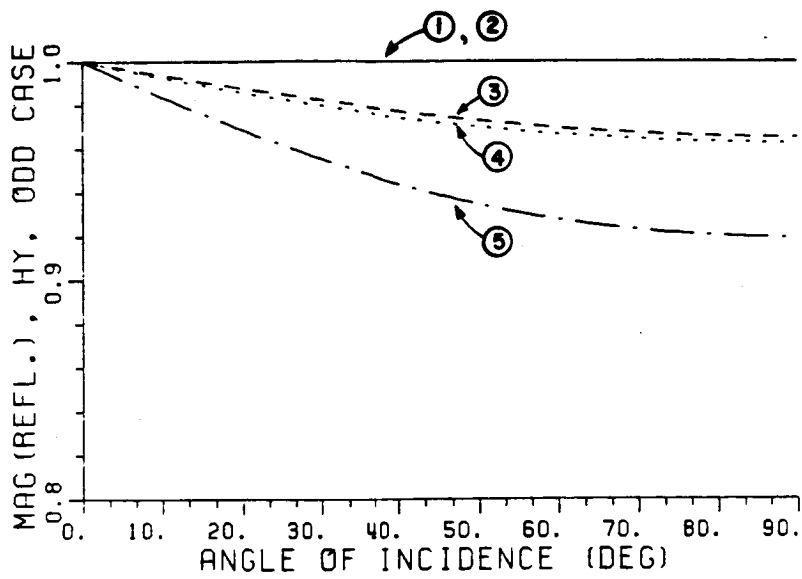


Magnitude of Reflection Coefficient

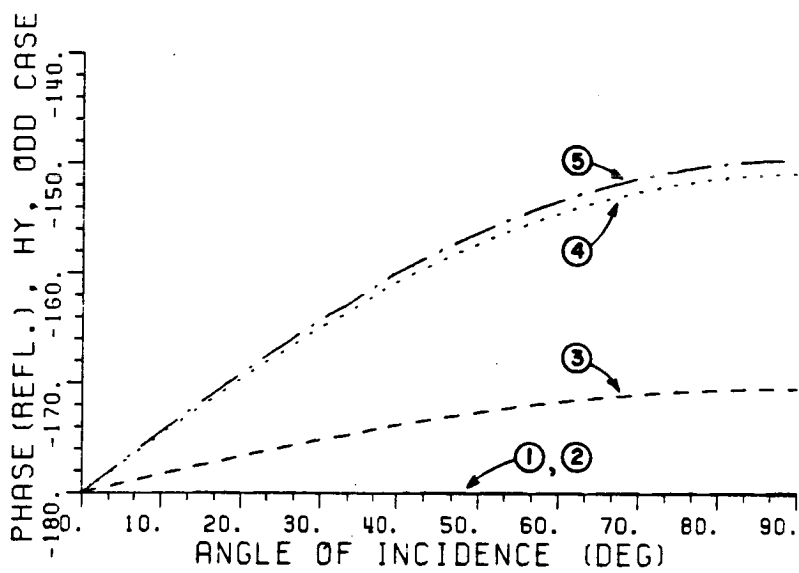


Phase of Reflection Coefficient (Degrees)

Figure 5.4. Reflection coefficient for TE_y polarization (H_y), even case.



Magnitude of Reflection of Coefficient



Phase of Reflection Coefficient (Degrees)

Figure 5.5. Reflection coefficient for TE_y polarization (H_y), odd case.

Note that the reflection coefficients shown in Figures (5.2) through (5.5) can be controlled (magnitude and phase) by varying the values of ϵ_r , μ_r and d . The reason for referring the reflection coefficients to the x - z plane is because the edge diffracted field from the dielectric/ferrite half-plane is assumed to originate from an equivalent edge located half way between the two geometrical edges of the half-plane of finite thickness.

Since the geometrical optics field has been modified, the diffracted field has to be modified also to have a continuous total field at the boundary $\phi=\pi-\phi$, where the reflected field becomes discontinuous. First, the diffraction coefficients (for plane and surface wave incidence) and the surface wave launching coefficients for the 2-D (normal incidence) impedance bisection problem will be modified. In Section C, the more general 3-D results obtained in Chapter IV will also be modified, however, unlike the 2-D case, a combination of the first and second approaches will be used.

2. Diffraction Coefficients for the Normal Incidence Case ($\theta'=\pi/2$)

Recall that the diffraction coefficients D_e^d and D_o^d obtained in Chapter III are a function of ξ , which is related to the normalized impedance or admittance as shown in Equations (3.96) and (3.156). The goal of this section is to find an equivalent $\tilde{\xi}$ for the

dielectric/ferrite slab depicted in Figure 5.1. Unlike ξ , the new $\tilde{\xi}$ will be a function of ϕ' and θ' .

In order to obtain the new function $\tilde{\xi}$, note that near the boundary $\phi=\pi-\phi'$, the diffraction coefficients D_e^d and D_o^d for the impedance bisection problem (see Chapter III) are equal to

$$D_{e,o}^d(\phi=\pi-\phi', \phi', \theta'=\pi/2) = \left[\frac{1-R_{e,o}}{2} \right] \text{sign}(\tilde{\epsilon}) + CT^{e,o} \quad (5.25)$$

where $CT^{e,o}$ is a continuous term at the boundary $\phi=\pi-\phi'$ and

$$\tilde{\epsilon} = \phi + \phi' - \pi \quad . \quad (5.26)$$

The sign that $\tilde{\epsilon}$ takes on both sides of the shadow boundary is depicted in Figure 5.6. Note that $R_{e,o}$, defined in (3.20), is the Fresnel reflection coefficient for an impedance wall.

Furthermore, it is easy to prove that D_e^d and D_o^d satisfy the Lorentz reciprocity theorem, that is [47]

$$D_{e,o}^d(\phi, \phi') = D_{e,o}^d(\phi', \phi) \quad , \quad 0 < (\phi, \phi') < \pi \quad . \quad (5.27)$$

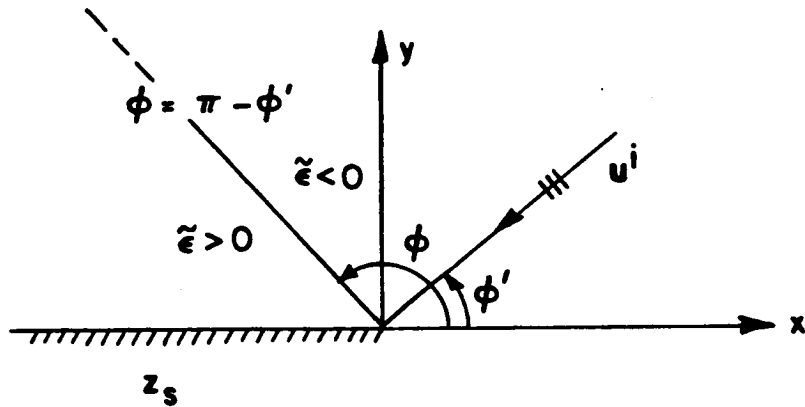


Figure 5.6. Sign of $\tilde{\epsilon}$ near the reflection shadow boundary.

Now, let \tilde{D}_e^d and \tilde{D}_o^d be the even and odd diffraction coefficients for the dielectric/ferrite bisection problem, respectively. These two diffraction coefficients also satisfy Equation (5.27). In addition to that, they satisfy an equation similar to (5.25), that is

$$\tilde{D}_{e,0}^d(\phi \approx \pi - \phi', \phi', \theta' = \pi/2) = \left[\frac{1 - \tilde{R}_{e,0}}{2} \right] \text{sign}(\tilde{\epsilon}) + \tilde{C}T^{e,0} \quad (5.28)$$

where $\tilde{R}_{e,0}$ is the reflection coefficient defined in the previous section and $\tilde{C}T^{e,0}$ is a continuous term at the boundary $\phi = \pi - \phi'$.

The first step in finding the function $\tilde{\xi}$ is to define a new function $\tilde{R}_{e,0}^d$ which assumes the value of $\tilde{R}_{e,0}$ at the boundary $\phi=\pi-\phi'$, that is

$$\tilde{R}_e^d(\phi, \phi') = \frac{\sin \phi' - \cos \tilde{\xi}^e}{\sin \phi' + \cos \tilde{\xi}^e} e^{-ik\tilde{\psi}} \quad (5.29)$$

$$\tilde{R}_0^d(\phi, \phi') = \frac{\sin \phi' - \cos \tilde{\xi}^0}{\sin \phi' + \cos \tilde{\xi}^0} e^{-ik\tilde{\psi}} \quad (5.30)$$

where $\cos \tilde{\xi}^e$ and $\cos \tilde{\xi}^0$ are defined as follows:

$$\begin{aligned} \tilde{\delta}_{e,0}(\phi, \phi', \theta'=\pi/2) &= \tilde{\delta}_{e,0}(\phi', \phi, \theta'=\pi/2) = \cos \tilde{\xi}^{e,0} \\ &= \begin{bmatrix} \mu_r & -1 \\ \epsilon_r & -1 \end{bmatrix} \tilde{\gamma}^{e,0}(\phi, \phi, \theta'=\pi/2); \begin{bmatrix} E_z \\ H_z \end{bmatrix} \end{aligned} \quad (5.31)$$

and

$$\begin{aligned} \tilde{\gamma}^e(\phi', \phi, \theta'=\pi/2) &= -i[N^2 - |\cos \phi \cos \phi'|]^{1/2} \\ &\cdot \tan \left[(N^2 - |\cos \phi \cos \phi'|)^{1/2} kd/2 \right] \end{aligned} \quad (5.32)$$

$$\begin{aligned} \tilde{\gamma}^0(\phi', \phi, \theta'=\pi/2) &= i[N^2 - |\cos \phi \cos \phi'|]^{1/2} \\ &\cdot \cot \left[(N^2 - |\cos \phi \cos \phi'|)^{1/2} kd/2 \right] \end{aligned} \quad (5.33)$$

$$\tilde{\psi}(\phi, \phi', \theta' = \frac{\pi}{2}) = \tilde{\psi}(\phi', \phi, \theta' = \frac{\pi}{2}) = \frac{d}{2} \sin \theta' (\sin \phi + \sin \phi') \Big|_{\theta' = \pi/2} = \frac{d}{2} (\sin \phi + \sin \phi') \quad (5.34)$$

Note that $\tilde{\gamma}^e$ and $\tilde{\gamma}^o$ are functions of ϕ and ϕ' , while γ^e and γ^o were not. Moreover, $\tilde{\gamma}^{e,o}$ is equal to $\gamma^{e,o}(\phi', \theta' = \pi/2)$ at the boundary $\phi = \pi - \phi'$. For the lossless case (N real) and for ϕ, ϕ' in the interval $0 < (\phi, \phi') < \pi$, it is desirable that $\tilde{\delta}_e$ and $\tilde{\delta}_o$ do not change sign. It follows that

$$0 < [N^2 - |\cos \phi \cos \phi'|]^{1/2} \frac{kd}{2} < \frac{\pi}{2}, \quad 0 < (\phi, \phi') < \pi \quad (5.35)$$

which implies that

$$\frac{d}{\lambda} < \frac{1}{2N} \quad (5.36)$$

where λ is the free space wavelength. Note that if Equation (5.36) is satisfied, Equation (5.12) will also be satisfied. The above restriction is due to the fact that $\tilde{\delta}_{e,o}$ plays the role of an equivalent normalized reactance (or susceptance) for the dielectric/ferrite slab depicted in Figure 5.1.

Replacing $\tilde{R}_{e,o}$ by $\tilde{R}_{e,o}^d$ in the term $(1 \pm \tilde{R}_{e,o})/2$, one gets

$$\left[\frac{1 - \tilde{R}_e^d}{2} \right] = \left[\frac{1 - e^{-ik\tilde{\psi}}}{2} \right] \frac{\sin \phi'}{\sin \phi' + \cos \tilde{\xi}^e} + \left[\frac{1 + e^{-ik\tilde{\psi}}}{2} \right] \frac{\cos \tilde{\xi}^e}{\sin \phi' + \cos \tilde{\xi}^e} \quad (5.37)$$

and

$$\begin{aligned}
\left[\frac{1+\tilde{R}_0^d}{2} \right] \frac{\cos(\phi/2)}{\sin(\phi'/2)} &= (1+e^{-ik\tilde{\psi}}) \frac{\cos(\phi'/2) \cos(\phi/2)}{\sin\phi'+\cos\tilde{\xi}^0} \\
+ \left[\frac{1-e^{-ik\tilde{\psi}}}{2} \right] \frac{\cos\tilde{\xi}^0}{(\sin\phi'+\cos\tilde{\xi}^0)} \frac{\cos(\phi/2)}{\sin(\phi'/2)} & \quad (5.38)
\end{aligned}$$

Recall that \tilde{D}_e^d and \tilde{D}_0^d have to satisfy Equation (5.27), however, (5.37) and (5.38) do not satisfy these two equations, so one more modification is necessary. The new quantities $(1-\tilde{R}_e^d)/2$ and $(1+\tilde{R}_0^d)/2$ which satisfy Equation (5.27), are defined in Equations (5.39) and (5.40) as follows:

$$\left[\frac{1-\tilde{R}_e^d}{2} \right] = \left[\frac{1+e^{-ik\tilde{\psi}}}{2} \right] \frac{\cos\tilde{\xi}^e}{\sin\phi'+\cos\tilde{\xi}^e} + \left[\frac{1-e^{-ik\tilde{\psi}}}{2} \right] \frac{(\sin\phi\sin\phi')^{1/2}}{\sin\phi'+\cos\tilde{\xi}^e} \quad (5.39)$$

and

$$\begin{aligned}
\left[\frac{1+\tilde{R}_0^d}{2} \right] &= \left[\frac{1+e^{-ik\tilde{\psi}}}{2} \right] \frac{2\cos(\phi'/2)\cos(\phi/2)}{\sin\phi'+\cos\tilde{\xi}^0} \\
+ \left[\frac{1-e^{-ik\tilde{\psi}}}{2} \right] \frac{\cos\tilde{\xi}^0 e^{-f}}{\sin\phi'+\cos\tilde{\xi}^0} & \quad (5.40)
\end{aligned}$$

where

$$f(\phi', \phi) = f(\phi, \phi') = \frac{|\sin(\phi + \phi')|}{(\pi - \phi)^2 (\pi - \phi')^2} \quad (5.41)$$

The new function $f(\phi', \phi)$ was introduced because the term $\cos(\phi/2)/\sin(\phi'/2)$ in (5.38) becomes unbounded at $\phi'=0$. Note that the function e^{-f} assumes the following values when $\phi = \pi$ or $\phi = \pi - \phi'$:

$$e^{-f} = \begin{cases} 1 & \text{at } \phi = \pi - \phi' \\ 0 & \text{as } \phi \rightarrow \pi \end{cases} \quad (5.42)$$

and

$$\left[\frac{1 - \tilde{R}_e^d}{2} \right] = \left[\frac{1 - \tilde{R}_e}{2} \right], \quad \left[\frac{1 + \tilde{R}_0^d}{2} \right] = \left[\frac{1 + \tilde{R}_0}{2} \right] \quad (5.43)$$

as required. Furthermore, when d is very small

$$\hat{\psi} \approx 0 \quad (5.44)$$

and

$$\left[\frac{1 - \tilde{R}_e^d}{2} \right] = \frac{\cos \tilde{\xi}^e}{\sin \phi' + \cos \tilde{\xi}^e}; \quad \left[\frac{1 + \tilde{R}_0^d}{2} \right] = \frac{2 \cos(\phi/2) \cos \phi'/2}{\sin \phi + \cos \tilde{\xi}^e} \quad (5.45)$$

The modifications made above may appear arbitrary, however, as shown in Chapter VIII, they give very good results when compared with solutions obtained using the method of moments.

Using the results obtained above, the new diffraction coefficients \tilde{D}_e^e and \tilde{D}_0^d for the geometry depicted in Figure 5.7 can be written as follows:

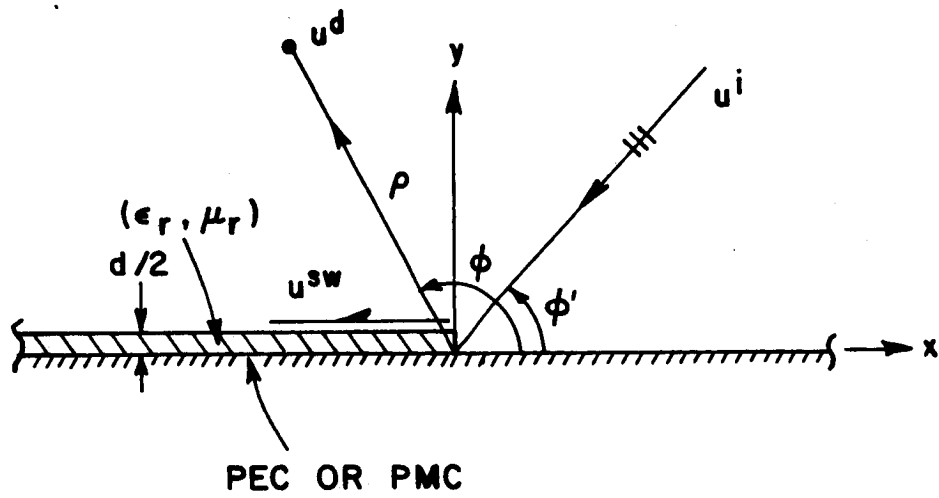


Figure 5.7. Dielectric/ferrite bisection problem.

$$\begin{aligned}
 \hat{D}_{ez}^d(\phi, \phi') = \hat{D}_{ez}^d(\phi', \phi) = & - \left[\frac{1 - R_e^d}{2} \right] \frac{e^{i\pi/4}}{\sqrt{2\pi k}} \\
 & \cdot \frac{[(\sin \tilde{\xi}^e - \cos \phi)(\sin \tilde{\xi}^e - \cos \phi')]^{1/2}}{\sin \phi + \cos \tilde{\xi}^e} e^{-\frac{\tilde{J}_1^e(\phi) + \tilde{J}_1^e(\phi')}{2\pi}} \\
 & \cdot \left[\sec(\beta^+/2) F(-kLa^+) + \sec(\beta^-/2) F(-kLa^-) \right], \quad 0 < \phi < \pi
 \end{aligned} \tag{5.46}$$

$$\begin{aligned}
\hat{D}_{oz}^d(\phi, \phi') = \hat{D}_{oz}^d(\phi', \phi) = & \frac{-e^{i\pi/4}}{\sqrt{2\pi k}} \left[\frac{1 + \hat{R}_0^d}{2} \right] \\
& \cdot \frac{[(\sin \hat{\xi}^0 - \cos \phi)(\sin \hat{\xi}^0 - \cos \phi')]^{1/2}}{\sin \phi + \cos \hat{\xi}^0} e^{-\frac{\hat{J}_1^0(\phi) + \hat{J}_1^0(\phi')}{2\pi}} \\
& \cdot \left[\sec(\beta^-/2) F(-kLa^-) - \sec(\beta^+/2) F(-kLa^+) \right]
\end{aligned} \tag{5.47}$$

where

$$\hat{J}_1^{0,e}(w) = \int_{\pi/2 - w + \hat{\xi}^{0,e}}^{3\pi/2 - w - \hat{\xi}^{0,e}} \frac{t}{\sin t} dt \tag{5.48}$$

3. Modification of Surface Wave Field Excited by a Plane Wave (Normal Incidence)

From the results given in Chapter III, the expressions for the surface wave fields u_e^{sw} and u_o^{sw} can be completely specified in terms of ξ and w_s which is the pole of $G_-(-k\cos w)$. Since $\xi^{e,0}$ can be expressed in terms of $w_s^{e,0}$, the fields u_e^{sw} and u_o^{sw} can be represented as a function of w_s only.

Thus, the first step is to rewrite u_e^{SW} and u_o^{SW} in terms of w_s . Substituting Equations (3.167) and (3.215) into (3.200) and (3.233), respectively, yields

$$u_e^{SW}(\rho, \phi, w_s^e) = u^i(QE) L_{ze}^{SW}(\phi', w_s^e) \exp[ik(x \cos w_s^e + y \sin w_s^e)] U(\phi - \tilde{\phi}_s^e) \quad (5.49)$$

$$u_o^{SW}(\rho, \phi, w_s^o) = u^i(QE) L_{zo}^{SW}(\phi', w_s^o) \exp[ik(x \cos w_s^o + y \sin w_s^o)] U(\phi - \tilde{\phi}_s^o) \quad (5.50)$$

where L_{ze}^{SW} and L_{zo}^{SW} are the even and odd surface wave launching coefficients, respectively, and

$$u^i(QE) = u^i(\rho=0) = v e^{-ik\rho \cos(\phi - \phi')} \Big|_{\rho=0} = v \quad (5.51)$$

The coefficients L_{ze}^{SW} and L_{zo}^{SW} are given by the following two expressions:

$$L_{ze}^{SW}(\phi', w_s^e) = \frac{\sin(w_s^e)}{\sin \phi' - \sin w_s^e} \left[\frac{2(\cos w_s^e + \cos \phi')}{\cos w_s^e} \right]^{1/2} \cdot \exp \left[\frac{-1}{2\pi} [J_1^e(w_s^e) + J_1^e(\phi')] \right] \cdot \left[\sec((w_s^e - \phi')/2) + \sec((w_s^e + \phi')/2) \right] \quad (5.52)$$

$$L_{oz}^{sw}(\phi', w_s^0) = \frac{-2\cos(\phi'/2)\cos(w_s^0/2)}{\sin\phi' - \sin w_s^0} \left[\frac{2(\cos w_s^0 + \cos\phi')}{\cos w_s^0} \right]^{1/2} \cdot \exp \left[\frac{-1}{2\pi} [J_1^0(w_s^0) + J_1^0(\phi')] \right] \cdot \left[\sec((w_s^0 - \phi')/2) - \sec((w_s^0 + \phi')/2) \right] \quad (5.53)$$

where

$$J_1(\alpha) = \int_{w_s^0 - \alpha}^{2\pi - w_s^0 - \alpha} \frac{t}{\sin t} dt \quad . \quad (5.54)$$

Note that QE is the point where u^{sw} is excited, which in this case happens to be the origin.

It is shown in [21] that for the grounded dielectric/ferrite slab depicted in Figure 5.1, the propagation constants $\cos(w_s)$ and $\sin(w_s)$ of a surface wave field are a function of the poles (on the proper Riemann surface) of the reflection coefficients defined in Equations (5.16), (5.17), (5.20) and (5.21) with ϕ' replaced by the complex variable w . In other words, for the grounded dielectric/ferrite slab of thickness $d/2$, w_s is the root of the equations:

$$\sin w_S^e - i \begin{bmatrix} \mu_r - 1 \\ \epsilon_r - 1 \end{bmatrix} (N^2 - \cos^2 w_S^e)^{1/2} \tan \left[(N^2 - \cos^2 w_S^e)^{1/2} k \frac{d}{2} \right] = 0; \begin{bmatrix} E_z \\ H_z \end{bmatrix} \quad (5.55)$$

and

$$\sin w_S^o + i \begin{bmatrix} \mu_r - 1 \\ \epsilon_r - 1 \end{bmatrix} (N^2 - \cos^2 w_S^o)^{1/2} \cot \left[(N^2 - \cos^2 w_S^o)^{1/2} k \frac{d}{2} \right] = 0; \begin{bmatrix} E_z \\ H_z \end{bmatrix} \quad (5.56)$$

Since Equations (5.55)-(5.56) have many solutions, the roots w_S have to lie in the correct location of the periodic w -domain so they will correspond to physically possible surface wave fields (see Figure 3.11). Furthermore, it was assumed at the beginning of Section B, that the parameters of the dielectric/ferrite slab (ϵ_r , μ_r , d) are chosen so that only the lowest order even mode can propagate. Thus, only Equation (5.55) has to be solved for the root w_S^e corresponding to the lowest order even mode, and the field u_0^{sw} given in (5.50) is not allowed to exist. Once w_S^e is calculated in (5.55), then u_e^{sw} can be easily computed by substituting w_S^e into (5.49) and (5.52).

4. Modification of Reflected and Diffracted Surface Wave Fields Excited by an Incident Surface Wave (Normal Incidence)

The procedure for modifying the reflected and diffracted surface wave fields is the same as in Section 3. In other words, the

expressions for the reflected and diffracted surface wave fields are rewritten in terms of w_s only, where w_s is calculated by solving Equations (5.55) and (5.56). It follows from (3.278) and (3.291) that

$$u_e^{rsw}(\rho, \phi) = u_e^{isw}(QR) R_{ez}^{sw}(w_s^e) \exp[ik(x \cos w_s^e + y \sin w_s^e)] \quad (5.57)$$

$$u_o^{rsw}(\rho, \phi) = u_o^{isw}(QR) R_{oz}^{sw}(w_s^o) \exp[ik(x \cos w_s^o + y \sin w_s^o)] \quad (5.58)$$

where w_s^e and w_s^o are the roots of Equations (5.55) and (5.56), respectively. The functions R_{ez}^{sw} and R_{oz}^{sw} , given by

$$R_{ez}^{sw}(w_s^e) = \left[\frac{1 + \cos w_s^e}{\cos w_s^e} \right] \exp \left[\frac{-1}{\pi} \int_0^{2\pi - 2w_s^e} \frac{t}{\sin t} dt \right] \quad (5.59)$$

and

$$R_{oz}^{sw}(w_s^o) = \tan(w_s^o) \exp \left[\frac{-1}{\pi} \int_0^{2\pi - 2w_s^o} \frac{t}{\sin t} dt \right], \quad (5.60)$$

are the even and odd reflection coefficients, respectively. $u^{isw}(QR)$ is the incident surface wave field evaluated at the point of reflection QR, which in this problem happens to be the origin. That is,

$$u^{isw}(QR) = v e^{ik(-x \cos w_s + y \sin w_s)} \Big|_{x=y=0} = v \quad (5.61)$$

The diffracted surface wave fields can be rewritten as follows:

$$u_e^{dsw}(\rho, \phi) = u_e^{isw}(QE) D_{ez}^{swd} \frac{e^{ik\rho}}{\sqrt{\rho}} \quad (5.62)$$

$$u_o^{dsw}(\rho, \phi) = u_o^{isw}(QE) D_{oz}^{swd} \frac{e^{ik\rho}}{\sqrt{\rho}} \quad (5.63)$$

where D_{ez}^{swd} and D_{oz}^{swd} are the surface wave diffraction coefficients which can be obtained from Equations (3.318) and (3.332) such that

$$D_{ez}^{swd} = \frac{ie^{-i\pi/4}}{\sqrt{2\pi k}} \frac{\sin(w_s^e)}{(\cos w_s^e + \cos \phi)} \left[\frac{2\cos(w_s^e)(1 + \cos \phi)}{(\cos w_s^e - 1)(\cos \phi - \cos w_s^e)} \right]^{1/2} \\ \cdot \left[\frac{\sin \phi + \sin w_s^e}{\sin \phi - \sin w_s^e} \right]^{1/2} \cdot \exp \left[\frac{-1}{2\pi} [J_1^e(\phi) + J_1^e(w_s^e)] \right] \quad (5.64)$$

$$D_{oz}^{swd} = \frac{ie^{-i\pi/4}}{\sqrt{2\pi k}} \frac{\sin \phi}{(\cos w_s^0 + \cos \phi)} \left[\frac{2\cos(w_s^0)}{\cos w_s^0 - \cos \phi} \right]^{1/2} \\ \cdot \left[\frac{\sin \phi + \sin w_s^0}{\sin \phi - \sin w_s^0} \right]^{1/2} \cdot \exp \left[\frac{-1}{2\pi} [J_1^0(\phi) + J_1^0(w_s^0)] \right] \quad (5.65)$$

The point QE is the point of diffraction which in this particular problem is equal to QR. Thus,

$$u^{isw}(QE) = v \quad . \quad (5.66)$$

As in Section 3, if only the lowest order even mode is allowed to exist, R_0^{sw} and D_{0z}^{swd} are equal to zero.

C. MODIFICATION OF DIFFRACTED FIELD FOR PLANE WAVE INCIDENCE (OBLIQUE INCIDENCE CASE)

As shown in Chapter IV, the diffraction coefficients for the fields E_z^d and H_z^d can be expressed in terms of the two-dimensional diffraction coefficients (obtained in Chapter III) and the \tilde{F}_i -functions. Note that all the \tilde{F}_i -functions are multiplied by $(\cos\phi + \cos\phi')$ which is zero at the shadow boundary $\phi = \pi - \phi'$. This means that the \tilde{F}_i -functions do not play a very important role near the shadow boundary. Consequently, the two approaches described in Sections A and B will be combined to modify the diffraction coefficients for the case of oblique incidence.

The diffraction coefficients $\{D_{ye}^{da}, D_{ye}^{dh}, D_{yo}^{da}, D_{yo}^{dh}\}$ will be modified following an approach similar to that in Section B.2. First, the functions $\tilde{\delta}_e$ and $\tilde{\delta}_o$ are defined as follows:

$$\cos \tilde{\xi}_{e,0}^{(a)} = \frac{\tilde{\delta}_{e,0}^{(h)}(\phi, \phi', \theta')}{\sin \theta'} = \begin{bmatrix} \epsilon_r^{-1} \\ \mu_r^{-1} \end{bmatrix} \tilde{\gamma}_{e,0}(\phi', \phi, \theta') / \sin \theta'; \begin{bmatrix} E_y \\ H_y \end{bmatrix} \quad (5.67)$$

where

$$\tilde{\gamma}^e(\phi', \phi, \theta') = -i[N^2 - (|\cos \phi \cos \phi'| + |\sin \phi \sin \phi'| \cos^2 \theta')]^{1/2} \cdot \tan \left[\frac{[N^2 - (|\cos \phi \cos \phi'| + |\sin \phi \sin \phi'| \cos^2 \theta')]^{1/2} kd/2}{1} \right] \quad (5.68)$$

$$\tilde{\gamma}^o(\phi', \phi, \theta') = i[N^2 - (|\cos \phi \cos \phi'| + |\sin \phi \sin \phi'| \cos^2 \theta')]^{1/2} \cdot \cot \left[\frac{[N^2 - (|\cos \phi \cos \phi'| + |\sin \phi \sin \phi'| \cos^2 \theta')]^{1/2} kd/2}{1} \right] \quad (5.69)$$

As in the 2-D case, $\tilde{\gamma}^{e,o}(\phi', \phi, \theta')$ is equal to $\gamma^{e,o}$ when $\phi = \pi - \phi'$.

Next, the expressions $(1 + \tilde{R}_0^d) \cos(\phi/2) / (2 \sin(\phi'/2))$ and $(1 - \tilde{R}_e^d)/2$ are replaced by two new functions $(1 + \tilde{R}_0^d)/2$ and $(1 - \tilde{R}_e^d)/2$ given in Equations (5.40) and (5.39), respectively, except that the functions $\cos \tilde{\xi}^e$ and $\cos \tilde{\xi}^o$ which appear in (5.39)-(5.40) are replaced by the ones defined in (5.67). Furthermore, the function $\tilde{\psi}(\phi, \phi', \theta')$ given in (5.34) replaces $\tilde{\psi}(\phi, \phi', \theta' = \pi/2)$ in (5.39)-(5.40). Therefore, the new diffraction coefficients $\{D_{ye}^{da}, D_{ye}^{dh}, D_{yo}^{da}, D_{yo}^{dh}\}$ are similar to those in (5.46)-(5.47), except for the changes mentioned above and the fact that k is replaced by K .

Since the \tilde{F}_i -functions are multiplied by a function which is zero at the boundary $\phi=\pi-\phi'$, they are modified as indicated in Section A; i.e., "the first approach". In other words, the parameters $\{\xi^{ae}, \xi^{ao}, \xi^{he}, \xi^{ho}\}$ which appear in the F_i -functions will be replaced by the new set of parameters $\{\tilde{\xi}^{ae}, \tilde{\xi}^{ao}, \tilde{\xi}^{he}, \tilde{\xi}^{ho}\}$ which are calculated as follows:

$$\cos \tilde{\xi}^{he} = \frac{-i(N^2-1)kd}{2 \mu_r \sin \theta'} \quad , \quad 0 < \theta' < \pi \quad (5.70)$$

$$\cos \tilde{\xi}^{ho} = \frac{i2}{\mu_r k d \sin \theta'} \quad , \quad 0 < \theta' < \pi \quad (5.71)$$

$$\cos \tilde{\xi}^{ae} = \frac{-i(N^2-1)kd}{\epsilon_r 2 \sin \theta'} \quad , \quad 0 < \theta' < \pi \quad (5.72)$$

$$\cos \tilde{\xi}^{ao} = \frac{i2}{\epsilon_r k d \sin \theta'} \quad , \quad 0 < \theta' < \pi \quad (5.73)$$

Note that the real part of the parameter $\tilde{\xi}$ is restricted to the interval $0 < \text{Re}(\tilde{\xi}) < \pi/2$.

D. MODIFICATION OF SURFACE WAVE FIELD EXCITED BY A PLANE WAVE (OBLIQUE INCIDENCE)

Recall that the surface wave fields E_y^{sw} and H_y^{sw} are expressed in terms of the incident fields E_y^i and H_y^i . In order to express E_y^{sw} and H_y^{sw} in terms of launching coefficients similar to those defined in Section B.3, it is necessary to rewrite E_y^i and H_y^i in terms of E_z^i and H_z^i .

PEC Case

Substituting (4.194)-(4.195) into (4.121) and (4.135) yields

$$\begin{aligned} E_{ye}^{sw}(\phi', \phi, \xi^{ae}) &= L_{ye}^{swa}(\phi', w_s^{ae}) \cdot [\cos \theta' p_{2s}^{ae} E_{cz} + \eta_0 p_{1s}^{ae} H_{cz}] \\ &\cdot U(\phi - \phi_s^{ae}) \cdot e^{ik_z z} \cdot \exp [ik(x \cos w_s^{ae} + y \sin w_s^{ae})] \end{aligned} \quad (5.74)$$

$$\begin{aligned} H_{yo}^{sw}(\phi', \phi, \xi^{ho}) &= L_{yo}^{swh}(\phi', w_s^{ho}) \cdot [\cos \theta' p_{2s}^{ho} H_{cz} + \gamma_0 p_{1s}^{ho} E_{cz}] \\ &\cdot U(\phi - \phi_s^{ho}) \cdot e^{ik_z z} \cdot \exp [ik(x \cos w_s^{ho} + y \sin w_s^{ho})] \end{aligned} \quad (5.75)$$

The surface wave launching coefficients L_{ye}^{swa} and L_{yo}^{swh} are given by

$$L_{ye}^{swa}(\phi', w_s^{ae}) = L_{ze}^{sw}(\phi', w_s^e) / \sin \theta' \quad (5.76)$$

$$L_{yo}^{swh}(\phi', w_s^{ho}) = L_{zo}^{sw}(\phi', w_s^o) / \sin \theta' \quad (5.77)$$

where L_{ze}^{sw} and L_{zo}^{sw} were defined in (5.52) and (5.53), respectively.

The constants $\{p_{1s}^{ae}, p_{2s}^{ae}, p_{1s}^{ho}, p_{2s}^{ho}\}$ can be expressed as follows:

$$p_{1s}^{ae} = -\cos \phi' + (\cos \phi' + \cos w_s^{ae}) \tilde{F}_2^{ce} \quad (5.78)$$

$$p_{2s}^{ae} = -\sin \phi' + (\cos \phi' + \cos w_s^{ae}) \tilde{F}_4^{ce} \quad (5.79)$$

$$p_{1s}^{ho} = \cos \phi' - (\cos \phi' + \cos w_s^{ho}) \tilde{F}_1^{ce} \quad (5.80)$$

$$p_{2s}^{ho} = -\sin \phi' + \sin \phi' (\cos \phi' + \cos w_s^{ho}) \tilde{F}_3^{ce} \quad (5.81)$$

where the functions $\{\tilde{F}_i^{ce}\}$ were defined in Chapter IV.

The constants w_s^{ae} and w_s^{ho} which appear in the launching coefficients $\{L_{ye}^{swa}, L_{yo}^{swh}\}$ are the roots of the following equations:

$$\sin w_s^{ae} + \epsilon_r^{-1} \gamma^e(w_s^{ae}, \theta') / \sin \theta' = 0 \quad (5.82)$$

$$\sin w_s^{ho} + \mu_r^{-1} \gamma^o(w_s^{ho}, \theta') / \sin \theta' = 0 \quad (5.83)$$

where

$$\begin{aligned} \gamma^e(w, \theta') &= -i [N^2 - \cos^2 \theta' \sin^2 w - \cos^2 w]^{1/2} \\ &\cdot \tan \left[\frac{[N^2 - \cos^2 \theta' \sin^2 w - \cos^2 w]^{1/2} \frac{kd}{2}}{1} \right] \end{aligned} \quad (5.84)$$

$$\begin{aligned} \gamma^o(w, \theta') &= i [N^2 - \cos^2 \theta' \sin^2 w - \cos^2 w]^{1/2} \\ &\cdot \cot \left[\frac{[N^2 - \cos^2 \theta' \sin^2 w - \cos^2 w]^{1/2} \frac{kd}{2}}{1} \right] \end{aligned} \quad (5.85)$$

The constants $\{\hat{F}_1^{ce}, \hat{F}_2^{ce}, \hat{F}_3^{ce}, \hat{F}_4^{ce}\}$ can be modified in two ways.

The first approach is the same as in Section C, which is to calculate the parameters $\{\xi^{ae}, \xi^{ho}\}$ from Equations (5.71) and (5.72). The second approach is to express $\{\xi^{ae}, \xi^{ho}\}$ in terms of $\{w_s^{ae}, w_s^{ho}\}$ which are the roots of (5.82)-(5.83). The latter approach is considered to be more accurate.

PMC Case

By duality, it follows that

$$E_{y0}^{sw}(\phi', \theta', \xi^{ao}) = L_{y0}^{swa}(\phi', w_s^{ao}) \left[\cos \theta' p_{2s}^{ao} E_{cz} + p_{1s}^{ao} \eta_0 H_{cz} \right] \\ \cdot U(\phi - \phi^{ao}) \cdot e^{ik_z' z} \exp \left[iK(x \cos w_s^{ao} + y \sin w_s^{ao}) \right] \quad (5.86)$$

$$H_{ye}^{sw}(\phi', \theta', \xi^{he}) = L_{ye}^{swh}(\phi', w_s^{he}) \left[p_{1s}^{he} \gamma_0 E_{cz} + p_{2s}^{he} \cos \theta' H_{cz} \right] \\ \cdot U(\phi - \phi^{ao}) \cdot e^{ik_z' z} \exp \left[iK(x \cos w_s^{he} + y \sin w_s^{he}) \right] \quad (5.87)$$

where

$$L_{y0}^{swa}(\phi', w_s^{ao}) = L_{y0}^{swh}(\phi', w_s^{ho}) \quad (5.88)$$

$$L_{ye}^{swh}(\phi', w_s^{he}) = L_{ye}^{swa}(\phi', w_s^{ae}) \quad (5.89)$$

$$p_{1s}^{ao} = -\cos \phi' + (\cos w_s^{ao} + \cos \phi') \hat{F}_1^{co} \quad (5.90)$$

$$p_{2s}^{ao} = -\sin \phi' + \sin \phi' (\cos w_s^{ao} + \cos \phi') \hat{F}_3^{co} \quad (5.91)$$

$$p_{1s}^{he} = \cos \phi' - (\cos \phi' + \cos w_s^{he}) \hat{F}_2^{co} \quad (5.92)$$

$$p_{2s}^{he} = -\sin \phi' + (\cos \phi' + \cos w_s^{he}) \hat{F}_4^{co} \quad (5.93)$$

The constants w_s^{ao} , w_s^{he} are the roots of the following equations:

$$\sin w_s^{he} + \mu_r^{-1} \gamma^e(w_s^{he}, \theta') / \sin \theta' = 0 \quad (5.94)$$

$$\sin w_s^{ao} + \epsilon_r^{-1} \gamma^o(w_s^{ao}, \theta') / \sin \theta' = 0 \quad (5.95)$$

Again, the constants $\{\tilde{F}_1^{co}, \tilde{F}_2^{co}, \tilde{F}_3^{co}, \tilde{F}_4^{co}\}$ can be modified in two ways.

That is, one can obtain $\{\tilde{\xi}^{ao}, \tilde{\xi}^{he}\}$ from (5.70) and (5.73), or one can first express $\{\xi^{ao}, \xi^{he}\}$ in terms of $\{w_s^{ao}, w_s^{he}\}$ which satisfy Equations (5.94) and (5.95).

E. MODIFICATION OF REFLECTED AND DIFFRACTED SURFACE WAVE FIELDS (OBLIQUE INCIDENCE)

Since the expressions for the reflected and diffracted surface wave fields are given in terms of $\{w_s^{ae}, w_s^{he}, w_s^{ao}, w_s^{ho}\}$ only (see Chapter IV), it is very simple to modify them. The only modification that is needed is to let the constants w_s^{ae} , w_s^{ho} , w_s^{he} and w_s^{ao} be the roots of Equations (5.82), (5.83), (5.94) and (5.95), respectively. This is the same procedure that was followed in Section B.4 for the special case of normal incidence.

CHAPTER VI

THE DIELECTRIC/FERRITE HALF-PLANE PROBLEM

A. STATEMENT OF THE PROBLEM

The solutions for the even and odd dielectric/ferrite bisection problems were obtained in Chapter V by modifying the solutions of Chapters III and IV. As shown in Chapter II, once the even and odd bisection problems have been solved, it is very simple to get the solution for the dielectric/ferrite half-plane problem depicted in Figure 2.1. It is shown in Chapter II that the total field for plane wave excitation can be expressed as follows:

$$\vec{E}(\rho, \phi, z) = 1/2 \vec{E}^e(\rho, |\phi|, z) + 1/2 \vec{E}^o(\rho, |\phi|, z) \text{ sign } (\phi) , \quad (6.1)$$

$$\begin{aligned} 0 < \theta' < \pi \\ -\pi < \phi < \pi \\ 0 < \phi' < \pi \end{aligned}$$

$$\vec{H}(\rho, \phi, z) = 1/2 \vec{H}^e(\rho, |\phi|, z) + 1/2 \vec{H}^o(\rho, |\phi|, z) \text{ sign } (\phi) , \quad (6.2)$$

where the angles ϕ, ϕ' and θ' are shown in Figure 2.1. Note that by combining the even and odd solutions, which are restricted to the half-space $0 < \phi < \pi$, their sum turns out to be valid in the entire space $-\pi < \phi < \pi$. As mentioned before, it is assumed that there is only one diffracting edge.

B. GEOMETRICAL OPTICS FIELD

As shown in (6.1) and (6.2), the geometrical optics fields can be written as follows:

$$\begin{aligned}
 E_y^{GO}(\rho, \phi, z) = & E_{cy} e^{-ik\rho\cos(\phi-\phi')} e^{ik_z' z} U(\pi+\phi-\phi') \\
 & + E_{cy} \frac{\tilde{R}_a^e + \tilde{R}_a^o}{2} e^{-ik\rho\cos(\phi+\phi')} e^{ik_z' z} U(\pi-\phi-\phi') \\
 & + E_{cy} \frac{\tilde{R}_a^e - \tilde{R}_a^o}{2} e^{-ik\rho\cos(\phi-\phi')} e^{ik_z' z} U(\phi'-\pi-\phi)
 \end{aligned} \quad (6.3)$$

$$\begin{aligned}
 H_y^{GO}(\rho, \phi, z) = & H_{cy} e^{-ik\rho\cos(\phi-\phi')} e^{ik_z' z} U(\pi+\phi-\phi') \\
 & + H_{cy} \frac{\tilde{R}_h^e + \tilde{R}_h^o}{2} e^{-ik\rho\cos(\phi+\phi')} e^{ik_z' z} U(\pi-\phi-\phi') \\
 & + H_{cy} \frac{\tilde{R}_h^e - \tilde{R}_h^o}{2} e^{-ik\rho\cos(\phi-\phi')} e^{ik_z' z} U(\phi'-\pi-\phi)
 \end{aligned} \quad (6.4)$$

To write the GO fields in standard form, i.e., in terms of dyadic reflection and transmission coefficients, it is necessary to define a "ray-fixed" coordinate system [2,19] which is depicted in Figure 6.1. The unit vector \hat{n} is normal to the surface at the point of incidence, \hat{s}^i is the incident unit vector, and \hat{s}^r is the reflection unit vector from the point of reflection to the observation point. The unit vectors \hat{u}_\parallel^i , \hat{u}_\parallel^r , and \hat{u}_\perp are defined the following way:

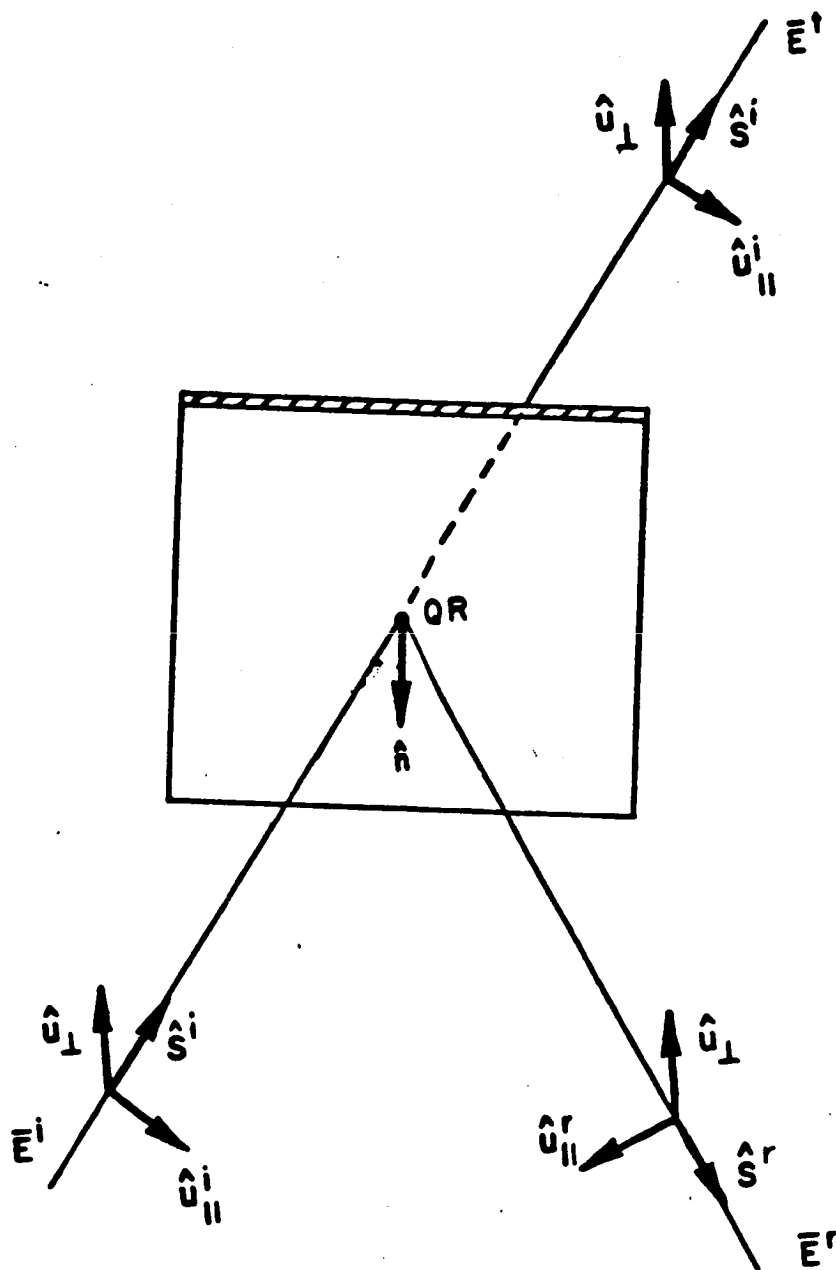


Figure 6.1. Ray fixed coordinate system used for 3D reflection and transmission.

$$\hat{u}_{\parallel}^i = \frac{\hat{s}^i \times (\hat{n} \times \hat{s}^i)}{|\hat{n} \times \hat{s}^i|} \quad (6.5)$$

$$\hat{u}_{\parallel}^r = \frac{\hat{s}^r \times (\hat{n} \times \hat{s}^r)}{|\hat{n} \times \hat{s}^r|} \quad (6.6)$$

$$\hat{u}_{\perp} = \hat{u}_{\parallel}^i \times \hat{s}^i = \hat{u}_{\parallel}^r \times \hat{s}^r \quad (6.7)$$

Note that (\perp) and (\parallel) indicate vectors perpendicular and parallel, respectively, to the plane of incidence which is the plane containing \hat{s}^i and \hat{n} . The unit vectors ($\hat{s}^i, \hat{u}_{\parallel}^i, \hat{u}_{\perp}$) define an orthonormal coordinate system for the incident and transmitted fields. Likewise, the unit vectors ($\hat{s}^r, \hat{u}_{\parallel}^r, \hat{u}_{\perp}$) define an orthonormal coordinate system for the reflected field.

It is shown in Appendix K that the fields ($E_{\parallel}^{i,r}, E_{\perp}^{i,r}, E_s^{i,r}$) can be expressed in terms of the $E_y^{i,r}$ and $H_y^{i,r}$ fields as follows:

$$E_s^i = 0 \quad (6.8)$$

$$E_s^r = 0 \quad (6.9)$$

$$E_{\parallel}^i = \frac{E_y^i}{|\hat{n} \times \hat{s}^i|} \quad (6.10)$$

$$E_{\perp}^i = \frac{\eta_0 H_y^i}{|\hat{n} \times \hat{s}^i|} \quad (6.11)$$

$$E_{\perp}^r = \frac{\eta_0 H_y^r}{|\hat{n} \times \hat{s}^i|} \quad (6.12)$$

$$E_{\parallel}^r = \frac{E_y^r}{|\hat{n} \times \hat{s}^i|} \quad (6.13)$$

In vector form, the reflected field \vec{E}^r can be expressed in terms of the dyadic reflection coefficient \bar{R} such that

$$\vec{E}^r(s^r) = \hat{u}_{\perp} E_{\perp}^r + \hat{u}_{\parallel} E_{\parallel}^r = \vec{E}^i(QR) \cdot \bar{R} e^{iks^r} \quad (6.14)$$

where s^r is the distance from the point of reflection QR to the observation point. The incident field $\vec{E}^i(QR)$ is given by

$$\vec{E}^i(QR) = \hat{u}_{\parallel}^i E_{\parallel}^i(QR) + \hat{u}_{\perp}^i E_{\perp}^i(QR) \quad (6.15)$$

which is evaluated at QR. It is shown in Appendix K that the dyadic reflection coefficient can be written the following way:

$$\bar{R} = \hat{u}_{\parallel}^i \hat{u}_{\parallel}^r R^{\parallel} + \hat{u}_{\perp}^i \hat{u}_{\perp}^r R^{\perp} \quad (6.16)$$

where

$$R^{\parallel} = \frac{\tilde{R}_a^e + \tilde{R}_a^o}{2} \quad (6.17)$$

$$R^{\perp} = \frac{\tilde{R}_h^e + \tilde{R}_h^o}{2} \quad (6.18)$$

The transmitted field can also be expressed in terms of a dyadic transmission coefficient \bar{T} such that

$$\vec{E}^t(s^t) = \hat{u}_\perp E_\perp^t + \hat{u}_\parallel E_\parallel^t = \vec{E}(QR) \cdot \bar{T} e^{iks^t} \quad (6.19)$$

where s^t is the distance from the point of incidence QR to the point of observation and

$$\bar{T} = \hat{u}_\parallel^i \hat{u}_\parallel^i T^\parallel + \hat{u}_\perp^i \hat{u}_\perp^i T^\perp \quad (6.20)$$

where

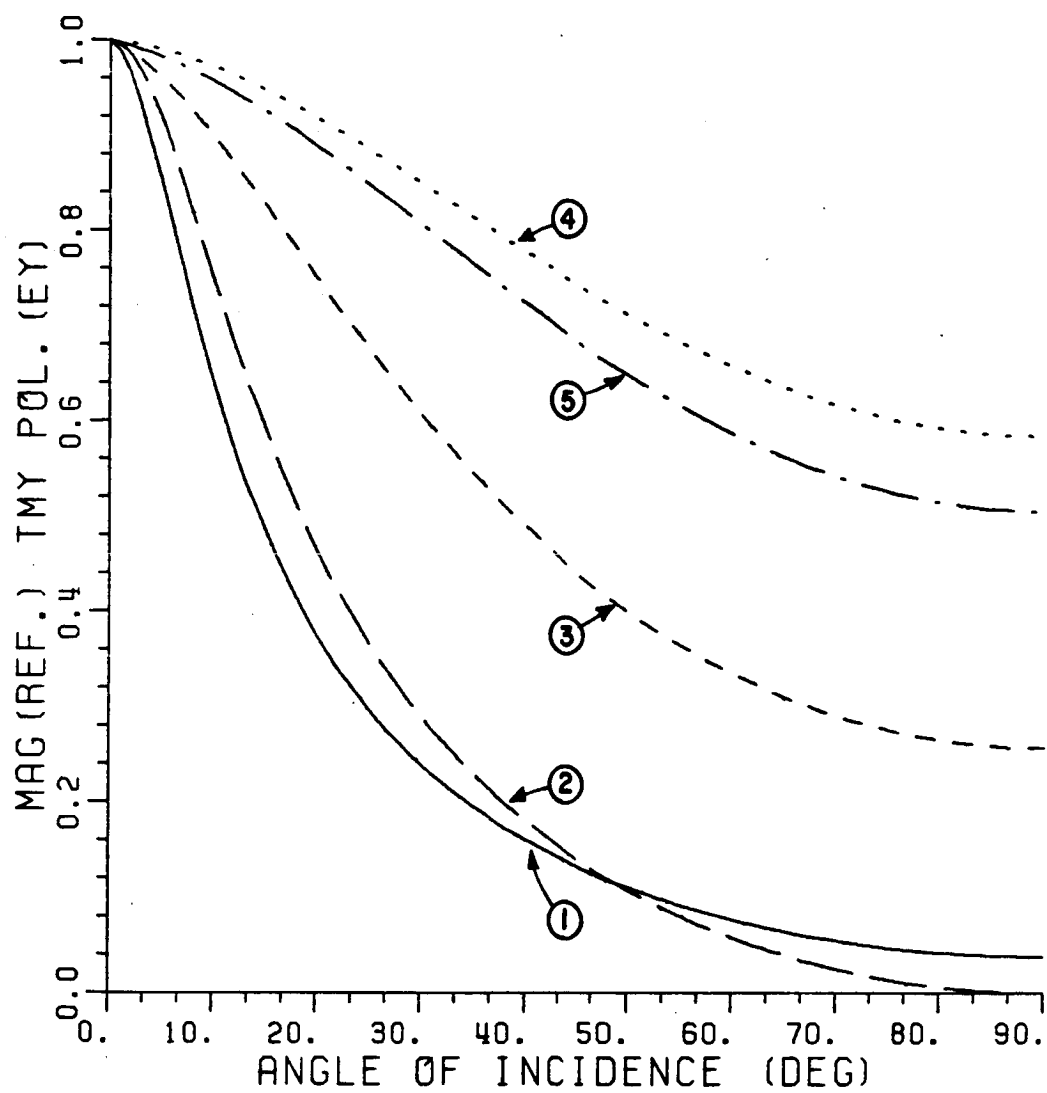
$$T^\parallel = \frac{\tilde{R}_a^e - \tilde{R}_a^o}{2} \quad (6.21)$$

$$T^\perp = \frac{\tilde{R}_h^e - \tilde{R}_h^o}{2} \quad (6.22)$$

The reflection coefficients R^\parallel , R^\perp and the transmission coefficients T^\parallel , T^\perp are depicted in Figures 6.2 - 6.5, respectively, for five different combinations of ϵ_r and μ_r :

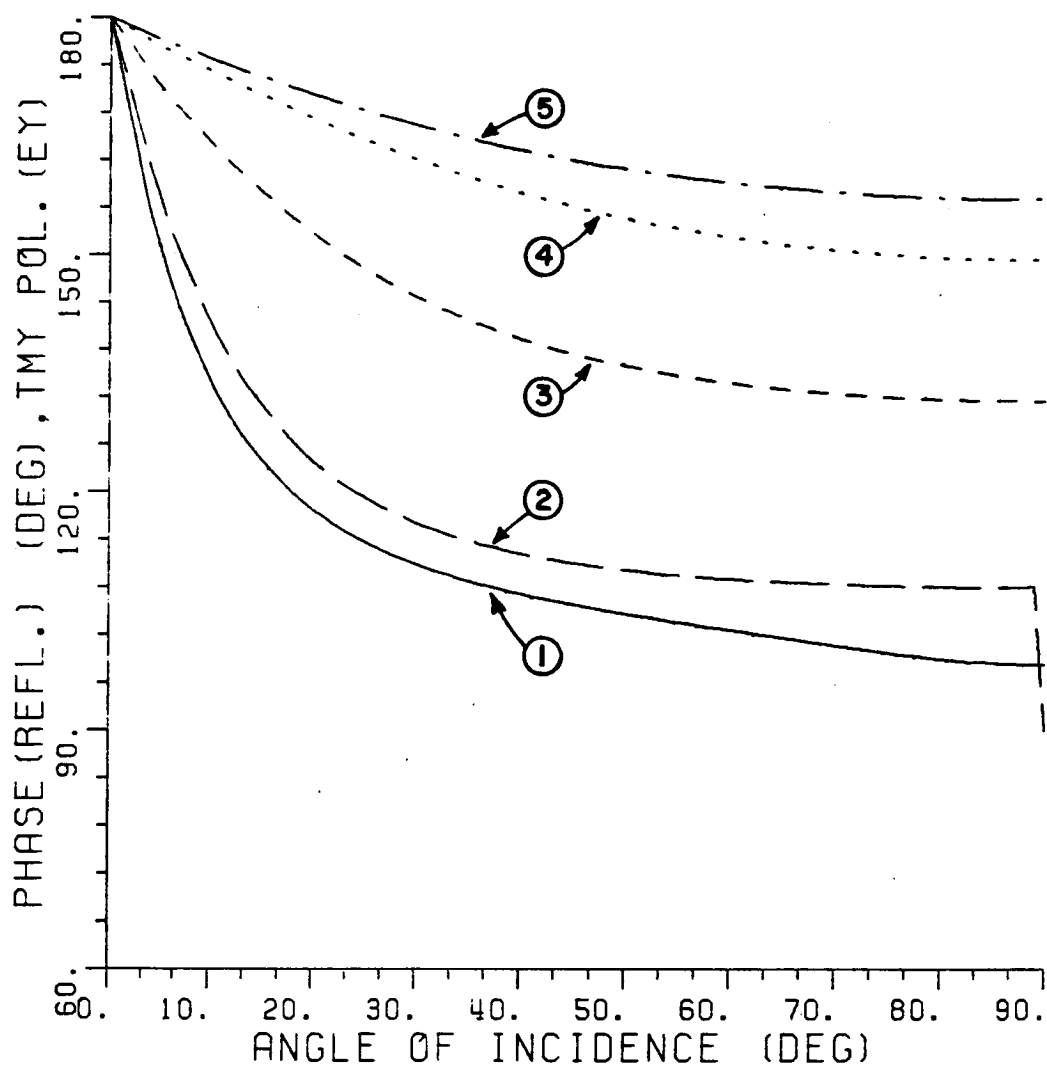
- | | |
|---------------------------------|------------------------|
| (1) $\epsilon_r = 2.(1.+i0.05)$ | $\mu_r = 1.(1.+i0.)$ |
| (2) $\epsilon_r = 3.(1.+i0.)$ | $\mu_r = 1.(1.+i0.)$ |
| (3) $\epsilon_r = 3.(1.+i0.1)$ | $\mu_r = 2.(1.+i0.1)$ |
| (4) $\epsilon_r = 3.(1.+i0.05)$ | $\mu_r = 4.(1.+i0.05)$ |
| (5) $\epsilon_r = 4.(1.+i0.1)$ | $\mu_r = 4.(1.+i0.1)$ |

In all five cases, $\theta' = \pi/6$ and $d = 0.005\lambda$.



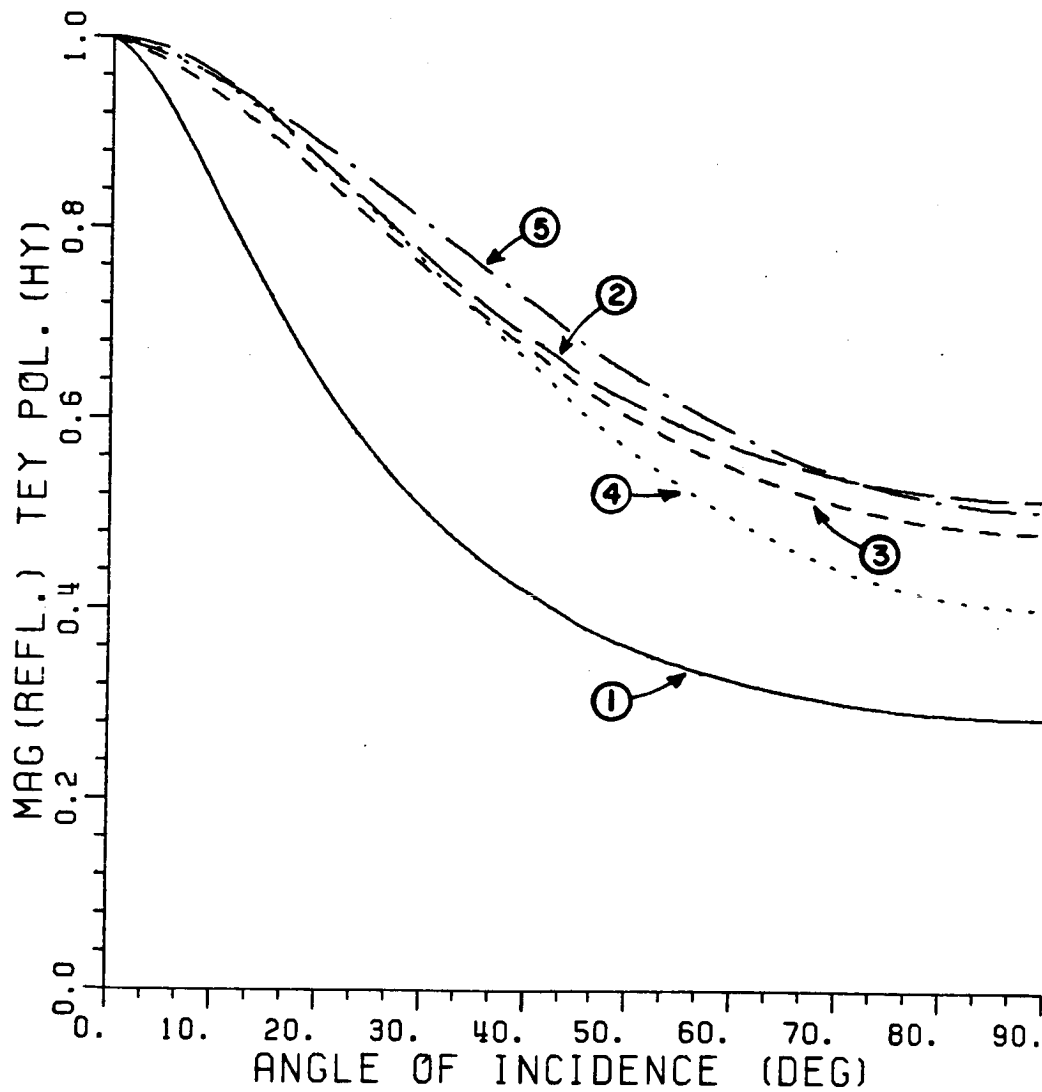
Magnitude of Reflection Coefficient R^H

Figure 6.2. Reflection coefficient of R^H .



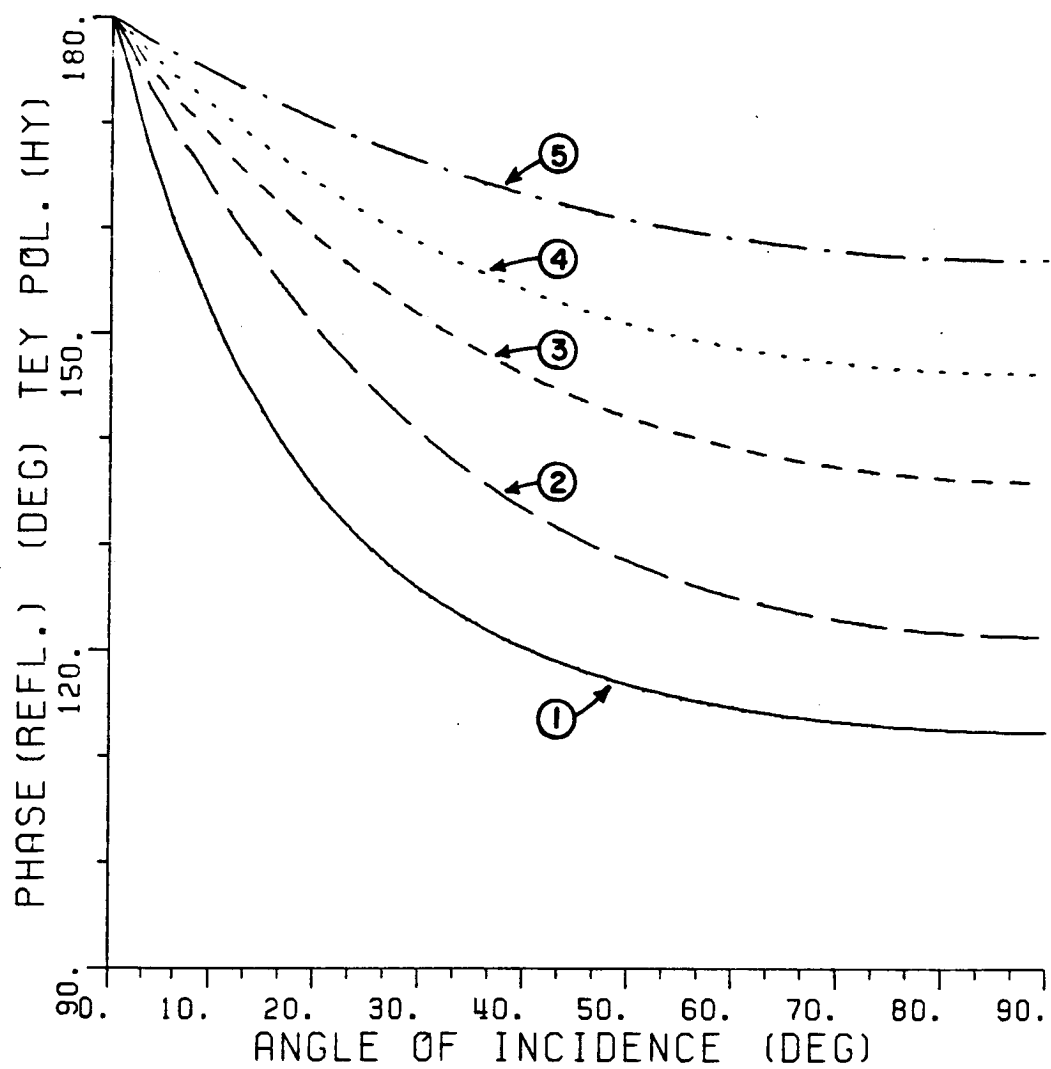
Phase of Reflection Coefficient R^{\parallel} (Degrees)

Figure 6.2. (continued)



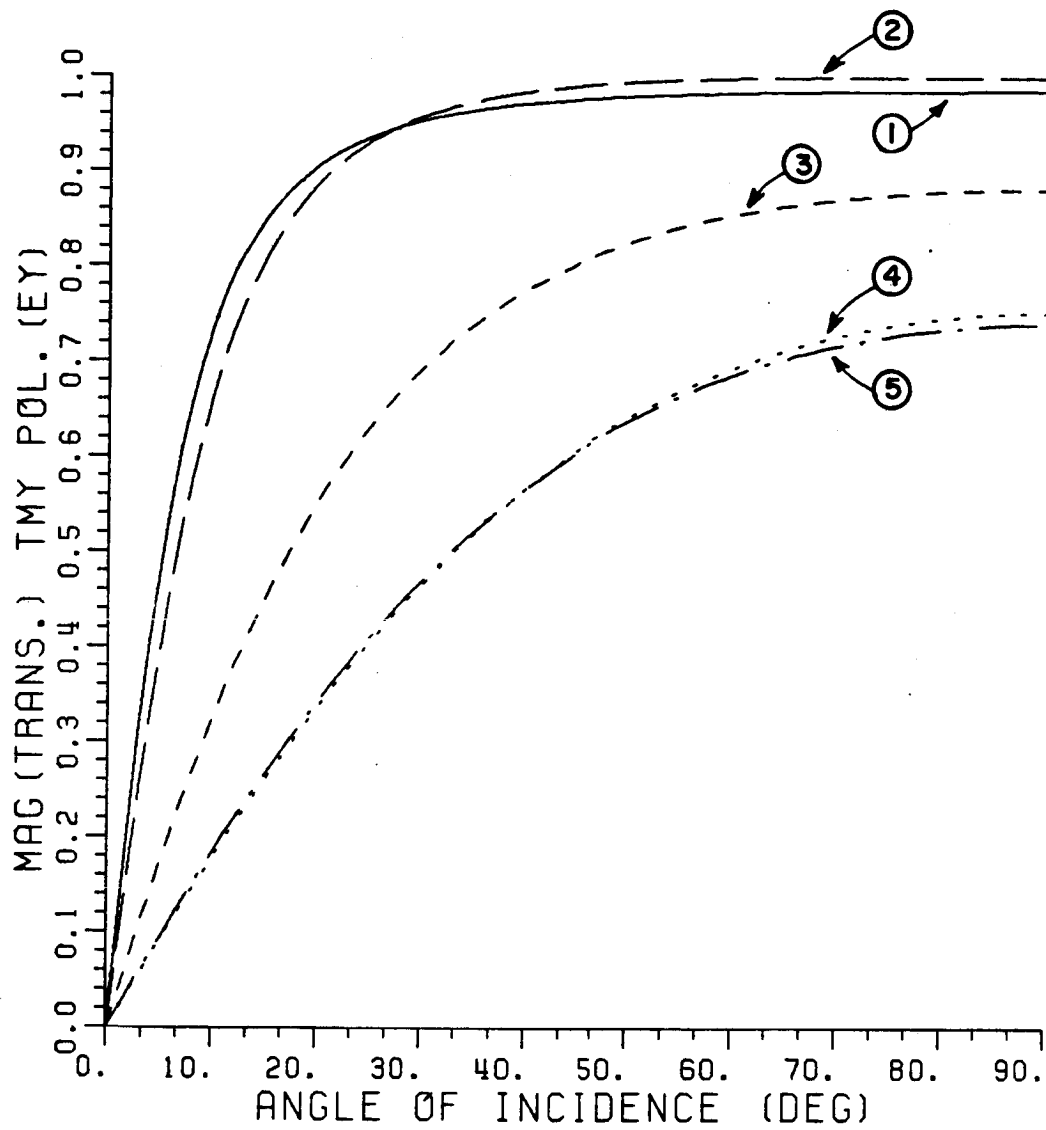
Magnitude of Reflection Coefficient R^{\perp}

Figure 6.3. Reflection Coefficient R^{\perp} .



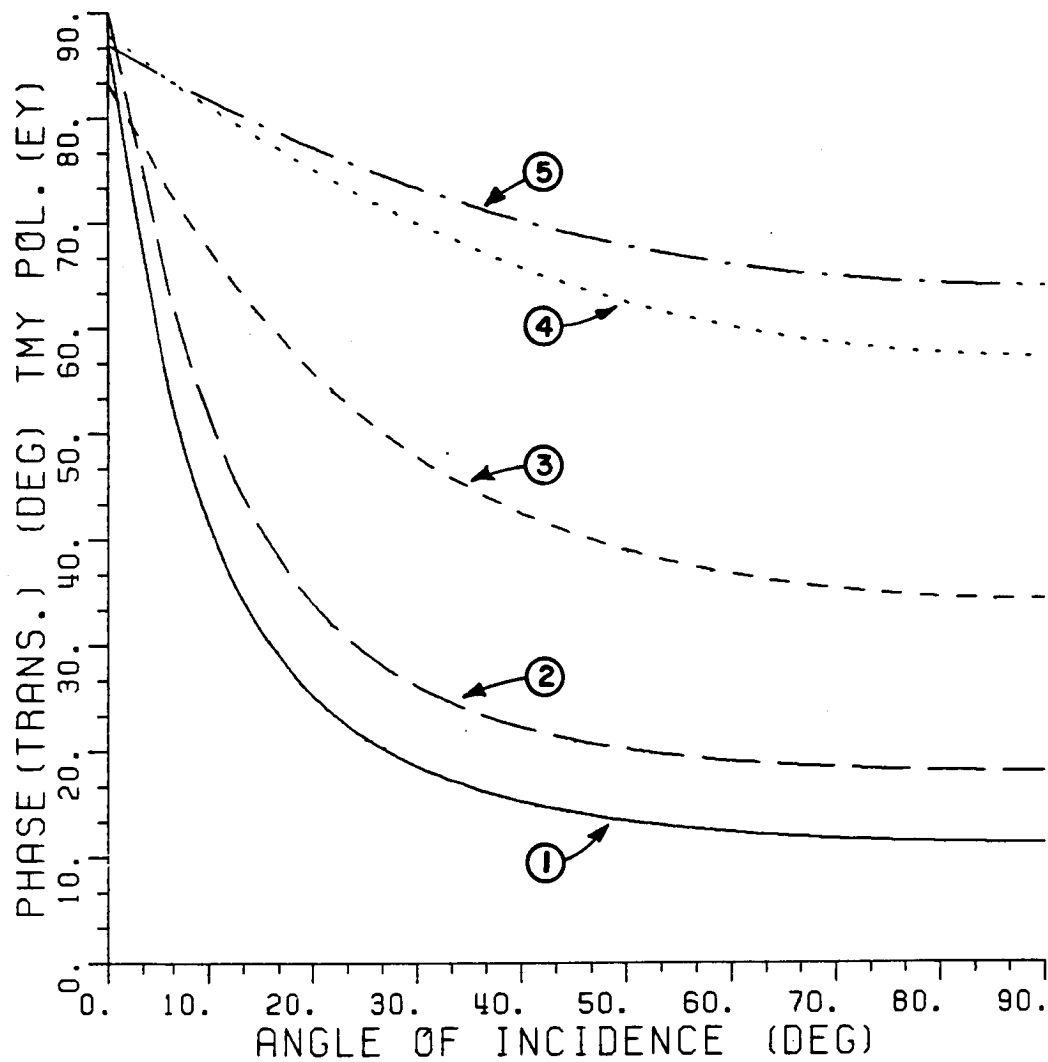
Phase of Reflection Coefficient R^{\perp}

Figure 6.3. (continued)



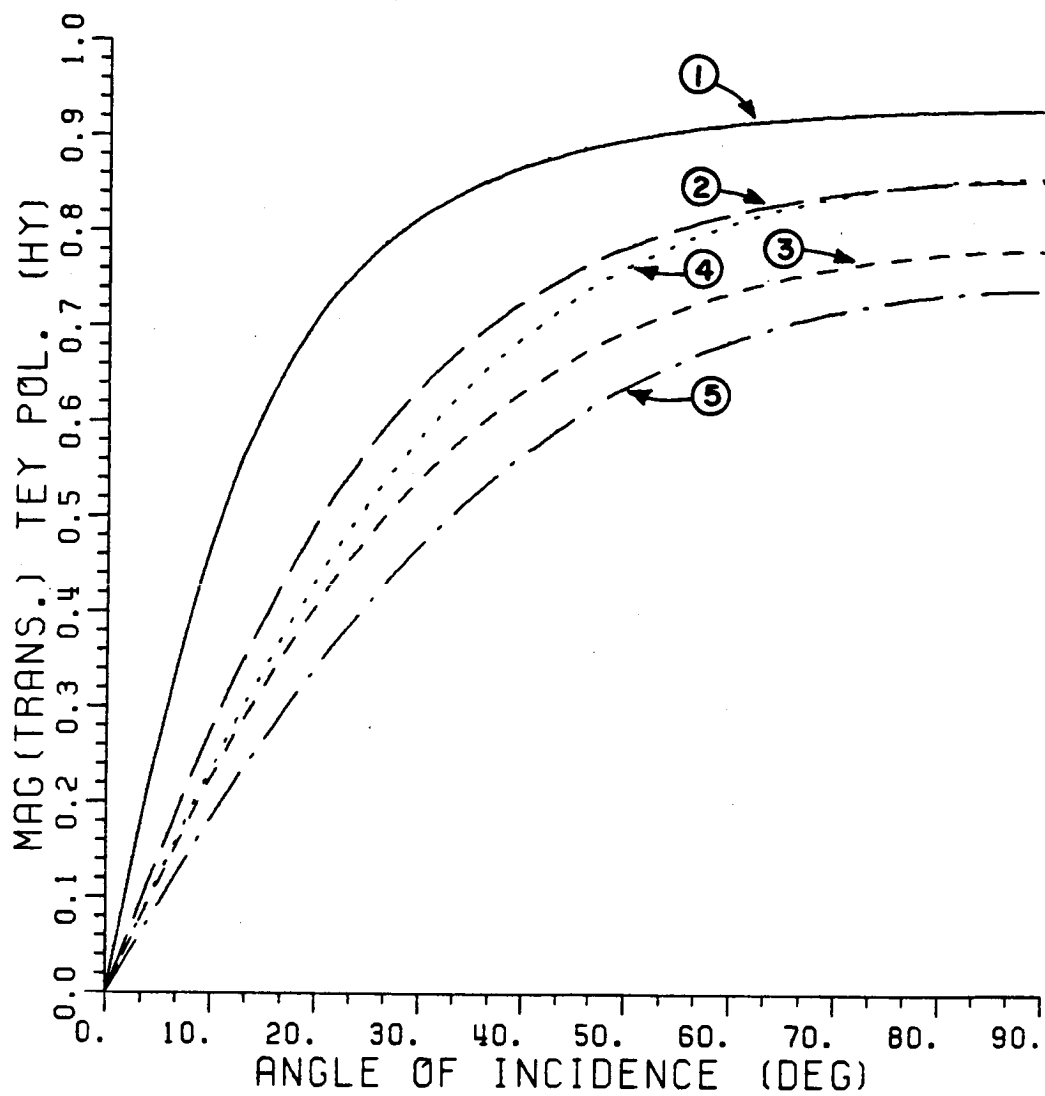
Magnitude of Transmission Coefficient T^I

Figure 6.4. Transmission Coefficient T^I .



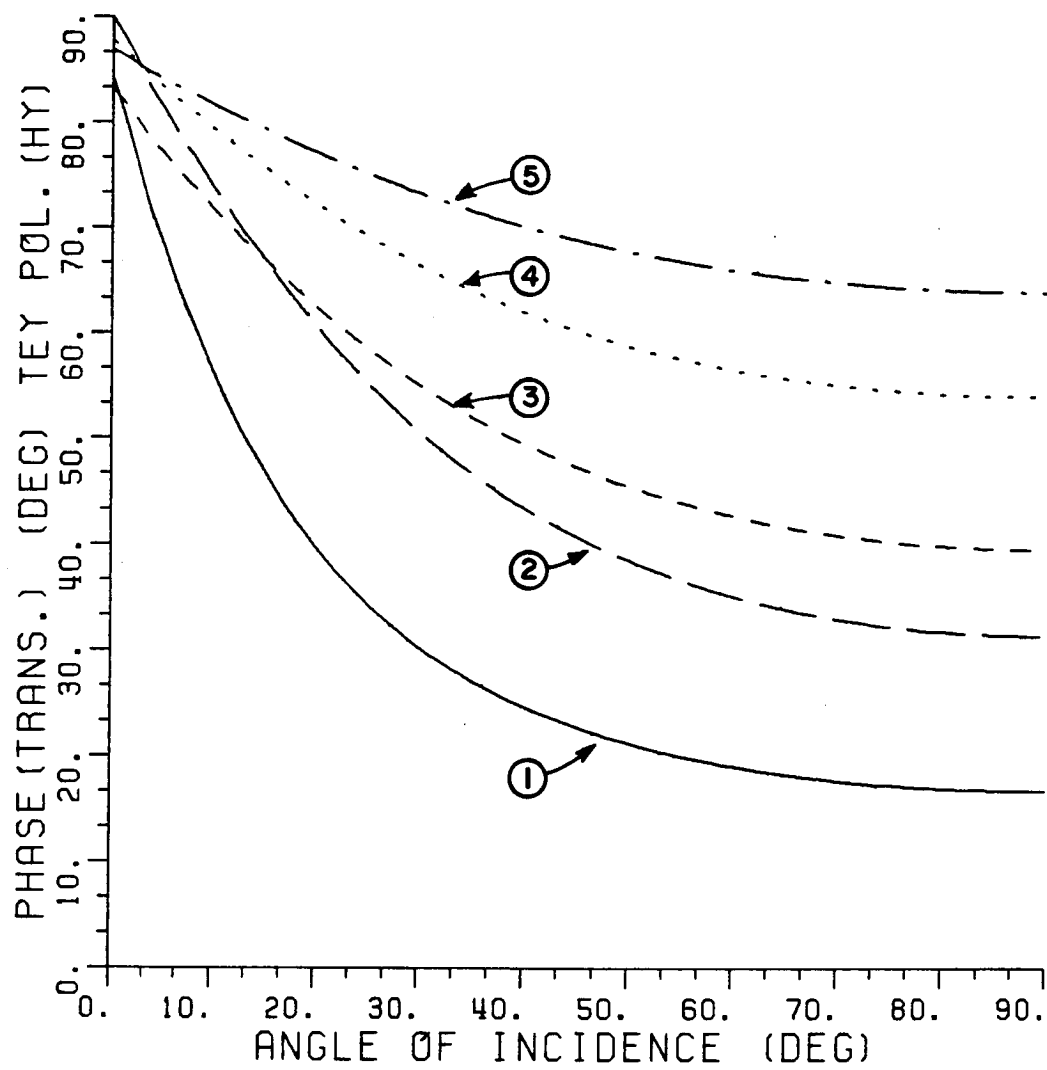
Phase of Transmission Coefficient T^H

Figure 6.4. (continued).



Magnitude of Transmission Coefficient T^{\perp}

Figure 6.5. Transmission Coefficient T^{\perp} .



Phase of Transmission Coefficient T^{\perp}

Figure 6.5. (continued).

C. DIFFRACTED FIELD

The diffracted H_Z^d and E_Z^d fields for the dielectric/ferrite half-plane can be obtained by adding the even and odd solutions and then dividing by 2, that is

$$E_Z^d(\rho, \phi, z) = \frac{1}{2} E_Z^{de}(\rho, |\phi|, z) + \frac{1}{2} E_Z^{do}(\rho, |\phi|, z) \text{sign}(\phi), \quad -\pi \leq \phi \leq \pi \quad (6.23)$$

$$H_Z^d(\rho, \phi, z) = \frac{1}{2} H_Z^{de}(\rho, |\phi|, z) + \frac{1}{2} H_Z^{do}(\rho, |\phi|, z) \text{sign}(\phi), \quad -\pi \leq \phi \leq \pi. \quad (6.24)$$

In order to express the diffracted field in terms of a dyadic diffraction coefficient, it is necessary to define a suitable coordinate system. It is mentioned in [11] that the correct coordinate system is the ray-fixed coordinate system depicted in Figure 6.6. The plane of incidence for edge diffraction, which is simply referred to as the edge-fixed plane of incidence, contains the incident ray and the unit vector \hat{e} tangent to the edge at the point of diffraction QE. The plane of diffraction contains \hat{e} and the diffracted ray. The unit vectors $\hat{\beta}_0'$ and $\hat{\beta}_0$ which are parallel to the edge-fixed plane of incidence and the plane of diffraction, respectively, are given by

$$\hat{\beta}_0' = \frac{\hat{s}' \times (\hat{e} \times \hat{s}')}{|\hat{e} \times \hat{s}'|} \quad (6.25)$$

$$\hat{\beta}_0 = \frac{-\hat{s} \times (\hat{e} \times \hat{s})}{|\hat{e} \times \hat{s}|} \quad (6.26)$$

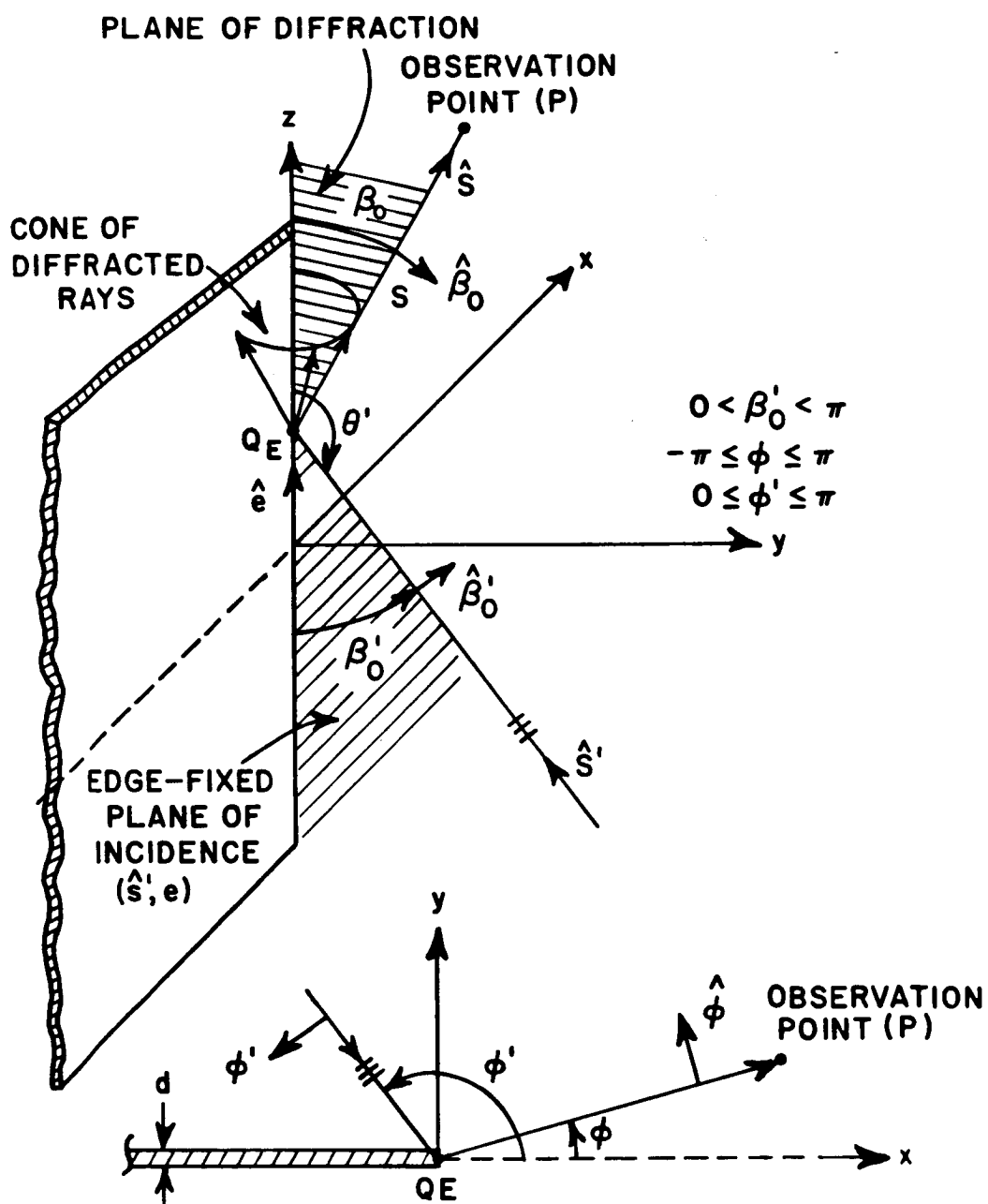


Figure 6.6. Ray fixed coordinate system used for 3D diffraction.

where the unit vector \hat{s}' is in the direction of incidence, and the unit vector \hat{s} is in the direction of diffraction. The unit vectors $\hat{\phi}'$ and $\hat{\phi}$ which are perpendicular to the edge-fixed plane of incidence and the plane of diffraction, respectively, are defined as follows:

$$\hat{\phi}' = \hat{\beta}_0' \times \hat{s}' \quad (6.27)$$

$$\hat{\phi} = \hat{\beta}_0 \times \hat{s} \quad (6.28)$$

It is shown in Appendix L that

$$E_{\phi}'^i = \frac{-\eta_0 H_z^i}{\sin \beta_0'} \quad (6.29)$$

$$E_{\beta_0}'^i = \frac{E_z^i}{\sin \beta_0'} \quad (6.30)$$

$$E_{s'}^i = 0 \quad (6.31)$$

$$E_s^d = 0 \quad (6.32)$$

$$E_{\phi}^d = \frac{\eta_0 H_z^d}{\sin \beta_0'} \quad (6.33)$$

$$E_{\beta_0}^d = \frac{-E_z^d}{\sin \beta_0'} \quad (6.34)$$

Rewriting the diffracted field in terms of the dyadic diffraction coefficient $\bar{\bar{D}}$, one gets

$$\vec{E}^d(s) = \hat{\phi} E_{\phi}^d + \hat{\beta}_0 E_{\beta_0}^d = \vec{E}^i(QE) \cdot \bar{\bar{D}} \frac{e^{iks}}{\sqrt{s}} \quad (6.35)$$

where s is the distance from the point of diffraction (QE) to the observation point, and

$$\vec{E}(QE) = \hat{\phi} E_{\phi}^i(QE) + \hat{\beta}_0 E_{\beta_0}^i(QE) \quad (6.36)$$

As shown in Appendix L, the dyadic diffraction coefficient can be written as follows:

$$\bar{\bar{D}} = \hat{\phi} \hat{\phi} \tilde{D}_{h1}^d - \hat{\beta}_0 \hat{\phi} \cos \beta_0 \tilde{D}_{h2}^d - \hat{\phi} \hat{\beta}_0 \cos \beta_0 \tilde{D}_{a2}^d + \hat{\beta}_0 \hat{\beta}_0 \tilde{D}_{a1}^d \quad (6.37)$$

where

$$\tilde{D}_{hi}^d(|\phi|, \phi', \theta') = \frac{1}{2} \left[\tilde{D}_{ze}^{hi}(|\phi|, \phi', \theta') + \tilde{D}_{zo}^{hi}(|\phi|, \phi', \theta') \text{sign} \phi \right], \quad i=1,2 \quad (6.38)$$

$$\tilde{D}_{ai}^d(|\phi|, \phi', \theta') = \frac{1}{2} \left[\tilde{D}_{ze}^{ai}(|\phi|, \phi', \theta') + \tilde{D}_{zo}^{ai}(|\phi|, \phi', \theta') \text{sign} \phi \right], \quad i=1,2 \quad (6.39)$$

Note that the diffraction coefficients $\{\tilde{D}_{ze}^{hi}, \tilde{D}_{zo}^{hi}, \tilde{D}_{ze}^{ai}, \tilde{D}_{zo}^{ai}\}_{i=1}^2$ are defined in Equations (L.31)-(L.49) in Appendix L. Furthermore, the angle of diffraction β_0 is equal to the angle β_0' as predicted by Keller's law of edge edge diffraction, [11]. The latter can be expressed mathematically as

$$\hat{s}' \cdot \hat{e} = \hat{s} \cdot \hat{e} \quad (6.40)$$

Equation (6.40) is used to find the point of diffraction QE for a given point of observation away from the edge and a unit vector \hat{s}' . In some cases this must be done by a computer search procedure as shown in [48].

D. SURFACE WAVE FIELD EXCITED BY A PLANE WAVE (OBLIQUE INCIDENCE)

As mentioned in Chapter V, the parameters of the dielectric/ferrite half-plane are adjusted such that only the lowest order even mode can exist. This implies that only the fields E_{ye}^{SW} and H_{ye}^{SW} given in Equations (5.74) and (5.87), respectively, are allowed to exist. Therefore, the total surface wave field can be expressed as

$$E_y^{SW} = \frac{1}{2} E_{ye}^{SW} (|y|, \phi, ' \theta ') \quad , \quad |y| > \frac{d}{2} \quad (6.41)$$

$$H_y^{SW} = \frac{1}{2} H_{ye}^{SW} (|y|, \phi, ' \theta ') \quad , \quad |y| > \frac{d}{2} \quad . \quad (6.42)$$

In general, the TE_y and TM_y fields have different propagation and attenuation constants. Thus, assuming Q_w is the point where the surface waves are launched, they will propagate in different directions as shown in Figure 6.7. Note that β_w^a and β_w^h are always bigger than β_0' . However, β_w^a can be larger or smaller than β_w^h depending on the parameters of the dielectric/ferrite half-plane.

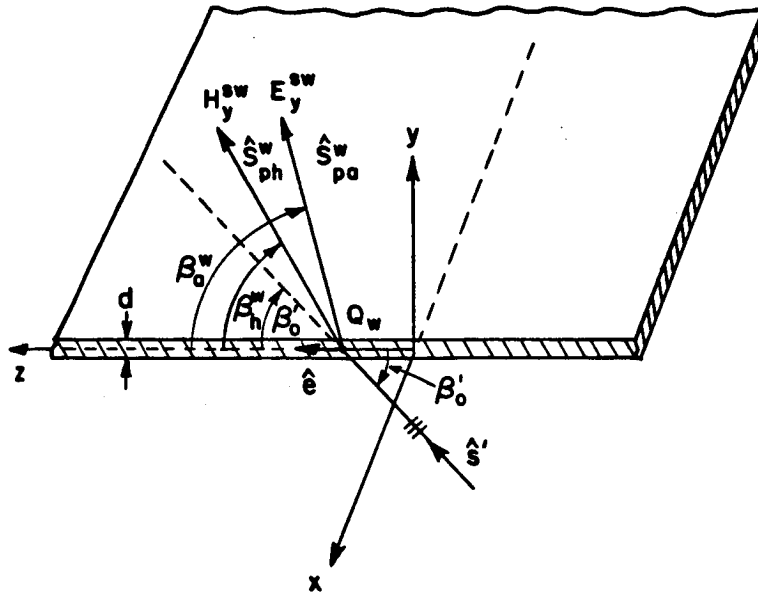


Figure 6.7. Edge excited surface waves E_y^{sw} and H_y^{sw} where $\beta_0' < \beta_a^w$, $\beta_0' < \beta_h^w$.

It can be shown that, for a given point of observation and unit vector \hat{s}' , one can determine the point Q_w and the relationship between the angles β_0' and β^w from the following equation:

$$\hat{s} \cdot \hat{e} = \hat{s}_p^w \cdot \hat{e} = \frac{\hat{s}' \cdot \hat{e}}{[\cosh^2(w_{sI}) - (\hat{s}' \cdot \hat{e})^2 \sinh^2(w_{sI})]^{1/2}} \quad (6.43)$$

where w_{sI} is the imaginary part of w_s . The unit vector \hat{s}_p^w is in the direction of propagation of the surface wave fields from the point Q_w , and \hat{s} is the unit vector in the direction from the point Q_w to the point of observation. That is,

$$\hat{s}_p^w = \hat{\rho}_p^w \sin \beta^w + \hat{e} \cos \beta^w \quad (6.44)$$

$$\hat{s} = \hat{p} \sin \beta^w + \hat{e} \cos \beta^w \quad (6.45)$$

$$\hat{\rho}_p^w = \hat{x} \cos w_{sr} + \hat{y} \sin w_{sr} \quad , \quad \pi < w_{sr} < 3\pi/2 \quad (6.46)$$

$$\hat{p} = \hat{x} \cos \phi + \hat{y} \sin \phi \quad (6.47)$$

where w_{sr} is the real part of w_s .

Note that the expressions in Equations (6.41) and (6.42) are valid outside the dielectric/ferrite medium.

E. REFLECTED SURFACE WAVE (OBLIQUE INCIDENCE)

As in Section D, only the even reflected surface wave field can propagate in the dielectric/ferrite half-plane. The total E_y^{rsW} and H_y^{rsW} fields are given by

$$E_y^{rsW} = E_{ye}^{rsW} (|\phi|, w_s^{ae}, \theta') \quad , \quad -\pi < \phi < \pi \quad (6.48)$$

$$H_y^{rsW} = H_{ye}^{rsW} (|\phi|, w_s^{he}, \theta') \quad , \quad -\pi < \phi < \pi \quad (6.49)$$

where E_{ye}^{rsW} and H_{ye}^{rsW} were defined in Equations (4.162) and (4.184), respectively. Furthermore, w_s^{ae} and w_s^{he} are the roots of Equations (5.82) and (5.94), respectively. It follows from either (4.162) or (4.184) that the propagation and attenuation vectors for the incident and reflected surface wave fields are given by

$$\vec{k}^{wi} = k_p^{wi} \hat{s}_p^{wi} + i k_a^{wi} \hat{s}_a^{wi} \quad (6.50)$$

for the incident field, and

$$\hat{k}^{wr} = k_p^{wr} \hat{s}_p^{wr} + i k_a^{wr} \hat{s}_a^{wr} \quad (6.51)$$

for the reflected field, where

$$k_p^w = k(\sin^2 \beta_0' \cosh^2 w_{sI} + \cos^2 \beta_0')^{1/2} \quad (6.52)$$

$$k_a^w = -k \sin \beta_0' \sinh w_{sI} \quad , \quad w_{sI} < 0 \quad (6.53)$$

$$\hat{s}_p^{wi} = \sin \beta_0' (-\hat{x} \cos w_{sr} + \hat{y} \sin w_{sr}) + \hat{e} \cos \beta_0' \quad , \quad \pi < w_{sr} < 3\pi/2 \quad (6.54)$$

$$\hat{s}_a^{wi} = -\hat{x} \sin w_{sr} - \hat{y} \cos w_{sr} \quad (6.55)$$

$$\hat{s}_p^{wr} = \sin \beta_0' (\hat{x} \cos w_{sr} + \hat{y} \sin w_{sr}) + \hat{e} \cos \beta_0' \quad (6.56)$$

$$\hat{s}_a^{wr} = \hat{x} \sin w_{sr} - \hat{y} \cos w_{sr} \quad . \quad (6.57)$$

The angle β_0' is depicted in Figure 6.8. It is easy to conclude by studying Equations (6.52)-(6.57) that the angle of incidence is equal to the angle of reflection such that

$$(-\hat{s}_p^{wi}) \cdot (-\hat{x}) = \cos \theta_w' = -\cos w_{sr} \sin \beta_0' = \hat{s}_p^{wr} \cdot (-\hat{x}) \quad (6.58)$$

where the angle of incidence θ_w' is depicted in Figure 6.8. It follows from (6.58) that

$$\theta_w' = \arccos [-\cos(w_{sr}) \sin \beta_0'] \quad , \quad \pi < w_{sr} < 3\pi/2 \quad (6.59)$$

$$0 < \theta_w' < \pi/2$$

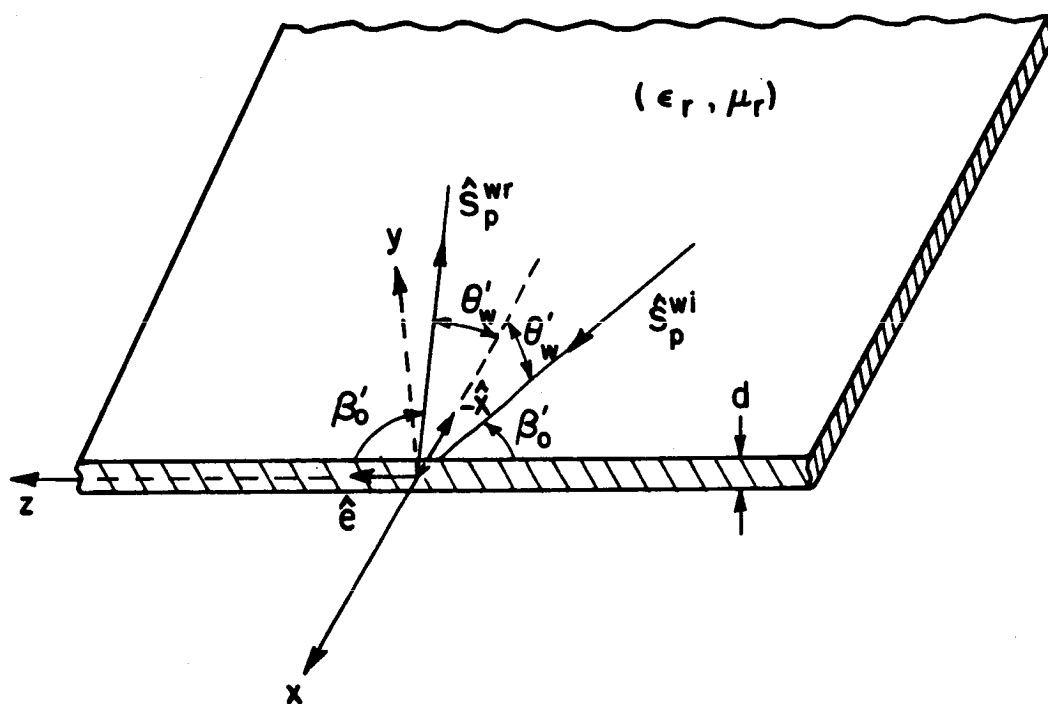


Figure 6.8. Reflected surface wave field.

F. DIFFRACTED SURFACE WAVE (OBLIQUE INCIDENCE)

The E_y and H_y diffracted surface wave fields for the dielectric/ferrite half-plane can be expressed as follows:

$$E_y^{\text{dsw}}(\rho, \phi, z) = E_{ye}^{\text{dsw}}(\rho, |\phi|, z) + E_{yo}^{\text{dsw}}(\rho, |\phi|, z) \text{sign}(\phi), \quad -\pi < \phi < \pi \quad (6.60)$$

$$H_y^{\text{dsw}}(\rho, \phi, z) = H_{ye}^{\text{dsw}}(\rho, |\phi|, z) + H_{yo}^{\text{dsw}}(\rho, |\phi|, z) \text{sign}(\phi), \quad -\pi < \phi < \pi \quad (6.61)$$

where $\{E_{ye}^{\text{dsw}}, E_{yo}^{\text{dsw}}, H_{ye}^{\text{dsw}}, H_{yo}^{\text{dsw}}\}$ are given by Equations (4.163), (4.181), (4.185), and (4.167), respectively, with the modifications indicated in Section E of Chapter V.

An equation similar to (6.43) can also be obtained for this case. It is easy to show that

$$\hat{s}^{\text{d}} \cdot \hat{e} = \frac{(\cosh w_{sI}) (\hat{s}_p^{\text{wi}} \cdot \hat{e})}{(1 + (\hat{s}_p^{\text{wi}} \cdot \hat{e})^2 (\sinh^2 w_{sI}))^{1/2}} \quad (6.62)$$

where \hat{s}^{d} is the unit vector in the direction from Q_w to the observation point, as depicted in Figure 6.9.

G. LINE SOURCE EXCITATION

Consider the geometry illustrated in Figure 6.10 showing a line source radiating in the presence of a dielectric/ferrite half-plane. It is assumed that the line source is far enough from the edge so its field can be represented by a cylindrical wave. The total field at the observation point (P) can be expressed as the sum of the incident, reflected, transmitted, diffracted and surface wave fields such that

$$u(\rho, \phi) = u^i(\rho, \phi) + u^r(\rho, \phi) + u^d(\rho, \phi) + u^{SW}(\rho, \phi) \quad (6.63)$$

Note that u represents the electric field if an electric line source is used, or the magnetic field, if a magnetic line source is present.

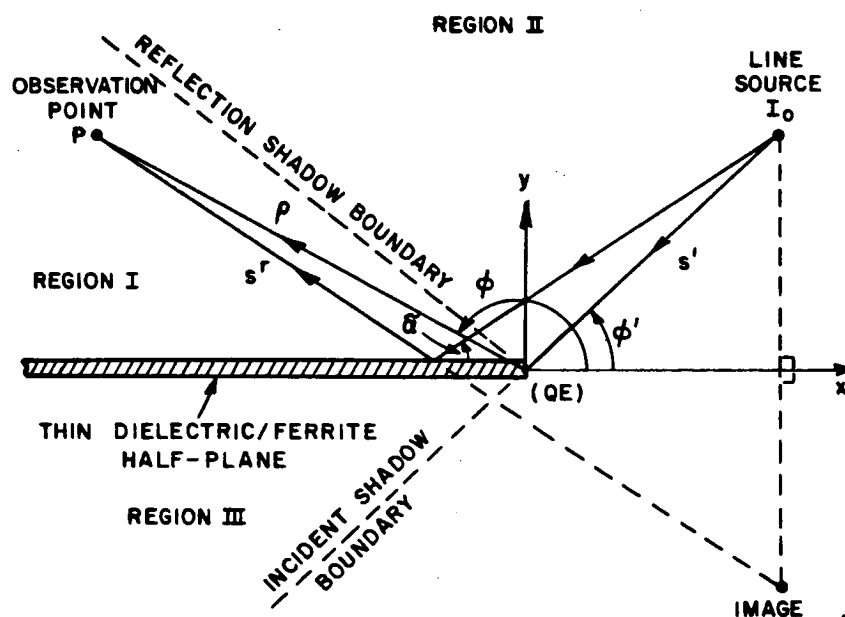


Figure 6.10. Line Source Excitation

Using the same notation as in [2], the individual terms in (6.63) may be expressed as follows:

$$u^i(P) = \begin{cases} I_0 \frac{e^{iks^i}}{\sqrt{s^i}} & \text{Regions I and II} \\ 0 & \text{Region III,} \end{cases} \quad (6.64)$$

$$u^r(P) = \begin{cases} I_0 \tilde{R} \frac{e^{iks^r}}{\sqrt{s^r}} & \text{Region I} \\ 0 & \text{Region II and III,} \end{cases} \quad (6.65)$$

$$u^t(P) = \begin{cases} I_0 \tilde{T} \frac{e^{iks^i}}{\sqrt{s^i}} & \text{Region III} \\ 0 & \text{Regions I and II,} \end{cases} \quad (6.66)$$

and

$$u^d(\rho, \phi) = u^i(QE) \left[\frac{1}{2} \tilde{D}_e^d(|\phi|, \phi') + \frac{1}{2} \tilde{D}_0^d(|\phi|, \phi') \sin(\phi) \right] \frac{e^{ik\rho}}{\sqrt{\rho}}, \quad -\pi < \phi < \pi \quad (6.67)$$

where s^i is the distance from the source to the observation point and s^r is the distance from the image point to the observation point. The diffraction coefficients \tilde{D}_e^d and \tilde{D}_0^d are given in Equations (5.46) and (5.47), respectively, except that the L parameter becomes [11]

$$L = \frac{s^i \rho}{s^i + \rho} \quad (6.68)$$

where s^i is the distance from the source point to QE.

The incident field evaluated at QE is

$$u^i(QE) = I_0 \frac{e^{iks'}}{\sqrt{s'}} \quad (6.69)$$

where I_0 is an arbitrary constant.

The reflection and transmission coefficients are given by

$$\hat{R} = \frac{1}{2} [\hat{R}^e(\tilde{\alpha}) + \hat{R}^0(\tilde{\alpha})] \quad (6.70)$$

$$\hat{T} = \frac{1}{2} [\hat{R}^e(\tilde{\alpha}) - \hat{R}^0(\tilde{\alpha})] \quad (6.71)$$

where \hat{R}^e and \hat{R}^0 are defined in (5.16) and (5.20), respectively, for an electric line source. If the source is a magnetic line source, \hat{R}^e and \hat{R}^0 are defined in (5.17) and (5.21), respectively.

Since it is assumed that only the lowest order even mode can propagate in the half-plane, u^{SW} is equal to

$$u^{SW}(x,y) = \frac{1}{2} u^i(QE) L_{ze}^{SW}(\phi', w_S^e) \exp [ik(x \cos w_S^e + |y| \sin w_S^e)] U(\phi - \phi_S^e), \quad (6.72)$$

$$|y| > \frac{d}{2}$$

where L_{ze}^{SW} is defined in (5.52).

In Chapter VIII, where a dielectric/ferrite slab is considered, the fields excited by the geometry illustrated in Figure 6.11 will also be needed. As shown in [21,49], the total field is the sum of the incident, reflected, transmitted, surface wave, and leaky wave fields. The last two fields are pole wave contributions, so they will exist only if the poles are captured when the original contour of integration is deformed to the steepest descent path in evaluating the integral

representation for u . The surface wave field (lowest order even mode) outside the dielectric/ferrite medium can be expressed as follows:

$$u_{(x,y)}^{SW} = 2\pi i e^{i\pi/4} I_0 F(w_s) \exp \left[ik[(|y|+h-d) \sin w_s \pm x \cos w_s] \right],$$

$$|y| > \frac{d}{2} \quad (6.73)$$

where

$$F(w_s) = \frac{\sin w_s + i \begin{bmatrix} -1 \\ \epsilon_r \\ -1 \\ \mu_r \end{bmatrix} \gamma(w_s) \tan[\gamma(w_s) kd/2]}{\cos w_s - i \begin{bmatrix} -1 \\ \epsilon_r \\ -1 \\ \mu_r \end{bmatrix} \frac{k d \sin(2w_s)}{4} \left[\frac{\tan[\gamma(w_s) kd/2]}{\gamma(w_s) kd/2} + \sec^2[\gamma(w_s) kd/2] \right]}; \begin{bmatrix} H_z \\ E_z \end{bmatrix} \quad (6.74)$$

and

$$\gamma(w_s) = (N^2 - \cos^2 w_s)^{1/2} \quad (6.75)$$

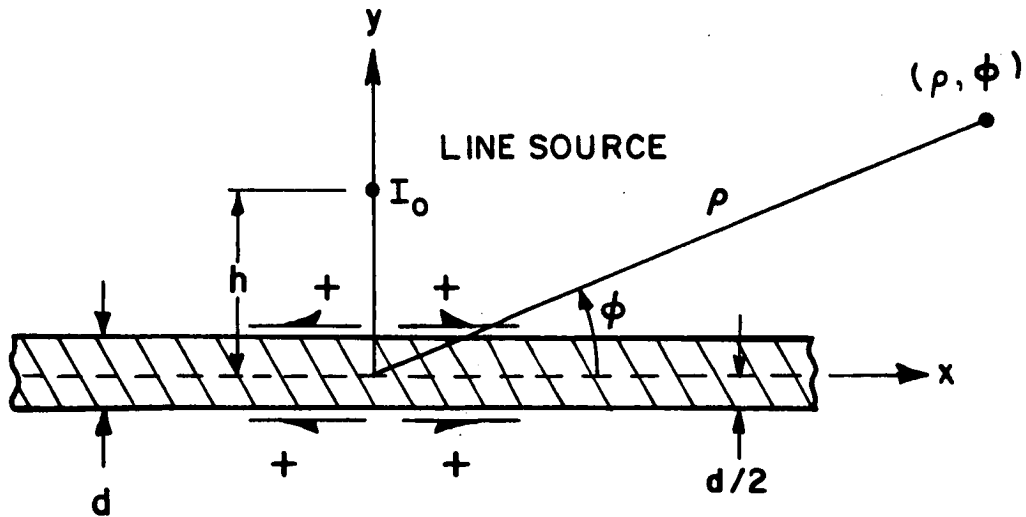


Figure 6.11. Surface waves excited by a line source above a dielectric/ferrite slab.

CHAPTER VII

MOMENT METHOD

It is crucial to ascertain the validity of the UTD solutions presented in the previous chapters. The geometry used to test the validity of these UTD ray solutions is a dielectric slab of finite width, which can be excited by a line source or an obliquely incident plane wave because the latter geometry can be analyzed via the moment method. A brief description of the development of the moment method solution to this problem will be given in this chapter. For a more general and complete treatment of this method refer to [50].

The technique employed here is an extension of the one developed by Richmond [51,52] for the case where the incident field is normally incident to the edges of the slab. In the more general case of oblique incidence (plane wave excitation) the problem is more complicated, but the solution proceeds in a similar manner. The dielectric material is assumed to be linear, isotropic, nonmagnetic ($\mu=\mu_0$), and homogeneous ($\epsilon=\text{constant}$).

This technique is based on the integral equation for the total field excited by a source in the presence of the dielectric slab [51,52].

Assume that the field (\vec{E}^i, \vec{H}^i) is incident on a dielectric material as depicted in Figure 7.1. Let (\vec{E}, \vec{H}) represent the total field; that is, the field excited by the incident field in the presence of the dielectric object. The difference between the total and incident fields is usually referred to as the scattered field (\vec{E}^s, \vec{H}^s) . Thus,

$$\vec{E} = \vec{E}^i + \vec{E}^s \quad (7.1)$$

$$\vec{H} = \vec{H}^i + \vec{H}^s \quad (7.2)$$

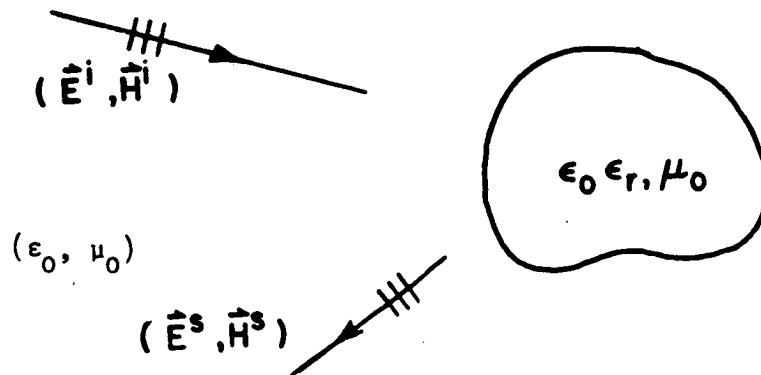


Figure 7.1. Plane wave (\vec{E}^i, \vec{H}^i) incident on a dielectric object.

It is assumed that the medium exterior to the dielectric obstacle is free space. It follows from Maxwell's equations that the scattered field (\vec{E}^S, \vec{H}^S) may be considered as the field generated by an equivalent electric current \vec{J} radiating in unbounded free space, where

$$\vec{J} = -i\omega(\epsilon - \epsilon_0) \vec{E} = -ikY_0(\epsilon_r - 1) \vec{E} \quad (7.3)$$

and ω is the angular frequency. This current is usually referred to as the volume polarization current.

The dielectric slab in this problem is a two-dimensional object, and since the incident field has an $e^{-ik\cos\theta'z}$ variation, the polarization current and scattered field will also have the same variation along the z -axis. Except for the $e^{-ik\cos\theta'z}$ factor, this problem is still considered a two-dimensional problem.

The scattered field \vec{E}^S can be expressed in terms of the electric dyadic Green's function as follows [53]:

$$\vec{E}^S(\vec{\rho}) = ik\eta_0 \lim_{\delta \rightarrow 0} \int_{A_J - A_\delta} \vec{g}_e^0 \cdot \vec{J} dA' + \frac{\vec{\ell} \cdot \vec{J}}{ikY_0} \quad (7.4)$$

where A_J and A_δ are depicted in Figure 7.2. The area A_δ , which excludes the singularity of \vec{g}_e^0 is called the "principal area". It becomes infinitesimally small in the limit as its maximum chord length δ approaches zero. Since the value of $\vec{\ell}$ and the integral in (7.4) depend on the geometry of A_δ [53], the area A_δ is assumed to be a circle here.

The electric dyadic Green's function is given by

$$\vec{g}_e^0 = \frac{i}{4} \left(\vec{I} + \frac{1}{k^2} \nabla \nabla \right) H_0^{(1)}(k|\vec{\rho} - \vec{\rho}'|) \quad , \quad \vec{\rho} \neq \vec{\rho}' \quad (7.5)$$

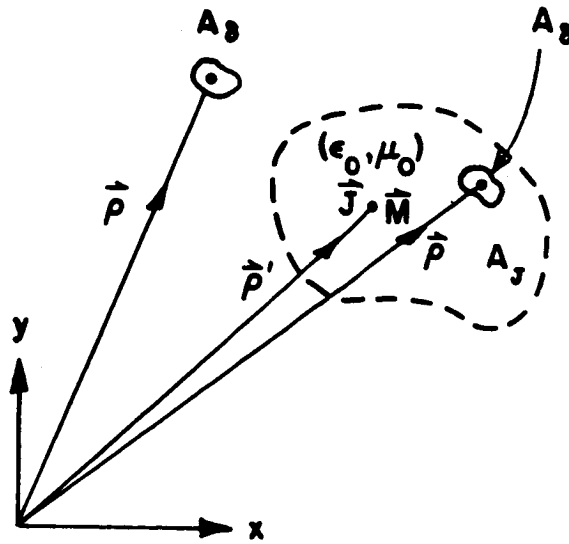


Figure 7.2. Polarization current \vec{J} replaces dielectric object.

where

$$\bar{\bar{I}} = \hat{x} \hat{x} + \hat{y} \hat{y} + \hat{z} \hat{z} \quad (7.6)$$

$$K = k \sin \theta' \quad (7.7)$$

$$\nabla = \hat{x} \frac{\partial}{\partial x} + \hat{y} \frac{\partial}{\partial y} + \hat{z} i k_z' \quad (7.8)$$

Substituting (7.3) and (7.4) into (7.1) yields

$$\vec{E}(\vec{\rho}) - k^2 (\epsilon_r - 1) \lim_{\delta \rightarrow 0} \int_{A_J - A_\delta} \bar{g}_e^0 \cdot \vec{E}(\vec{\rho}') dA' + (\epsilon_r - 1) \bar{\bar{k}} \cdot \vec{E}(\vec{\rho}) = \vec{E}^i(\vec{\rho}) \quad (7.9)$$

where the dyadic term $\bar{\bar{k}}$ is equal to [53]

$$\bar{\bar{k}} = \frac{1}{2} (\hat{x} \hat{x} + \hat{y} \hat{y}) \quad (7.10)$$

when A_δ is a circle. The integral Equation (7.9) is solved numerically using the moment method.

The first step in the solution of (7.9) is to divide the dielectric slab into square cells (see Figure 7.3) small enough so that the electric field intensity is nearly uniform in each cell. This is equivalent to choosing the pulse functions $\{f_n(\vec{\rho}')\}_{n=1}^N$ as the basis functions. That is, let

$$E_p(\vec{\rho}') = \sum_{n=1}^N E_{pn} f_n(\vec{\rho}') \quad , \quad p = x, y, z \quad (7.11)$$

where

$$f_n(\vec{\rho}') = \begin{cases} 1 & \text{in cell } n \\ 0 & \text{elsewhere} \end{cases} \quad (7.12)$$

and $\{E_{pn}\}$ are unknown coefficients.

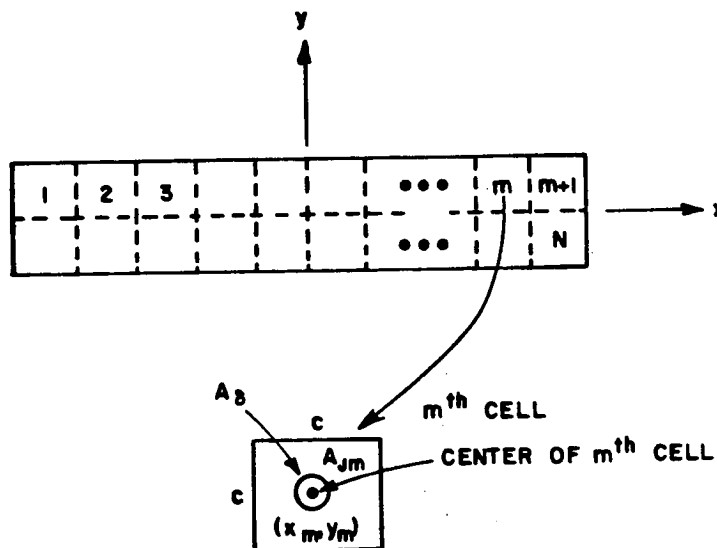


Figure 7.3. Dielectric slab divided into square cells.

In order to obtain a system of linear equations to solve for $\{E_{pn}\}_{n=1}^N$, it is necessary to define a set of testing functions. Here, the Dirac "delta" functions $\{\delta(x-x_n)\delta(y-y_n)\}_{n=1}^N$ are chosen as the testing functions. This is equivalent to enforcing the condition that at the center of each square cell, the total field must be equal to the sum of the incident and scattered fields.

Substituting (7.11) and the testing functions into (7.9) and enforcing Equation (7.9) at the center of each m^{th} cell, the following set of $3N$ simultaneous equations with $3N$ unknowns is obtained:

$$\sum_{n=1}^N \{A_{mn} E_{xn} + B_{mn} E_{yn} + C_{mn} E_{zn}\} = E_{xm}^i, \quad m = 1, 2, \dots, N \quad (7.13)$$

$$\sum_{n=1}^N \{B_{mn} E_{xn} + P_{mn} E_{yn} + F_{mn} E_{zn}\} = E_{ym}^i, \quad m = 1, 2, \dots, N \quad (7.14)$$

$$\sum_{n=1}^N \{C_{mn} E_{xn} + F_{mn} E_{yn} + M_{mn} E_{zn}\} = E_{zm}^i, \quad m = 1, 2, \dots, N \quad (7.15)$$

where for $m \neq n$

$$A_{nm} = A_{mn} = \tilde{K}' \left\{ K\rho(y_m - y_n)^2 H_0^{(1)}(K\rho) + [(x_m - x_n)^2 - (y_m - y_n)^2] H_1^{(1)}(K\rho) + \frac{k_z'^2 \rho^3}{K} H_0^{(1)}(K\rho) \right\} \quad (7.16)$$

$$B_{mn} = B_{nm} = \tilde{K}' \{ (x_m - x_n)(y_m - y_n) [2H_1^{(1)}(K\rho) - K\rho H_0^{(1)}(K\rho)] \} \quad (7.17)$$

$$C_{mn} = \tilde{K}' \{ -ik_z' \rho^2 (x_m - x_n) H_1^{(1)}(K\rho) \} = -C_{nm} \quad (7.18)$$

$$P_{mn} = \tilde{R}' \left[K\rho(x_m - x_n)^2 H_0^{(1)}(K\rho) + [(y_m - y_n)^2 - (x_m - x_n)^2] H_1^{(1)}(K\rho) + \frac{k_z'^2 \rho^3}{K} H_0^{(1)}(K\rho) \right] = P_{nm} \quad (7.19)$$

$$F_{mn} = \tilde{R}' \left[-ik_z' (y_m - y_n) \rho^2 H_1^{(1)}(K\rho) \right] = -F_{nm} \quad (7.20)$$

$$M_{mn} = \tilde{R}' \rho^3 K H_0^{(1)}(K\rho) = M_{nm} \quad (7.21)$$

$$\tilde{R}' = -i\pi a J_1(Ka)(\epsilon_r - 1)/(2\rho^3) \quad (7.22)$$

$$\rho = \left[(x_n - x_m)^2 + (y_n - y_m)^2 \right]^{1/2} \quad (7.23)$$

For $m = n$

$$B_{mm} = C_{mm} = F_{mm} = 0 \quad (7.24)$$

$$M_{mm} = 1 - i(\epsilon_r - 1)/2 \left[\pi Ka H_1^{(1)}(Ka) + 2i \right] \quad (7.25)$$

$$P_{mm} = A_{mm} = 1 + \frac{\epsilon_r - 1}{2} - \frac{i(\epsilon_r - 1)}{4} \left[\pi Ka H_1^{(1)}(Ka) + 2i \right] \left[1 + \frac{2k_z'^2}{K^2} \right] \quad (7.26)$$

Note that it is not possible to obtain a closed form result for the integral of the Hankel function over a square cell. However, a simple solution is available if the region of integration is a circle [51]. It has been shown [51] that the error in approximating square cells with circular cells of the same cross section area as shown in Figure 7.4 is very small.

Once the 3N simultaneous equations are obtained, they can be solved with the aid of a digital computer to evaluate the electric field at the center of each cell. Note that by inserting the appropriate equations for the incident field, one obtains solutions for any two-dimensional source (line source, array of line sources, plane wave) in the presence of the dielectric slab. Furthermore, the solution approaches the exact solution if a sufficiently large number of cells are employed [51].

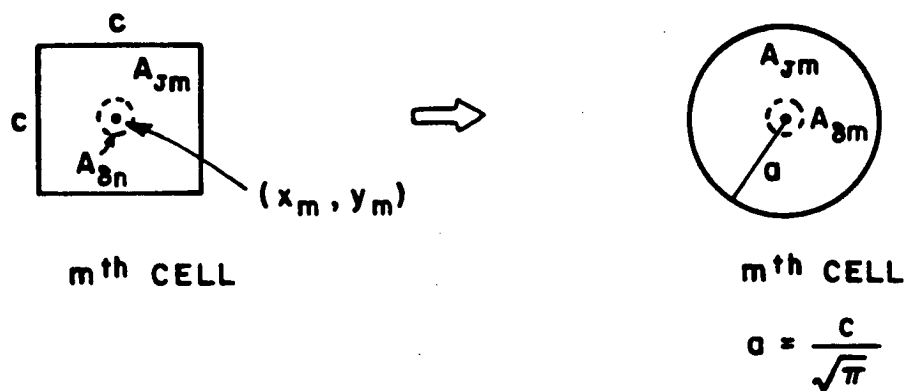


Figure 7.4. Square cell is replaced by a circular cell of the same area.

Assuming that the simultaneous equations have been solved, the scattered fields E_Z^S and H_Z^S are given by

$$E_Z^S(\rho, \phi, z) = i(\epsilon_r - 1) (-\pi i/2)^{1/2} (Ka) J_1(Ka) \cdot \sum_{n=1}^N \left[E_{zn} - (k_z'/K)(\rho_0/\rho_n) [(\cos \phi - x_n/\rho_0)E_{xn} + (\sin \phi - y_n/\rho_0)E_{yn}] \right] \cdot \exp(iK\rho_n + ik_z'z)/(K\rho_n)^{1/2} \quad (7.27)$$

$$H_Z^S(\rho, \phi, z) = -iY_0 (-\pi i/2)^{1/2} (ka) J_1(Ka) (\epsilon_r - 1) \cdot \sum_{n=1}^N (\rho_0/\rho_n) \left[(\sin \phi - y_n/\rho_0)E_{xn} - (\cos \phi - x_n/\rho_0)E_{yn} \right] \frac{\exp(iK\rho_n + ik_z'z)}{(K\rho_n)^{1/2}} \quad (7.28)$$

where

$$\rho_n = [(x - x_n)^2 + (y - y_n)^2]^{1/2}, \quad \rho_0 = (x^2 + y^2)^{1/2} \quad (7.29)$$

As mentioned by Richmond [52], in order to obtain accurate results, the dimensions of each cell should not exceed

$$\frac{c}{\lambda} < \frac{0.2}{\sqrt{\epsilon_r}} \quad (7.30)$$

where c was defined in Figure 7.4.

To calculate the elements of the impedance matrix, it is necessary to evaluate the following two integrals:

$$\hat{I}_1 = \lim_{b \rightarrow 0} \int_b^a \int_0^{2\pi} H_0^{(1)}(K\rho') \rho' d\rho' d\phi' , \quad a > 0 \quad (7.31)$$

$$\hat{I}_2 = \int_0^a \int_0^{2\pi} H_0^{(1)}(K|\vec{\rho} - \vec{\rho}'|) \rho' d\rho' d\phi' , \quad \rho' < a < \rho . \quad (7.32)$$

By using the integral tables in [54], the integral in (7.31) can be easily evaluated. One gets

$$\hat{I}_1 = \frac{2}{K^2} [\pi Ka H_1^{(1)}(Ka) + 2i] , \quad a > 0 . \quad (7.33)$$

The integral in (7.32) can be evaluated by first using the addition theorem for the function $H_0^{(1)}(K|\vec{\rho} - \vec{\rho}'|)$, and then integrating term by term. After some simplification, one obtains

$$\hat{I}_2 = \frac{2\pi a}{K} J_1(Ka) H_0^{(1)}(K\rho) , \quad a < \rho . \quad (7.34)$$

CHAPTER VIII

RESULTS AND DISCUSSION

As stated in the previous chapter, it is important to ascertain the validity of the UTD solutions developed in Chapters III through VI. The dielectric/ferrite strip geometry shown in Figures 8.1 and 8.2 has been chosen for this purpose. The fields scattered by the strip are then calculated using the UTD solutions as well as the corresponding MM solutions discussed in the previous chapter. The results obtained by these two distinct methods are shown to agree very closely, which gives a good indication of the accuracy of the new UTD results.

The scattering and diffraction of an object which is large in terms of a wavelength is essentially a local phenomenon associated with specific parts of the object [6,7,8,10,59]. Therefore, the UTD results obtained for the dielectric/ferrite half-plane can be used to analyze the strip as long as the width of the strip is generally more than about one wavelength [10].

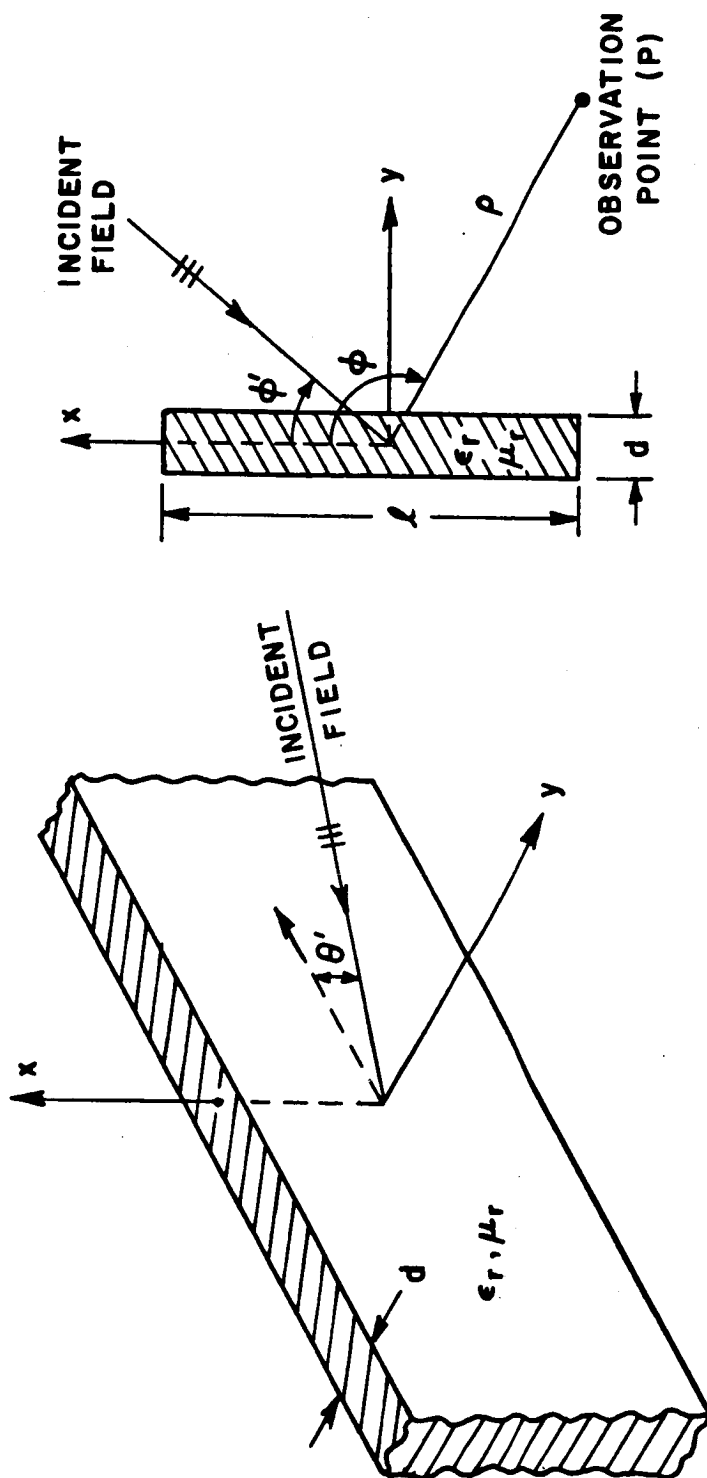


Figure 8.1. Plane wave excitation.

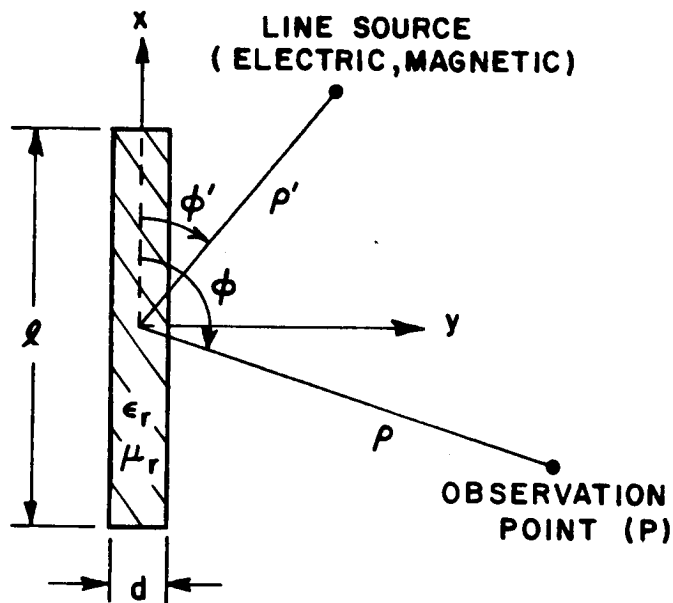


Figure 8.2. Line source excitation.

The total field at a point of observation (P) is equal to the superposition of the following field components as depicted in Figure 8.3.

- (I) Direct field from the source
- (II) Reflected field from the finite dielectric/ferrite strip
- (III) Transmitted field through the finite dielectric/ferrite strip
- (IV) Edge Diffracted fields from both edges of the strip
- (V) Edge diffracted surface waves
- (VI) Reflected surface waves which are subsequently diffracted by the opposite edges of the strip.

If additional terms are needed, one can add them to the solution; however, as will be shown in the examples, the six field components

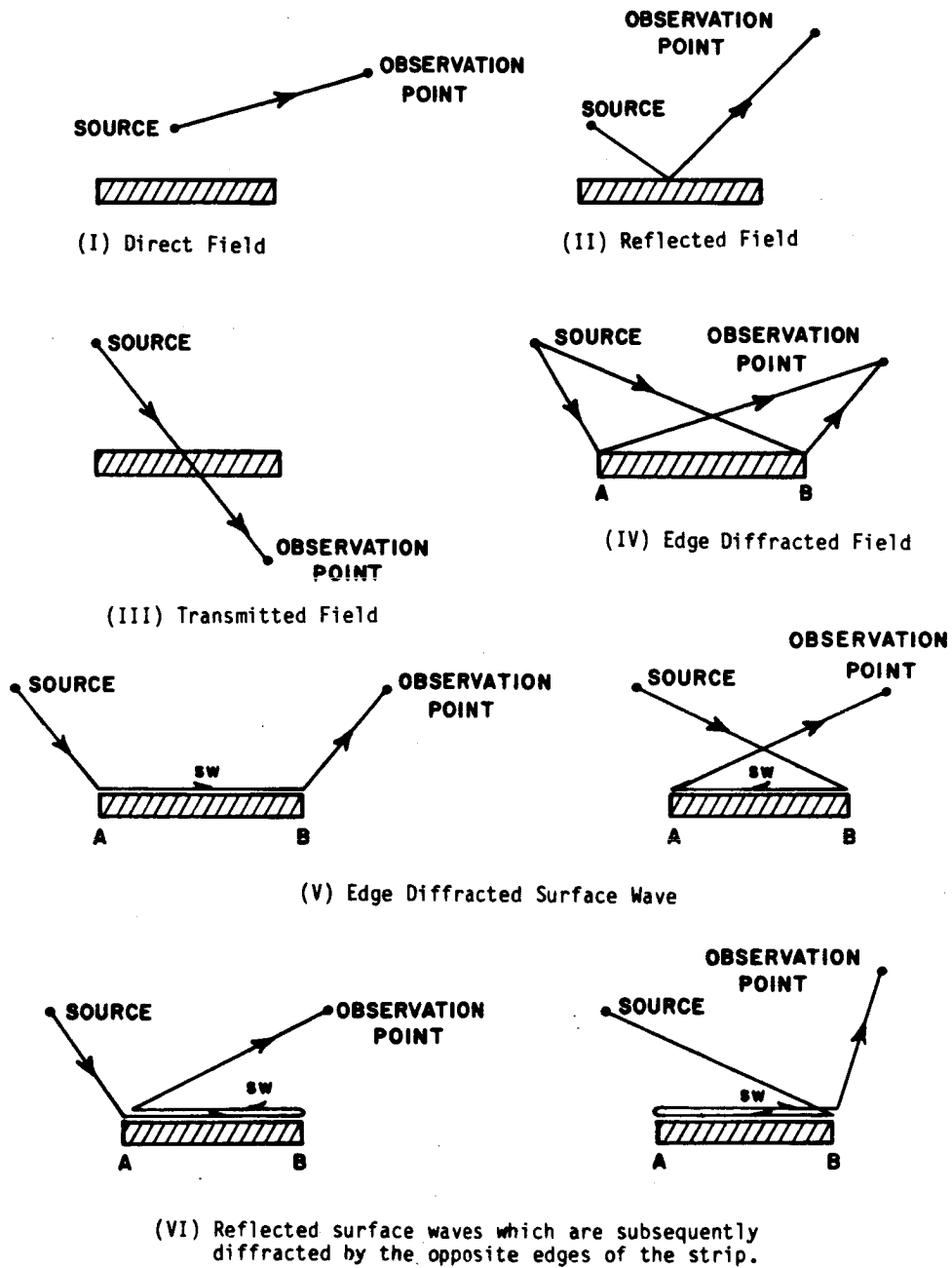


Figure 8.3. Field components that contribute to the total field at the observation point.

listed above are more than sufficient for the problems considered here. Because the total field is obtained from the superposition of the various field components listed above, UTD provides a very valuable physical insight into the radiation and scattering mechanisms involved. Furthermore, the UTD solutions for the problems developed here (Figures 1.2 and 1.3) serve to extend the applicability of the UTD method to analyze the radiation and scattering by complex structures containing dielectric/ferrite panels. It is noted that UTD can solve high frequency radiation and scattering problems (for which exact analytical solutions are not available) once the pertinent UTD diffraction coefficients are known for that problem.

In order to provide a more stringent test on the validity of the results obtained here, the scattered field is calculated instead of the total field. The reason for this is that the direct source field is usually much stronger than the other field components and could possibly conceal errors in the scattered field.

The scattered fields (\vec{E}^S, \vec{H}^S) are easily obtained from the total fields (\vec{E}, \vec{H}) as follows:

$$\vec{E}^S = \vec{E} - \vec{E}^i \quad (8.1)$$

$$\vec{H}^S = \vec{H} - \vec{H}^i \quad (8.2)$$

where the fields \vec{E}^i and \vec{H}^i are the incident electric and magnetic fields, respectively, in the absence of the dielectric/ferrite strip. Most of the results shown here will be the scattered fields, except for a few results where the total field will be calculated.

All the patterns shown here are calculated in the x-y plane shown in Figures 8.1 and 8.2 where the point of observation (P), which is at a distance ρ from the origin, rotates clockwise from $\phi=0$ to $\phi=2\pi$. Note that for the case of oblique incidence ($\theta' \neq \pi/2$, plane wave excitation), the field evaluated at a given x-y plane ($z=z_0$), differs from the field evaluated at another x-y plane ($z=z_1$) by the factor $\exp(-ik\cos\theta'(z_1-z_0))$. For the case of line source excitation depicted in Figure 8.2, the distance from the origin to the line source is ρ' . The dielectric/ferrite strip has a width ℓ , thickness d , with a relative permittivity ϵ_r , and relative permeability μ_r . Throughout this chapter, unless otherwise stated, only the magnitude of the calculated fields will be plotted. As mentioned before, a heuristic approach was suggested by Burnside [2] to solve the dielectric strip problem by modifying the solution of the perfectly conducting half-plane. This heuristic solution does not include surface waves, reflected surface waves, or diffracted surface waves. This solution will be referred to as the old UTD solution. Figures 8.4-8.6 depict the total field of a line source in the presence of a lossless dielectric strip computed by three different methods. Note that new UTD solutions developed in this study are the ones that were obtained by modifying the impedance bisection solutions using the "second approach". That is, the GO fields are the exact fields, while the diffracted fields were obtained by heuristically modifying the impedance half-plane diffracted fields using the UTD recipe. Furthermore, the surface wave reflected and diffracted fields were obtained from the impedance bisection solutions by replacing the impedance surface wave propagation and attenuation constants by the

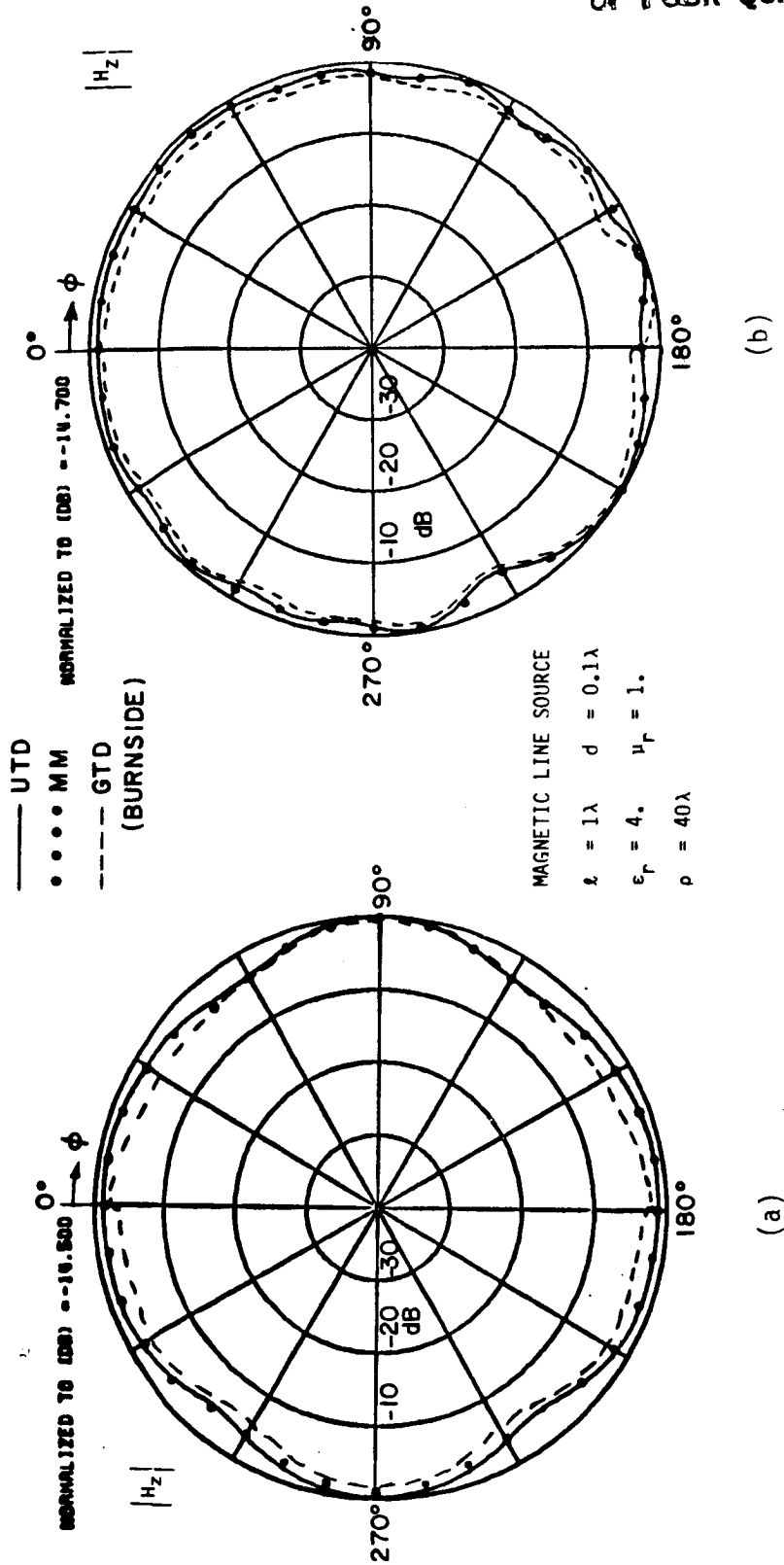


Figure 8.4. Magnitude of the total H_z field for the geometry shown in

Figure 8.2. (a) $\phi' = 90^\circ$, $\rho' = 1\lambda$. (b) $\phi' = 30^\circ$, $\rho' = 2\lambda$.

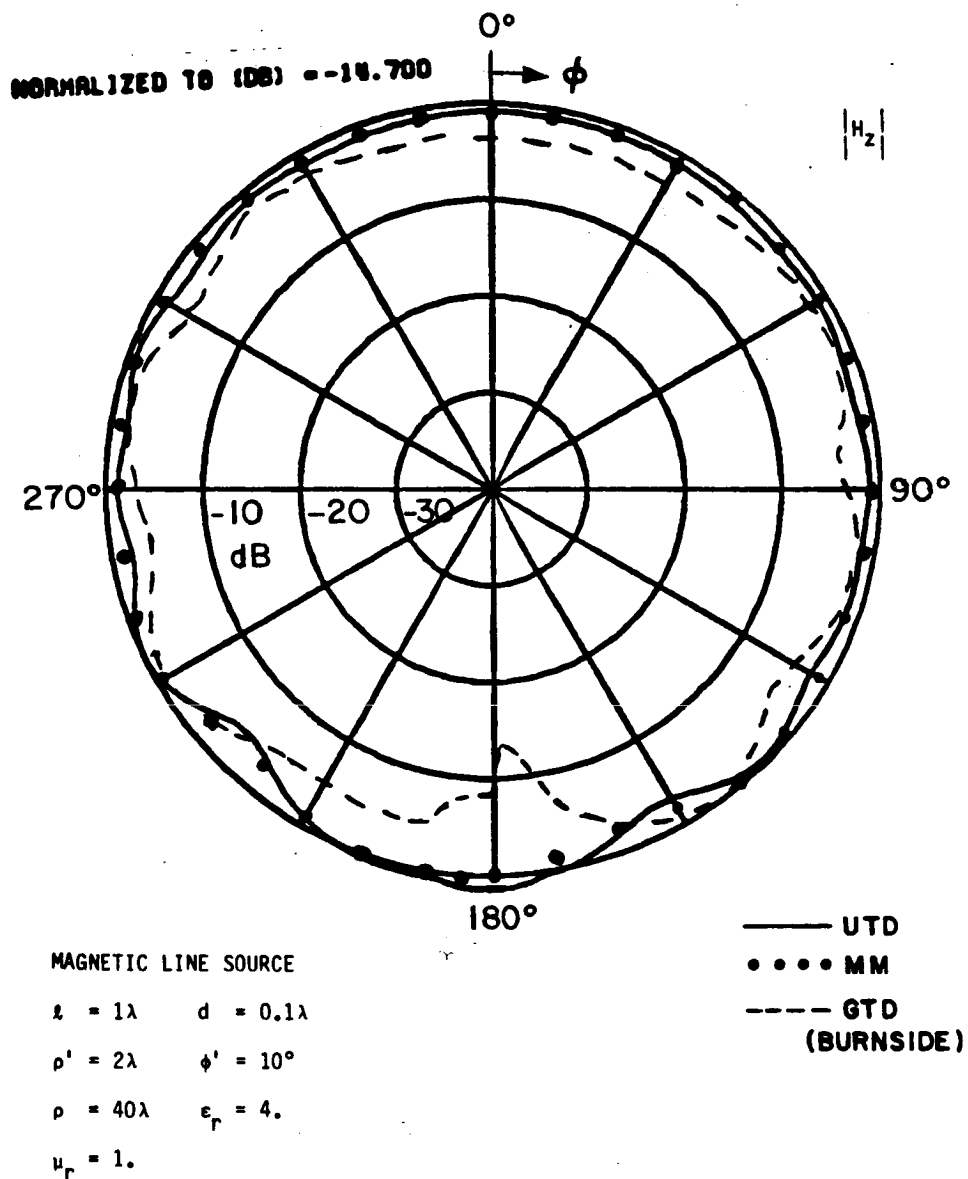


Figure 8.5. Magnitude of the total H_z field for the geometry shown in Figure 8.2.

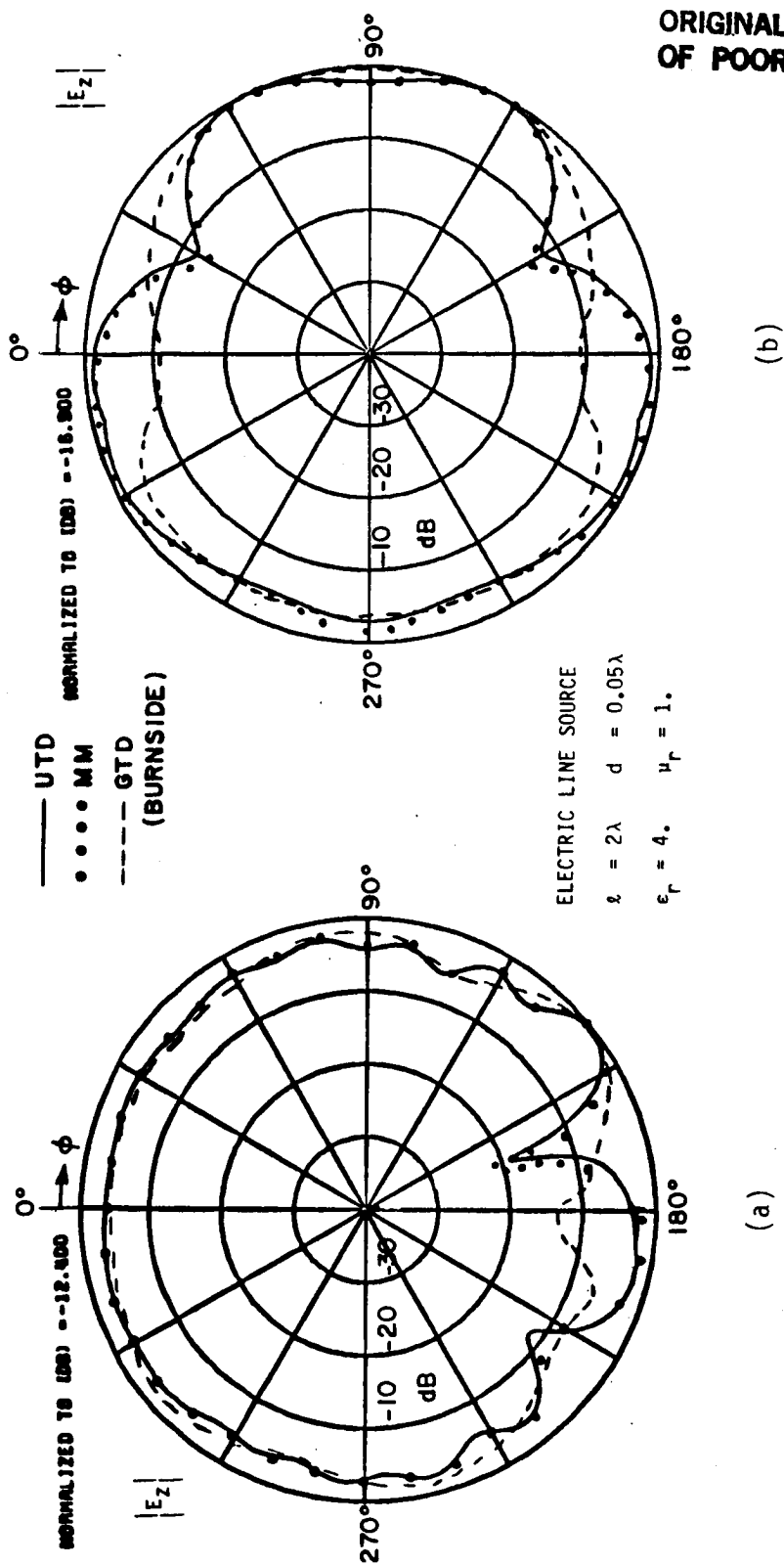


Figure 8.6. Magnitude of the E_z field for the geometry shown in Figure 8.2.

(a) $\phi' = 10^\circ$, $\rho = 40\lambda$. (b) $\phi' = 90^\circ$, $\rho = 0.25\lambda$.

more accurate corresponding exact coefficients for the grounded dielectric/ferrite slab.

It is obvious from Figures 8.4-8.6, that there is better agreement between the new UTD and MM solutions than between the old UTD and MM solutions. In Figures 8.4b-8.6a, where the angle of incidence is either 30 or 10 degrees, there is a big improvement with the new UTD solutions, especially around 180 degrees, where the diffracted surface waves play an important role. However, even in Figure 8.4a, where the diffracted surface wave is not important, because the angle of incidence is 90 degrees, the new UTD solution seems to agree more closely with the MM solution. This means that not only is there an improvement in the new UTD solution because of the inclusion of the surface wave effects, but the new UTD edge diffraction coefficients also provide more accurate results than the old ones. In Figure 8.6b where the electric line source is only 0.25λ away from the middle of the slab, there is a big disagreement between the old UTD and MM solutions, especially around 0 and 180 degrees. The reason for this disagreement is that the line source excites two surface waves which travel in opposite directions toward the edges of the strip (see Figure 6.11) where they are diffracted. Since the amplitude of the surface wave is inversely proportional to the distance of the line source from the strip, these surface wave contributions become important for $\rho'=0.25\lambda$. Since the new UTD solution includes these contributions, it agrees very well with the MM solution as shown in Figure 8.6b.

In Figures 8.7a-8.8a, the total field of a magnetic line source is depicted for increasing values of the electric loss tangent, and for the

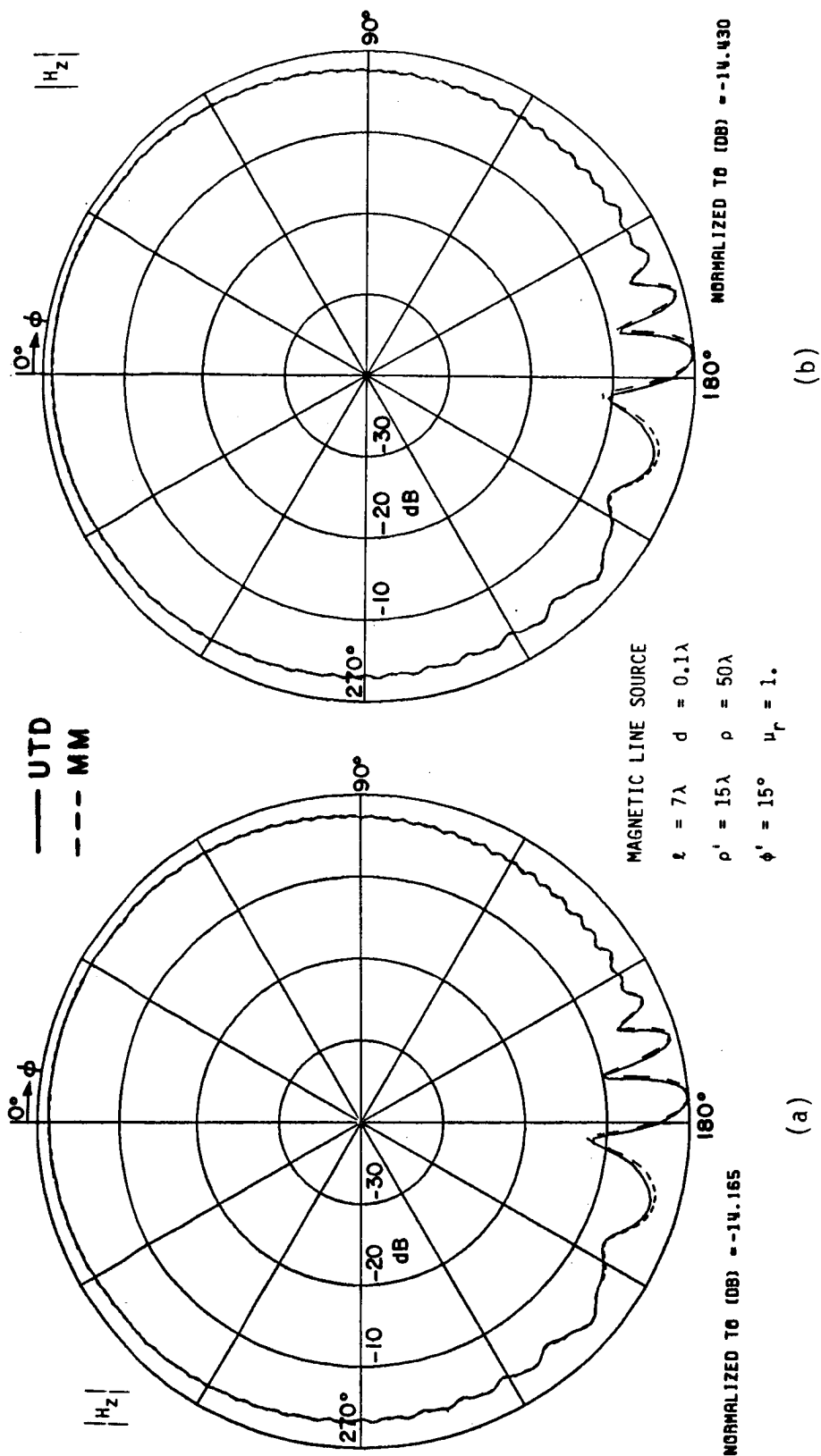


Figure 8.7. Magnitude of the total H_z field for the geometry shown in

Figure 8.2. (a) $\epsilon_r = 4 + i0$. (b) $\epsilon_r = 4 + i0.8$

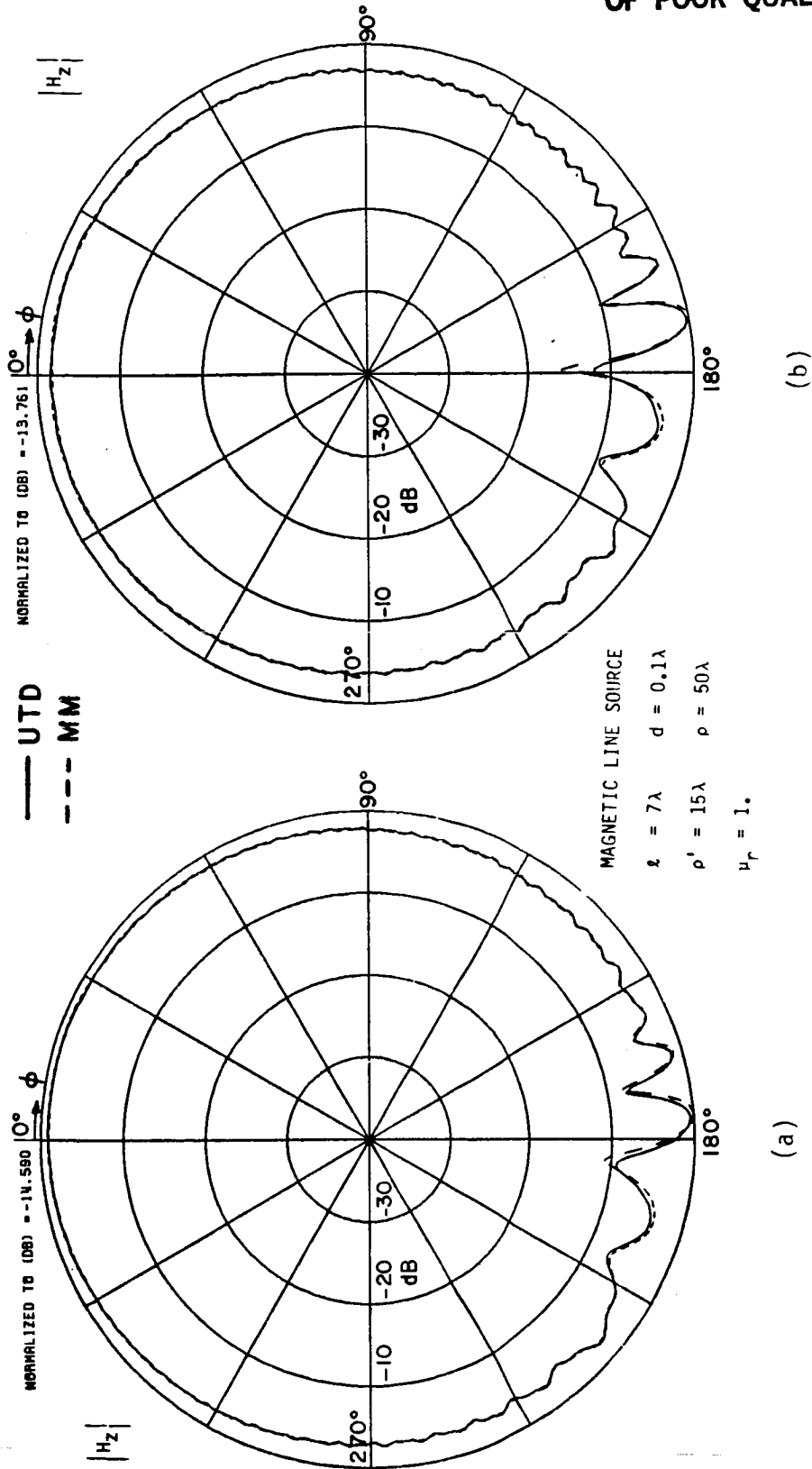


Figure 8.8. Magnitude of the total H_z field for the geometry shown in

Figure 8.2. (a) $\epsilon_r = 4. + i2.$, $\phi' = 15^\circ$ (b) $\epsilon_r = 4. + i0.$, $\phi' = 10^\circ$

case where the angle of incidence is 15 degrees. In Figures 8.8b-8.9b, the angle of incidence is 10 degrees, and still there is very good agreement between the new UTD and MM solutions. Figures 8.10a-8.13b show the total field of an electric line source for different values of the electric loss tangent, angle of incidence, and length of the strip.

As the angle of incidence becomes smaller, the diffracted surface waves become significant. For example, in Figure 8.13a, the total field of an electric line source is depicted without the diffracted surface wave fields. Since the angle of incidence is only 1 degree, the new UTD solution without the above surface wave contribution is not very accurate, especially around 180 degrees where the diffracted surface wave is important. When the diffracted surface wave is added, the two solutions agree very well everywhere, except near 180 degrees as illustrated in Figure 8.13b. When the angle of incidence becomes smaller, not only does the diffracted surface wave become important, but the doubly edge diffracted field also becomes significant. The doubly edge diffracted field is the field diffracted from the second edge after being diffracted by the first one as depicted in Figure 8.14. This field diffracted by the first edge at near grazing angles of incidence, which is then incident on the second edge, is in general not a ray optical field. Consequently, its diffraction by the second edge must be handled carefully near the forward scatter direction. The present UTD solution does not include this doubly edge diffracted term; however, it will be added in the future. It can be shown [55] that as the length of the strip increases, this doubly edge diffracted field becomes less important.

ORIGINAL PAGE IS
OF POOR QUALITY

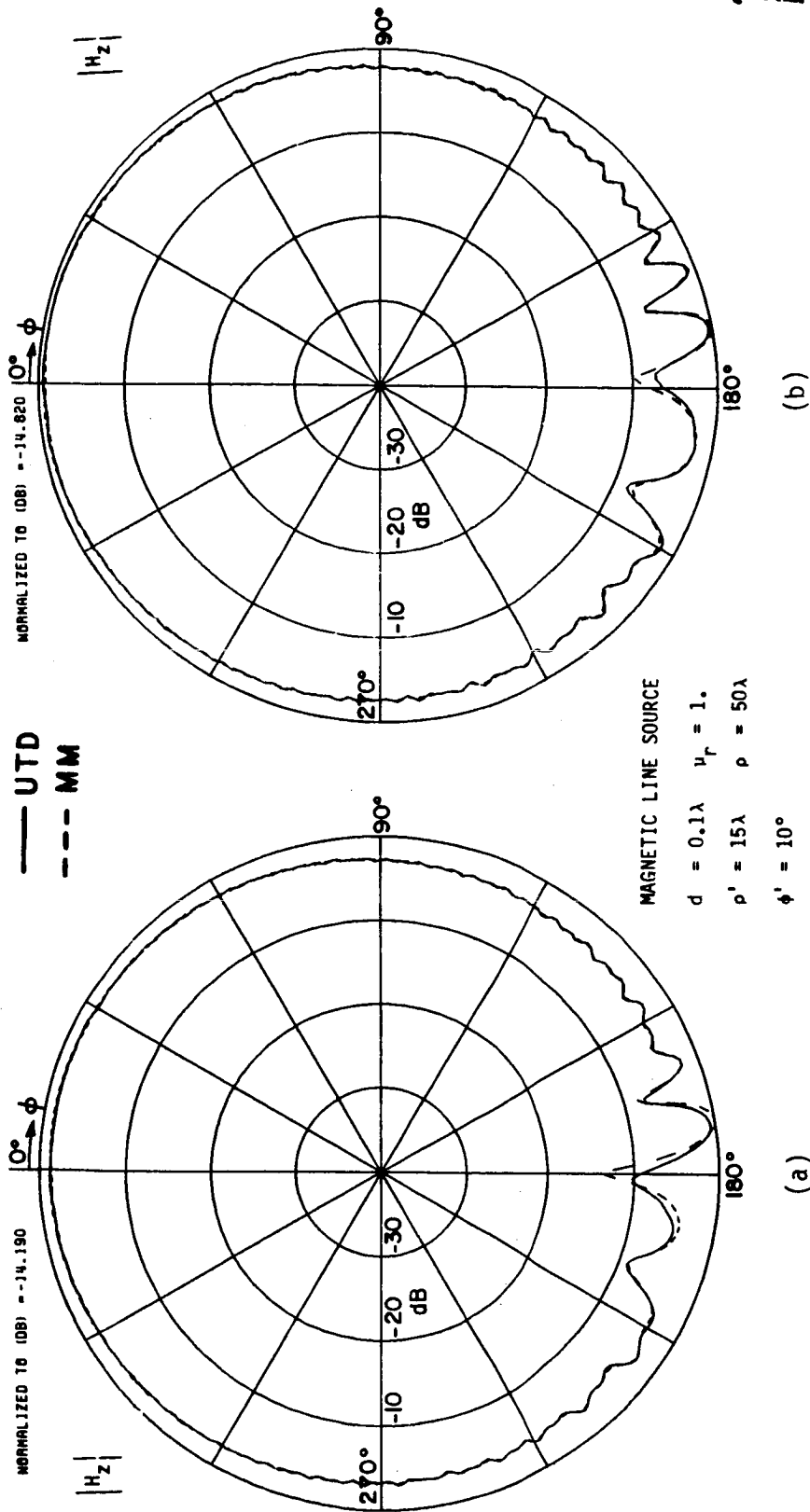


Figure 8.9. Magnitude of the total H_z field for the geometry shown in

Figure 8.2. (a) $l=7\lambda$, $\epsilon_r=4.+i2$. (b) $l=5\lambda$, $\epsilon_r=4.+i0$.

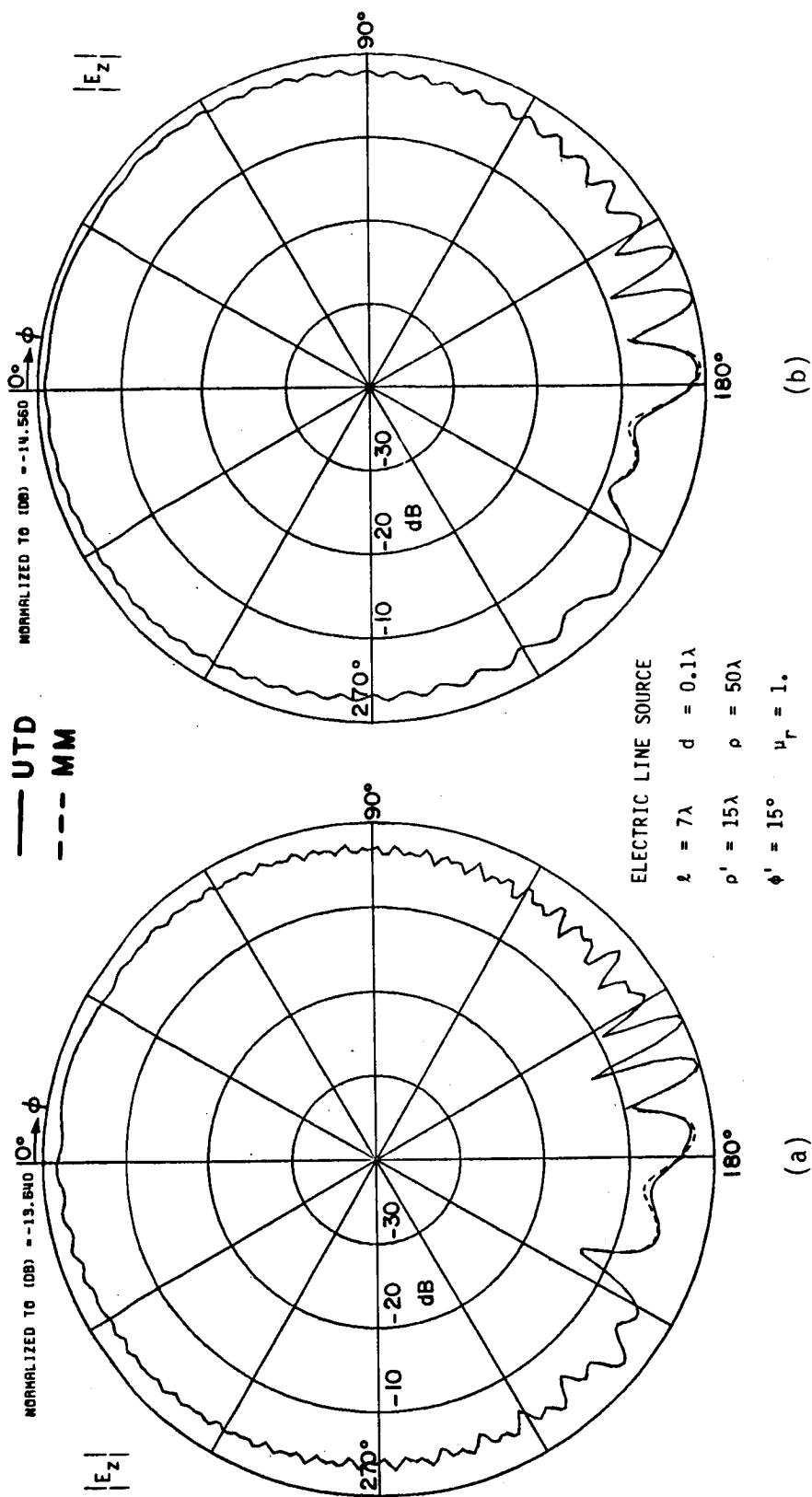


Figure 8.10. Magnitude of the total E_z field for the geometry shown in

Figure 8.2. (a) $\epsilon_r = 4 + i0$. (b) $\epsilon_r = 4 + i2$.

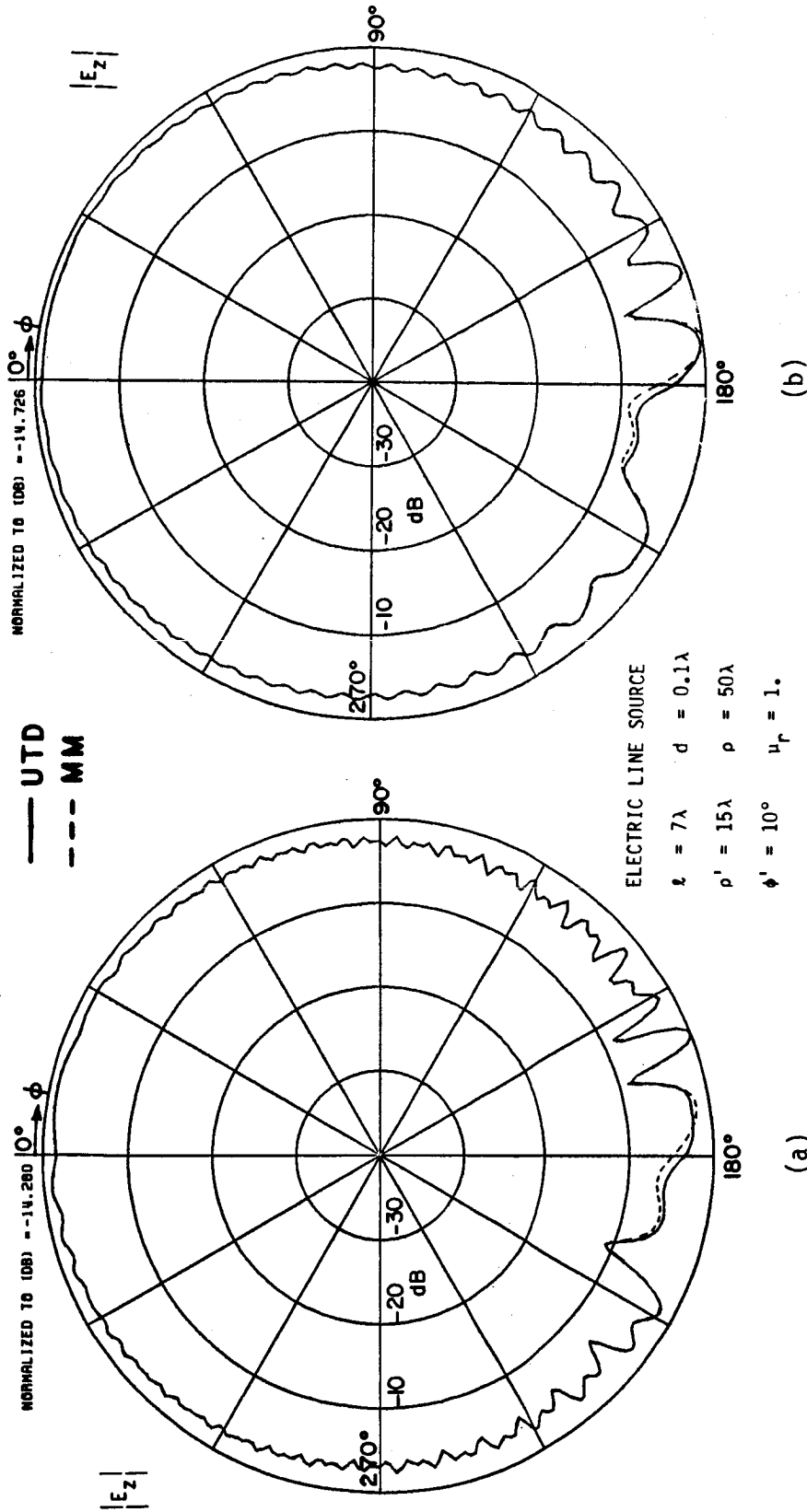


Figure 8.11. Magnitude of the total E_z field for the geometry shown in

Figure 8.2. (a) $\epsilon_r = 4 + i0$. (b) $\epsilon_r = 4 + i2$.

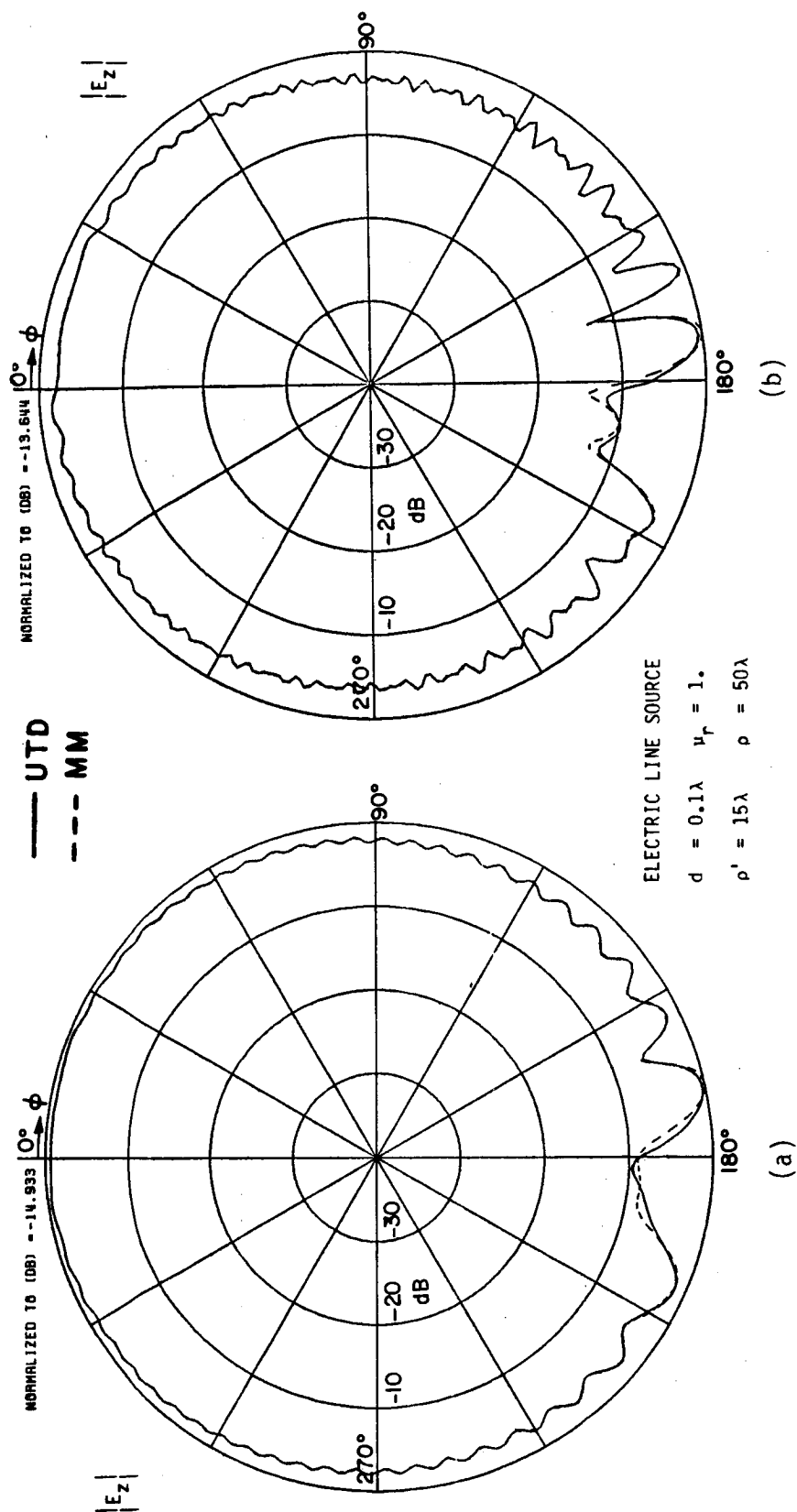


Figure 8.12. Magnitude of the total E_z field for the geometry shown in

Figure 8.2. (a) $\ell=7\lambda$, $\epsilon_r=4.+i2.8$, $\phi'=5^\circ$ (b) $\ell=5\lambda$,
 $\epsilon_r=4.+i0.$, $\phi'=10^\circ$

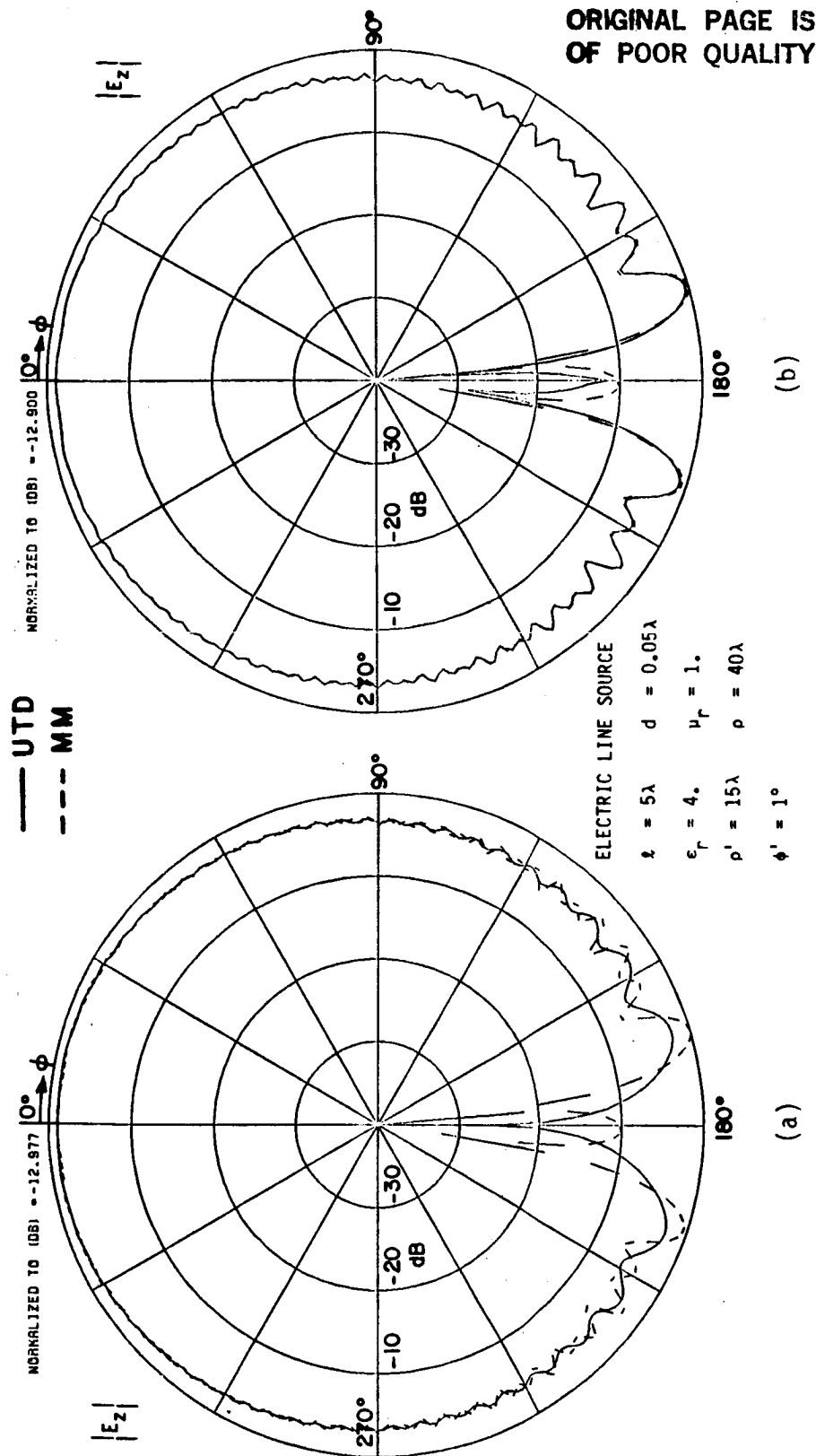


Figure 8.13. Magnitude of the total E_z field for the geometry shown in Figure 8.2. (a) Without diffracted surface wave, (b) Field components V and VI included (diffracted surface wave included).

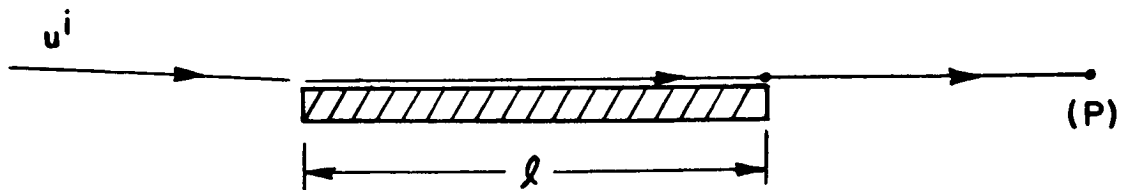


Figure 8.14. Doubly Edge Diffracted Field.

Even though there is an improvement when the diffracted surface wave is added, the agreement between the UTD and MM solution is not perfect due to the absence of the doubly edge diffracted field. In Figure 8.15a, the dielectric strip becomes lossy and the diffracted surface wave becomes less important. However, the doubly edge diffracted field is still important, and its absence causes the disagreement between the new UTD and MM solutions around 180 degrees. Additional plots are depicted in Figures 8.15b through 8.17b for three different lengths of the dielectric strip.

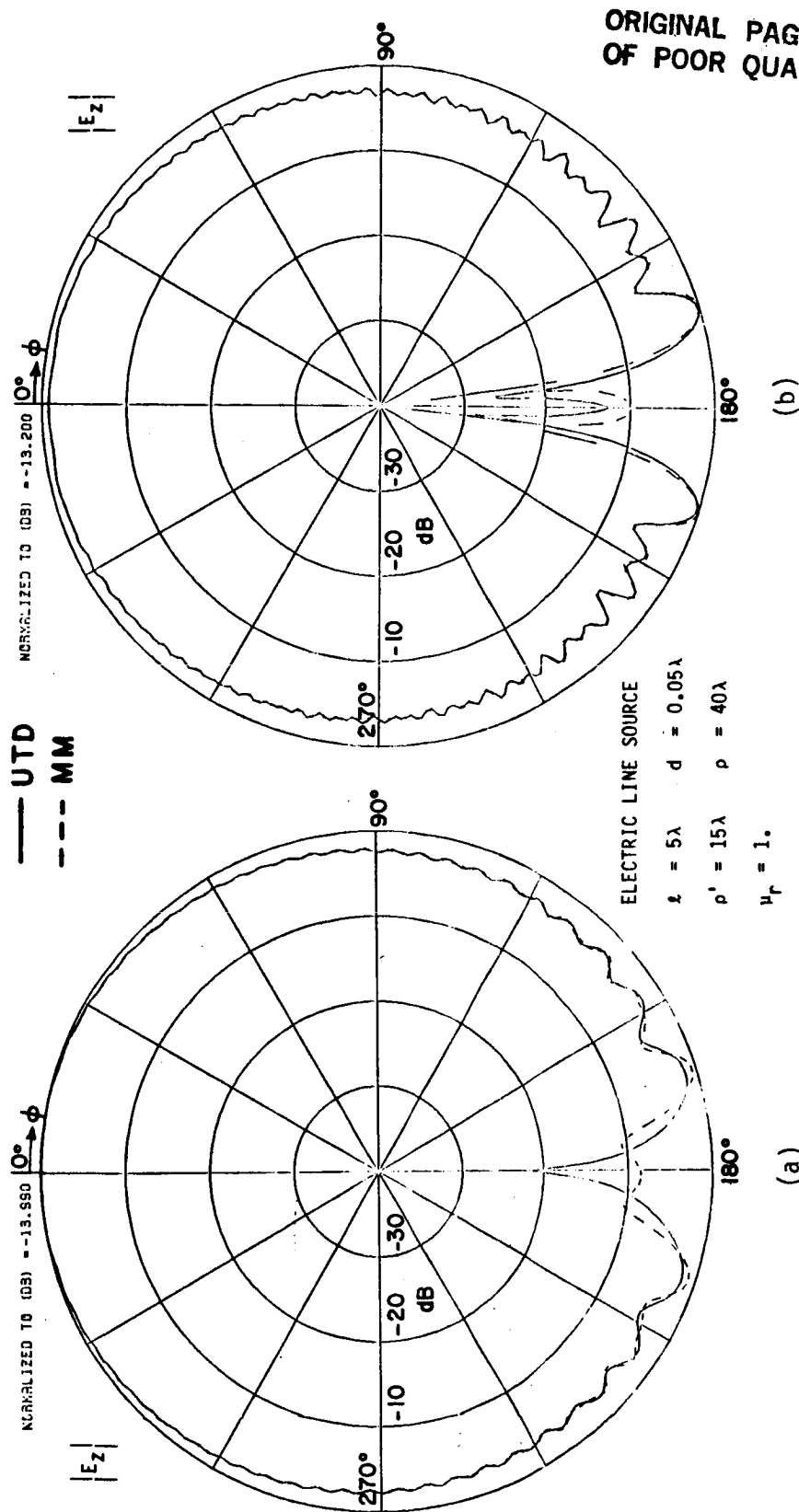


Figure 8.15. Magnitude of the total E_z field for the geometry shown in

Figure 8.2. (a) $\epsilon_r = 4. + i1.$, $\phi' = 1^\circ$, (b) $\epsilon_r = 4. + i0.$, $\phi' = 0.1^\circ$

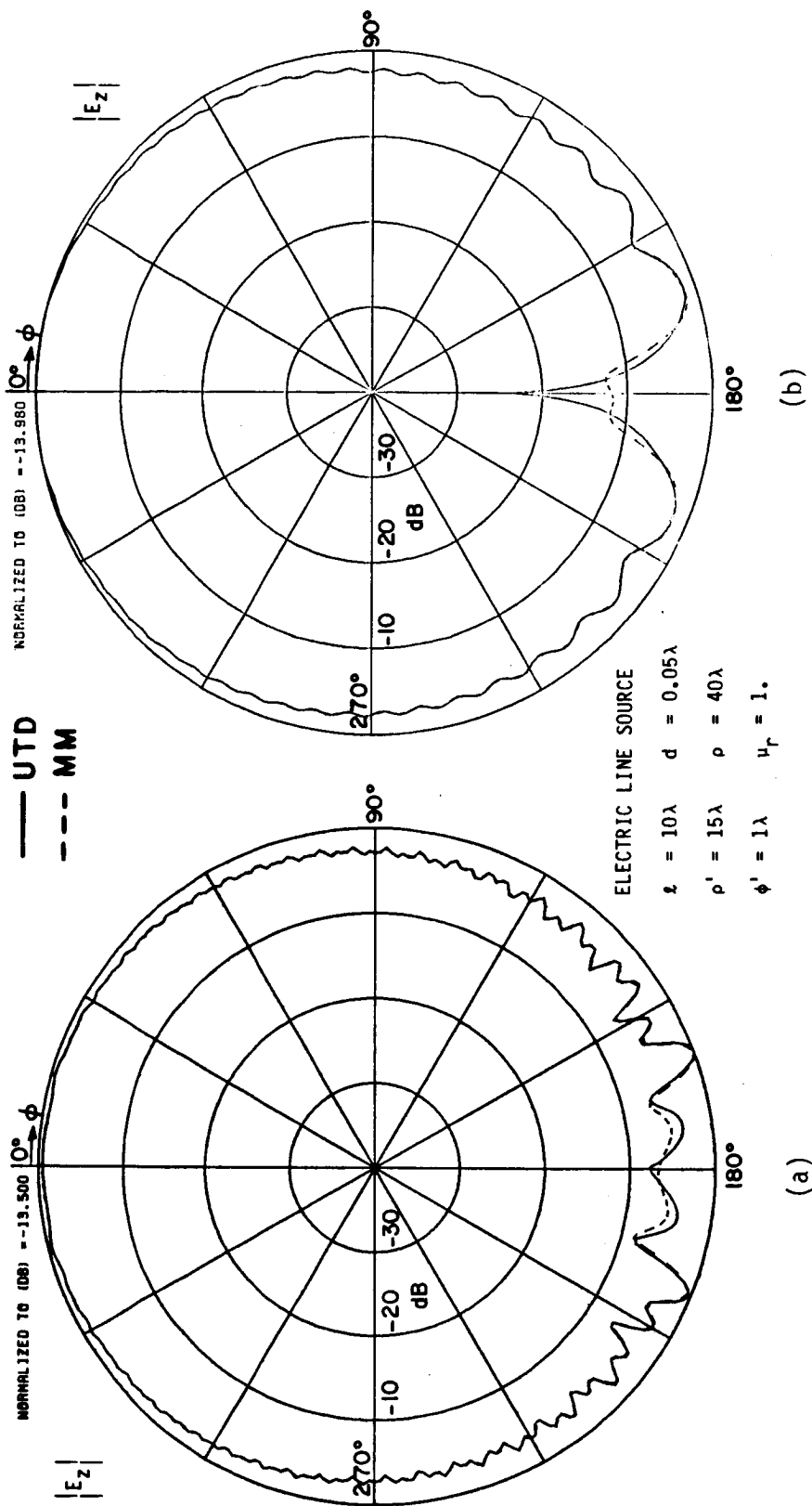


Figure 8.16. Magnitude of the total E_z field for the geometry shown in

Figure 8.2. (a) $\epsilon_r = 4. + i0.$, (b) $\epsilon_r = 4. + i1.$

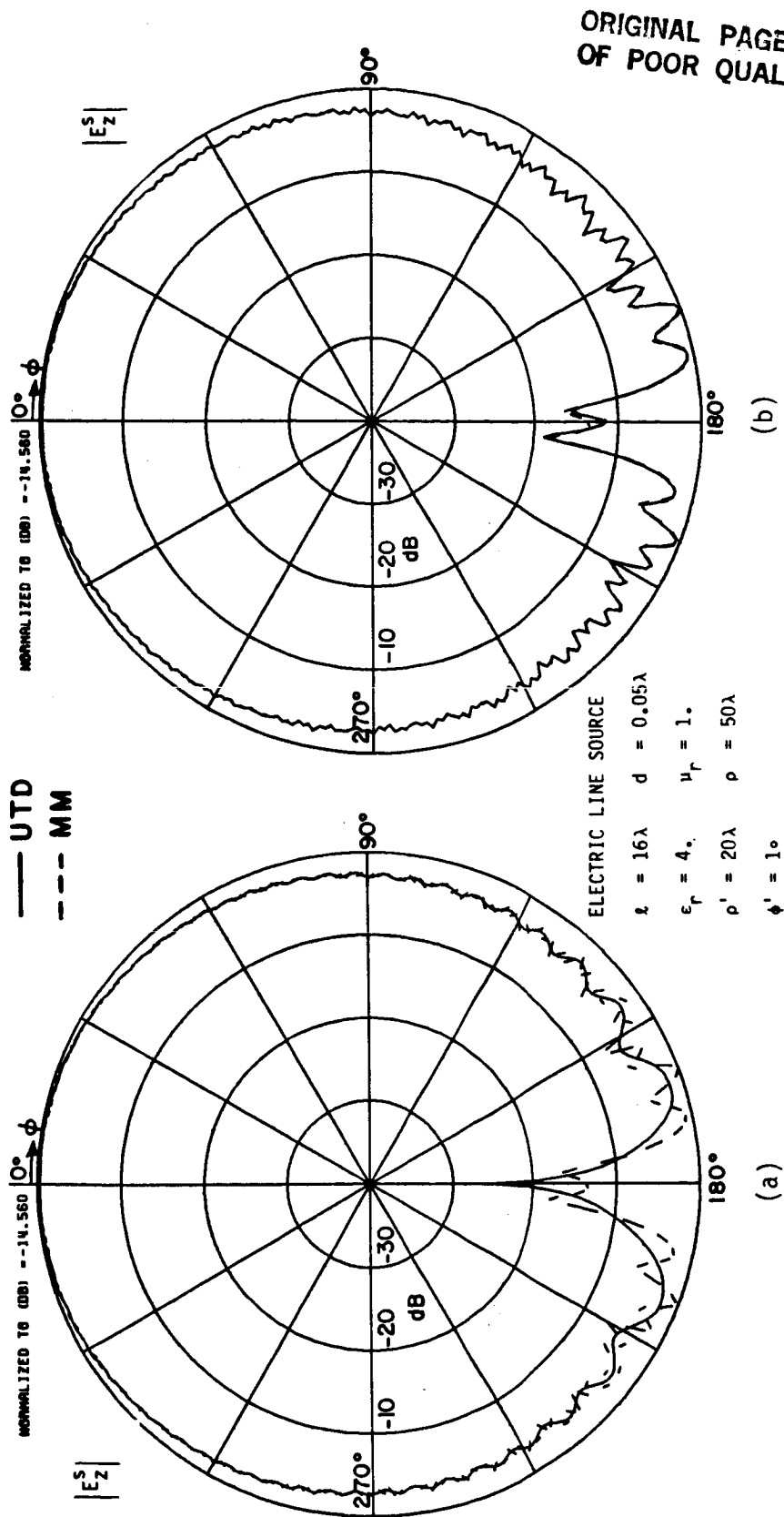


Figure 8.17. Magnitude of the total E_z field for the geometry shown in Figure 8.2.
 (a) Without diffracted surface wave, (b) Field components V and VI included (diffracted surface wave included).

So far, the total field of a line source in the presence of the strip has been calculated for various angles of incidence. It is obvious that the incident field is the dominant term, and in order to very carefully test the accuracy of the new UTD solutions, the scattered field should be calculated instead of the total field. From now on, only the scattered fields will be shown, unless otherwise stated. The electric scattered field \vec{E}^S and the magnetic scattered field \vec{H}^S were defined in Equations (8.1) and (8.2), respectively. Note that the incident fields defined in these equations are the fields that would exist in the absence of the strip.

Figures 8.18a and 8.18b depict the field scattered by a dielectric strip for an E_Z^i -polarized incident plane wave where $\phi'=65^\circ$ and $\theta'=45^\circ$. The scattered E_Z^S field is shown in Figure 8.18a. Since $\theta' \neq 90^\circ$, there is coupling between the E_Z^S and H_Z^S fields. Figure 8.18b shows the $\eta_0 H_Z^S$ field, which as expected, is not zero. Figures 8.19a and 8.19b depict the scattered H_Z^S and $Y_0 E_Z^S$ fields, respectively. The incident field is H_Z^i -polarized, where $\phi'=65^\circ$ and $\theta'=45^\circ$. Again, since $\theta' \neq 90^\circ$, there is coupling between the H_Z^S and E_Z^S fields. Figures 8.20-8.25 show additional examples where $\theta' \neq 90^\circ$.

Figures 8.26a and 8.26b depict the field scattered by a strip where the line source is at a distance of 7λ and 15λ , respectively, from the center of the strip. Figure 8.27a shows the field scattered by a dielectric strip of length 5λ and $\epsilon_r=5.0+i0.5$, $\mu_r=1.0$. The source is a magnetic line source located at a distance of 15λ from the origin. In the Figure 8.27b the source is also a magnetic line source, however, the

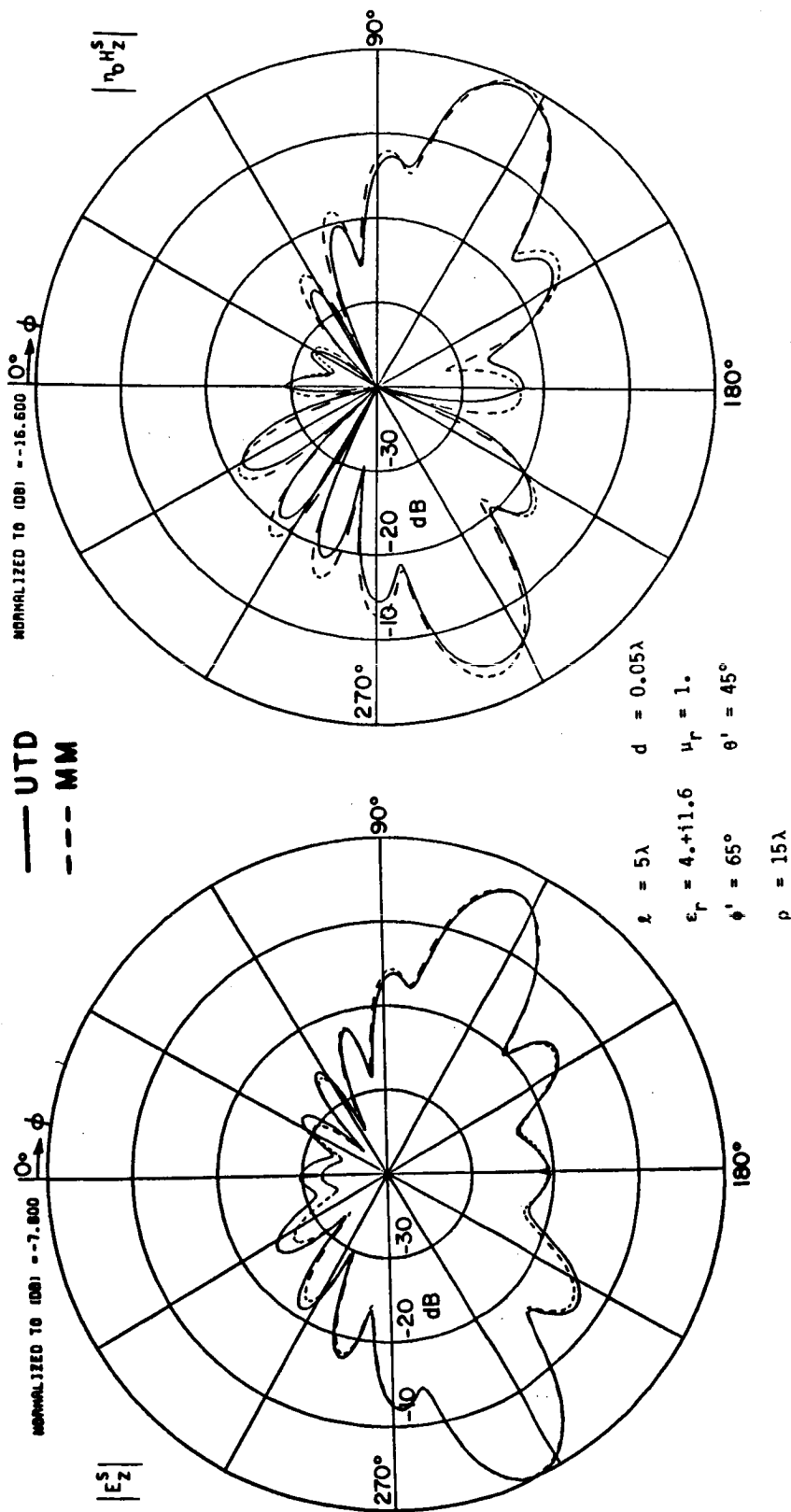


Figure 8.18. Magnitude of the scattered E_z^S and H_z^S fields for an E_z^i -polarized plane wave incident on the geometry shown in Figure 8.1.

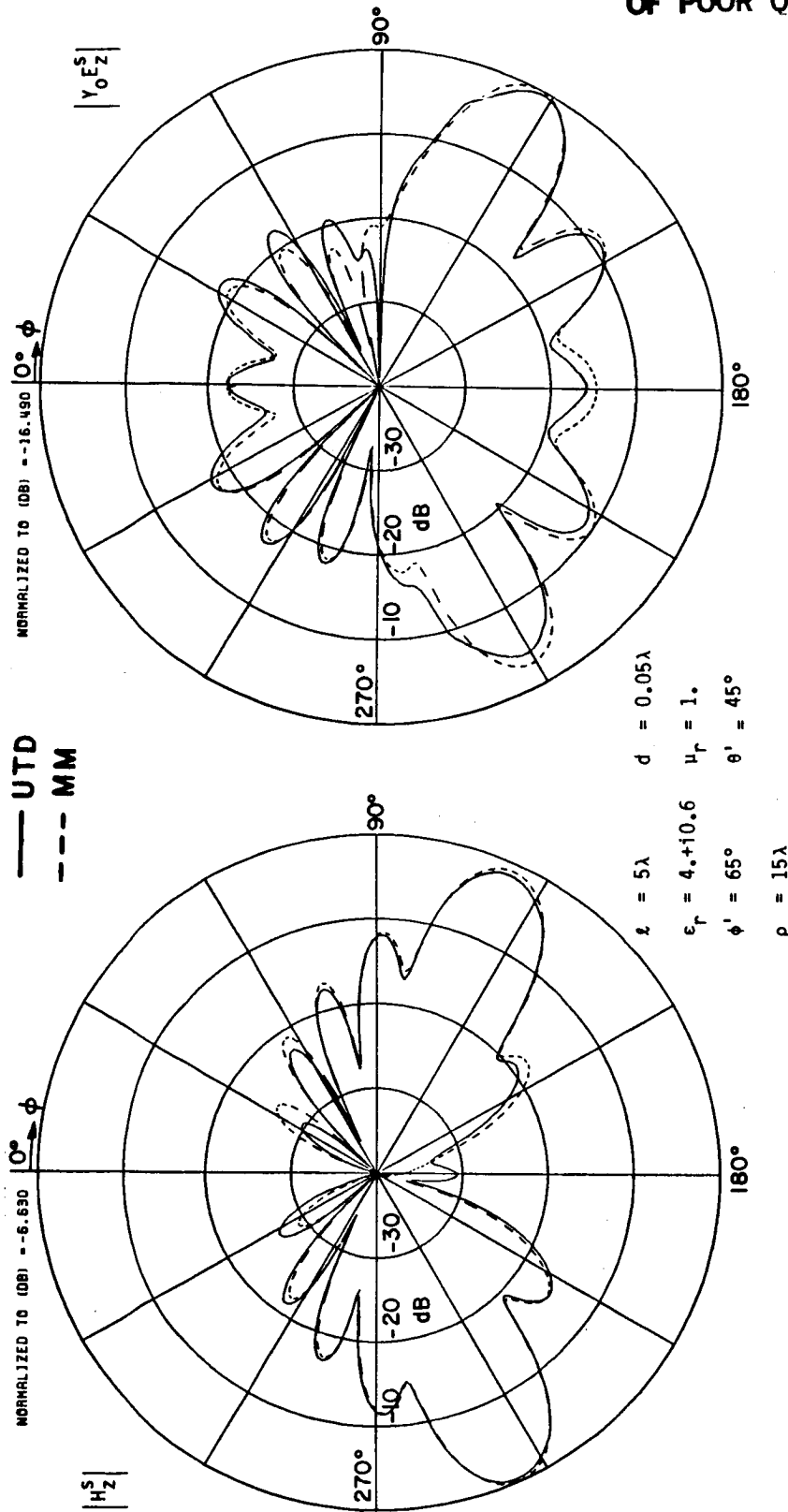


Figure 8.19. Magnitude of the scattered H_z^S and E_z^S fields for an H_z^i -polarized plane wave incident on the geometry shown in Figure 8.1.

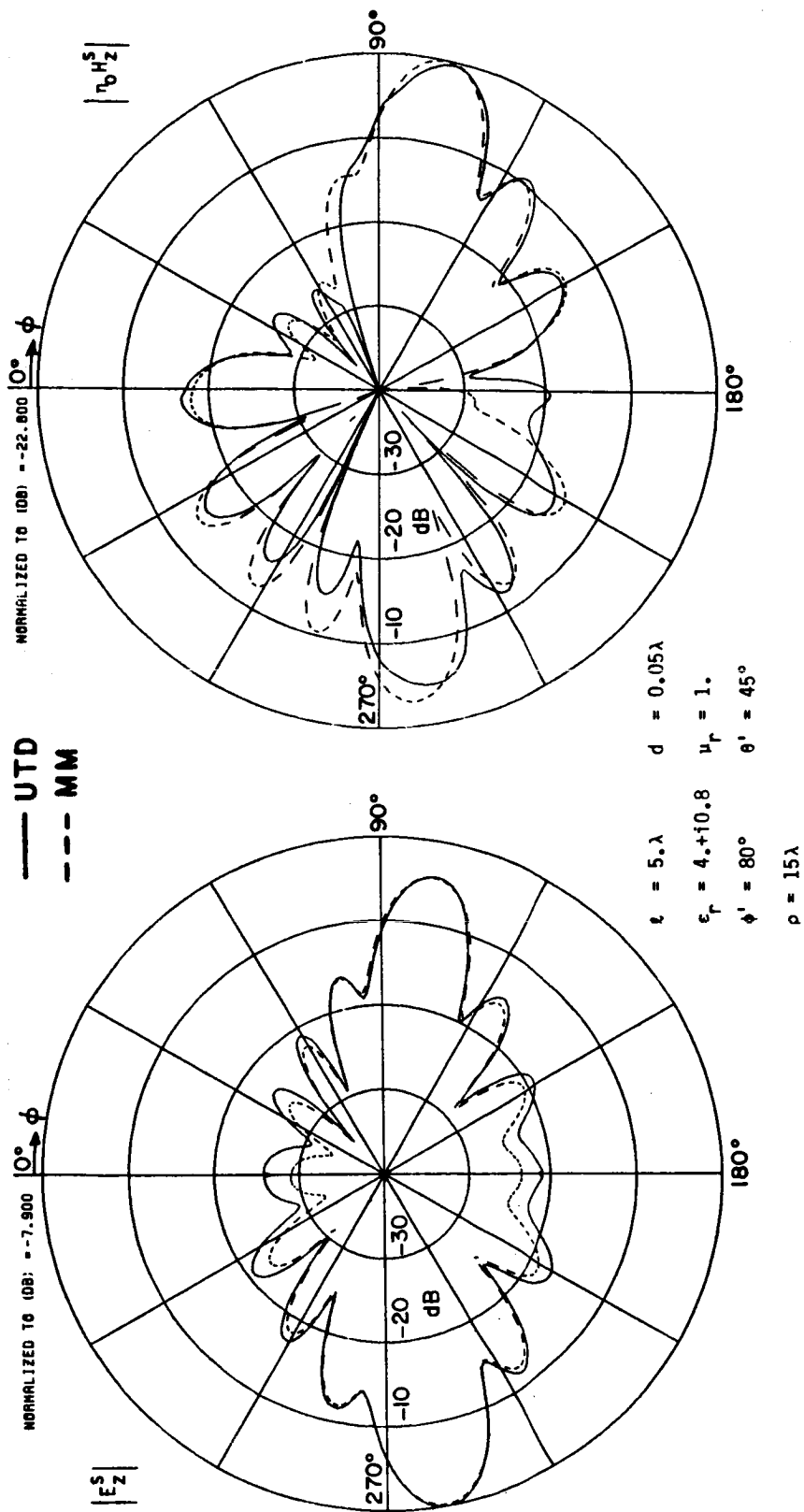


Figure 8.20. Magnitude of the scattered \mathbf{E}_Z^S and \mathbf{H}_Z^S fields for an \mathbf{E}_Z^i -polarized plane wave incident on the geometry shown in Figure 8.1.

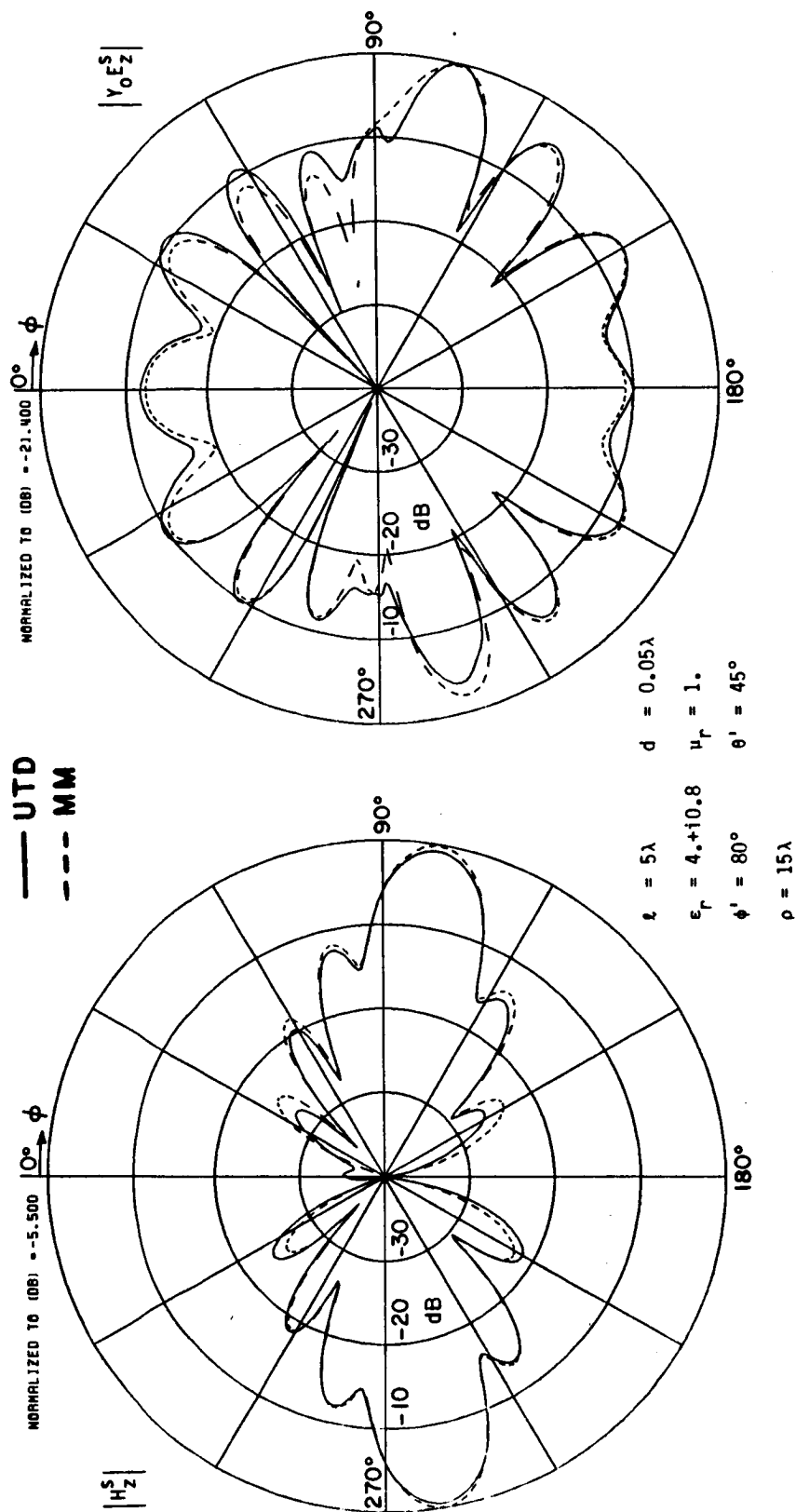


Figure 8.21. Magnitude of the scattered H_z^S and E_z^S fields for an H_z^i -polarized plane wave incident on the geometry shown in Figure 8.1.

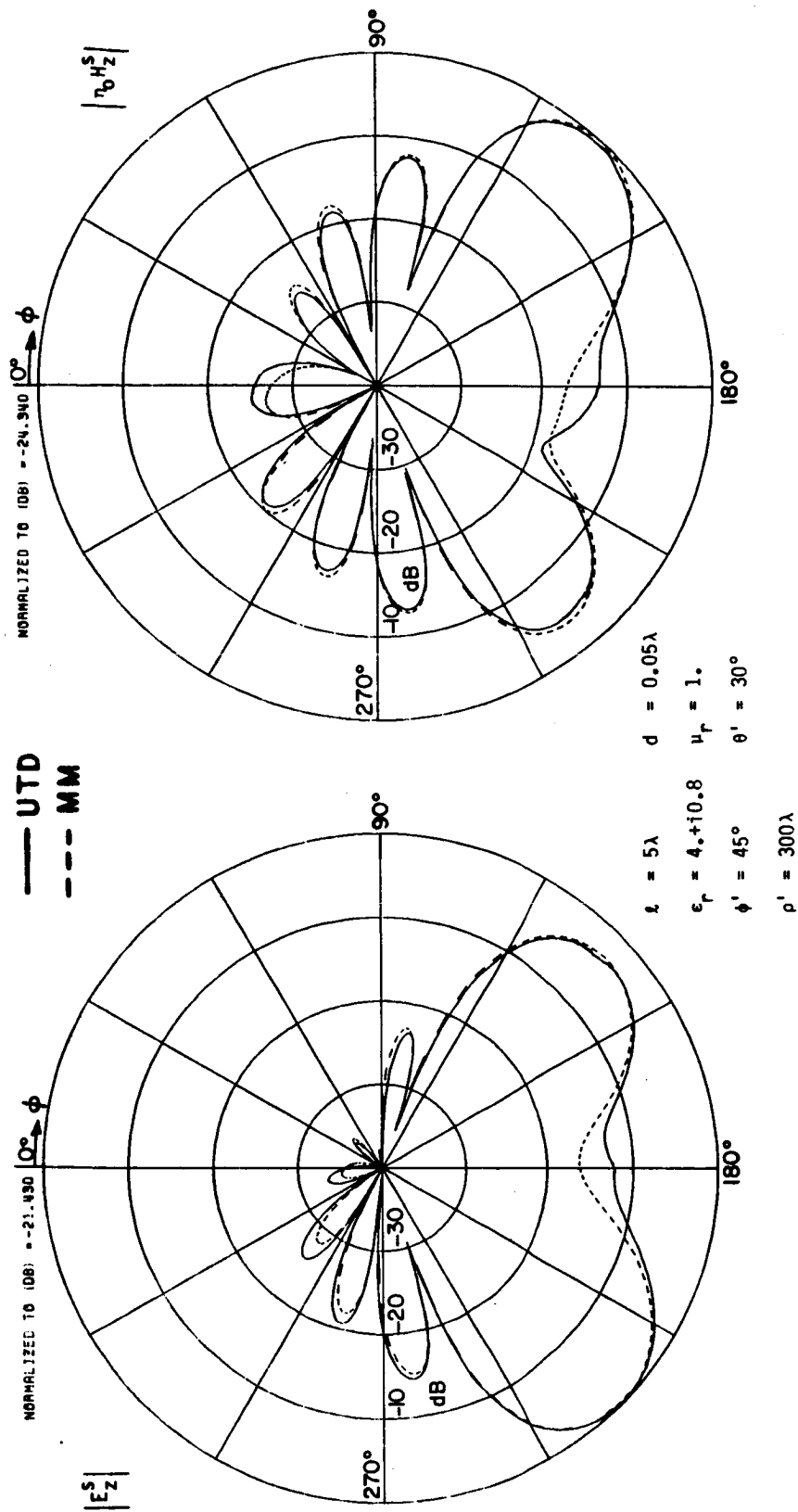


Figure 8.22. Magnitude of the scattered E_z^S and H_z^S fields for an E_z^i -polarized plane wave incident on the geometry shown in Figure 8.1.

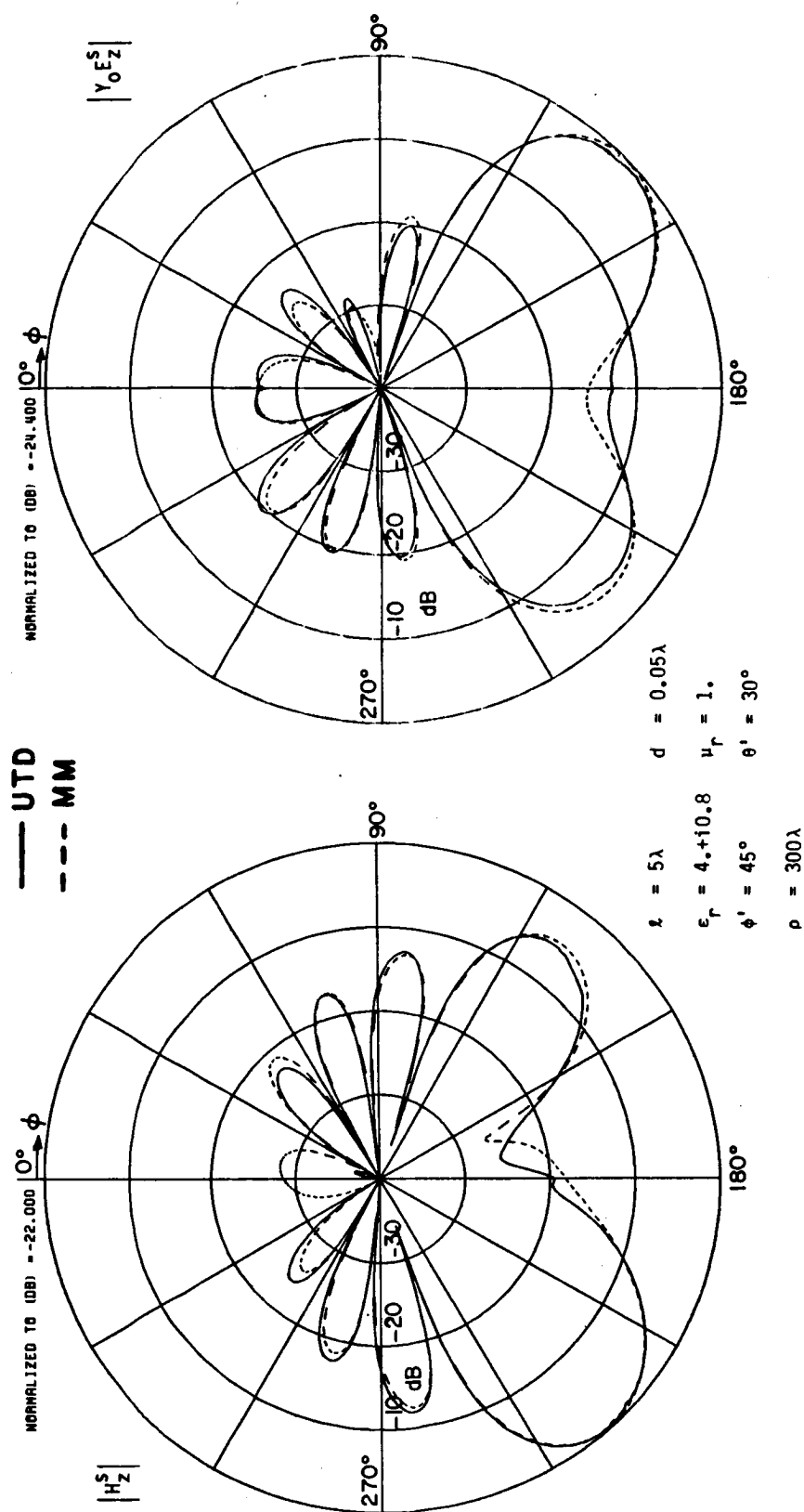


Figure 8.23. Magnitude of the scattered H_z^S and E_z^S fields for an H_z^i -polarized plane wave incident on the geometry shown in Figure 8.1.

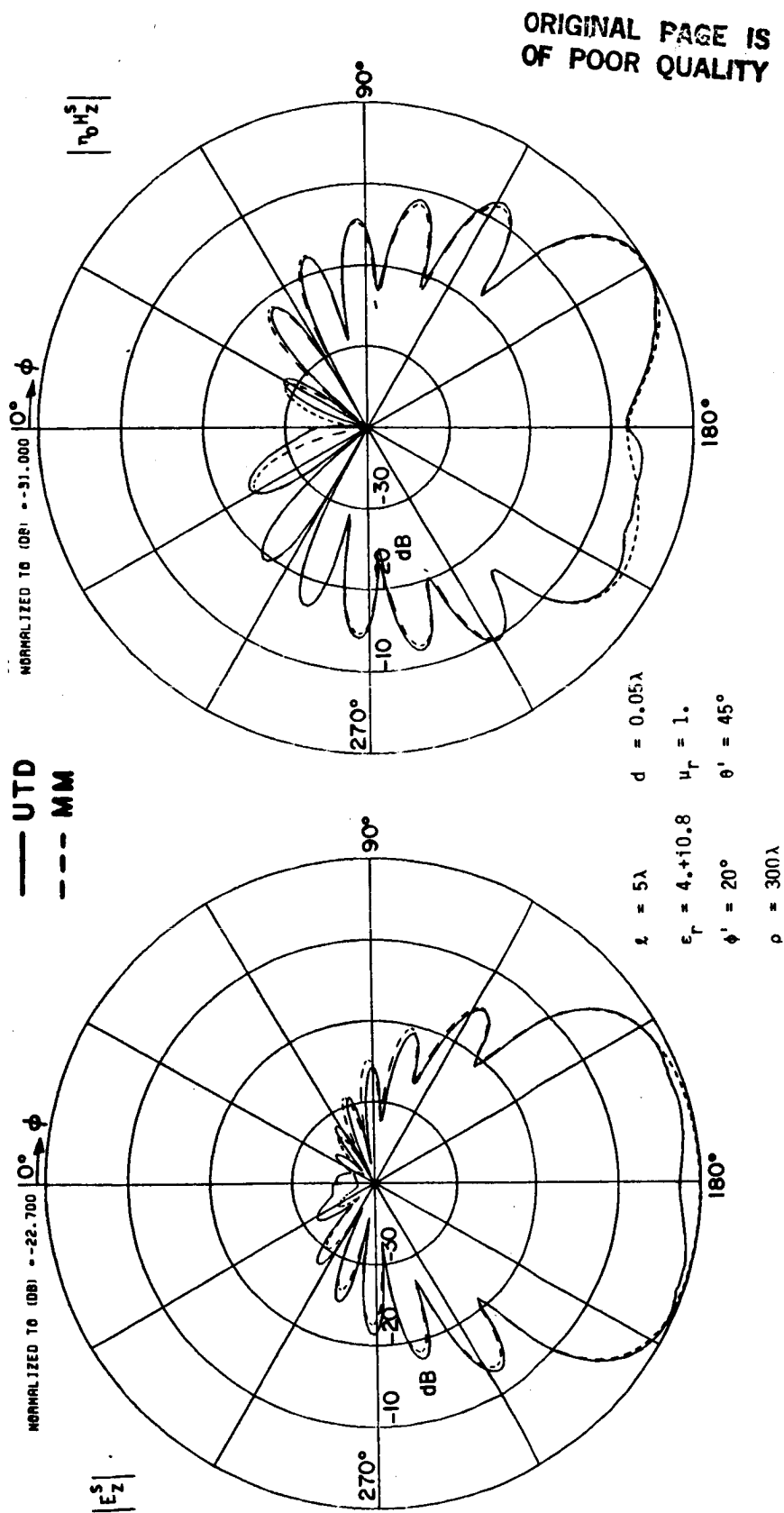


Figure 8.24. Magnitude of the scattered E_z^S and H_z^S fields for an E_z^i -polarized plane wave incident on the geometry shown in Figure 8.1.

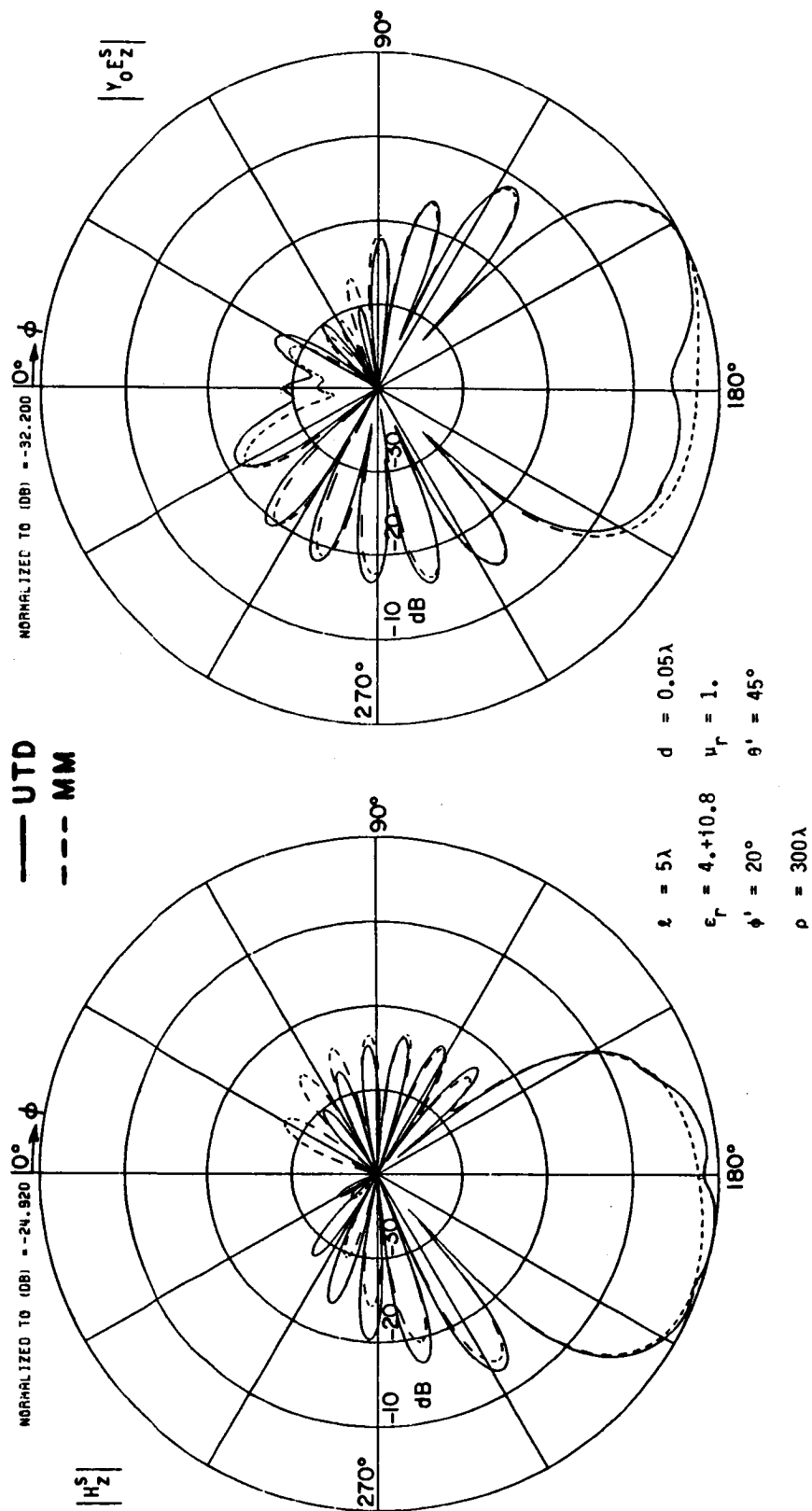


Figure 8.25. Magnitude of the scattered H_z^S and E_z^S fields for an H_z^i -polarized plane wave incident on the geometry shown in Figure 8.1.

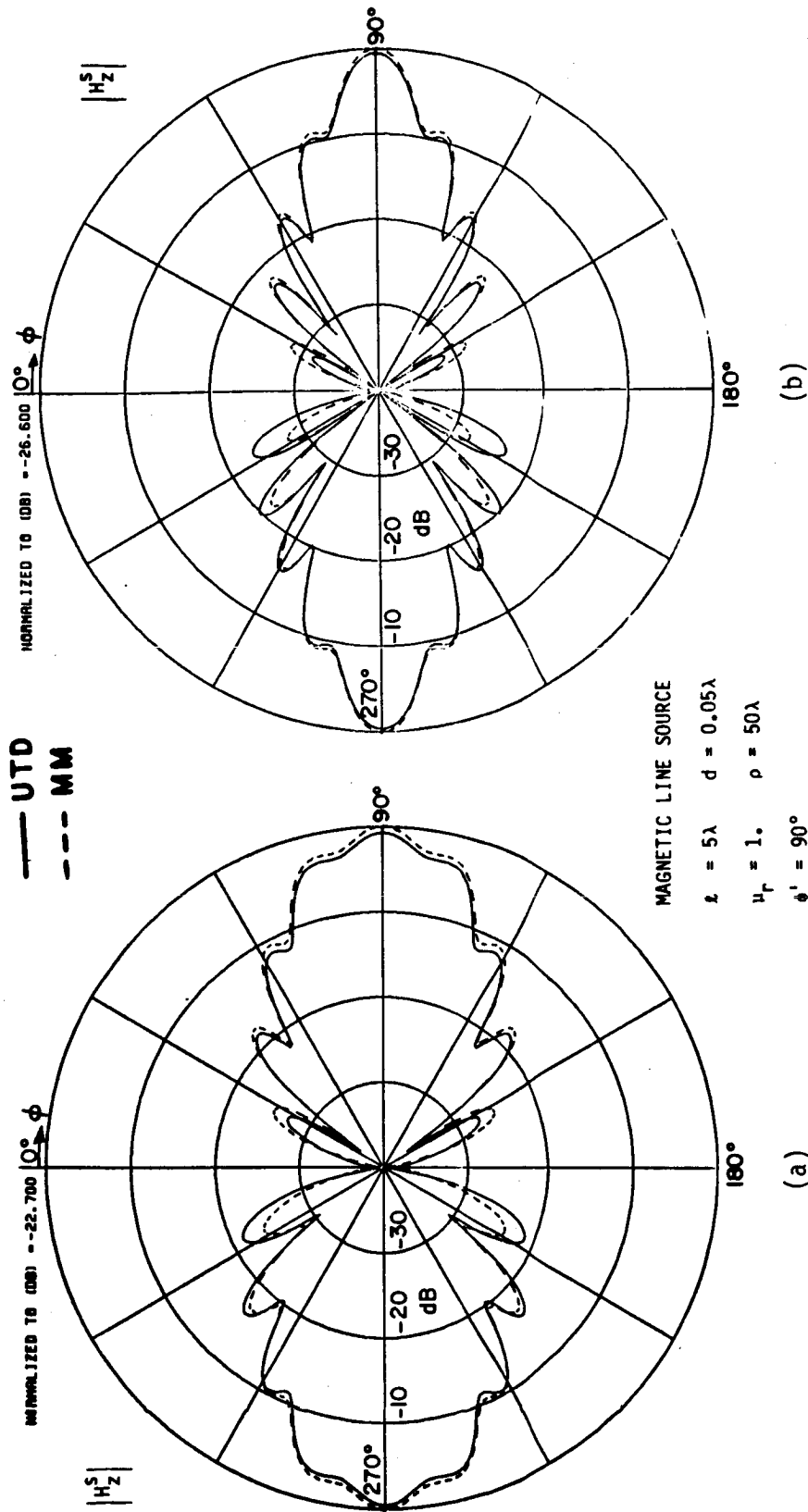


Figure 8.26. Magnitude of the scattered field H_z^S for the geometry depicted in Figure 8.2. (a) $\epsilon_r = 4. + i0.$, $\rho' = 7\lambda$,
 (b) $\epsilon_r = 3. + i0.3$, $\rho' = 15\lambda$.

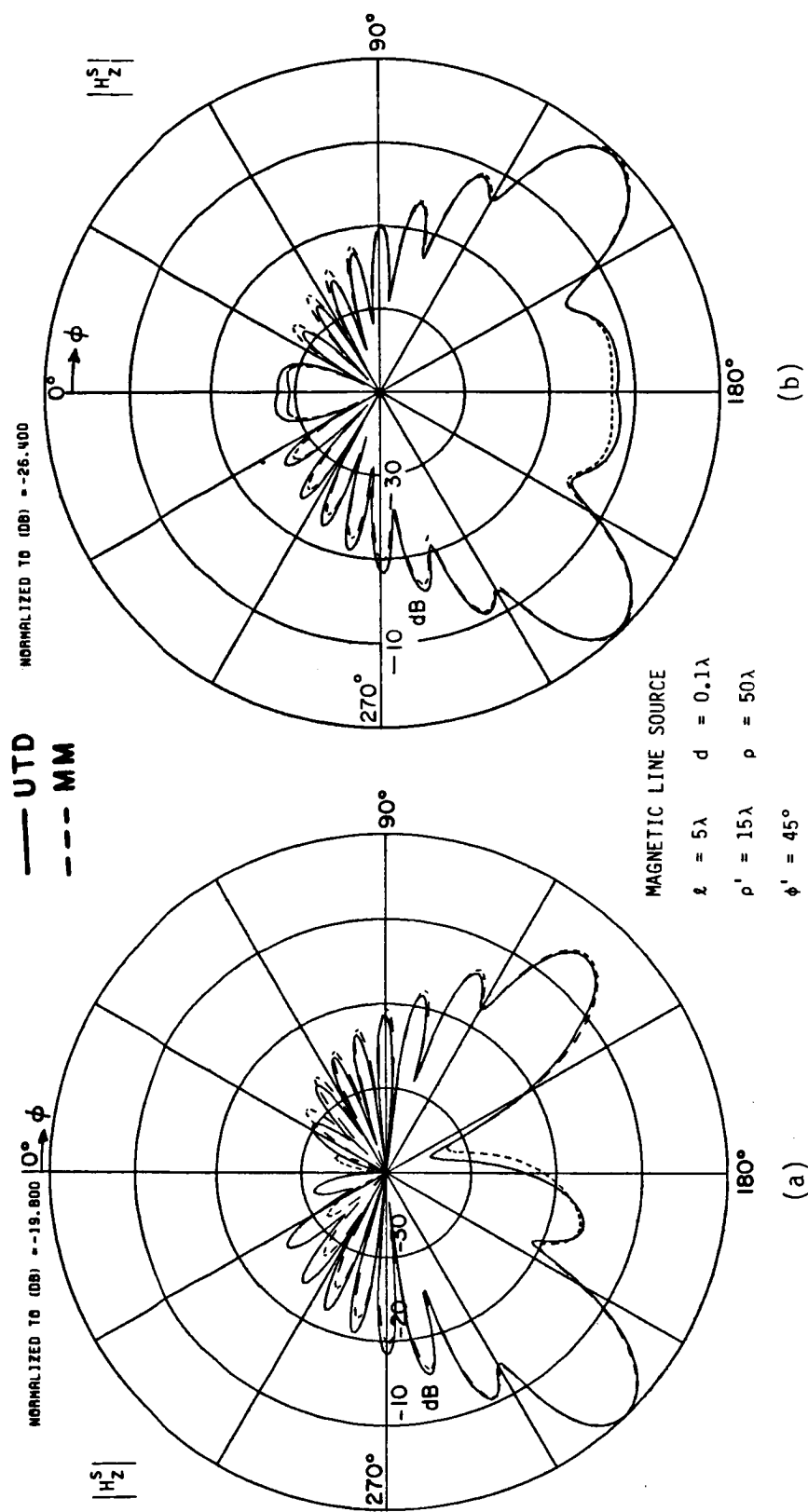


Figure 8.27. Magnitude of the scattered H_z^S field for the geometry depicted in Figure 8.2. (a) $\epsilon_r = 5. + i0.5$, $\mu_r = 1. + i0.$,
 (b) $\epsilon_r = 1. + i0.$, $\mu_r = 3. + i0.3$.

strip is a ferrite with $\mu_r = 3.0 + i0.3$, $\epsilon_r = 1.0$. The length of the strip is $l = 5\lambda$ and its thickness $d = 0.1\lambda$. Figures 8.28a and 8.28b depict the H_z^S -scattered field where the incident field is a H_z^i -polarized plane wave. The values of ϕ' , and θ' are 45 and 90 degrees, respectively, and as expected, in both cases the field E_z^S is zero.

Figures 8.29a through 8.29c show the E_z^S -field scattered by a dielectric strip for increasing values of the electric loss tangent. The incident field here is an E_z^i -polarized plane wave where $\phi' = 90^\circ$ and $\theta' = 90^\circ$.

As mentioned several times already, the total or scattered field can be obtained by adding the different terms depicted in Figure 8.3. In other words, UTD is a method in which rays are employed in a systematic way to obtain the field at a given observation point. For example in Figure 8.30a, there is an E_z^i -polarized plane wave, incident on a lossy dielectric strip where the angle of incidence ϕ' is 45 degrees and $\theta' = 90$ degrees. In order to obtain the total field, the first four terms shown in Figure 8.3 are added together. Next, the scattered E_z^S -field which is shown in Figure 8.30a has been obtained by subtracting the unperturbed incident field \tilde{E}_z^i from the total field. It is obvious by observing Figure 8.30a that the agreement between the UTD and MM solutions is not good. Thus, the next step is to add more terms to the UTD solution. The field obtained by adding the diffracted surface wave (field component V) plus the diffracted-reflected surface wave (field component VI) is shown in Figure 8.30b. Note that this field is important in the regions around 0 and 180 degrees, which is

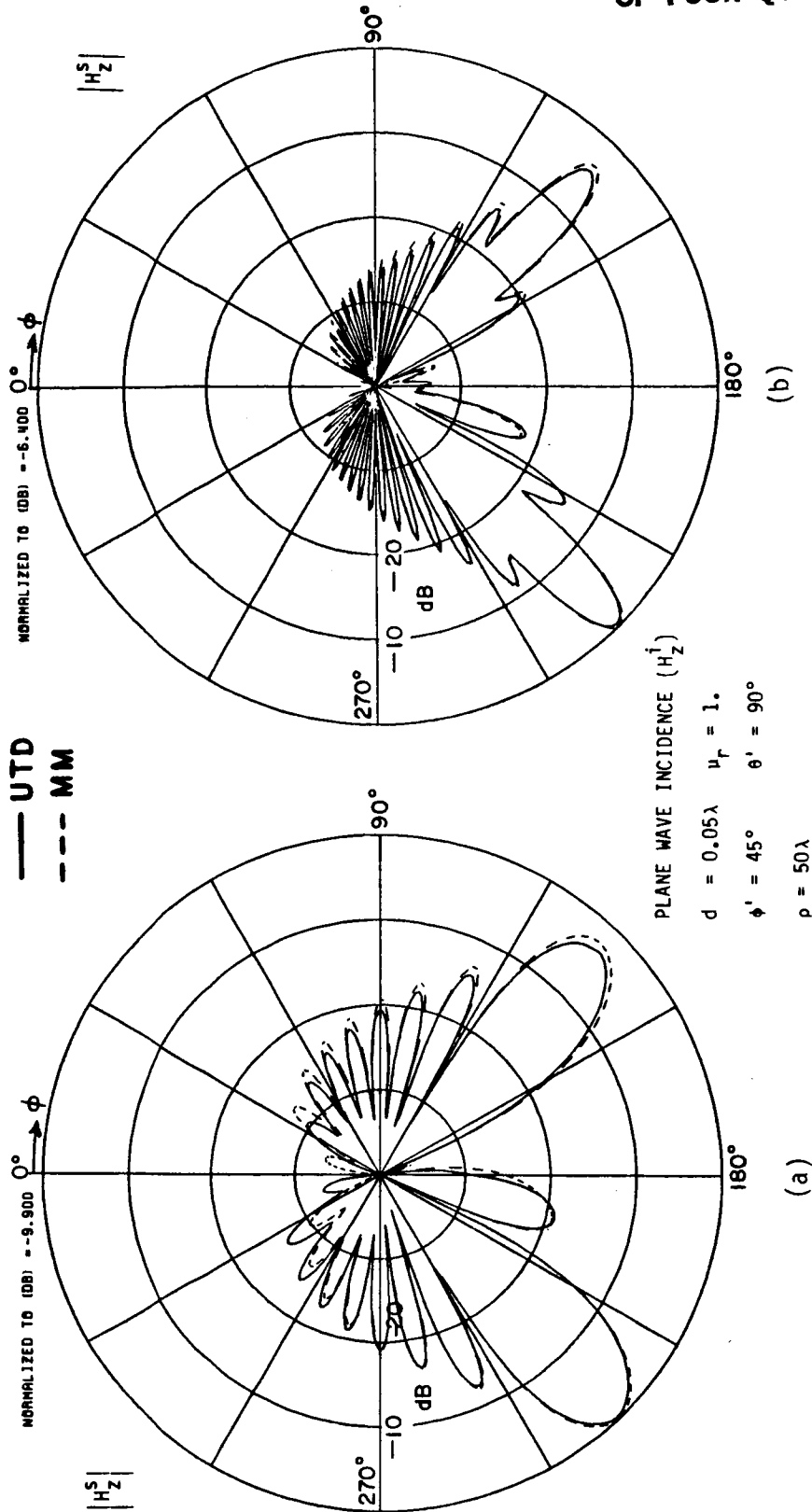


Figure 8.28. Magnitude of the scattered H_z^s field for the geometry depicted in Figure 8.1 (normal incidence).

(a) $\ell=5\lambda$, $\epsilon_r=7.+i0.7$, (b) $\ell=10\lambda$, $\epsilon_r=5.+i0.5$.

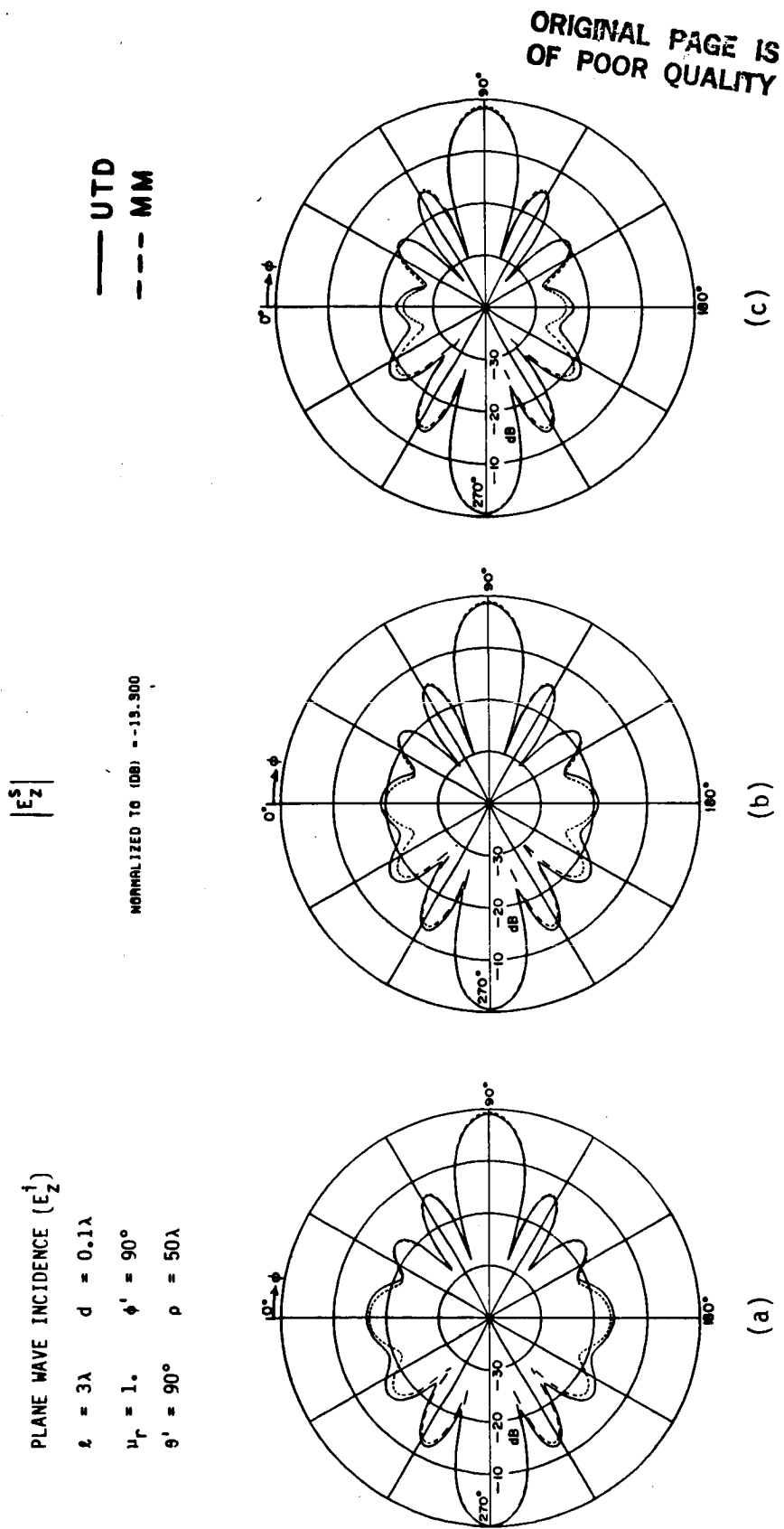


Figure 8.29. Magnitude of the scattered E_z^s field for the geometry depicted in Figure 8.2.

(a) $\epsilon_r = 3. + i0.$, (b) $\epsilon_r = 3. + i0.3$, (c) $\epsilon_r = 3. + i1.2$.

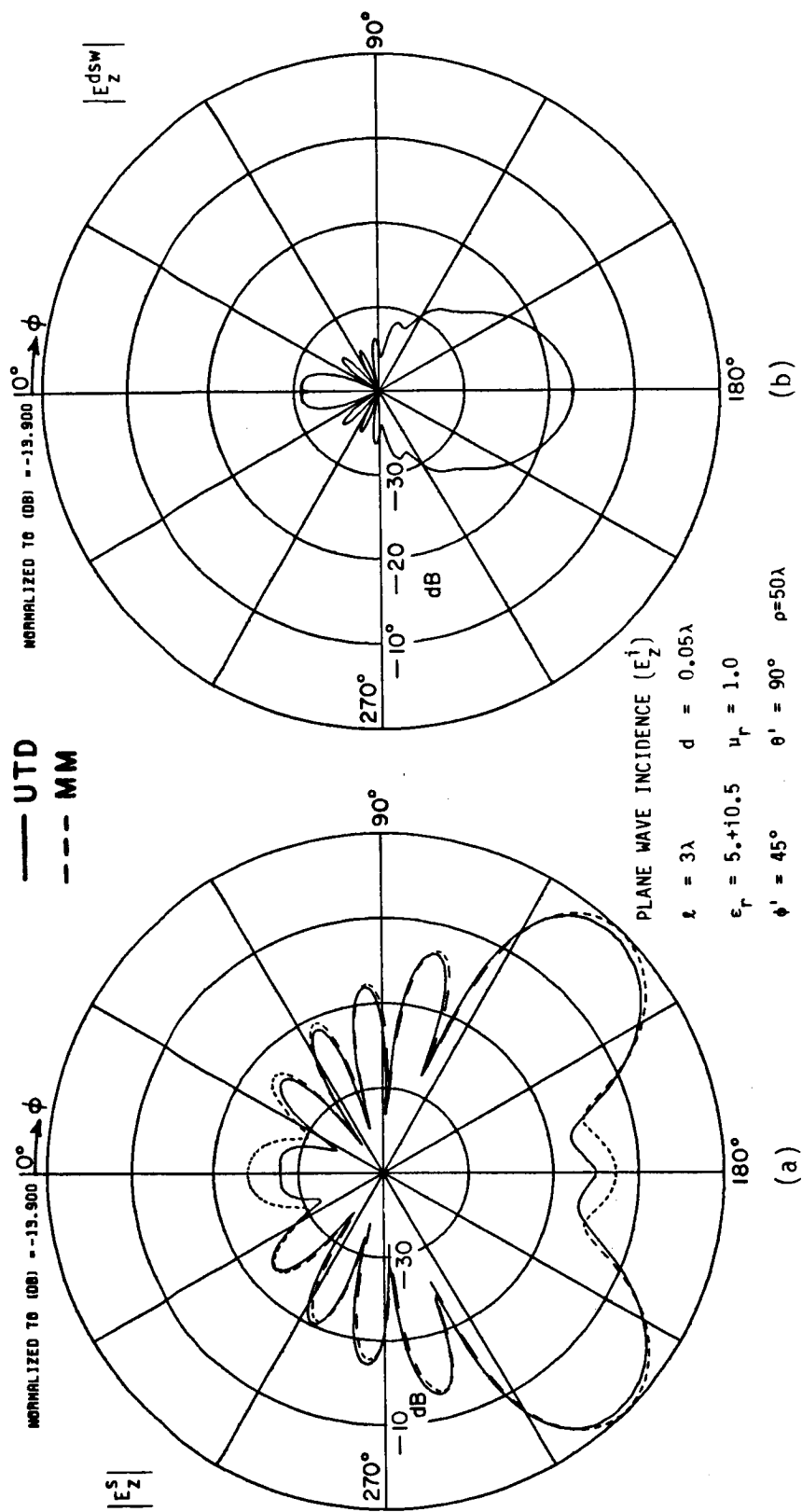
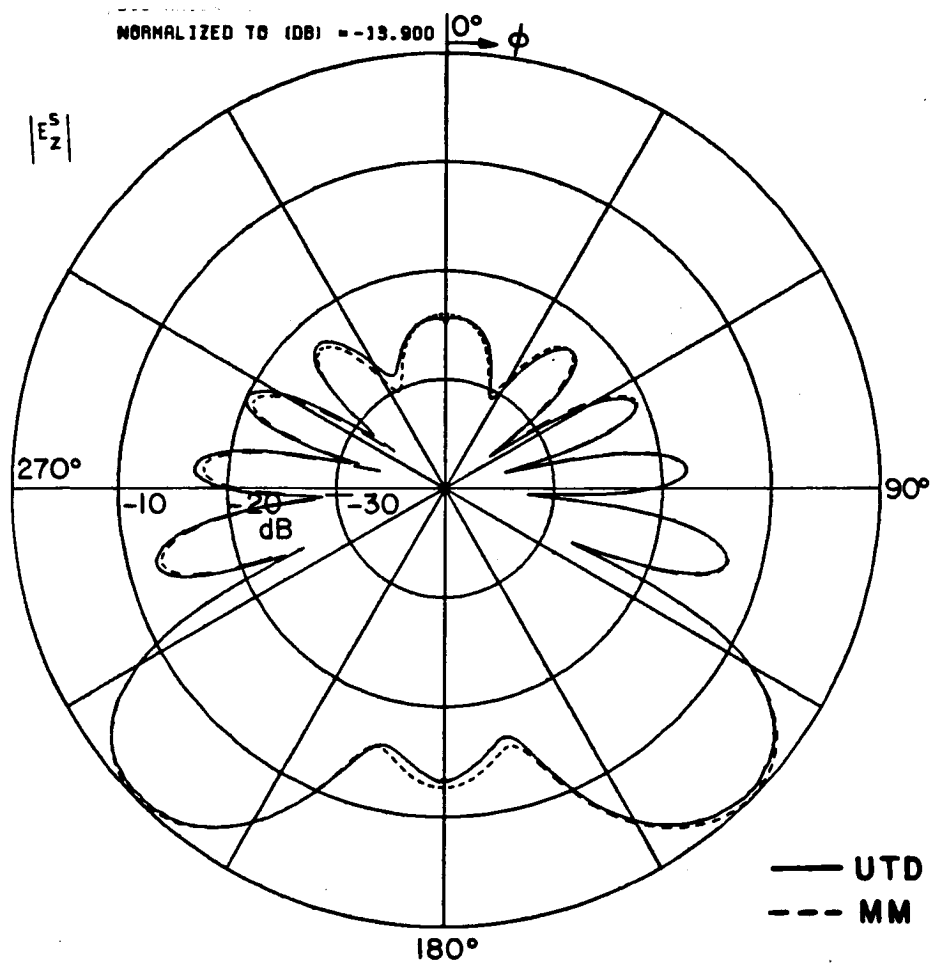


Figure 8.30. Magnitude of the field E_Z for the geometry depicted in Figure 8.1. (a) Scattered field E_Z^S without diffracted surface wave, (b) diffracted surface wave E_Z^{dsw} (field components V and VI).

where the UTD and MM solutions disagree. Adding the V and VI terms to the scattered field one obtains the field shown in Figure 8.31. As expected, the agreement between the new scattered field and the MM solution is much better when the various diffracted surface waves are added. Additional results where the diffracted surface wave is important are shown in Figures 8.32 through 8.44 for both, normal and oblique (on the edge) angles of incidence. Note that the strength of the surface wave excited by a line source radiating above a dielectric slab is inversely proportional to the distance of the line source from the slab (see Figure 6.11) as indicated by the results depicted in Figures 4.41 through 4.44.

As stated before, the diffracted surface wave is important as long as the dielectric strip is lossless and the incident field is near grazing. In Figure 8.45a the scattered field of a lossless strip of length $\ell=10\lambda$ is shown where the source is an E_z^i -polarized plane wave with $\phi'=1^\circ$ and $\theta'=90^\circ$. The many sidelobes of the field are due to the interaction between the edge diffracted and diffracted surface wave fields. When the strip becomes lossy ($\tan\delta_e=0.25$), the diffracted surface wave becomes insignificant and the scattered field shown in Figure 8.45b is mostly the contribution from the edge diffracted fields. The agreement between the UTD and MM solutions is good except in the region around 180 degrees where the doubly diffracted field is important, but it has not been included here. One additional example is shown in Figures 8.46a and 8.46b where the electric line source is 20λ from the origin, $\ell=16\lambda$ and $\phi'=1^\circ$.



PLANE WAVE INCIDENCE (E_z^i)

$l = 3.0\lambda$ $d = 0.05\lambda$

$\epsilon_r = 5. + i0.5$ $\mu_r = 1.$

$\phi^i = 45^\circ$ $\theta^i = 90^\circ$

$\rho = 50\lambda$

Figure 8.31. Magnitude of the scattered field E_z^s with the diffracted surface wave field E_z^{dsw} included (see Figure 8.30).

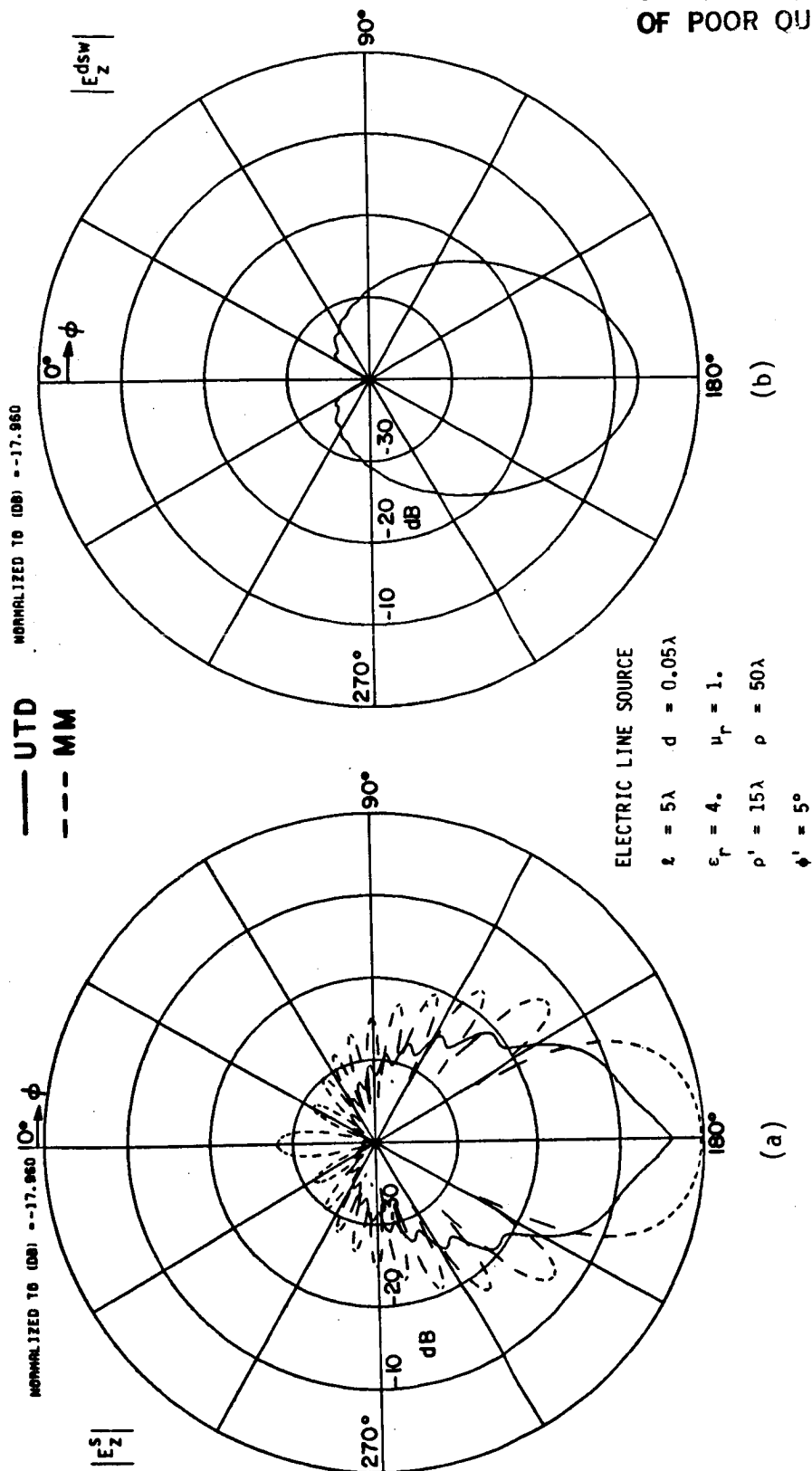


Figure 8.32. Magnitude of the field E_z for the geometry depicted in Figure 8.2.

(a) Scattered field E_z^S without diffracted surface wave,

(b) Diffracted surface wave field E_z^{dsw} (field component V).

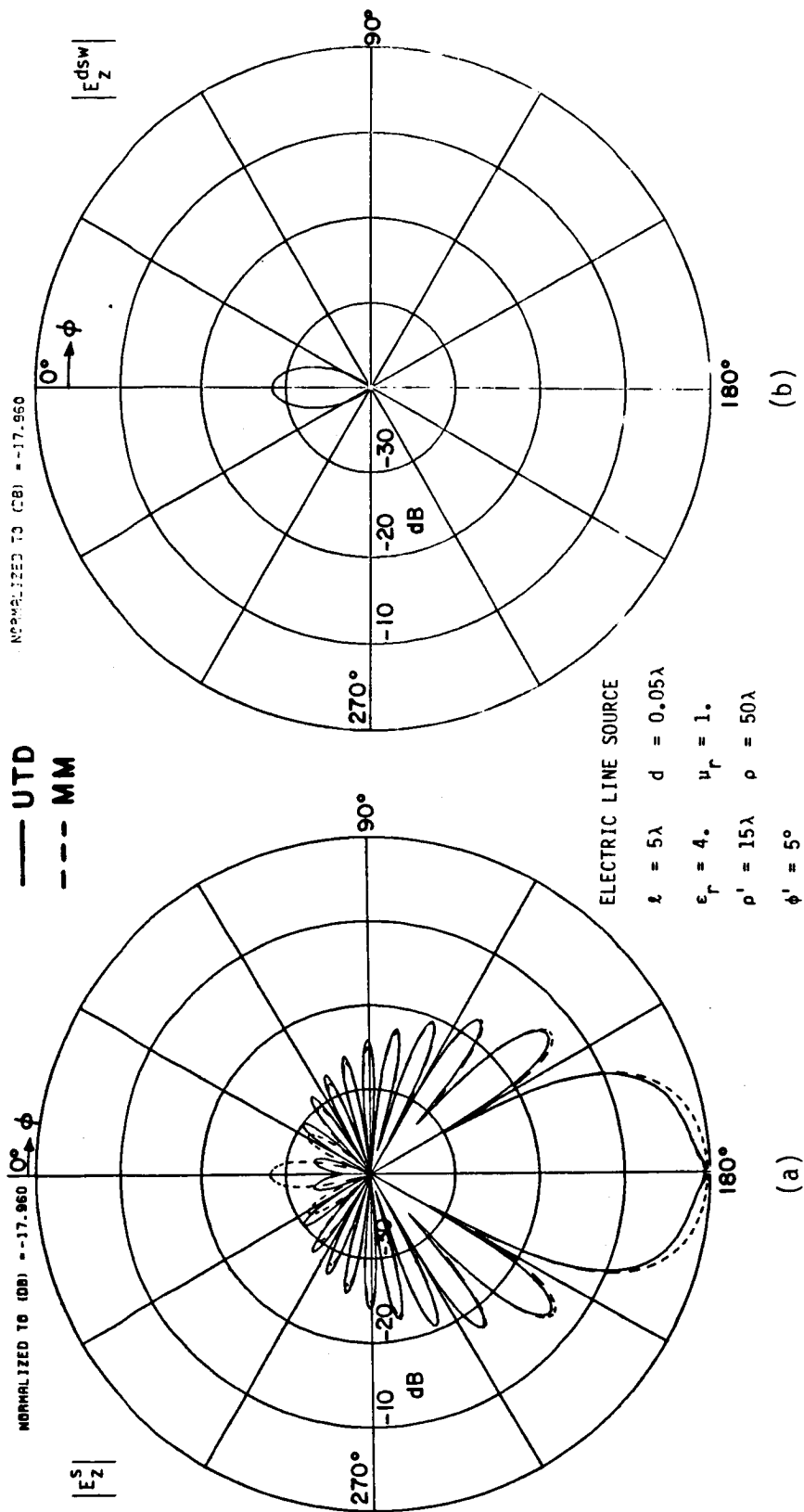


Figure 8.33. Magnitude of the field E_z for the geometry depicted in Figure 8.2.

- (a) Scattered field E_z^S with field component V included,
 (b) Diffracted surface wave field E_z^{dsw} (field component VI).

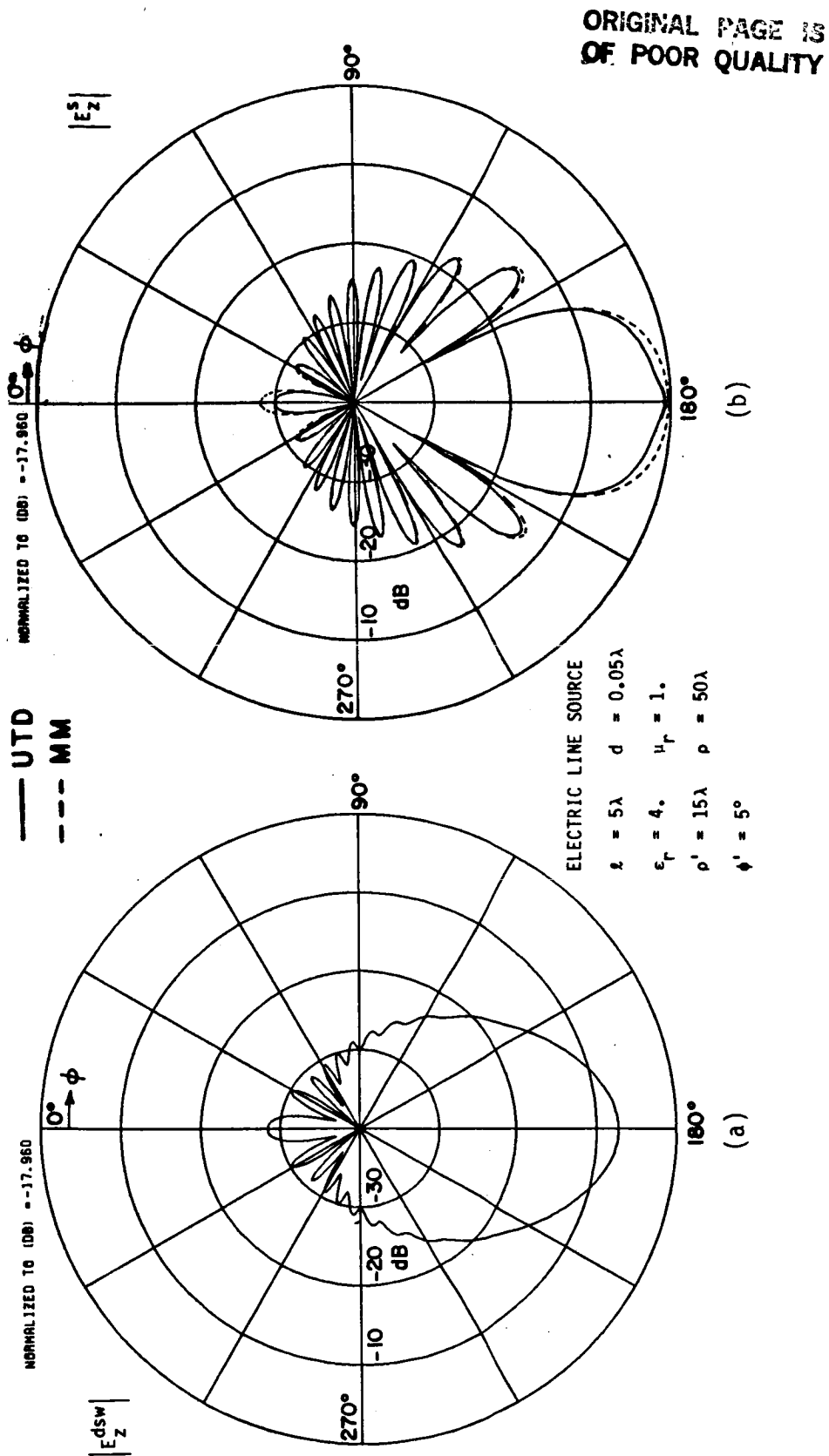


Figure 8.34. Magnitude of the field E_z for the geometry depicted in Figure 8.2.
 (a) Diffracted surface wave field E_z^{dsw} (field components V+VI),
 (b) Scattered field E_z^s with the field components V and VI included.

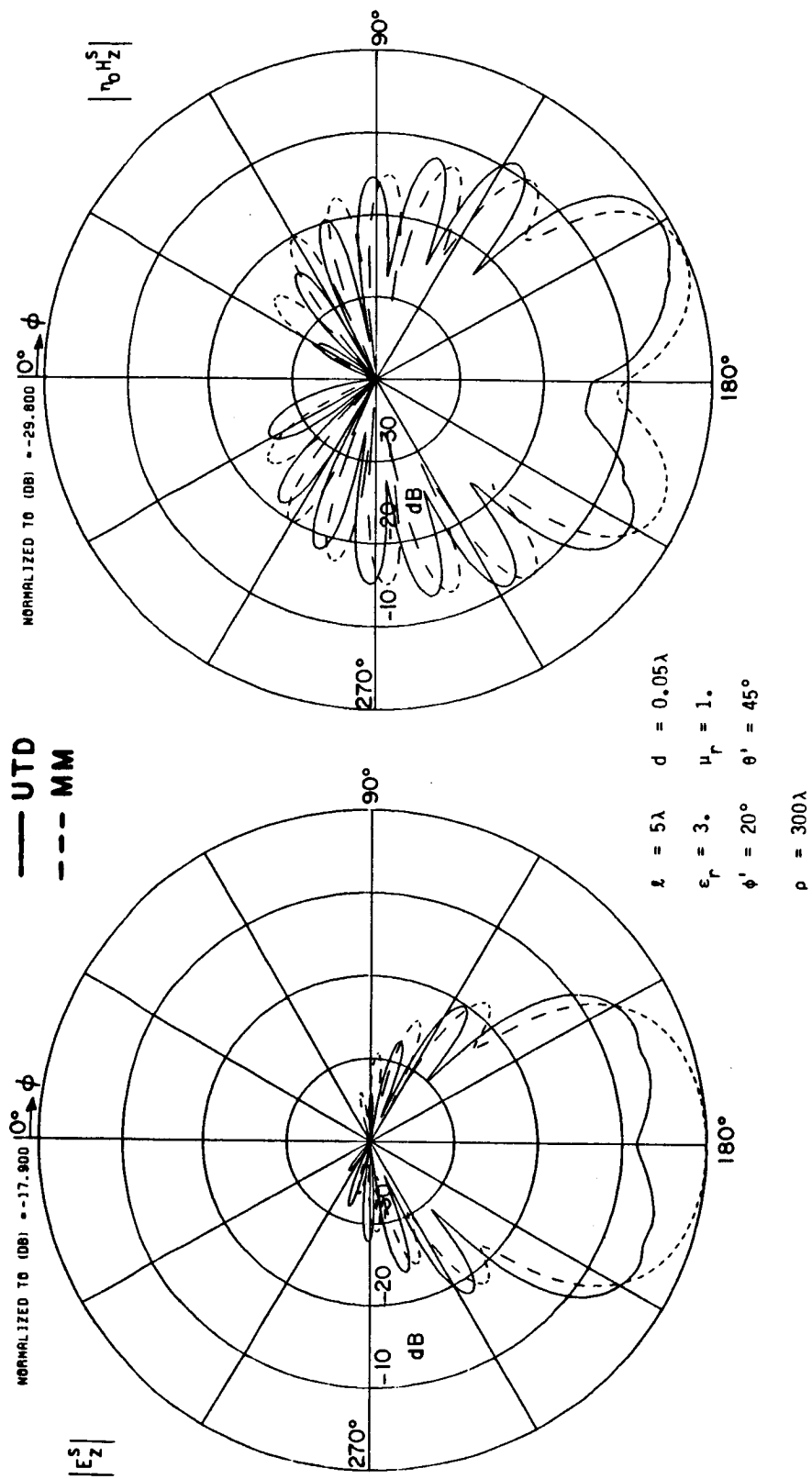
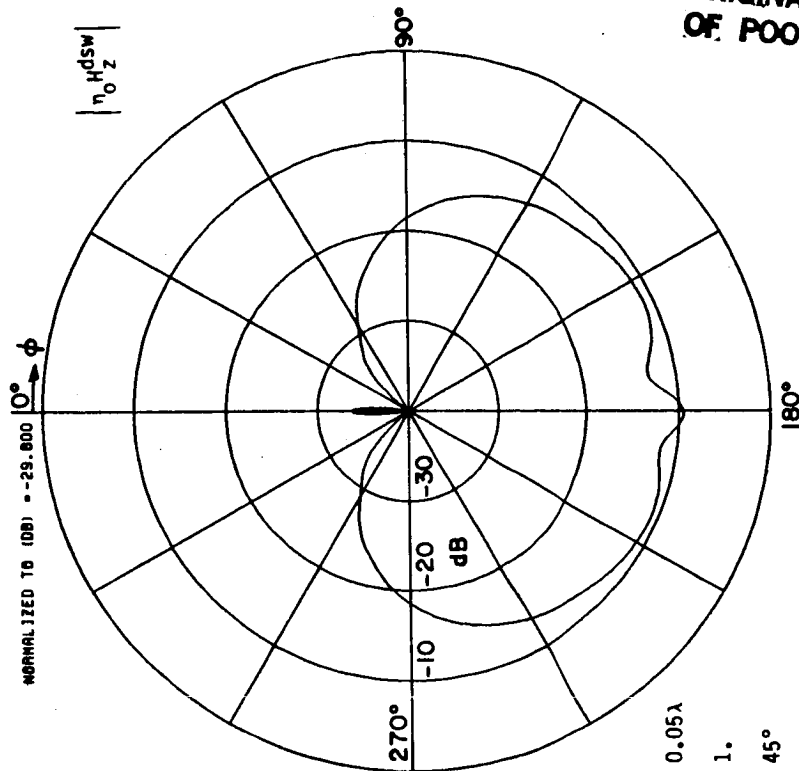
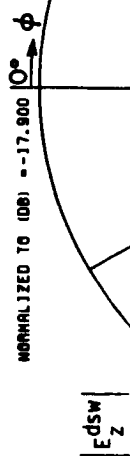


Figure 8.35. Magnitude of the scattered E_z^S and H_z^S fields for an E_z^i -polarized plane wave incident on the geometry shown in Figure 8.1. The diffracted surface wave is not included in the solution.

— UTD



$z = 5\lambda$ $d = 0.05\lambda$
 $\epsilon_r = 3$ $\mu_r = 1$
 $\phi' = 20^\circ$ $\theta' = 45^\circ$
 $\rho = 300\lambda$

ORIGINAL PAGE IS
OF POOR QUALITY

Figure 8.36. Magnitude of the diffracted surface wave fields E_z^{dsw} and H_z^{dsw} (field component V) for a E_z^i -polarized plane wave incident on the geometry shown in Figure 8.1.

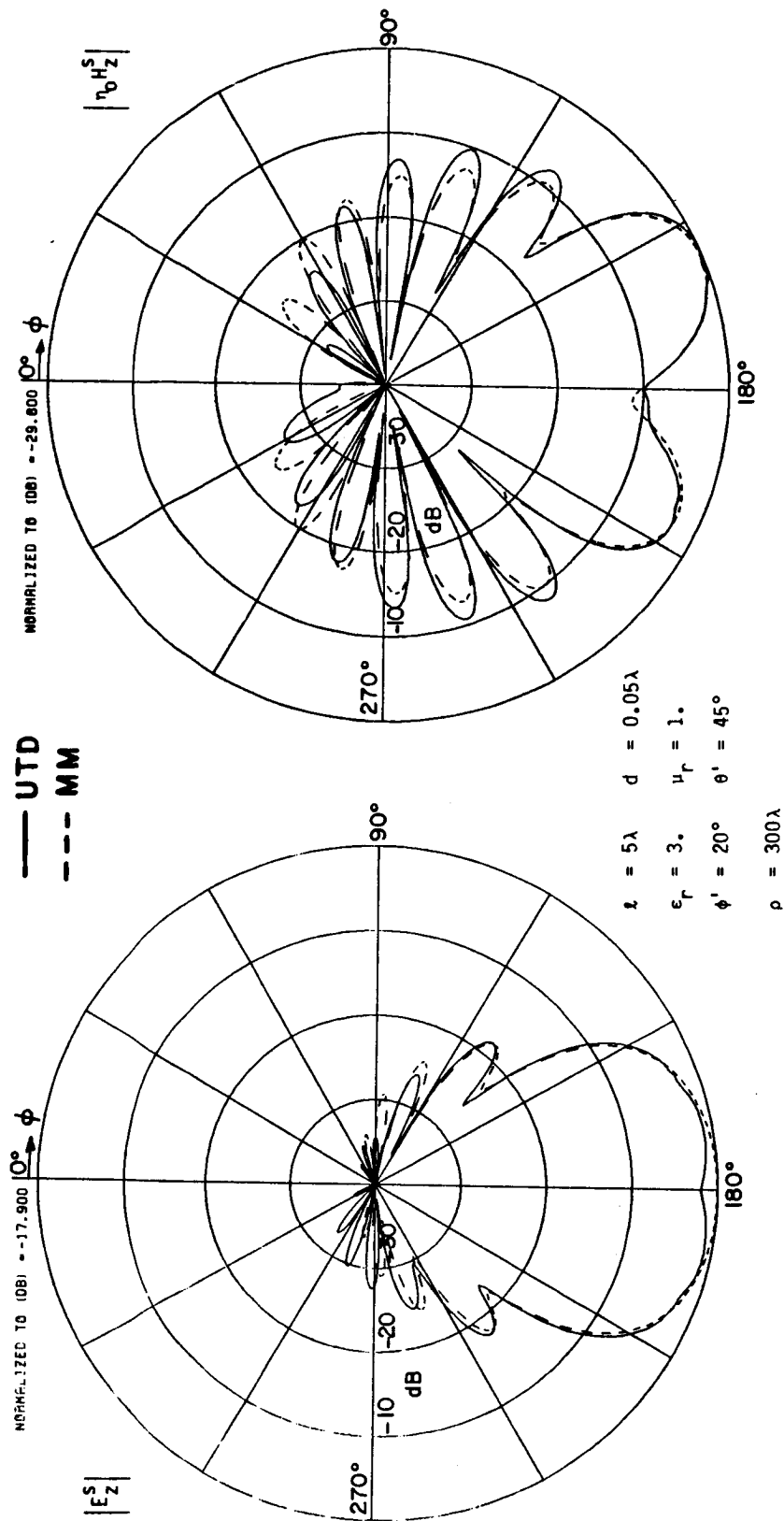


Figure 8.37. Magnitude of the scattered fields E_z^S and H_z^S for an E_z^i -polarized plane wave. The diffracted surface wave (see Figure 8.36) is included in the solution.

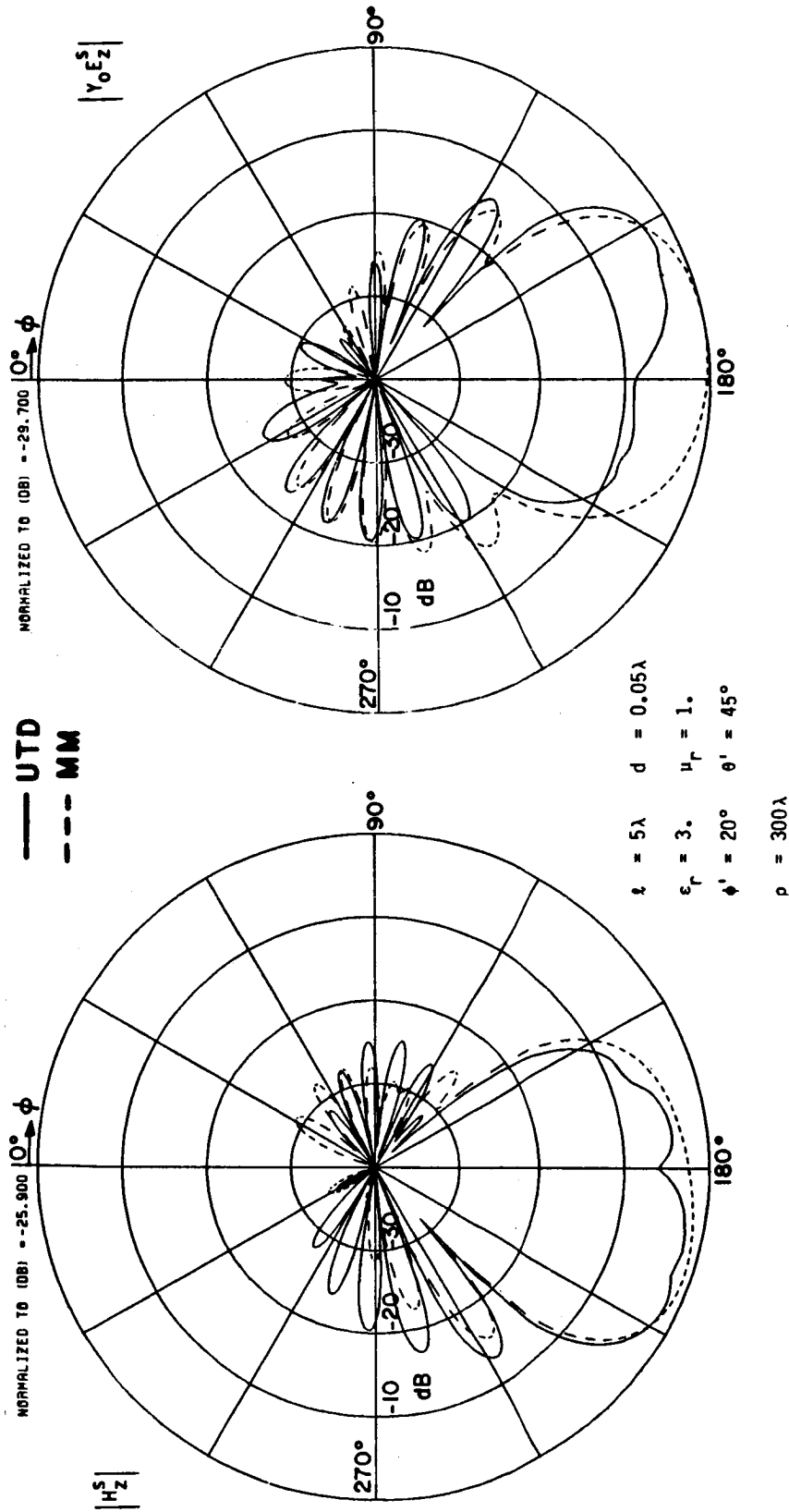


Figure 8.38. Magnitude of the scattered fields H_z^S and E_z^S for a H_z^i -polarized plane wave incident on the geometry depicted in Figure 8.1. The diffracted surface wave is not included in the solution.

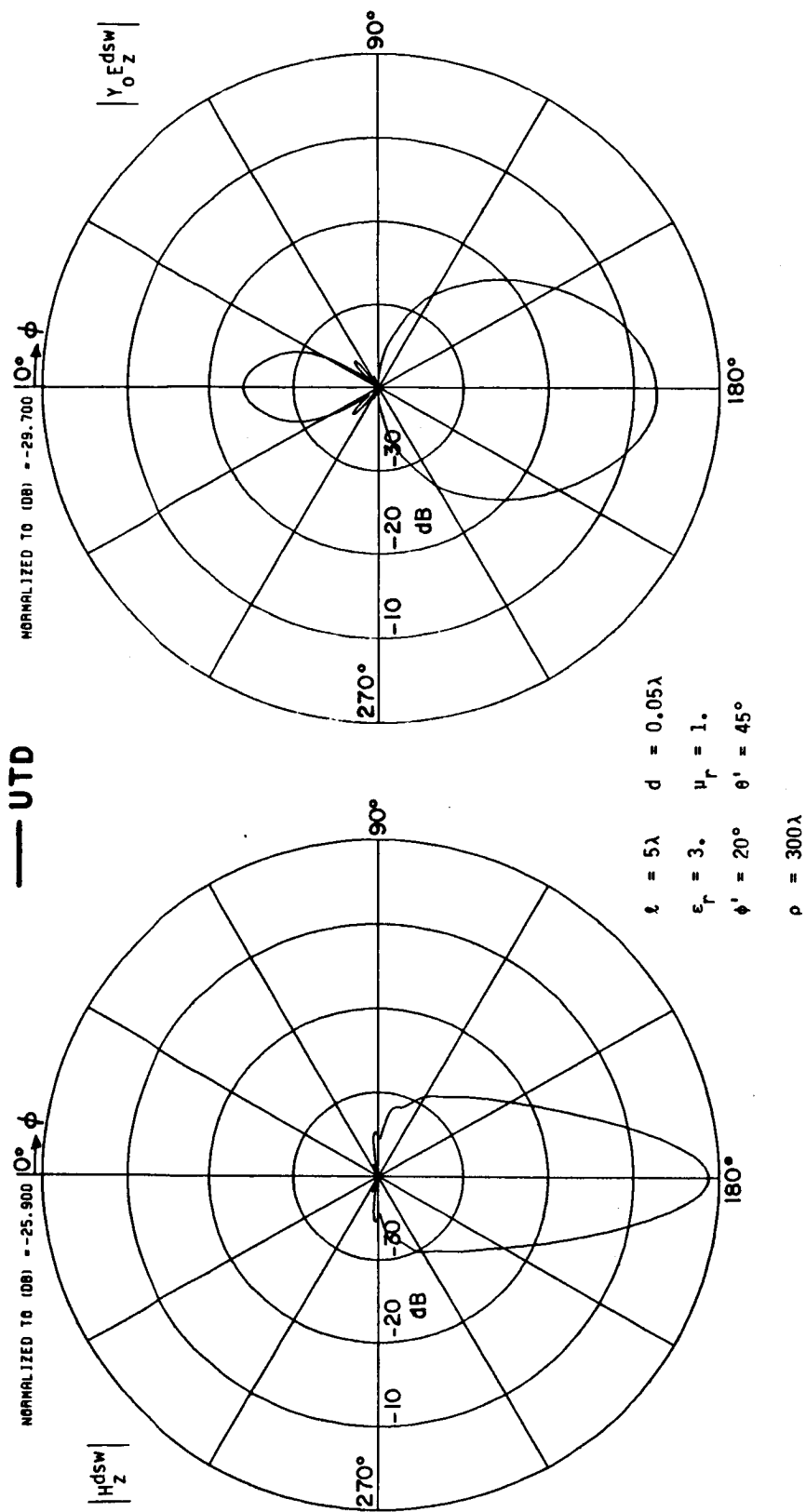


Figure 8.39. Magnitude of the diffracted surface wave fields H_z^{dsw} and E_z^{dsw} (component V) for a H_z -polarized plane wave.

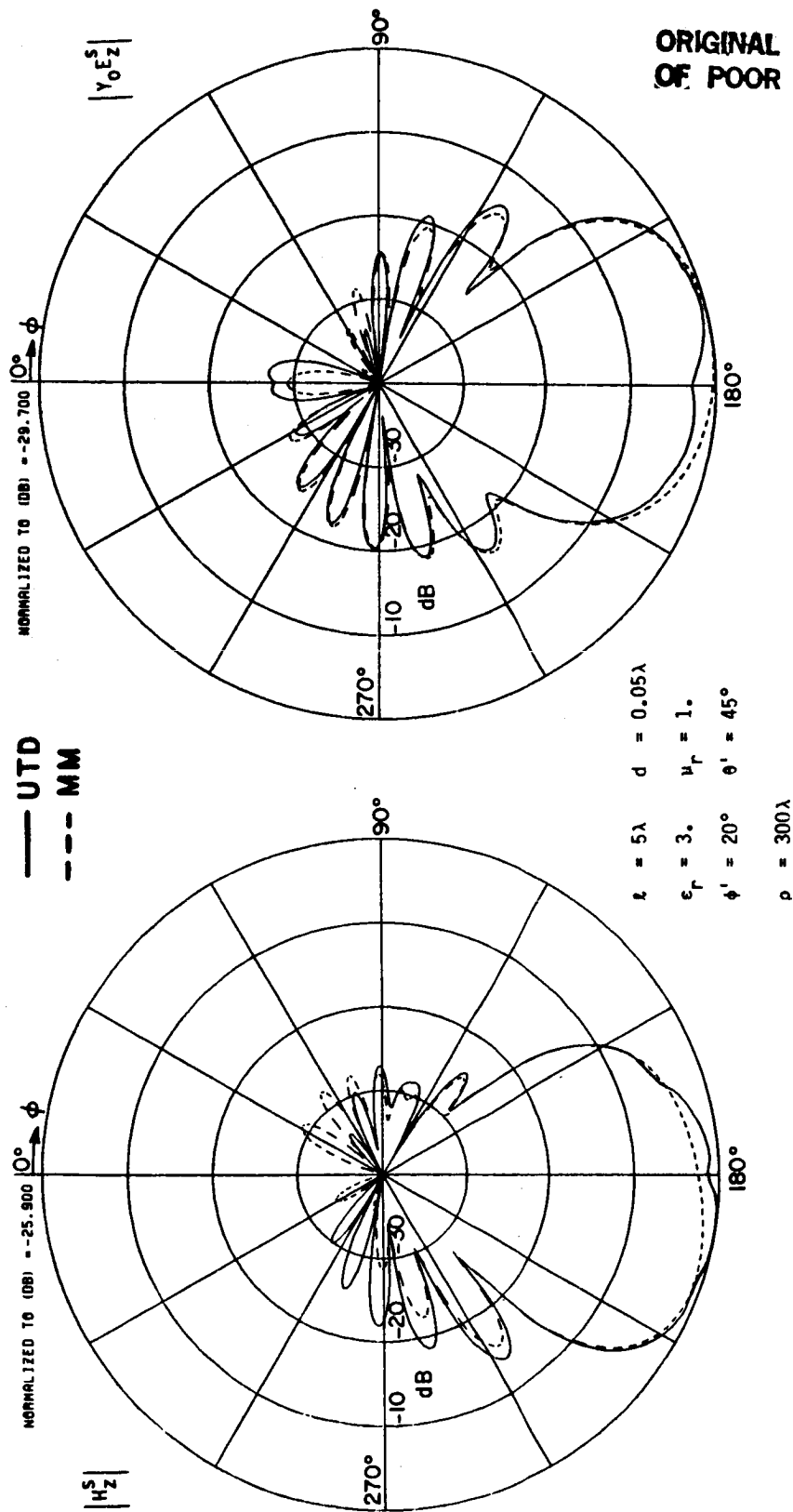


Figure 8.40. Magnitude of the scattered fields H_z^S and E_z^S for a H_z^i -polarized plane wave. The diffracted surface wave field (see Figure 8.39) is included in the solution.

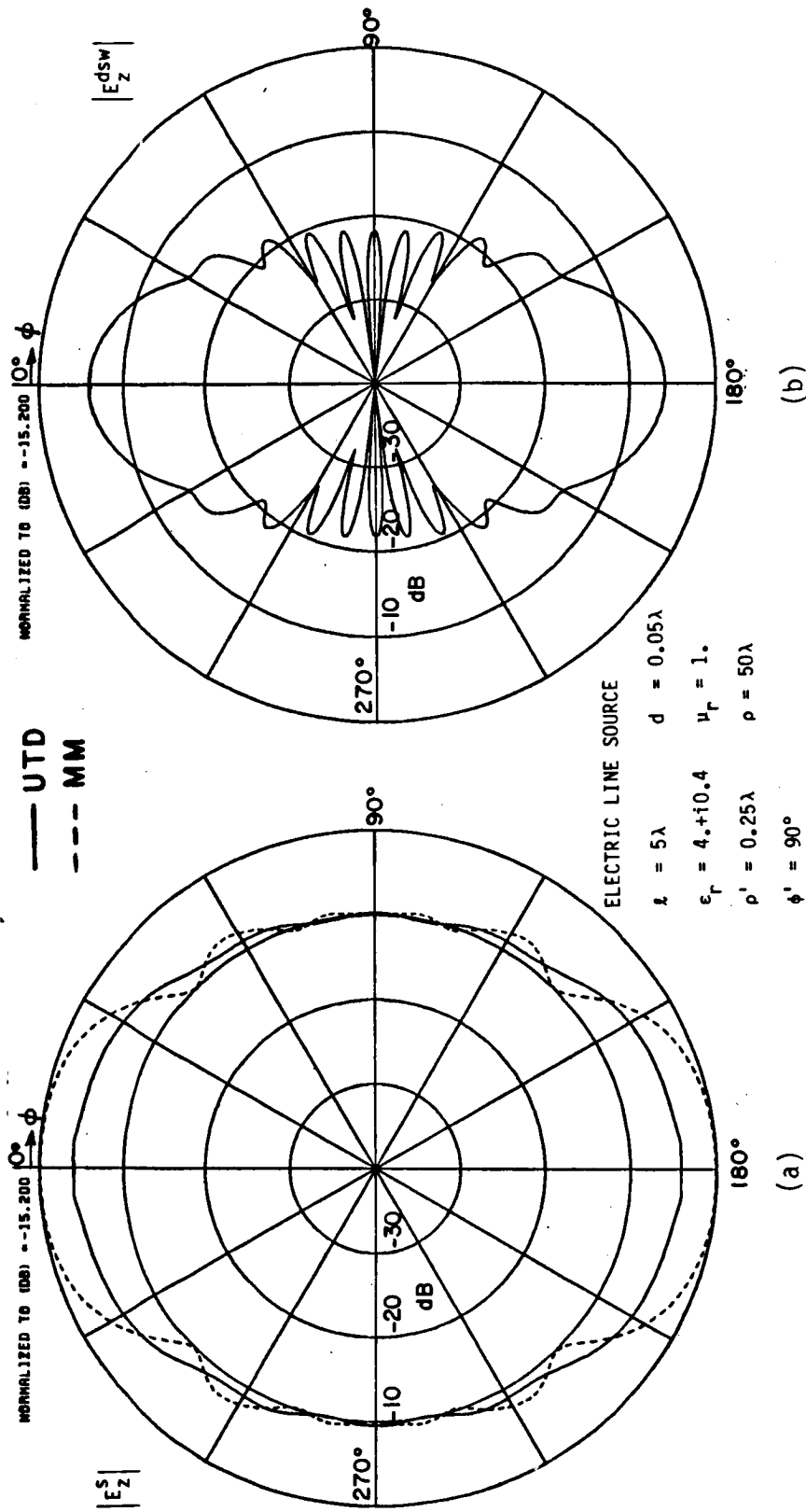
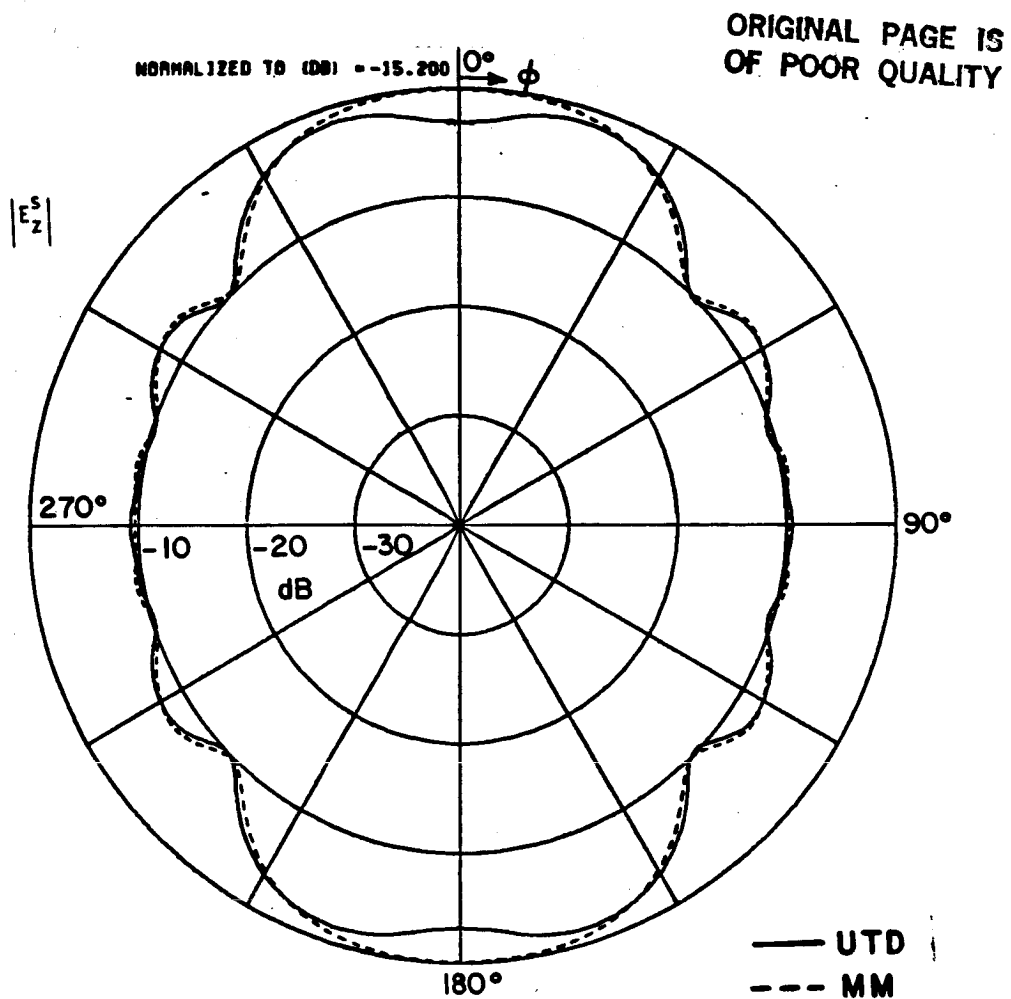


Figure 8.41. Magnitude of the E_z field for the geometry depicted in Figure 8.2.

(a) Scattered E_z^S field without the diffracted surface wave field,

(b) Diffracted surface wave field E_z^{dsw} (see Figure 6.11).



ELECTRIC LINE SOURCE

$$L = 5\lambda \quad d = 0.05\lambda$$

$$\epsilon_r = 4 + j0.4 \quad \mu_r = 1.$$

$$\rho' = 0.25\lambda \quad \rho = 50\lambda$$

$$\phi' = 90^\circ$$

Figure 8.42. Magnitude of the scattered E_z^S field with the diffracted surface wave field E_z^{dsw} included (see Figure 8.41).

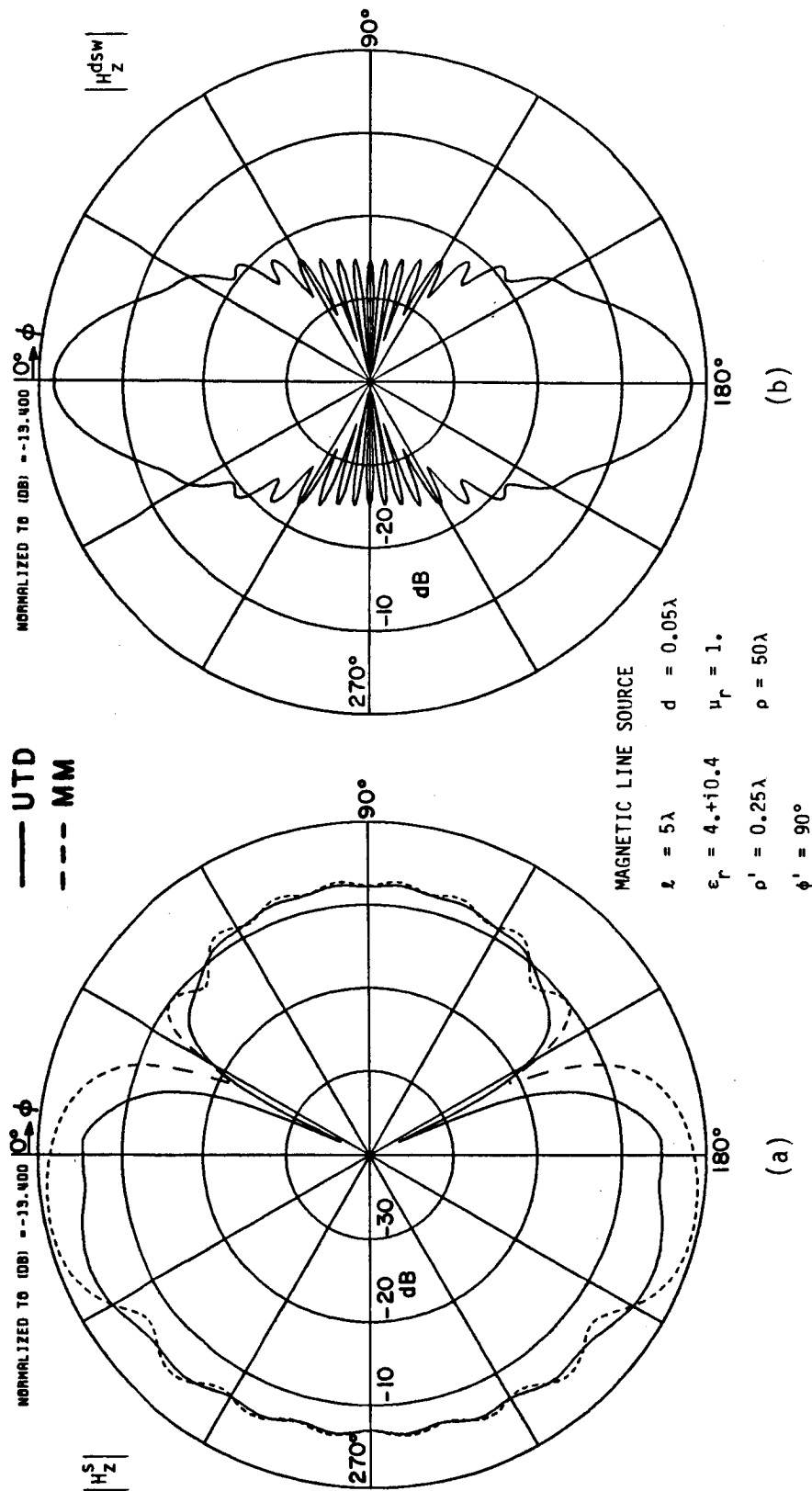
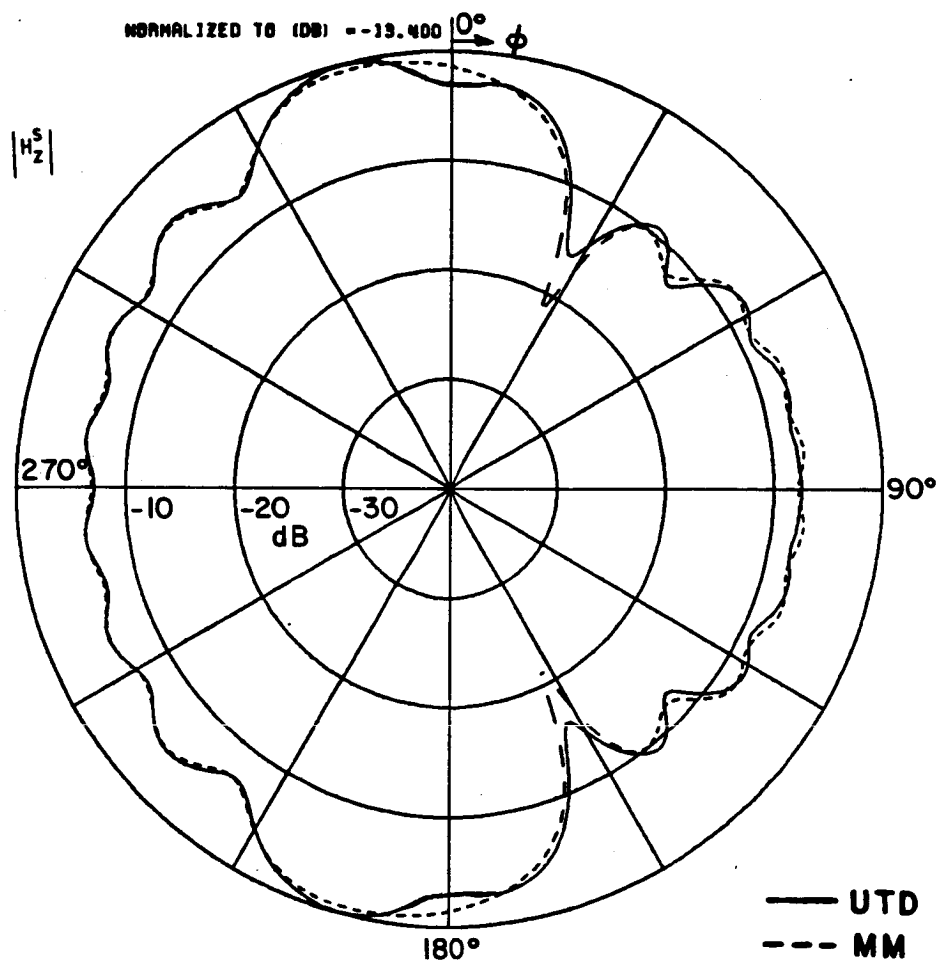


Figure 8.43. Magnitude of the H_z field for the geometry depicted in Figure 8.2.

(a) Scattered H_z^S field without the diffracted surface wave field.

(b) Diffracted surface wave field H_z^{dsw} (see Figure 6.11).



MAGNETIC LINE SOURCE

$$\begin{aligned}
 l &= 5\lambda & d &= 0.05\lambda \\
 \epsilon_r &= 4. + j0.4 & \mu_r &= 1. \\
 \rho' &= 0.25\lambda & \rho &= 50\lambda \\
 \phi' &= 90^\circ
 \end{aligned}$$

Figure 8.44. Magnitude of the scattered H_z^S field with the diffracted surface wave field H_z^{dsw} included (see Figure 8.43).

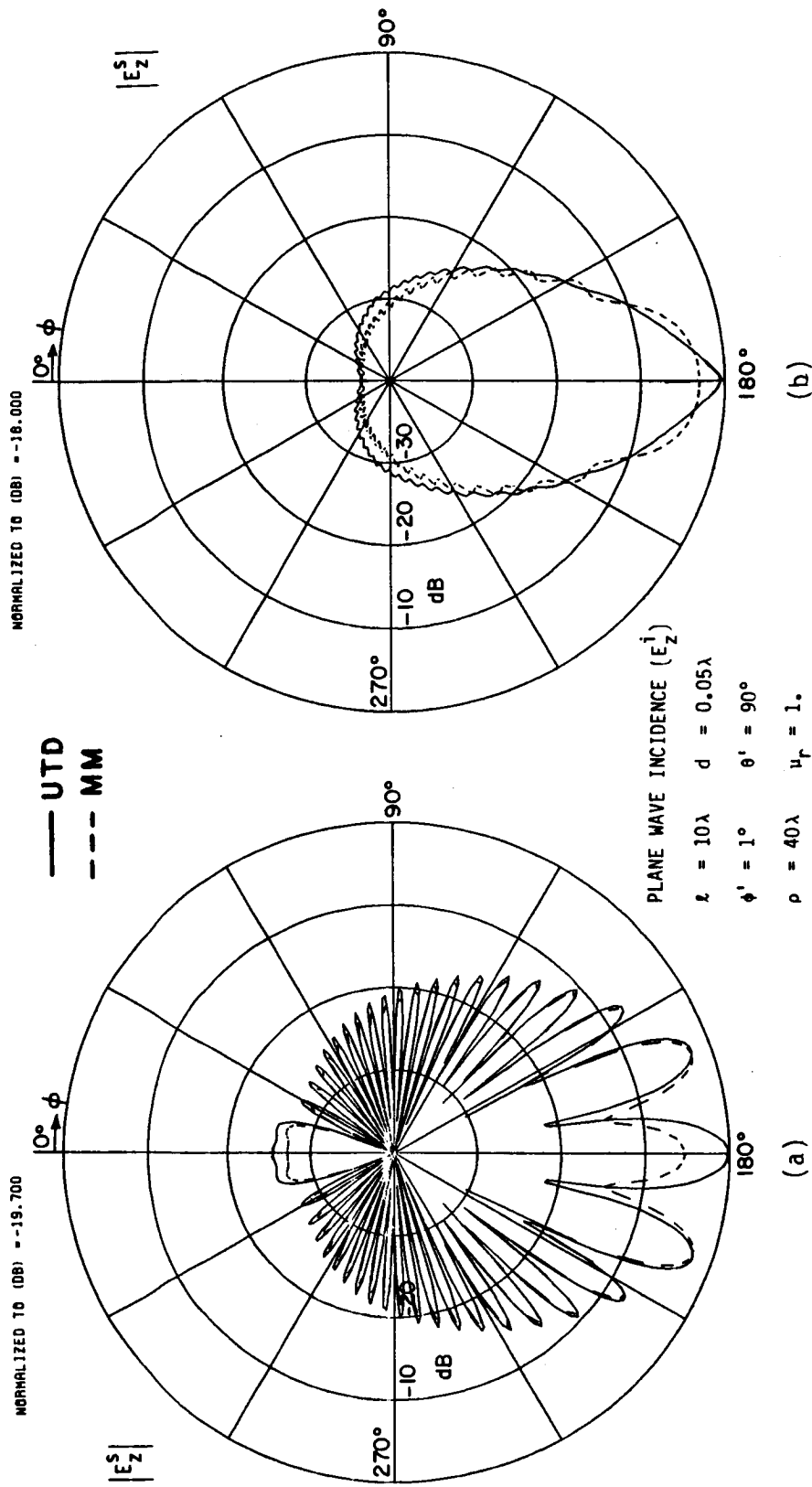


Figure 8.45. Magnitude of the scattered E_z^S field for the geometry depicted in Figure 8.1 (normal incidence).
 (a) $\epsilon_r = 4. + i0.$, (b) $\epsilon_r = 4. + i1.$

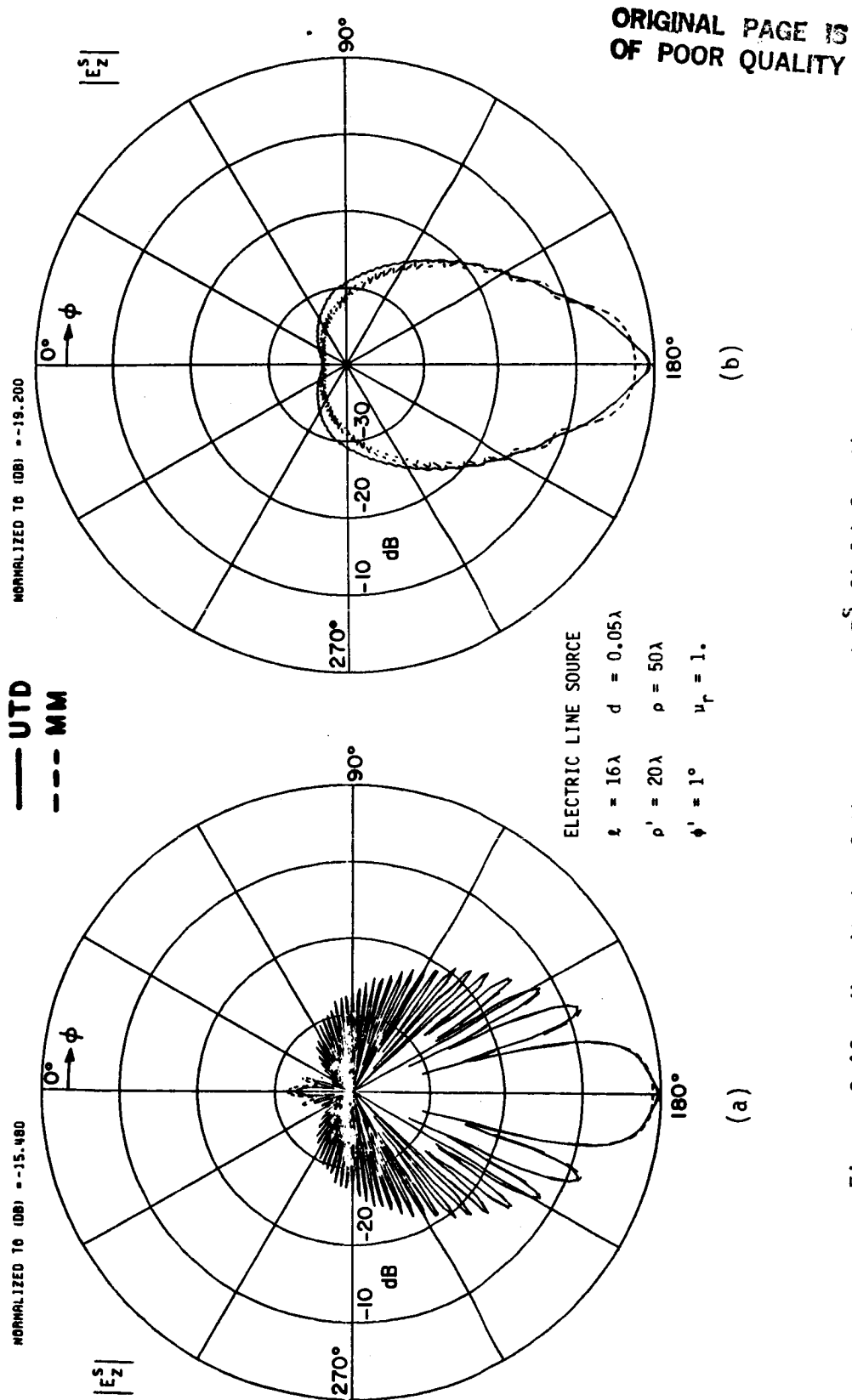
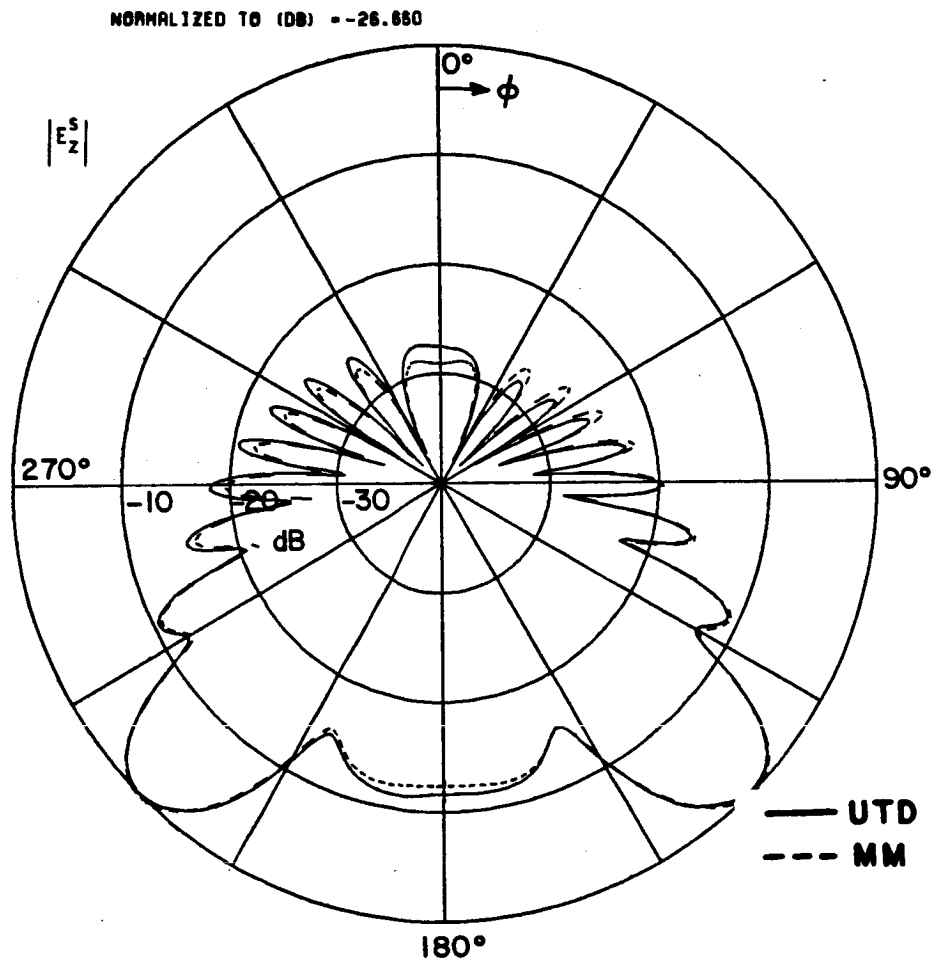


Figure 8.46. Magnitude of the scattered E_z^S field for the geometry depicted in Figure 8.2. (a) $\epsilon_r = 4. + i0.$, (b) $\epsilon_r = 4. + i1.$

In Chapter II, when the dielectric/ferrite half-plane problem was being considered, it was first broken down into two problems with symmetric and asymmetric excitations. The problem with symmetric excitation was referred to as the even problem, whereas, the one with asymmetric excitation was referred to as the odd problem. Note that the scattered field of the even problem is symmetric with respect to the x-axis, while the scattered field of the odd problem is asymmetric with respect to the x-axis. The diffracted field of either configuration is proportional to the difference in the reflection coefficients between the grounded dielectric/ferrite slab ($\tilde{R}^{e,0}$) and the conductor ($R_c = \pm 1$). Thus, by studying the reflection coefficients $\tilde{R}^{e,0}$ and R_c one can predict whether the even, odd, or both diffracted fields will be the dominant contributors to the scattered field. For example, in Figure 8.47 the scattered field is symmetric, which means that the dominant contributor is either the even or odd scattered field, but not both. In order to determine which is the dominant one, the reflection

coefficients for the even and odd configurations have to be examined. For the even configuration $R_c^e = 1$ and \tilde{R}^e is depicted in Figure 8.48. For the odd configuration $R_c^o = -1$ and \tilde{R}^o is depicted in Figure 8.49. Since \tilde{R}^o is very close to -1 for $\phi' = 45^\circ$, the dominant term is the one corresponding to the even configuration. This can be verified by calculating the even and odd diffracted fields which are shown in Figure 8.50a. When the permeability is increased to $3. + i0.3$, R_d^e does not change much, however, R_d^o is no longer close to -1 and one can expect the odd diffraction coefficient to become more important. This is confirmed in Figure 8.50b where the diffracted fields are depicted. As expected,



ELECTRIC LINE SOURCE

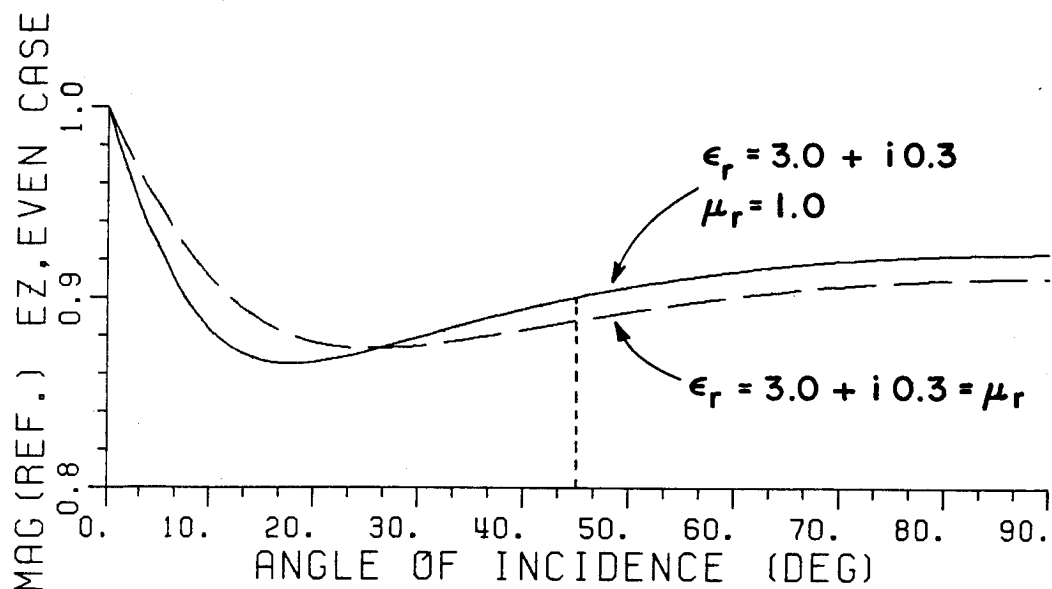
$$z = 5\lambda \quad d = 0.05\lambda$$

$$\epsilon_r = 3. + j0.3 \quad \mu_r = 1.$$

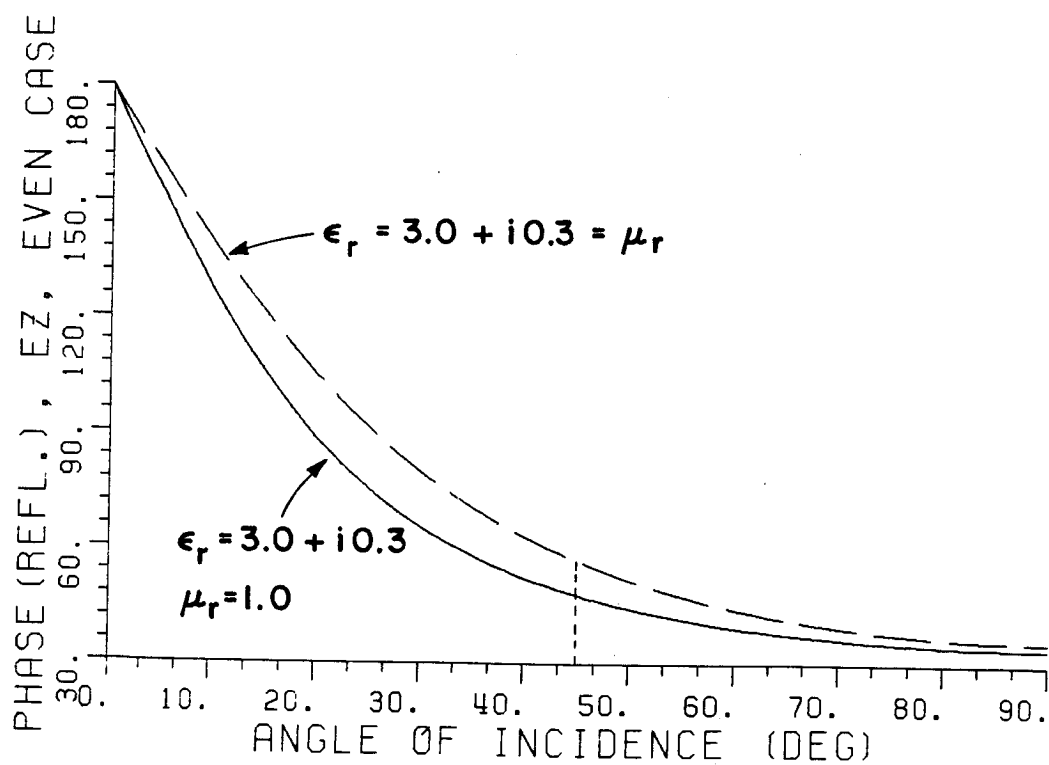
$$\rho' = 15\lambda \quad \rho = 50\lambda$$

$$\phi' = 45^\circ$$

Figure 8.47. Magnitude of the scattered E_z^s field for the geometry depicted in figure 8.2.

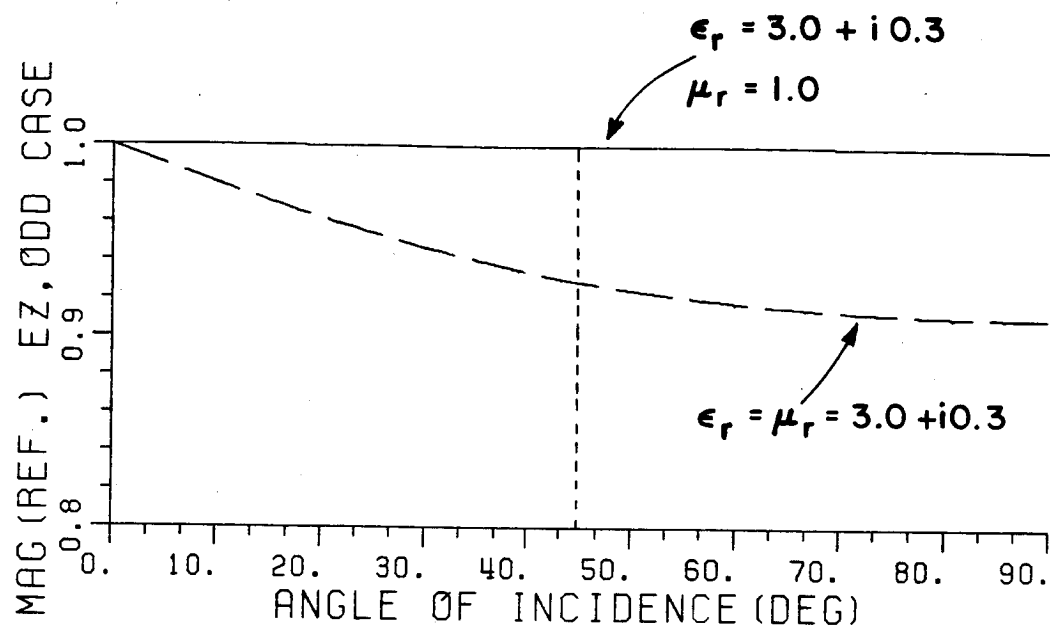


MAGNITUDE

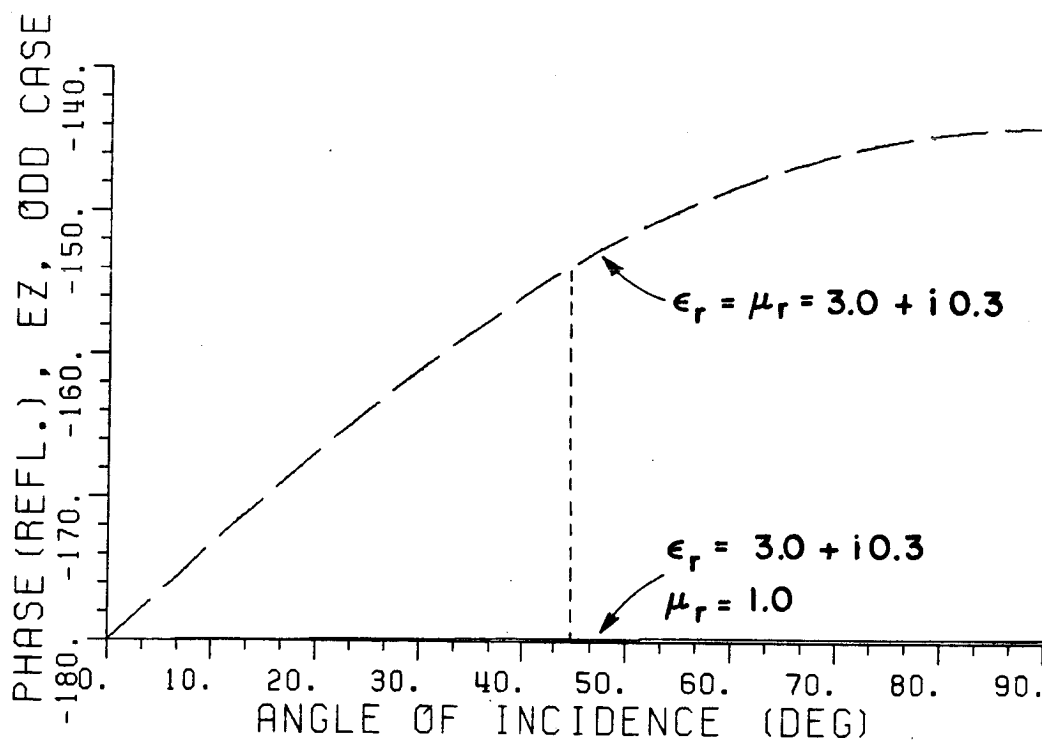


PHASE (DEG.)

Figure 8.48. Even reflection coefficient (TM_z polarization) for a grounded (PMC) dielectric/ferrite slab.



MAGNITUDE



PHASE (DEG.)

Figure 8.49. Odd reflection coefficient (TM_z polarization) for a grounded (PEC) dielectric/ferrite slab.

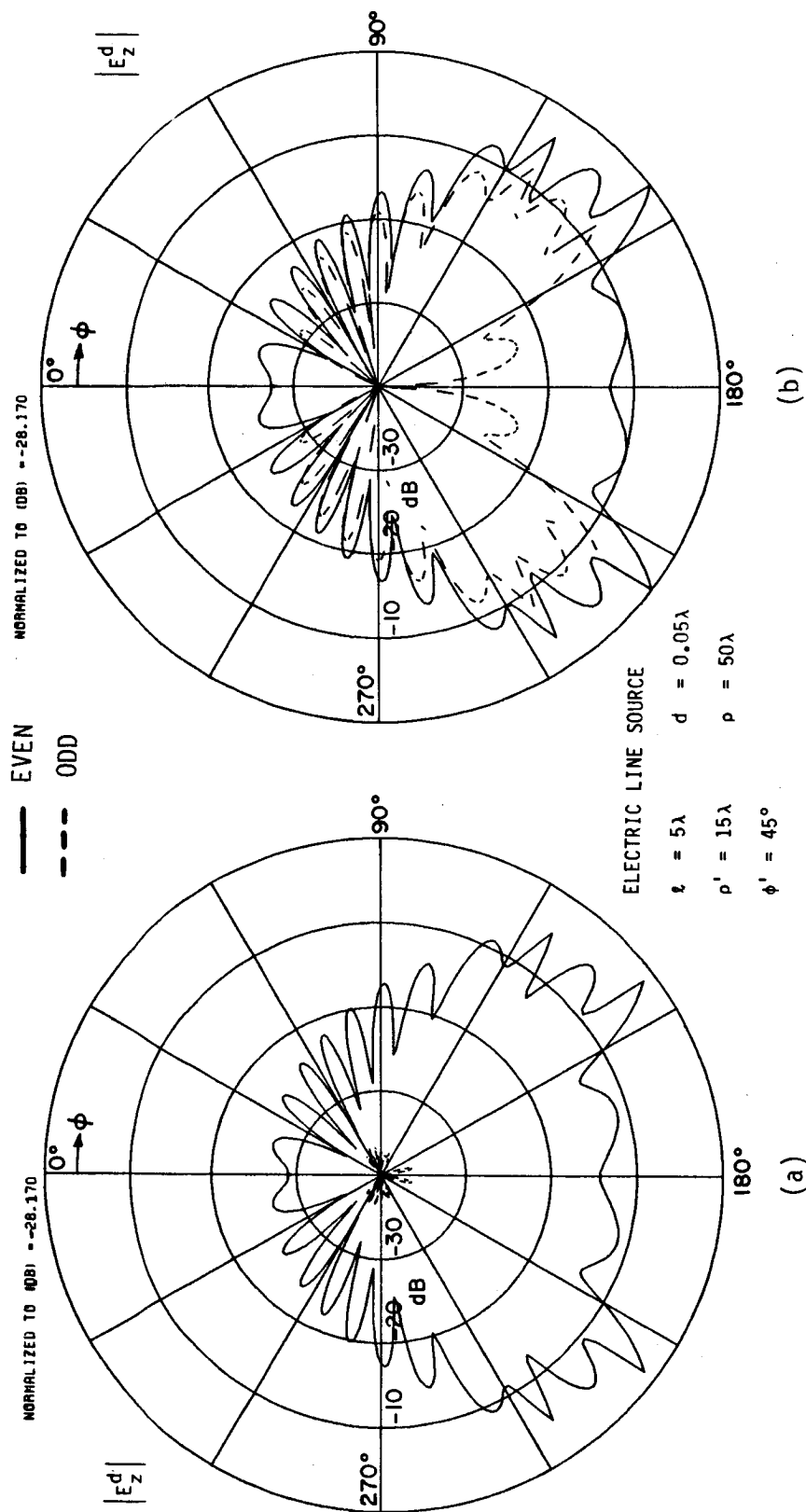


Figure 8.50. Magnitude of diffracted E_z^d field for the geometry depicted

in Figure 8.2. (a) $\epsilon_r = 3 + i0.3$, $\mu_r = 1 + i0$,

(b) $\epsilon_r = 3 + i0.3$, $\mu_r = 3 + i0.3$.

the new scattered field which is shown in Figure 8.51 is no longer symmetric. This example shows that one can predict whether the even, odd, or both solutions will be the dominant contributors by examining the reflection coefficients \tilde{R}^e , \tilde{R}^o , R_C^e , and R_C^o .

Another application of the solutions presented in Chapters III to VI is in the calculation of the echo width of two-dimensional targets. The echo width is defined as follows:

$$e(\phi) = \lim_{\rho \rightarrow \infty} 2\pi\rho \frac{\left| \frac{\vec{E}^s}{E} \right|^2}{\left| \frac{\vec{E}^i}{E} \right|^2} \quad (8.3)$$

where \vec{E}^s and \vec{E}^i are the scattered and incident electric fields, respectively. Figures 8.52 to 8.55 depict the echo width of a dielectric strip for various angles of incidence and for both E_z^i and H_z^i polarizations of the incident plane wave. In all cases the agreement between the UTD and MM solutions is very good.

Besides the dielectric/ferrite half-plane, UTD solutions are also directly available for the diffraction by the dielectric/ferrite bisection problem since the former solution was actually constructed from the latter. These solutions can be used to obtain the fields scattered by a grounded dielectric/ferrite slab as depicted in Figure 8.56.

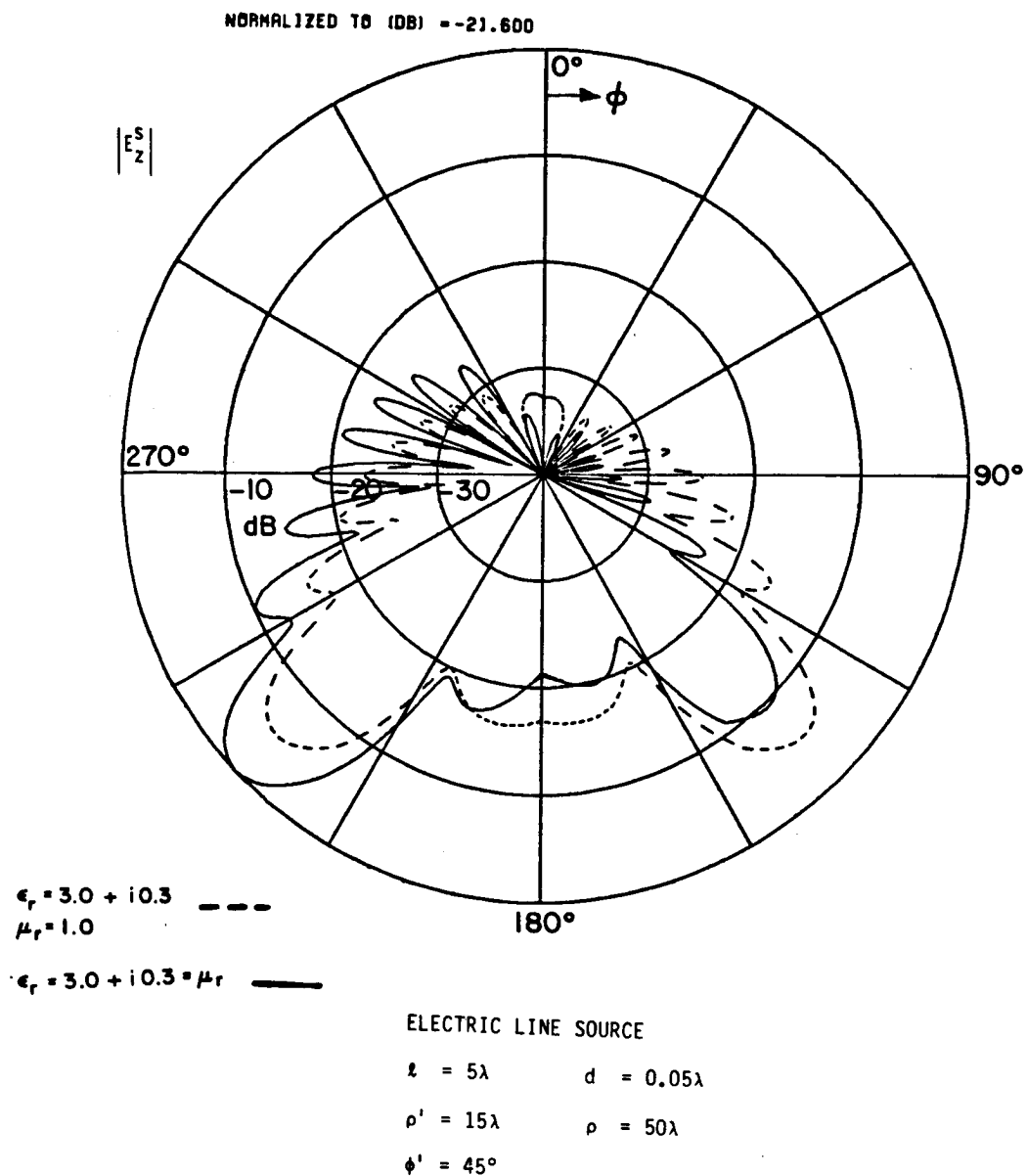


Figure 8.51. Magnitude of the scattered E_z^S field for the geometry depicted in Figure 8.2.

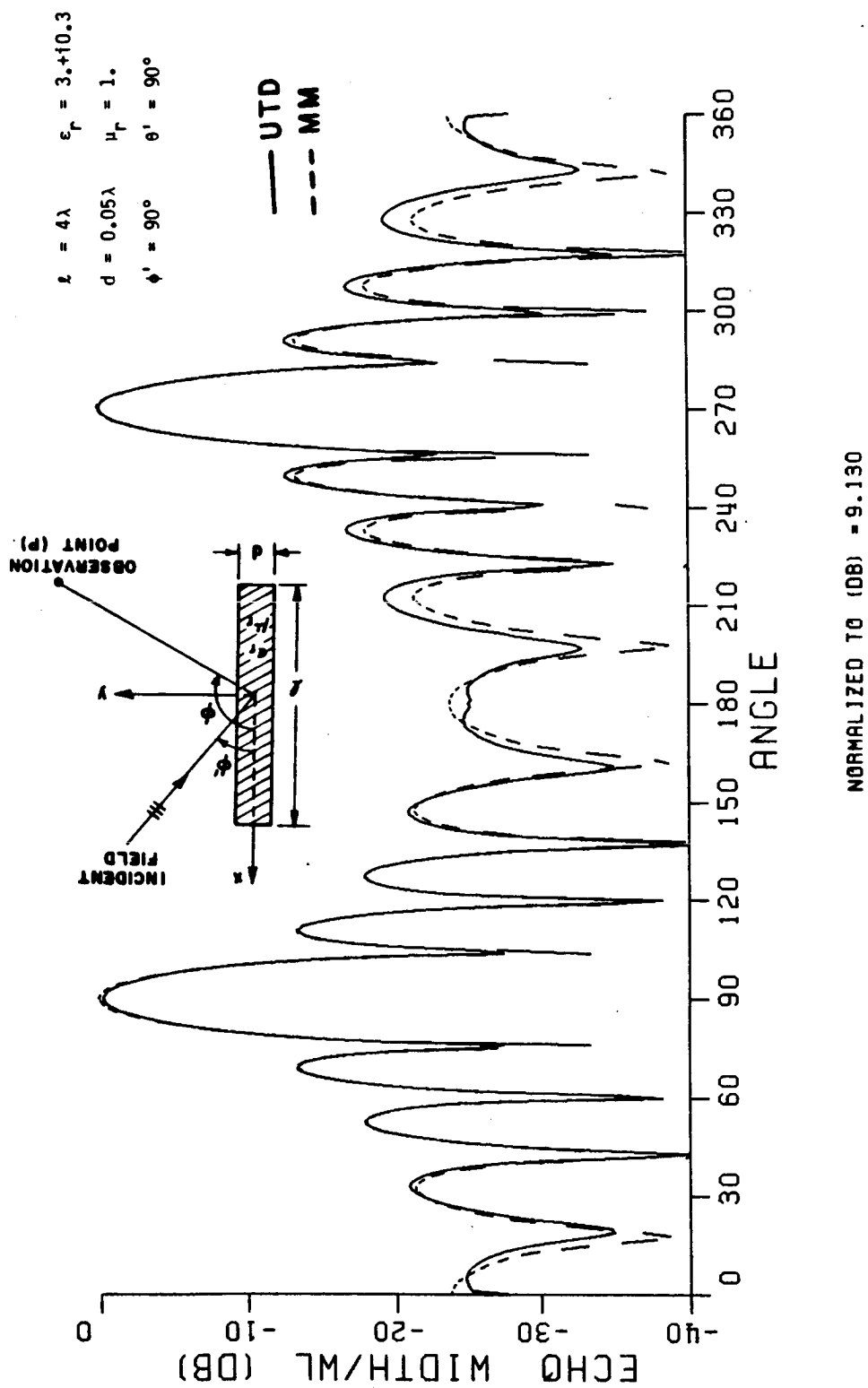


Figure 8.52. Echo width per wavelength of a thin dielectric strip, TM_z polarization.

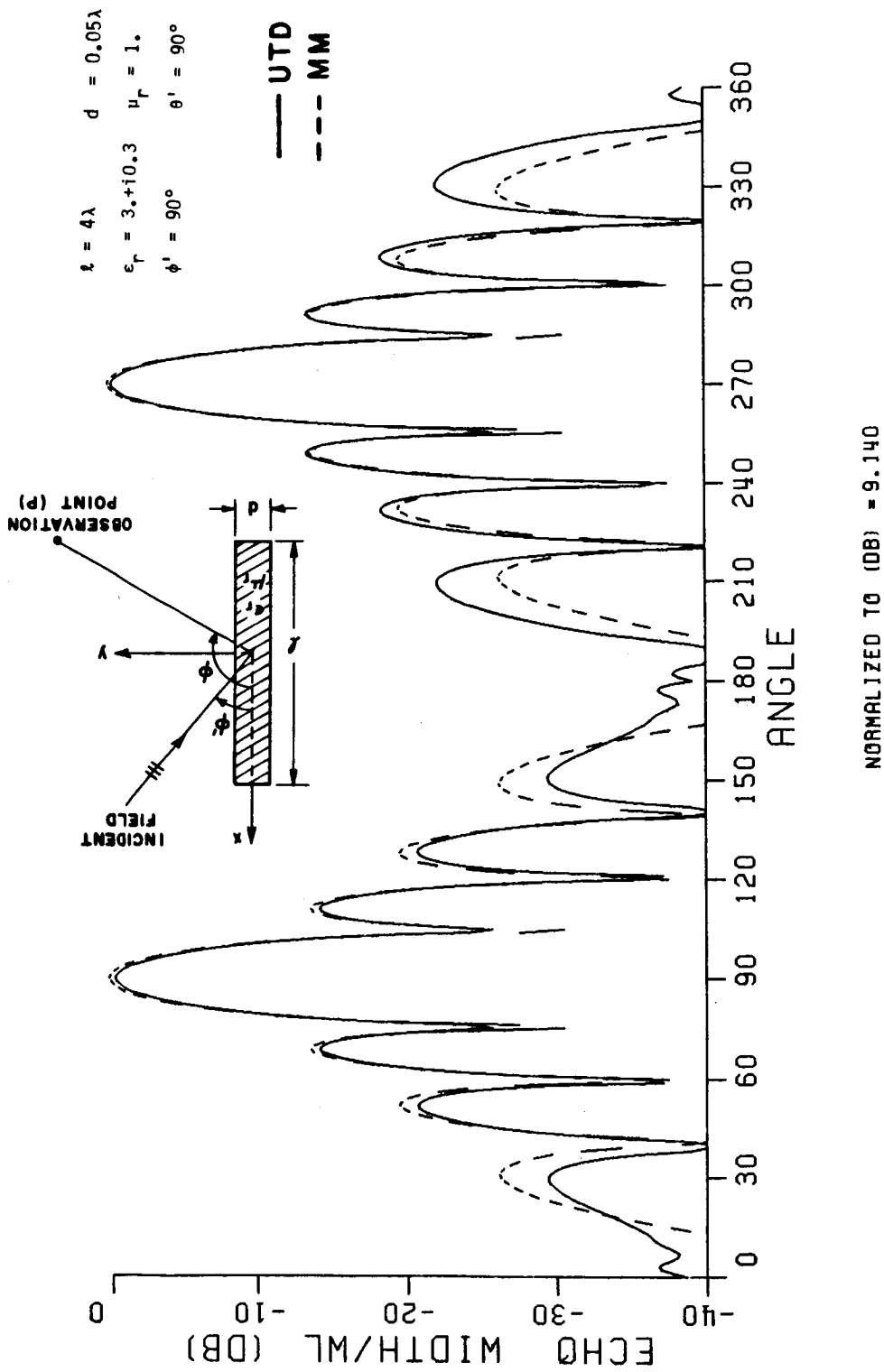


Figure 8.53. Echo width per wavelength of a thin dielectric strip, TE_z polarization.

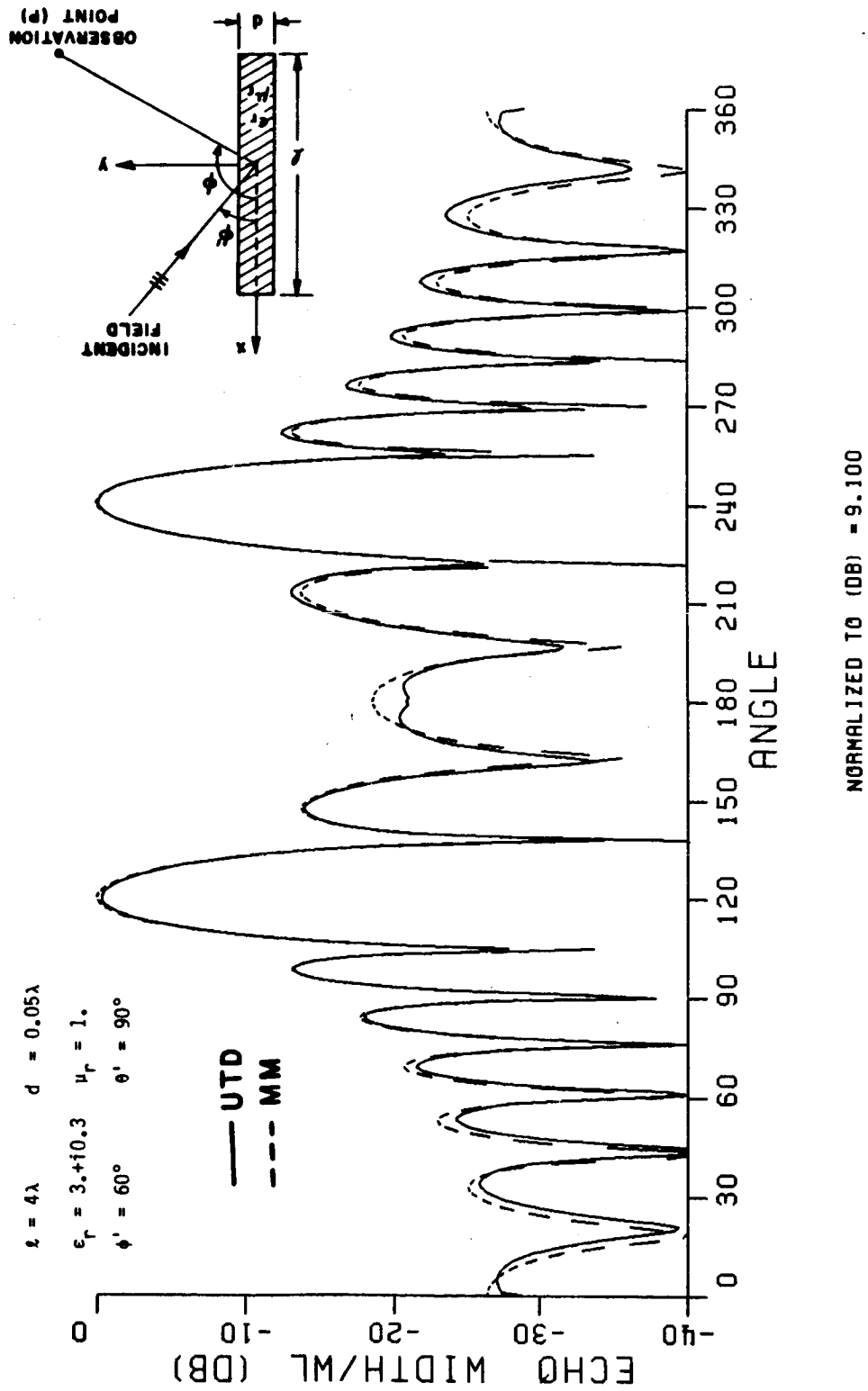


Figure 8.54. Echo width per wavelength of a thin dielectric strip, TM_z polarization.

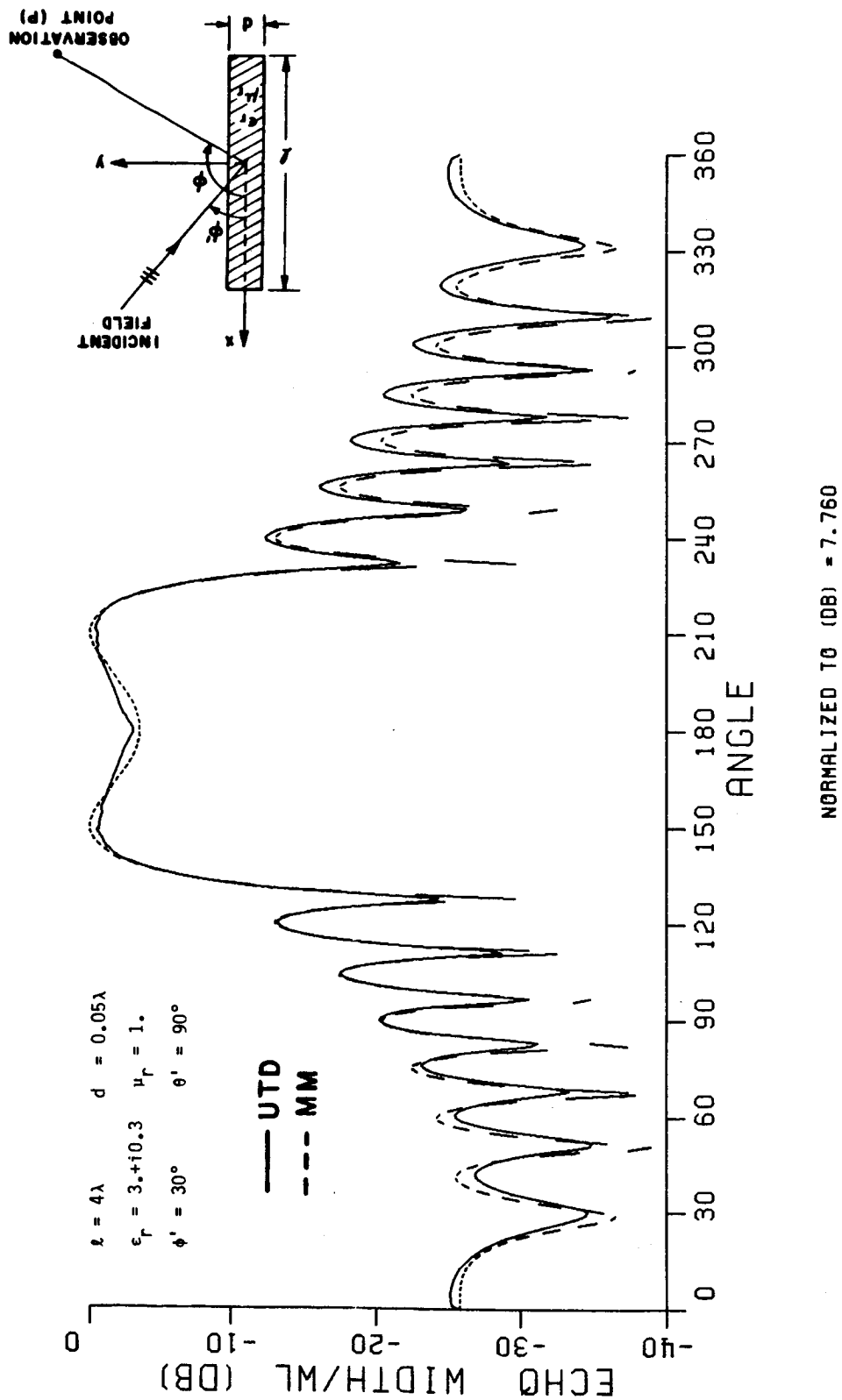


Figure 8.55. Echo width per wavelength of a thin dielectric strip, TM_z polarization.

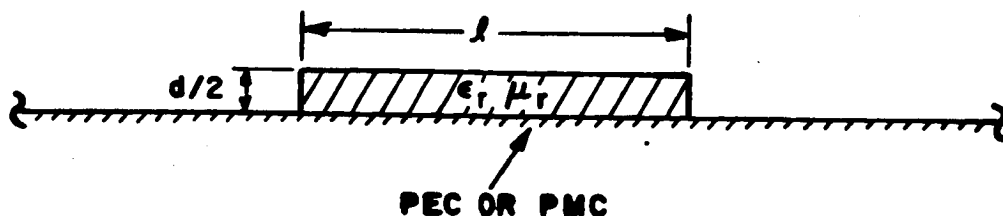


Figure 8.56. Grounded dielectric slab.

This report has examined the scattering by a thin dielectric/ferrite half-plane. The half-plane solution was obtained by appropriately combining the solutions to the even and odd dielectric/ferrite bisection (DFB) problems. Both normal and oblique (or skew) incidence on the edge was considered and it was shown that for oblique incidence there is coupling between the TE and TM fields. However, for the special case of normal incidence, the TE and TM fields become decoupled. As stated in Chapter I, this is an important canonical problem for the UTD, since it extends the UTD edge diffraction solutions from perfectly conducting to penetrable geometries.

In order to obtain the solution to the DFB problem, the impedance bisection problem was considered first. The impedance bisection problem

(plane wave incidence) was solved rigorously via the Wiener-Hopf technique. The Wiener-Hopf equation was obtained by Jones' method [32], and the Wiener-Hopf factorization was accomplished by following a procedure similar to Weinstein [37]. The other crucial step in the solution of the Wiener-Hopf equation is the decomposition of a function. There is a formal decomposition formula [34], however, for the problems considered here, the functions were simple enough so that the decomposition was achieved by inspection.

The solution for the case of surface wave incidence can also be obtained by repeating the same procedure described above for the plane wave excitation problem. However, there is a simpler way (which was used here) of obtaining the former solution from the latter one; namely, the angle of incidence is simply extended to the complex domain, i.e., Brewster angle. From this second solution, the surface wave launching, reflection, and diffraction coefficients were obtained.

It was important to cast the impedance bisection solutions into the UTD form involving reflection and transmission coefficients, and also the surface wave propagation and attenuation constants. Once this was done, the DFB solutions were obtained in the UTD format from the impedance bisection solutions as described in Chapter V. These UTD solutions are valid for illumination by ray optical plane and cylindrical waves, and also by a surface wave.

All of the UTD results shown in this chapter agree very well with the MM-based solutions, except for the case of grazing incidence and aspects near forward scatter, where the doubly edge diffracted field

becomes important. This doubly diffracted field can be obtained by following a procedure similar to that in [55]. That is, the singly diffracted field (diffracted by the first edge) incident on the second edge can be represented as a sum of ray optical wave components because it is non-ray optical there, and hence, its diffraction at the second edge cannot be obtained directly via the use of the above UTD solutions. However, the diffraction of each of these ray optical components by the second edge can be calculated by the UTD. This work is worthy of future investigation.

Another area of future research is to extend the solution to the problem of the diffraction by an impedance wedge which was initially developed by Maliuzhinets [24] in 1959. Since his solution is restricted to the special case of normal incidence, it would be very useful to obtain a solution to this problem for the more general case of oblique (skew) incidence on the edge. However, it may be very difficult to scalarize the original vector problem as it was done here. The problem becomes even more difficult if one allows the surface impedance to be a tensor, i.e., anisotropic impedance sheet, in which case an approximate solution is usually the best one can hope to obtain.

An additional area of future research related to this work is to extend the solutions obtained here to curved surfaces which have many practical applications in the analysis of flush mounted antennas, surface wave antennas and flush mounted radomes to name a few.

In order to facilitate the use of the new solutions developed here, Tables 1 through 3 summarize the most important results.

TABLE 8.1
IBS SOLUTIONS

	<u>Equation Number</u>
A. Plane Wave Incidence (2-D)	
1. Even problem, edge excited surface wave	3.200
2. Even problem, reflected field	3.206
3. Even problem, diffraction coefficient	3.210
4. Odd problem, edge excited surface wave	3.233
5. Odd problem, reflected field	3.238
6. Odd problem, diffraction coefficient	3.242
7. Slope diffraction coefficient (even problem)	3.255
8. Slope diffraction coefficient (odd problem)	3.257
B. Surface Wave Excitation (2-D)	
1. Even problem, incident surface wave	3.301
2. Even problem, reflected surface wave	3.315
3. Even problem, diffracted surface wave	3.312
4. Odd problem, incident surface wave	3.324
5. Odd problem, reflected surface wave	3.329
6. Odd problem, diffracted surface wave	3.330

TABLE 8.1 (CONTINUED)

	Equation Number
C. Plane Wave Incidence (3-D)	
1. Even problem, PEC case, reflected field (E_y^{re})	4.119
2. Even problem, PEC case, edge excited surface wave (E_{ye}^{sw})	4.121
3. Even problem, PEC case, diffracted field (E_y^{de})	4.123
4. Odd problem, PEC case, reflected field (H_y^{ro})	4.133
5. Odd problem, PEC case, edge excited surface wave (H_{yo}^{sw})	4.135
6. Odd problem, PEC case, diffracted field (H_y^{de})	4.137
D. Surface Wave Excitation (3-D)	
1. Even problem, PEC case, reflected surface wave (E_{ye}^{rsw})	4.162
2. Even problem, PEC case, diffracted surface wave (E_{ye}^{dsw})	4.163, 4.175
3. Odd problem, PEC case, reflected surface wave (H_{yo}^{rsw})	4.171
4. Odd problem, PEC case, diffracted surface wave (H_{yo}^{dsw})	4.167, 4.172
E. Edge Diffracted E_z^d and H_z^d Fields	
1. PEC case, E_z^{do}	4.200
2. PEC case, H_z^{de}	4.201
3. PMC case, E_z^{de}	4.216
4. PMC case, H_z^{do}	4.217

TABLE 8.2
DFB SOLUTIONS

	<u>Equation Number</u>
A. Fresnel Reflection Coefficients	5.14 through 5.21
B. 2-D Problems	
1. Even diffraction coefficient	5.46
2. Odd diffraction coefficient	5.47
3. Even surface wave launching coefficient	5.52
4. Odd surface wave launching coefficient	5.53
5. Even surface wave reflection coefficient	5.59
6. Odd surface wave reflection coefficient	5.60
7. Even surface wave diffraction coefficient	5.64
8. Odd surface wave diffraction coefficient	5.65
C. 3-D Problems	
1. Edge excited surface wave, E_{ye}^{sw}, E_{yo}^{sw} (plane wave incidence)	5.74, 5.86
2. Edge excited surface wave, H_{ye}^{sw}, H_{yo}^{sw} (plane wave incidence)	5.75, 5.87

TABLE 8.3
DIELECTRIC/FERRITE HALF-PLANE SOLUTIONS

	<u>Equation Number</u>
1. Reflected field	6.14
2. Dyadic reflection coefficient	6.16, 6.17, 6.18
3. Transmitted field	6.19
4. Dyadic transmission coefficient	6.20, 6.21, 6.22
5. Edge diffracted field	6.35
6. Dyadic diffraction coefficient	6.37, 6.38, 6.39
7. Surface wave field excited by a plane wave (oblique incidence)	6.41, 6.42
8. Reflected surface wave (oblique incidence)	6.48, 6.49
9. Diffracted surface wave (oblique incidence)	6.60, 6.61
10. Line source excitation	6.63 through 6.75

APPENDIX A

FOURIER TRANSFORM IN COMPLEX S-PLANE

In the development of the Wiener-Hopf technique, one can use the two-sided Laplace transform or the Fourier transform because in the complex plane both transforms are completely equivalent [32]. Here the Fourier transform is used. In this appendix certain properties of the Fourier transform that are relevant to the Wiener-Hopf technique are summarized. A detailed discussion of this topic can be found in many excellent books such as Titchmarsh [56].

Let $f(x)$ be a function of the real variable x . Define the half-range functions $f_+(x)$ and $f_-(x)$ as follows:

$$f_+(x) = \begin{cases} f(x) & x > 0 \\ 0 & x < 0 \end{cases} \quad (\text{A.1})$$

$$f_-(x) = \begin{cases} 0 & x > 0 \\ f(x) & x < 0 \end{cases} \quad (\text{A.2})$$

where the subscript (+) in the function $f_+(x)$ signifies that the function is identically zero for $x < 0$, and the subscript (-) in the

function $f_-(x)$ means that this second function is identically zero for $x > 0$. Therefore, $f(x)$ can be represented as

$$f(x) = f_+(x) + f_-(x) \quad . \quad (A.3)$$

Furthermore, assume $f_+(x)$ and $f_-(x)$ have the following asymptotic behavior:

$$f_+(x) \sim Ae^{\tau_- x} \quad \text{as } x \rightarrow \infty \quad (A.4)$$

$$f_-(x) \sim Be^{\tau_+ x} \quad \text{as } x \rightarrow -\infty \quad . \quad (A.5)$$

Next, let s be a complex variable such that

$$s = \sigma + i\tau \quad (A.6)$$

where σ and τ are real variables.

The Fourier transform of $f_+(x)$ is defined by [32]

$$\hat{F}_+(s) = \frac{1}{\sqrt{2\pi}} \int_{-\infty}^{\infty} f_+(x) e^{isx} dx = \frac{1}{\sqrt{2\pi}} \int_0^{\infty} f_+(x) e^{isx} dx \quad (A.7)$$

where $\hat{F}_+(s)$ is regular in the upper s -plane defined by $\tau > \tau_-$ [32].

The above integral is interpreted as a Riemann integral [34] and it will exist provided $f_+(x)$ satisfies certain conditions [32,56]. Since most of the functions in engineering applications are sufficiently well behaved, their Fourier transforms usually exist.

Similarly, the Fourier transform of $f_-(x)$ is defined by

$$\hat{F}_-(s) = \frac{1}{\sqrt{2\pi}} \int_{-\infty}^{\infty} f_-(x) e^{isx} dx = \frac{1}{\sqrt{2\pi}} \int_{-\infty}^0 f_-(x) e^{isx} dx \quad (A.8)$$

where $\hat{F}_-(s)$ is regular in the lower s -plane defined by $\tau < \tau_+$ [32].

Finally, the Fourier transform of $f(x)$ can be written the following way:

$$\hat{F}(s) = \frac{1}{\sqrt{2\pi}} \int_{-\infty}^{\infty} f(x) e^{isx} dx \quad (\text{A.9})$$

where $\hat{F}(s)$ is regular in the strip defined by $\tau_- < \tau < \tau_+$, and the inverse transform of $\hat{F}(s)$ is given by [34]

$$f(x) = \frac{1}{\sqrt{2\pi}} \int_{-\infty+ia}^{\infty+ia} \hat{F}(s) e^{-isx} ds, \quad \tau_- < a < \tau_+. \quad (\text{A.10})$$

It follows from Equations (A.7), (A.8) and (A.9) that

$$\hat{F}(s) = \hat{F}_+(s) + \hat{F}_-(s) \quad . \quad (\text{A.11})$$

In solving the Wiener-Hopf equation, it will be necessary to know the asymptotic behavior of $\hat{F}_+(x)$ and $\hat{F}_-(s)$ which is related to the behavior of $f_+(x)$ and $f_-(x)$ as follows [34]:

$$\text{if } f_+(x) \sim x^p \text{ as } x \rightarrow 0+, \text{ then} \quad (\text{A.12})$$

$$\hat{F}_+(s) \sim s^{-p-1} \quad \text{as } |s| \rightarrow \infty \text{ in } \tau > \tau_- \quad ; \quad (\text{A.13})$$

$$\text{if } f_-(x) \sim x^p \text{ as } x \rightarrow 0-, \text{ then} \quad (\text{A.14})$$

$$\hat{F}_-(s) \sim s^{-p-1} \quad \text{as } |s| \rightarrow \infty \text{ in } \tau < \tau_+ \quad . \quad (\text{A.15})$$

In Chapters III and IV the Fourier transform is applied to the scalar Helmholtz differential equation. Thus, it is important to define the Fourier transform of the second derivative of $f(x)$. This is done in [32] and only the result will be shown here. If $\hat{F}(s)$ is the Fourier transform of $f(x)$, it follows that the Fourier transform of $\frac{d^2 f(x)}{dx^2}$ is given by [32]:

$$\mathcal{F} \left[\frac{d^2 f(x)}{dx^2} \right] = -s^2 \hat{F}(s) \quad , \quad \tau_- < \tau < \tau_+ \quad (\text{A.16})$$

where \mathcal{F} is the Fourier transform operator such that

$$\mathcal{F} [f(x)] = \frac{1}{\sqrt{2\pi}} \int_{-\infty}^{\infty} f(x) e^{isx} dx \quad , \quad \tau_- < \tau < \tau_+ \quad . \quad (\text{A.17})$$

APPENDIX B

RADIATION AND EDGE CONDITIONS

In Chapters III and IV it is necessary to solve the following scalar Helmholtz equation:

$$\left[\frac{\partial^2}{\partial x^2} + \frac{\partial^2}{\partial y^2} + K^2 \right] f(x,y) = 0 \quad (\text{B.1})$$

where K is a complex constant with its real and imaginary parts positive, and where the region of interest in the x - y plane will involve boundaries at infinity and geometrical singularities. In order to obtain unique solutions it is necessary to apply two physical constraints. The first condition known as the radiation condition [57] deals with the behavior of the fields at infinity due to real or equivalent sources contained in a finite area of the x - y plane (for 2-D problems). If the medium is lossy, i.e., $k_2 \neq 0$, the radiation condition dictates that the fields have to vanish at infinity. On the other hand, if the medium is lossless, i.e., $k_2 = 0$, and isotropic [34], the solutions of Equation (B.1) have to represent traveling waves propagating toward infinity. Mathematically, this condition dictates that the solutions of (B.1) have to satisfy the Sommerfeld radiation condition given by [45]

$$\lim_{\rho \rightarrow \infty} (\rho)^{1/2} \left[\frac{\partial}{\partial \rho} - iK \right] f(x,y) = 0 \quad (B.2)$$

where

$$\rho = (x^2 + y^2)^{1/2} \quad (B.3)$$

It follows from Equation (B.2) that

$$f(x,y) \sim \frac{c e^{iK\rho}}{(\rho)^{1/2}} \quad \text{as } \rho \rightarrow \infty \quad (B.4)$$

where c is an arbitrary constant. Note that it was emphasized that the sources have to be confined to a finite area of the x - y plane, however, in Chapters III and IV it is assumed that a plane wave is incident on the diffracting geometry. Thus, the asymptotic behavior of the fields (for plane wave incidence) has to be interpreted carefully.

The second physical constraint which deals with the behavior of the fields near geometrical singularities is the edge condition. First introduced by Meixner [58], it insures that the total electric and magnetic energy stored in any finite neighborhood of an edge will be finite.

For the geometry considered in this study which is depicted in Figure 3.1, it is difficult to obtain the edge conditions. However, as shown in Chapters III and IV it is enough to know the following information:

The most singular behavior of the fields near the origin (see Figure 3.1) is [34,21]:

$$E_z, H_z = O(\rho^\tau) \quad (\text{B.5})$$

for the tangential components (E_z, H_z) , and

$$E_y, H_y = O(\rho^{-1+\tau}) \quad (\text{B.6})$$

for the transverse components (E_y, H_y) . The edge condition is satisfied if the constant τ is restricted to the domain $\tau > 0$.

APPENDIX C

SPECIFICATION OF THE VALUE OF $\beta = (K^2 - s^2)^{1/2}$

In this appendix, the double-valued function β defined by

$$\beta = (K^2 - s^2)^{1/2} \quad (C.1)$$

will be uniquely specified. Recall that s is the complex variable in the Fourier transformed domain given by

$$s = \sigma + i\tau \quad (C.2)$$

and K is equal to

$$K = K_1 + iK_2 = k \sin \theta' = (k_1 + ik_2) \sin \theta', \quad 0 < \theta' < \pi. \quad (C.3)$$

It follows from Chapter I, that

$$K_1, K_2 > 0 \quad (C.4)$$

and it will be assumed that the following constraint is satisfied for analytic convenience

$$K_1 \gg K_2. \quad (C.5)$$

Because of the radiation condition given in Appendix B, the double-valued function β has to satisfy the following two conditions along the Fourier inversion path:

$$\text{Im } (\beta) < 0 \quad (\text{C.6})$$

and

$$\text{Re } (\beta) > 0 \quad (\text{C.7})$$

Conditions (C.6) and (C.7) will insure that the solutions of the Fourier transformed wave equation will represent either outgoing or evanescent waves for large $|y|$. Note that the function β has two branch points located at

$$s = \pm K \quad (\text{C.8})$$

To specify β uniquely, it is convenient to view the complex s -plane as a two sheeted surface with the sheets connected along the branch cuts. In each sheet, β is a single-valued analytic function of s . The choice of branch cuts is arbitrary, but for the problems considered here, a particular set of branch cuts will be defined based on the restrictions given by Equations (C.6) and (C.7).

The branch cut of β in the s -plane is defined such that $\text{Im } (\beta) > 0$ on one sheet, which will be called the top or proper sheet, and $\text{Im } (\beta) < 0$ on the bottom or improper sheet [34]. This definition implies that the two sheets are connected by the curve defined by $\text{Im } (\beta) = 0$ which locates the desired branch cut.

In order to obtain the branch cut curve, it is necessary to first write β^2 as

$$\beta^2 = K^2 - s^2 = (K_1 + iK_2)^2 - (\sigma + i\tau)^2 \quad (\text{C.9})$$

or

$$\beta^2 = (K_1^2 - K_2^2 - \sigma^2 + \tau^2) + 2i(K_1 K_2 - \sigma\tau) \quad (\text{C.10})$$

Next, the complex s -plane is divided by the curves $\text{Re}(\beta^2) = 0$ and $\text{Im}(\beta^2) = 0$ as shown in Figures C.1 where the horizontally shaded regions correspond to $\text{Re}(\beta^2) < 0$ and the vertically shaded regions correspond to $\text{Im}(\beta^2) < 0$. The unshaded region corresponds to both $\text{Re}(\beta^2) > 0$ and $\text{Im}(\beta^2) > 0$. Note that the $\text{Re} \beta^2 = 0$ implies that

$$K_1^2 - K_2^2 - \sigma^2 + \tau^2 = 0 \quad (\text{C.11})$$

which is the equation of a hyperbola. On the other hand, the condition $\text{Im}(\beta^2) = 0$ implies that

$$K_1 K_2 = \sigma \tau \quad (\text{C.12})$$

and solving for τ one obtains

$$\tau = K_1 K_2 / \sigma \quad . \quad (\text{C.13})$$

Furthermore, the constraint $\text{Im}(\beta^2) > 0$ can be expressed as

$$K_1 K_2 > \sigma \tau \quad (\text{C.14})$$

or

$$\tau \begin{cases} < \frac{K_1 K_2}{\sigma} & \sigma > 0 \\ > \frac{K_1 K_2}{\sigma} & \sigma < 0 \end{cases} \quad . \quad (\text{C.15})$$

To insure that $\text{Im}(\beta) > 0$ on the entire top-sheet, it is required that the argument of β^2 be restricted to the domain given by

$$0 < \text{Arg}(\beta^2) < 2\pi \quad (\text{C.16})$$

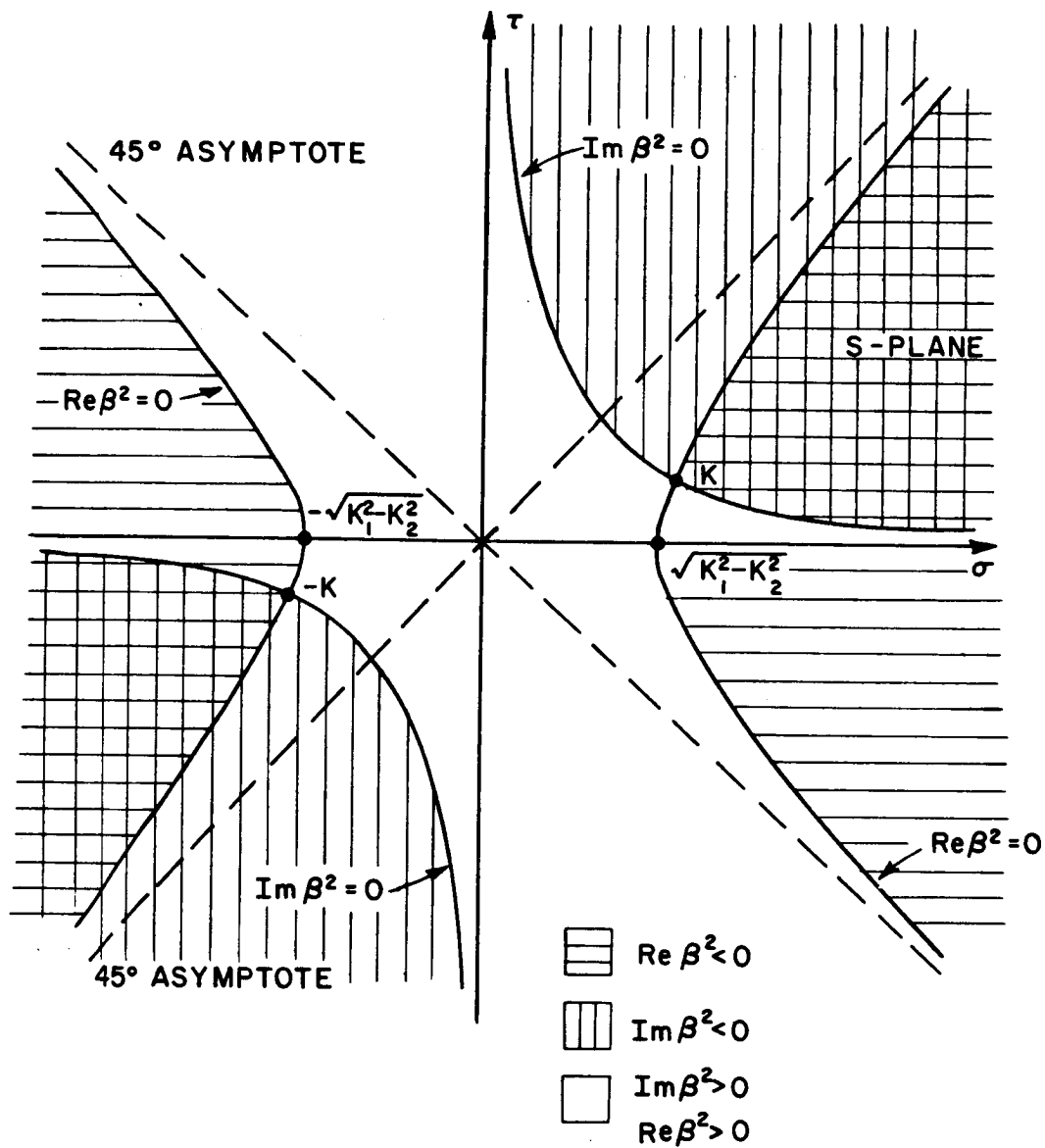


Figure C.1. Domain of $\beta = (K^2 - s^2)^{1/2}$.

on the top-sheet. This dictates that along the branch cut

$$\text{Arg} (\beta^2) = 2\pi \quad . \quad (\text{C.17})$$

It follows that the branch cut is described by the equations

$$\text{Im} (\beta^2) = 0 \quad \text{and} \quad \text{Re} (\beta^2) > 0 \quad . \quad (\text{C.18})$$





Thus, the branch cut of the function β depicted in Figure C.2 has been uniquely determined. It follows from Equation (C.16) that

$$2\pi < \text{Arg} (\beta^2) < 4\pi \quad (\text{C.18})$$

and $\text{Im} (\beta) < 0$ on the entire bottom sheet as required. The bottom sheet is shown in Figure C.3 and the signs of $\text{Re} (\beta)$ and $\text{Im} (\beta)$ on the entire two-sheeted s -plane are summarized in Table C.1. For the special case of $k_2 = 0$, the two sheets of the s -plane are depicted in Figures C.4 and C.5.

TABLE C.1

SIGNS OF $\text{Re} (\beta)$ and $\text{Im} (\beta)$

$\text{Re} (\beta)$			$\text{Im} (\beta)$
TOP SHEET		-	+
		+	
BOTTOM SHEET		+	-
		-	

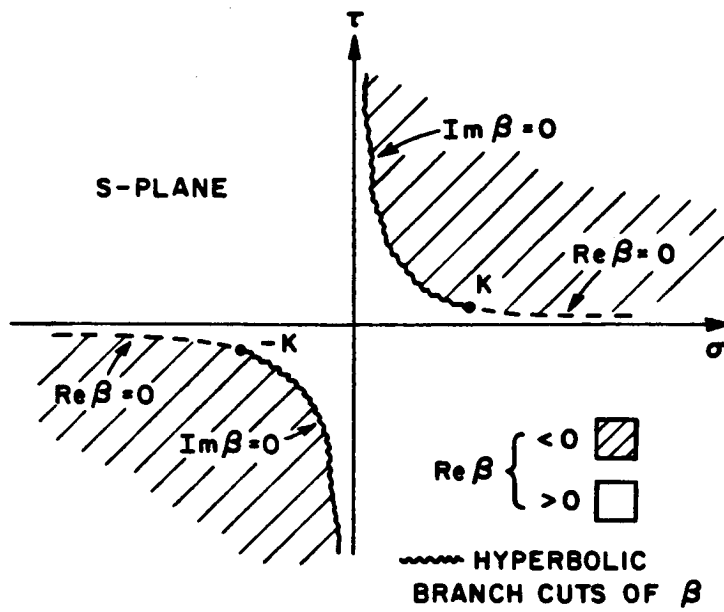


Figure C.2. Top sheet: $\text{Im}(\beta) > 0$.

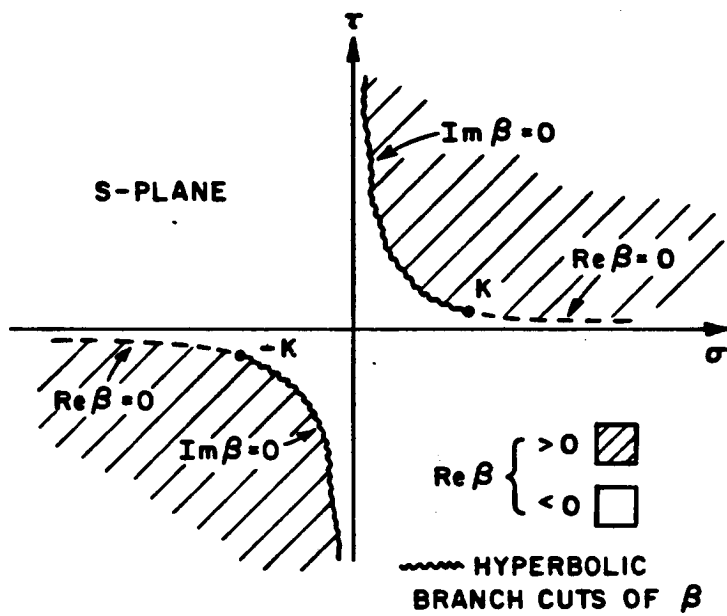


Figure C.3. Bottom sheet: $\text{Im}(\beta) < 0$.

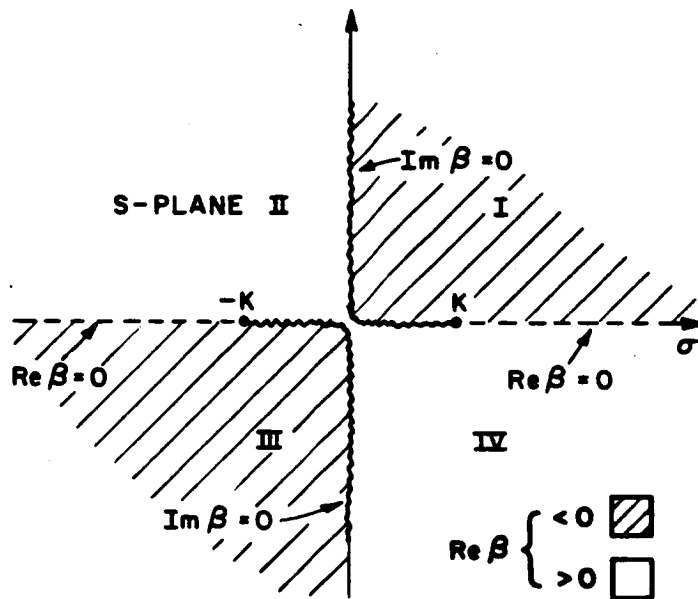


Figure C.4. Top sheet: $\text{Im}(\beta) > 0$, $K = K_1$.

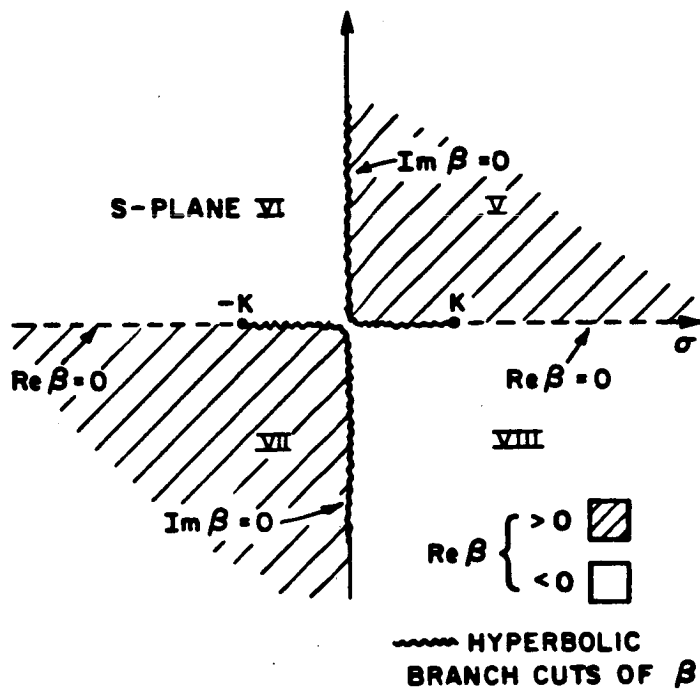


Figure C.5. Bottom sheet: $\text{Im}(\beta) < 0$, $K = K_1$.

APPENDIX D

FACTORIZATION OF THE FUNCTIONS $G^e(s)$ AND $G^0(s)$

The factorization of a function $G(s)$, which is regular and free of zeros in a strip $\tau_- < \tau < \tau_+$, means that $G(s)$ can be expressed as the product of two functions such that

$$G(s) = G_+(s) G_-(s) \quad (D.1)$$

where $G_+(s)$ and $G_-(s)$ are regular and free of zeros in the upper and lower half s -planes $\text{Im}(s) > \tau_-$, and $\text{Im}(s) < \tau_+$, respectively. There is a formal procedure for obtaining $G_+(s)$ and $G_-(s)$ [32,34]. That is, if $G(s)$ has the properties mentioned above, and $G(s) \rightarrow 1$ uniformly as $|s| \rightarrow \infty$ inside the strip $\tau_- < \text{Im}(s) < \tau_+$, then [32,34]

$$G_+(s) = \exp \left[\frac{1}{2\pi i} \int_{-\infty + ic}^{\infty + ic} \frac{\text{Log}[G(u)]}{u-s} du \right], \quad \tau_- < c < \tau < \tau_+ \quad (D.2)$$

is regular and free of zeros in the upper half s -plane defined by $\text{Im}(s) > \tau_-$, and

$$G_-(s) = \exp \left[\frac{-1}{2\pi i} \int_{-\infty + id}^{\infty + id} \frac{\text{Log}[G(u)]}{u-s} du \right], \quad \tau_- < \tau < d < \tau_+ \quad (D.3)$$

is regular and free of zeros in the lower half s -plane defined by $\text{Im}(s) < \tau_+$. Note that a branch of the logarithm is chosen so that $\lim_{|s| \rightarrow \infty} \text{Log}[G(s)] = 0$ within the strip $\tau_+ < \tau < \tau_-$. Furthermore, the functions

$G_+(s)$ and $G_-(s)$ have the following properties:

$$G_-(s) = G_+(-s) \quad (\text{D.4})$$

and each tends to unity in that half-plane in which it is analytic [37].

1. EVEN Function

In this case, the function $G^e(s)$ is given by

$$G^e(s) = \frac{\beta}{\beta + k\delta} \quad (\text{D.5})$$

which is regular in the strip defined by $-\text{Im}(K) < \text{Im}(s) < \text{Im}(K)$. Define the function $\psi(s)$ as

$$\psi(s) = G^{e-1}(s) = 1 + \frac{K\delta}{\beta} \quad (\text{D.6})$$

where β was defined in Appendix C. The function $\psi(s)$ will be factorized into the product of the functions $\psi_+(s)$ and $\psi_-(s)$ such that

$$\psi(s) = \psi_+(s) \psi_-(s) \quad (\text{D.7})$$

It follows from D.7 that

$$G_+^e(s) = \psi_+^{-1}(s) \quad (\text{D.8})$$

and

$$G_-^e(s) = \psi_-^{-1}(s) \quad (\text{D.9})$$

The first step in the factorization of $\psi(s)$ is to take the logarithm of (D.7), that is

$$\text{Log}[\psi(s)] = \text{Log}[\psi_+(s)] + \text{Log}[\psi_-(s)] \quad . \quad (\text{D.10})$$

As suggested by Weinstein [37], it is easier to factorize the function $\psi'(s)/\psi(s)$. Thus, taking the derivative of (D.10), one gets

$$X(s) = \frac{\psi'(s)}{\psi(s)} = \frac{\psi'_+(s)}{\psi_+(s)} + \frac{\psi'_-(s)}{\psi_-(s)} = X_+(s) + X_-(s) \quad . \quad (\text{D.11})$$

Substituting (D.6) into (D.11) yields

$$X(s) = \frac{K\delta s}{\beta^2(\beta + K\delta)} \quad . \quad (\text{D.12})$$

Note that the branch points $\pm K$ of β are also poles of $X(s)$. Thus, the factorization of the function $\psi(s)$ reduces to the decomposition of $X(s)$.

It follows from [32,37], that

$$X_-(s) = \frac{-1}{2\pi i} \int_{-\infty+id}^{\infty+id} \frac{X(u)}{u-s} du \quad , \quad \tau_- < \tau < d < \tau_+ \quad (\text{D.13})$$

and

$$X_+(s) = \frac{1}{2\pi i} \int_{-\infty+ic}^{\infty+ic} \frac{X(u)}{u-s} du \quad , \quad \tau_- < c < \tau < \tau_+ \quad (\text{D.14})$$

where $\tau_- = -\text{Im}(K)$ and $\tau_+ = \text{Im}(K)$. The function $X_-(s)$ will be computed first, followed by $X_+(s)$. First of all, the path of integration is deformed upward in (D.13), so that it encloses the branch cut $K \rightarrow i\infty$ as shown in Figure D.1. Next, assume there is a pole u_p (that is,

$\beta(u_p) = -K\delta$ enclosed by the contour. Note that u_p is enclosed by the contour if $\text{Im}(K\delta) < 0$. Then,

$$X_-(s) = 2\pi i [\text{Res}(u_p) + \text{Res}(+K)] - \int_{\Gamma} - \int_{c_1} - \int_{c_2} \quad (\text{D.15})$$

where the contours Γ , c_1 , and c_2 are depicted in Figure D.1. It can be shown that the integration along the contour Γ does not contribute to $X_-(s)$, that is

$$\int_{\Gamma} \frac{X(u)}{u-s} du = 0 \quad . \quad (\text{D.16})$$

Define the constant ξ such that

$$\cos \xi = \delta \quad 0 < \text{Re}(\xi) < \pi/2 \quad (\text{D.17})$$

where $\text{Im}(\delta) < 0$ implies $\text{Im}(\xi) > 0$. It follows from (C.1) that

$$u_p = K \sin \xi \quad . \quad (\text{D.18})$$

Now, the residues at u_p and $+K$ can be computed such that

$$\text{Res}(+K) = \frac{1}{2\pi i 2(K-s)} \quad (\text{D.19})$$

and

$$\text{Res}(u_p) = \frac{-1}{2\pi i (K \sin \xi - s)} \quad . \quad (\text{D.20})$$

Substituting (D.19) and (D.20) into (D.15) yields

$$X_-(s) = \frac{1}{2(K-s)} + \frac{1}{s - K \sin \xi} + \frac{K\delta}{\pi i} \int_{c_2} \frac{udu}{\beta(u-s)(\beta^2 - K^2 \delta_e^2)} \quad . \quad (\text{D.21})$$

Note that along the contour c_2 , $\text{Im}(\beta) = 0$, and $\text{Re}(\beta) > 0$.

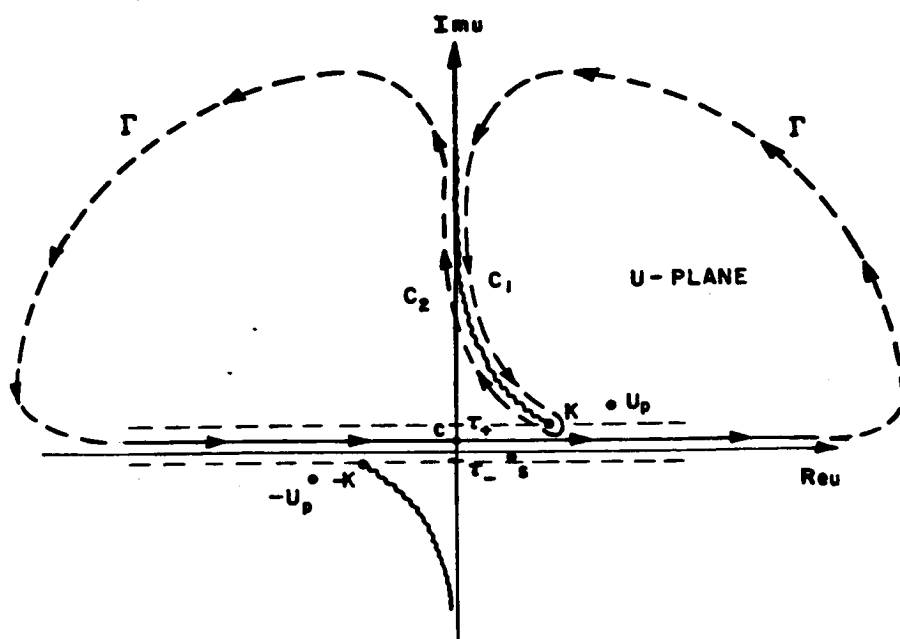


Figure D.1. Integration path of Equation D.15.

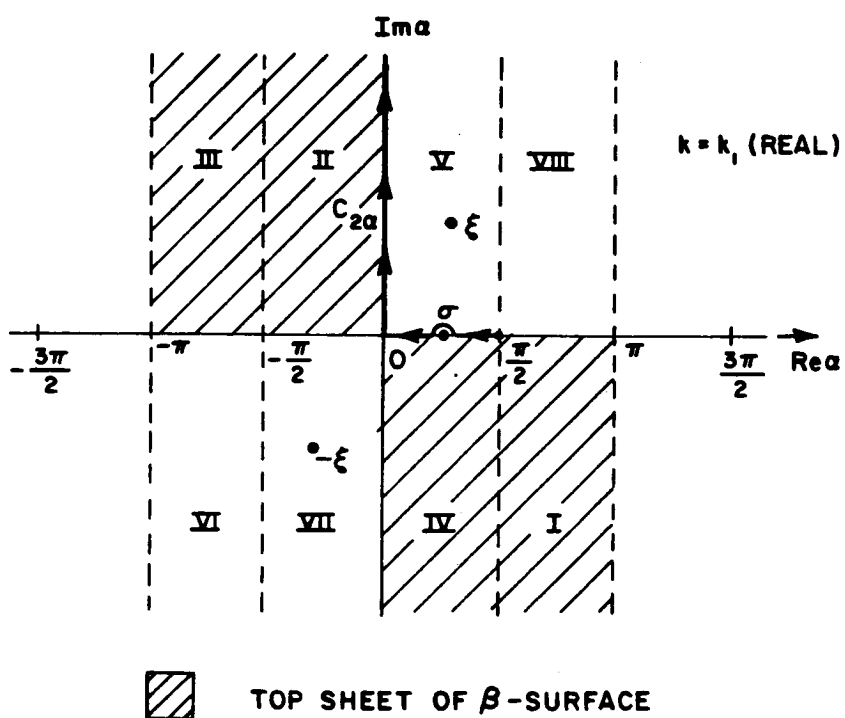


Figure D.2. Integration path of Equation D.25 in periodic α -plane.

The next step in the analysis is to map from the u -plane to the α -plane.

That is,

$$u = K \sin \alpha \quad , \quad -\pi < \operatorname{Re}(\alpha) < \pi \quad (\text{D.22})$$

$$\beta = K \cos \alpha \quad (\text{D.23})$$

and

$$s = K \sin \tilde{\sigma} \quad (\text{D.24})$$

where it is assumed that $\operatorname{Im}(K)=0$ for convenience. The mapping in (D.22) and (D.23) is discussed in more detail in Appendix F. Substituting (D.22), (D.23) and (D.24) into (D.21), the last term in (D.21) becomes

$$\frac{K\delta}{\pi i} \int_{c_2} \frac{udu}{\beta(u-s)(\beta^2-K^2\delta^2)} = \frac{-\cos \xi}{\pi i K} \int_{c_{2\alpha}} \frac{\sin \alpha d\alpha}{(\sin \alpha - \sin \tilde{\sigma})(\sin^2 \alpha - \sin^2 \xi)} \quad (\text{D.25})$$

where $c_{2\alpha}$ is shown in Figure D.2. Evaluating the integral along $c_{2\alpha}$, one finally gets [37]

$$X_-(s) = \frac{1}{2(K-s)} + \frac{1}{2(s-K\sin)} - \frac{1}{2\pi K \cos \tilde{\sigma}} \left[\frac{\tilde{\sigma} + \xi}{\sin(\tilde{\sigma} + \xi)} - \frac{\pi + \tilde{\sigma} - \xi}{\sin(\pi + \tilde{\sigma} - \xi)} \right] \quad (\text{D.26})$$

Substituting (D.26) into (D.11), and integrating $X_-(s)$, one obtains

$$\psi_-(K \sin \alpha) = \left[\frac{\sin \xi - \sin \alpha}{1 - \sin \alpha} \right]^{1/2} \exp \left[\frac{-1}{2\pi} J(\alpha) \right], \quad 0 < \operatorname{Re}(\xi) < \pi/2 \quad (\text{D.27})$$

where

$$J(\alpha) = \int_{\alpha + \pi - \xi}^{\alpha + \xi} \frac{t}{\sin t} dt \quad (\text{D.28})$$

Note that the fact that $\psi_-(-i\infty) = 1$ has been used to obtain (D.27).

Using the identity $\psi_+(s) = \psi_-(-s)$, it follows that $\psi_+(s)$ is given by

$$\psi_+(Ks\alpha) = \left[\frac{\sin\xi + s\alpha}{1 + s\alpha} \right]^{1/2} \exp \left[\frac{-1}{2\pi} J(-\alpha) \right], \quad 0 \leq \text{Re}(\xi) \leq \pi/2. \quad (\text{D.29})$$

Substituting (D.27) and (D.29) into (D.9) and (D.8), respectively, yields

$$G_+^e(Ks\alpha) = \left[\frac{1 + s\alpha}{\sin\xi + s\alpha} \right]^{1/2} \exp \left[\frac{1}{2\pi} J(-\alpha) \right], \quad 0 \leq \text{Re}(\xi) \leq \pi/2 \quad (\text{D.30})$$

which is regular in the upper half s-plane defined by $\text{Im}(s) > -\text{Im}(K)$, and

$$G_-^e(Ks\alpha) = \left[\frac{1 - s\alpha}{\sin\xi - s\alpha} \right]^{1/2} \exp \left[\frac{1}{2\pi} J(\alpha) \right], \quad 0 \leq \text{Re}(\xi) \leq \pi/2 \quad (\text{D.31})$$

is regular in the lower half s-plane $\text{Im}(s) < \text{Im}(K)$.

2. ODD Function

The odd function is given by

$$G^o(s) = \frac{1}{\beta + K\delta} = \frac{G^e(s)}{\beta} \quad (\text{D.32})$$

Note that the function β can be expressed as

$$\beta = (K-s)^{1/2} (K+s)^{1/2} \quad (\text{D.33})$$

where $(K-s)^{1/2}$ is analytic in the lower half s -plane defined by $\text{Im}(s) < \text{Im}(K)$, while $(K+s)^{1/2}$ is analytic in the upper s -plane $\text{Im}(s) > -\text{Im}(K)$. Substituting (D.33) into (D.32) yields

$$G^0(s) \frac{G_+^e(s)}{(K+s)^{1/2}} - \frac{G_-^e(s)}{(K-s)^{1/2}} = 0. \quad (\text{D.34})$$

It follows from (D.30), (D.31), and (D.34) that

$$G_+^0(K \sin \alpha) = \frac{\exp[1/2\pi J(-\alpha)]}{[K(\sin \xi + \sin \alpha)]^{1/2}}, \quad 0 < \text{Re}(\xi) < \pi/2 \quad (\text{D.35})$$

is regular in the upper half s -plane $\text{Im}(s) > -\text{Im}(K)$, and

$$G_-^0(K \sin \alpha) = \frac{\exp[1/2\pi J(\alpha)]}{[K(\sin \xi - \sin \alpha)]^{1/2}}, \quad 0 < \text{Re}(\xi) < \pi/2 \quad (\text{D.36})$$

is regular in the lower half s -plane $\text{Im}(s) < \text{Im}(K)$.

APPENDIX E

DECOMPOSITION OF THE FUNCTIONS $D^e(s)$ AND $D^o(s)$

The decomposition of the function $D(s)$, which is regular in the strip $\tau_- < \text{Im}(s) < \tau_+$, means that $D(s)$ can be expressed as the sum of two functions $D_+(s)$ and $D_-(s)$ such that

$$D(s) = D_+(s) + D_-(s) \quad (\text{E.1})$$

where $D_+(s)$ and $D_-(s)$ are regular in the upper and lower half s -plane defined by $\tau > \tau_-$ and $\tau < \tau_+$, respectively.

There is a formal procedure for obtaining (E.1) [32,34], however, for the functions needed in this study, the decomposition can be achieved by inspection. First, the function in Equation (3.62) will be considered, followed by the one defined in (3.128).

1. EVEN Function

The function $D^e(s)$ is given by

$$D^e(s) = \Phi^e(s) G_+^e(s) = \frac{ivk'_y(1-R_e) G_+^e(s)}{\sqrt{2\pi} \beta (s+k_x)} \quad (\text{E.2})$$

where $G_+^e(s)$, which was computed in Appendix D, is regular in the half-plane $\text{Im}(s) > -\text{Im}(k)$. Substituting (3.83) into (E.2) yields

$$D^e(s) = \frac{ivk_y'(1-R_e)}{\sqrt{2\pi} k \delta_e} \left[\frac{-G_+^e(s)}{(s+k_x')} + \frac{1}{G_-^e(s) (s+k_x')} \right] \quad (E.3)$$

where $\tau_- = -\text{Im}(k_x')$, $\tau_+ = \text{Im}(k)$, and $G_-^e(s)$ is regular in the lower half plane $\text{Im}(s) < \text{Im}(k)$. The second term in (E.3) can be rewritten as follows:

$$\frac{1}{G_-^e(s) (s+k_x')} = \frac{1}{(s+k_x')} \left[\frac{1}{G_-^e(s)} - \frac{1}{G_-^e(-k_x')} \right] + \frac{1}{(s+k_x') G_-^e(-k_x')} \quad (E.4)$$

Substituting (E.4) into (E.3), one obtains

$$D^e(s) = \frac{ivk_y'(1-R_e)}{\sqrt{2\pi} k \delta_e} \left[\frac{1}{(s+k_x')} \left[\frac{1}{G_-^e(-k_x')} - G_+^e(s) \right] + \frac{1}{(s+k_x')} \left[\frac{1}{G_-^e(s)} - \frac{1}{G_-^e(-k_x')} \right] \right] \quad (E.5)$$

After studying carefully the expression in (E.5), one concludes that the first term in (E.5) is regular in the upper half-plane $\text{Im}(s) > \tau_-$, while the second term is regular in the lower half-plane $\text{Im}(s) < \tau_+$. Thus, $D_+^e(s)$ and $D_-^e(s)$ are given by

$$D_+^e(s) = \frac{ivk_y'(1-R_e)}{\sqrt{2\pi} k \delta_e} \left[\frac{1}{(s+k_x')} - \frac{G_+^e(s)}{G_-^e(-k_x')} \right] \quad (E.6)$$

and

$$D_-^e(s) = \frac{ivk_y'(1-R_e)}{\sqrt{2\pi} k \delta_e (s+k_x')} \left[\frac{1}{G_-^e(s)} - \frac{1}{G_-^e(-k_x')} \right] \quad (E.7)$$

2. ODD Function

It follows from (3.128) that

$$D^0(s) = \Phi^0(s) G_+^0(s) = \frac{v}{\sqrt{2\pi}} (1+R_0) i \frac{\beta}{(s+k_x')} G_+^0(s) \quad (E.8)$$

where $G_+^0(s)$, which is defined in Appendix D, is regular in the upper half-plane $\text{Im}(s) > -\text{Im}(k)$. Solving for β in (3.121), one gets

$$\beta = \frac{1}{G^0(s)} - k \delta_0 \quad (E.9)$$

Substituting (E.9) into (E.8) yields

$$D^0(s) = \frac{vi(1+R_0)}{\sqrt{2\pi}} \left[\frac{1}{(s+k_x') G_-^0(s)} - \frac{k \delta_0 G_+^0(s)}{(s+k_x')} \right] \quad (E.10)$$

where $G_-^0(s)$, which is also defined in Appendix D, is regular in the lower half-plane $\text{Im}(s) < \text{Im}(k)$. The first term in (E.10) can be rewritten as follows:

$$\frac{1}{(s+k_x') G_-^0(s)} = \frac{1}{(s+k_x')} \left[\frac{1}{G_-^0(s)} - \frac{1}{G_-^0(-k_x')} \right] + \frac{1}{(s+k_x') G_-^0(-k_x')} \quad (E.11)$$

Substituting (E.11) into (E.10), one obtains

$$D^0(s) = \frac{v i (1+R_0)}{\sqrt{2\pi}} \left[\frac{1}{(s+k'_x)} \left[\frac{1}{G_-^0(s)} - \frac{1}{G_-^0(-k'_x)} \right] + \frac{1}{(s+k'_x)} \left[\frac{1}{G_-^0(-k'_x)} - k \delta_0 G_+^0(s) \right] \right] \quad (E.12)$$

It follows from (E.12) that $D_+^0(s)$ is given by

$$D_+^0(s) = \frac{i v (1+R_0)}{(s+k'_x) \sqrt{2\pi}} \left[\frac{1}{G_-^0(-k'_x)} - k \delta_0 G_+^0(s) \right] \quad (E.13)$$

which is regular in the upper half-plane defined by $\text{Im}(s) > \tau_-$, and $D_-^0(s)$ can be expressed as follows:

$$D_-^0(s) = \frac{i v (1+R_0)}{\sqrt{2\pi} (s+k'_x)} \left[\frac{1}{G_-^0(s)} - \frac{1}{G_-^0(-k'_x)} \right] \quad (E.14)$$

which is regular in the lower half-plane defined by $\text{Im}(s) < \tau_+$.

APPENDIX F

ANGULAR SPECTRAL MAPPING

1. Mapping to the periodic ψ -plane.

To simplify the analysis, assume that $K=K_1$ is real, that is, $\text{Im}(K)=K_2=0$. Next, let

$$s = K \sin \psi \quad (F.1)$$

where s was defined in (C.2) and ψ is given by

$$\psi = u + iv \quad (F.2)$$

Substituting (F.2) and (C.2) into (F.1) yields

$$\sigma = K \sin u \cosh v \quad ; \quad \tau = K \cos u \sinh v \quad (F.3)$$

It follows from (C.1) and (F.1) that

$$\beta = \beta_r + i\beta_I = (K^2 - K^2 \sin^2 \psi)^{1/2} = K \cos \psi \quad (F.4)$$

where

$$\beta_r = K \cos u \cosh v \quad ; \quad \beta_I = -K \sin u \sinh v \quad (F.5)$$

Note that Equations (F.3) and (F.5) map a finite-width strip (width of 2π) in the ψ -plane to the entire two-sheeted plane of $\beta(s)$ depicted in Figures (C.4) and (C.5).

In order to have a one-to-one mapping, the real part of ψ is restricted to the interval $-\pi < \text{Re}(\psi) \leq \pi$. This can be achieved by an inverse mapping from the two-sheeted plane of $\beta(s)$ to the ψ -plane. The inverse mapping can be obtained by solving for ψ in terms of s and $\beta(s)$ such that

$$\cos \psi = \frac{\beta}{K} \quad (\text{F.6})$$

and

$$i \sin \psi = \frac{is}{K} \quad (\text{F.7})$$

Adding (F.6) and (F.7), one gets

$$\cos \psi + i \sin \psi = e^{i\psi} = \frac{\beta + is}{K} \quad (\text{F.8})$$

Taking the logarithm of both sides of (F.8) and dividing by i yields

$$\psi = -i \text{Log} \left[\frac{\beta + is}{K} \right] \quad (\text{F.9})$$

where

$$\text{Log}(z) = \text{Log}|z| + i \text{Arg}(z) \quad ; \quad -\pi < \text{Arg}(z) < \pi \quad (\text{F.10})$$

It follows from (F.9) and (F.10) (or from (F.3) and (F.5)) that the two-sheeted plane of $\beta(s)$ maps to the ψ -plane as shown in Figure (F.1). The top-sheet maps into the region indicated with cross-hatching, and the branch cuts of $\beta(s)$ in the s -plane become the lines depicted in Figure (F.1). It is obvious that the effect of the mapping is to open up the function $\beta(s)$ so that the branch cuts of $\beta(s)$ are replaced by lines in the ψ -plane.

One of the reasons for mapping into the ψ -plane is that it is easier and more natural to perform the asymptotic evaluation of the inverse Fourier-Transform in the ψ -plane. This mapping is usually referred to as the Angular Spectral mapping.

2. Mapping to the w -plane

In order to have the saddle point of the integrands in the inverse-Fourier Transform integrals equal to the observation angle ϕ , it is necessary to make one more mapping, which is a simple translation of the imaginary axis of ψ . That is, let w be equal to

$$w = \alpha + i\gamma = \psi + \frac{\pi}{2} = u + \frac{\pi}{2} + iv \quad . \quad (F.11)$$

Substituting (F.11) into (F.1) and (F.4) yields

$$s = -K \cos w = -K \cos(\alpha + i\gamma) \quad (F.12)$$

and

$$\beta = K \sin w = K \sin(\alpha + i\gamma) \quad . \quad (F.13)$$

Expanding Equations (F.12) and (F.13) one obtains

$$\sigma = -K \cos \alpha \cosh \gamma \quad , \quad \tau = K \sin \alpha \sinh \gamma \quad (F.14)$$

$$\beta_r = K \sin \alpha \cosh \gamma \quad , \quad \beta_I = K \cos \alpha \sinh \gamma \quad . \quad (F.15)$$

The w -plane is depicted in Figure 3.7. Note that the real part of w is restricted to the interval

$$-\frac{\pi}{2} < \text{Re}(w) = \alpha < \frac{3\pi}{2} \quad . \quad (F.16)$$

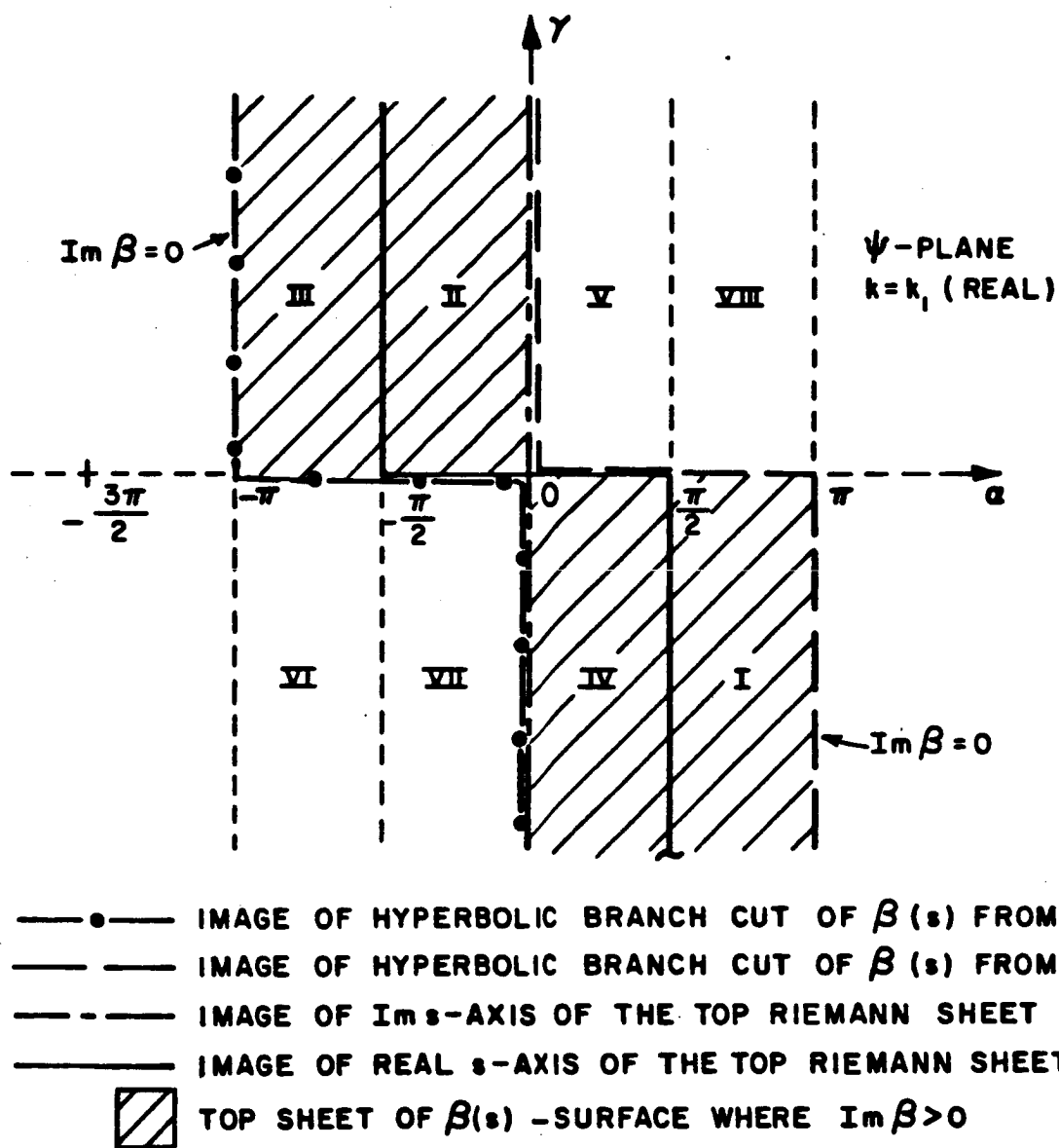


Figure F.1. Periodic ψ -plane.

APPENDIX G

SADDLE POINT METHOD I

1. One Pole Near Saddle Point

In this section a method is discussed for evaluating a particular integral by the saddle point approximation technique. This method is discussed in more detail in [38].

Assume that the integral is of the form

$$I(K) = \int_C M(z) e^{Kf(z)} dz \quad (G.1)$$

where K is real and positive, and the path C is chosen so that the integral converges. Let z_s be an isolated, first order saddle point of the analytic function $f(z)$. That is,

$$f'(z_s) = 0 \quad \text{and} \quad f''(z_s) \neq 0 \quad . \quad (G.2)$$

Also assume that $M(z)$ is an analytic function, except at a finite number of singular points which are not close to the point z_s . Furthermore, assume $M(z)$ has one simple pole z_1 close to the saddle point. Next, define the transformation

$$f(z) = f(z_s) - u^2 \quad (G.3)$$

from the z -plane to the u -plane, where the descending part of C is mapped onto the positive real u -axis. It follows from (G.3) that

$$I(K) = e^{Kf(z_s)} \int_{-\infty}^{\infty} M(z) \frac{dz}{du} e^{-Ku^2} du \quad (G.4)$$

where one assumes that $\frac{dz}{du}$ has no poles close to the saddle point.

Therefore, the function $N_1(u)$ given by

$$N_1(u) = \left[M(z) \frac{dz}{du} \right] (u-u_1) \quad (G.5)$$

is analytic in the neighborhood of u_1 and $u=0$, which means that it can be expanded in a Taylor series such that

$$N_1(u) = \sum_{m=0}^{\infty} A_m u^m \quad (G.6)$$

Now, define a_1 such that

$$a_1 = i [f(z_s) - f(z_1)] \quad (G.7)$$

Substituting (G.6) into (G.4), and assuming K is large, yields

$$I_s(K) \sim e^{Kf(z_s)} \sum_{m=0}^{\infty} A_m I_m \quad (G.8)$$

where

$$I_m = \int_{-\infty}^{\infty} \frac{u^m e^{-Ku^2} (u+u_1) du}{u^2 + ia_1} \quad (G.9)$$

In practice, usually the first term in (G.8) is computed. That is, for K sufficiently large

$$I_s(K) \sim \exp(Kf(z_s)) A_0 I_0 \quad (G.10)$$

It is shown in [38] that

$$A_0 = N_1(0) = -u_1 M(z_s) \left| \left[\frac{-2}{f''(z_s)} \right]^{1/2} \right| e^{i\phi_s} \quad (G.11)$$

and

$$I_0 = 2 u_1 e^{ika_1} \left[\frac{\pi}{a_1} \right]^{1/2} \int_0^\infty e^{-it^2} dt \quad (G.12)$$

$(Ka_1)^{1/2}$

where ϕ_s is depicted in Figure G.1. Substituting (G.11) and (G.12) into (G.10) yields

$$I_s(K) \sim M(z_s) \exp(Kf(z_s)) \left| \left[\frac{-2\pi}{Kf''(z_s)} \right]^{1/2} \right| e^{i\phi_s} F(Ka_1) \quad (G.13)$$

where $F(Ka_1)$, which is referred to as the transition function [11], is defined given in (3.197). In order for $F(x)$ to converge, the argument of $x^{1/2}$ is restricted to [41] $-3\pi/4 < \arg(x^{1/2}) < \pi/4$.

2. Two poles near the saddle point

Now assume $M(z)$ has two poles, z_1 and z_2 , near the saddle point z_s . In this case, the function $N_2(u)$ given by

$$N_2(u) = M(z) \frac{dz}{du} (u-u_1) (u-u_2) \quad (\text{G.14})$$

is analytic in the neighborhood of $u=0$, u_1 , and u_2 . Thus, $N_2(u)$ can be expanded in a Taylor series such that

$$N_2(u) = \sum_{m=0}^{\infty} c_m u^m \quad (\text{G.15})$$

around the point $u=0$. Substituting (G.15) into (G.4) and for large K , one obtains

$$I_s(K) \sim \exp(Kf(z_s)) \sum_{m=0}^{\infty} c_m \tilde{I}_m \quad (\text{G.16})$$

where

$$\tilde{I}_m = \int_{-\infty}^{\infty} \frac{u^m e^{-Ku^2}}{(u-u_1)(u-u_2)} du \quad (\text{G.17})$$

and

$$a_2 = i [f(z_s) - f(z_2)] \quad (\text{G.18})$$

The denominator of the integrand in (G.17) can be expanded in partial fractions such that

$$\frac{1}{(u-u_1)(u-u_2)} = \frac{1}{u-u_1} \left[\frac{u+u_1}{u^2+ia_1} - \frac{u+u_2}{u^2+ia_2} \right] \quad (\text{G.19})$$

Thus, \tilde{I}_m can be rewritten as follows:

$$\tilde{I}_m = \frac{1}{u_1 - u_2} \int_{-\infty}^{\infty} u^m e^{-Ku^2} \left[\frac{u+u_1}{u^2+ia_1} - \frac{u+u_2}{u^2+ia_2} \right] du \quad . \quad (G.20)$$

Again, keeping only the first term in (G.16), $I_s(K)$ is given by

$$I_s(K) \sim \exp(Kf(z_s)) c_0 \tilde{I}_0 \quad (G.21)$$

where

$$\begin{aligned} \tilde{I}_0 = \frac{2(\pi)^{1/2}}{u_1 - u_2} & \left[u_1 \frac{e^{iKa_1}}{(a_1)^{1/2}} \int_{-\infty}^{\infty} \frac{e^{-it^2}}{(Ka_1)^{1/2}} dt \right. \\ & \left. - \frac{e^{iKa_2}}{(a_2)^{1/2}} u_2 \int_{-\infty}^{\infty} \frac{e^{-it^2}}{(Ka_2)^{1/2}} dt \right] \quad . \quad (G.22) \end{aligned}$$

The constant c_0 is easily evaluated by setting $z=z_s$ ($u=0$) in (G.14) such that

$$c_0 = N_2(0) = M(z_s) \frac{dz}{du} \Big|_{z=z_s} (-u_1)(-u_2) \quad . \quad (G.23)$$

Furthermore, it is shown in [38] that

$$\frac{dz}{du} \Big|_{z=z_s} = \left| \left[\frac{-2}{f''(z_s)} \right]^{1/2} \right| e^{i\phi_s} \quad . \quad (G.24)$$

Substituting (G.22)-(G.24) into (G.21) yields

$$I_s(K) \sim M(z_s) \exp(Kf(z_s)) e^{i\phi_s} \left| \frac{-2\pi}{Kf''(z_s)} \right|^{1/2} \left| \frac{(Ka_2)^{1/2} F(Ka_1) - (Ka_1)^{1/2} F(Ka_2)}{(Ka_2)^{1/2} - (Ka_1)^{1/2}} \right|$$

(G.25)

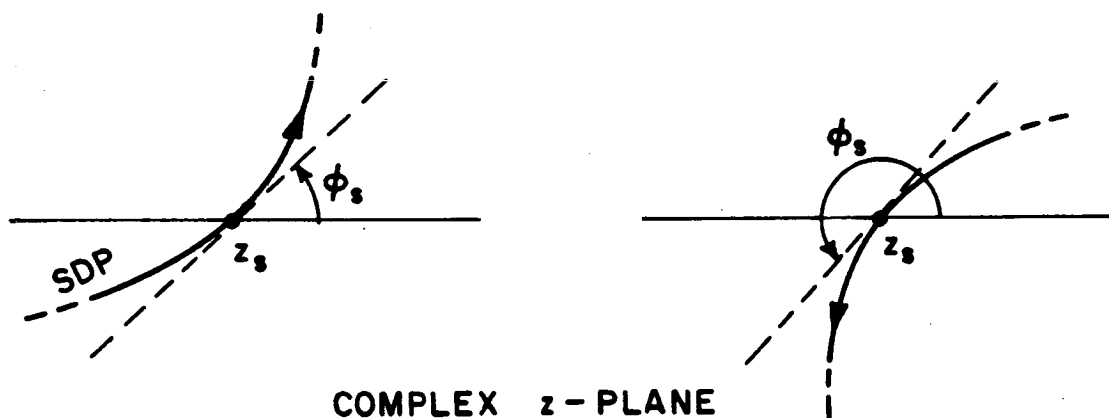


Figure G.1. Definition of the angle ϕ_s . The direction of integration along the path SDP is indicated by the arrowhead.

(Figure copied from: Proceedings of the IEEE Vol. 55, August 1967, pp. 1496-1497, R.H. Schafer, R.G. Kouyoumjian)

APPENDIX H
SADDLE POINT METHOD II
(One Pole Near Saddle Point)

In this section, the evaluation of (3.231), when the saddle point z_s is $z_s = \pi$, is discussed. The saddle point method used here is the one developed by Felsen and Marcuvitz [42]. It is shown in [42], that the first term in the asymptotic expansion of (G.1) when a simple pole z_1 of $M(z)$ is near the saddle point, is given by

$$I_s(K) \sim \exp(Kf(z_s)) \left[\pm 2ia\sqrt{\pi} e^{-Kb^2} Q[\mp ib\sqrt{K}] + \left(\frac{\pi}{K}\right)^{1/2} T(0) \right],$$

$$\text{Im}(b) \geq 0, K \rightarrow \infty \quad (\text{H.1})$$

where

$$a = \lim_{z \rightarrow z_1} [M(z)(z - z_1)] \quad (\text{H.2})$$

$$b = (f(z_s) - f(z_1))^{1/2}; \quad h = \left[\frac{-2}{f''(z_s)} \right]^{1/2} = \left[\frac{2}{f''(z_s)} \right]^{1/2} e^{i\phi_s}$$

$$(\text{H.3})$$

$$T(0) = hM(z_s) + \frac{a}{b} \quad (\text{H.4})$$

and

$$Q(y) = \int_y^{\infty} e^{-x^2} dx \quad . \quad (H.5)$$

The argument of b is defined [42] so that $b \rightarrow \frac{z_1 - z_s}{h}$ as $z_1 \rightarrow z_s$.

Since the function $M_0(z)$, defined in (3.227) is equal to zero when $z_s = \pi$, it follows that

$$T(0) = \frac{a}{b} \quad . \quad (H.6)$$

Since $M_0(z)$ has two simple poles at $z_1 = \pi - \phi'$ and $z_2 = \pi + \phi'$ ($\phi' \neq 0$), the asymptotic evaluation of (3.231) is given by

$$I_s(K) \sim \exp(k\rho f(z_s)) \left[\begin{aligned} & 2ia_2\sqrt{\pi} \exp(-k\rho b_2^2) Q[-ib_2\sqrt{k\rho}] + (\pi/(k\rho))^{1/2} \frac{a_2}{b_2} \\ & - \left[-2ia_1\sqrt{\pi} \exp(-k\rho b_1^2) Q[ib_1\sqrt{k\rho}] + (\pi/(k\rho))^{1/2} \frac{a_1}{b_1} \right] \end{aligned} \right] \quad (H.7)$$

where

$$b_1 = -\sqrt{2} e^{i\pi/4} \sin(\phi'/2) \quad , \quad \text{Im}(b_1) < 0 \quad (H.8)$$

$$b_2 = \sqrt{2} e^{i\pi/4} \sin(\phi'/2) = -b_1 \quad , \quad \text{Im}(b_2) > 0 \quad (H.9)$$

and

$$f(z_s) = i \quad . \quad (H.10)$$

Since $b_2 = -b_1$, Equation (H.7) can be rewritten as follows:

$$I_s(K) \sim e^{ik\rho} \left[2i\sqrt{\pi} \exp(-k\rho b_2^2) Q[-ib_2\sqrt{k\rho}] + (\pi/(k\rho))^{1/2}/b_2 \right] (a_1 + a_2) . \quad (H.11)$$

Next, the constants a_1 and a_2 are evaluated. Substituting (3.227) into (H.2), one obtains

$$a_1 = \frac{-v}{2\pi i} \frac{\sin\phi'[(\sin\xi^0 - \cos\phi')(\sin\xi^0 + \cos\phi')]^{1/2}}{(\sin\phi' + \sin\xi^0)^2} \cdot \exp \left[\frac{-1}{2\pi} [J_1^0(\pi - \phi') + J_1^0(\phi')] \right] \quad (H.12)$$

and

$$a_2 = \frac{v}{2\pi i} \frac{\sin\phi'[(\sin\xi^0 - \cos\phi')(\sin\xi^0 + \cos\phi')]^{1/2}}{(\cos\xi^0 - \sin\phi')(\cos\xi^0 + \sin\phi')} \cdot \exp \left[\frac{-1}{2\pi} [J_1^0(\pi + \phi') + J_1^0(\phi')] \right] \quad (H.13)$$

where

$$b_2^2 = 2i \sin^2(\phi'/2) = i(1 - \cos\phi') \quad . \quad (H.14)$$

For large $|\sqrt{k\rho} b_2|$, the first term in (H.11) becomes [42]

$$2i\sqrt{\pi} \exp(-k\rho b_2^2) Q[-ib_2\sqrt{k\rho}] \sim -(\pi/(k\rho))^{1/2}/b_2 \text{ as } |\sqrt{k\rho} b_2| \rightarrow \infty. \quad (H.15)$$

Thus, when $|\sqrt{k\rho} b_2|$ is very large, $I_s(K)$ which is approximated by only the first term of its asymptotic expansion, approaches zero as expected.

APPENDIX I

EXPRESSIONS FOR $\hat{E}_{x,z}$ AND $\hat{H}_{x,z}$ IN TERMS OF \hat{H}_y AND \hat{E}_y

Evaluating Equations (1.1) and (1.2) in rectangular coordinates one obtains the following six equations:

$$ik\eta_0 H_z = \frac{\partial E_y}{\partial x} - \frac{\partial E_x}{\partial y} \quad (I.1)$$

$$ik\eta_0 H_y = \frac{\partial E_x}{\partial z} - \frac{\partial E_z}{\partial x} \quad (I.2)$$

$$ik\eta_0 H_x = \frac{\partial E_z}{\partial y} - \frac{\partial E_y}{\partial z} \quad (I.3)$$

$$ikY_0 E_z = \frac{\partial H_x}{\partial y} - \frac{\partial H_y}{\partial x} \quad (I.4)$$

$$ikY_0 E_y = \frac{\partial H_z}{\partial x} - \frac{\partial H_x}{\partial z} \quad (I.5)$$

$$ikY_0 E_x = \frac{\partial H_y}{\partial z} - \frac{\partial H_z}{\partial y} \quad (I.6)$$

Taking the Fourier transform of (I.1) through (I.6) with respect to x , and assuming all the field components have a z -dependence of the form $\exp(ik'_z z)$ yields

$$ik\eta_0\hat{H}_z = -is\hat{E}_y - \frac{\partial\hat{E}_x}{\partial y} \quad (I.7)$$

$$ik\eta_0\hat{H}_y = ik_z'\hat{E}_x + is\hat{E}_z \quad (I.8)$$

$$ik\eta_0\hat{H}_x = \frac{\partial\hat{E}_z}{\partial y} - ik_z'\hat{E}_y \quad (I.9)$$

$$ikY_0\hat{E}_z = \frac{\partial\hat{H}_x}{\partial y} + is\hat{H}_y \quad (I.10)$$

$$ikY_0\hat{E}_y = is\hat{H}_z - ik_z'\hat{H}_x \quad (I.11)$$

$$ikY_0\hat{E}_x = ik_z'\hat{H}_y - \frac{\partial\hat{H}_y}{\partial y} \quad (I.12)$$

Furthermore, it follows from (3.31) that

$$\frac{\partial^2\hat{E}_i}{\partial y^2} = \beta^2\hat{E}_i \quad \text{for } y > 0, \quad i = x, y, z \quad (I.13)$$

and

$$\frac{\partial^2\hat{H}_i}{\partial y^2} = -\beta^2\hat{H}_i \quad \text{for } y > 0, \quad i = x, y, z \quad (I.14)$$

Taking the derivative of both sides of (I.9) with respect to y and using (I.13) yields

$$ik\eta_0\frac{\partial\hat{H}_x}{\partial y} = -\beta^2\hat{E}_z - ik_z'\frac{\partial\hat{E}_y}{\partial y} \quad (I.15)$$

Substituting (I.15) into (I.10) and after some simplification one obtains

$$\hat{E}_z(s, y, z) = \frac{k\eta_0s\hat{H}_y(s, y, z) + ik_z'\frac{\partial\hat{E}_y(s, y, z)}{\partial y}}{(s^2 + k_z'^2)} \quad (I.16)$$

The expression for \hat{H}_z can be obtained in a similar fashion, however, it is easier to use duality [20]. That is, substituting (I.16) into (4.109) (where y is replaced by z), one obtains

$$\hat{H}_z(s,y,z) = \frac{ik_z' \frac{\partial \hat{H}_y(s,y,z)}{\partial y} - kY_0 s \hat{E}_y(s,y,z)}{(s^2 + k_z'^2)} \quad (I.17)$$

The first step in solving for \hat{E}_x in terms of \hat{E}_y and \hat{H}_y is to take the derivative of (I.17) with respect to y such that

$$\frac{\partial \hat{H}_z}{\partial y} = \frac{-ik_z' s \hat{H}_y - kY_0 s \frac{\partial \hat{E}_y}{\partial y}}{(s^2 + k_z'^2)} \quad (I.18)$$

where equation (I.14) has been used to simplify (I.18). Substituting Equation (I.18) into (I.12) and after some simplification, one gets

$$\hat{E}_x(s,y,z) = \frac{ik_z' \hat{H}_y(s,y,z) + sY_0 \frac{\partial \hat{E}_y(s,y,z)}{\partial y}}{iY_0 (s^2 + k_z'^2)} \quad (I.19)$$

Again, to get the expression for \hat{H}_x , one can follow a similar procedure as the one used to obtain \hat{E}_x . However, it is much simpler to use duality. Thus, substituting (I.19) into (4.109) (where y is replaced by x) yields

$$\hat{H}_x(s,y,z) = \frac{s\eta_0 \frac{\partial \hat{H}_y(s,y,z)}{\partial y} - ik_z' kE_y(s,y,z)}{i\eta_0 (s^2 + k_z'^2)} \quad (I.20)$$

APPENDIX J

CALCULATION OF THE FRESNEL REFLECTION COEFFICIENTS OF A GROUNDED DIELECTRIC/FERRITE SLAB USING THE TRANSVERSE RESONANCE METHOD

Figure (J.1) illustrates the geometry for the problem considered in this appendix. The dielectric/ferrite slab has a thickness t , and it can be backed by either a perfect electric conductor (PEC) or a perfect magnetic conductor (PMC). Region 1, which is characterized by (ϵ_1, μ_1) is the region $\tilde{y} > 0$, while Region 2, characterized by (ϵ_2, μ_2) is the region $-t < \tilde{y} < 0$. A plane wave is incident on the slab at an angle θ_1 from the y -axis. The transverse resonance method [21] models the geometric depicted in Figure J.1 by an equivalent transmission line circuit as shown in Figure J.2.

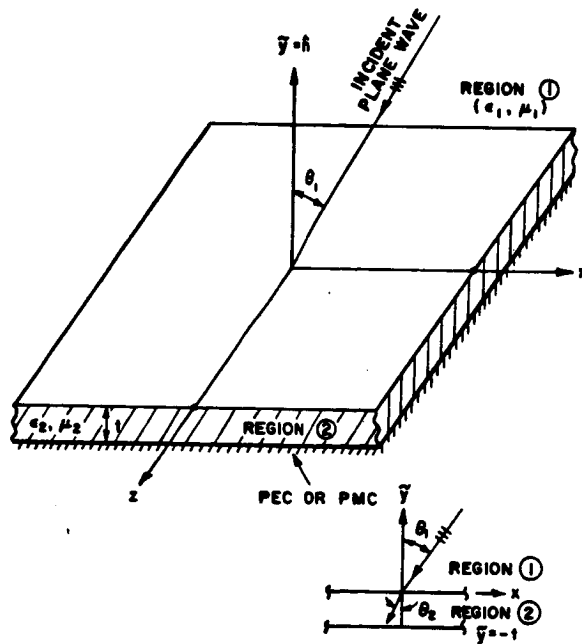


Figure J.1. Grounded Dielectric/ferrite slab.

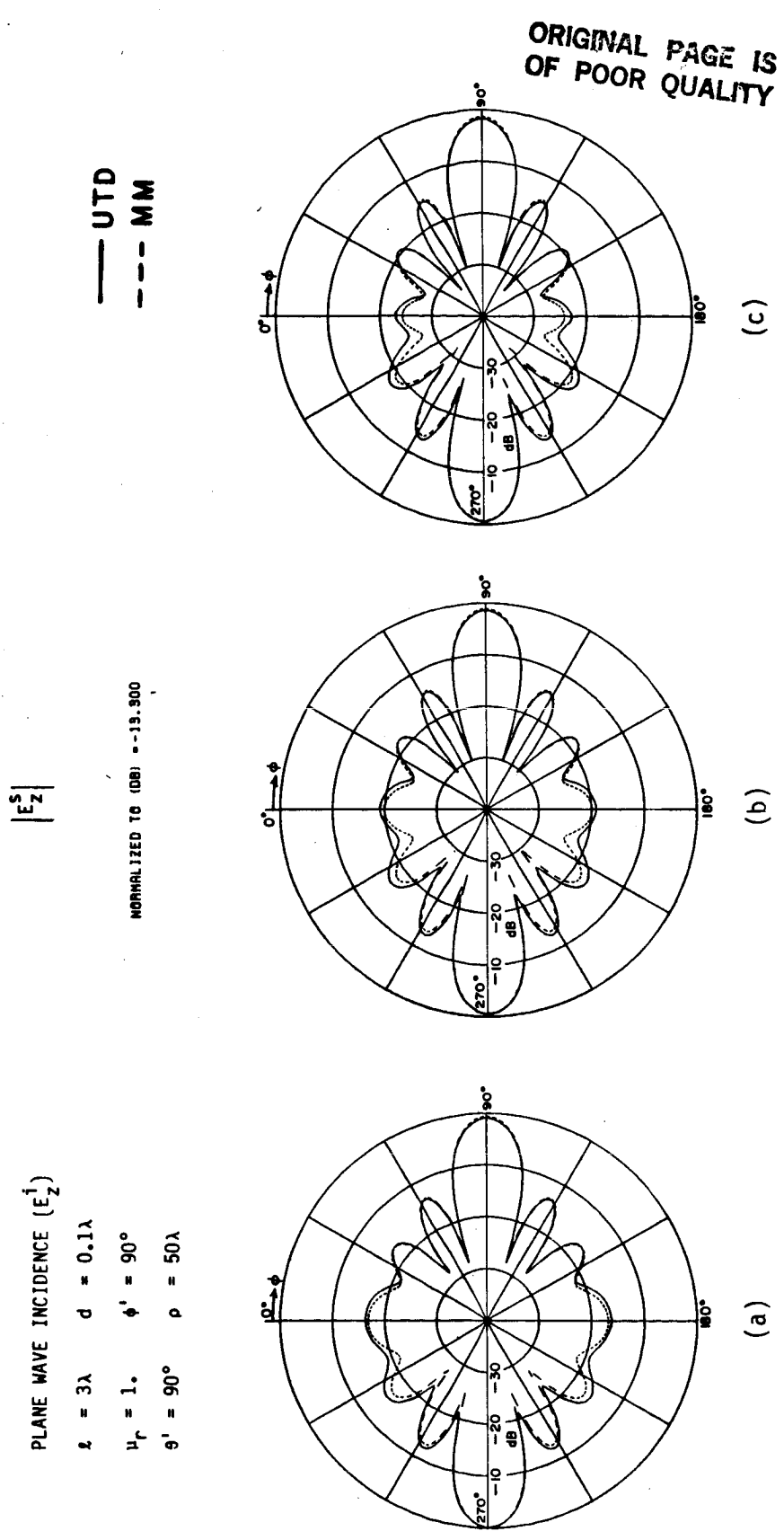


Figure 8.29. Magnitude of the scattered E_z^s field for the geometry depicted in Figure 8.2.

(a) $\epsilon_r = 3. + i0.$, (b) $\epsilon_r = 3. + i0.3$, (c) $\epsilon_r = 3. + i1.2$.

where

$$\hat{k}_1 = (-\hat{x}\sin\theta'\cos\phi' - \hat{y}\sin\theta'\sin\phi' - \hat{z}\cos\theta') k_1 \quad (J.4)$$

$$\cos\theta_1 = \sin\theta' \sin\phi' \quad . \quad (J.5)$$

It follows from Snell's law that

$$\sin\theta_1 = N \sin\theta_2 \quad (J.6)$$

where

$$N = \left[\frac{\epsilon_2 \mu_2}{\epsilon_1 \mu_1} \right]^{1/2} \quad . \quad (J.7)$$

The characteristic impedances for both polarizations are as follows:

$$\text{TE}_y \text{ wave } (H_y): Z_{1,2}^h = \frac{k_{1,2} \eta_{1,2}}{\beta_{1,2}} \quad (J.8)$$

$$\text{TM}_y \text{ wave } (E_y): Z_{1,2}^a = \frac{k_{1,2} \beta_{1,2}}{\eta_{1,2}} \quad (J.9)$$

where

$$\eta_{1,2} = \left[\frac{\mu_{1,2}}{\epsilon_{1,2}} \right]^{1/2} ; k_{1,2} = \omega(\epsilon_{1,2} \cdot \mu_{1,2})^{1/2} \quad (J.10)$$

$$\beta_1 = k_1 \cos\theta_1 \quad (J.11)$$

and

$$\beta_2 = k_2 \cos\theta_2 = k_2 (1 - \sin^2 \theta_2)^{1/2} = k_1 (N^2 - \sin^2 \theta_1)^{1/2} \quad (J.12)$$

Note that Z_s , the equivalent load impedance at $\tilde{y}=-t$ is given by

$$Z_s = \begin{cases} 0 & \text{for PEC} \\ \infty & \text{for PMC} \end{cases} \quad (J.13)$$

Substituting (J.13) into (J.1) yields

$$Z_{in}(\tilde{y}=0) = \begin{cases} -iZ_2 \tan(\beta_2 t) & \text{for PEC} \\ iZ_2 \cot(\beta_2 t) & \text{for PMC} \end{cases} \quad (J.14)$$

Next, the Fresnel reflection coefficients for both polarizations are computed.

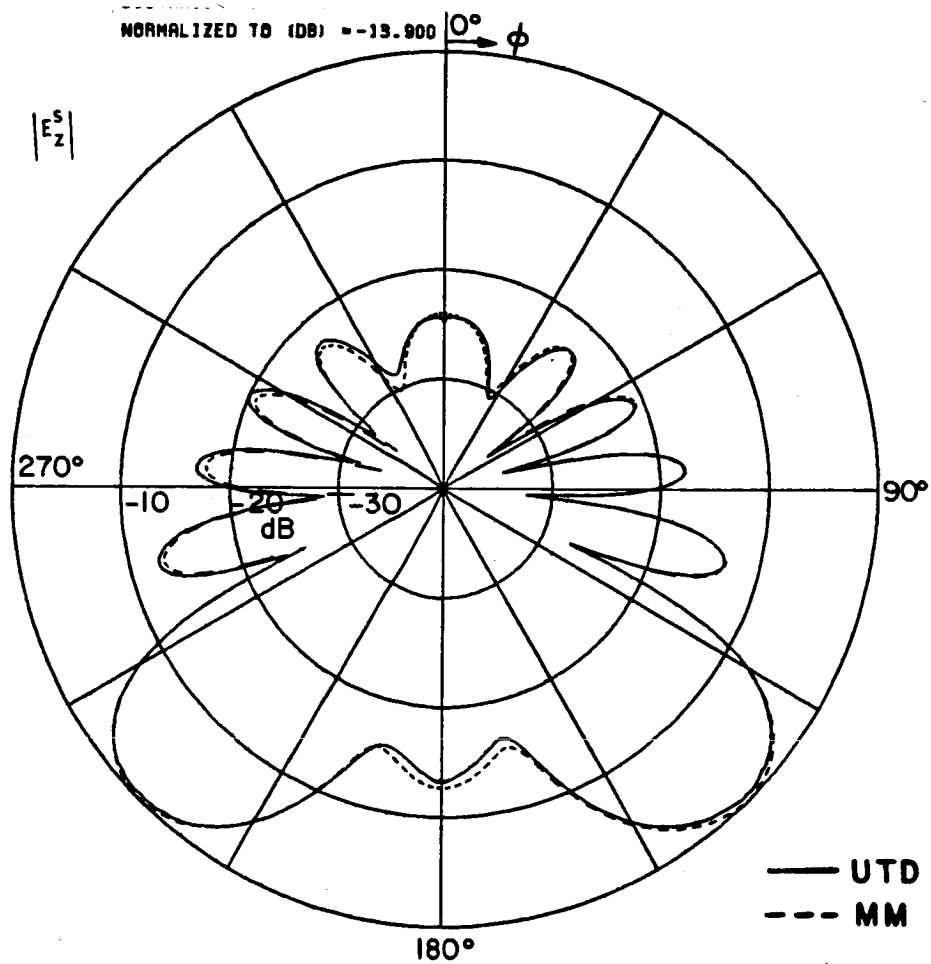
I. TE_y POLARIZATION (H_y)

The reflection coefficient for this polarization at $\tilde{y}=0$ can be written as follows:

$$R_h(\tilde{y}=0) = \frac{Z_{in}(\tilde{y}=0) - Z_1^h}{Z_{in}(\tilde{y}=0) + Z_1^h} = \left. \frac{H_y^r}{H_y^i} \right|_{\tilde{y}=0} \quad (J.15)$$

When there is an electric wall (PEC) at $\tilde{y}=-t$, the reflection coefficient is

$$R_h^0(\tilde{y}=0) = \frac{-iZ_2^h \tan(\beta_2 t) - Z_1^h}{-iZ_2^h \tan(\beta_2 t) + Z_1^h} \quad (J.16)$$



PLANE WAVE INCIDENCE (E_z^i)

$l = 3.0\lambda$ $d = 0.05\lambda$

$\epsilon_r = 5. + i0.5$ $\mu_r = 1.$

$\phi' = 45^\circ$ $\theta' = 90^\circ$

$\rho = 50\lambda$

Figure 8.31. Magnitude of the scattered field E_z^s with the diffracted surface wave field E_z^{dsw} included (see Figure 8.30).

When there is an electric wall (PEC) at $\tilde{y}=-t$, the reflection coefficient can be written as follows:

$$R_a^e(\tilde{y}=0) = \frac{Z_1^a + iZ_2^a \tan(\beta_2 t)}{Z_1^a - iZ_2^a \tan(\beta_2 t)} \quad (J.21)$$

Substituting (J.9) into (J.21), one obtains

$$R_a^e(\tilde{y}=0) = \frac{\cos\theta_1 + i \frac{\epsilon_1}{\epsilon_2} (N^2 - \sin^2 \theta_1)^{1/2} \tan[k_1 t (N^2 - \sin^2 \theta_1)^{1/2}]}{\cos\theta_1 - i \frac{\epsilon_1}{\epsilon_2} (N^2 - \sin^2 \theta_1)^{1/2} \tan[k_1 t (N^2 - \sin^2 \theta_1)^{1/2}]} \quad (J.22)$$

Finally, if there is a magnetic wall (PMC) at $\tilde{y}=-t$, the reflection coefficient becomes

$$R_a^o(\tilde{y}=0) = \frac{Z_1^a - iZ_2^a \cot(\beta_2 t)}{Z_1^a + iZ_2^a \cot(\beta_2 t)} \quad (J.23)$$

Substituting (J.9) into (J.23) yields

$$R_a^o(\tilde{y}=0) = \frac{\cos\theta_1 - i \frac{\epsilon_1}{\epsilon_2} (N^2 - \sin^2 \theta_1)^{1/2} \cot[k_1 t (N^2 - \sin^2 \theta_1)^{1/2}]}{\cos\theta_1 + i \frac{\epsilon_1}{\epsilon_2} (N^2 - \sin^2 \theta_1)^{1/2} \cot[k_1 t (N^2 - \sin^2 \theta_1)^{1/2}]} \quad (J.24)$$

APPENDIX K

RAY-FIXED COORDINATE SYSTEM FOR GO FIELDS

It is well known that the natural coordinate system for the GO fields is the one depicted in Figure 6.1. The propagation vector \vec{k}^i for the incident field defined in Equation (4.4) is given by

$$\vec{k}^i = k \hat{s}^i, \quad (K.1)$$

where

$$\hat{s}^i = -\hat{x} \sin \theta' \cos \phi' - \hat{y} \sin \theta' \sin \phi' - \hat{z} \cos \theta'. \quad (K.2)$$

It follows from (6.5) - (6.7) that the unit vectors $\{\hat{u}_{\parallel}^i, \hat{u}_{\perp}, \hat{u}_{\parallel}^r\}$, and \hat{s}^r are given by

$$\hat{u}_{\parallel}^i = \frac{-\hat{x} \sin^2 \theta' \sin \phi' \cos \phi' + \hat{y} (1 - \sin^2 \theta' \sin^2 \phi') - \hat{z} \sin \theta' \cos \phi' \sin \phi'}{|\hat{n} \times \hat{s}^i|} \quad (K.3)$$

$$\hat{u}_{\perp} = \frac{\hat{z} \sin \theta' \cos \phi' - \hat{x} \cos \theta'}{|\hat{n} \times \hat{s}^i|} \quad (K.4)$$

$$\hat{u}_{\parallel}^r = \frac{\hat{x} \sin^2 \theta' \sin \phi' \cos \phi' + \hat{y} (1 - \sin^2 \theta' \sin^2 \phi') + \hat{z} \sin \theta' \cos \phi' \sin \phi'}{|\hat{n} \times \hat{s}^i|} \quad (K.5)$$

and

$$\hat{s}^r = -\hat{x}\sin\theta'\cos\phi' + \hat{y}\sin\theta'\sin\phi' - \hat{z}\cos\theta' \quad , \quad (K.6)$$

where $\hat{n}=\hat{y}$, and

$$|\hat{n} \times \hat{s}'| = (1 - \sin^2\theta' \sin^2\phi')^{1/2} \quad . \quad (K.7)$$

Thus, the field components $E_{s'}^i$, E_{\parallel}^i , and E_{\perp}^i can be expressed as follows:

$$E_{s'}^i = (-E_x^i \sin\theta'\cos\phi' - E_y^i \sin\theta'\sin\phi' - E_z^i \cos\theta') \quad (K.8)$$

$$E_{\parallel}^i = (-E_x^i \sin^2\theta'\sin\phi'\cos\phi' + E_y^i (1 - \sin^2\theta'\sin^2\phi') - E_z^i \sin\theta'\cos\theta'\sin\phi') \frac{1}{|\hat{n} \times \hat{s}'|} \quad (K.9)$$

and

$$E_{\perp}^i = (-E_x^i \cos\theta' + E_z^i \sin\theta'\cos\phi') \frac{1}{|\hat{n} \times \hat{s}'|} \quad . \quad (K.10)$$

The fields E_x^i and E_z^i can be written in terms of E_y^i and H_y^i only such that

$$E_x^i = - \frac{\eta_0 \cos\theta' H_y^i + \sin^2\theta' \cos\phi' \sin\phi' E_y^i}{|\hat{n} \times \hat{s}'|^2} \quad (K.11)$$

$$E_z^i = \frac{\sin\phi' (\eta_0 \cos\phi' H_y^i - \cos\theta' \sin\phi' E_y^i)}{|\hat{n} \times \hat{s}'|^2} \quad . \quad (K.12)$$

Substituting (K.11) and (K.12) into (K.8) through (K.10) yields

$$E_{S'}^i = 0 \quad (K.13)$$

$$E_{\parallel}^i = \frac{E_y^i}{|\hat{n} \times \hat{s}'|} \quad (K.14)$$

$$E_{\perp}^i = \frac{\eta_0 H_y^i}{|\hat{n} \times \hat{s}'|} \quad (K.15)$$

where E_y^i and H_y^i were defined in (4.4) and (4.42), respectively.

Furthermore, the field components for the reflected field, that is, E_S^r , E_{\parallel}^r and E_{\perp}^r are given by

$$E_S^r = -E_X^r \sin\theta' \cos\phi' + E_Y^r \sin\theta' \sin\phi' - E_Z^r \cos\theta' \quad (K.16)$$

$$E_{\perp}^r = \frac{-\cos\theta' E_X^r + E_Z^r \sin\theta' \cos\phi'}{|\hat{n} \times \hat{s}'|} \quad (K.17)$$

$$E_{\parallel}^r = \frac{E_X^r \sin^2\theta' \sin\phi' \cos\phi' + E_Y^r (1 - \sin^2\theta' \sin^2\phi') + E_Z^r \sin\theta' \cos\theta' \sin\phi'}{|\hat{n} \times \hat{s}'|} \quad (K.18)$$

where

$$E_X^r = - \frac{\eta_0 \cos\theta' H_Y^r - \sin^2\theta' \cos\phi' \sin\phi' E_Y^r}{|\hat{n} \times \hat{s}'|^2} \quad (K.19)$$

$$E_z^r = \frac{\sin \theta'}{|\hat{n} \times \hat{s}'|^2} (E_y^r \cos \theta' \sin \phi' + \eta_0 \cos \phi' H_y^r) \quad (K.20)$$

Substituting (K.19) and (K.20) into (K.16) through (K.18) yields

$$E_s^r = 0 \quad (K.21)$$

$$E_{\perp}^r = \frac{\eta_0 H_y^r}{|\hat{n} \times \hat{s}'|} \quad (K.22)$$

$$E_{\parallel}^r = \frac{E_y^r}{|\hat{n} \times \hat{s}'|} \quad (K.23)$$

It follows from (6.3) and (6.4) that

$$\vec{E}^r(x,y,z) = \left[E_{cy} \hat{u}_{\parallel}^r \left[\frac{\tilde{R}_a^e + \tilde{R}_a^o}{2} \right] + H_{cy} \hat{u}_{\perp} \eta_0 \left[\frac{\tilde{R}_h^e + \tilde{R}_h^o}{2} \right] \right] \frac{e^{i\vec{k}^r \cdot \vec{r}}}{|\hat{n} \times \hat{s}'|} \quad (K.24)$$

and

$$\vec{E}^i(x,y,z) = (\hat{u}_{\parallel}^i E_{cy} + \eta_0 \hat{u}_{\perp} H_{cy}) \frac{e^{i\vec{k}^i \cdot \vec{r}}}{|\hat{n} \times \hat{s}'|} \quad (K.25)$$

where

$$\vec{k}^r = k \hat{s}^r \quad (K.26)$$

$$\vec{r} = \hat{x} x + \hat{y} y + \hat{z} z \quad (K.27)$$

Let \vec{r}_r be the point of reflection (QR) on the x-z plane, that is

$$\vec{r}_r = \hat{x} x_r' + \hat{z} z_r' \quad . \quad (K.28)$$

It follows from (K.28) that

$$\vec{k}^i - \vec{r}_r = -k(x_r' \sin\theta' \cos\phi' - z_r' \cos\theta') \quad (K.29)$$

and

$$\vec{r} = \vec{r}_r + \hat{s}^r s^r \quad (K.30)$$

where s^r is the distance from the point of reflection QR to the observation point. Substituting (K.30) into (K.27), one obtains

$$x = x_r' - s^r \sin\theta' \cos\phi' \quad (K.31)$$

$$y = s^r \sin\theta' \sin\phi' \quad (K.32)$$

$$z = z_r' - s^r \cos\theta' \quad . \quad (K.33)$$

Solving for s^r from (K.32) yields

$$s^r = \frac{y}{\sin\theta' \sin\phi'} \quad , \quad y > 0 \quad . \quad (K.34)$$

It follows from (K.29) through (K.34) that

$$\vec{k}^r \cdot \vec{r} = k \hat{s}^r \cdot \vec{r}_r + s^r k = k \hat{s}' \cdot \vec{r}_r + k s^r = \vec{k}^i \cdot \vec{r}_r + k s^r \quad . \quad (K.35)$$

Finally, substituting (K.35) into (K.24), one gets

$$E(\vec{s}^r) = E^i(QR) \cdot \frac{1}{R} e^{i k s^r} \quad (K.36)$$

where

$$\vec{E}^i(QR) = \hat{u}_\parallel^i E_\parallel^i(QR) + \hat{u}_\perp^i E_\perp^i(QR) \quad (K.37)$$

and

$$\vec{R} = \hat{u}_\parallel^i \hat{u}_\parallel^r \left[\frac{\tilde{R}_a^e + \tilde{R}_a^o}{2} \right] + \hat{u}_\perp^i \hat{u}_\perp^r \left[\frac{\tilde{R}_h^e + \tilde{R}_h^o}{2} \right] \quad (K.38)$$

Following the same procedure as above, it can be shown that the transmitted field can be written as follows:

$$\vec{E}^t(s^t) = \vec{E}^i(QR) \cdot \vec{T} e^{iks^t} \quad (K.39)$$

where

$$\vec{T} = \hat{u}_\parallel^i \hat{u}_\parallel^t \left[\frac{\tilde{R}_a^e - \tilde{R}_a^o}{2} \right] + \hat{u}_\perp^i \hat{u}_\perp^t \left[\frac{\tilde{R}_h^e - \tilde{R}_h^o}{2} \right] \quad (K.40)$$

and s^t is the distance from (QR) to the observation point.

APPENDIX L

RAY-FIXED COORDINATE SYSTEM FOR DIFFRACTED FIELD

The ray fixed coordinate system for the diffracted fields is depicted in Figure 6.6. It follows from Equations (6.25) through (6.28) that

$$\hat{s}' = -\hat{x} \sin \beta_0' \cos \phi' - \hat{y} \sin \beta_0' \sin \phi' + \hat{z} \cos \beta_0' = -\hat{R}' \quad (\text{L.1})$$

$$\hat{\phi}' = -\hat{x} \sin \phi' + \hat{y} \cos \phi' \quad (\text{L.2})$$

$$\hat{\beta}' = \hat{x} \cos \phi' \cos \beta_0' + \hat{y} \cos \beta_0' \sin \phi' + \hat{z} \sin \beta_0' \quad (\text{L.3})$$

Therefore, the field components $E_{s'}^i$, $E_{\phi'}^i$, and $E_{\beta'}^i$ can be expressed as follows:

$$E_{s'}^i = -E_x^i \sin \beta_0' \cos \phi' - E_y^i \sin \beta_0' \sin \phi' + E_z^i \cos \beta_0' \quad (\text{L.4})$$

$$E_{\phi'}^i = -E_x^i \sin \phi' + E_y^i \cos \phi' \quad (\text{L.5})$$

$$E_{\beta'}^i = E_x^i \cos \phi' \cos \beta_0' + E_y^i \cos \beta_0' \sin \phi' + E_z^i \sin \beta_0' \quad (\text{L.6})$$

The field components E_x^i and E_y^i can be expressed in terms of E_z^i and H_z^i only. Thus, it follows from (4.186) that

$$E_x^i = \frac{1}{\sin \theta'} (\eta_0 \sin \phi' H_z^i - \cos \theta' \cos \phi' E_z^i) \quad (\text{L.7})$$

$$E_y^i = -\frac{1}{\sin\theta'} (\eta_0 \cos\phi' H_z^i + \cos\theta' \sin\phi' E_z^i) \quad (L.8)$$

where $\theta' = \pi - \beta_0'$. Substituting (L.7) and (L.8) into (L.4) - (L.6) yields

$$E_{s'}^i = 0 \quad (L.9)$$

$$E_{\phi'}^i = \frac{-\eta_0 H_z^i}{\sin\beta_0'} \quad (L.10)$$

$$E_{\beta'}^i = \frac{E_z^i}{\sin\beta_0'} \quad (L.11)$$

Next, the fields E_s^d , E_ϕ^d , and E_β^d are computed. The unit vector \hat{s} and $\hat{\beta}$ depicted in Figure (L.1) can be expressed in terms of the spherical unit vectors \hat{R} and $\hat{\theta}$ as follows:

$$\hat{s} = -\hat{R} \cos(\theta+\theta') + \hat{\theta} \sin(\theta+\theta') \quad (L.12)$$

$$\hat{\beta} = -\hat{\theta} \cos(\theta+\theta') - \hat{R} \sin(\theta+\theta') \quad (L.13)$$

The point of diffraction QE is given by

$$z_d = \frac{R \sin(\theta+\theta')}{\sin\theta'}, \quad 0 < \theta' < \pi \quad (L.14)$$

and s , which is the distance from the point of diffraction QE to the observation point (P), is equal to

$$s = \frac{R \sin \theta}{\sin \theta'} , \quad 0 < \theta' < \pi \quad . \quad (L.15)$$

It follows from (L.12) and (L.13) that

$$E_S^d = -E_R^d \cos(\theta + \theta') + E_\theta^d \sin(\theta + \theta') \quad (L.16)$$

and

$$E_\beta^d = -E_R^d \sin(\theta + \theta') - E_\theta^d \cos(\theta + \theta') \quad . \quad (L.17)$$

Furthermore, it can be shown that

$$E_R^d = E_Z^d \left[\cos \theta + \frac{\cos \theta' \sin \theta}{\sin \theta'} \right] \quad (L.18)$$

$$E_\theta^d = E_Z^d \left[\frac{\cos \theta' \cos \theta}{\sin \theta'} - \sin \theta \right] \quad (L.19)$$

and

$$E_\phi^d = \frac{\eta_0 H_Z^d}{\sin \beta_0} \quad . \quad (L.20)$$

Substituting (L.18) and (L.19) into (L.16) and (L.17) yields

$$E_S^d = 0 \quad (L.21)$$

$$E_\beta^d = \frac{-E_Z^d}{\sin \beta_0} \quad . \quad (L.22)$$

Thus, the diffracted fields E_ϕ^d and E_β^d are given by

$$\begin{bmatrix} E_{\phi}^d \\ E_{\beta}^d \end{bmatrix} = \begin{bmatrix} \tilde{D}_{h1}^d & -\cos\beta_0' \tilde{D}_{h2}^d \\ -\cos\beta_0' \tilde{D}_{a1}^d & \tilde{D}_a^d \end{bmatrix} \begin{bmatrix} E_{\phi}^0 \\ E_{\beta}^0 \end{bmatrix} \frac{e^{-ikR\cos(\theta+\theta')}}{(1-\sin^2\theta'\sin^2\phi)\sqrt{\rho}} \quad (L.23)$$

Furthermore, it follows from (L.14) and (L.15) that

$$E_{\phi}^0 e^{-ikR\cos(\theta+\theta')} = E_{\phi}^0 e^{+ik_z z_d} e^{iks} = E_{\phi}^{i,(QE)} e^{iks} \quad (L.24)$$

$$E_{\beta}^0 e^{-ikR\cos(\theta+\theta')} = E_{\beta}^0 e^{+ik_z z_d} e^{iks} = E_{\beta}^{i,(QE)} e^{iks} \quad (L.25)$$

and

$$|\hat{n} \times \hat{s}|^2 = |\hat{y} \times \hat{s}|^2 = (1-\sin^2\theta'\sin^2\phi) \quad (L.26)$$

$$\sqrt{\rho} = \sqrt{R\sin\theta} = \sqrt{\sin\beta_0'} \left[\frac{R\sin\theta}{\sin\beta_0'} \right]^{1/2} = \sqrt{\sin\beta_0'} \sqrt{s} \quad (L.27)$$

Substituting (L.24) - (L.27) into (L.23), one obtains

$$\begin{bmatrix} E_{\phi}^d(s) \\ E_{\beta}^d(s) \end{bmatrix} = \begin{bmatrix} \tilde{D}_{h1}^d & -\cos\beta_0' \tilde{D}_{h2}^d \\ -\cos\beta_0' \tilde{D}_{a1}^d & \tilde{D}_{a2}^d \end{bmatrix} \begin{bmatrix} E_{\phi}^{i,(QE)} \\ E_{\beta}^{i,(QE)} \end{bmatrix} \frac{e^{-iks}}{\sqrt{s}} \quad (L.28)$$

where

$$\begin{aligned} \tilde{D}_{hi}^d(\phi, \phi', \beta_0') &= 1/2 [\tilde{D}_{ze}^{hi}(|\phi|, \phi', \beta_0') + \tilde{D}_{zo}^{hi}(|\phi|, \phi', \beta_0') \text{sign}\phi], \\ i &= 1, 2, \\ 0 &< \beta_0' < \pi, \\ -\pi &< \phi < \pi \end{aligned} \quad (L.29)$$

$$\begin{aligned}\tilde{D}_{ai}^d(\phi, \phi', \beta_0') &= 1/2 [\tilde{D}_{ze}^{ai}(|\phi|, \phi', \beta_0') + \tilde{D}_{zo}^{ai}(|\phi|, \phi', \beta_0') \text{sign} \phi], \\ i &= 1, 2, \\ 0 &< \beta_0' < \pi, \\ -\pi &< \phi < \pi\end{aligned}\quad (\text{L.30})$$

$$\begin{aligned}\tilde{D}_{ze}^{h1} &= \{ \cos \phi \tilde{D}_{ye}^{da}(\phi, \phi', \beta_0') [\cos \phi' - (\cos \phi + \cos \phi')] \tilde{F}_2^{ce} \\ &+ \cos^2 \beta_0' \sin \phi \sin \phi' \tilde{D}_{yo}^{dh}(\phi, \phi', \beta_0') [1 - (\cos \phi + \cos \phi')] \tilde{F}_3^{ce} \} / |\hat{n} \times \hat{s}|^2\end{aligned}\quad (\text{L.31})$$

$$\begin{aligned}\tilde{D}_{ze}^{h2} &= \{ \sin \phi \tilde{D}_{yo}^{dh}(\phi', \phi, \beta_0') [\cos \phi' - (\cos \phi + \cos \phi')] \tilde{F}_1^{ce} \\ &+ \cos \phi \tilde{D}_{ye}^{da}(\phi', \phi, \beta_0') [-\sin \phi' + (\cos \phi + \cos \phi')] \tilde{F}_4^{ce} \} / |\hat{n} \times \hat{s}|^2\end{aligned}\quad (\text{L.32})$$

$$\begin{aligned}\tilde{D}_{zo}^{a1} &= \{ \cos \phi \tilde{D}_{yo}^{dh}(\phi', \phi, \beta_0') [\cos \phi' - (\cos \phi + \cos \phi')] \tilde{F}_1^{ce} \\ &+ \cos^2 \beta_0' \sin \phi \tilde{D}_{ye}^{da}(\phi', \phi, \beta_0') [\sin \phi' - (\cos \phi + \cos \phi')] \tilde{F}_4^{ce} \} / |\hat{n} \times \hat{s}|^2\end{aligned}\quad (\text{L.33})$$

$$\begin{aligned}\tilde{D}_{zo}^{a2} &= \{ \cos \phi \sin \phi' \tilde{D}_{yo}^{dh}(\phi', \phi, \beta_0') [1 - (\cos \phi + \cos \phi')] \tilde{F}_3^{ce} \\ &+ \sin \phi \tilde{D}_{ye}^{da}(\phi', \phi, \beta_0') [-\cos \phi' + (\cos \phi + \cos \phi')] \tilde{F}_2^{ce} \} / |\hat{n} \times \hat{s}|^2\end{aligned}\quad (\text{L.34})$$

$$\tilde{D}_{ye}^{da}(\phi, \phi', \beta_0') = \frac{-e^{i\pi/4} (1 - \tilde{R}_a^e)/2 [(\sin \tilde{\xi}^{ae} - \cos \phi)(\sin \tilde{\xi}^{ae} - \cos \phi')]^{1/2}}{\sqrt{2\pi k} \sin \beta_0' (\sin \phi + \cos \tilde{\xi}^{ae})}$$

$$\cdot \exp(-(\tilde{J}_1^{ae}(\phi) + \tilde{J}_1^{ae}(\phi'))/(2\pi)) \cdot (\sec(\beta^+/2)F(-KL a^+) + \sec(\beta^-/2)F(-KL a^-))$$

(L.35)

$$\tilde{D}_{yo}^{dh}(\phi, \phi', \beta_0') = \frac{-e^{i\pi/4} (1 + \tilde{R}_h^o)/2 [(\sin \tilde{\xi}^{ho} - \cos \phi)(\sin \tilde{\xi}^{ho} - \cos \phi')]^{1/2}}{\sqrt{2\pi k} \sin \beta_0' (\sin \phi + \cos \tilde{\xi}^{ho})}$$

$$\cdot \exp(-(\tilde{J}_1^{ho}(\phi) + \tilde{J}_1^{ho}(\phi'))/(2\pi)) \cdot (\sec(\beta^-/2)F(-KL a^-) - \sec(\beta^+/2)F(-KL a^+))$$

(L.36)

$$L = s \sin^2 \beta_0' \quad (L.37)$$

$$\tilde{F}_1^{ce}(\phi', \beta_0') = \cos \phi' F_1^{ce} + 2 \cos^2 \beta_0' \cos(\phi'/2) \sin(\phi') F_2^{ce} \quad (L.38)$$

$$\tilde{F}_2^{ce}(\phi', \beta_0') = \cos \phi' F_3^{ce} + \cos^2 \beta_0' \sin \phi' F_4^{ce} \quad (L.39)$$

$$\tilde{F}_3^{ce}(\phi', \beta_0') = F_1^{ce} - F_2^{ce} \cos \phi' / \sin(\phi'/2) \quad (L.40)$$

$$\tilde{F}_4^{ce}(\phi', \beta_0') = \sin \phi' F_3^{ce} - \cos \phi' F_4^{ce} \quad (L.41)$$

$$F_1^{ce}(\phi', \beta_0') = \sin \beta_0' (\sin \beta_0' \cos \phi' - i \cos \beta_0' |\bar{A}_{ce}| / |\bar{B}_{ce}|) / |\hat{n} \times \hat{s}'|^2 \quad (L.42)$$

$$F_3^{ce}(\phi', \beta_0') = \sin \beta_0' (\sin \beta_0' \cos \phi' + i \cos \beta_0' |\bar{A}_{ce}| / |\bar{B}_{ce}|) / |\hat{n} \times \hat{s}'|^2 \quad (L.43)$$

$$F_2^{ce}(\phi', \beta_0') = \frac{\sin \beta_0' \cos \xi^{ae} (\sin \phi' + \cos \xi^{\tilde{ho}}) \exp([J_1^{\tilde{ho}}(\phi') - J_1^{ae}(\phi')]/(2\pi))}{|\hat{n} \times \hat{s}'|^2 k |\bar{B}_{ce}| (\sin \phi' + \cos \xi^{ae}) (1 + \sin \beta_0' \cos \xi^{ae})} \\ \cdot \sqrt{2K^-} ((\sin \xi^{ae} - \cos \phi') / (\sin \xi^{\tilde{ho}} - \cos \phi'))^{1/2} / \sin \phi' \quad (L.44)$$

$$F_4^{ce}(\phi', \beta_0') = \frac{2 \sin(\phi'/2) (\sin \phi' + \cos \xi^{\tilde{ae}}) \exp([J_1^{ae}(\phi') - J_1^{\tilde{ho}}(\phi')]/(2\pi))}{|\hat{n} \times \hat{s}'|^2 k |\bar{B}_{ce}| (\sin \phi' + \cos \xi^{\tilde{ho}}) (1 + \sin \beta_0' \cos \xi^{\tilde{ho}})} \\ \cdot \sqrt{2K^-} ((\sin \xi^{\tilde{ho}} - \cos \phi') / (\sin \xi^{ae} - \cos \phi'))^{1/2} / \cos(\xi^{ae}) \quad (L.45)$$

$$\tilde{D}_{zo}^{h1}(\tilde{\xi}^{ao}, \tilde{\xi}^{he}) = \tilde{D}_{zo}^{a1}(\tilde{\xi}^{ho}, \tilde{\xi}^{ae}) \quad (L.46)$$

$$\tilde{D}_{zo}^{h2}(\tilde{\xi}^{ao}, \tilde{\xi}^{he}) = -\tilde{D}_{zo}^{a2}(\tilde{\xi}^{ho}, \tilde{\xi}^{ae}) \quad (L.47)$$

$$\tilde{D}_{ze}^{a1}(\tilde{\xi}^{ao}, \tilde{\xi}^{he}) = \tilde{D}_{ze}^{h1}(\tilde{\xi}^{ho}, \tilde{\xi}^{ae}) \quad (L.48)$$

$$\tilde{D}_{ze}^{a2}(\tilde{\xi}^{ao}, \tilde{\xi}^{he}) = -\tilde{D}_{ze}^{h2}(\tilde{\xi}^{ho}, \tilde{\xi}^{ae}) \quad (L.49)$$

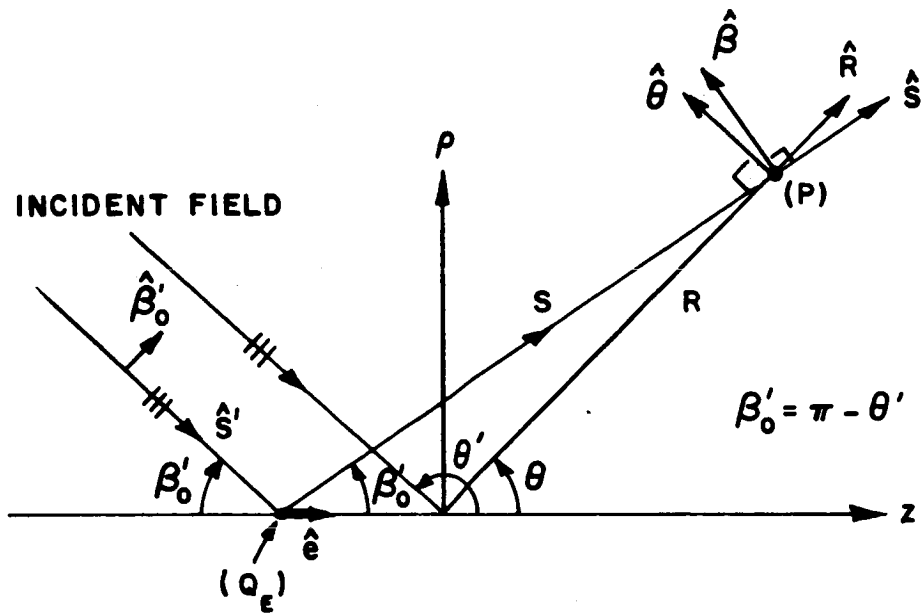


Figure L.1 Relationship between the unit vectors $\hat{\theta}$, $\hat{\beta}$, \hat{R} and \hat{s} .

REFERENCES

- [1] T.B.A. Senior, "Some Problems Involving Imperfect Half-Planes," in Electromagnetic Scattering, P.L.E. Uslenghi, Editor, New York: Academic Press, pp. 185-219, 1978.
- [2] W.D. Burnside, Ken W. Burgener, "High Frequency Scattering by a Thin Lossless Dielectric Slab," IEEE Trans. on Antennas and Propagation, Vol. AP-31, No. 1, pp. 104-110, January 1983.
- [3] G.T. Ruck, Editor, Radar Cross-Section Handbook, Volume 2, New York: Plenum, 1970.
- [4] E.F. Knott, V.V. Liepa and T.B.A. Senior, Non-Specular Radar Cross Section Study, The University of Michigan Radiation Laboratory Report No. 011062-1-F (1973).
- [5] E.F. Knott, V.V. Liepa and T.B.A. Senior, Non-Specular Radar Cross Section Study, The University of Michigan Radiation Laboratory Report No. 011764-1-T (1974).
- [6] J.B. Keller, "A Geometrical Theory of Diffraction," in Calculus of Variations and its Applications, L.M. Graves, Ed., New York, McGraw-Hill, pp. 27-52, 1958.
- [7] J.B. Keller, "The Geometric Optics Theory of Diffraction," presented at the 1953 McGill Microwave Optics Symposium, A.F. Cambridge Research Center, Report TR-59-118 (II), pp. 207-210, 1959.
- [8] J.B. Keller, "Geometrical Theory of Diffraction," J. Opt. Soc. Amer., Vol. 52, pp. 116-130, 1962.
- [9] R.G. Kouyoumjian, "The Geometrical Theory of Diffraction and its Applications," in Numerical and Asymptotic Techniques in Electromagnetics, R. Mittra, Ed., New York, Springer-Verlag, 1975.
- [10] R.G. Kouyoumjian, P.H. Pathak, and W.D. Burnside, "A Uniform GTD for the Diffraction by Edges, Vertices, and Convex Surfaces," in Acoustic, Electromagnetic and Elastic Wave Scattering - Focus on the T-Matrix Approach, V.K. Varadan, V.V. Varadan, Eds., New York: Pergamon Press, pp. 373-397, 1980.
- [11] R.G. Kouyoumjian and P.H. Pathak, "A Uniform Geometrical Theory of Diffraction for an Edge in a Perfectly Conducting Surface," Proc. IEEE, Vol. 62, No. 11, pp. 1448-1461, November 1974.

- [12] A.A. Pistol'kors, V.A. Kaplun and L.V. Knyazeva, "On the Diffraction of Electromagnetic Waves at Dielectric or Semi-conducting Sheets," Radio Eng. and Electronic Physics (USSR), Vol. 4, pp. 1-13, 1959.
- [13] N.G. Khrebet, "Diffraction of Plane Electromagnetic Waves on the Edge of a Dielectric Half Plane," Radio Eng. and Electronic Physics (USSR), Vol. 13, pp. 331-338, 1968.
- [14] F. Oberhettinger, "Diffraction of Waves by a Wedge," Communications on Pure and Applied Mathematics, 7, pp. 551-563, 1954.
- [15] A. Mohsen and M.A.K. Hamid, "Diffraction by a Dielectric-Loaded Wedge," Radio Science, Volume 8, No. 1, pp. 71-80, January 1973.
- [16] M.A.K. Hamid, "Diffraction Coefficient of a Conducting Wedge Loaded with a Dielectric Slab on the Illuminated Surface," IEEE Trans. on Antennas and Propagation, Vol. AP-21, No. 5, pp. 728-729, September 1973.
- [17] Iain Anderson, "Plane Wave Diffraction by a Thin Dielectric Half-Plane," IEEE Trans. on Antennas and Propagation, Vol AP-27, No. 5, pp. 584-589, September 1979.
- [18] K.W. Burgener, W.D. Burnside, "High Frequency Scattering from a Thin Lossless Dielectric Slab," The Ohio State University, ElectroScience Laboratory, Department of Electrical Engineering, prepared under Grant NSG 1498 for NASA; Langley Research Center, Master's Thesis, 1979.
- [19] Roberto G. Rojas and W.D. Burnside, "GTD Analysis of Airborne Antennas Radiating in the Presence of Lossy Dielectric Layers," The Ohio State University, ElectroScience Laboratory, Department of Electrical Engineering; prepared under Grant NSG 1498 for NASA, Langley Research Center, Master's Thesis, August, 1981.
- [20] Roger F. Harrington, Time Harmonic Electromagnetic Fields, McGraw-Hill Book Company, New York, 1961.
- [21] Robert E. Collin, Field Theory of Guided Waves, McGraw-Hill Book Company, New York, 1960.
- [22] T.B.A Senior, "Impedance Boundary Condition for Imperfectly Conducting Surfaces," Apply Scientific Research, Section B, Vol. 8, pp. 418-436, 1960.
- [23] Y.M. Hwang, "The Diffraction at the Edge of a Uniform Impedance Surface," Ph.D. Dissertation, The Ohio State University, Department of Electrical Engineering, 1973.

- [24] G.D. Maliuzhinets, "Excitation, Reflection and Emission of Surface Waves from a Wedge with Given Face Impedances," Soviet Physics Dokl. Volume 3, pp. 752-755, 1959.
- [25] O.M. Bucci and G. Franceschetti, "Rim Loaded Reflector Antennas", IEEE Trans. on Antennas and Propagation, Vol. 28, pp. 297-305, May 1980.
- [26] Ovidio M. Bucci and Giorgio Franceschetti, "Electromagnetic Scattering by a Half-Plane with Two Phase Impedances," Radio Science, Vol. 11, No. 1, pp. 49-59, January 1976.
- [27] V.G. Vaccara, "Electromagnetic Diffraction from a Right-Angled Wedge with Soft Conditions on One Face," Opt. Acta, Vol. 28, pp. 293-311, March 1981.
- [28] R. Tiberio, F. Bessi, G. Manara, and G. Pelosi, "Scattering by a Strip with Two Face Impedances at Edge-On Incidence," Radio Science, Vol. 17, No. 5, pp. 1199-1210, September-October 1982.
- [29] R. Tiberio, G. Pelosi, "High-Frequency Scattering from the Edges of Impedance Discontinuities on a Flat Plane," IEEE Trans. on Antennas and Propagation, Vol. AP-31, No. 4, pp. 590-596, July 1983.
- [30] John J. Bowman, "High Frequency Backscattering from an Absorbing Infinite Strip with Arbitrary Face Impedances," Canadian Journal of Physics, Vol. 45, pp. 2409-2430, 1967.
- [31] R. Tiberio, G. Pelosi, and G. Manara, "A Uniform GTD Formulation for the Diffraction by a Wedge with Impedance Faces," IEEE/APS Symposium and National Radio Science Meeting in Boston, Massachusetts, June 1984.
- [32] B. Noble, Methods Based on the Wiener-Hopf Technique, Pergamon Press, Inc., New York, 1958.
- [33] D.S. Jones, "A Simplifying Technique in the Solution of a Class of Diffraction Problems," Quarterly Journal of Mathematics, pp. 189-196, 1952.
- [34] R. Mittra and S.W. Lee, Analytical Techniques in the Theory of Guided Waves, MacMillan Co., New York, Collier-MacMillan Ltd., London, 1971.
- [35] T.B.A. Senior, "Diffraction by an Imperfectly Conducting Half-Plane at Oblique Incidence," Apply Scientific Research, Section B, Vol. 8, pp-35-61, 1959.
- [36] George Arfken, Mathematical Methods for Physicists, Second Edition, Academic Press, Inc., New York, 1970.

- [37] Lev A. Weinstein, The Theory of Diffraction and the Factorization Method, The Golem Press, Boulder, Colorado, 1969.
- [38] EE 819 notes, Spring Quarter 1981, Prof. R.G. Kouyoumjian.
- [39] Robert E. Collin and F.J. Zucker (editors), Antenna Theory, Part II, McGraw-Hill, 1969.
- [40] P.H. Pathak, Private Communication.
- [41] P.C. Clemmow, The Plane Wave Spectrum Representation of Electromagnetic Fields, Pergamon Press, Ltd., 1966.
- [42] Leopold B. Felsen and Nathan Marcuvitz, Radiation and Scattering of Waves, Prentice-Hall, Inc., Englewood Cliffs, New Jersey, 1973.
- [43] P.H. Pathak, "A GTD Analysis of the Radiation from Slots in Planar and Cylindrical Perfectly-Conducting Structures with a Surface Impedance Patch," ElectroScience Laboratory Report 4396-2, pp. 46-54, February 1977.
- [44] William H. Beyer, Editor, CRC Standard Mathematical Tables, 25th Edition, CRC Press, West Palm Beach, Florida, 1978.
- [45] J.J. Bowman, T.B. Senior, P.L.E. Uslenghi, Electromagnetic and Acoustic Scattering by Simple Shapes (Part I), North-Holland Publishing Company, 1969.
- [46] P.H. Pathak, "TM Surface Wave Diffraction by a Truncated Dielectric Slab Recessed in a Perfectly Conducting Surface," Ph.D. Dissertation, The Ohio State University ElectroScience Laboratory, Department of Electrical Engineering, pp. 3-4, 1973.
- [47] R.G. Kouyoumjian, and P.H. Pathak, "The Dyadic Diffraction Coefficient for a Curved Edge," The Ohio State University ElectroScience Laboratory, Department of Electrical Engineering; prepared under Grant No. NGR36-008-144 for National Aeronautics and Space Administration, Annual Report 3001-3, August 1973.
- [48] W.D. Burnside, N. Wang, and E.L. Pelton, "Near Field Pattern Computations for Airborne Antennas," IEEE Trans., Vol. AP-28, pp. 318-327, May 1980.
- [49] C.T. Tai, "The Effect of a Grounded Slab on the Radiation from a Line Source," Journal of Applied Physics, Vol. 22, No. 4, pp. 405-414, April 1951.
- [50] Roger F. Harrington, Field Computation by Moment Methods, Robert E. Krieger Publishing Company, Malabar, Florida, 1982.

- [51] Jack H. Richmond, "Scattering by a Dielectric Cylinder of Arbitrary Cross Section Shape," *IEEE Trans. on Antennas and Propagation*, Vol. AP-13, No. 3, pp. 334-341, May 1965.
- [52] Jack H. Richmond, "TE-Wave Scattering by a Dielectric Cylinder of Arbitrary Cross-Section Shape," *IEEE Trans. on Antennas and Propagation*, Vol. AP-14, No. 4, pp. 460-464, July 1966.
- [53] Arthur D. Yaghjian, "Electric Dyadic Green's Functions in the Source Region," *Proceedings of the IEEE*, Vol. 88, No. 2, pp. 248-263, February 1980.
- [54] M. Abramowitz and I.A. Stegun (editors), Handbook of Mathematical Functions with Formulas, Graphs, and Mathematical Tables, National Bureau of Standards, Applied Mathematics Series, December 1972.
- [55] R. Tiberio and R.G. Kouyoumjian, "A Uniform GTD Solution for the Diffraction by Strips Illuminated at Grazing Incidence," *Radio Science*, Volume 14, Number 6, pp. 933-941, November-December 1979.
- [56] E.C. Titchmarsh, Theory of Fourier Integrals, New York: Oxford University Press, 1937.
- [57] Julius A. Stratton, Electromagnetic Theory, McGraw-Hill Book Company, New York, 1941.
- [58] J. Meixner, "The Behavior of Electromagnetic Fields at Edges," *Ins. Math. Sci. Research. Report EM-72*, New York University, New York, Dec. 1954.
- [59] P.H. Pathak, "Techniques for High Frequency Problems," to appear in *Antenna Handbook*, eds., Y.T. Lo and S.W. Lee, Publisher: ITT-Howard W. Sams and Co., Inc.